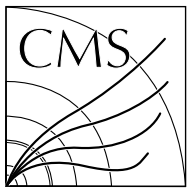

CMS U1TDR

2011/05/23

2011/05/23
Head Id: 16688
Archive Id: 56952M
Archive Date: 2010/08/31
Archive Tag: trunk

TECHNICAL PROPOSAL FOR THE UPGRADE OF THE CMS DETECTOR THROUGH 2020

The Large Hadron Collider at CERN has begun operations at 7 TeV center of mass energy. CERN plans to run at this energy until the end of 2012 with the goal of providing an integrated luminosity of a few fb $^{-1}$ to the CMS and ATLAS experiments.The LHC will then shut down for 1.5 to 2 years to make the revisions necessary to run at $\sim$14 TeV. Operation resumes in 2014. In 2017/18, there will be another long shutdown to prepare the LHC to operate at and eventually above the design luminosity of $10^{34}\,\mathrm{cm}^{-2}\,\mathrm{s}^{-1}$. Operation will then resume with the luminosity rising gradually during this period to $2\times\ 10^{34}\,\mathrm{cm}^{-2}\,\mathrm{s}^{-1}$. The two long shutdowns provide CMS an opportunity to carry out improvements to make the experiment more efficient, to repair problems that have been uncovered during early operations, and to upgrade the detector to cope with the ultimate luminosity that will be achieved during this period. The detector work involves the hadron calorimeters, the muon detectors, the pixel detector, the beam radiation monitoring and luminosity measurement system, the trigger, the data acquistion system, and the CMS infrastructure and facilities. The purpose of this report is to explain the need for these improvements, repairs and upgrades and the plans for carrying them out and installing them in the two long shutdowns forseen in 2013/14 and 2017/18.

Contents

Chapter 1

Introduction

The CERN Large Hadron Collider (LHC) is designed to reach a luminosity of $10^{34}\,\mathrm{cm}^{-2}\,\mathrm{s}^{-1}$ at a center of mass energy of 14 TeV. It is already the world's highest energy particle collider and opening a new frontier in particle physics. When it achieves its design performance, experiments will be able to fully probe the TeV energy scale relevant to electroweak symmetry breaking and the Higgs phenomenon and increase significantly the discovery reach for supersymmetry, extra dimensions of space and time, and other "Beyond the Standard Model (BSM)" physics. This is expected to lead to an unparalleled opportunity for discovery and a revolution in our understanding of particle physics.

The LHC began operation in late 2009 and is now producing collisions at 7 TeV center of mass energy until the end of 2012 (or perhaps into the beginning of 2013). In July of 2010, CERN released a technical plan for LHC operations describing the expected luminosity growth over the next two decades. The plan was further refined in January/February of 2011. The main change is that 7 TeV operation, which was to be completed in 2011 in the July 2010 plan, will now continue through 2012. The 2012 shutdown to increase the LHC energy to 14 TeV will be delayed by one year until 2013 with operations resuming a few months into 2014.

The twenty year period divides roughly into two equal parts:

Phase 1 In this period, which started in March of 2010 and extends until at least 2020, the LHC will achieve its design energy and luminosity. Towards the end of this period, the luminosity should increase beyond the original design value to over $2\times10^{34}\,\mathrm{cm}^{-2}\,\mathrm{s}^{-1}$. Two major "long shutdowns", called LS1 and LS2, of at least a year each will be needed to accomplish these objectives. Improvements and upgrades to some CMS sub-detectors will be necessary to fully exploit the luminosity, especially towards the end of this phase. The two long LHC shutdowns provide the access to the CMS collision hall needed to make improvements. The pixel detector will be replaced and the trigger upgraded in 2016 but CMS will utilize the present outer microstrip tracker throughout the Phase 1 period.

Phase 2: After 2020, there will be a major machine upgrade with an extended long shutdown, LS3, to achieve considerably higher annual integrated luminosity, perhaps by a factor of 5, over that achieved in the last part of Phase 1. At the same time as the accelerator is upgraded, the experiment will also undergo major transformations to handle the higher luminosity. In particular, CMS will completely replace the tracking detector and will make many other changes to sub-detectors and the trigger and data acquisition systems.

It is the goal of CMS always to have a detector capable of profiting fully from the LHC performance. Each shutdown for machine upgrades provides an opportunity to carry out improvements to make the experiment more efficient, to repair problems uncovered during operations,

and to upgrade the detector to cope with the luminosity that will be achieved during the subsequent running period(s).

This Technical Proposal presents the improvements, replacements, and upgrades to the detector to optimize CMS performance during Phase 1 of LHC operations and thereby maximize its physics output. The work foreseen involves muon detectors, hadron calorimeters, the pixel detector, the trigger and data acquistion, and the beam radiation monitoring and luminosity measurement system. A series of improvements to CMS infrastructure will ensure efficient implementation of the upgrades and maintenance of the upgraded detectors.

This proposal is based on the following key inputs:

1. the CERN "10 Year Technical Plan" for LHC operations presented in July of 2010 and modified in January/February of 2011, which specifies luminosity goals and also shutdown periods during which major changes to the detector can be made;

2. the challenges that arise from higher luminosities and the practical issues of maintaining the detector for a decade or more;

3. the design of the CMS detector, its actual performance so far, and its projected performance as the instantaneous luminosity rises above the design value and as the integrated lumnosity increases; and

4. practical considerations of how to modify an operating detector, which could be participating in a "discovery in progress". Example issues are the inability to make major changes to the on-detector infrastructure, problems of working in an irradiated environment; the beam time sacrificed to commission a new detector, which must be compared with the gains from superior performance of the replacement; and the risk of causing damage while making modifications.

The outline of this Technical Proposal is as follows: First in the remaining parts of this introductory chapter, a brief description of CMS detector is given, emphasizing features relevant to this proposal, and the items enumerated above are discussed. There follows a brief summary of each of the subdetector upgrade programs. In chapter 2, the physics motivation for the Phase 1 upgrade is outlined and selected sub-detector performance plots presented to demonstrate benefits gained from the upgrades; this chapter should be viewed as a work in progress, as will be explained. Chapter 3 presents the proposal for the upgrade for the CMS muon detection subsystems. Chapter 4 presents the upgrades to the hadron calorimeters at low pseudorapidity (less than 3). Chapter 5 discusses improvements to the calorimeters in the high pseudorapidity regions. Chapter 6 presents the upgrade of the pixel detector, the only part of the CMS Tracker that can be modified during Phase 1. Chapters 7 and 8 explain the changes required by the Trigger and Data Acquisition systems to handle higher instantaneous rates and larger event sizes arising from increased event pileup and larger channel counts that will be present towards the end of Phase 1. Chapter 9 describes improvements to the beam monitoring system, which protects the detector from beam-related accidents, provides inputs to the zero and minimum bias triggers, measures the luminosity, and produces many measurements of beam quality and beam-related backgrounds that are fed back to the accelerator teams. Chapter 10 discusses infrastructure improvements and facilities necessary for construction and commissioning of upgraded detectors, installation into CMS, and sustained operations thereafter. Finally, chapter 11 provides a provisional estimate of the total cost, a preliminary schedule of the major installation activities, and guidelines on organization of the project.

To complete the picture, an appendix explains the R&D required for the Phase 2 upgrade, which must proceed in parallel with Phase 1 developments in order to have upgraded detectors ready for installation soon after 2020. The Phase 2 upgrades represent a serious challenge as requirements are in many ways more difficult than those of Phase 1.

1.1 A brief introduction to CMS

An exploded view of CMS is shown in Fig. 1.1. CMS was assembled on the surface in sections that were lowered 100m through a large shaft into the collision hall. At the heart of the experiment is a 13m long, 6m diameter, 4T superconducting solenoid providing large bending power (12 T-m) for tracking measurements and whose return field is large enough to saturate the 1.5 m iron plates in the return yoke, used for muon track reconstruction. The gaps between the plates provide slots for the four muon tracking stations, each of which consists of several layers of aluminum drift tubes (DT) in the barrel region and cathode strip chambers (CSCs) in the endcap region. Each system is complemented by resistive plate chambers (RPCs).

The bore of the magnet is large enough to accommodate the inner tracker and the calorimetry systems. The tracking volume is contained in a cylinder of 5.8m length and 2.6 m diameter. CMS employs ten layers of silicon microstrip detectors, which provide the required granularity and precision to reconstruct efficiently high multiplicity events. The silicon microstrip tracker with its long bending path, combined with the strong solenoidal field, provides excellent momentum resolution. In addition three layers of silicon pixel detectors in the barrel region, complemented by two forward disks at each end, seed the track reconstruction and improve the measurement of the impact parameter measurements, as well as providing points to reconstruct secondary vertices.

The electromagnetic calorimeter (ECAL) provides coverage up to $|\eta| = 3$ and uses lead tungstate ($PbWO_4$) crystals whose scintillation light is detected by silicon avalanche photodiodes (APDs) in the barrel and vacuum phototriodes (VPTs) in the endcaps. A preshower system is installed in front of the endcap ECAL for π^o rejection.

The ECAL is surrounded by a brass/scintillator sampling hadron calorimeter (HCAL) with coverage up to $|\eta| = 3$. The light is converted by wavelength shifting (WLS) fibres embedded in the scintillator tiles and channeled via clear fibres to hybrid photodiodes (HPDs) that provide some gain and can operate in high axial magnetic fields. This central calorimetry is complemented by a "tail-catcher" (HO) in the barrel region insuring that hadronic showers are sampled with nearly eleven interaction lengths. Coverage from $\eta = 3$ to $\eta = 5$ is provided by an iron/quartz-fibre calorimeter (HF). The Cherenkov light emitted in the quartz fibres is detected by photomultipliers. The HF ensures full geometric coeverage for measurement of the transverse energy in the event. Two additional calorimeters, called CASTOR and the Zero Degree Calorimeter (ZDC), not shown in Fig. 1.1, provide coverage at even higher rapidities than the HF.

The modular construction of CMS is the key element for maintenance and provision of access for detector upgrades. The solenoid and the central yoke block, called YB0, are the only fixed structures in CMS. The other large slices through the experiment, either "rings" or "disks", all move to permit access to the interior. The endcap disks can be pulled back and separated for access to the CSCs and endcap RPCs. The rings of the solenoid return yoke can be separated to provide access to the muon DTs. With the disk pulled back, it is possible to access the endcap HCAL, ECAL, and preshower, all of which are mounted on the disk closest to the Interaction Point. Also, with all disks retracted, there is access to the vacuum tank region. It is possible to

remove the pixel detector, which is inserted in two halves around the beam pipe. This was a requirement because of the need to bake out the beam pipe. The pixel detector can be removed or reinstalled in a few days.

While the ECAL, HCAL and Silicon Strip tracker slide on rails, they cannot easily be extracted because it would require removal of a very large number of power and control cables, optical fibers and cooling pipes. However, the front end electronics of the HCAL is accessible when the vacuum tank is opened. The front end electronics of the HO is accessible when the return yoke rings are separated. The HF can be lowered and moved to a special garage for maintenance. Finally, CASTOR and the ZDC can be removed from the beam line by cranes.

CMS is triggered by dedicated custom electronics located in an underground control room USC55, which forms various partial triggers using trigger primitives from the front ends of the calorimeters and muon detectors. These are then sent to the Global Level 1 trigger, which processes up to 40 million beam crossings per second and can accept up to 100,000 of them for further processing. The latency of the Level 1 trigger is 3.6 μs and data must be stored on the detectors during this time. When a Level 1 Accept occurs, data fragments from individual detectors are sent to the High Level Trigger (HLT), operating on a large computer cluster to build complete events. The HLT performs a lean version of the offline reconstruction using full event data and uses the result to decide if the event should be written, together with trigger information, to mass storage for subsequent analysis. CMS writes out up to 300 events/second.

A detailed description of the CMS detector is given elsewhere [1].

1.2 The CERN "10 Year Technical Plan" for operation of the LHC

The CERN 10 Year Technical Plan is shown schematically in Fig. 1.2. It has long periods of collider operation interleaved with shutdowns of a year or more each in 2013 and 2016. The major intervals are:

2010-2012: 7 TeV operation to commission the LHC and the experiments and make early measurements of physics at this energy;

2013/14: Long Shutdown 1 (LS1) to repair magnet splices to allow the LHC to operate safely at 14 TeV and to improve collimation to permit operation at high luminosity;

2014-2016: 14 TeV run to explore Terascale physics at moderate luminosity within the capability of existing detectors;

2017: Long Shutdown 2 (LS2) to improve collimation in the LHC to enable operation at highest Phase 1 luminosities; to prepare the LHC for the addition of Crab Cavities and RF cryo-systems needed for Phase 2; to connect Linac4 into the injector complex; and to upgrade the energy of the PS Booster to reduce the beam emittance; and

2018- 2020: 14 TeV high luminosity run to more thoroughly explore Terascale physics and to study in more detail new phenomena observed in the preceding runs using the upgraded detectors.

The LHC goal for peak instantaneous luminosity defines the number of interactions per beam crossing that the experiments must handle; and the goal for integrated luminosity determines how radiation-resistant the detectors must be. The expected luminosity of the LHC is shown in Figs 1.3 and 1.4. The projections provided in July of 2010 have been modified by us to account

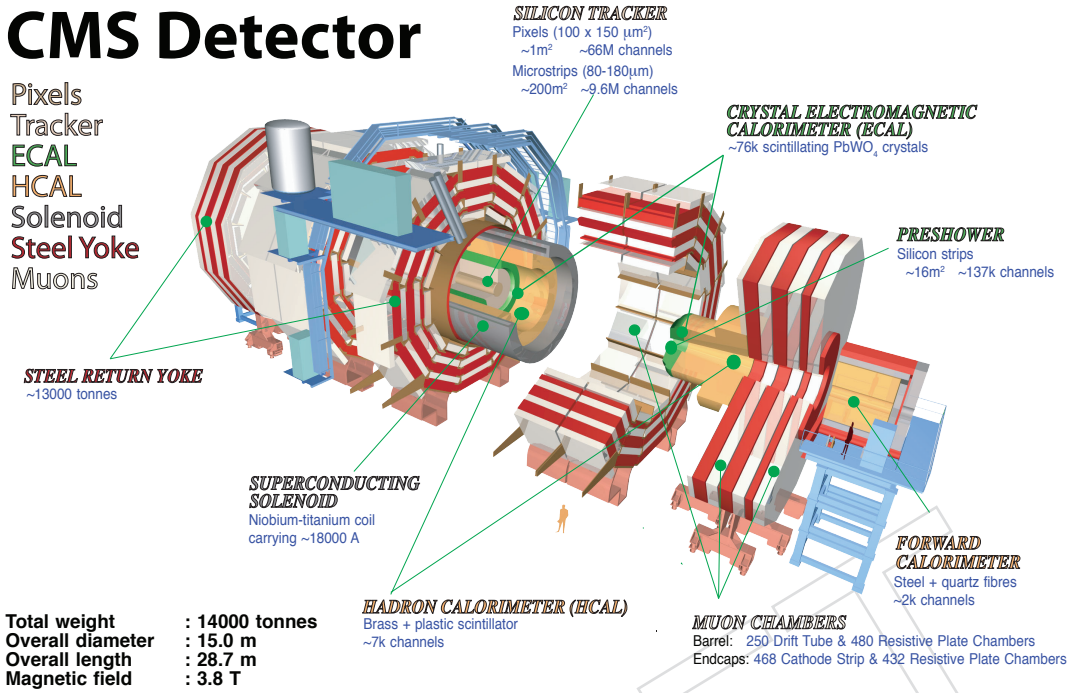

Figure 1.1: A schematic representation of the CMS Detector, with its various sections in retracted positions. The central yoke block is called YB0. The next yoke block 1 (YB+1, with a corresponding YB-1 on the other side of YB0), is shown partially moved away from YB0. The yoke block 2 (YB+2, with a corresponding YB-2 on the other side) is shown fully moved past the vacuum tank of the solenoid. The endcap calorimeters are shown attached to endcap disk YE+1, then the endcap CSCs and RPCs, then YE+2, more muon chambers, and YE+3, with additional muon chambers on the front and back. Eventually, another disk, YE+4 will be added at the end to provide shielding from beam-related backgrounds. This configuration is repeated on the other end, with designations now changed to YE-1, YE-2, YE-3, and eventually YE-4. In operation, the detector is closed by moving all the pieces together.

Figure 1.2: CERN technical plan for operations over the next decade as modified in January/February 2011

for the change in plan in 2011 based on the latest operational experience from 2011 and its projection to 2012. For the 14 TeV operation starting in 2014, we have used the projections from July of 2010 but moved them ahead by one year to account for the extra year of 7 TeV operation. We have left the second long shutdown in 2016, which makes the first 14 TeV run shorter than originallly forseen.

It is worth noting that in the first half of 2011 the LHC luminosity has exceeded the July 2010 projection by more than a factor of 4 and is likely to go higher. The LHC has succeeded in accelerating bunches of $1.7\times10^{1}0$ protons, which is 1.5 times the design value. The LHC is also operating with a bunch crossing interval of 50 ns rather than 25 ns. Consequently, the number of interactions per crossing is much higher than expected in the orginal 2010 plan. If it proves to be impossible to run at 25 ns, the number of interactions per crossing after 2017 would be twice the number in Fig. 1.3 and would create an even more severe challenge for the detectors. Figure 3 is based on the July 2010 version of the LHC schedule and has not been adjusted for running

in 2012. It however does give a reasonable indication of the challenges that the upgrades must respond to over the decaade.

Towards the end of Phase 1 the LHC will run at or above the original LHC design luminosity of $1\times10^{34}\,\mathrm{cm}^{-2}\,\mathrm{s}^{-1}$; about 80% of the total Phase 1 integrated luminosity will be delivered in the three year run starting in 2017. About half of the total will be delivered in annual periods with a peak luminosity **above** what the detectors were designed to handle. The two long shutdowns provide CMS with the opportunity to make improvements to cope with the evolution of the machine performance.

Year	TeV	OEF	β*	Nb	Ib	Itot	MJ	Peak luminosity	Pile up	pb-1/day	Physics Days	Integrated (fb-1/year)	Total Int (fb-1)
2010	3.50	0.20	2.00	796	8.0E+10	6.4E+13	36.0	1.886E+32	1.2643	3.3	20.0	0.1	0.07
2011	3.50	0.25	2.00	796	8.0E+10	6.4E+13	36.0	1.886E+32	1.2643	4.1	240.0	0.98	1.04
2012												0.0	1.0
2013	6.50	0.20	0.55	796	1.15E+11	9.2E+13	96.1	2.632E+33	17.6429	45.5	180.0	8.2	9.2
2014	7.00	0.20	0.55	1404	1.15E+11	1.6E+14	182.5	5.000E+33	19.0000	86.4	240.0	20.7	30.0
2015	7.00	0.20	0.55	2808	1.15E+11	3.2E+14	365.0	1.000E+34	19.0000	172.8	210.0	36.3	66.3
2016											0.0	0.0	66.3
2017	7.00	0.25	0.55	2808	1.15E+11	3.2E+14	365.0	1.000E+34	19.0000	216.0	240.0	51.8	118.1
2018	7.00	0.28	0.55	2808	1.50E+11	4.2E+14	476.1	1.701E+34	32.3251	411.6	240.0	98.8	216.9
2019	7.00	0.30	0.55	2808	1.70E+11	4.8E+14	539.6	2.185E+34	41.5198	566.4	210.0	118.9	335.8
2020											0.0	0.0	335.8
2021	7.00	0.20	0.30	2808	1.70E+11	4.8E+14	539.6	4.006E+34	76.1197	692.3	150.0	103.8	439.7
2022	7.00	0.27	0.25	2808	1.80E+11	5.1E+14	571.3	5.390E+34	102.4060	1257.3	220.0	276.6	716.3
2023	7.00	0.27	0.25	2808	1.80E+11	5.1E+14	571.3	5.390E+34	102.4060	1257.3	220.0	276.6	992.9
2024	7.00	0.29	0.25	2808	1.80E+11	5.1E+14	571.3	5.390E+34	102.4060	1350.5	220.0	297.1	1290.0
2025	7.00	0.29	0.25	2808	1.80E+11	5.1E+14	571.3	5.390E+34	102.4060	1350.5	220.0	297.1	1587.1
2026	7.00	0.29	0.25	2808	1.80E+11	5.1E+14	571.3	5.390E+34	102.4060	1350.5	220.0	297.1	1884.2
2027	7.00	0.29	0.25	2808	1.80E+11	5.1E+14	571.3	5.390E+34	102.4060	1350.5	220.0	297.1	2181.3
2028	7.00	0.29	0.25	2808	1.80E+11	5.1E+14	571.3	5.390E+34	102.4060	1350.5	220.0	297.1	2478.4
2029	7.00	0.29	0.25	2808	1.80E+11	5.1E+14	571.3	5.390E+34	102.4060	1350.5	220.0	297.1	2775.5
2030	7.00	0.29	0.25	2808	1.80E+11	5.1E+14	571.3	5.390E+34	102.4060	1350.5	220.0	297.1	3072.6

13

Figure 1.3: The expected luminosity for each year of LHC operations between 2010 and 2020. Shown are the energy per beam in TeV ; the operational efficiency fraction (OEF); the β^* at the CMS/ATLAS IRs in meters; the number of colliding bunches (Nb) in each beam; the number of protons (Ib) in each bunch; the total number of protons in each beam (Itot); the energy in each beam (MJ); the peak luminosity in $\mathrm{cm}^{-2}\mathrm{s}^{-1}$; the pile up, that is the average number of interactions per crossing at the peak luminosity; the luminosity/day in pb^{-1}; the number of days of running for physics; and the integrated luminosity/year in fb^{-1}. The last column shows the integrated luminosity from the beginning of the LHC program in 2010 in fb^{-1}.

Following the 10 year Phase 1 period, there will be a long shutdown for further improvements to the LHC to enable it to deliver up to $300\,\mathrm{fb}^{-1}$ per year. This will be a new era, referred to as the Phase 2 LHC or sometimes as the High Luminosity LHC (HL-LHC), characterized by ultra-high luminosity. The detectors, including the main tracking systems, must be rebuilt to deal with the extreme radiation levels and large numbers of interactions per beam crossing. There follows another ten years of operation at this new higher luminosity. During "Phase 2" of LHC Operation the experiments would integrate up to $3000\,\mathrm{fb}^{-1}$, allowing them to complete

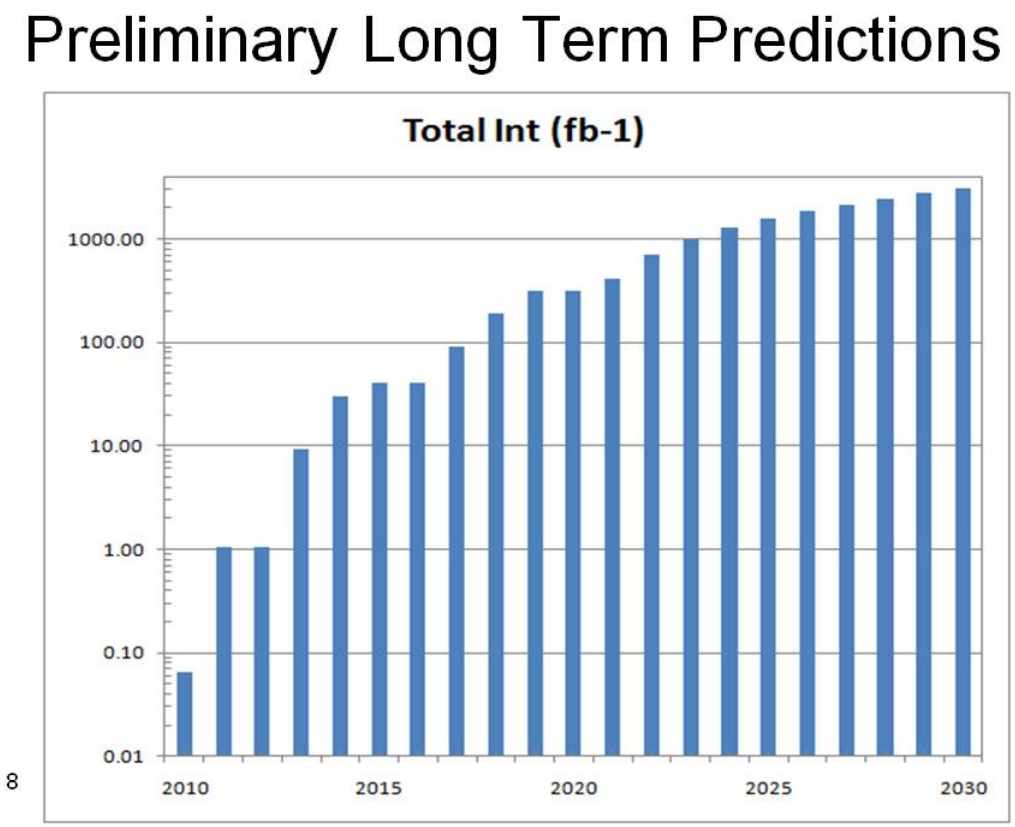

Figure 1.4: Log plot of the integrated luminosity as a function of year from 2010 to 2030

their exploration and study of physics at the Terascale. The construction of detectors that can operate in Phase 2 is beyond the scope of this document except for the appendix on upgrade R&D noted above.

1.3 Challenges Addressed by the Phase 1 Upgrade Plan

At the end of the Phase 1 period, the peak luminosity is expected to exceed what CMS was designed for by a factor of two. Here follows a brief summary of the problems that must be addressed to operate successfully throughout Phase 1. Chapters 3-9 provide the details of the sub-detector challenges to be addressed, many of which are related to operating at high luminosity.

1.3.1 Issues related to collisions

1.3.1.1 Issues related to instantaneous luminosity

Bunches of approximately 1.15×10^{11} protons collide in the LHC every 25ns. About 20 interactions take place each crossing when the luminosity is $10^{34}\,\mathrm{cm}^{-2}\,\mathrm{s}^{-1}$, for which 2808 bunches are required, and 40 interactions/crossing towards the end of Phase 1, using an increased number of protons. The occurrence of many interactions in a crossing is called "pileup".

Most of the interactions are "soft" or "peripheral" interactions which do not make high mass states or contribute to the study of Electroweak or BSM physics. Very rarely a "hard collision" capable of making a high mass state and therefore of interest occurs. The CMS trigger recog-

nizes such events (actually the crossing containing the event) and preserves it for subsequent analysis. For successful analysis, the detector must discriminate well between hard and soft collisions, which is more difficult in the presence of pileup. Dealing with pileup as the peak luminosity increases above the original design value is the motivation for several of the upgrades.

High instantaneous luminosity can confuse the CMS Level 1 trigger. To keep up with the 40 MHz rate, it uses partial data from events in each beam crossing and dedicated, custom hardware. At very high luminosity, With 20-40 interactions superimposed, and with only some of the event information available, trigger performance will degrade. Upgrades to the muon system and the hadron calorimeters aim to preserve the Level 1 trigger capability by providing it with more and higher quality inputs.

The CMS Higher Level Trigger (HLT) that follows Level 1 has access to the full event data and is performed on a large computer cluster so it is better able to cope with the confusion caused by high pileup.

Pileup can also confuse the offline analysis. Interactions are distributed along the collision region over several cm in z (direction parallel to the beams). CMS tracking has z-resolution better than a 1 mm and should usually associate charged tracks correctly to individual separated vertices, although efficiency will worsen in extreme conditions. However, calorimeters lack precise directional capability and hence cannot associate neutral particles, which appear as deposits of energy, with vertices. Hence some confusion and overlap between various interactions in the crossing is inevitable.

Fortunately, most soft interactions deposit very little energy in the CMS calorimeters and many of the events of real physics interest deposit large amounts. Discrimination using transverse energy thresholds requires clear separation of high energy deposits in the calorimeters from lower energies in surrounding regions, referred to as "isolation". Energy sums are constructed using data from considerable areas of ECAL and HCAL, especially for jets, and the ability to separate energy clusters inevitably worsens in the presence of pileup owing to the prsence of more neutral pions. Some improvements can, nevertheless, be made to the calorimeters to improve trigger performance.

The pileup discussed previously is from interactions in the same crossing as the interesting, triggered event, referred to as "in-time-pileup." "Out-of-time pileup" refers to the case when signals from a preceeding or following crossing contaminate the triggered crossing. This can happen because the intrinsic response of the sensor, or electronics is longer than the 25 ns bunch crossing interval. If the occupancy of a given channel is small, there is unlikely to be another particle traversing it close enough in time to contaminate the triggered bunch. Increasing the segmentation of a detector is one way to combat out-of-time pileup. Another method is to carry out more sophisticated time analysis to try to unravel signals overlapping in time. Each of these tactics is employed in the proposed upgrades.

Other sources of out-of-time pileup also exist. These include signals from very slow particles, mainly neutrons, that have scattered multiple times in the detector and may eventually deposit energy in an active element.

1.3.1.2 Integrated luminosity

Ionizing radiation in CMS also damages the detectors, so that over time the signals may decline and the noise levels may rise, compromising the performance by degrading the resolution or efficiency. Detectors may become less effective at detecting real signals and more vulnerable to

creating fake ones with serious consequences for the overall physics capability of CMS.

The understanding of radiation damage mechanisms in particle detectors and the development of radiation hard or radiation tolerant sensors and electronics was a major R&D effort for the LHC experiments. Most CMS detectors can sustain the integrated luminosity of Phase 1 with at most slight degradation.

There are two cases where radiation damage is sufficiently severe that it might be necessary to replace damaged detectors before Phase 2: one is at the inner radius of the Forward Hadron Calorimeter (HF) which receives very large doses that will reduce the transmission of the windows of the Photomultiplier Tubes (PMTs); the other is the inner layer of the barrel pixel detector which is only 4 cm from the colliding beams. The strategy to deal with these detectors is discussed in chapters 5 and 6, respectively.

1.3.2 Issues related to non-collisional background

There are backgrounds from sources other than proton collisions at the interaction point, such as

- **beam halo:** particles that migrate out of the beam and strike material such as a beam pipe or collimator and eventually produce muons that leave the LHC beam pipe and spread out. These particles are especially troublesome to large area systems such as the muon detectors.
- **beam-gas interactions:** protons in one of the beams can hit a residual gas molecule inside the vacuum pipe. The collision products may reach the detector on a direct path or may strike other material producing more secondaries that eventually reach the detector.
- **cosmic rays:** cosmic rays are always passing through the detector. Occasionally, they will occur in time with a trigger and may be overlaid on the event and be recorded as part of the crossing data. Some may pass through the pixel detector and be close enough to beam spot to mimic genuine tracks from interactions.
- **residual radiation:** the particles passing through CMS can activate the elements of the detector producing various radionuclides. Their decay products may cause signals in some detectors.

Most of these backgrounds can be rejected by topological or timing cuts or both. However, sometimes especially in the case of cosmics, the background will mimic a real track and can cause confusion to the analysis.

1.3.3 Other issues

1.3.3.1 Minimizing downtime

Downtime refers to periods when the LHC is producing collisions but CMS is not in a condition to record them. Examples are problems with the trigger or data acquisition system or one of the subdetectors. What counts for the physics productivity is the integrated luminosity recorded with a physics capable detector. If there is a failure, CMS should be able to recover from it quickly. In some cases, this means having a good supply of working spares and being able to install them quickly. Improvements to the detector and the experiment infrastructure to prevent failures that would cause downtime or help recover from failures more quickly all contribute to a successful CMS physics program. The relocation of electronics for the Drift Tube Muon trigger (Sector Collectors) from a high radiation to a low radiation area is an example of

an upgrade to eliminate a potential source of failure. Many of the infrastructure improvements discussed in chapter 10 are aimed at reducing downtime. CMS has a requirement to reduce downtime below 10% and eventually as an advanced goal below 5%.

1.3.3.2 Coping with Obsolescence

CMS construction started in the late 1990's. The technology in CMS dates back, in many cases, more than 15 years. Maintenance of the detector sometimes depends on the availability of spare components that have become obsolete and may be in short supply in coming years, which puts the operation of CMS and its physics program at risk. Possible problems must be identified and replacement electronics based on more modern and available technology must be designed and built or otherwise obtained.

1.3.3.3 Schedule uncertainty

The current schedule of shutdowns is tied directly to necessary and well-understood upgrades needed by the LHC with the biggest uncertainty probably at the transition between Phase 1 and Phase 2. One possible occurence could be that there is an indication of a physics discovery that might become conclusive with another factor of two in data, which would take about 2-3 years. If the detector or machine upgrades were behind schedule, not impossible given their complexity, it might make sense to continue to run. If that were to happen radiation damage would be an issue for the pixel detector and perhaps some other detectors. This makes it highly desirable that there be contingency in the expected lifetime of the detectors to deal with schedule variations, especially at the end of Phase 1.

1.3.3.3.1 Flexibility and agility of CMS Because of its modular design, CMS has some detectors that can be repaired or replaced in relatively short shutdowns of three to four months. The pixel detector was designed for fast installation, extraction, repair and re-installation; this has been demonstrated. The upgraded detector will be designed to facilitate rapid replacement of the first and even the second layers. If the pixel detector inner barrel layer needed to be replaced once more, it should be possible to do it with only a modest change to the LHC operating schedule. The endcap muon systems can be worked on also in short shutdown and the last disk, on which new detectors will be installed, can be worked on without opening the detector. Thus if the work to install the last endcap disk is not completed in the 2013 shutdown as planned, it can be completed during the short technical stops that occur in operations after the startup in 2014.

1.3.3.3.2 Preparing for the unexpected As experience is gained in operating the experiment, it is likely that experts will continue to identify improvements in performance that could be gained by making changes not foreseen in the original design, most of which was carried out far in the past. Recent examples are the small fraction of beam gas events whose secondaries are highly visible in the pixel detector, and the knock on recoil atoms in the ECAL APDs, whose impact on operation was larger than expected. They will now be taken into account in future ASIC or FPGA firmware developments. Another potential development concerns the accelerator where operation with 50 ns bunch spacing has been discussed as an effective means of reaching the highest luminosity. Such a change has serious impact on pileup and the performance of CMS should be carefully studied, as well as being taken into account in new ASIC designs, for e.g., the pixel system.

1.4 Issues arising from the design of the CMS detector and its actual and projected performance

By early November 2010, CMS had recorded $>40\,\mathrm{pb}^{-1}$ of data. The peak luminosity was rising quickly and had reached over $10^{32}\,\mathrm{cm}^{-2}\,\mathrm{s}^{-1}$. Even at this low luminosity, CMS was able to observe the whole known family of Standard Model particles and to begin serious physics studies at 7 TeV. For some final states, it was able to look for physics beyond the Standard Model with unprecedented sensitivity. Sub-detectors performed according to expectations in almost all respects. Collision data agree very well with Monte Carlo simulations and the detector behaves as expected. In particular, the pattern of photon conversions and nuclear interactions in the data is well reproduced by the material distribution in the simulation.

With the luminosity acquired so far, radiation damage is not seen. However, because of the way the LHC operated in this period, the detectors began to see "in time" pileup. The LHC plans to collide low-emittance bunches with at least 1.15×10^{11} protons every 25 ns. There will eventually be 2808 bunches colliding. The LHC quickly reached and exceeded the design protons/bunch. In the spring of 2011, it was colliding about 600 bunches in CMS, with a peak luminosity of $8.4\times10^{32}\,\mathrm{cm}^{-2}\,\mathrm{s}^{-1}$. Most bunches were separated from adjacent bunches by 50 ns. In this configuration, the collisions of pairs of bunches had a luminosity similar to what one would experience at 3-4$\times10^{33}\,\mathrm{cm}^{-2}\,\mathrm{s}^{-1}$. The average number of interactions per crossing is 6-8; in the data collected so far we already have many crossings containing 12 or more interactions. Hence, it is already possible to study the behavior of the detector with "in-time" pileup.

Since the luminosity will grow in steps, many projections, justifications for the upgrades, and design optimizations will continue to rely on the simulation studies and, in the case of radiation damage, on exposure studies in low energy accelerators with intense beams. Validating the simulations with collision data is presently underway so a set of runs to finalize the details of upgrade designs can be undertaken. Meanwhile, the current simulation is adequate to demonstrate the value of the proposed upgrades.

1.5 Practical considerations for upgrading an operating detector

CMS adopted the strategy of assembling the major infrastructure components of the detector - the solenoid and the iron return yoke, and the detectors - on the surface near the experiment site, and to commission and operate them above ground first and then later to lower them into the Collision Hall. This approach also guaranteed that CMS could be easily opened for maintenance and upgrades.

The installation of the upgraded detector components (discussed later in this report) presents a serious challenge that is discussed in chapter 10. However, the ability to open the detector quickly at the beginning of a shutdown and the accessibility of many components once the detector is opened provides CMS with the flexibility to incrementally upgrade the detector in a series of shutdowns. Some detectors, however, are not readily accessible and upgrading them within the planned shutdowns is not possible.

Considerations of accessibility shape the approach to the upgrades planned for CMS and presented in this document. Several other issues that shape the upgrade are discussed next.

1.5.1 Radiation Safety

The Point 5 area is now a radiation zone and there are access controls, restrictions on the removal and storage of equipment, and requirements to track and document any such move-

ments. In addition, there is the potential for exposure to ionizing radiation and contamination of the workers maintaining the detector, removing old equipment and installing new equipment.

Even though activation levels are expected to be fairly low, CERN has rather stringent limits on the exposure permitted to its staff and experimenters, very similar to those in effect at other accelerator laboratories and are well below the limits established for general radiation workers. This will limit the amount of time individuals can work on removal, in situ maintenance, and installation activities. This problem will increase as the integrated and instantaneous luminosity rise for each run. Early installation of the upgrades is therefore highly desirable. Possible exposures must be considered in the planning process using the guiding principle of ALARA ("as low as reasonably achievable") that requires that personnel exposures must be carefully monitored and minimized. Resources for the implementation of the ALARA principle and for safe decommissioning of equipment that is replaced must be accounted for either in this upgrade project or in the ongoing maintenance and operation of CMS.

1.5.2 Constraints to the Design of the Upgrades

The key constraints on the individual detector upgrades are

1. each must be capable of being installed in one of the two long shutdowns planned in 2012 and 2016 or in one of the short annual technical stops of 3 to 4 months that will occur between the major shutdowns and after 2016. CMS must be in a physics-ready state at the end of each shutdown;
2. the risk of physical damage to the detector due to upgrade activity must be minimized;
3. the risk to the program through excess startup time for physics or compromised performance must be minnimized; and
4. radiation exposure and accident risk must be minimized.

One practical aspect of these requirements is that the upgraded detectors must use the existing services. These include cables for power and high voltage, cables and fibres for signals, controls and monitoring, gas lines, and piping for cooling fluids. All the cable trays and tubes that carry these utilities are essentially full. The cables, pipes and cable trays will also become activated. The extraction of long cables running through YB0 would be incompatible with constraints (1) and (4) and possibly (3). Electrical ratings for existing power cables must be respected or, in a few cases, derogations obtained.

Another practical constraint is that some detectors cannot be removed and replaced. The pixel detector was designed to be extracted during a short shutdown for beam pipe bake-out. However, the other detectors inside the solenoid - the silicon strip tracker, the ECAL and the HCAL - cannot be removed. What can be replaced in the case of the HCAL is the front end electronics which is accessible when the detector is opened. The muon detector is outside the solenoid and is accessible, especially the endcaps, which are part of this upgrade. The back end electronics are in the underground control room, USC55. The main issue there is to integrate new electronics without incurring down time or creating a discontinuity in the data quality and consistency.

1.5.3 Physics Issues

When the upgrades are ready to be installed, CMS will be a physics experiment in progress. Many important topics require large integrated luminosity. Since the data from many years will need to be combined in a consistent way, changes have to be introduced very carefully. The new detectors or electronics will be replacing well-understood devices that, even if they are beginning to degrade, may be participating in a discovery in progress. Under that circumstance, the new detector, in order to be inserted, must demonstrate

- that it is physics-ready and will take quality data quickly without a long period of commissioning, alignment and calibration with collisions that would result in lost data; and
- that the data from it can be combined with data taken from the previous runs.

Even then, if the experimenters feel a discovery is imminent and that data from the next run are likely to confirm it, the collaboration might well be reluctant to change parts of the detector or the electronics, especially those used in the trigger. In order to avoid conflict over the value of replacements, each upgrade detector must demonstrate significant benefits compared to running with the detector it is replacing, each detector must be ready for physics with very little loss of beam time, and the software for its integration into the analysis must be available and tested before it is installed.

1.5.4 Implications for the Upgrades

This discussion above highlights the problems of making changes to an experiment in progress. They can be addressed by adequate testing before insertion into CMS, by developing tested and efficient installation procedures, quick and reliable alignment and calibration techniques, and accurate cross calibration with the devices that are being replaced. Achieving these goals requires good design and in many cases special test stands and procedures. Test beam setups with substantial detector modules may be needed to cross calibrate replacement detectors against existing ones. The costs of equipment, facilities, and activities needed to accomplish this must be included in the project costs and planning.

In the case of the off-detector trigger electronics, new devices can be installed alongside the ones they are replacing. By sending the new devices a copy of the input signals, the new and the old system trigger decisions can be compared for identical results. Only when it is established that the new components perform as well or better than the original ones can the new devices be used in the experiment and the old devices removed. For all electronics, test and burn-in facilities will be needed.

CMS addresses these issues by requiring early delivery of detectors to CERN, assembly, commissioning and operation above ground, including demonstrations using cosmic rays if possible. For off-detector trigger and data acquistion components, CMS requires detailed emulation and a means of parallel operation of existing and upgrade components (using split signals or copies of information packets). CMS also requires the provision of complete calibration and alignment procedures available in advance, complete detector simulation packages, and complete reconstruction programs. The procedure for installing the detector should be complete and designed to minimize risks. Trial insertions in mock ups are performed if possible. Some improvements to the infrastructure for carrying out installation activites in Point 5 will be undertaken as part of the upgrade program and are described in Chapter 10. When all these conditions, which are very demanding, are met, there should be consensus to install the new detector.

1.6 Summary of the proposed detector upgrades and improvements

The specific changes that the CMS Collaboration proposes to carry out between now and 2016 to optimize data taking during the Phase 1 operating period of the LHC are summarized briefly below.

1.6.1 Muon System

By 2015, the luminosity will reach $10^{34}\,\mathrm{cm}^{-2}\,\mathrm{s}^{-1}$. The in-time pileup will be right at the edge of the CMS design envelope and will present special challenges for the Muon System to trigger on muons with high tranverse momenta, which represent one of the key indicators of interesting electroweak interactions.

1.6.1.1 Cathode Strip Chambers (CSCs)

The CSC upgrade is driven by considerations of the impact of peak instantaneous luminosity on the muon trigger. It includes

1. Addition of a fourth layer of chambers (ME4/2) and associated readout and triggering electronics and services to reduce the accidental trigger rate and to preserve a low P_T threshold for the Level 1 Muon Trigger at high instantaneous luminosity;

2. Upgrade of the layer 1 (ME1/1) electronics with a new CSC "Digital" Front End Board (DCFEB) so every strip can be read out separately (they are now ganged into groups of three). This will allow ME1/1 to continue to contribute effectively to the muon trigger at high instantaneous luminosity so CMS can retain four-plane coverage from $2.1 < |\eta| < 2.5$; and

3. Deployment of new muon trigger primitive electronics to deliver the additional muon track segments, which will be produced at high lumniosity and by the additional planes, to the upgraded CSC Trigger Track-Finder.

1.6.1.2 Barrel Muon Drift Tubes (DTs)

The work on the DTs is driven by maintenance considerations over the life of the experiment. The proposed work includes

1. Generation of a supply of BTIM chips (DT front end trigger primitive chip) which are in short supply due to unexpectedly high mortality. This is achieved by replacing the Theta Trigger Boards by an FPGA-based board (or new ASIC) and recovering the BTIM chips from them; and

2. Relocation of the Sector Collector boards from the periphery of the detector where they are exposed to radiation and high magnetic fields, and where the cooling is marginal to the Underground Control Room where the environment is more congenial.

1.6.1.3 Endcap Resistive Plate Chambers (RPCs)

The RPC upgrade is driven by considerations of peak instantaneous luminosity on the muon trigger. The proposed work includes

1. Addition of a fourth layer of RPCs to extend coverage to $\eta = 1.6$ to preserve a low P_T threshold for the Level 1 Muon Trigger at high instantaneous luminosity

2. R&D to develop detectors that can extend coverage to the region $1.6 < |\eta| < 2.1$ or even higher. Possible technologies include RPCs optimzed to handle the high rate or Multi-Pattern Gas Detectors.

1.6.2 Hadron calorimeters

This upgrade is directed at handling instantaneous luminosity, integrated luminosity, overall robustness and efficiency and providing opportunities to make improvements to the trigger at all luminosities.

1.6.2.1 Calorimeters inside the CMS Solenoid (HB/HE/HO)

The following work will be done to upgrade the calorimeters inside the solenoid:

1. Replacement of the HPDs in all three detectors with an improved photodetector, the Silicon Photomultiplier (SiPM). SiPMs have better quantum efficiency, higher gain, and better immunity to magnetic fields than HPDs. Since SiPMs operate at relatively low voltages, they do not produce large pulses from high voltage breakdown that mimic energetic showers like HPDs do. These features of the SiPMS together with their low cost and compact size compared to HPDs enable several major changes to the HCAL.

2. Implementation of depth segmentation which has advantages in coping with higher luminosities and compensating for radiation damage to the scintillators. This is made possible by the use of SiPMs;

3. Use of timing to clean up backgrounds, made possible by the extra gain and better signal-to-noise of the SiPMs

4. New backend electronics designed to provide enhanced information to the upgraded Regional Calorimeter Trigger (RCT).

1.6.2.2 Forward calorimeters

The following work will be done to upgrade the forward calorimeters:

1. Replacement of the photomultipliers of the Forward Hadron Calorimeter with new photomultipliers that have thinner glass windows and metal envelopes to reduce the amount of Cherenkov light generated by charged particles passing through the glass. The Cherenkov light from the glass creates large pulse heights that look like energetic particles to the trigger and analysis. The new PMTS also have 4-way segmented anodes that provide additional rejection of these spurious signals. These PMTs also have higher quantum efficiency so the resolution of the HF will improve, and HF will last longer under irradiation. Timing electronics may eventually be installed to further reject backgrounds.

2. Replacement of the PMTs of the CASTOR detector with more radiation tolerant PMTs and improvement of the calibration and monitoring systems. In addition, improvements will be made to CASTOR's mechanical support system so it will not move when the CMS Solenoid is energized. This motion currently brings it very close to the fragile LHC vacuum pipe.

1.6.3 Pixel System

The goal of the Phase 1 upgrade is to replace the present pixel detector with one that can maintain a high tracking efficiency at luminosities up to $2 \times 10^{34}\,\mathrm{cm}^{-2}\mathrm{s}^{-1}$. The present pixel system was designed for operation with a maximum luminosity of $1 \times 10^{34}\,\mathrm{cm}^{-2}\mathrm{s}^{-1}$. Due to severe data losses in the read out chip (ROC), the present system will not sustain the extreme operating conditions expected in Phase 1 after 2016. The replacement is therefore planned in the long shutdown of 2016, which is the best and perhaps only opportunity before the luminosity exceeds $1 \times 10^{34}\,\mathrm{cm}^{-2}\mathrm{s}^{-1}$. The main features of the upgraded detector are:

1. Replacement of the current 3-layer barrel (BPIX), 2-disk endcap (FPIX) system with a 4-layer barrel, 3-disk endcap system for four hit coverage.
2. Ultra-lightweight support with CO_2 cooling and displacement of the electronic boards and connections out of the tracking volume for material reduction.
3. Development of a new readout chip with reduced data loss at higher collision rates expected in Phase 1.
4. Development of high bandwidth readout electronics and links as well as DC-DC power converters, which allow reuse of the existing fibers and cables.

The addition of the fourth barrel layer at a radius of 16 cm and the third set of forward disks will maintain the present level of tracking performance even in the high occupancy environment of the upgraded LHC. In addition, it provides a safety margin in case the first silicon strip layer of the Tracker Inner Barrel degrades more rapidly than expected. The upgraded pixel system will have a reduced mass, a reduced innermost radius and increased lever arm, altogether resulting in a significant improvement over the present system in terms of tracking, vertexing and b jet identification.

1.6.4 Trigger

The trigger system will migrate to a new technology which is more maintainable and more flexible with respect to data interconnection than the current VME system. The candidate is μ-TCA, which has become important in many commerical areas, including telecommunications and other applications requiring high speed and bandwidth, and has been used in the current version of the Global Calorimeter Trigger. The trigger upgrade includes:

1. rebuilding the Regional Calorimeter Trigger (RCT) using advanced technologies, such as μ-TCA to take advantage of the full granularity of the data available from the calorimeter front end and to implement more sophisticated clustering and isolation algorithms. This will permit the trigger to handle higher rates and more complex events;
2. rebuilding the CSC Trigger Track-Finder to accomodate the additional information from ME4/2 and ME1/1, to use more input segments and to combine a greater variety of tracks to enhance performance amidst greater occupancy and backgrounds;
3. rebuilding the RPC track finder to accomodate the additional plane of RPCs;
4. modification of the DT track finder to accomodate the move of the Sector Collectors and convert to the new trigger technology; and
5. eventual implementation of a new Timing and Trigger Control system based on more modern technology.

1.6.5 Data Acquisition System

It will be necessary to increase the bandwidth of the DAQ by a factor of 2 to 5 to handle the larger data volume produced at $2\times10^{34}\,\mathrm{cm}^{-2}\,\mathrm{s}^{-1}$ and the larger number of detector channels. It will be achieved as a result of several major technological improvements:

1. Several systems will have to be upgraded since the commercial components they use will become obsolete and unobtainable;
2. The complete Event Builder will have to be replaced in 2016 using more modern technologies capable of handling the data volumes and rates that will be encountered after the shutdown; and
3. The processors of the High Level Trigger must be replaced with faster processors to handle the increasingly complex calculations that will be needed to select events.

1.6.6 Beam monitoring system

The system that is used to monitor the beam, generate abort signals if the beam condition degrades so that it could endanger the detector, and measures beam backgrounds will require the following upgrades:

1. Construction of the Pixel Luminosity Telescope (PLT), a dedicated luminosity monitor consisting of two sets, one on each side at ±1.8 m from the interaction point, of 3 rings of 8 diamond pixel detectors. The detectors, which are at radius of 5 cm relative to the beams, are organized into 8 towers each giving a three-fold coincidences when a particle from a collision traverses it. The detector is read out every beam crossing. The number of three-fold coincidences is proportional to the luminosity. The PLT also provides information about beam backgrounds and beam quality;
2. Replacement of the Beam Scintillation Counters (BSC), which have been used to provide minimum bias triggers and measurements of the beam background. The current BSCs will suffer radiation damage and are not optimally designed for the important role they are currently playing in CMS, which was not originally foreseen. Several options are being considered; and
3. Replacement of BC1F, a diamond detector also near the location where the PLT will go, that provides single bunch readout to identify pathological beam conditions, such as serious beam losses. It will suffer radiation damage and will need to be replaced in 2016. More radiation hard devices are being evaluated.

1.6.7 Common Systems, Infrastructure Upgrades and Facilities

There are now more than two years of experience in operating the CMS detector and maintaining it. This operational experience has revealed a number of vulnerabilities that can cause downtime that can result in data loss. There are also well-understood ways to reduce the risk of opening the detector to do maintenance work or to install upgrades. The activties to strengthen the infrastructure at Point 5 both above and below ground and to develop the facilities needed to execute the upgrades, including assembly areas, test beam setups, and comissioning and "burn-in" areas, are an important part of this proposal.

CMS Common Systems include:

1. safety systems for protection of personnel and equipment;
2. the CMS solenoid and associated systems;
3. yoke, shielding, and moving systems;
4. the section of beampipe through the experiment;
5. beam and radiation monitoring systems;
6. equipment for support of logistics and integration;
7. experiment services infrastructure – power, cooling, supply systems for various gases, cabling, piping, networking, the various control rooms, and test facilities; and
8. surface assembly buildings, workshops and laoboratories.

Each of these is described and the need and plans for related upgrades and improvements is explained. Organizations that provide resources crucial to the support of CMS and the upgrade, including an "Engineering Integration Centre (ENIC)" and an "Electrical systems Integration Centre (ELIC)" are discussed. Development of facilities at the CMS surface assembly building, SX5, at Point 5, and a detector assembly and electronics integration facility in Building 904 on the CERN/Prevessin campus are described.

1.7 Other Projects under Development in this Period

The CMS collaboration is composed of a large number of energetic, creative and knowledgeable people. While the plans presented in this document form the core of the upgrade, there are many additional ideas on how to improve the CMS detector or give it features that will enable it to address new physics topics. These ideas are not as far along as the ones presented in this Technical Proposal. In some cases, the CMS collaboration has not yet endorsed the physics goals. In other cases, the R&D is at an early stage and technical feasibility has not yet been established. The current set of projects under development but not yet approved parts of the upgrade is summarized in a document that is available from CMS Upgrade management[2]. It is expected that some of these projects will become part of the Phase 1 upgrade; others may fall by the wayside for technical, scientific, or financial (priority) reasons and still others may be deferred until Phase 2. In addition, we expect still other projects to emerge and to follow a similar path. This is all part of the life of a healthy scientific enterprise.

1.8 The Challenge Ahead

The remainder of this document presents in detail the proposed CMS Upgrade Technical Plan for Phase 1 of LHC operations. It will be a challenge for the CMS collaboration to operate the experiment and analyze the data while completing R&D and designs, and then constructing and installing these upgrades. At the same time, work must continue on the R&D for the Phase 2 upgrade. However, the CMS detector has demonstrated in its early operation at the LHC that it is a remarkable scientific device. The prospects of doing physics with hundreds and eventually thousands of inverse femtobarns of data taken with the upgraded CMS is wonderfully exciting and will be well worth the effort!

Chapter 2

Physics Justification for the CMS Upgrade

A detailed physics case for the upgrade awaits crucial information that will be obtained at the LHC and CMS over the first few years of operation. Once the outlines of the new physics become visible, it will be possible to complete the applicable studies and to quantify the physics benefits of the CMS upgrade. At that time, a complete Phase 1 Upgrade Physics Technical Design Report will be written.

What is certain is that the objects that CMS is designed to detect, electrons, muons, taus, light quark and gluon jets, b-jets, top quarks, W and Z bosons, and missing E_{T}, will be the states into which these objects decay. Preserving the ability to reconstruct these objects at high luminosity with large pileup is a crucial goal of the upgrade. Moreover, the Trigger system must achieve similar high efficiency and high rejection to today's version. This chapter therefore presents physics object level summary for each of the proposed upgrades, extracted from the subsequent chapters, in one place for convenience. It also presents one physics channel studied using parameterizations of the object level performance as a first indication of what the physics will look like. The actual CMS simulation software program is now being configured with the upgraded detector choices presented in this document. It will be used for simulation studies in the future to fully prepare the physics case for the proposed upgrades.

By 2015, CMS will have seen few tens of fb^{-1} luminosity at nominal center of mass energy. It is quite likely that signatures of the Standard Model like Higgs and new physics at TeV scale will already have been discovered. In that case, the physics program beyond 2016 will be primarily for thorough exploration of Higgs sector and any new physics phenomena discovered earlier. Whether CMS has discovered something or not, the program continues with searches for rarer processes with higher mass objects, which requires higher luminosities.

The CMS detector is designed to integrate several hundred fb^{-1} of luminosity at instantaneous luminosities up to $1 \times 10^{34}\mathrm{cm}^{-2}\mathrm{s}^{-1}$ with 25 ns bunch spacing. It was not designed to operate at $2 \times 10^{34}\mathrm{cm}^{-2}\mathrm{s}^{-1}$ with 25 ns bunch spacing or at $1 \times 10^{34}\mathrm{cm}^{-2}\mathrm{s}^{-1}$ with 50 ns bunch spacing. The improvement of the muon system by the addition of the fourth station of chambers achieves the original muon trigger rate and efficiency goals under these more demanding conditions. An upgrade of the calorimeter photo-detectors and electronics is needed to mitigate its noise problems. An upgrade of the pixel system is needed to avoid serious data losses for 50 ns operation at design luminosity or at twice design luminosity with 25 ns bunch spacing. The 50-ns operation or potentially twice the instantaneous luminosity will require an additional factor of two reduction in trigger rate to keep the thresholds at the same level as planned for nominal operations, requiring a rebuilding of the trigger electronics. Besides meeting these necessary goals, we intend to further enhance the CMS physics capability by benefiting from the evolution in technologies since the time we originally built these parts of CMS.

The forward muon upgrades will provide additional muon hit measurements to achieve higher

efficiency and better resolution for muons in certain pseudo-rapidity regions, providing the necessary control on the trigger rates in those regions, in addition to significant additional acceptance for muons at the trigger level. The upgraded hadron calorimeter will provide more robustness in handling pileup by the use of appropriate weights for its different longitudinal depths in the upgraded system, improving the jet energy resolution, and providing better isolation of leptons. This will restore or even enhance the original performance of CMS. The upgraded pixel system will provide improved b-tagging, pixel track seeding and stand-alone tracking capabilities, which will enhance CMS physics reach in exploring the Higgs, where b-jets and τ-leptons are often produced in association with the Higgs boson or in its decays, and the SUSY sector where third generation sparticle masses are expected to be lighter resulting in enhanced production of b-jets and τ-leptons. The enhanced trigger system will provide necessary factor of two reduction in rate allowing CMS to operate at low enough lepton, especially τ-lepton, trigger thresholds to enable the study of the Higgs boson properties in both Standard Model and MSSM scenarios, and to better explore SUSY states. Somewhat imporoved signal efficiencies are an added bonus.

2.1 Simulation Setup

In order to establish the physics justification for the proposed CMS upgrades we have begun a simulation exercise. A detailed simulation program with updated geometries, detector materials and detector response to particles is used to make choices amongst several possible detector upgrade scenarios, whereas a parameterized fast simulation program is used to make trigger/physics studies because the full simulation is too time consuming. The standard CMS fast simulation is used for trigger/physics studies with modifications to the parameterizations of performance of upgraded systems. In both cases the options are built as part of current CMS software, so that bulk of the detector description remains as is, and the analysis infrastructure is reused. Pileup of multiple events in a bunch crossing at the level expected during high luminosity operation beyond 2016, i.e., ~ 50 inelastic interactions per crossing, is simulated. While the detailed studies using the full simulation include both in-time and out-of-time pileup for 50ns operation, the fast simulation considers only the in-time pileup for simplicity. A summary of detailed detector studies made is presented here, and further elaborations are provided in the sub-detector chapters. The fast simulation results of expected physics benefits from L1 trigger studies are presented below.

Finally, a study of Higgs production in association with Z bosons with the Higgs decaying to b-jets, using a parameterization of b-tagging performance obtained from detailed simulation, is also presented. This early study indicates substantial improvement with the upgraded pixel detector.

2.2 Muon System Completion Simulation Summary

The physics case for addition of forward muon chambers is also straight forward. The CSC system has reduced muon acceptance at trigger level in the region $1.6 < |\eta| < 1.8$ that can be restored with the addition of a fourth layer of chambers. These chambers enable efficient 3 out of 4 logic at the Level-1 trigger restoring loss of trigger efficiency in this region. The installation of RPC chambers in the region $1.2 < |\eta| < 1.6$ provide the finer timing and redundancy for the corresponding CSC system, improving the quality of muons reconstructed in this region. Upgrade of ME1/1 chamber electronics improves the muon trigger in the $2.1 < |\eta| < 2.4$, especially in the high luminosity regime where the present ganging of some channels in these

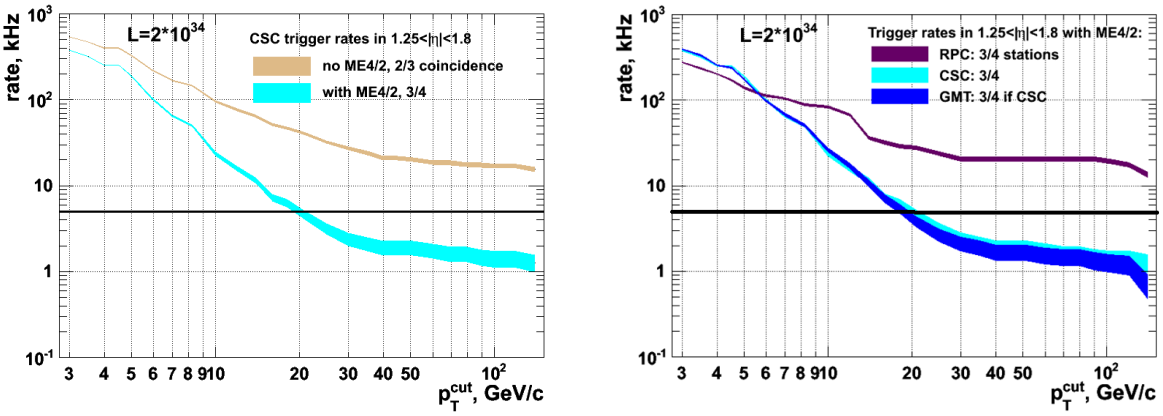

Figure 2.1: (a): Simulation predictions for the contribution to the CSC inclusive muon trigger rate from the region $1.25 < |\eta| < 1.8$ as a function of trigger p_T threshold. The curves demonstrate that the CSC trigger performance critically depends on the ME4/2. The target single-muon trigger rate of 5 kHz is indicated by the horizontal line; (b) Trigger rate of the upgraded standalone RPC and CSC systems (including the proposed RE4 and ME4/2 upgrades) as well as the Global Muon Trigger (GMT) rate. The RPC curve shown corresponds to the configuration optimized for high efficiency and not for rate rejection. In this configuration, the GMT trigger rate nearly entirely relies on the ME4/2 upgrade, making it critical from the standpoint of maintaining acceptable trigger performance.

chambers results in an unacceptable number of spurious tracks. The improvements to the muon trigger are quantified by detailed simulations and are discussed in Section 3. The main benefit from the CSC upgrade is significantly lower rate with the use of ME4/2 and also ability to control the muon trigger background rate at the expected thresholds of about 30 GeV as shown in the Figure 2.1. The upgraded CMS configuration shows a decrease in rate as the threshold is increased compared to the expectations for the existing CMS muon system. Without such control we would be forced to prescale and randomly throw out good events. While the CSC upgrade provides bulk of the improvement the RPC upgrade provides the redundancy that we seek in the high background environment expected at high lumionsities.

2.3 Hadron Calorimeter Simulation Summary

The physics case for the outer hadron calorimeter (HO) was presented in original HCAL TDR [**?**]. The addition of energy leaked into the HO for the high p_T jets is especially important in the case where new physics masses are very high. Similarly, the physics case for endcap (HE) and forward (HF) hadron calorimeters is also justified in the original CMS TDRs [**? ?**]. For instance the jets used to tag the vector-boson fusion process that results in production of a central Higgs accompanied by fairly soft ($p_T \approx 30$ GeV) jets in the $2 < |\eta| < 5$, requires good quality jet reconstruction. The existing detector suffers from poor performance of the HPDs in magnetic environment of the HO, occasional coherent noise in the HPDs of the HB and HE, and large spurious energy deposits in HF because of Cherenkov light produced in the glass windows and walls of its photomultipliers. The software algorithms designed to identify the spurious energy deposits by examining the pattern of energy deposits and their signal time profiles are likely to become ineffective as the pileup increases at high luminosity. Therefore, mitigation of these problems in the hadron calorimeter by replacement of the HO/HB/HE HPDs with higher quality SiPMs and phototubes in HF with thinner window phototubes is necessary to restore the original performance.

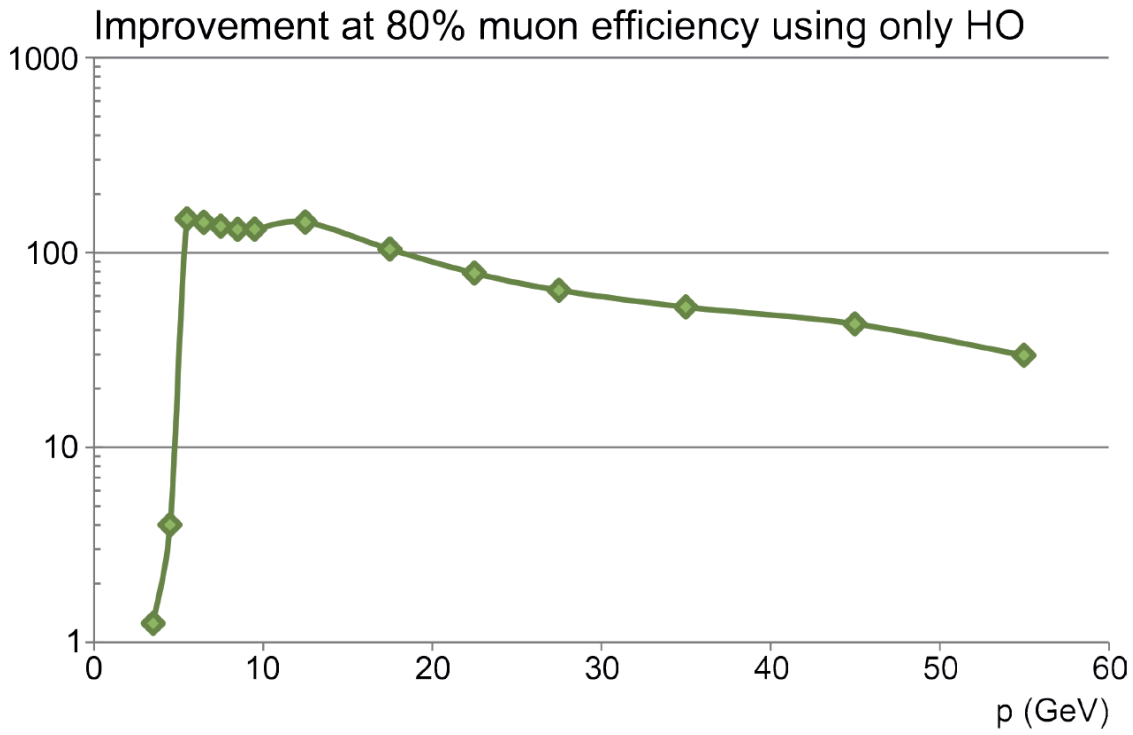

Figure 2.2: Improvement in π/μ rejection for a fixed muon efficiency of 80% due to replacement of HO photo-detectors.

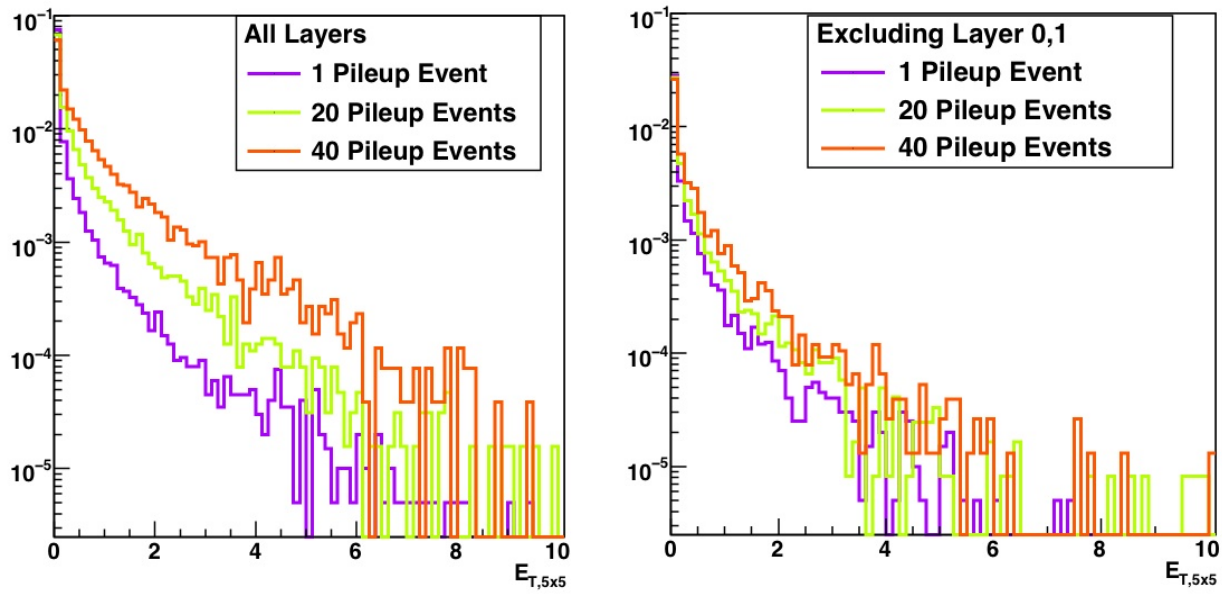

Figure 2.3: Energy distribution in the HB as a function of pileup when considering all layers (left) and when excluding the first two layers (right).

Simulations of upgraded HCAL indicate significant improvements in the detector response. For instance, the HO upgrade provides a better minimum ionizing particle response, thereby improving π/μ rejection as shown in Figure 2.2. In HB and HE there is degradation due pileup

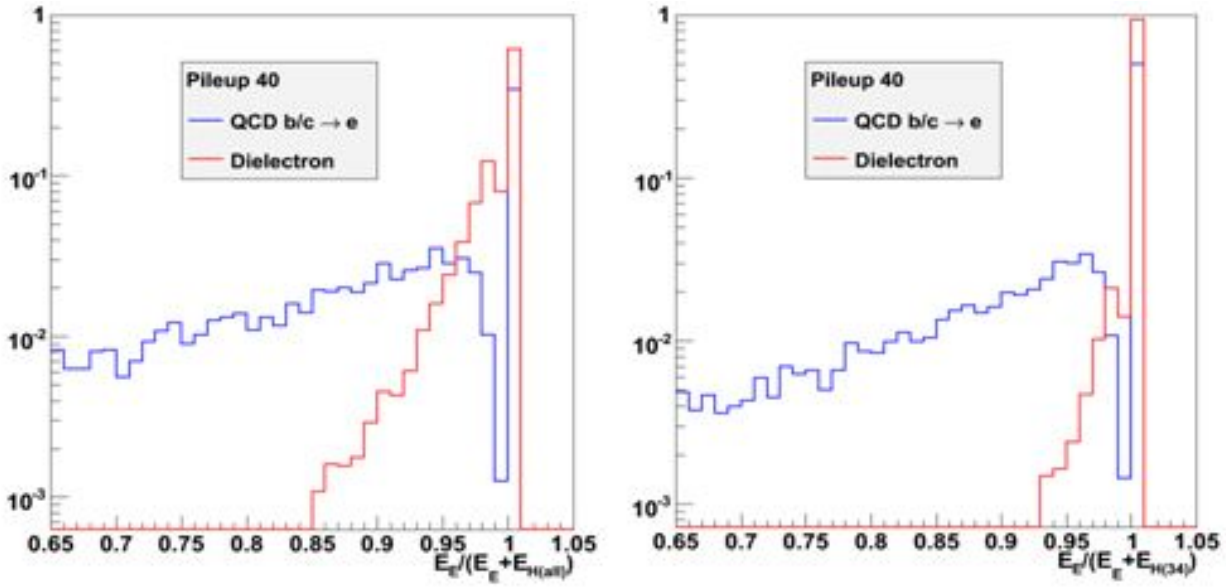

Figure 2.4: HCAL isolation variable computed using all layers (left) and ignoring the first layer (right).

energy deposits, which can be mitigated by examining the longitudinal shower profile as it develops in the detector. Ignoring the first layers of the HCAL improves the detector response as shown in Figure 2.3. For electron/photon identification one can use only the latter layers of the HCAL to restore the discrimination capability as shown in Figure 2.4.

2.4 Pixel Upgrade Simulation Summary

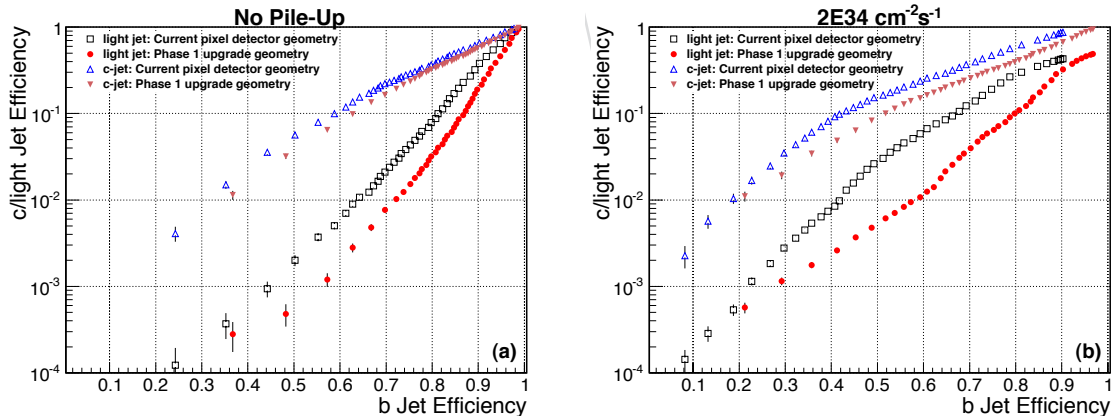

Figure 2.5: The efficiency for b-tagging, using secondary vertex tag, for true b-jets is plotted versus fake light and charm quark jet efficiency in $t\bar{t}$-events with zero (left) or with 50 pileup events per crossing (right) for nominal and upgraded CMS configurations.

The upgraded pixel system with four barrel layers and three forward disks provides improved b-tagging capability and stand-alone tracking capability with higher efficiency. The mass reduction in the upgraded tracker reduces the photon conversion and electron bremsstrahlung probability, enhancing the electron tracking and pixel based isolation of leptons. Full simu-

lation results of the improvement in b-tagging are presented in Chapter 6. The expected improvement in b-tagging is shown in the Figure 2.5. At operating point with fixed light jet fake efficiency, the absolute b-jet tagging efficiency improves as much as 20%, which is quite substantial. Pixel-only tracking and b-tagging capability in the high level trigger are yet to be explored.

2.5 Trigger Upgrade Simulation Summary

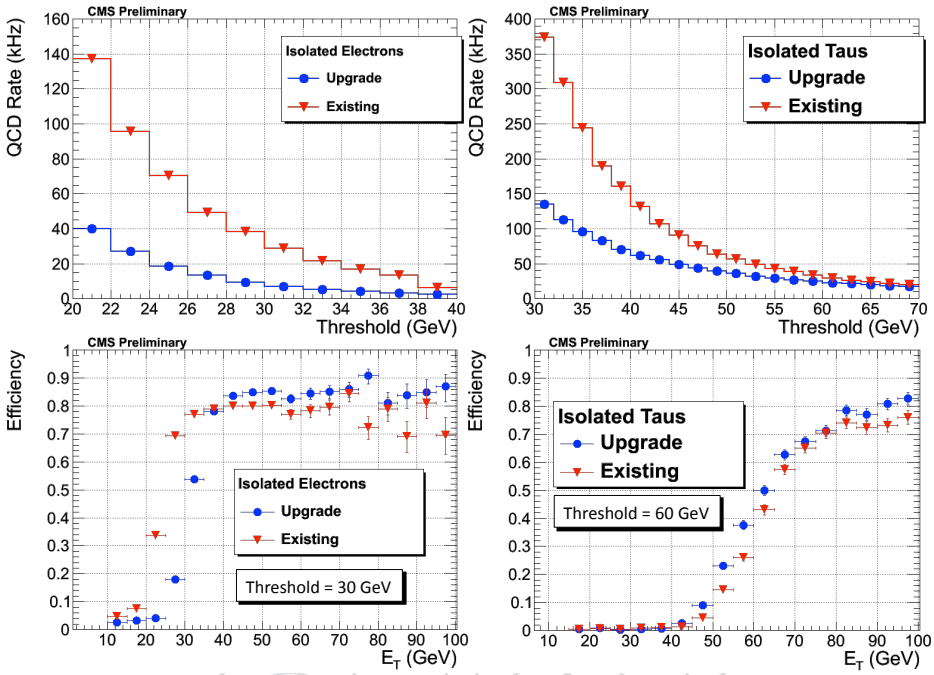

Figure 2.6: Integrated QCD rate (kHz) for electron (top-left) and tau (top-right) triggers is plotted versus trigger E_T cut for current LHC and upgraded algorithms with improved clustering. Corresponding efficiencies for isolated electrons (bottom-left) and hadronically decaying taus (bottom-right) are also plotted.

The main benefit of the trigger upgrade is the improved performance for isolated electron, muon and τ triggers. Details of algorithms and their performance are given in chapter 7. Here we present results if simulation studies which used fast simulation with pileup of $\tilde{2}5$ inelastic interactions per crossing. We defined two configurations of software, the existing CMS calorimeter trigger system and the upgraded calorimeter trigger.

The efficiency turn-on and the integrated trigger rate versus the chosen threshold is shown for electrons and taus in Figure 2.6. The expected rate from the endcap muon system is shown in Figure 2.1.

Sample Level-1 (HLT) trigger tables with thresholds and rates corresponding to 100 kHz (300 Hz) total rate dominated by QCD (EWK) are shown in Table 2.1 for the case of instantaneous luminosity of 10^{34} cm^{-2} s^{-1} where an average of 25 pileup events are seen. [Currently only the Level-1 calorimeter trigger data is available. Muon and HLT simulation results are still under preparation.] The thresholds values represent energies where there is 80% (75%) efficiency for the electron/photon (tau) object. The rates corresonding to these thresholds for existing and upgraded calorimeter trigger system are shown. The total rate reduction is better than a factor of four. Note that the upgraded trigger system has more parameters that can be tuned to keep

Table 2.1: A sample trigger table showing 80% (75% for τ) thresholds and rates which add up to 100 kHz (300 Hz) at Level-1 (HLT) for existing and upgraded CMS trigger systems.

Trigger Object	Threshold		Rate			
			Existing CMS		Upgraded CMS	
	Level-1 (GeV)	HLT (GeV)	Level-1 (kHz)	HLT (Hz)	Level-1 (kHz)	HLT (Hz)
Single Photon	37		28		8	
Double Photon	20		12		2	
Single Electron	37		28		8	
Double Electron	20		12		2	
Single Muon						
Double Muon						
Single Tau	85		29		23	
Double Tau	45		29		5	
Electron + Tau	20, 45					
Muon + Tau						
H_T (with b-jet)						

Table 2.2: Level-1 trigger efficiencies for a sample set of physics channels corresponding to the thresholds chosen with 80% efficiency for electron and 75% efficiency for taus for existing and upgraded CMS trigger systems. Note that the efficiency is calculated for those events that have generated object(s) above the selected thresholds in Table 2.1 within the fiducial volume of the detector.

Physics Process	Trigger Efficiency (%)					
	Existing CMS			Upgraded CMS		
	Single	Double	Cross	Single	Double	Cross
$W \rightarrow e\nu$	79.6	-	-	80.0	-	-
$Z \rightarrow ee$	83.7	68,8	-	88.9	71.4	-
$Z \rightarrow \tau_h\tau_h$	63.8	53.4	-	82.3	58.6	-
$Z \rightarrow \tau_e\tau_h$	69.9	62.9	46.7	82.3	64.4	48.6
$H(130) \rightarrow \gamma\gamma$	92.1	73.1	-	92.8	71.2	-
$H(135) \rightarrow \tau_h\tau_e$	69.1	44.1	39.0	79.5	49.4	40.2
$H(135) \rightarrow \tau_h\tau_h$	72.3	44.8	-	82.2	52.9	-
$tbH^+(200) \rightarrow \tau_h X$	62.6	-	-	88.0	-	-

the rate at an acceptable level. Efficiencies corresponding to this reduced trigger table for a representative set of physics channels is shown in Table 2.2. Because we want to show the efficiency for triggerable events only we show the efficiency for each trigger for those events which have generated objects above the thresholds shown in Table 2.1, within the fiducial volume of the detector. Absolute efficiencies for some of the triggers is rather low, e.g., the double τ thresholds is quite high (45 GeV), and therefore only significantly boosted Z bosons would have generated τ-leptons above that cut.

We conclude that the calorimeter trigger upgrade will meet the required factor of two better rate performance while slightly improving the physics yield for several physics processes.

2.6 HLT and Physics Simulations

The higher level trigger development and offline physics analysis studies with upgraded detector are beginning, now that the upgrade plans are more firm and sub-detector level software is becoming available.

2.7 Physics Studies

While waiting for the completion of simulation software in the official CMSSW framework, which first requires detailed characterization of physics object reconstruction, we have embarked on a separate parameterized simulation for an early study. This study used Pythia8 for generation of the signal, ZH production with Z decays to muons and H(120 GeV) to b-jets, and largest two expected backgrounds, Z+Jets production and ZZ diboson production. Expected pileup (50 events on average) of QCD interactions have been superimposed on these events. We have smeared the four-vectors of the visible particles using the expected CMS performance. We also folded in degraded track finding efficiency for muons in the case of high 50-event pileup environment, where 15% of the muons are lost with the non-upgraded situation. We used the FastJet [3] program, with the anti-KT algorithm, to reconstruct jets. We have then used b-tagging performance from detailed simulation presented earlier to tag b-jets including expected fakes from the light quark jets. The smeared/parameterized output was used to study the ZH signal and background. The reconstructed dimuon pairs, with $P_T^{\mu} > 20$ GeV, invariant mass within ± 20 GeV of M_Z, and $P_T^{\mu\mu} > 100$ GeV were selected. Two jets with $P_T^{j} > 20$ GeV and di-jet $P_T^{jj} > 120$ GeV were required to be identified as b-tagged. Three b-tag operating points were tried, and the optimal choice had a 60% b-tagging efficiency with a light (charm) quark mis-tagging probability of 1% (15%) for the upgraded detector configuration, which is labeled as Phase-1, and 6% (20%) for the non-upgraded configuration, which is labeled as StdGeom, for the situation where we had 50 PU events. For comparison, in the zero pileup situation, the 60% b-tag efficiency point corresponded to light (charm) quark mis-tag efficiencies of 0.2% (10%) for Phase-1 and 0.6% (10%) for StdGeom. The invariant mass distributions for the four cases, (StdGeom, Phase-1) $\times$ (0 PU, 50 PU) are shown in Figure 2.7. Note that the jet energy scales are not calibrated, resulting in 5 GeV downward shift for zero pileup situation compared to 10 GeV upward shift for the 50 pileup, with additional degradation of the resolution. These effects can be mitigated with specialized cleaning algorithms eventually. Additional selection cuts for reducing the dominant Z+Jets background are still under development. At this stage of analysis the signal significance ($S/\sqrt{(S+B)}$) is 2.3 for 400 fb^{-1} collected, in the case where there is no pileup. While the absolute value of this significance can be improved with analysis optimization, it is already useful for making comparisons. This 2.3 σ significance degrades to 1.1 with the current detector if no upgrade is made. However, we conclude from this quick study that the Phase-1 upgrade doubles the significance to 2.0σ essentially restoring the performance when there is a pileup at the level of 50 events per crossing.

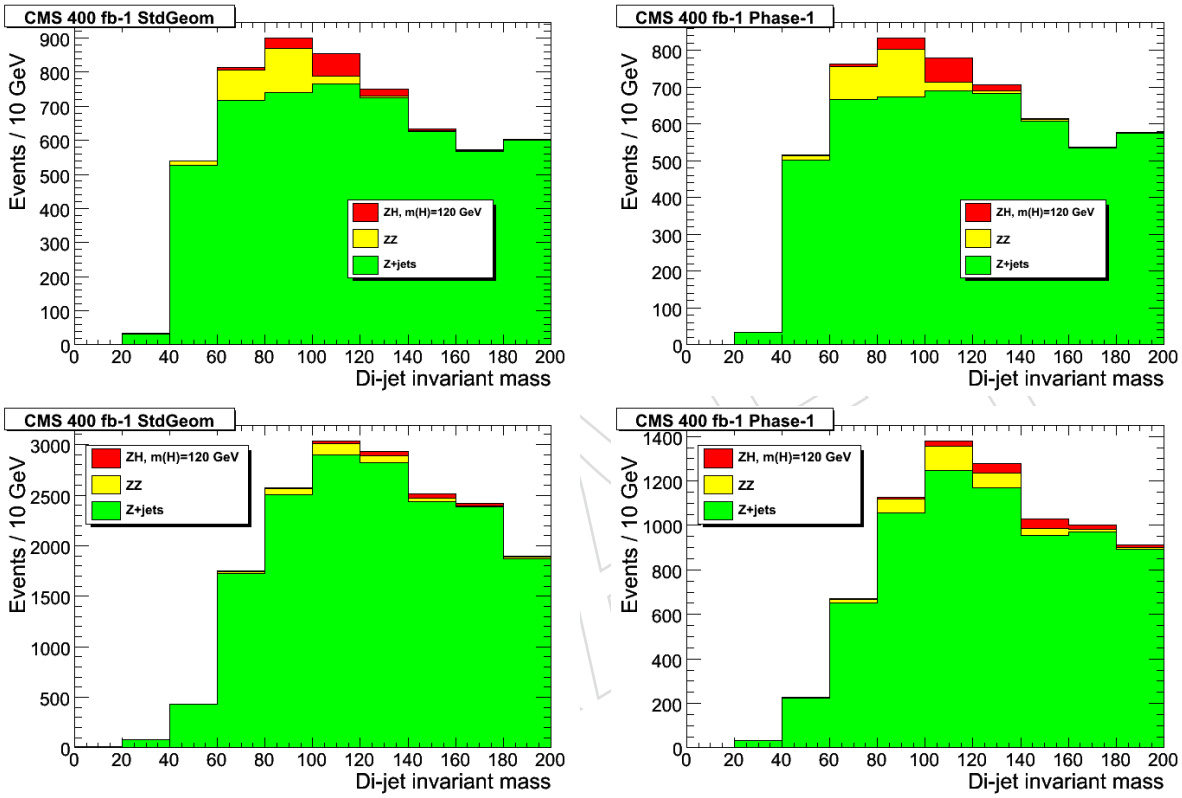

Figure 2.7: Di-jet invariant mass after b-tag selection produced in association with a Z boson for degraded current detector with standard geometry (left) and Phase-1 upgraded detector (right) for no pileup (top) and 50 pileup events per crossing (bottom).

Chapter 3

The CMS Muon System Upgrades

3.1 Introduction

Muon detection is a powerful tool for recognizing signatures of interesting processes over the very high background rate expected at the LHC. This is particularly true as the luminosity increases. The CMS muon system has three functions: muon identification, momentum and charge measurement, and triggering. Good muon momentum resolution and triggering are enabled by the high-field solenoidal magnet and the flux-return yoke. This flux-return yoke also serves as a hadron absorber, which enables the identification of the muons.

The CMS muon system (Fig. 3.1) is designed to reconstruct the momentum and charge of muons over the entire kinematic range of the LHC. CMS uses 3 types of gaseous particle detectors for muon identification arranged as a cylindrical barrel region and planar endcaps. Because of the large area to be covered and the inaccessibility of the detector, it is important that the muon detectors be cost-effective, reliable, and robust.

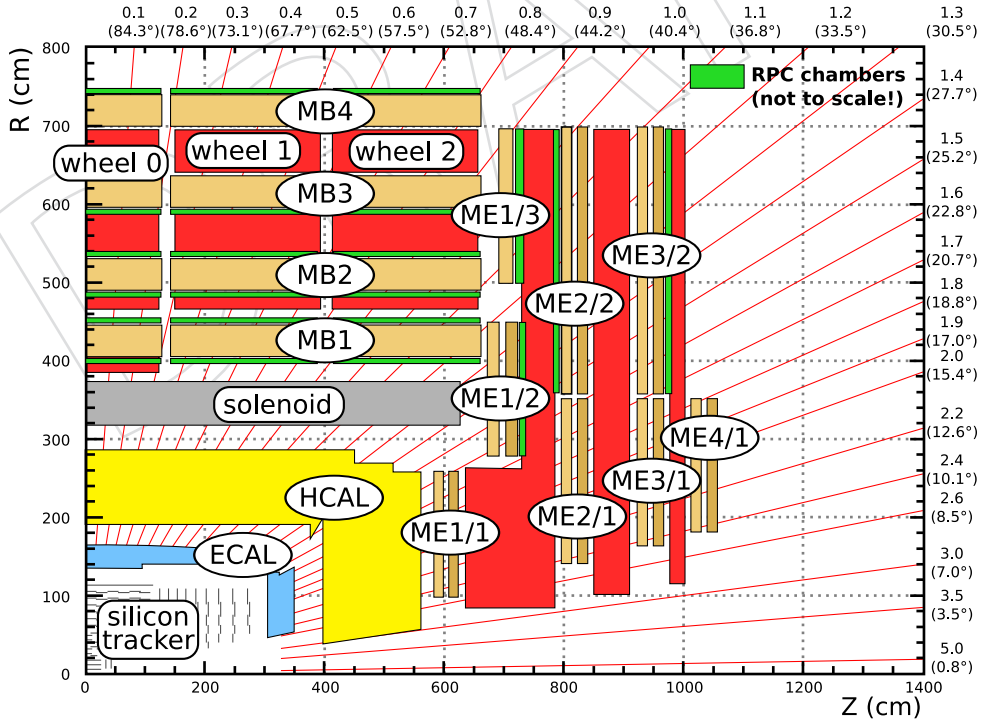

Figure 3.1: An r-z cross-section of one quadrant of the CMS detector with the axis parallel to the beam (z) running horizontally and radius (r) increasing upward. The interaction region is at the lower left. Shown are the locations of the various muon stations and the steel disks.

In the barrel region, where the muon rate is low, the neutron background is relatively small, and the magnetic field is mostly uniform, drift chambers with rectangular cells are employed. The barrel drift tube (DT) chambers cover the pseudorapidity region $|\eta| < 1.2$. They are organized into 4 stations at different radii and mounted parallel to the beam between the flux return plates of the solenoid.

In the two endcap regions of CMS, where the muon rates and background levels are high and the magnetic field is high and non-uniform, CMS uses cathode strip chambers (CSC). These chambers have a fast response time, fine segmentation, and relative immunity to the non-uniform field. The CSCs cover the region of $0.9 < |\eta| < 2.4$. Each endcap has 4 stations of chambers mounted on the faces of the endcap disks, and perpendicular to the beam. The cathode strips run radially outward and provide a precision measurement in the $r - \phi$ bending plane. The wires are roughly perpendicular to the strips.

In addition to these muon detectors, CMS has added a complementary, dedicated triggering detector with excellent time resolution to measure the correct beam-crossing time at the highest LHC luminosities. The resistive plate chambers (RPC) are located in both the barrel and endcap regions, and they provide a fast, independent trigger over a large portion of the rapidity range ($|\eta| < 1.6$). The RPCs are double-gap chambers, operated in avalanche mode to ensure good performance at high rates.

These muon detector elements cover the full pseudorapidity interval $|\eta| < 2.4$ with no acceptance gaps, ensuring good muon identification over an angular range of $10^\circ < \theta < 170^\circ$, where θ is the polar angle between the beam and the muon track. Offline reconstruction efficiency for the muons with p_T greater than 3 GeV/c is typically 96-99% except in gaps between the DT station elements ($|\eta| = 0.25$ and 0.8) and the transition region between the DTs and the CSCs ($|\eta| \sim 0.9$). Due to the large amount of material before the first muon station, punchthrough is negligible. A crucial characteristic of the DT and CSC systems is that they can trigger on muons with good efficiency and high background rejection. DT and CSC triggers are combined in the overlap region ($0.9 < |\eta| < 1.2$).

Thus, in CMS the triggering scheme for muons relies on independent and complementary triggering technologies: cathode strip chambers (CSC) in the endcaps plus drift tubes (DT) in the barrel, and resistive plate chambers (RPC) in both endcaps and barrel. The CSC and DT systems provide good momentum resolution and reasonable timing, while the RPC system provides excellent timing with somewhat worse momentum resolution. To be effective, the muon trigger must achieve good enough resolution to identify high-p_T tracks. Three stations are essential for the fast, accurate, and robust measurement of the muon momentum. With a primary-vertex constraint, two stations are sufficient to measure momentum in principle. However, the third station is highly desirable to provide for gaps in coverage, missing or dead chambers, muon bremsstrahlung, and multiple scattering. In the proposed system with 4 stations, any gaps in coverage within individual stations are complemented by good coverage in other stations, so that, in general, at least three stations will be hit by any muon.

The original plans for the CMS endcaps included four stations for each of the CSC and RPC systems. However, only part (ME4/1) of the 4th CSC station was constructed, so we are now proposing to complete the 4th station with 72 ME4/2 chambers (36 on each endcap). We also propose to construct a new 4th station for the RPCs. In addition to these systems, which are now operating very effectively, CMS is considering adding a new system, the Micropattern Gas Detectors (MPGD) in the region $1.6 < |\eta| < 2.4$ (described elsewhere) not covered by the RPC system.

Without a 4th station, the CSC system does not have the necessary redundancy to control the trigger rate at the increased luminosity while preserving high trigger efficiency. With the trigger requiring segments in two out of three stations (requiring three will lead to a large efficiency loss due to inefficiencies and gaps in the coverage), the problem stems from momentum mismeasurements of low p_T muons contributing to the trigger rate. With the much higher flux of low-momentum muons at increased luminosity, these poorly measured muons dominate the trigger rate making it unacceptably high. The same effect occurs in the RPC system without the 4th station. Without a proper measurement, these low p_T muons cannot be eliminated with p_T cuts, so the muon trigger rate increases. With an additional station we will have four potential measurements. Since we only need three out of the four stations to get a good momentum measurement, we can be both correct and efficient in identifying high-p_T muons in the trigger.

The chamber construction for the 4th stations of both CSC and RPC will be done at CERN. A large fraction of the CERN building B904 has been allocated as a production facility for the CSC and RPC. The chambers will be assembled and tested in this building before being installed in CMS. At this time, the building is being refurbished and is expected to be ready for occupancy in early 2011.

The space available for the 4th station is very tight and we will need to plan the integration of this area carefully. The CSCs will be mounted on the back of the YE3 disk, and the RPCs will be mounted just behind the CSCs. As a consequence, the installation sequence requires the CSCs be installed first, then the RPCs. Once these chambers are installed and commissioned, a YE4 shielding wall will be mounted behind the 4th station and will protect the muon chambers from the spray of neutrons caused by losses in the LHC elements in the upstream beam lines.

An important consequence for the planning is that the installation of the CSCs must occur before the RPCs. The conservative schedule for the CSC construction requires roughly two years for the production of one endcap station (36 chambers), then an additional year for the next 36 chambers of the remaining endcap. The next long-term LHC stop is scheduled for 2012, so it is unlikely that the CSCs will be ready for installation at that time. Moreover, the funding for the CSCs is not yet in place. In contrast, the proposed 4th station of RPCs will be built by a large collaboration from many countries and much of the required funding has been pledged. Work has already begun on ordering materials. The RPC system expects to be ready for installation in a few years, possibly by 2012. This mismatch and possible resolutions are discussed in section 3.5.

In addition to the proposal for constructing additional CSC and RPC chambers, we propose replacing the ME1/1 front-end cathode electronics with new digital boards and upgrading the associated readout boards to increase the rate capability. The Drift Tube (DT) system electronics will also undergo some important changes, namely the replacement of some electronic components and the relocation of others, to make the system more reliable and robust and to resolve some problems with availability of spare components.

When these improvements and upgrades, described in detail in the following sections, are made to the three muon systems, CMS will be able to trigger on, identify, and reconstruct high-p_T muons with high efficiency and purity throughout the period until 2020.

3.2 CSC Muon Detector Upgrades and Repairs

The endcap Cathode Strip Chamber (CSC) muon system has been designed to provide robust triggering and muon identification over a wide rapidity range of $0.9 < |\eta| < 2.4$, and to

improve the momentum measurement for ultrahigh energy muons with momenta of several hundred GeV/c or greater. The current CSC detector consists of 468 large 6-layer chambers arranged in Muon Endcap (ME) stations, as shown in Fig. 3.2(a) (note that the drawing also includes station ME-4/2 proposed in this document, which is not part of the current system). The full system contains more than 2 million wires and nearly half a million readout channels, whiich are processed by a multi-layer readout and trigger electronics systems. The six layers of each chamber provide a track segment that gives an excellent measurement of the azimuthal angle, ϕ, of the muon track impact point in the plane of the station. The difference of the azimuthal angle between stations provides a measurement of the transverse momentum. The layout of the CSC electronics system is shown in Figure 3.2(b). On-detector boards digitize the data and send it to a system of 60 nearby VME crates, which form trigger primitives, store the data blocks, and send them to the underground service cavern over optical fibers.

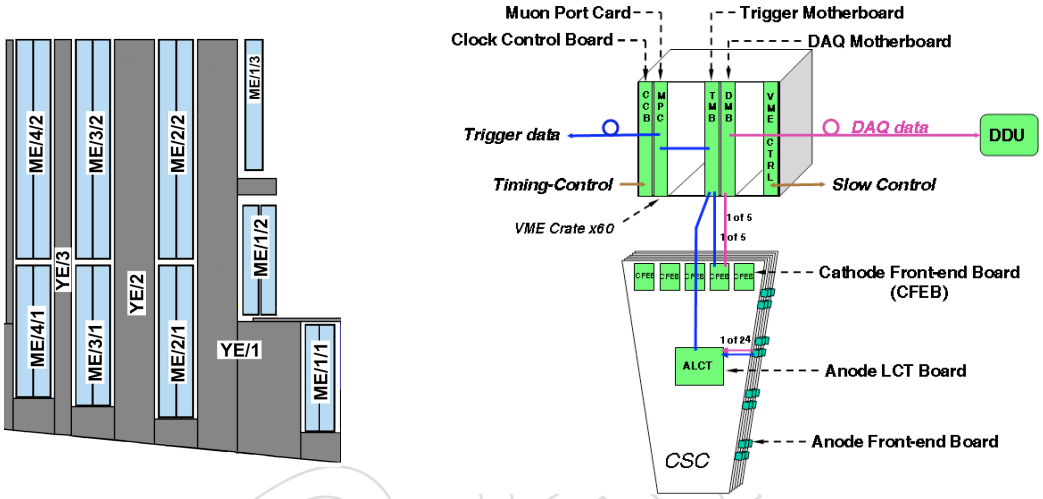

Figure 3.2: (a) An r-z cross-section of one endcap of the CSC muon system showing the new station ME4/2 (upper left) proposed in this document. In the drawing, the axis parallel to the beam (z) runs horizontally and radius (r) increasing upward, the interaction region is on the right, off the page. Shown are the locations of the various muon stations in blue and the steel disks between them in gray. Both station ME4/2 and ME1/1 (lower right) are specifically mentioned in the text; (b) A block diagram of the CSC electronics system.

The CSC system is one of the principal systems for triggering the CMS experiment on muon particles that pass through the endcap region. The task of the Level-1 CSC trigger is to efficiently select events with muons of a high enough transverse momentum, p_T, while reducing the rate of incoming events by about four orders of magnitude by rejecting background events. For the trigger to measure p_T, the CSC trigger electronics reconstructs muon tracklets (stubs) in CSC chambers and passes this information to the CSC Track Finder (CSC TF). The CSC TF electronics (further discussed in the Trigger/DAQ section of this proposal) measures the differences between ϕ values in the various CSC muon stations (i.e., ME1, ME2, ME3, and ME4) and translates that information into muon candidate p_T.

While the CSC chambers themselves are expected to survive the increased radiation levels from the LHC luminosity upgrades, the current system will not be able to sustain its performance in the face of increasing luminosity. Apart from a smaller scale electronics replacement needed to maintain the system performance at current luminosities (the TMB daughtercard replacement will take advantage of newly available technologies), continued robust performance of the CSC

system at the SLHC luminosities will require increasing the redundancy of the system. The key elements are building a new station ME4/2 and upgrading station ME1/1. While meeting these goals requires replacing several electronics components for station ME1/1, such replacement is also necessary on its own merits in order to maintain the CSC trigger and reconstruction efficiencies. Replacement electronics will meet all the requirements of operating the upgraded CSC system.

From a physics perspective, not upgrading the current CSC system will cause a dramatic decrease in the CMS acceptance in the range of $0.9 < |\eta| < 2.1$ for physics signatures with muons due to inefficiencies at increased luminosity and a complete shutdown of triggering capabilities in the region of $2.1 < |\eta| < 2.4$. Because muons are critical for most signatures of Higgs or new physics including Supersymmetry, the CMS physics reach in those areas will be severely diminished. Shutdown of the very forward region ($2.1 < |\eta| < 2.4$) will have a substantial reduction in acceptance for signatures with one triggerable muon (e.g. SUSY, or $h \rightarrow \tau\tau$ in the "golden" muon plus hadronic tau channel) and diminished acceptance for two-muon signatures. The very forward region is also critical for the measurement of $\sin^2\theta_{eff}$ and Parton Distribution Functions using forward-backward asymmetry A_{FB} in $Z \rightarrow \mu\mu$ events. Accurate knowledge of PDFs plays a key role in predicting Standard Model backgrounds in searches for new physics. Today's technologies allow us to remove these deficiencies and provide robust muon triggering and reconstruction up to $|\eta| = 2.4$.

3.2.1 Performance Limitations

At higher instantaneous luminosities, the much increased hit occupancies lead to both an unacceptable increase in the CSC trigger rates as well as a significant decrease of muon trigger efficiencies. Without an upgrade, preserving the muon trigger rate within the allowed range would require unacceptably high muon Level-1 trigger thresholds, which will severely diminish CMS physics reach. The root cause of the rate problem is the lack of redundancy of the system, which prevents us from tightening trigger purity without unacceptable sacrifices in efficiency. Construction of the new station ME4/2 and unganging of channels in station ME1/1 will alleviate these shortcomings.

Apart from the trigger rate problems, the particularly high rate and occupancy of hits in the CSC chambers in station ME1/1 will cause a significant decrease in trigger reconstruction efficiency in the forward half of the CSC region due to the limitations of the existing electronics system. The CSC electronics was not designed for instantaneous luminosity beyond the nominal LHC range and was limited by the technology available at the time of the original system design. A specific example of technology limitations is a less than powerful TMB daughtercard FPGA. If the TMB FPGA is not replaced, the muon trigger will have to be shut down in the region of $2.1 < |\eta| < 2.4$ at already nominal LHC luminosities.

3.2.1.1 Lack of Redundancy in the Region $1.2 < |\eta| < 1.8$

With the current CSC detector, the CSC Track Finder selects muons using a two-out-of-three-station triggering configuration. Two stations supply a single difference in ϕ positions; this is the minimal coincidence that measures muon momentum, leaving no redundancy for multiple scattering or mis-measurement. At high luminosity simulations show that the two-out-of-three-station triggering configuration needed for high efficiency suffers from a high rate of background from mis-measured low-p_T muon tracks, as shown in Fig. 3.3. A three-out-of-three-station triggering configuration cannot be used because of large and uncertain losses due to requiring perfect muon information from every muon station, because it suffers the third

power of the per-station efficiency, which comes from many factors:

- chamber geometry gaps.
- high-voltage isolation gaps within chambers where the gas gain is lower.
- position determination errors due to muon bremsstrahlung, which increases dramatically at high momentum.
- electronics dead-time at higher luminosity and timing errors due in part to early background hits including those from neutrons.
- "real-world" losses due to individual chamber problems such as high-voltage breakdown and electronics malfunctions.

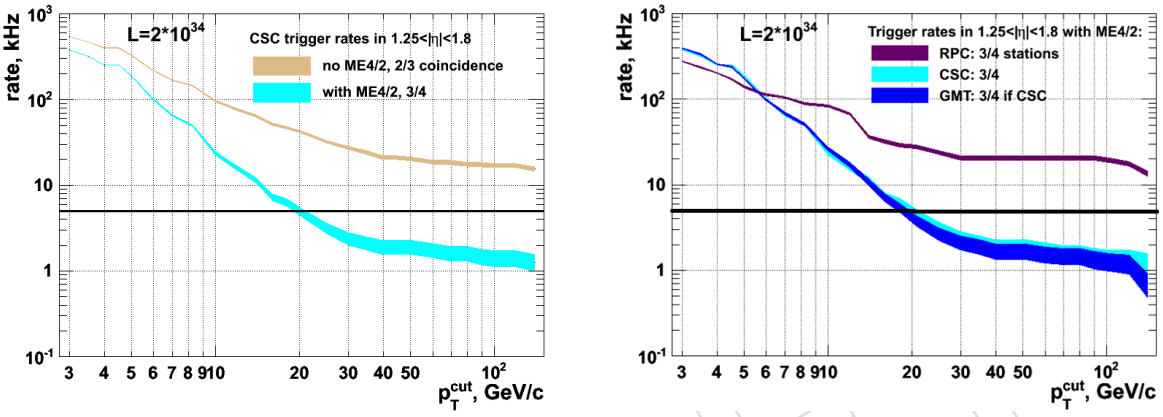

Figure 3.3: (a): Simulation predictions for the contribution to the CSC inclusive muon trigger rate from the region $1.25 < |\eta| < 1.8$ as a function of trigger p_T threshold. The curves demonstrate that the CSC trigger performance critically depends on the ME4/2. The target single-muon trigger rate of 5 kHz is indicated by the horizontal line; (b) Trigger rate of the upgraded RPC and CSC systems (including the proposed RE4 and ME4/2 upgrades) as well as the Global Muon Trigger (GMT) rate. The RPC curve shown corresponds to the configuration optimized for high efficiency and not for rate rejection. In this configuration, the GMT trigger rate nearly entirely relies on the ME4/2 upgrade, making it critical from the standpoint of maintaining acceptable trigger performance.

With an upgrade to build the ME4/2 CSC chamber station covering the rapidity range 1.2 to 1.8, the CSC Track Finder will be able to select muons using a highly efficient three-out-of-four-station triggering configuration. Figure 3.3(a) shows the expected rate curves from simulation with and without the ME4/2 station at SLHC Phase-1 luminosity, with the target rate of 5 kHz for the Level-1 muon trigger rate as indicated. Without the upgrade, the increase and flattening of the trigger rates leads to an effective loss of triggering in that region. With the upgraded ME4/2, the trigger p_T threshold can be maintained at 20 GeV/c, allowing for efficient triggering on W, Z, and top quark muonic decays. The W, Z, and top particles in turn are some of the best signals for Higgs, Supersymmetric, and other sought-after particles.

Figure 3.3(b) shows the performance of the GMT with both upgraded RPCs and CSCs. The presented RPC trigger rate curve is based on the 3/4 layer coincidence that will be possible only after the RPC upgrade and, in accord with current practice, was optimised for efficiency rather than rate rejection. With a different optimization, the RPCs could contribute more to the over all trigger rate reduction at a loss of efficiency. However the pseudorapidity interval $1.24 < |\eta| < 1.6$ presents special difficulty for the RPCs. Moreover, all the rate curves shown are very optimistic, as they take into account only the real muon (primary or secondary) spectrum.

It is known that background rates in the endcap region from neutrons, albedo particles, and beam-halo muons have caused serious problems for other collider detectors lacking sufficient redundancy in the past. Figure 3.3(b) indicates that the ME4/2 upgrade remains critical even with the RPC RE4 upgrade, since the performance of the CSC muon trigger has such a strong impact on the CMS Global Muon Trigger (GMT) rate.

3.2.1.2 Loss of Performance in the Region $1.6 < |\eta| < 2.4$

The ME1/1 muon station shown in the lower right portion of Fig. 3.2(a) covers the forward half of the CSC rapidity range. Because of its proximity to the interaction point (least multiple scattering compared to other stations) and its location in the region before the magnetic field changes direction, ME1/1 is the most important station for standalone momentum resolution for muons with $|\eta| = 1.6 - 2.4$. The standalone muon momentum resolution is, in turn, crucial to the Level-1 and Level-2 trigger event selection, and is also used offline for muon identification. This makes it imperative to maintain high local track reconstruction efficiency in ME1/1 chambers. Because of the proximity to the beam line, the ME1/1 chambers receive the highest particle rates of any of the CMS muon chambers. In addition to the prompt muons, ME1/1 is exposed to high long-lived neutron and beam backgrounds that are particularly significant in the very forward region. As an illustration, Fig. 3.4(a) shows the density of hits sharply peaking in station ME1/1 as observed in early LHC beam-halo events. At higher luminosity, the high background rates cause significant losses in efficiency due to shortcomings of station ME1/1 electronics.

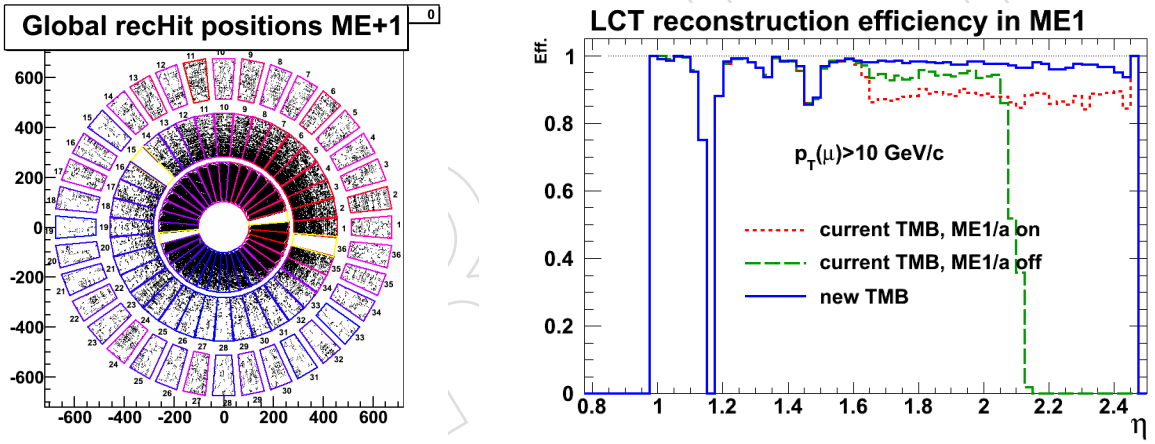

Figure 3.4: (a): The distribution of beam-halo muon hits in station ME1 using actual LHC data shows the rate is highly peaked in station ME1/1, which is closest to the beam; (b) Simulation prediction for the efficiency of finding a local muon track in station ME1 as a function of muon pseudorapidity for muons with $p_T > 10$ GeV/c. The decrease in efficiency is due to backgrounds from pile-up (note that this calculation includes prompt contributions only, i.e. no beam or neutron backgrounds). Because of the features of the TMB board, the efficiency over the entire range of $|\eta| = 1.6 - 2.4$ is sensitive to the background rate in the region of $|\eta| = 2.1 - 2.4$. Upgrade of the TMB board allows recovering robust muon triggering in the entire range of $1.6 < |\eta| < 2.4$.

Furthermore, technology constraints at the time the system was originally designed led to a decision to divide all ME1 chambers into two halves covering regions $1.6 < |\eta| < 2.1$ and $2.1 < |\eta| < 2.4$ and to implement a 3:1 ganging of cathode strips in the high-η part of the chambers. The ganging is done at intervals of 16 strips so that, for example, strips 1, 17, and 33 are directly connected to electronics channel 1; strip 2, 18, and 34 are connected to electronics

channel 2, etc. At higher luminosity, such grouping leads to a rapid increase in the trigger rate, which cannot be controlled by tightening trigger requirements due to an effective loss in system redundancy caused by ganging.

3.2.1.2.1 Sub-optimal Trigger Segment Reconstruction Performance An important issue was identified with the muon trigger that is relevant for the region $|\eta| = 2.1 - 2.4$ already at nominal LHC luminosities. One of the key elements of the muon trigger sequence is the reconstruction of local muon tracks in chambers, which is handled by the Trigger MotherBoard (TMB). Because of a feature of the board (driven by the limitations in FPGA technology at the time of the board design), the board becomes blind to any new muons for several bunch-crossings after reconstructing a local track anywhere in the chamber. Since both the high- and low-η regions of the ME1/1 chambers are handled by a single TMB board, the efficiency of muon triggering in the entire region of $|\eta| = 1.6. - 2.4$ becomes highly sensitive to the rate of backgrounds in the region of $|\eta| = 2.1 - 2.4$. Even though the current simulation lacks critical contributions from neutron and beam-induced backgrounds, the effect is apparent, as demonstrated in Fig. 3.4(b) showing a large decrease in muon trigger efficiency in the entire region of $|\eta| = 1.6 - 2.4$. While it is possible to improve performance in the lower η region by turning off triggering in the region of $|\eta| = 2.1 - 2.4$, this option fails due to physics reach considerations. Apart from a lower efficiency, the strong susceptibility of trigger performance to the precise level of backgrounds in the region with highest and most difficult-to-predict backgrounds diminshes the robustness of the trigger.

Resolving this problem requires an upgrade of the current TMB boards used in station ME1/1 to utilize a new generation of FPGA chips and deploy a new nearly deadtime-less algorithm with additionally developed background suppression options. While the new TMB algorithm will recover efficiency, one still needs to address the high contribution to the trigger rate coming from the region of $|\eta| = 2.1 - 2.4$ as shown in Fig. 3.5(a). To control the rate, the CSC Track Finder (CSCTF) will be configured to require 3-out-of-4 station coincidence for candidate tracks with $|\eta| > 2.1$. Because of the much increased robustness of reconstruction in station ME1/1, this will present a safe and efficient solution (solid line in Fig. 3.5(a)).

3.2.1.2.2 Front-End Readout Dead Time with Increasing Luminosity An important element of the CSC front-end readout is the Switched Capacitor Array (SCA) cells that form the analog charge storage pipeline. They hold the data until they can be digitized and read out. At higher luminosities, the SCA cells can become fully occupied by data before they are digitized, so effectively the board is dead for a time. Also, the pedestal for each time sample can be disturbed by the presence of earlier hits, so that the accuracy of the position determination is degraded. Alleviating the high-data-rate readout problems in ME1/1 requires replacing the existing cathode front-end boards (CFEBs). We propose that the current "analog" CFEBs that use the SCA and 16:1 multiplexing digitizers (ADCs) be replaced by "digital" DCFEB boards that flash-digitize data from every channel simultaneously and store the results in a digital pipeline.

3.2.1.2.3 Rapid Trigger Rate Growth in $2.1 < |\eta| < 2.4$ with Increasing Luminosity While an upgraded TMB restores robust triggering for the near term, at Phase 1 luminosities the 3:1 ganging of ME1/1 channels presents a fundamental problem as it leads to a large increase in muon trigger rate as well as complicating the reconstruction due to combinatorics. The CSC trigger depends on the measured ϕ difference between muon stations and the desirable high-p_T muons have very small ϕ differences. Because of the ganging, there is a high rate of low-p_T muons that will be seen as nearly straight (infinite momentum) if their bending in

the magnetic field takes them roughly 16 or even 32 strips away. Fig. 3.5(b) shows the large enhancement in the number of muon trigger candidates at $|\eta| > 2.1$ even with the three out of four station coincidence requirement for the current system. This problem also exists in offline muon identification, where muon stubs are matched in position with inner-detector tracks. At Phase 1 luminosities, the trigger rate from that region will become unacceptable.

Maintaining muon trigger performance in the region $2.1 < |\eta| < 2.4$ will require the removal of channel ganging and mounting additional DCFEB boards on each ME1/1 chamber so that every strip can be read out separately. The TMB and DMB boards, which receive trigger and data readout information from the CFEBs in ME1/1, will concurrently need to be modified to handle the additional DCFEBs. A backward/forward compatible design of the new TMB daughtercard discussed in Section 3.2.2.2.1 will allow upgrading the system without replacing the TMB boards themselves. Instead, the TMB boards will undergo only minor modifications to route optical links directly to the new TMB daughtercard and will be ready to operate with the new DCFEB boards using a new version of the firmware.

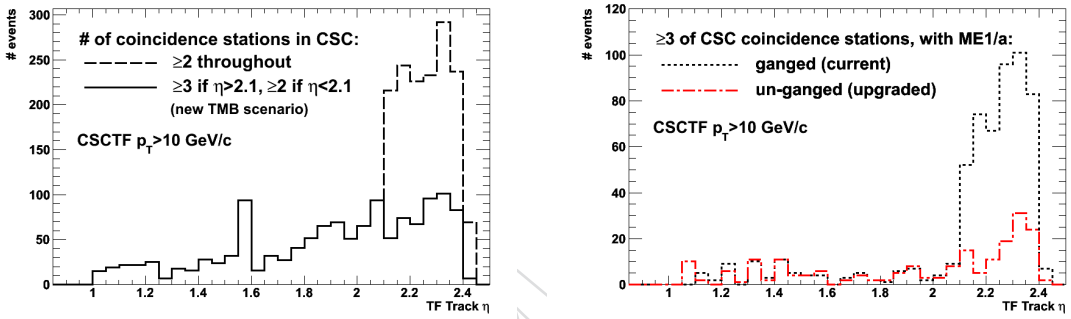

Figure 3.5: (a) Simulation predictions for the pseudorapidity distribution for background events passing the current L1 trigger (dashed line). The enhancement in the region $|\eta| > 2.1$ is due to the strip ganging in ME1/1a. For LHC luminosities, the requirement of a three-out-of-four station coincidence and an improved TMB algorithm (solid line) help decrease the rate to an acceptable level. (b) For the highest Phase 1 luminosities, the trigger purity will have to be substantially improved again. Addition of station ME4/2 and requiring a three station match in the entire CSC detector (dotted line) will bring the rate in the lower $|\eta|$ range to acceptable level. Suppressing the large remaining contribution to the trigger rate from $|\eta| > 2.1$ requires unganging the strips in ME1/1a chambers (dash-dotted line), which in turn necessitates the DCFEB upgrade.

3.2.2 Description of the Muon Detector Upgrade Plan

The proposed upgrade of the CSC detector consists of three specific activities, which have important interdependencies:

- The constuction and installation of a new CSC station ME4/2 to provide the badly needed redundancy in the region of $1.2 < |\eta| < 1.8$. New chambers will require either new electronics or the recovered electronics from station ME1/1 (after ME1/1 electronics replacement).
- The design and installation of new digital front-end boards (DCFEBs) for station ME1/1 and unganging of cathode strip channels in the high-η half of the chambers. This will also require a replacement of the readout and trigger electronics for ME1/1 chambers (i.e. TMB and DMB boards) with more powerful chips to implement improvements to the reconstruction algorithm. This will provide a long-term solution

for triggering in the region of $1.6 < |\eta| < 2.4$.

- The replacement of the TMB boards responsible for the formation of trigger primitives for station ME1/1 will recover triggering in the region of $2.1 < |\eta| < 2.4$ at nominal LHC luminosity without a degradation of efficiency in the region of $1.6 < |\eta| < 2.1$.

3.2.2.1 Construction of ME4/2 Chambers

For the ME4/2 chambers, detailed engineering designs already exist, as these chambers are identical to the existing ME2/2 and ME3/2 chambers that were built at Fermilab and assembled and tested at UCLA and University of Florida. Space for the ME4/2 chambers on the YE3 iron disks already exists. Therefore, these chambers should be straightforward to build and deploy. Each ME4/2 chamber subtends 10 degrees in ϕ, and the full system with two endcaps contains 72 CSC chambers. Two spare chambers will also be built.

In 2008 it was found that the previous vendor no longer produces the large 5'x12' flat FR4 panels. After much difficulty, a replacement vendor was found, and these panels and other parts were procured to build a new ME4/2 prototype chamber. Most of the necessary chamber-building tooling was restored from the previous production of ME2/2 and ME3/2 chambers, and during FY09 this prototype was assembled, tested at Fermilab, and then shipped to CERN, where it was installed on the back side of the YE+3 disk. Thus, we have demonstrated that the tooling and expertise currently exists for production of the chambers and that suitable parts can still be acquired.

It is anticipated that Fermilab and Wisconsin will handle the bulk of chamber parts procurement and the modest amount of engineering associated with reviving the tooling and the drawings. Panel production (including precision milling of cathode strips patterns) will take place at FNAL. Assembly of the ME4/2 chambers will be done at a factory that will be set up in Building 904 at CERN, which will be available for first occupancy in early 2011. This offers some advantages, such as the possibility of strong contributions of manpower from foreign collaborators and CERN, the presence of substantial U.S.-funded manpower resident at CERN, and the ability for hands-on training of CMS graduate students with a substantial detector-building and testing project.

A management plan for the ME4/2 construction project is being developed. An overall ME4/2 upgrade manager will coordinate activities at the FNAL and CERN sites. There will be site managers at FNAL and CERN who supervise appropriate personnel (site-specific project engineer, floor manager, QA/QC technicians, etc.), as well as a Final ASsembly and Test (FAST) facility. Discussions have already taken place regarding specific personnel, including CERN and non-U.S. collaborators such as Russia (PNPI, Dubna) and China (IHEP).

Associated with the new ME4/2 chambers are a variety of electronics boards and other infrastructure associated with each CSC. The electronics board acronyms are: Anode Front End Board (AFEB), Cathode Front End Board (CFEB), DAQ Motherboard (DMB), Anode Local Charged Track Board (ALCT), Trigger Motherboard (TMB), Low Voltage Distribution Board (LVDB), and Low Voltage Monitoring Board (LVMB). Unoccupied slots for these boards are available in existing electronics crates for all associated readout and trigger electronics. Besides electronics boards, there are cables, cooling plates, HV, LV, cooling, and gas infrastructure items.

While the expertise and capabilities to build additional quantities of these boards are both available, one money-saving element of the muon upgrade plan as a whole is that as ME1/1 chambers are pulled out to install the new DCFEBs, the current CFEBs will be removed from

ME1/1 and then subsequently installed on the new ME4/2 chambers. Other electronics boards freed up as a part of the ME1/1 electronics replacement plan (old DMB, TMB, LVDB, LVMB) will also be moved to station ME4/2 as they become available.

3.2.2.2 Improving Trigger Performance in the Region $|\eta| = 1.6 - 2.4$

There are several specific improvements needed to address suboptimal trigger performance in the higher $|\eta|$ half of the ME1/1 region. These improvements focus on improving efficiency and robustness of the trigger as well as preserving trigger rates within the acceptable range, which is particularly difficult in the forward region.

3.2.2.2.1 Replacement of the TMB Board Daughter Cards The first part of the upgrade of the TMB board is the replacement of the mezzanine card holding the FPGA chip to allow for a more complex algorithm required to restore reliable triggering in the region of $|\eta| > 2.1$. With the deployment of the new DCFEB boards (described next), the TMB board itself will undergo some minor modifications to accommodate new optical fibers bringing data from the front-end boards. No changes to the mezzanine cards holding FPGAs will be required at that time. The total number of mezzanine cards needed is 72 plus 20% spares, all of which will rely on XILINX Virtex-6 FPGA chips. Neither procedure (the first one being essentially a repair) requires a long shutdown or any significant LHC down-time, since the new TMB cards can be installed during one of the many LHC short technical stops.

With the new algorithm, the efficiency of reconstructing stubs will be assured for the entire station ME1/1 and pseudorapidity up to $|\eta| = 2.4$, as shown in Fig. 3.4(b). For luminosities approaching $\simeq 10^{34}$ cm^{-2}s^{-1} (still prior to Phase I LHC upgrade), the acceptable trigger rate can be achieved by improved background rejection in the TMB algorithm and a requirement of three (out of four) stubs for muon tracks in the CSC Track Finder (CSCTF) (see Fig. 3.5(a)). For Phase-1 luminosities, removal of cathode strip ganging will provide another powerful tool in reducing the trigger rate by removing the ambiguity in selecting muon stubs, and will also further improve the efficiency by reducing the effective TMB dead-time in the high-η portion of the chamber.

3.2.2.2.2 DCFEB Boards and Removal of Channel Ganging in ME1/1 Chambers The "digital" Cathode Front-End Boards (DCFEBs) for ME1/1 that flash-digitize every channel simultaneously have a very simple architecture: low-noise amplifiers are connected directly to flash ADCs, whose output is fed in parallel into memories in a programmable gate array for storage until readout. The current CFEB boards can handle a steady input rate of 2 kHz, while the new boards will be able to handle 50 kHz (the rate of the local muon trigger in coincidence with the Level-1 trigger) with no deadtime.

The ganging of cathode strips in the inner portion of the ME1/1 chambers was done using a small passive printed circuit board. The outer portion of ME1/1 chambers covers $|\eta| = 1.5 - 2.1$ and contains 64 cathode strips per layer, while the inner portion contains 48 strips per layer. The outer portion can be read out by four CFEB boards, while the 3:1 ganging of the inner section allowed it to be read out by a single CFEB board. With the removal of the ganging of strips in ME1/1, three DCFEB boards will replace one CFEB on each ME1/1 chamber for readout of the inner portion, making a total of seven DCFEB boards per ME1/1 chamber, or a total of 504 DCFEB boards to be built for the 72 ME1/1 chambers, plus 20% spares.

It is anticipated that the outputs of the CFEB boards, currently two SCSI-50 connectors, will be retained on the DCFEB boards for "legacy" purposes, but supplemented in parallel by two

high-speed optical connectors. The optical links from the DCFEB will allow easier cable installation in CMS, as well as more reliable data transmission. Using the legacy connections and up to five boards per chamber, the DCFEBs could be connected to the current DMB and TMB boards. However, with seven boards per ME1/1 chamber and with optical links, the DMB and TMB boards must be revised. The CFEB, TMB, and DMB cards currently operating on ME1/1 chambers will be recycled by moving them to the new ME4/2 chambers.

3.2.2.2.3 DCFEB Compatible Electronics for Station ME1/1 Deployment of the new DCFEB boards with new optical links for station ME1/1 will necessitate replacement of certain electronics components, most notably the TMB and DMB boards. The prevously described repairs to the TMB board will make the new TMB board compatible with the new links after some minor modifications to the board. This will require 72 new modified DMB boards to operate with the new DCFEB and optical links. In addition, 72 updated LVMB and LVDB boards will have to be built, which will likely require only small design changes to enable the handling of seven (instead of five) front-end boards per chamber. For each board type, 20% spare boards will be produced to allow stable operations of the system in the long term.

3.2.3 R&D needed in preparation for the Phase 1 TDR

The ME4/2 chambers use an existing design, and therefore the R&D needs related to chamber construction are modest. One area we are working on is evaluation of vendors and currently available technologies related to building the panels for new chambers as the original vendor is no longer available. In FY09, a new fully operational ME4/2 prototype chamber was built using panels from a new vendor. Since then, another potential vendor has been identified and the studies aimed at evaluating long term reliability and physical aging of the panels have started. In order to build additional electronics boards, cables, etc. that are needed for use on ME4/2, we anticipate a modest amount of engineering R&D related to re-evaluating parts availability, vendors, PC boards and assembly houses. For example, the requirement to transition from leaded to non-leaded ICs happened since the original boards were built.

The DCFEB board is a new design and work has begun on evaluating this device. It has been found that the outputs of the existing low-noise amplifiers need to be buffered before serving as inputs to the new flash-ADC devices. We anticipate production of a DCFEB prototype board for evaluation in 2011. Work on improving the performance of the TMB boards in station ME1/1 has also begun and the first prototype of the replacement mezzanine board is expected in 2010. Engineering effort will be needed to finalize the design of the daughter card, implement the new algorithm in firmware, and to work out modifications of the main TMB board that allow it to receive data over optical links and communications with the trigger electronics downstream from TMB. Similarly, in order to build a revised DMB board for the ME1/1 electronics replacement, engineering effort will be needed to address issues related to optical link technology, board redesign, and FPGA evaluation. For all board types, engineering will be needed for prototype design, production, production supervision, deployment, and commissioning of the new system.

In addition to electronics engineering work specific to the CSC system, certain generic R&D studies related to the deployment of new generation of electronics components will be necessary. A number of radiation tolerance and hardness studies need to be planned and performed to ensure that both the new FPGA chips (Virtex-6 family) as well as optical-link components will be able to operate reliably throughout the lifetime of the experiment.

A high priority is the simulation studies of the high-rate conditions for the CSC detector. Those studies are ongoing and have already been critical in identifying the shortcomings of the cur-

rent system, developing solutions and evaluating robustness of the proposed solutions. Moreover, extensive studies of muon system backgrounds, such as neutrons, albedo particles, and beam-halo are also ongoing. Apart from improving simulations to include these effects, the measured LHC data on these backgrounds needs to be fed back into the high-rate simulation software. Neutron-induced hits in particular, while not penetrating like muons, produce large numbers of hits everywhere in the muon system. Present uncertainty of a factor of three in the rates of these hits is obtained from comparing existing simulation parameterizations, and reducing this uncertainty using the real data is important for Phase 1 upgrades and will become a dominant concern for proper planning of further Phase 2 upgrades.

3.2.4 Alignment with a possible Phase 2 upgrade

Based on previous irradiation studies, we expect the CSC muon chambers to perform as designed and not to degrade intrinsically to any significant degree even at SLHC Phase 2 luminosities. However, the current trigger and readout schemes were not designed for such high luminosities, and we may anticipate that other electronics upgrades than those instituted for Phase 1 will be necessary. The Phase 1 upgrades will, in any case, be critical for Phase 2. The additional ME4/2 station will help reject low-momentum muons and other backgrounds, and the engineering put into building DCFEBs, upgraded TMBs, and upgraded DMBs will prove very useful, since additional boards of these types may need to be built for CSC stations other than ME1/1 as the background rates increase.

An additional board, the Muon Port Card (MPC) may become a CSC muon trigger bottleneck and, if so, will have to be replaced in order to use dramatically faster optical links. The MPCs must be upgraded at the same time as the Trigger system's CSC Track Finder cards to which they link.

Additionally, it is possible that on-chamber anode trigger and readout boards (ALCT) will need replacement due to degraded performance. If these on-chamber CFEB and/or ALCT boards need to be replaced, it will require a large program of removing chambers to obtain the necessary access.

The numbers of CSC muon electronics boards involved in a full program of electronics replacement for Phase 2 include: 2196 DCFEBs; 468 each of TMBs, DMBs, and ALCTs; 60 MPCs, and a large number of optical fibers.

If a Level-1 track trigger is implemented for Phase 2, it will probably allow a somewhat degraded performance of muon-only triggering. On the other hand, some of the backgrounds, such as from neutron overlaps with muons, may scale as a power of the luminosity and become surprisingly large. These factors will need to be carefully evaluated with simulations and background-rate determinations from LHC collisions.

3.2.5 Schedule

The schedule of the two tasks related to production of chambers for the new station ME4/2 and electronics replacements for station ME1/1 are presented in this section. While the two activities are mostly independent, the installation and commissioning of the ME4/2 chambers on both endcaps requires the production of additional electronics boards (CFEB, TMB, DMB, LVMB and LVDB) to equip the new chambers. To reduce the overall costs, our plan calls for recycling the existing electronics, which will be freed-up as a result of the ME1/1 electronics replacement, on station ME4/2. This creates a dependency of the schedules of the two upgrades and emphasizes importance of planning as discussed in what follows.

3.2.5.1 ME4/2 Chamber Production

The schedule is well-understood: the process of producing ME4/2 chambers requires first procurement of parts, then the production of panels and chamber assembly can proceed. This will be a pipelined process in which the early chambers are being equipped with electronics and tested, while later chambers are being built. Installation of the chambers in CMS is relatively rapid and can be accomplished in a few weeks. Access to CMS, on the other hand, is expected to be quite difficult, especially in the 2016 shutdown, because of the major improvements scheduled by the Technical Coordinator.

From the start of Project funding, it will take approximately one year for production of the first chamber, and it will then be 2 additional years until production is complete. Additional time will, of course, be needed to install the chambers in CMS, and to connect the cables and other services needed for full operation. Time will also be needed for testing and commissioning. Some of the details of this schedule are shown in Section 3.5.

The muon upgrade plan couples the schedule for DCFEB production for ME1/1 to that of the ME4/2 chambers, due to the recycling of ME1/1 CFEB boards on the ME4/2 chambers. Because of difficult access to the ME1/1 region and the production schedule for the new DCFEB boards, the replacement of the ME1/1 CFEB boards can occur only in the 2016 shutdown. While the first endcap of ME4/2 chambers can be populated with spare electronics, the second endcap cannot be installed until the recovery of the CFEB boards from ME1/1. Specifically, the first endcap of ME1/1 chambers must undergo CFEB to DCFEB replacement before the installation of ME4/2 chambers for the second endcap. In order to remove this dependency of the second ME4/2 station, we would need to produce additional CFEB boards of the old style.

3.2.5.2 ME1/1 Electronics Repairs and Improvements

The ME1/1 system will need 504 new DCFEB boards (7 boards per each of the 72 chambers), 72 redesigned TMB boards, and 72 new DMB boards. In addition, the LVDB and LVMB boards will require modest modifications to account for the increase in the number of front-end boards per chamber.

The installation of the new ME1/1 electronics will be accomplished during the 2016 shutdown. The requirement of a shutdown is mainly driven by the necessity to access the ME1/1 chambers to install the new DCFEB boards. While it is more convenient to perform all replacements simultaneously from the logistics stand point, some of the ME1/1 repairs do not require a shutdown and can be installed during LHC technical stops. One such example is the TMB replacement, which will allow us to alleviate chamber level trigger efficiency concerns and which can be done even before the DCFEBs are replaced.

3.3 DT Muon Detector

3.3.1 Introduction

The barrel muon system forms the central, outer part of CMS. It is composed of 5 roughly identical wheels centered on the beam pipe. Each wheel contains 4 layers of drift chambers (DT) interspersed with the iron of the return yoke and 50 drift chambers, so the barrel system has 250 chambers.

The Drift Tube (DT) Muon system is a wide area detector with distributed on-detector readout and trigger electronics accessible only when the detector is open. See Figure 3.6 for a schematic view of the readout and trigger electronics. All the devices located on the Minicrate, as defined

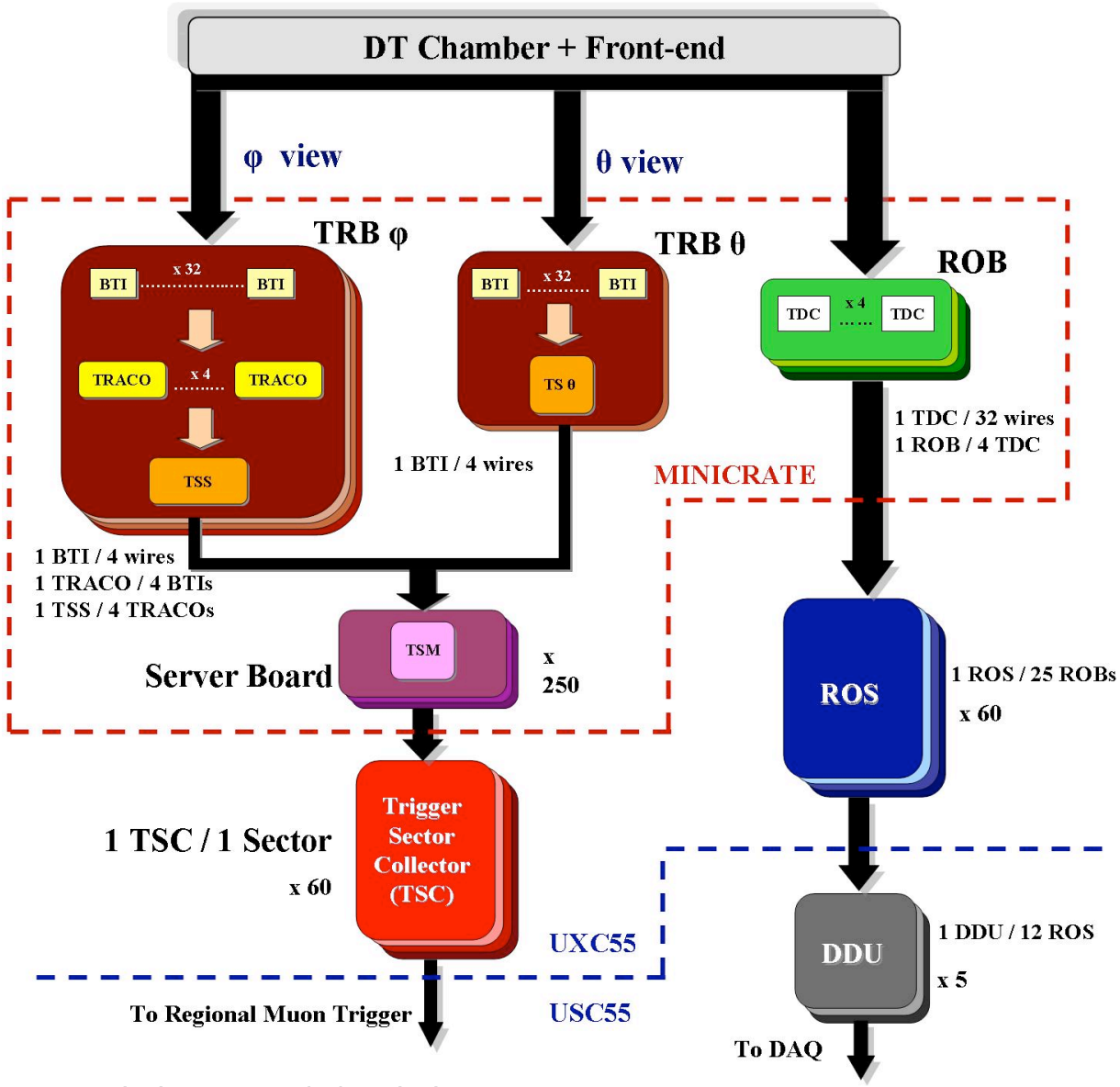

Figure 3.6: A schematic view of the readout and trigger electronics of the DT system.

by the dashed shape in Figure 3.6, are not accessible without opening the detector. Any foreseen upgrade should therefore cope with the limited access time and should aim to interventions that have limited impact on the single detector. This means that unless a really critical problem is found, the chamber itself and the on-detector electronics should not be touched.

A long cosmic ray data acquisition campaign and the first data registered from pp collisions provided information about system performance and permitted the evaluation of the weaknesses of the detector.

The study did not reveal any relevant weakness in the overall detector performance (resolutions, tracking capabilities, efficiencies), but spotted a few problems for the electronics. They were found in three devices:

- Trigger Boards
- Sector Collector

- Drift Tubes Track Finder

While the Sector Collector and the Track Finder boards are always accessible during any shutdown, the Trigger Boards are instead placed close to the detector. The difficult access to them requires a careful plan to allow an intervention. Details of the problems found in Trigger Boards and Sector Collector, together with proposed solutions are reported in the following paragraphs, while the Drift Tubes Track Finder ones are described in the Trigger section of the proposal.

3.3.2 Theta Trigger Board replacement

3.3.2.1 Motivation

The weakest point of the DT electronics is the BTIM hybrid circuit, a device carrying four Silicone-topped BTI ASICs (the front end barrel muon trigger device) bonded on a ceramic support (Figure 3.7).

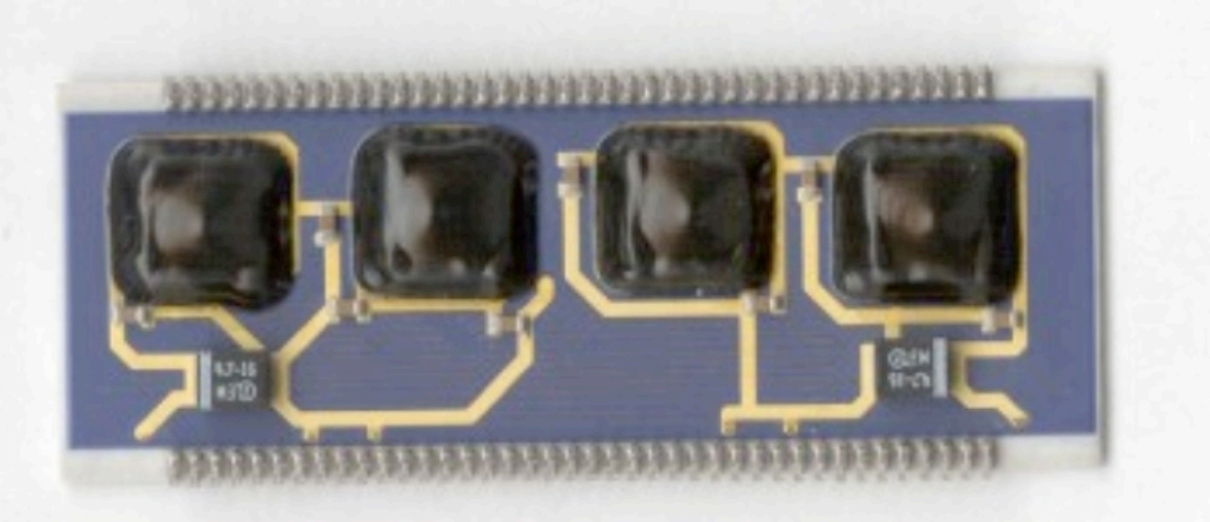

Figure 3.7: Picture of the BTIM hybrid module.

Eight BTIMs are placed on each Trigger Board (TRB). After detector installation TRBs were replaced at a rate of approximately 1%/year (19 boards were replaced during the detector commissioning phase and 24 in the setup period). Failures are probably related to thermal stresses of the BTI ASIC bonds caused by the continuous power cycling of the electronics during the commissioning and detector setup phases. Although we produced a large number of BTI spares (25%), the BTIM mortality was very high already during BTIM production tests and currently we are left with about 3% spare devices (Table 3.1) obtained, with high yield, by recovering good parts from faulty boards.

With the measured failure rate we will be running out of spares in about three years. But some caution must be taken since the unusual detector operation of the past years may have reduced the device lifetime and therefore the failure rate needs to be understood during steady operation. However, the two long shutdowns in 2012 and 2016, followed by startups, may subject the detector to conditions similar to those experienced in 2007-2009 with similar results.

3.3.2.2 Proposed solution

The BTI was fabricated in the ATMEL 0.5μ technology, which is now obsolete. Thus there is no chance for new production. Hence the only possibility left to solve this spares crisis is

Table 3.1: Available spares of boards carrying BTIM devices. The number of spares is estimated asuming a 80% yield on BTIM recovery from discarded boards and includes those mounted on good spare boards.

Board type	TRBPHI128	TRBPHI32	TRBTHETA	BTIM
Total installed	1080	60	360	10640
Spares	12	6	4	370

Table 3.2: Results of the radiation test of FPGA candidates with 60 MeV protons at PSI.

FPGA type	test fluence (p/cm^2)	MTBF (LHC years)	Comments
XILINX Virtex 5 LX 110 with SEU Controller Macro	$6x10^8$	0.1	Current increase detected
XILINX Virtex 5 LX 110 with Blind Scrubbing	$2.7x10^9$	0.5 - 0.8	Current increase detected
ACTEL A3PE1500 std com	$2.6x10^{11}$	150	Stopped working at 360 Gy
ACTEL A3PE3000L-1 com low power	$1x10^{11}$	85	Still working after 130 Gy

a migration to a more recent ASIC technology or to an FPGA device. We have investigated the second choice, since migrating to an FPGA optimizes the production timescale and leaves space for possible modifications that may be needed for the future high luminosity operation. Once the migration to an FPGA is completed, its conversion to an ASIC can be reasonably fast.

The TRBs are installed close to the detector in an environment that is not hostile in terms of radiation dose ($\sim$ 0.4Gy in 10 years of LHC operation), but subject to a substantial probability of Single Event Effects (expected fluence $5x10^{10}$ p/cm^2 in 10 years of LHC operation). Hence, after the BTI algorithm was migrated to a few possible FPGAs and its performance was verified using the old ASIC test vectors, the prototype boards were irradiated at PSI with 60 MeV protons.

Each FPGA under test was running two BTI cores at nominal frequency (80/40 MHz) and was fed by a monitor board with the same test vectors. Error counting was done comparing the trigger parameters on output of both BTIs to the expected benchmark results. The test results are reported in Table 3.2. The Xilinx FPGA is not suitable as a BTI replacement, while both ACTEL devices showed very good performance and are indeed fit also for operation in the SLHC environment.

Now that we have an appropriate FPGA device, a long term replacement strategy should be developed. Indeed the new boards production plan must consider detector survival and possible trigger algorithm improvements for future high luminosity scenarios. The best-suited action is the replacement of all currently installed THETA TRBs with the newly produced FPGA-based ones. The removed boards could be used as a source of spare BTIMs to be used to repair the failing PHI TRBs. If we follow this option, 2300 spare devices would be available allowing survival of PHI TRBs to the Phase 2 luminosity era. However, this replacement is an expensive option and is probably not worth it if the new BTI is performing exactly like the old one. Hence an alternative option could be the replacement of only a part of the boards: changing

for instance one full station layer (e.g. MB1) we could recover 780 BTIM so that even assuming a steady failure rate, there would be enough to cover the detector needs until the Phase 2 luminosity upgrade.

In the meantime it will be possible to understand if the theta trigger projection logic needs modifications for SLHC, as discussed later. The new algorithm could be uploaded to the already installed FPGAs, while choosing a less expensive ASIC option for the production of the remaining boards, which could be installed during the long LHC shutdown in 2020 preceding the beginning of the high luminosity run.

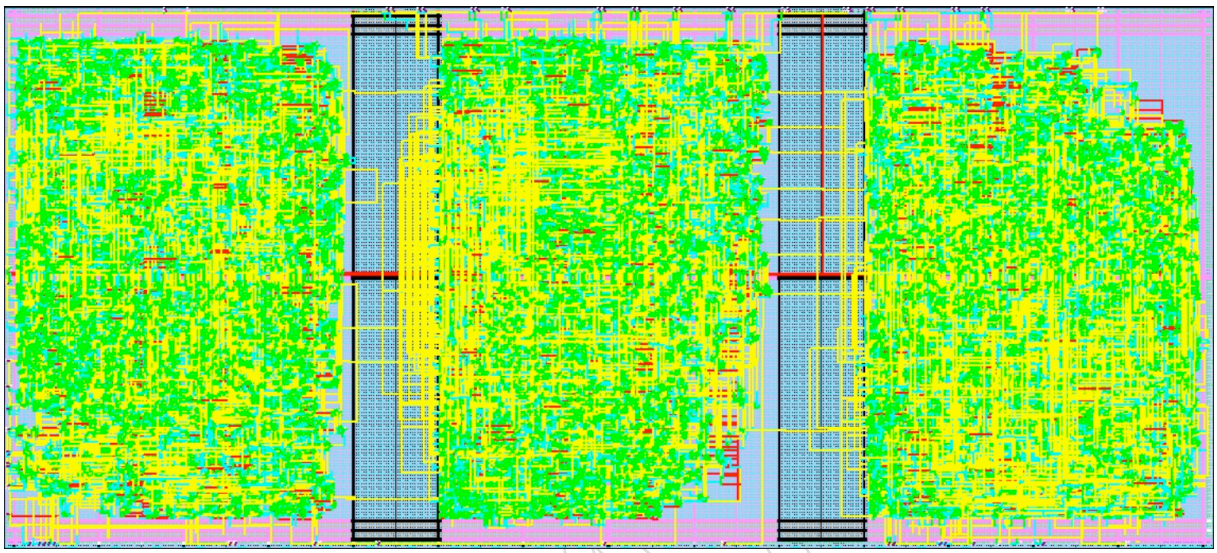

Figure 3.8: Layout of 3 BTIs included in an ACTEL A3PE3000L FPGA.

The cost of the replacement will depend on the number of FPGAs needed which in turn depends on the number of BTIs that can be programmed inside each of them. An ACTEL A3PE3000L can easily contain 2 BTIs while it is far more difficult to include 3 or even 4 of them. Currently 3 BTIs have been included in one chip (Figure 3.8) although the timing is not yet correct (76 MHz against 80 MHz), while inclusion of 4 of them is really at the limit since $\sim$ 90%of the FPGA resources are used. The number of FPGAs needed for each TRB is 16 if two BTIs/FPGA are included, while it is 11 if three BTIs/FPGA are included. Although rather problematic the inclusion of 4 BTIs/FPGA is still an option being pursued. A prototype board is being developed in order to understand if there is any critical aspect in the project and eventually solve it. Main problems currently being addressed are power supply schemes, power dissipation and network configuration of the board.

There is, in fact, only one major improvement that can be made in a new THETA TRB. Currently the triggers in this projection are OR-ed in groups of 8 BTIs, leading to a local z-position resolution of 16 cm, while the intrinsic resolution of the chamber is $\sim$1.2 mm. The new board could then be programmed to transmit a more accurate value allowing a better resolution. The polar angle resolution for a few different cases, assuming a beam spot with 5 cm z-spread, is shown in Figure 3.9. There is room to halve the current polar angle resolution. Incorporating this improved resolution will require changes to the DT Track Finder.

3.3.2.3 Schedule

The actual implementation program will largely depend on the final decision about access to the Minicrates. The main bottleneck is access to the minicrates since the detector must be

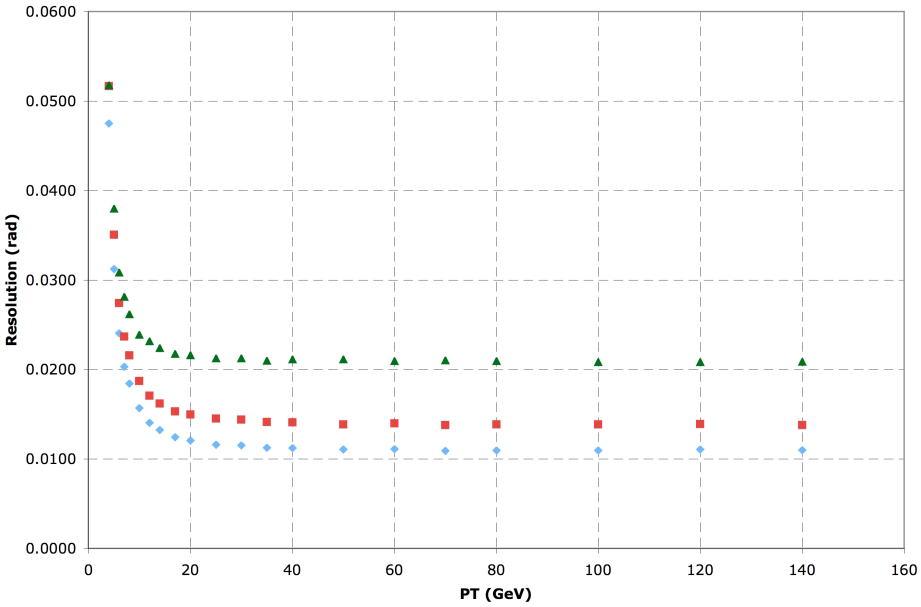

Figure 3.9: Expected resolution of the polar angle θ as a function of the muon momentum for current resolution (green), only BTI number transmitted (red), full resolution (blue). The primary vertex z- position is smeared with a Gaussian of $\sigma = 5$ cm.

Table 3.3: Upgrade schedule

2010	production of 2 prototype boards
2011	bench tests and decision on replacement strategy
2012-2013	mass production and test
2014-2015	installation
2015	decision about strategy in high luminosity operation

opened to allow board replacements. The interventions should be easier on external wheels, but on average we expect to be able replace and test two minicrates/week. From the detector performance point of view the best solution is the replacement by stations in such a way that the detector preserves a uniform response. This choice optimizes the access time, since the replacement on any wheel can be done in parallel with the interventions on other detectors, thus adapting the work to the general CMS maintainance schedule. Taking into account all the constraints the total access time needed to replace all boards of one station is about 6 months. We propose to replace all the boards in one full station (e.g. MB1) with the FPGA version by 2015. The replacement in the other stations will be decided only if needed and when it will be clear which one will be the best option to pursue. We propose the schedule shown in Table 3.3.

3.3.3 Sector Collector Upgrade

3.3.3.1 Overview of present Sector Collector system

The Sector Collector (SC), second level of DT trigger and read-out electronics, is sitting in the tower racks on one side of the CMS wheels. It is made of 10 VME crates that host 60 ROS (Read-Out Server) boards, 60 TSC (Trigger Sector Collector) boards and 10 TIM (TTC Interface Module) boards.

Each ROS board is in charge of data merging and data quality monitoring, reducing data over-

head to build a synchronized event fragment of one sector. They collect the information from 25 ROBs (Read-Out Boards), which are located inside the Minicrates. Each ROB sends its read-out information to the ROS through an LVDS copper link, up to 40 meters long, at 240 Mbps. Merged data is sent from each ROS through a 60 meters optical link at 800 Mbps to the DDU (Device Dependent Units), located in the Underground Service Cavern (USC55) at the S1 floor.

Local trigger data of each chamber are output using serial LVDS running at 480 Mbps on two FTP cables, up to 40 m long. The TSC boards collect and synchronize the trigger information from one sector (4 or 5 chambers). They send the encoded information of position, transverse momentum and track quality through 1.6 Gbps optical links (about 60 m long path) to the counting room, where optical receiver boards (Opto-RX) fan out the trigger data to the Drift Tube Track Finder (DTTF).

3.3.3.2 Motivations for Sector Collector upgrade

The proposed upgrade of the Sector Collector is not motivated by the physics performance of the sub-detector as of today, but by the fact that aging and other risks may jeopardize detector operation and contribute to an accelerated degradation.

The Sector Collector is a complex electronic system located in an environment with significant magnetic fields and radiation doses up to 0.2 Gy per year of LHC run (charged particle fluxes of 20 cm^{-2} s^{-1}) that intrinsically becomes a weak point in terms of maintenance of the detector. A failure in one ROS or TSC board may handicap a large fraction of the detector (one sector out of 60) and a failure in one TIM board turns into half a wheel lost both in the trigger and read-out chains. A fast reaction time is needed in order to minimize the impact of such failures. However, limited access to the CMS cavern, which is subject to technical stops in LHC operation and radiation protection issues, increases dramatically the impact of a failure in the system, and renders a significant fraction of the DT system useless in the meantime.

Another point of concern is the power consumption due to the limited cooling capacity of the tangential turbines capable of operating under such magnetic fields. Aging of the present turbines, will lead to operation of SC electronics at higher temperature, and thus, accelerated aging and increased failures. The power dissipation of the present Sector Collector electronics is already marginal for the CMS cooling system, so any increase in performance cannot be accompanied by an increase of power consumption if these electronics remain in their present location.

Furthermore substitution of the present electronics with higher performance designs that may improve functionality is subject to the constraints of being able to operate in the radiation environment. This requires identification of proper devices through radiation campaigns, which increase significantly the design timescale and price. Moreover, in some cases, increased performance may be limited itself by the radiation tolerance of the devices. On top of previous arguments, the accumulated experience points to several aspects related to the Sector Collector electronics that leave room for performance improvement.

3.3.3.2.1 ROS boards The read-out electronics was designed to work beyond the expected data rates at LHC. However, during the last years we have observed the presence of bursts of noise affecting large areas of the detector (more than one sector) that have an impact on buffer occupancies throughout the read-out chain. In fact, the maximum number of hits per HPTDC (High Performance TDC chip produced by CERN) in the ROB boards has been limited at present to be able to cope with the present noise without flooding the data acquisition system.

Table 3.4: Number of links between Minicrates and Sector Collector electronics.

	Per Sector	Per Wheel	Totals
ROB to **ROS**	25	300	1500
SB to **TSC**	32/40	400	2000
Total	57/65	700	3500

ROS design includes some parallelism in channel processing, but each group of 6 input channels is processed sequentially since input FIFOs are external to the FPGA controller. The programmable logic devices market has evolved to allow embedded deserializers and placement of large memories inside each device. Profiting from these higher performance devices, ROS functionality could be improved significantly by increasing its parallelization and thus, reducing its processing time. The benefit could be twofold; not only will the effect of noise be reduced at this level by means of larger buffer capabilities, but also, higher performance FPGAs could allow suppression mechanisms that filter out noise events avoiding saturation of higher level buffers. However these new devices cannot suvive in the cavern radiation environment.

3.3.3.2.2 TSC boards The Opto-RX boards that collect TSC information turned out to be very sensitive to the clock frequency shifts intrinsic to LHC energy ramps, which by unlocking the links create high rate input noise that propagates through all the trigger chain resulting in an unsustainable trigger rate. Unfortunately slow control of these Opto-RX boards through a JTAG interface is also unstable and allows very limited programmability in the devices. It is also worth noting that DT trigger latency is one of the largest in the CMS trigger system and reducing the serialization/deserialization stages may allow a faster triggering mechanism. This may be achieved by the integration of TSC and Opto-RX devices in one single module.

3.3.3.3 Description of the proposed upgrade

The proposed solution to Sector Collector electronics problems consists of its relocation to the USC counting room, freeing it from the hazardous environment in the cavern and minimizing the downtime in case of failure. Since SC inputs are based on copper links whose length cannot be increased without compromising its reliability, a simple copper to optical fiber conversion should be placed in the cavern. As a first approach, a suitable place to allocate this optical converter is in the present SC tower racks. The total number of copper-pair differential links reaching the SC crates is 3500, distributed as shown in Table 3.4.

Several options for this optical conversion are under study. The preferred one at present is a direct 1-to-1 copper to optical fiber conversion. This implies 3500 optical fibers to be routed from the cavern to the counting room. Taking as a reference the DT optical links currently installed between SC and USC, consisting of 10 multi-ribbon cables 48 fibers each, the minimal number of cables to route is 73 (plus spares). Each of these cables is 10 mm diameter, so the total cross section required would be in the order of 100 cm^2.

Present SC crates space would be replaced by an array of 3500 electrical to optical converters, by means of a very simple (and, therefore, robust) electronics system based on a line equalizer, laser driver and laser diode. The actual implementation of this solution is still under study, but the main components are already identified and some of them are already in operation in the current system, so no further characterization may be required. It is also possible that the solutions under study in the CERN Versatile Link project may fit our requirements.

Accordingly, present SC electronics would be moved to USC, where it would be necessary to

implement a conversion back from optical to electrical signals. The input stages of the present TSC and ROS boards are implemented in mezzanine boards, so they can be replaced to receive the appropriate optical links instead of the present copper ones with minor modifications of the SC boards and thus reduced cost. Moreover, the interface with present DDU and DTTF would remain unchanged, avoiding dependencies with upgrading different parts of the system simultaneously. The basic schematic of this proposal is shown in Figure 3.10 for an individual DT sector. The reverse optical to copper conversion is represented as an independent module to emphasize that ROS and TSC main functionality does not necessarily need to be fully redone.

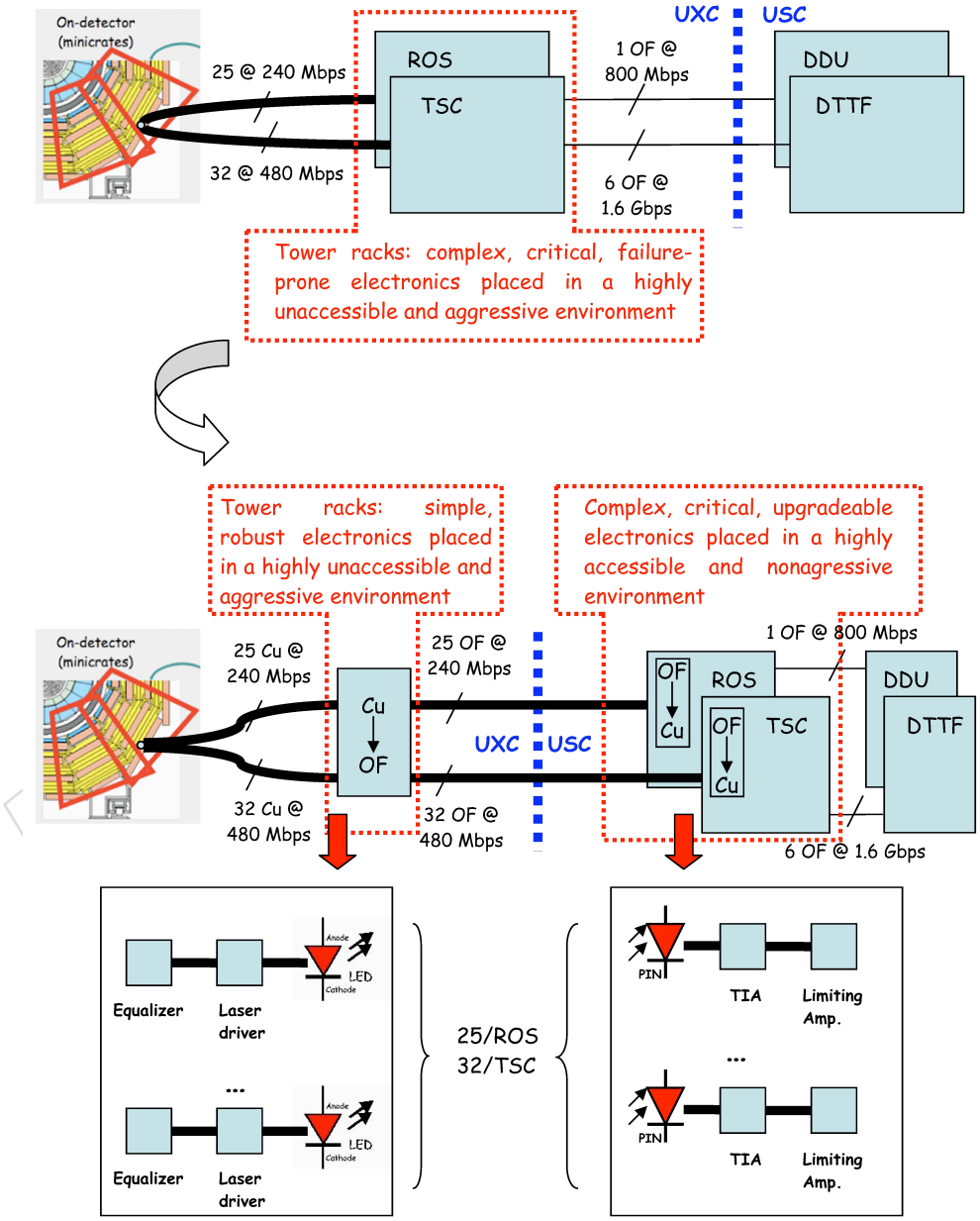

Figure 3.10: Schematic view of the proposed upgrade for Sector Collector electronics. The top part of the figure shows the current situation, while the bottom part sketches the situation after the proposed upgrade.

3.3.3.4 Examination of the upgrade and alternatives

There are many advantages of this proposal:

1. The complex SC electronics is located in a less hostile environment where the possibility of failure is reduced.
2. Access on demand in case of failure can easily take place, thus, minimizing downtime.
3. Copper to optical conversion in tower racks is much simpler and more robust than present SC electronics, with much smaller power consumption, so the probability of failure is minimized.
4. The solution allows a gradual, controlled replacement plan for current SC electronics in order to implement future upgrades.
5. The relocation of SC electronics in USC provides great benefits in view of future upgrades to improve the physics performance of the system by allowing the use of commercial off-the-shelf devices without radiation tolerance requirements. New designs will profit from a reduced price at a higher performance.

The main disadvantage of the proposal is the increased number of fibers and optical transmitters that need to be installed. Solutions allowing the minimization of the number of optical links by means of multiplexing are under study. Direct multiplexing the 240 or 480 Mbps serial links may not be feasible due to timing constraints: the high speed and phase difference of the various independent inputs does not allow a proper sampling of the links guaranteeing signal integrity.

An alternative could be multiplexing the input links once deserialized by means of a large data-width high-speed serializer. Accordingly, the number of optical fiber links to be routed can be reduced by a factor N, where N can be at most 3 to 4 for devices available on the market (even GBTx). It has to be also noted that the added complexity in the copper to optical fiber conversion system will compromise the advantage of this design compared to present SC electronics. On top of that, it is unclear if the reduction in the number of optical components entails a cost reduction. What is clear is that cost will not be reduced by a factor N, due to several factors: the higher number of components that will be required to perform the copper to optical multiplexed conversion; their increased performance requirements; the higher speed of the new link which is directly associated with its grade requirements. Moreover, the demultiplexing will have to be done within the new SC electronics, also increasing accordingly the complexity and cost of the new design. Furthermore, additional multiplexing and demultiplexing stages will increase trigger latency as compared with a direct copper to optical conversion. The impact of a latency increase is critical in our case, since DT trigger latency is already the largest one in CMS and will have a non negligible impact in other CMS subdetectors. Finally, this approach is much less compatible with a possible future upgrade that would allocate the copper to optical conversion nearby or within Minicrates.

3.3.3.5 Implementation and infrastructure issues

The feasibility of the relocation of the Sector Collector from UXC is subject to various constraints from the infrastructure point of view. The most relevant ones are the routing of a large amount of fibers between the cavern and the counting room and the availability of the space required to allocate present Sector Collector electronics in USC.

3.3.3.5.1 Routing of new fibers As previously mentioned, the number of links if TSC and ROS were to be moved to the counting room can be up to 3500 fibers. By using multi-ribbon fibers the required cross section could be minimized down to 100 cm^2. Enough space should be made available not only in the tunnels that exit the cavern, but also in the cable chains of the external wheels and in the Patch Panel frames below the tower racks. Preliminary inspections indicate that space is available for the cables, but more detailed studies should be done about connector fanouts and proper integration. Furthermore, the available space to recover extra cable lengths below the S1 floor in USC55 needs to be verified.

One important point to be taken into account is that trigger fibers must follow the shortest possible path to avoid increasing trigger latency. Therefore, at least trigger fibers should be routed through the fast channels that provide a short path of less than 60 meters. We are also investigating the possibility to install all those fibers with the "blowing tecnique" by means of a specialized CERN group.

3.3.3.5.2 Relocation of crates in USC55 The Relocation of Sector Collector electronics is a complex operation that should be planned carefully to be fully compatible with the present system throughout all of the upgrade steps. A gradual approach would be much more convenient in some cases, minimizing system failure risks and allowing proper testing of the new solution before full installation. In order to decouple copper to optical conversion and redesign of new Sector Collector electronics, a feasible proposal is to reuse at a first stage present SC boards in USC with modified mezzanines that host the receivers for the Minicrate data with optical receivers. In either case, the required space to allocate Sector Collector electronics in USC remains constant. Accordingly, at least the same amount of space presently used in UXC should be made available in USC: 10 VME 9U crates, i.e., 120 U, would be needed. Roughly, that would imply using 3.5 racks. At present, about half of that space could be available among racks S1D10, S1D08 and S1D03, presently assigned to the DT system. Again, it is important to take into account that to minimize trigger latency, at least, TSC boards should be placed near the DTTF rack. The previously mentioned racks accomplish this.

3.3.3.5.3 Interferences and dependencies The installation of new fibers is a major task that requires a long shutdown and could not be accomplished before 2012. However, fiber installation and Sector Collector relocation are two tasks that can be decoupled in time. In fact, relocation of Sector Collector in USC could be split into several tasks that are independent from the opening of CMS wheels, and thus, from LHC long shutdowns. Accordingly, this operation can be performed during the short end-of-year technical stops. The minimal advisable granularity is half a wheel, i.e., one Sector Collector crate.

In a first scenario, the plan would be to reuse the present SC boards in USC but modify the mezzanines that host the receivers for the Minicrate data. In this way, a complete redesign of the system, if desired, does not need to be tied to the schedule in the present proposal. The tower rack space, presently used for Sector Collector electronics, will accomodate the copper to optical fiber conversion modules, which would be simple and robust. The number of components to be used is minimal and therefore, less prone to failures. Power consumption will also be strongly reduced, ensuring longer term operation.

3.3.3.6 Proposed schedule

There are 5 major tasks that must be done:

1. Installation of fibers between UXC and USC (up to 3500 links distributed in 73 multi-

ribbon cables). This can be divided into three stages:

- 30 cables through YB+ tunnel
- 15 cables through YB0 tunnel
- 30 cables through YB- tunnel

2. Relocation of TSC and ROS in USC according to the space made available.
3. Modification of TSC and ROS input mezzanines to support optical link reception.
4. Redesign of ROS electronics with a new slow control interface and higher performance.
5. Redesign of TSC and Opto-RX electronics integrated in a single unit compatible with the new DTTF design.

The optical fibers installation requires opening the cable chains. Such an intervention is quite time-consuming and can be done only by an experienced team. The cost of installation is also largely dependent on the technique used. If we were to redesign completely ROS and TSC an extra cost of 600 kEuros should be added assuming the costs are similar to those of the currently installed boards.

3.4 RPC Muon Detector

3.4.1 Introduction

3.4.1.1 The CMS muon trigger system

At the LHC, the bunch crossing frequency is 40 MHz, which, at the nominal luminosity of 10^{34} cm^{-2}s^{-1}, leads to about 800 million proton-proton collisions per second. CMS has put emphasis on the detection and identification of muons. Every 25 ns some 1000 particles emerge from the interaction point into the CMS spectrometer. In less than 3 μs a first level trigger has to reduce this rate to 100 kHz without losing potentially interesting collisions requiring further analysis. The CMS muon system described in the CMS Muon Technical Design Report [CERN/LHCC 97-32] contains two complementary technologies:

- Wire chambers that track the muons with precision through the iron yoke and return field: Drift Tubes (DT) in the barrel part; Cathode Strip Chambers (CSC) in the end caps. In both cases, there are four layers of chambers and they provide a reasonable estimate of the trigger timing.
- Resistive Plate Chambers (RPC) that determine precisely the time of passage of the muons as well as an estimate of their transverse momentum.

3.4.2 Physics motivation for the forward up-scope

The first level trigger based on the RPCs provides CMS with the most precise timing in both the barrel and endcap region. Six concentric layers of chambers are used in the barrel part, while four layers have been foreseen in total for the end caps to cover a rapidity up to $|\eta| = 2.1$. A Memorandum Of Understanding (MOU) commitment for the production of the forward RPC system was signed with university groups in Islamabad (Pakistan), Peking (China) and Seoul (Korea). Due to insufficient funding availability, only 3 layers were built in the endcap which provided a limited rapidity coverage up to $|\eta| = 1.6$ as shown in Figure 3.11. It was expected that the fourth layer chambers could be constructed later so that coverage of the full rapidity

range of the original design could be achieved. The key element of this proposal is to construct the 4th layer of RPCs in the endcap.

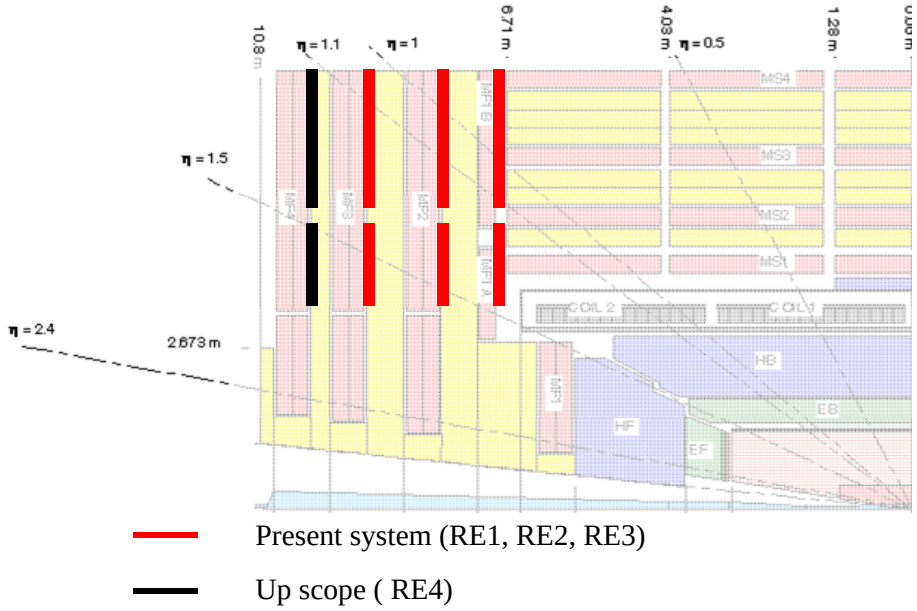

Figure 3.11: Profile of the CMS endcap region showing the existing RPC stations (RE1, RE2, and RE3) and the proposed upgrade station RE4.

In Figure 3.12 the simulated trigger efficiency as a function of η is shown in case of the present 3 layers and compared to the result for a 4-layer system. The advantage in extending the detector to include the fourth station is clearly evident.

The completion of the forward RPC system to 4 layers per end cap is therefore a priority. CMS has decided to split the up-scope project into two distinct phases:

- Phase 1: completion of the low $|\eta|$ part ($|\eta| < 1.6$).
- Phase 2: completion of the high $|\eta|$ part ($1.6 < |\eta| < 2.1$).

This section will be focused on the restoration of a full low η system which will provide an efficient and robust trigger operation at the LHC design luminosity. The groups from Pakistan, China and Korea have already committed themselves to this completion. In addition, groups from Belgium, India, and Egypt have confirmed their involvement in the project while negotiations with Italy are under way to provide the off-detector electronics. Other countries (Finland, Poland) have expresed an interest in joining the project, although they have not yet committed to any financial contribution. Nonetheless, their participation and expertise is an important aspect of the project. Recently interest has been expressed from Iran and Colombia and negotiations have started to define possible contributions and areas of involvement.

3.4.3 Detector design and layout

3.4.3.1 Description of the detector geometry

The forward stations are wedge-shaped detectors with a double gap RPC. A schematic layout is shown in Figure 3.13a. The actual system consists of 432 chambers mounted in a staggered way in two concentric rings on the endcap disks to cover its surface ($\sim$ 150 m^2 per disk) as illustrated in Figure 3.13b. A photograph of the RPC third layer on the +z endcap is shown

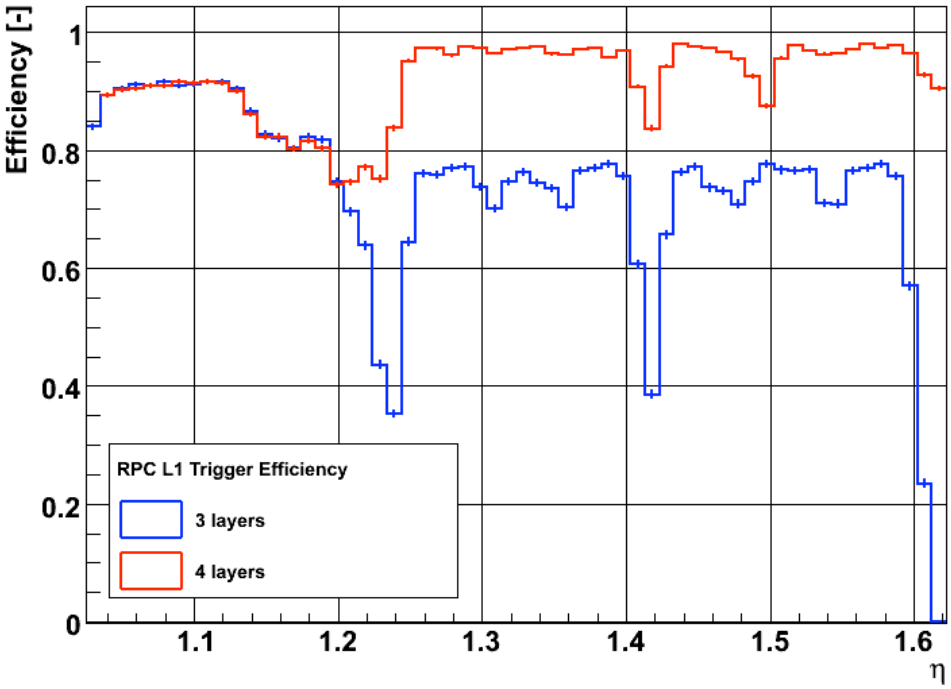

Figure 3.12: Simulated trigger efficiency as a function of the number of layers of RPCs.

Figure 3.14. The completion of the forward RPC system for $|\eta| < 1.6$ region will require an additional layer, (RE4), composed of 144 new chambers. These new RE4 chambers will be composed of two concentric rings (RE4/2 and RE4/3) of RPC chambers. Each ring is therefore composed of 36 chambers. These new RPC chambers will be of the standard CMS forward design.

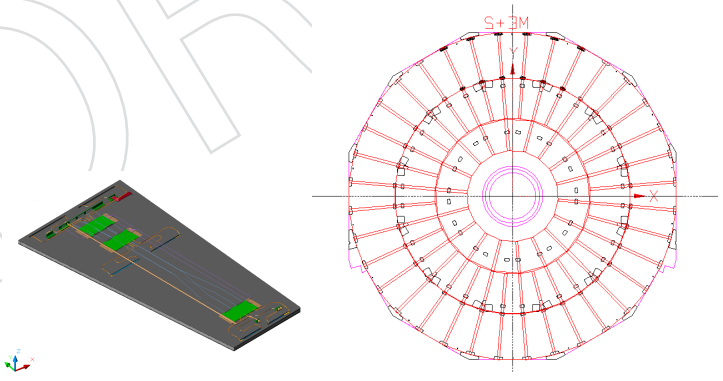

Figure 3.13: a) Schematic layout of a forward double gap chamber; b) Layout of an RPC station on the endcap yoke disk.

3.4.3.2 Integration of station RE4

The new RE4 station will be installed on the back of the YE3 yoke, mounted independently of the CSC chambers. The RE4 detectors will be mounted on an aluminum interface frame, supported on the existing threaded M16 holes at the extension of the CSC mounting posts, as illustrated in Figure 3.15. This solution decouples the installation of RE4 from the existence of

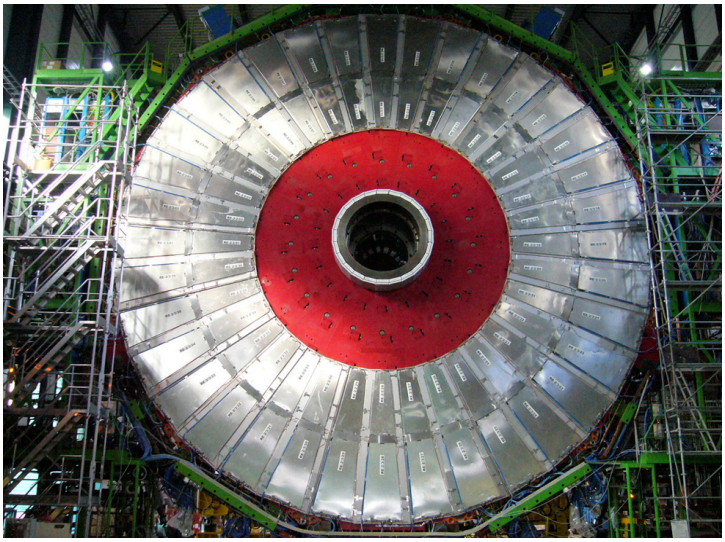

Figure 3.14: The third station of RPC chambers on the +z endcap disk.

the YE4 shielding wall. The nominal clearance to the shielding wall will be 9 mm provided the interface frames have a thickness of 8 mm.

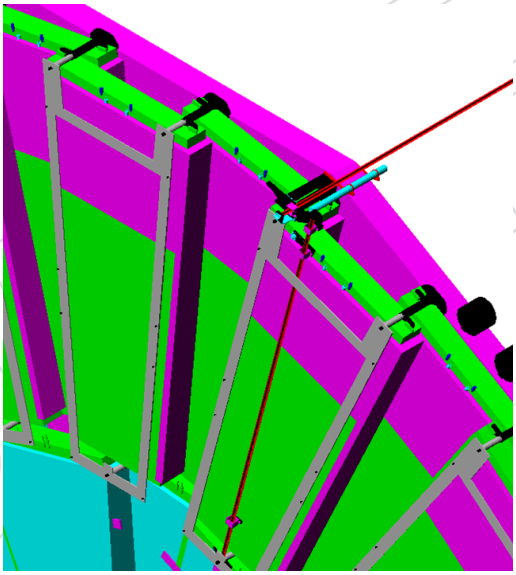

Figure 3.15: Mounting of the RE4 chambers on the back side of the YE3 disk with the interface frame attached to the disks.

The services to RE4 will be housed on the YE3 towers where the infrastructure will need to be completed. No services to RE4 have been installed since they were part of the staging scenario that originally involved mounting the RE4 chambers on the YE4 shielding wall. The infrastructure services that now must be added to YE3 are:

- A gas distribution rack with 72 channels and the necessary pipe work to the local bulkheads.
- The manifold and pipe work for the proper distribution of the cooling fluid.
- The low voltage (LV) system, including crates and cabling to the power supply sys-

tem in the YE3 towers.

- The HV cabling to the YE1 Patch Panel (requires insertion in the minicable chain) and to USC (requires insertion in the main cable chain).
- The necessary Link Board Boxes and the related cables and optical fibers.

As a consequence the endcap main cable chains will have to be opened to install the missing HV umbilical links to the SX5 cavern (this will be a major intervention that requires an expert team). It will be possible only when the main cable chain will be accessible, which will require the complete opening of YE1s. Adequate space for these cables has been reserved in the main- and mini- cable chains in the original construction of CMS.

3.4.4 Electronics

The layout of the RPC electronics is shown in Figure 3.16. The chamber readout data are initially analyzed at the Front-End electronics Boards (FEB), which forms LVDS digital signals and sends them to the Link Boxes, which are located on the balconies at the yoke periphery. Here synchronization and data reduction is performed before transmitting the information via optical fiber to the trigger electronics in the control room.

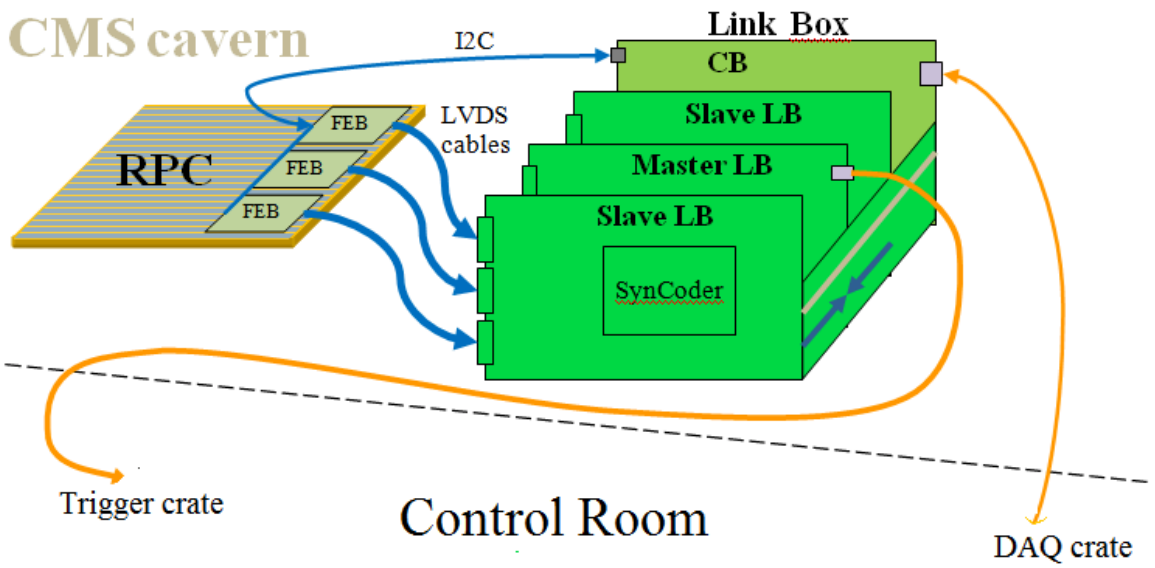

Figure 3.16: Layout of the RPC electronics.

3.4.4.1 Front-end boards

The same RPC Front-End Board (FEB) that was developed in the past and mounted on the current chambers will be employed. The front end has four 8-channel ASIC Front-End Chips (FEC) each consisting of an amplifier, discriminator, monostable and differential LVDS line driver. The connection between the RPC strips and the FEB is made with 50-Ohm coaxial cables, that are soldered on small adapter boards such that they are easily pluggable to the FEBs. FECs are available from the past production. However, new boards will be necessary to instrument the new RE4 layer and production is scheduled to be done in Pakistan. Figure 3.17 shows a picture of one 32-channel FEB.

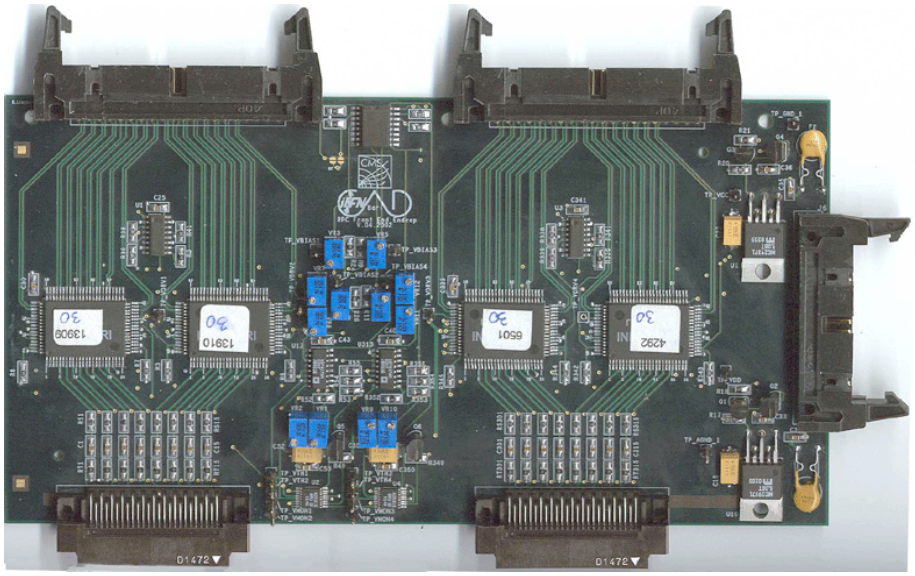

Figure 3.17: Front-end board.

Pakistan will be responsible for FEB mass production in Pakistan. Plans call for 50 FEBs to be produced by the end of October 2010. After a complete validation of FEBs, mass production will be started at the beginning of 2011. We require 600 FEBs, which includes 10% contingency. The required production time is approximately three months, which includes the time of procuring of components, developing of PCBs, mounting the components, and testing of final FEBs. Before shipment to CERN, validation tests, such as voltage threshold setting (VTH), voltage biasing setting (VBIAS), voltage monitoring (VMON) and I2C for quality assurance, will be performed in Pakistan.

Each chamber also contains one Distribution Board (Figure 3.18) that receives power and slow control communication through power cables and I2C bus and distributes them to the FEBs using flat cables. 200 additional Distribution boards will be required.

3.4.4.2 Off-detector electronics

The output of the FEBs is sent to the Link Board system (LB) where the synchronization with the LHC clock, the optical conversion and the transmission to the Trigger Electronics are performed. The new layer, RE4, has to be equipped with a complete new set of LBs. Table 3.5 gives the number of additional components needed to complete the LB system on the detector side. The new electronics will include minor design improvements to overcome a few problems observed during operation. However, it will be fully compatible with the present system. A special role is played by the Control Board (CB) which drives each LB crate, provides inter-crate communication and hosts the main software for the connection to the readout and the trigger systems. While only minor improvement will be considered for the additional CBs to be procured in the present upscope project, a major redesign is planned for the 2016 upgrade. INFN is willing to take responsibility for the production and to gain expertise in the operation of the new system. The tests and the installation of the new boards should be done under Italian responsibility. Poland is expected to provide expertise to allow the transfer of knowledge and to take the responsibility for the integration of the trigger system of the new electronics.

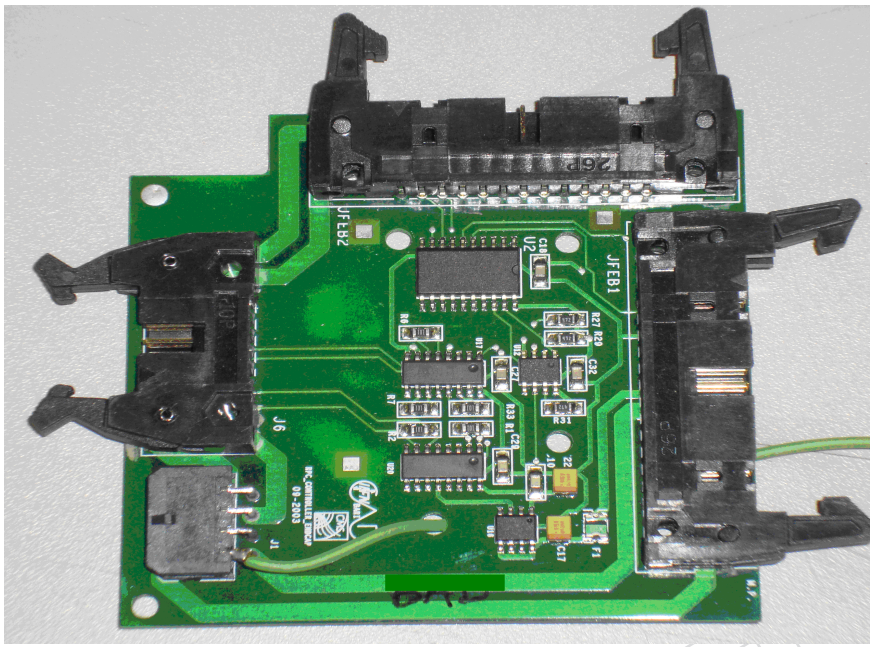

Figure 3.18: Distribution board.

Table 3.5: List of Link Board system components needed for RE4.

	RE4/2,RE4/3 on YE3		
	needed	spare	total
LB mechanics	12	2	14
LB Back Plane	12	2	14
MLB	48	10	58
SLB	96	10	106
CB	24	6	30
FP	24	6	30

3.4.5 Services

3.4.5.1 Gas system

At present no work has been done for the fourth station besides the necessary piping for the control of the intended gas rack. The supply and return piping to RE3 chambers has been designed to allow RE4 chambers to be connected to it. It will be necessary to find the space for an additional gas rack. Space is available next to the RE3 gas rack, while space above is slightly obstructed by the existing RE3 piping.

3.4.5.2 Cooling

Cooling has been a difficulty in the past. Our experience indicates that most of the heating is due to external sources, not to the heating of the gaps themselves. Now we are confident that the present cooling setup is adequate to compensate for the heat produced by RPC electronics, which is only 12 watts, but we know that RPC gaps are still suffering from temperature

increase. We are requesting a cooling connection every 10 degrees on the manifold so we do not have 3 chambers on a cooling circuit. Moreover we will have 2 pipes on each side of a copper plate. As stated before there are no spigots at present available on YE3 for RE4. Significant reworking of the manifold must be considered. In addition, we are considering mounting thermal insulation between the CSC and RPC chambers. We know that RPC operation is quite temperature sensitive. Best thermal working conditions for RPC are with chambers at 18°C. 23°C is the maximum temperature where we must switch off the chambers. Given the present performance, the current cooling system in CMS endcap demands significant revision to insure the best working conditions for RPC. Hence quality assurance procedures in the cooling system will be particularly important.

3.4.5.3 Signal read out

The data readout and transmission to the trigger crate will need some additional cables that have to be procured, connectorised, labelled, tested and installed:

- 864 signal cables and 72 DCS (I2C) cables between the RE4 chambers and the Link Board boxes.
- 48 fibers from LB boxes to RE3 tower patch panels in UXC.
- 24 single-mode TTC fibers from the Link Board boxes to the TTCOC.
- 84 DCS Ethernet (class 7) cables between the Link Board.
- 96 multimode fibers between the Splitter boards and Trigger Boards in USC.

3.4.5.4 High voltage

For the 144 RE4 chambers, a total of 288 HV channels are needed (each gas gap is supplied separately). However, the number of channels can be reduced by using distribution boxes. This allows cost reduction while still maintaining the ability to handle problems in case of a single gap failure. Each distributor (Figure 3.19) will transform 10 input channels into 40 output channels. A total of 8 HV distribution boxes will be needed.

Figure 3.19: HV Distribution board.

A total of 12 HV CAEN A3512 boards (72 channel in total) will be necessary to complete the system. The existing HV EASY Crates have enough free slots to allow installation of these new boards. New HV cables need to be pulled from the RE4 chambers to HV patch panel (PP) at the base of the YE1 disk through mini-cable chains, while additional umbilical cables need to be installed from PP to reach the USC HV racks. The HV cables from chambers to the PP will be connectorized and tested before installation, whereas umbilical cables from PP to USC

will be connectorized and tested after installation. Extensive quality tests on the cables will be performed prior the installation following the same protocols already developed.

3.4.5.5 Low voltage

The Low Voltage (LV) system supplies power to Link Board Boxes (LBBs) as well as Front End Boards (FEBs). In the case of LBB supply, 8 new A3016 boards will be installed in the existing EASY Crate (Figure 3.20). The FEB supply would need 12 additional A3009s. In this case, 4 new EASY Crates (3000S) will be installed in each near and far side tower at suitable levels. The choice of level depends on available space in racks and cable length. New cables from the CAEN A3009 power supplies to the RE4 chambers will have to be procured, connectorised, tested and routed in mini-cable chains. The FEB's LV Crates will take the 48V from the existing RE3 MAO by using a special type of splitter at the PP75 connector. Two new branch controllers are required, each one controlling near and far side LV-FEB EASY Crates of the same yoke.

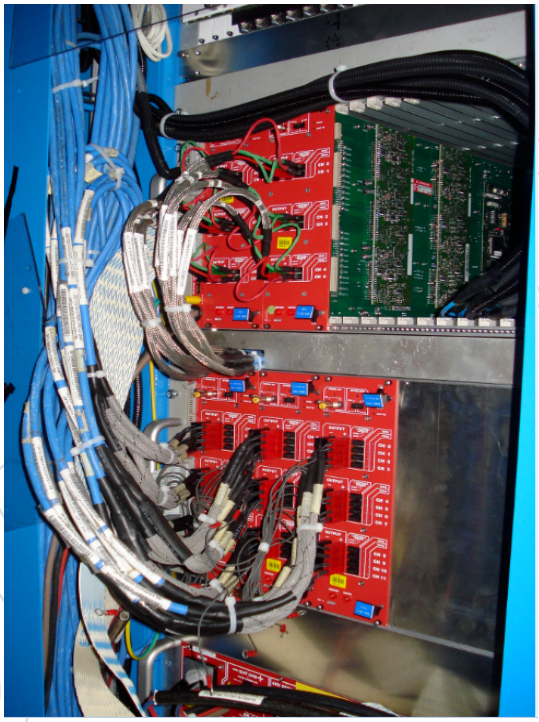

Figure 3.20: Available slots for the RE4 LBB boards.

3.4.5.6 Temperature and Humidity sensors

Temperature and relative humidity are parameters that affect the response of RPC detectors. Several studies on dark current monitoring carried out during CMS commissioning in 2008 and 2009 have shown that the thermal stabilisation of RPCs in the 21-23°C range is essential for the operation and that the working point depends strongly on temperature. The dependence on humidity is less crucial. However, the stabilization is much more critical due to the dimensions of SGX5 and the cavern humidity variation range. Presently temperature and humidity monitoring is performed with six conventional electrical sensors in each of the existing RE stations, while each Barrel chamber has one temperature and humidity sensor. The typical desired precision is ± 0.2°C for temperature monitoring and 2% for humidity monitoring.

The development of optical sensors based on the Fiber Bragg Grating (FBG) technique for temperature measurement has provided a better solution than the electrical sensors with respect to radiation hardness, insensitivity to magnetic field, lack of electrical noise, ease of installation, minimal cabling, and precision ($\pm 0.2^{\circ}$C). Two Italian groups, Frascati and Naples, have extensive experience in the development and deployment of FBG sensors for a variety of measurements. Each RE4 chamber will be equipped with one optical sensor for temperature measurement. The sensors will be purchased bare and enclosed in a heat conducting housing. The sensors will be tested in Frascati for radiation hardness, and installed at CERN on the RE4 chambers. The design of housings will allow ease of disassembly from chambers prior to chamber removal from disks for maintainance and repair. Optical fibers will be routed to the existing CERN system for readout and integrated into the CMS sensors slow-control framework. Humidity monitoring will be performed via conventional electrical sensors, identical to those employed in the existing RE disks (4 sensors/disk).

Finally, an R&D programme has started in early 2010 for the development of optical sensors for hydrofluoridric acid detection in the RPC gas mixture. Options will be considered in case of positive results to install a few sensors in the USC gas distribution racks, upstream and downstream of the RPC detectors in the closed loop recirculation gas system.

3.4.6 Production facilities

In the following, the main aspects relevant to the chamber production will be briefly reviewed. All the numbers quoted below refer to the production of 200 new chambers, out of which 144 will be needed for the RE4 station and the remaining 56 will be kept as spares for the RE2/RE3/RE4 forward system.

3.4.6.1 High Pressure Laminate production

Production of High Pressure Laminate (HPL) will follow the same procedure already established in the past. The main steps are:

- Production of the HPL foils.
- Quality check for resistivity measurement and surface quality.
- Cutting the foils to the required size and finally surface cleaning of the obtained components.

Raw material production will take place at the Puricelli industry near Milan. This company has the necessary expertise and experience to produce low resistivity (1-6 x 10^{10} Ω cm) HPL as required (they have hired some expert personnel from PamPla firm, a previous supplier of HPL for the particle physics community). Recently a small production with the same CMS specifications has been successfully achieved at the Puricelli site, ensuring that the proper production set parameters can be reproduced. About six hundred 1620 x 3200 mm^2 foils for a total of 3110 m^2 are necessary. A preliminary planning draft discussed with the producer shows that about 2 months are required for the production assuming a 3 week cycle for the production and quality control of batches of 200 foils. A quality check will be performed at the Pavia INFN site. Here the resistivity measurement table already used in the past will be re-commissioned and made available for operation. The Pavia group will provide supervision for the operation of the device, while measurement operations will be under RPC community responsibility. Successive cutting and surface cleaning procedures will follow according to the scheme already established in the past respectively at RIVA (Milano) and General Tecnica (Frosinone).

3.4.6.2 Gap production

The gas gaps for the forward upgrade RPC chambers will be produced by KODEL at Korea University. KODEL will use the same technology as developed for the production of the initial 432 forward RPC chambers. A total of about 660 gaps are needed for the proposed new RE4 station production (including spares). The general production procedures can be divided into several sequential steps:

- Initially HPLs will be inspected for defects in color, scratches on the surface and any mechanical damage on the edges and corners. The surfaces of all selected HPLs will be properly cleaned before the graphite coating. The next step is to insulate the graphite surface with PET film. PET film is glued to the graphite surface by the machine shown in Figure 3.21a. The gaps are then assembled and placed under a pressing machine (Figure 3.21b) for 24 hours for glue hardening.
- All assembled gas gaps are treated with linseed oil mixed with heptane. The rate of linseed oil administration into the gas gap placed in its vertical position is 100 cm^3/hour. After the completion of the linseed oil administration, a small compressor is used to immediately remove the remaining oil in the gas gap. Then, dry air at 40° C is circulated over the oiled surfaces of the gaps. The flow rate of air is from 60 to 100 liters/hour. The period of the air circulation is from 48 to 72 hours.
- A check of the mechanical and electrical quality of the gas gap is finally performed. The criteria for accepting the gas gap are very strict. For the mechanical test, no pop-up spacer should be found when the gas gap is pressurized with +20 hPa for 10 minutes. In addition, the rate of leakage of the gas gap should be less than 0.2 hPa for 10 minutes. For the electrical test of the gas gaps, high voltage is applied to the gas gap and the amount of current drawn is recorded. First a voltage of 8.5 kV is applied for 12 hours, then a voltage 9.4 kV is applied for 96 hours. The current limit for accepting large gaps is 3.0 μA. For the gas gaps which pass the tests, transportation is arranged. Wooden boxes are specially designed for safe transportation. The gaps inside the wooden box are stored vertically and are clamped by using partially prestressed bars.

Figure 3.21: a) Electrode insulation machine; b) Gas assembly machine.

Korea expects to have the preproduction gaps delivered to CERN for evaluation in October 2010. Mass production will then take place from January to December 2011.

3.4.6.3 Chamber mechanics

The chamber mechanical system is composed of several parts:

- honeycomb box
- auxiliary parts
- cooling circuit, FEB support and screen box
- readout strips plane

3.4.6.3.1 Honeycomb box The box is made of aluminium top and bottom honeycomb plates and four edge bars. The honeycomb plate is 6 mm thick, composed of 0.5 mm thick top and bottom Al cover sheets, and 5 mm thick Al honeycomb core. At the four edges and a few other positions (where slots or threaded holes will be located) 5 mm thick solid Al plates will be inserted in the honeycomb core. The cross section of the edge bar is 16 x 16 mm^2. Figure 3.22 shows the layout of a typical RE honeycomb plate.

Production of the honeycomb plate proceeds as following: the 0.5 mm thick Al sheets are cut to shape and the surfaces are oxidized; additional 5 mm thick Al plates and the Al honeycomb cores are glued at the edges and in the middle; the assembled plates are heated at 120° C temperature to cure the glue; finally the slots and holes are machined. We plan to use a CNC machine to make all parts interchangeable.

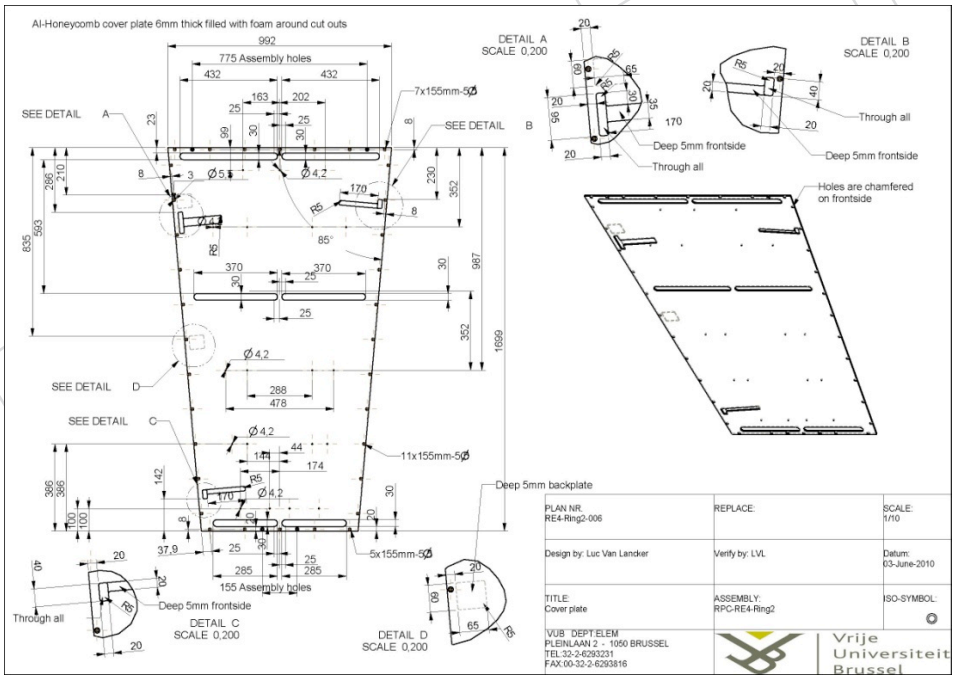

Figure 3.22: Layout of a typical RE honeycomb plate.

3.4.6.3.2 Auxiliary parts These parts include the front patch panel, the joint pieces for mounting the chamber in the yoke, the inside chamber fixation pieces etc.

3.4.6.3.3 Cooling circuit, FEB support and screen box This part is made of copper pipe soldered onto three copper plates, where the FEB will be mounted. The screen box made of 1 mm thick Al sheets will cover all cooling and FEB system.

Table 3.6: Chamber assembly responsibilities.

Type of chamber	numb. chambers	Assembly site
RE4/2	40	Mumbai, Chandigarh
RE4/2	60	CERN - B904
RE4/3	40	Gent
RE4/3	60	CERN - B904

3.4.6.3.4 Readout strip plane The readout strip planes are divided into three sections as shown in Figure 3.23, the gap between the strips is 2 mm. The plane is 0.3 mm thick, with a 0.035 mm thick copper cladding. Strips are produced by etching method. By request, the factory could heat-cover the strips plane with a 0.15 mm thick Mylar sheet for protection and insulation. The honeycomb boxes and auxiliary parts will be produced in "Beijing Axicomb Technology Co., Ltd" (China) and the readout strips will be produced in "Beijing Gaonengkedi SGT Co., Ltd" (China). We have a long term collaboration with both companies since they have already successfully provided good quality mechanics for the RE station built and installed in CMS. For the 200 RE4 chambers, the companies could complete the production of the mechanics within three months after signing the contract. Considering the time needed for the transportation, ordering the mechanics six months before the chamber assembly is recommended.

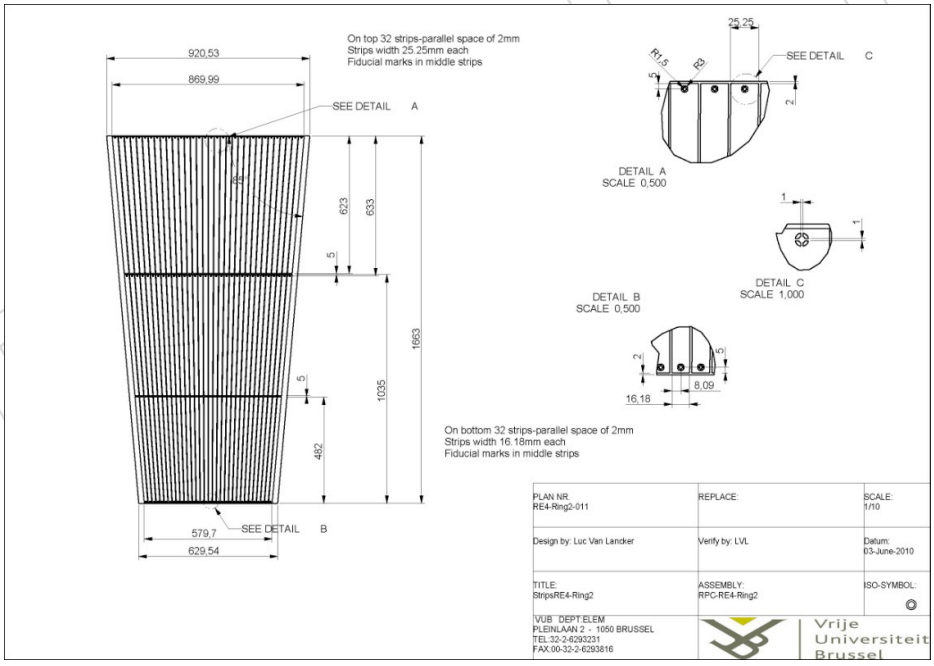

Figure 3.23: Layout of the RE chamber strip patterns.

3.4.6.4 Chamber assembly and test sites

The 200 new RE2 chambers will be assembled and tested at different sites according to Table 3.6.

3.4.6.4.1 CERN Building 904 site On the 904 premises at CERN, an assembly and test laboratory will be set up for the production of the RPC chambers. This facility will include

the assembly tables and tooling facilities for the gas gap QC/QA for leak tightness, popped spacers, and HV behaviour. A cosmic hodoscope will also be available to test up to 10 detectors at once and determine all physical working chamber parameters. The manpower to run this facility will be provided by the respective institutes when their detectors are being tested. The Pakistan group, which has experience in chamber assembly, will provide qualified manpower for the assembly and test. A more detailed description of the 904 infrastructure will be given in a dedicated section of the CMS upgrade technical proposal document.

3.4.6.4.2 Belgium site The chamber construction will be the main effort of the University of Gent. At this institute a chamber assembly and test facility is presently being set up. It is foreseen that in Gent 40 new RE4/3 chambers will be assembled to instrument an entire new RE4 outer ring station. The manpower to perform the assembly will be provided by both the University of Gent and the Vrije Universiteit Brussel. The fabrication of assembly tools, small mechanical detector pieces, signal readout cables, storage racks, etc. will be handled by the mechanical workshop in Brussels and Gent. All commercially available components, e.g. cooling lines, gas tubes, connectors, foils etc. that are required for the chamber assembly will be purchased in common orders with other sites to ensure a uniform chamber construction. The gas gaps will undergo a basic quality control before the assembly. The test procedures will be similar to those performed in the previous construction phase at the CERN ISR test facility. All gas gaps will be tested for unglued spacers and gas tightness using Argon. High voltage behaviour will also be tested with a gas mixture of Freon and Iso-butane (no SF6). Once the chambers are assembled, a complete test with a cosmic hodoscope will be performed before the transportation to CERN.

3.4.6.4.3 India sites Under India-CMS-RPC collaboration, RPC assembly and testing would be done at two sites: Nuclear Physics Division-Bhabha Atomic Research Centre (NPD-BARC) at Mumbai; and Panjab University at Chandigarh. The RPC Lab at NPD-BARC, Mumbai is fully operational and basic quality control procedures have been set up for assembly and testing. Recently ten RPCs which have been assembled and tested there, in collaboration with Panjab University and Delhi University, are at CERN. The lab has an associated storage area and is backed by a robust workshop for handling all the relevant mechanical jobs. The HV, LV, 4 channel gas mixing unit, 8 channel gas flow system and gas recovery unit are fully operational. The cosmic ray stand can handle eight RPCs of RE4/2 type at a time. Scintillators of the relevant sizes are under fabrication at BARC, Centre for Design and Manufacture and accordingly the cosmic hodoscope would be set up to study the chamber performance. Efforts are underway to have an independent air conditioning system for controlling the relative humidity at 45-50% level round the clock. Electronics and DAQ have to be upgraded to handle more chambers simultaneously. Expertise from CERN would be required for setting up the cosmic hodoscope to test up to 8 detectors together and determine all RPCs physical working parameters. The Panjab University RPC lab is also equipped with a 4-channel gas-mixing unit, DAQ for the Cosmic Ray test, scintillator hodoscopes, mechanical and electrical workshops, etc.

3.4.7 Project organization

3.4.7.1 Responsibility assignments

Restoration of the low η RPC forward system will involve a large community of physicists around the world. Besides the major responsibilities already discussed in this document for the chamber production, other relevant responsibilities related to important detector components

Table 3.7: Overview of the responsibilities of each of the institutes (legend: BL=Belgium, CH=CERN, CN=China, IN=India, IT=Italy, KL=Korea, FI=Finland, PK=Pakistan, PL=Poland).

Item	BL	CH	CN	IN	IT	KL	FI	PK	PL
HPL production/QA		x			x				
Gap production						x			
Cham. mechanics	x		x						
Chamber assembly	x	x		x					
Front-end production								x	
HV/LV system	x			x					
LB design					x				
LB production & testing					x				x
T/RH sensors		x			x				
Infrastructure		x							

or to infrastructure services should be acknowledged. Table 3.7 gives a complete overview of the responsibilities for all the items related to the RE re-scope.

As already mentioned some of these responsibilities will be related to deliverables and appropriate funding commitment of the funding agencies. In other cases they refer to the coordination of some relevant parts of the projects based on existing expertise and competence already available from the group involved in the design and construction of the initial system.

3.4.7.1.1 HPL production and certification CERN will coordinate the logistics for the HPL production and quality assurance. In this context INFN Pavia will make available the proper tooling for the QA and some expertise will be available for its maintenance during 2010.

3.4.7.1.2 Gap production KODEL has the primary responsibility for gap production, certification and delivery to the chamber assembly sites.

3.4.7.1.3 Front-end board Pakistan has the primary responsibility for FEBs production, certification and delivery to the chamber assembly sites. Fifty FEBs will be produced at the end of October. After complete validation of FEBs , mass production will be started at the beginning of 2011. We require 600 FEBs including a 10% contingency. Required time is approximately three months which include the time of procuring of components, developing of PCBs, mounting of components and testing of final FEBs. Before shipment to CERN, validation tests will be performed in Pakistan, such as voltage threshold setting (VTH), voltage biasing setting (VBIAS), voltage monitoring (VMON) and I2C for quality assurance. Pakistan will also take charge of preparing on-chamber signal cables and FEB adapter for signal transmission to the off-detector electronics.

3.4.7.1.4 Off detector electronics Italy will take major responsibility in the re-design, production and pre-test of the Link Boards and Control Boards. The final validation will take place at the CERN 904 CMS electronic lab with the initial help of Poland.

3.4.7.1.5 HV/LV system The power system is an obvious extension of the one already installed in CMS, produced by CAEN (Italy). The procurement responsibility will be shared

among all institutions contributing to the chamber delivery. CERN may play a role by centrally coordinating the procurement procedures.

3.4.7.1.6 Infrastructure

CERN will have a major role in the infrastructure definition and assessment such as cooling, signal cabling, HV/LV cabling. It will also have the responsibility of the 904 test site running and maintenance.

3.4.7.2 Schedule

The overall schedule for the RE up-scope project should foresee as final achievement the chambers installation during the 2011-2012 winter break. The schedule is shown in Figure 3.24.

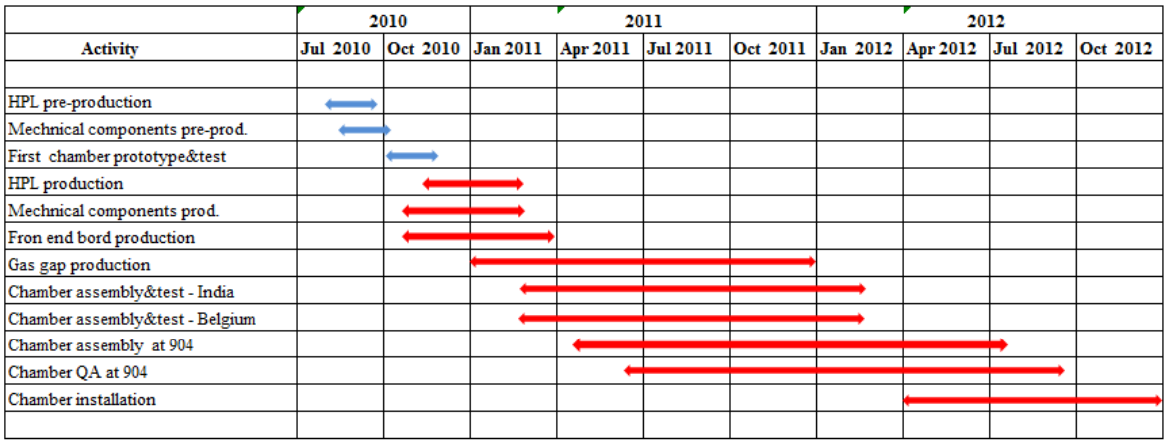

Figure 3.24: Schedule for RE4 production and installation during the 2012 LHC shutdown.

The major milestones are:

- Start up of the HPL production – September-November 2010
- Start up of the gap production – January 2011
- Start up of the FEB preproduction – October 2010
- Preparation of the assembly sites – end of 2010

3.4.7.3 Organization chart

A draft organization chart of the project in shown in Figure 3.25. An overall upscope manager will coordinate the project. A production manger will supervise the production at different sites with the help of local site managers who will train appropriate crews for assembly, QA and logistics. General procurement of components will be coordinated by the production manager, the technical coordinator and the electronic coordinator through appropriate responsible person designed for each given task. This organization will be fully integrated into the present RPC project to allow synergies between operation and upscope teams to be exploited.

3.5 Production and Installation Plans for the CMS Endcap Muon Upgrades

3.5.1 Introduction

As described in the preceding sections, the amount of upgrade work in the endcap region is quite large. As expected this will present challenges to the installation plans, which are

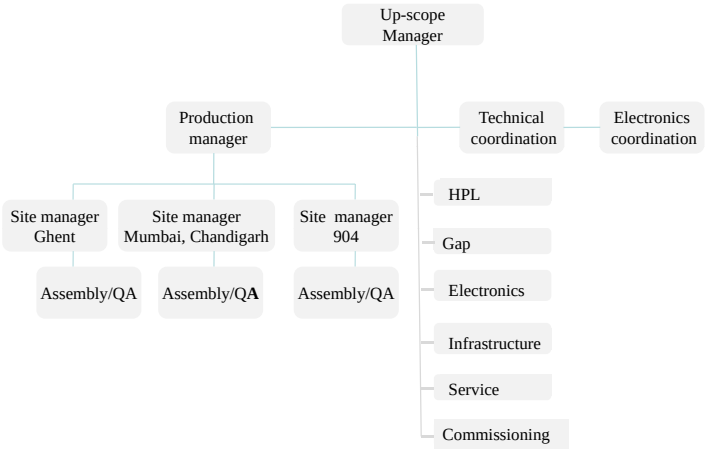

Figure 3.25: Organization chart of the RPC Upgrade Project.

already complicated by other subsystems such as HCAL and pixel. The DT upgrade occurs in the barrel region and is relatively independent of the endcap installations (except for crane usage of course). The basic endcap installation plan is that the ME4/2 chambers (CSC) must be installed prior to the RE4 chambers (RPC). After these are installed and commissioned, the YE4 wall is installed. However, this basic plan has a variety of complications:

- The full funding for the CSCs is not yet in place. At this time it appears possible to get some partial funding from CERN/CMS that would make it possible to complete one endcap by the end of 2012. A nominal schedule (typical of previous production) shows roughly two years from the start of funding to a point where one endcap is ready for installation. The other endcap will take roughly another year. Assuming the ME4/2 funding appears, it should be possible to get most of the chambers needed for one endcap ready for installation in 2012. Then the corresponding endcap of the RE4 chambers could be installed on top of the ME4/2.
- The LHC schedule foresees a shutdown for 16 months during 2011-2012 which would be a good opportunity to install the 2 muon systems. However, due to the lack of funding for CSCs, it is not realistic to expect that all the CSCs could be ready in time for this stop. This may block the installation of some of the RE4 chambers. If the proposed funding appears, it should be possible to install one of the CSC endcaps (and corresponding RE4 chambers) during the 2012 shutdown. The next foreseen LHC technical stop occurs during 2016, which would be a more reasonable match for the muon upgrade schedule. However, CMS is planning to replace the pixel detector and upgrade the HCAL during the 2016 shutdown so this would be a difficult addition. This makes it important that we install the first endcap of the CSCs (and subsequently the RE4 endcap) during the 2012 shutdown if at all posible.
- The first ME4/2 endcap can be fitted with the spare electronics that presently exist. However, the remaining endcap must derive its electronics from the boards removed from the ME1/1 replacements. Hence the installation of the digital CFEB boards on ME1/1 becomes linked to the completion of the second ME4/2 endcap. The ME4/2 chambers cannot be installed without the on-board electronics. Thus the second ME4 station cannot be installed until after recovering the electronics from the first ME1/1 station.
- The digital CFEB boards for ME1/1 are in design at the moment, but are not ex-

pected to be available for the 2012 shutdown. Hence, they must be installed during the next opportunity to open CMS: the 2016 shutdown. We estimate the refitting, testing, and installation of the new DCFEB boards will take roughly 12 weeks per endcap. This adds additional work to the already heavy installation schedule during this 2016 shutdown.

- After one (or both) CSC endcaps are installed, cabled, and commissioned, the overlaying RE4 chambers must also be installed, cabled, and commissioned. We expect that one RE4 station could be installed after the ME4/2 installation during the 2012 shutdown (or possibly during the 2013 Xmas stop since installation times are short and opening CMS is not required). The remaining RPC station would be installed following the installation of the second ME4 station in the 2016 shutdown.
- Finally, the YE4 wall must be installed. The heavy sections of the YE4 wall must be pieced together after all chambers (CSC and RPC) have been installed. The design of the YE4 wall allows it to be removed intact and "stored" on the end wall of the UXC cavern to allow for maintenance of the CSC and RPC chambers. If possible, one YE4 wall should be installed after the one endcap of ME4/2 and RE4 chambers during the 2012 shutdown. If the YE4 wall cannot be installed during the 2012 shutdowm it makes good sense to perform a trial construction of the YE4 wall in SX5 (upstairs assembly hall at point 5) to understand and fix any problems so the actual installation in UXC will be faster and easier. Clearly, delays in installing these chambers will increase the work necessary during the 2016 shutdown.

Of course, it is likely that the LHC schedule will change as we ramp up to the desired luminosity, and we must plan to be prepared for whatever occurs. Nonetheless, the amount of work required in the 2015-2016 shutdown is huge, and it will require a very detailed design plan for installation. The most important need at this time is to get the funding situation for the ME4/2 upgrade clarified. Any process that would allow us to speed up the procurement and production of the ME4/2 chambers could alleviate the foreseen logjam during the 2016 shutdown.

A large advantage we have is that the work required for the installation of the muon systems is essentially the same as for previous muon stations. To a large extent, the infrastructure is either in place or very similar to previous stations. Hence, the solutions are known and should be relatively straightforward to put in place. The actual installation of chambers will proceed quickly (roughly 2 weeks per endcap) and the cabling should also be fairly quick (3 weeks per endcap). Nonetheless, accessibility will be poor so the commissioning is an important step and may take more than a month per endcap. We can, of course, work multiple shifts to order to comply with the CMS schedules for the short stops in 2013 and 2014, and the long (16 month) shutdown in 2016.

3.5.2 CSC and RPC Production in Building 904

3.5.2.1 Introduction

CERN has agreed to provide assembly areas for both the CSC and RPC upgrades in Building 904. The area allocated for the CSCs is roughly 1100 m^2 of open, well-lighted space; the area for the RPCs is slightly less. This building was previously used for LHC production and is well-suited for chamber assembly and testing. Nonetheless, the building does require some renovation before it can be used for chamber assembly. In the latter part of 2010, repairs will be made to the roof and walls. The floor will be cleaned and repainted. Infrastructure for services (gas, water, air, network, etc.) will be updated to the levels required for chamber assembly

and the entire area will be air-conditioned. CERN will cover the majority of these costs. The subsystems (CSC and RPC) are requested to pay only for the new gas mixers (roughly 25 KCHF each). We expect that the infrastructure repairs and upgrading will be completed by the end of 2010, and that CMS will have beneficial occupancy beginning in January 2011.

However, the space available in B904 will not be adequate to store all the finished chambers. So additional space must be found at CERN. At this time CERN is considering a tent structure adjacent to Building 904.

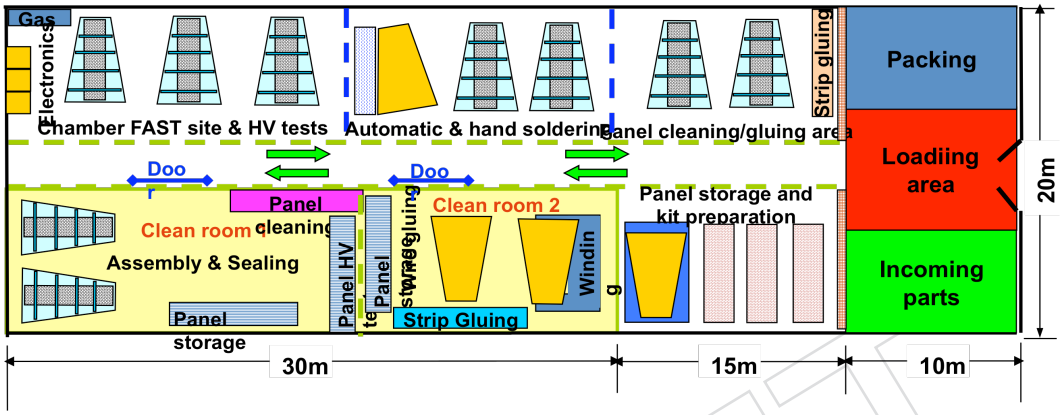

Figure 3.26: Layout for the CSC factory in Building 904.

3.5.2.2 CSC Production

We propose to assemble 75 ME4/2 chambers in Building 904 and expect to produce 4 chambers per month once the factory is operating at the rates achieved during the original production. Figure 3.26 shows a floor plan for the CSC factory. Each CSC chamber requires us to assemble 7 large honeycomb panels, 3 of which have wires wound with a spacing of 3.2 mm, with the correct spacers to produce a sandwich with 6 active wire planes. The panels will be manufactured commercially and machined at Fermilab. At CERN the first step is cleaning the panels, then winding wires and soldering. The wire work is done with a wire-winding machine and an automatic soldering machine, both of which were used for the original production of the CSC chambers. Once the HV and readout circuitry is added, a frame is attached. Then the chamber is tested for gas tightness and HV current. These chambers are identical to the 150 chambers built at Fermilab for the prior production.

Table 3.8: ME4/2 chamber production schedule.

t_0	Funding Approval
t_0 + 3 months	orders sent out for all parts
t_0 + 6 months	tooling assembled in B904
t_0 + 9 months	chamber parts delivered/ shipped to CERN
t_0 + 12 months	production begins at B904 2 CSC/month
t_0 + 15 months	production ramps to 4 CSC/month
t_0 + 18 months	FAST assembly/testing begins
t_0 + 24 months	42 CSCs finished and tested, install 1st endcap
t_0 + 33 months	all CSC production finished
t_0 + 36 months	all FAST assembly, testing finished

Then the chamber moves to the FAST (Final ASsembly & Test) area where the front-end electronics are added and the chamber is tested using cosmic rays. After passing the tests, it is crated and stored for installation. Table 3.8 shows the estimated production schedule, which is based on the experience of the original production at Fermilab.

3.5.2.3 RPC Production

The RPC upgrade requires 72 additional double-gap chambers per endcap, so the plan is to produce a total of 200 chambers (including spares). These chambers are identical to the chambers already produced and currently collecting data. The new RE4 chambers will be assembled according to Table 3.9. Regardless of where the chambers are assembled, all chambers will be brought to B904 at CERN for a quality-assurance test at the cosmic ray telescope site before the installation.

Table 3.9: RE4/2 assembly plan.

Chamber Type	Number of Chambers	Assembly Site
RE4/2	40	Mumbai, Chandigarh
RE4/2	60	CERN – B904
RE4/3	40	Gent
RE4/3	60	CERN – B904

Major components for the assembly will be delivered to B904 from different sites: gaps from Korea, mechanical parts and strips from China, front end electronics and signal cables from Pakistan. Additional minor components, such as gas and cooling circuits will be prepared in situ.

The B904 facility will include tooling for the gas gaps quality-control (QC) and quality-assurance (QA) (such as leak tightness, popped spacers, and HV behaviour) and proper tables for the chamber assembly. A cosmic hodoscope will also be available to test up to 10 detectors at once and thus determine all physical working chamber parameters. The manpower to run this facility will be provided by all institutes involved in the production. In addition, Pakistan, which has experience in chamber assembly, will provide qualified manpower for the assembly and testing.

The plan for the RE4 assembly station in B904 is being developed and is shown in Fig 3.27. Trucks can deliver materials through the large doors. The storage of raw materials (panels, aluminum cases, copper strips, Bakelite gaps, Mylar sheets, etc.) may be done on the shelving located close to the door. Scissor tables will be used to transport fragile or heavy materials from one part of the assembly line to the other. The assembly line comprises a granite table, and few other tables, on which the RPC is assembled by filling the aluminum case like a sandwich from the bottom up, starting with a Mylar sheet for insulation, copper sheet for ground, sensitive gaps, and readout strips, which are then connected to the electronics. All these activities take place on tables specifically designed for the activity. Plastic and copper tubing for gas and cooling inside the detectors are formed and then fitted.

Once all the predefined tasks like cable preparation, honeycomb panel milling for HV connections and services, gas tube forming etc. are done, the chamber assembly can start. According to the general schedule for the RPC upscope, we should be able to start the production in April 2011. We expect a production rate of 4 chamber/week once the operation reaches steady state.

After assembly, the chambers undergo rigorous cosmic tests at the test stand, also located in

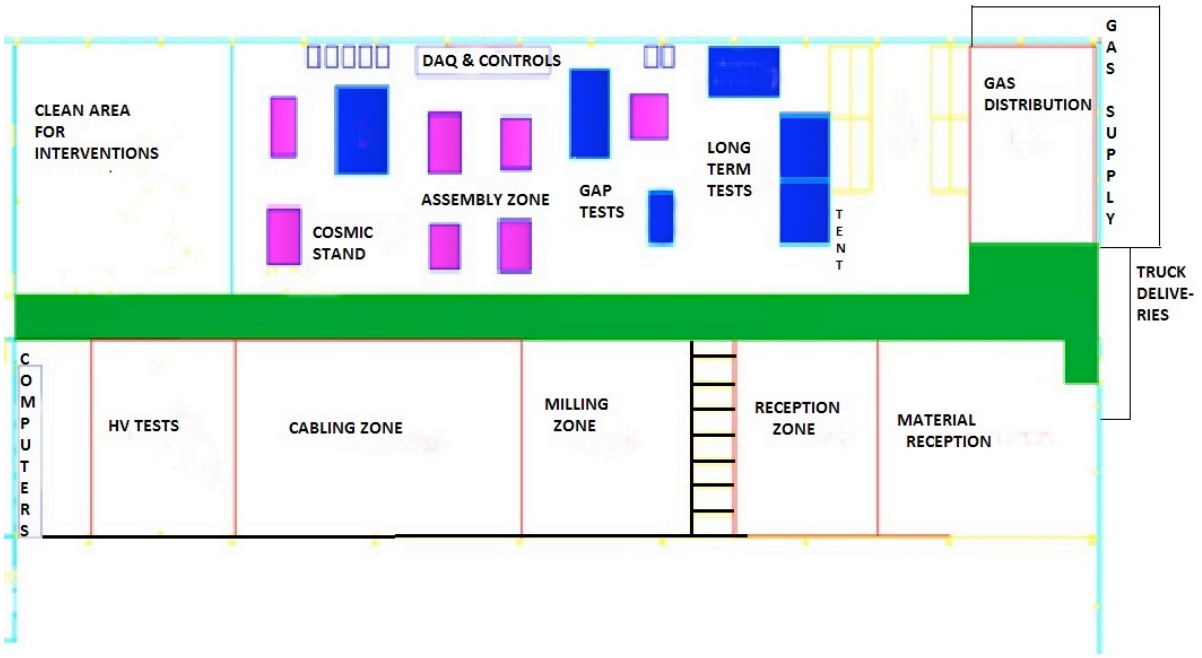

Figure 3.27: Layout of the RPC assembly area in Building 904.

Building 904. The cosmic stand has the capacity to certify 8/10 chambers simultaneously. The duty cycle for a complete test is roughly 2 weeks. We therefore expect to be able to test about 15 chambers/month. The QC and QA procedures also involve long term tests. Chambers, once past the cosmic test, must undergo long term current measurement under nominal operational voltage. A special area in B904 separated from the cosmic telescope will be instrumented for this purpose. Table 3.10 shows the expected production and test schedule starting from the t_o date, which is assumed to be April 2011.

3.5.3 Installation

3.5.3.1 CSC chambers

Last year a new ME4/2 prototype chamber and four previously built spare chambers were mounted with associated electronics, cables, etc. on the ME4/2 station of the plus z endcap of CMS (Figure 3.28). No particular problems were encountered, and the installation serves as an existence proof that the ME4/2 infrastructure in CMS (mounting holes and posts, HV, LV, gas, cooling services, cabling, etc.) is ready. These 5 chambers are currently operational and reading out data, along with the other CSC chambers.

Based on the experience of installing the first 473 chambers, we have made a conservative estimate of the time it will take to install the ME4/2 chambers on each endcap. The contingency is because the crane is not always available. The mounting posts are now being manufactured and they will be mounted during the 2012 shutdown. Table 3.11 shows the estimated times for installing one endcap with ME4/2 chambers.

We have also estimated the time it will take to replace the DCFEB boards (and LVDBs) on the ME1/1 chambers. This is a much more difficult task and is likely to be a critical path item for the entire sequence of operations during the 2016 shutdown. The ME1/1 chambers are not easily accessible since they are located in a slot in the nose. Each chamber must be removed completely to a location where the electronics can be replaced and tested. Then the

Table 3.10: RE4/2 and RE4/3 production schedule.

Date	RE4 Production in B904		Test Production in B904	
	number/month	total accumulated	number/month	total accumulated
April 2011	2			
May 2011	4		2	
June 2011	8		4	
July 2011	8	22	8	14
August 2011	8		8	
September 2011	12		12	
October 2011	12	54	12	46
November 2011	12		12	
December 2011	12		12	
January 2012	12	90	12	82
February 2012	12		12	
March 2012	12		16	
April 2012	6	120	18	128
May 2012			18	
June 2012			18	
July 2012			18	
August 2012			18	200

Table 3.11: Installation times for ME4/2 chambers per endcap

Mount back chambers (6/day+ contingency)	4 days
Cable back chambers (3/day)	6 days
Mount front chambers (6/day+contingency)	4 days
Cable front chambers (3/day)	6 days
Attach cooling, gas, HV, LV, test	10 days
total	30 days

chamber must be replaced in the slot where it can no longer be accessed for debugging, etc. At this time we are considering whether to remove all 36 chambers on one endcap at one time (minimizing the crane time) or to do the chamber replacement one at a time (minimizing the space needed for replacement). The correct approach is not clear at this time. Table 3.12 shows the estimated time for replacing DCFEBs on one endcap. Once one endcap of ME1/1 electronics has been replaced, the freed-up electronics is sufficient to equip and test the second ME4/2 station. Depending on the CMS schedule, the installation of the second ME4/2 station can then proceed.

During the 2016 shudown the major tasks are the installation of a new pixel detector and the replacement of HCAL sensors. These tasks require the endcap disks to be located against the far walls of the UXC cavern, so only the nose on YE1 is accessible. Hence, it looks possible that the replacement of the DCFEB boards can be done concurrently with the other prime tasks. It is important to configure the 2016 shutdown to ensure that all tasks can be completed in the available time.

Figure 3.28: 5 ME4/2 chambers installed on the back side of the YE+3 disk.

Table 3.12: Time for installing the DCFEB boards on one endcap.

Remove chambers (3/day)	12 days
Mount new DCFEB & test (4/day)	9 days
Install cables	9 days
Replace chambers (3/day)	12 days
Attach cooling, gas, HV, LV, test	10 days
total	52 days

3.5.3.2 RPC chambers

The new RE4 station will be installed on the back of the YE3 yoke but mounted independently of the CSC detector. The RE4 chambers will be mounted on an aluminum interface frame, which is supported on the existing threaded M24 holes on the CSC mounting posts. This solution decouples the installation of RE4 from the existence of the YE4 shielding wall. The nominal clearance to the shielding wall will be 12 mm provided the interface frames have a thickness of 8 mm. 2 RPC chambers will be preassembled on each Al interface frame. Thus a total of 36 such packages will constitute one RE4 station.

From our previous installation experience, we can mechanically mount 12 such 10° packages

per working day, which results in a total installation period of 6 working days for the two end-caps. Initial connection of the detectors to their services (HV, LV, signal cables and fibers, gas and cooling) on the YE3 yoke, is estimated to require 3 weeks per end-cap. Additional services to be routed through the YE1 main cable chains will have to be studied with an experienced team. Once these services have been installed and tested, removal and reinstallation of an entire RE4 station can be done in two working weeks per end-cap allowing for CSC installation with only 2 weeks overhead due to the RPC station.

3.5.3.3 Proposed Installation Plans

3.5.3.3.1 2012 shutdown Based on the funding situation, it seems possible that one end-cap of ME4/2 CSC chambers will be available for this shutdown. Of course, we will install as many as possible since it eases the work in subsequent stops. However, there is a substantial amount of infrastructure work required which must be done during the 2012 shutdown.

The cooling manifold is properly sized for the new stations, but there are not sufficient lateral connections. Hence, the manifolds (supply and return) must be removed from both YE3 disks, new holes drilled and half-couplings welded into place. Then the manifolds need to be reinstalled and commissioned. This is a more difficult task now with all the cabling and piping in place than when the manifold was originally installed on a bare disk.

The gas system for the RE4 station must be built and installed. This includes the standard gas rack and all the associated manifolds. In addition, LV and HV cables for the RE4 chambers must be installed in the cablechains.

As mentioned before, the remaining 134 mounting posts for installing all the CSC and RPC chambers can be installed during the 2012 shutdown. Both the CSCs and RPCs use the same posts. These posts have been funded and will be available.

We anticipate an opportunity to perform maintenance on the existing CSC chambers. For example, we have some dead CFEB boards which are under overlapped chambers. We expect to have time during the 2012 shutdown to remove the overlapped chambers, replace the faulty boards, and then replace the chambers.

Assuming one endcap of ME4/2 chambers is successfully installed during 2012, the RE4 chambers could be installed above this station of ME4/2 chambers. Once both ME4/2 and RE4 chambers are in place, the YE4 wall could be installed if time permits.

3.5.3.3.2 2013 and 2014 stops These are short stops at the end of each year and include parts of December and January. As a backup option is is possibe to install the ME4/2 chambers not installed during the 2012 shutdown since CMS does not need to be opened (and won't be over a short stop). It does require that the HF subsystem must be lowered to provide access to the back face of YE3. Installation during these Xmas stops provides an option to complete work not accomplished during the 2012 shutdown. Our schedule for installation is such that we should be able to fit into the available time window (see Table 3.11). RE4 installation also requires a short window so completion of one endcap before the 2016 shutdown is likely. Any installation, such as the YE4 wall, that we can complete during these short stops will be less work for the 2016 shutdown.

3.5.3.3.3 2016 shutdown At this time, the 2016 shutdown is scheduled to last for 16 months. We plan to replace all the ME1/1 electronics during this shutdown, as well as installing the ME4/2 and RE4 chambers not already installed. Since we expect that additional work (replacing the pixel detector and the HCAL sensors) will have priority and will consume

considerable time, we must be flexible and develop clear, efficient plans to make use of whatever time becomes available. It is essential that we end the 2016 shutdown with an operational 4th station for both ME4/2s and RE4s. At the end of the 2016 shutdown, we must add the remaining YE4 wall(s) to the back of the YE3 disk.

3.5.3.3.4 installation summary Coordination of all the conflicting requirements for installation will be very challenging. It would be best if the ME4/2 chambers were available first, then the RE4 chambers, and finally the YE4 wall. This is not likely to be the situation, and we must develop a set of options that work for each subsystem. At this time, the best option is to install one endcap of ME4/2 and RE4 chambers during the 2012 shutdown assuming the necessary funding becomes available. The final plans, of course, will depend on the delivery of items. We have been successful in past installations and it gives us confidence that we will accomplish this also.

Chapter 4

Central and Endcap Hadron Calorimeter Repairs, Improvements, and Upgrades

Introduction

In CMS, for central rapidities, the hadron calorimeters, along with the electromagnetic calorimeters, silicon tracking and muon systems, provide combined measurements of jet energies and Missing E_T. At higher rapidities beyond the coverage of the tracking systems, the calorimeters continue to provide rapidity coverage for energetic forward jets. Since the radiation hardness requirements vary significantly versus rapidity, a transition occurs in the detector technologies used for sampling hadronic calorimetry at a rapidity of $|\eta| = 3$ between the use of plastic scintillating tiles and quartz fibers/tiles as a source of scintillation and Cherenkov light, respectively. The high energies in the forward calorimeter make the use of Cherenkov light feasible, despite the relatively low light yield of the Cherenkov process. Table 4.1 describes these devices. At higher luminosities than originally foreseen at the LHC, the endcap regions near $|\eta| = 3$ of the plastic scintillator technology and the $|\eta| = 4.5 - 5.0$ regions of the quartz fiber with plastic cladding technology begin to degrade below the design performance.

The goal of measuring Missing E_T (MET) places strict performance requirements on the hadron calorimeters since any source of noise or inefficiency can become a false indicator of missing E_T and therefore a source of background to key searches, such as the search for collider-produced dark matter candidates. Similarly, the hadron calorimeters in the outer, barrel, and endcap regions provide critical isolation criteria to separate hadronic showers from leptons and photons measured in complementary detectors, electrons and photons in ECAL and muons in the central tracker and muon spectrometer. In addition, the calorimeters are one of the two main sources for selecting events through firmware-level trigger primitive generation in the hardware and through the full fine-granularity readout in the software level trigger. The primary trigger objects from the calorimeters are presented in chapter 2. The performance of the hadron calorimeter directly impacts the trigger capabilities of the experiment through measurements of jets, missing E_T, H_T, MH_T, τ leptons and isolation parameters for electrons, photons, and muons. Degradation of the calorimeter performance can lead to trigger inefficiencies or to high rates of false triggers impacting a wide range of physics analyses.

In the remainder of this section we discuss some of the issues that are common to more than one of these calorimeters. Then there follow sections describing the modifications planned through 2016 for the barrel, endcap, and outer hadron calorimeters. The plans for the Hadron Forward Calorimeter (HF), CASTOR, and the ZDC systems are presented in Chapter 5.

Table 4.1: Some Properties of CMS Hadron Calorimeters.

device	η range	absorber	active material	photo-detector
Barrel Hadron Calorimeter (HB)	$0 < \|\eta\| < 1.39$	brass	scintillator	HPD
Outer Hadron Calorimeter (HO)	$0 < \|\eta\| < 1.30$	cryostat	scintillator	HPD
Endcap Hadron Calorimeter (HE)	$1.39 < \|\eta\| < 3.0$	brass	scintillator	HPD
Forward Hadron Calorimeter (HF)	$3.0 < \|\eta\| < 5.0$	steel	quartz fiber	PMT
CASTOR	-6.6 $< \eta <$-5.2	tungsten	quartz plate	PMT
Zero Degree Calorimeter (ZDC)	$\|\eta\| > 8.3$	tungsten	quartz fiber	PMT

Improved Photon Detection with Silicon Photomultipliers

The Barrel Hadron Calorimeter (HB), the Endcap Hadron Calorimeter (HE), and the Outer Hadron Calorimeter (HO) all use Hybrid PhotoDiodes (HPDs) as their photodetector. At the time when it was necessary to commit to a photodetector for the construction of CMS, the HPD was the only technology that met all requirements, including the ability to run in a high (4T) magnetic field, radiation hardness, compactness, and cost. The performance of the HPDs has not been as good as expected forcing the devices to be operated at lower HV and, in some cases, the gain of the devices has fallen short of the original requirements. The low signal-to-noise in the outer hadron calorimeter prevents its use for muon identification, and similar performance reductions affect low energy measurements for lepton isolation in the barrel and endcap regions.

A new photodetector technology, the Silicon PhotoMultiplier (SiPM), has recently become available. SiPMs are a rapidly emerging technology that are replacing photomultipliers and other photodetectors for many applications, becoming common in commercial products such as PET scanners. SiPMs are pixel arrays of Avalanche Photodiodes operating in Geiger mode. Each pixel that is struck by a photon makes a single pulse of charge with uniform amplitude. The outputs of all the pixels are added together inside the chip to give a single output that is a measurement of the number of photons striking the SiPM, providing that more than one photon does not often strike the same pixel and that all pixels are active at the time of detection.

SiPMs have significant advantages relative to HPDs. SiPMs have quantum efficiences that are a factor of two higher than HPDs and the gain of a SiPM is similar to that of photomultipliers, ($\sim 10^5 - 10^6$ depending on the pixel size), a factor of 50–500 more than the HPDs. Compared to HPDs and their corresponding readout electronics, the SiPMs with an optimized readout electronics have a factor of 8 increase in signal-to-noise ratio. SiPMs are compact and relatively inexpensive. Pixel sizes as small as 10μm have been achieved while maintaining high photodetection efficiency. The SiPMs have lower operating voltages, of order 100V, compared to HPDs, which are vacuum tubes that run at $\sim$10KV. Low voltages have operational advantages, i.e. no high voltage breakdown as observed in the current HPDs. High voltages present safety hazards and can cause breakdowns that lower tube lifetime.

SiPMs are not affected by magnetic fields of up to 4T. The HPDs operate well at zero field and in strong fields of 3.5-4T. However, at lower fields of order 0.2-3.0T approximately 10% of the devices experience rapid breakdown. While the HPDs in the HB/HE are in high fields of 3.8T, the HO ring-1 and ring-2 are located in the problematic 0.2-0.3T range. The magnetic field value restrictions of the HCAL HPDs could potentially constrain CMS data-taking operations in situations where the solenoid field needs to be reduced. In addition, the performance of the HPDs is also affected by the alignment of the E-field in the tube with the external magnetic

field. It is difficult to control this alignment in the return flux and fringe fields outside of the CMS solenoid, especially for the HO.

For the HO, which is in a low rate environment and sees only a small fraction of the energy of a hadronic shower, there are already commercially-available SiPMs that meet the requirements of a replacement for the HPDs. The number of pixels, the time for a pixel to recover from its Geiger discharge, and radiation hardness are issues that must be addressed before one can confidently use SiPMs to replace HPDs in the HB and HE. No currently available SiPM meets all the requirements for the HB and HE.

The key issues for the SiPM R&D that must be addressed before they can be used as replacements for the HPDs in the HB and HE are:

- When a pixel fires, it is paralyzed for an interval of time until it can be recharged. The reset time must be reduced enough so that response to a subsequent signal is not affected.
- Pixel density is an important consideration. Each photon should hit a separate and active pixel or the linearity of the SiPM output will be affected. The number of pixels determines the dynamic range obtainable with the SiPM. The number of pixels must be significantly larger than the expected number of photons.
- SiPMs are sensitive to temperature and operating voltage, with the gain depending linearly on the voltage above the breakdown point, called the "overvoltage". Typical overvoltage values are 1-3V. These operating parameters must be adequately controlled for the gain to be stable and to minimize cell-to-cell variation.
- The rate of single-pixel self-firing must be kept low because a pixel becomes disabled briefly each time it emits a pulse.
- Crosstalk is possible when light or charged particles emerging from the Geiger breakdown fall on an adjacent pixel. This causes both extra deadtime and an error in the photon count. The crosstalk of the SiPM device will be minimized as part of the R&D program.
- Radiation tolerance. The amount of radiation that the SiPM must handle varies from relatively small in the HO, to moderate in the HB and HE. Long-term radiation exposure will increase the leakage currents and begin to degrade the signal-to-noise performance.

All these issues are being addressed by a systematic R&D program. Nearly every requirement for the HB and HE has been met by an available SiPM but no single device has been identified that satisifies all of the requirements. The R&D program is described below including the presentation of promising initial results on available devices.

Longitudinal Segmentation

An important attribute of the CMS HB and HE (and the HO) are that they are "tile-fiber" calorimeters. Tiles of scintillator are interleaved with absorbers (brass) to form calorimeter towers. Each tile has a wave length shifting (WLS) fiber embedded in it that absorbs a fraction of the light emitted by the tile and re-emits the light shifted to a longer wavelength. The wavelength of the emitted light is well-matched to the spectral response of an HPD (or SiPM) and the optical numerical aperature of the fiber, allowing it to be propagated over long distances through internal reflection in the fiber. The light from the WLS fiber is transmitted to the photodetector via an optically-spliced clear fiber with a long attenuation length.

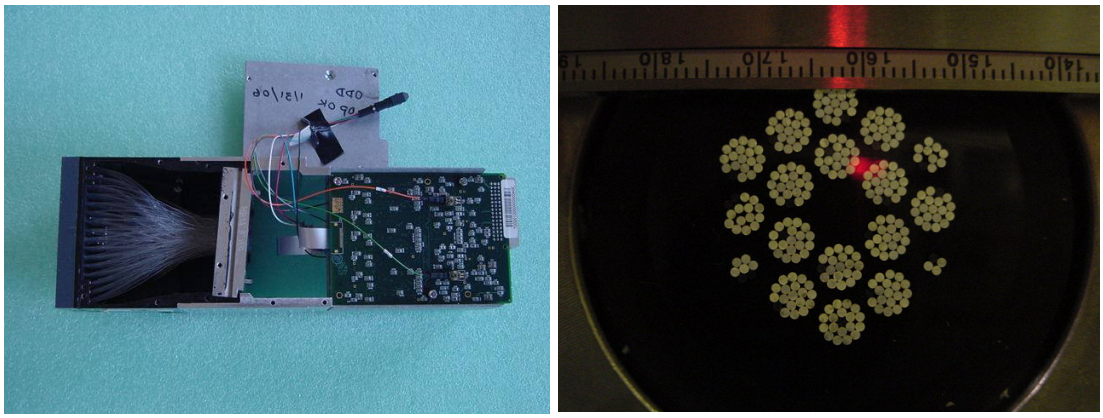

Figure 4.1: Each individual tile-fiber from the calorimeter is optically mapped to an element on the photodetector. The current optical decoding unit (ODU) is shown on the left, indicating how all of the 18-fiber ribbon cables from a barrel wedge are routed to the Hybrid PhotoDiode (HPD) photocathode surface. An end view of the ODU, on the right, shows how the depth segmentation was hardwired into the construction of the ODU with some depths having a small number of tiles (plus light calibration signals) and others having all 17 scintillators optically added into one readout channel and thereby limiting the barrel to one depth segmentation.

In the current HB and HE calorimeters, there are over an order of magnitude fewer photodetector elements than tile-fiber channels in the detector. This reduction is achieved by piping the light from groups of fibers to a single photodetector element, thereby optically summing the tile-fiber signals before the photodetector. For most of the HB and HE towers, all the light from the 17 tile-fibers of the tower are summed together resulting in a complete loss of information about the longitudinal development of the hadronic shower in the readout. This choice was made in the original calorimeter design due mainly to the low gain of the HPDs and corresponding low signal-to-noise of the readout and because finer segmentation was physically prohibitive due to the large mechanical size of the HPD.

Because SiPMs are compact, high gain and relatively inexpensive, it is possible to implement longitudinal segmentation of the fiber readout to obtain a calorimeter readout that provides more information than can be obtained from the HPDs. The optical grouping of channels in the HPD system is shown in Fig. 4.1 where the number of groups and number of fibers per group are constrained by the HPD geometry. Few geometric constraints are present in the SiPM upgrade and this opens up the possibility of increasing the number of longitudinal segments by either grouping a smaller number of fibers to illuminate a given SiPM device or by introducing separate SiPM devices for each optical fiber and electrically adding the outputs. The advantages of longitudinal segmentation are described in the section on the HB/HE. The compactness is crucial because the total space for the photodetectors and associated front-end electronics is fixed and cannot grow to accommodate the extra photodetectors needed to implement the additional segmentation.

Timing

Because of the nature of hadronc showers, the calorimetry does not have to be highly segmented for jet energy and angular measurements (except in particle flow based measurements, where finer transverse segmentation would have improved neutral hadron identification). In fact, the hadron calorimetry has by far the fewest channels of any of the CMS detectors. Consequently, its channels have the highest average occupancy.

When the LHC runs at or near design luminosity, there are multiple interactions in every bunch crossing. When the trigger selects a crossing of interest, it is possible for tile-fiber light emission from previous and subsequent crossings to pollute the "in-time" signal, where each signal in the HB/HE/HO has a duration of approximately 100ns affecting up to 4 bunch crossings. Similarly, the timing of a signal relies on there being no significant contribution from the neighboring bunch crossings, where overlapping pulses mean that more data must be collected and disentangled to separate out the data from each individual bunch crossing. The current version of the CMS calorimeter output provides timing information based on peak detection algorithms in the hardware trigger, and software fits that assume isolated signal pulses. The inherent capability of the calorimeter to provide fine-grained timing available in the analog pulse information in therefore not being utilized. It is a major theme of the hadron calorimeter upgrade to provide better timing resolution so as to maintain and improve the capabilities of the existing detector in a high instantaneous luminosity environment.

In addition to the problem discussed above there are other backgrounds such as beam halo and cosmic rays that produce signals in the calorimeters that come at random times with respect to the proton-proton collision. Timing information is also a crucial tool for rejecting these backgrounds. Non-collision backgrounds are especially pernicious in the search for very rare events signifying new physics. Many rare processes are detected using the calorimeters and in some cases only a few events per year are expected. For such investigations, cosmic rays and beam halo superimposed on collision data can mimic a rare event. This is discussed below in the section on the HB/HE calorimeters. Timing is a powerful tool for rejecting such backgrounds.

4.1 Outer Hadron Calorimeter (HO)

The outer hadron calorimeter is situated in the barrel return yokes (YB) in front of the first layer of muon chambers. The YBs consist of 5 rings (or wheels) of return iron: YB0, YB$\pm$1, and YB$\pm$2. Rings R0, $\pm$1 (R$\pm$1), and $\pm$2 (R$\pm$2) of the HO system are located in YB0, YB$\pm$1, and YB$\pm$2, respectively. The purpose of the HO is to measure any energy from showers due to particles hitting the HB that leaks out of the back end of the HB. Detectors that perform this function are often called "tail-catchers".

The HO uses HPDs for photo-detection. They are mounted on the rings of the muon detector and so are immersed in the stray return field of the solenoid coming from gaps in the iron return yoke. The HPDs have been found to produce large noise pulses when operated in the magnetic field environment of the outer rings ($\pm$1 and $\pm$2). The magnetic field at the HPDs in this region is in the range of 0.2-0.3T at the 3.8T operating field of the CMS magnet. Under these conditions a large fraction (10% or more) of the HPDs produce large discharges leading to permanent damage. The noise pulses are larger and more frequent if the E-field of the HPD is not well-aligned with the local B-Field. As a permanent solution to this problem, we are going to replace the HPDs in $\pm$R1 and$\pm$ R2 with SiPMs, devices that do not have these problems. While the HPDs in R0 experience fewer breakdowns, they are actually the most important detectors in the HO since they are located at 90° to the beam line, where the HCAL and ECAL present the least material. Consequently, we are also replacing the R0 HPDs due to the significant performance improvements on reducing leakage tails in the energy measurement for high energy jets in the central barrel. The improvement to the energy measurement of 500 GeV jets is shown in Figure 4.2.

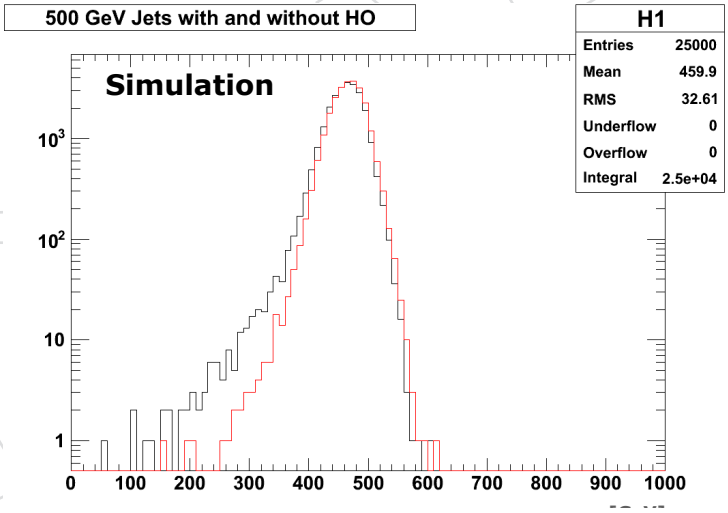

Figure 4.2: Comparison from simulation of the 500 GeV jet energy measurement in YB0 with (red) and without (black) the inclusion of the SiPM measured energy from the HO R0. The SiPM signals in HO R0 improve the containment of the central calorimeter and therefore provide a more Gaussian jet energy measurement. A clear reduction in the low energy mismeasurement tails is demonstrated and provides an essential improvement to the missing E_{T} measurements at high luminosity.

Because of operational problems with the HO in the fringe field regions, it has been necessary to run the HPDs at less than optimal HV. The lower HV results in lower gain and worsens the HO performance. Because of the low gain, electronics noise is more important and the HO is not as useful for jet and muon physics. The higher noise levels limit the utility of the HO for

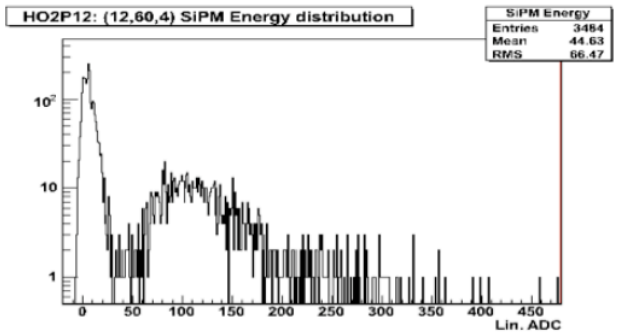

Figure 10a: Individual energy distribution, mwgr18, for a single HO channel, HO(ieta=12, iphi=60). Here energy E_a is not corrected for muon angle of incidence.

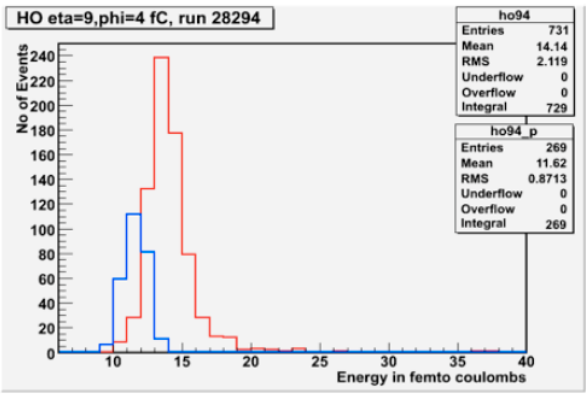

Figure 10b: For comparison, individual energy distribution, single HO channel read out with HPD, TB2007 data. Blue line: pedestal events, red line: muon signal.

Figure 4.3: Comparison of muon response in HO for SiPM and HPD. The top plot is the SiPM performance where the pedestal is in the lower peak and the muon signal is well separated from the pedestal. The bottom plot is for the HPD and due to the lack of separation, the pedestal triggers are plotted separately in the left distribution and the muon signal is plotted on the right indicating the HPD MIP is barely separated from the pedestal.

tagging shower leakage, the original goal of the detector. Replacing the HPDs with SiPMs re-establishes the baseline performance of the detector. An additional benefit of the replacement is that the much quieter detector provides for excellent muon identification, improving the CMS capabilities for low momentum central muons.

Figure 4.3 shows the distributions of signals for minimum ionizing particles (MIP) and pedestal values for SiPMs (above) and HPDs (below). The MIP signal is extremely clear in the SiPMs. This points to a marked improvement in MIP identification using the SiPMs. The higher gain of the SiPM relatively suppresses the electrical noise (pedestal) and makes the HO better suited for any energy measurement.

Figure 4.4 shows the improvement in π/μ rejection for SiPMs compared to HPDs. In this algorithm the HO alone is used for pion rejection. The rationale for this is that muons are deeply penetrating while pions shower and are absorbed in the calorimeter. Hence a MIP signal in HO is indicative of muons and absence of a MIP signal indicative of pions. Replacing HPDs with SiPMs vastly improves the MIP/pedestal separation and consequently improves the π/μ rejection. From this figure we see that the improvement is up to 150 times, depending on the momentum. This improved π/μ rejection will play an important role in low momentum muon identification, where the muon does not penetrate far enough into the steel yoke to record hits

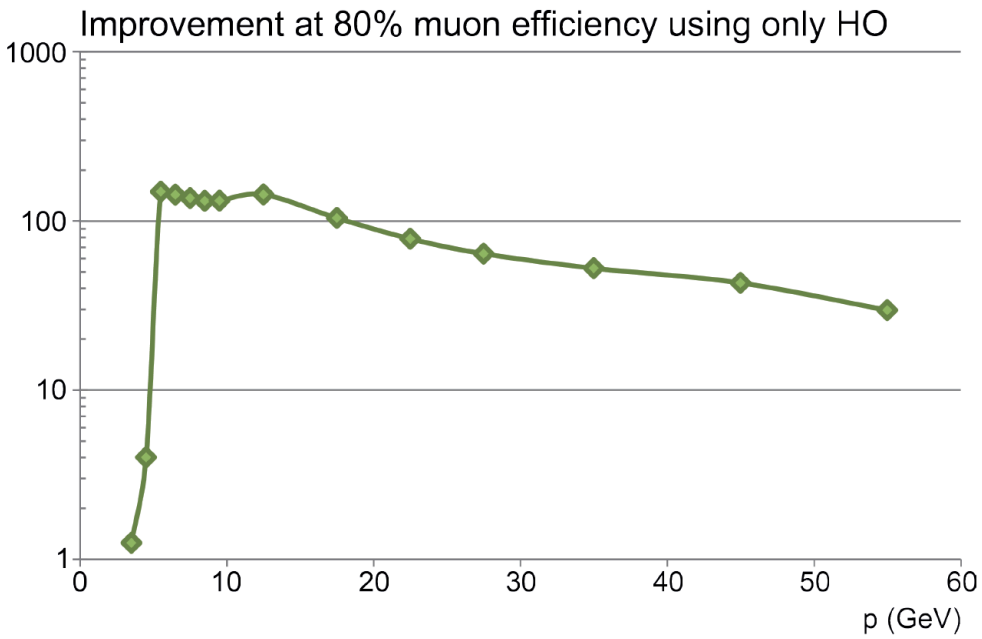

Figure 4.4: Improved π/μ rejection for a fixed muon efficiency of 80%. For low momentum the improvement is about 150 times. As the momentum increases pions become more likely to have shower leakage into the HO, and hence the rejection worsens.

in the Drift Tube muon system chambers. In addition, a muon identification algorithm that does not require the use of the muon chambers provides for an independent measurement of their efficiencies.

The plan for the HPD replacement is to remove the HPDs from the Readout Modules (RMs) and have "drop-in" SiPM packages that have the same pixel locations as the existing HPDs. The HPD in the RM is replaced with a 2-card "sandwich". One of the cards, the Mounting Card, contains the array of 18 SiPMs corresponding to the 18 pixels of the existing HPD, shown in Figure 4.5, and Peltier coolers for SiPM temperature control.

The second card, the Control Card, supplies needed voltages, control and monitoring functions. The control board is shown in Figure 4.6. It receives the analog signals from the SiPMs, shapes them, and then transmits them to the QIE (Charge Integrating and Encoding) cards. Bias voltages for the SiPMs are generated there, as well as the Peltier temperature control. SiPM leakage currents are also monitored here. Most parts of the RM (the ODU, structure, QIE card packs) remain unchanged and only the 2 card "sandwich" replaces the HPD.

HPDs in two HO Readout Box (RBXs) consisting of 8 RMs have been replaced with SiPMs and are currently installed in the CMS detector. In total they consist of 144 SiPMs out of which 36 channels are from the company Zecotek [4] and 108 channels from Hamamatsu [5]. They were installed in April 2009 and have been operated most of the time since then.

The SiPM replacement project is on schedule to replace the HO HPDs in all 5 rings during the next LHC shutdown, starting in the late fall of 2011 and extending through 2012 into early 2013. The RMs will be removed from the HO detector, taken to the surface hall at Point 5 where a small factory will be established. The RMs will have the HPDs replaced with the SiPM sandwich cards, and will be tested and burned in. Then the modified RMs will be taken back to the HO detector in SX5, re-installed and verified. Depending on detector access the

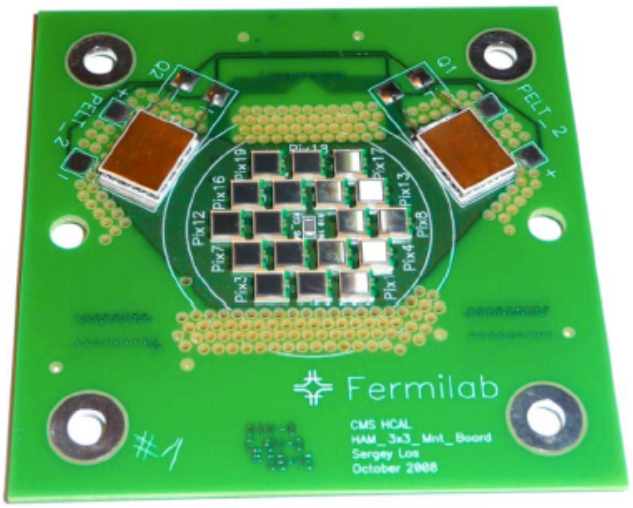

Figure 4.5: SiPM Mounting card. The larger rectangles are the 2 Peltier coolers. Also seen is a grid of 18 SiPMs with the same placement as the HPD pixels.

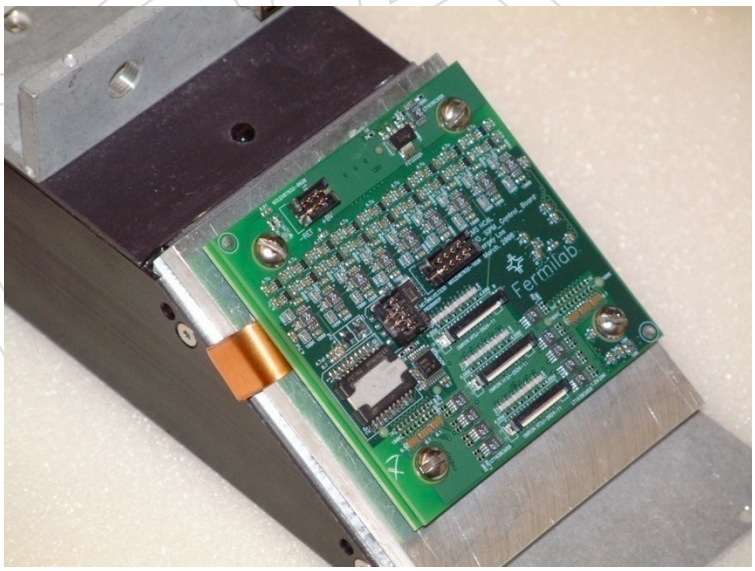

Figure 4.6: The Control Board. This board generates the SiPM bias voltages, measures the leakage currents, controls the Peltier cooler, and monitors voltages and temperatures.

Table 4.2: HO Schedule.

30-Aug-10	2000 Hamamatsu SiPMs ordered.
30-Aug-10	Design of final electronics cards complete.
30-Sep-10	Evaluations (radiation, reliability, noise) of final electronics cards complete.
31-Sep-10	Launch of fabrication of electronics.
30-Oct-10	Evaluation of first batch of assembled cards.
30-Nov-10	QC testing of SiPMs begins.
14-Nov-10	Electronics Production started.
30-Dec-10	All SiPMs delivered.
15-Jan-11	Electronics Production complete.
14-Mar-11	Start of fabrication of completed electronics and SiPMs (and burn-in).
14-May-11	Start of delivery of completed electronics and SiPMs to CERN.
17-Sep-11	Finish of fabrication of completed electronics and SiPMs.
14-Oct-11	Finish of Delivery of completed electronics/SiPMs to CERN.
15-Oct-11	Start development of Point 5 factory.
14-Nov-11	Ready for installation work.

Table 4.3: HO Project Task Assignments.

Lay out boards and test preproduction boards at FNAL
Specification of SiPMs (CERN/FNAL/TIFR/DESY)
Place SiPM order (FNAL/TIFR/DESY) (SiPMs to be delivered to CERN)
Receive and test initial batch of SiPMs (CERN/Boston/FNAL/TIFR/Aachen/DESY/ITEP)
Send SiPM samples to TIFR and DESY (CERN SiPM Team)
Production R1/R2 SiPM testing at Ooty (TIFR)
Production R0 SiPM testing at DESY (Aachen/DESY/ITEP)
Make trial run of boards (BEL/Ooty, TIFR)
Hand-load R1/R2 SiPMs on pre-production boards (Ooty, TIFR)
Hand-load R0 SiPMs on pre-production boards (Aachen/DESY/ITEP)
Initial tests of trial run (TIFR/Boston/FNAL, Boards sent to CERN and FNAL)
Production run (Ooty, TIFR)
Production tests (TIFR)
Production tests random verification done at CERN/FNAL
Inventory of components at CERN
Setup of factory at Point 5 (CERN/FNAL/TIFR/Aachen/DESY/ITEP)
Supply techs from TIFR, FNAL, Aachen, DESY, and ITEP (1-2 techs from each institution)

replacement can be made in a few months. The schedule for delivery of the HO electronics is show in Table 4.2.

The replacement activity for Rings ± 1 and ± 2 is planned as a joint effort between TIFR Mumbai and several U.S. CMS institutes. The replacement activity of R0 is a joint collaboration of DESY, RWTH Aachen University, III. Physik. Inst. A, and ITEP, Moscow. The team has developed a list of tasks and assigned them, shown in Table 4.3.

4.2 Barrel and Endcap Calorimeters (HB/HE)

4.2.1 Introduction

The barrel (HB) ($0 \leq |\eta| \leq 1.3$) and endcap (HE) ($1.3 \leq |\eta| \leq 3$) hadron calorimeters are made of alternating plates of brass absorber and scintillator with wave-length shifting (WLS) optical readout. As shown in Figure 4.7, there are 17-layers of scintillator with individual WLS fibers coming from nearly 72,000 individual tiles. Due to the intrinsic signal-to-noise limitations of the detected WLS light using hybrid photodiode (HPD) detectors and the corresponding front-end noise from the readout electronics, the analog calorimeter signals are digitized with a minimum number of individual electronics channels. The bulk of the η-φ barrel segmentation is read out with a single depth segmentation. Limited depth segmentation is present in the endcap, but is not optimally configured for radiation damage compensation foreseen in high luminosity SLHC operation. Since the development of the original calorimeter design, several physics analyses with initial LHC collision data have identified areas where an improvements in the hadron calorimeter will directly impact the physics productivity of the CMS experiment. The major performance limitations are all addressed in varying degrees by the upgrades and can be summarized as follows:

1) Need for calorimeter clean-up algorithms to reduce non-collision signals coming from numerous sources,
2) Limited discriminating power of the HCAL/ECAL energy ratio for separating pions from electrons,
3) Degradation of the electron isolation quantities with increasing instantantaneous luminosity,
4) Limited efficiency for muon isolation and identification using the HCAL barrel and endcap,
5) Large calibration biases using isolated hadrons below 5 GeV due to showering in dead material between ECAL and HCAL,
6) Inefficient bunch-crossing identification for low-energy signal impacting large area summations used for hardware trigger-level lepton isolation, jet energy and global energy sums,
7) Strong η-dependent radiation damage in the endcap scintillators at high luminosity introducing non-uniform light loss and constant term energy resolution degradation, and
8) Limited number of discriminating quantities to reject beam-related backgrounds not originating from the interaction region.

The degree to which the upgrades improve each of the performance issues listed above is described in more detail in the simulation section. The upgrade tackles these limitations by making the following physical changes in the on-detector instrumentation and front-end electronics:

a) Replacement of photodetector to eliminate the sources of anomalous signals and to improve the front-end signal-to-noise by an order of magnitude,
b) Four-fold increase in longitudinal segmentation to reduce pile-up/high-occupancy performance degradation coming from the first layer of scintillator, to improve clustering and geometric discrimination against non-collision backgrounds and to increase channel redundancy, and

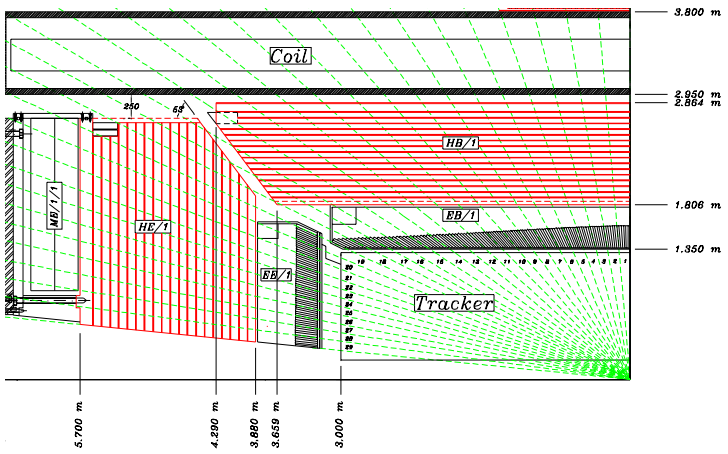

Figure 4.7: Quarter view of the barrel and endcap hadron calorimeters, showing the intrinsic longitudinal segmentation capabilities. The front-end readout electronics, the readout boxes or "RBX", are located directly behind tower 15 in the barrel and directly behind tower 18 in the endcap.

c) Scintillator time (TDC) measurements per bunch crossing with nanosecond timing resolution down to MIP energies to provide independent rejection for beam halo, cosmic ray, and other non-collision backgrounds.

To accomodate the front-end electronics upgrades and to fully benefit from the increased front-end capabilities, a complement of upgrades is proposed for the back-end trigger and readout electronics. The back-end electronics upgrades address the following new capabilities:

1) Front-end to back-end data bandwidth increases from increased longitudinal segmentation and TDC information in the readout of the HB and HE;
2) Data volume management and integration with the central DAQ;
3) Increased trigger processing needs to provide total energy sums, separate lepton isolation quantities and to apply the new front-end timing information;
4) Increased bandwidth to the trigger system to provide finer granularity information, including full granularity in the HF region, additional fine-grain information, and separate total energy and lepton isolation sums.

The goal of the HCAL upgrade plan for Phase 1 of the SLHC is to maintain and improve operation of the HCAL for physics. Our plan maximizes the inherent capability of the HB/HE for physics, especially for both high-p_T physics and luminosity increases beyond the LHC design luminosity of $10^{34}/cm^2/s$, where pileup becomes increasingly difficult. The proposal for Phase 1 consists of modifications to the front-end electronics (FE) and trigger/readout receiver back-end electronics (BE) for the barrel and endcap detectors. The front-end and back-end electronics are accessible and can be replaced without any modifications to the physical components of the barrel and endcap sampling calorimeters. For Phase 2, with a luminosity of $5 \times 10^{34}/cm^2/s$, we anticipate that the large integrated radiation doses might be sufficient to make high η regions of the endcap (HE) unusable. The Phase 1 upgrade components, photodetectors and on-detector electronics, will be specified and qualified to maintain performance standards through the entire Phase 2 period. For the physical components of the endcap calorimeter, ECAL and HCAL, R&D is needed to answer the questions of performance limitations from radiation damage. Overall, our Phase 1 upgrade plan is constructed to be able to meet the physics goals of the

LHC program and high instantaneous luminosity extensions to the program with the lowest possible cost.

4.2.2 Problems Motivating the Improvement and Upgrade Program

4.2.2.1 The Effects from Increasing Luminosity

CERN's plan for increasing the LHC's luminosity to the design value and beyond between now and 2020 is described above. When the luminosity increases, one has to consider the effects of an increased instantaneous luminosity and an increase in the overall integrated luminosity. For the former the effects are almost entirely due to an increase in the pileup, both in-time and out-of-time. Such pileup has the potential to severely compromise the detector performance and physics capability of CMS. For the latter (integrated luminosity increase), the main effect will be radiation damage to the detectors and front-end electronics.

In the CMS Upgrade, the upgraded detector must be able to handle up to 300-500 fb^{-1}, which will be accumulated through the end of Phase 1. This estimate takes into account the fraction of the year that the machine will be run for physics, peak luminosity vs integrated luminosity, live times, duty cycles, etc., and is sanctioned by the LHC machine group. Using the above schedule, we estimate that we will receive roughly 300 fb^{-1} for Phase 1, and roughly 3000 fb^{-1} for Phase 2. These numbers are important to the discussion of radiation damage.

Peak and integrated luminosities are obviously related, and as they increase CMS will become more sensitive to higher mass states, and smaller cross sections. As a result, it will be more important to have ways to reduce those backgrounds that are not from the beam crossing at the center of CMS, e.g. cosmic rays, beam gas and halo, neutron albedo, acute detector problems, etc. As will be explained shortly, the HCAL upgrade will take into account all of these backgrounds.

4.2.2.1.1 Effects Due to an Increase in Instantaneous Luminosity

At LHC design luminosities of 10^{34}, the average multiple interaction rate is approximately 20 per crossing. Note that for HB and HE, the HCAL towers are approximately 0.087 in η and exactly 1/72 in ϕ. As the instantaneous luminosity increases, the tower occupancy will increase, and the occupancy as a function of a fixed threshold cut will increase faster than linearly as more particles are included in the tower and the energy increases. Also for HCAL, as explained below, a larger DC level from the huge occupancies from multiple interactions will make it extremely difficult to use the current scheme for timing the arrival of showers, especially at lower transverse energies. These two effects, occupancy and timing, are detailed below, and dealing with them forms the basis of the HCAL upgrade.

Occupancy

At the original LHC design luminosity of 1×10^{34}, Monte Carlo simulations tell us that for HCAL, with a reasonably small zero suppression threshold the average tower occupancy can be limited to around 15% in the readout, dominated by the underlying event, and includes both in-time and out-of-time pileup. SLHC Phase 1 will have the same time structure (40MHz crossings) and so the multiple interaction rate will scale linearly with luminosity, rising to an average of ~ 40 at 2×10^{34}. We can estimate the effect this will have on the trigger and DAQ by using the same threshold and calculating the occupancy rate as approximately by $1 - (1 - 0.15)^3 = 39\%$, or just under a factor of 3 more particles (and more energy) per tower. Note, that for Phase 2, with a 50ns beam crossing and luminosity of 10 times the LHC design luminosity of 10^{34}, there

will be 20x more multiple interactions per event, increasing the in-time pileup. However, there will be no out-of-time pileup since most of the HCAL energy is contained within 2 of the 25ns buckets. This model results in a total occupancy of $1-(1-0.15)^{20}=96\%$, clearly suggesting that a higher threshold will need to be applied. Note also that this model is only valid when the occupancy is small. For a larger occupancy, where the pileup adds to the total amount of energy in a tower, one therefore has to apply a single threshold not to each particle individually but to the sum of all the particles, and this will make the occupancy rise more than linearly with luminosity. The CMS DAQ readout limits the data rate from any Front-End Driver (FED), which transmits the data from the readout VME crates to the DAQ). As we detail below, the amount of data for HCAL will increase by almost a factor of 4. With the same zero suppression threshold as for the 10^{34} running, the HCAL will be sending 4x more channels. The important point here is that the pileup will have a big impact on both the Level 1 trigger and the DAQ bandwidth requirement.

Timing

The current HCAL electronics is based on a linear current splitter for range determination, charge integration, and analog-to-digital conversion. Overall, the electronics needs approximately 3 beam crossings (75 ns) to deliver all the charge from real energy deposition in the HB and HE, as shown in Figure 4.8. By setting the phase of the integration clock relative to the LHC beam crossing, one can choose what fraction of the total charge is integrated in what beam crossing. For colliding beam running, the current plan is to tune to approximately 75%/20%/5% in the 3 successive beam crossings. Knowing these fractions allow one to fit the arrival time of the signal (which should be the same for all signals in any given tower) with a precision of approximately 2ns. However, as the amount of tower energy from the underlying event increases, the ability to do timing in this way diminishes for lower signal energies. This can be seen clearly in Figure 4.9, where the pileup begins to be comparable to the energy of particles from the hard scattering. At lower energies, the pileup completely dominates and and it is no longer possible to determine the timing from the shape.

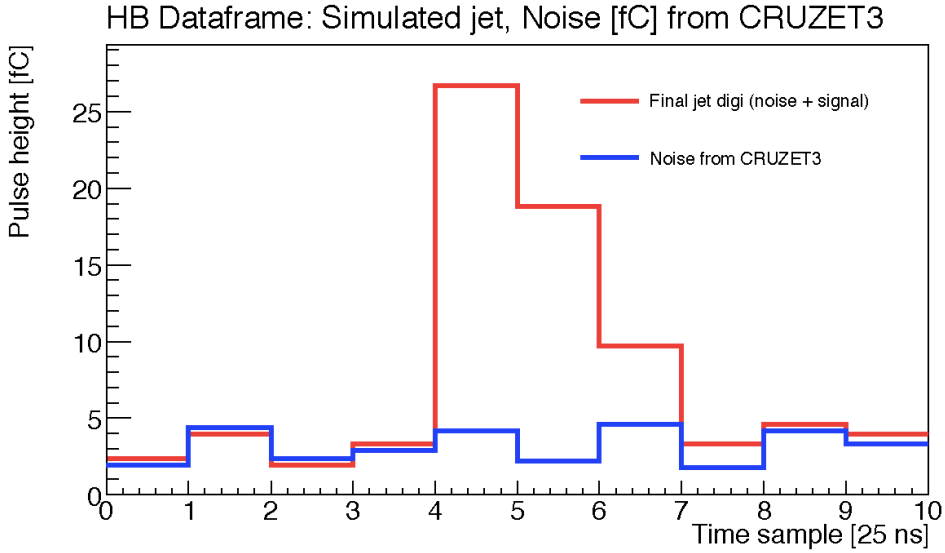

Figure 4.8: Energy in an HCAL tower needs 3 beam crossing times to fully integrate.

The use of HPDs made it impossible to have a separate TDC readout, as the devices have very

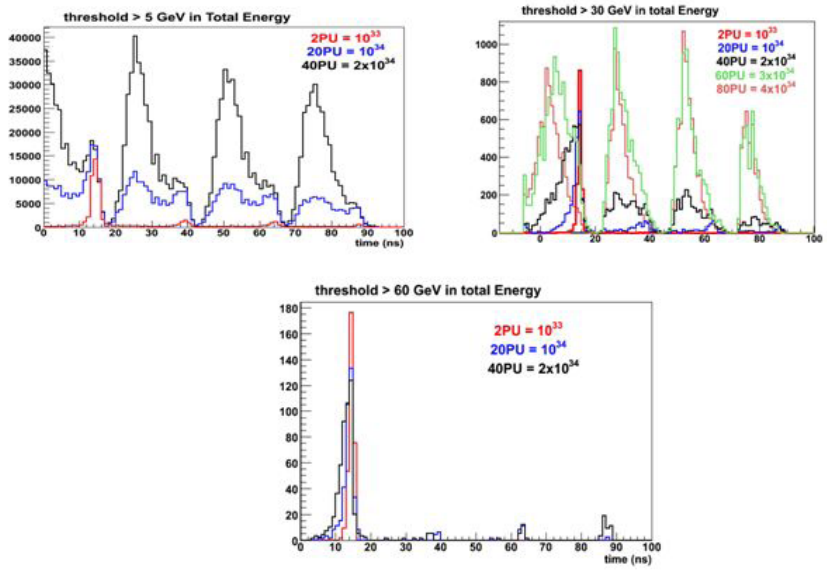

Figure 4.9: Determination of shower timing using 3-bucket fits for a 5 GeV, 30 GeV, and 60 GeV energy deposition. For all 3 plots, the time of the shower is in the first bucket, as seen in the 60 GeV deposition plot. Note that for the lower 2 energies, significant pileup causes the time to be incorrectly estimated to be in subsequent buckets, making such a technique ineffective

low gain (2000) and splitting the signal would have introduced unacceptably large electronic noise per channel. In order to achieve low front-end noise (about 4000 electrons at 40 MHz), compromises were made in the front-end ADC ASIC, called the QIE (Charge Integrating and Encoding). The QIE was designed to have a dynamic input impedance that depends on the amplitude of input pulse. This generates an apparent time slew in the output pulse sent to the flash ADC. Figure 4.10 shows the time slew vs input energy pulse. We see that at lower energies there is an increased time slew. This sets limits on our ability to localize in time the input event energy. For isolated large energy events this is not a problem as all the tower energies can be associated with the high-energy depositions of the event. As luminosity increases and the occupancy from the multiple interactions grows, our ability to correctly assign energies to the correct event will diminish. It will be extremely challenging to apply sensitive cuts as illustrated above.

Note that in the very forward (HF) region ($3 \leq |\eta| \leq 5$), PMT readout occurs on a time scale that is smaller than the 25ns between buckets, making any timing measurement impossible with the current electronics. We plan to introduce the same electronics into HF that we will introduce into HB and HE in order to have a similar timing measurement. Since we will not necessarily be increasing the number of channels in HF, it will constitute an increase in the timing electronics purchases of order 20% over the entire HCAL detector.

4.2.2.1.2 Radiation Damage Effects Due to an Increase in Integrated Luminosity

Although radiation map simulations indicate that the barrel (HB) and very forward (HF) calorimeters will be able to withstand Phase 1 radiation levels, this is most likely not the case for the endcap (HE) detector, which sits in the forward region $1.3 \leq |\eta| \leq 3$. We anticipate that damage from ionizing radiation will cause a reduction in the light from the inner HE layers. Introducing sufficient longitudinal segmentation in the HE will allow this effect to be mitigated by applying different weighting to the segments in the energy sum.

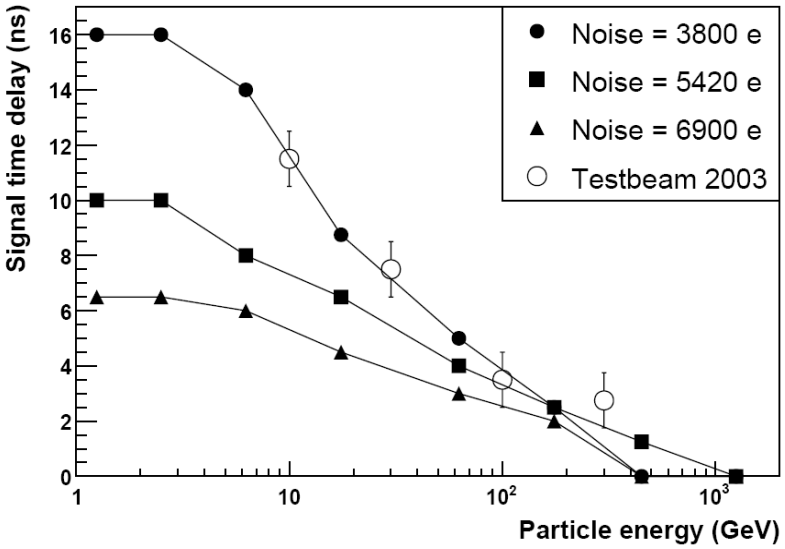

Figure 4.10: Time slew versus energy for the HCAL front end ASIC

Radiation damage considerations for Phase 1 require an understanding of the integrated ionization radiation in the scintillator for HE causing a reduction in number of photons per GeV, and radiation at the front-end readout boxes. For the former, an understanding of both the ionization and neutron fluence is required to be sure that the electronics will be able to last in that environment. Requirements for radiation tolerance for the HE scintillator will be set by the Phase 1 luminosity, however the radiation tolerance for the electronics for all of HCAL will be set by the Phase 2 luminosity, which is nominally 10 years at 5×10^{34} cm^{-2}s^{-1}. Similar studies for the ECAL endcap are also essential to understand the overall performance degradation with radiation dose for the combined calorimeter performance.

Figure 4.11 shows the radiation contours for 10 years of LHC running ($500 fb^{-1}$) for the HB and HE, with the contour units in Grays (100 rad = 1 Gray). From these maps we see that the ionization radiation levels of order one hundred Rad in the RBX region, and of order 10 kRad in the HB, all for integrated doses which are consistent with LHC and Phase 1 running. However in the lower part of HE, the radiation levels will approach 1 MRad, a significant amount. To understand the impact of these doses, we see in Figure 4.12 the effect of various ionization doses to the scintillator, and that for doses in excess of ∼few MRad the scintillator light output will be reduced by a non-trivial amount, to be checked with LHC running. This motivates the longitudinal separation of layers in order to apply re-weighting to adjust for the degradation. It is also clear that for Phase 2, where the radiation levels will be 10x higher for a long period of time, the light output from the HE scintillators will drop below a few percent, of their pre-radiation levels and the HE will no longer be viable. This motivates a completely new R&D effort for Phase 2, which is discussed in the appendix.

4.2.2.2 Problems with Backgrounds and Overall Sensitivity to Small Cross-sections

Effects from non-beam-crossing related signals (e.g. beam gas and halo, high energy muons from downstream scraping, cosmic rays, electronics problems, etc.) will become more critical as the focus turns to ever rarer physics processes with increased luminosity and data samples. Indeed at the Tevatron these effects are the highest contribution to the raw MET rate in the trigger and the offline. These upgrades will allow reweighting for radiation damage (from

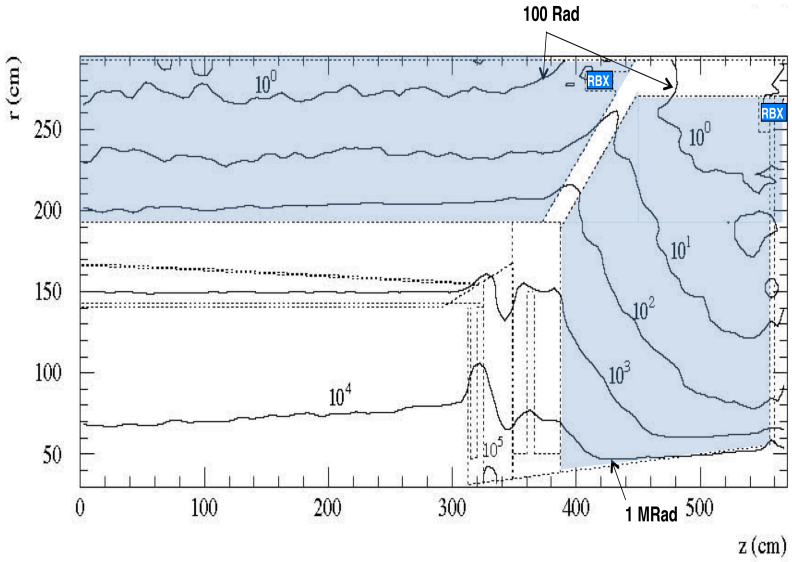

Figure 4.11: Radiation contours for CMS from FLUKA calculations, units of Grays, after $500 fb^{-1}$ (10 years at LHC design luminosity). HB and HE begins at $r > 180cm$ and $z >\sim 400cm$ respectively.

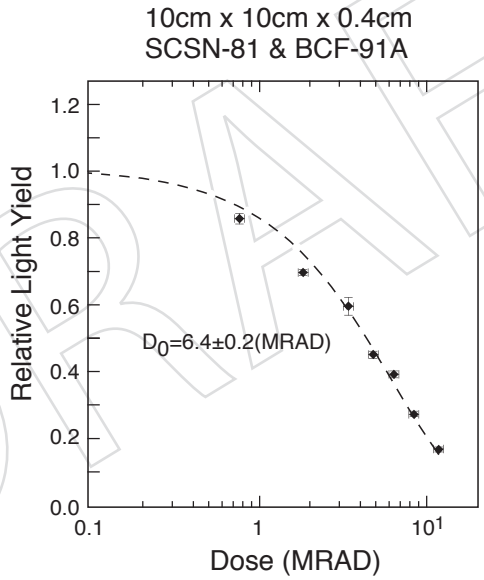

Figure 4.12: Scintillator degradation as a function of ionization radiation.

segmentation, mostly in HE), add redundancy and shower shape information (segmentation, in HB and HE), and timing (HB, HE, and HF) to help reduce non beam-crossing-related signals and out-of-time pileup. This proposal will increase the discovery potential of CMS, for example for long-lived heavy NLSPs such as gluinos from "Split SUSY" that decay asynchronously with the beam crossing.

Missing ET (MET) and missing HT (the vector sum over clustered energies and muons, MHT) is a very important signature for new physics such as SUSY and dark matter searches, and are extremely sensitive to contaminations from non-beam-related signals, the most important of

which are cosmic rays, beam halo, and detector malfunctioning. Good timing information in the calorimeters to reject out-of-time events and redundancy in the detector measurement to check for consistency in several readout channels are the classic handles for dealing with these contaminants. Since some of these very rare backgrounds are extremely difficult to simulate realistically, we can profit from the CDF and D0 experience at the Tevatron. Figure 4.13 illustrates the gain that CDF realizes by imposing timing (and jet) cuts in the MET distribution. One can clearly see the importance of removing these contaminations as the highest MET rate is reduced by about 2 orders of magnitude.

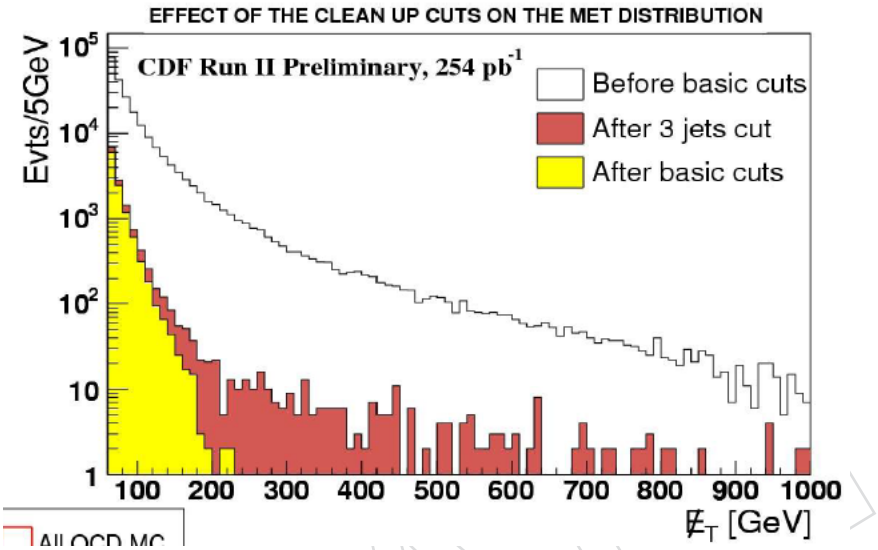

Figure 4.13: CDF MET distribution.

As the integrated luminosity of LHC increases, CMS will be sensitive to physics processes of lower and lower cross section. Hence flat or constant cross section backgrounds will become more and more important. In particular, the highest energy cosmic rays will start to be a problem for missing ET signals. Figure 4.14 from CDF shows signal + background for gamma-gamma + MET. Note that the non-collision background due to halo and cosmic ray events is roughly flat in MET out to 100 GeV/c and contribute a sizeable fraction of the total rate at higher MET.

In a recent CDF analysis [6], the highest E_T dijet event recorded (about 800 GeV per jet) was determined to be a cosmic ray event with a double bremsstrahlung. This event is shown in Figure 4.15. It was estimated that CDF would record only a few such events per year.

It is interesting to compare expected cosmic rates for CDF and CMS. CDF is sensitive to cosmics roughly 10ns out of each 396ns (bunch spacing). Correspondingly, CMS will be sensitive to 10ns out of each 25 ns or about a factor of 20 more than CDF. CMS sits under 100 meters of earth while CDF is under about 5 meters, however for energies greater than about 40 GeV, cosmic muons can easily penetrate the CMS overburden. Therefore we expect that CMS will have substantially more background due to cosmic rays in the multi-hundred GeV region. These events are rare and will not affect larger cross section measurements that will be done early in the CMS experiment lifetime. However as integrated luminosity increases, the effect of these rare events will become more important and techniques for detection and removal will have to be implemented.

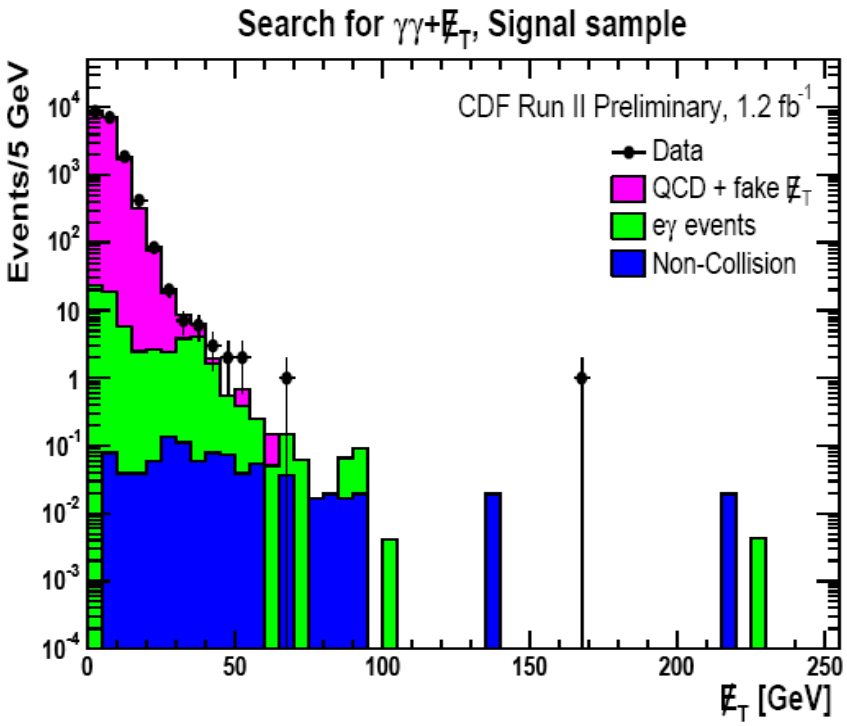

Figure 4.14: CDF MET distribution for $\gamma\gamma$+MET analysis showing irreducible backgrounds.

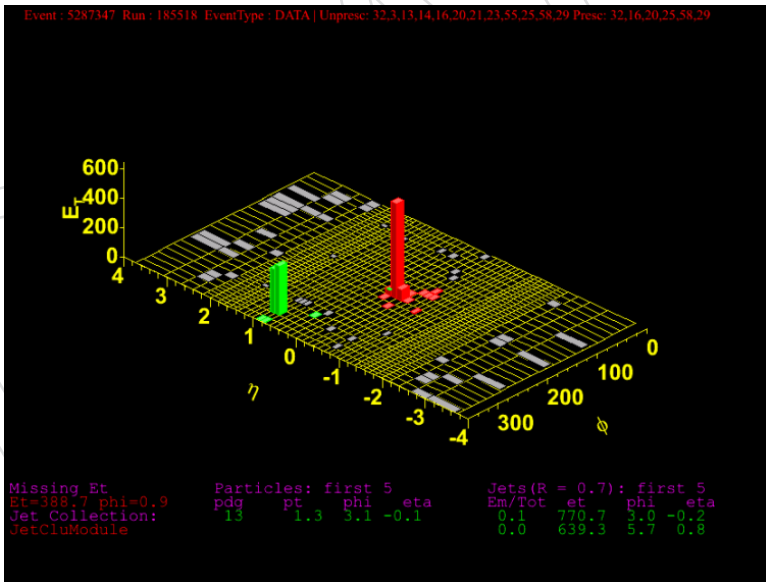

Figure 4.15: Highest ET dijet event seen by CDF determined to be from a cosmic ray.

Out-of-time events (due to cosmics and beam halo) are an important source of background in SUSY searches in D0 and CDF. An important upgrade for CDF was the addition of timing information in the calorimetry. Figure 4.16 on the left shows a CDF MET distribution for Monte Carlo and data (before cleanup cuts). Figure 4.16 on the right shows the same data after a requirement that less than 5 GeV was measured out of time with respect to the main event.

There is a very significant reduction in the tail. The rate of events with MET $>$ 100 GeV has been reduced by more than a factor of 10.

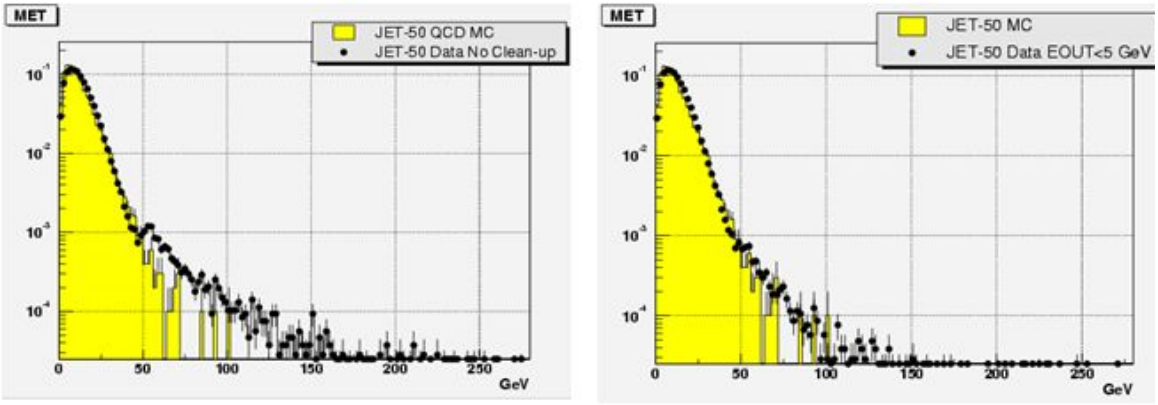

Figure 4.16: CDF missing ET distribution and effect of timing cut.

One of the largest backgrounds to isolated high E_T electrons will be from jet fluctuations. We studied this in the HE where the effect will be pronounced. By exploiting depth segmentation a much greater rejection factor can be achieved. For the plots in Figure 4.17, the HCAL was divided into 2 segments: a thin inner layer, and the rest in an outer layer, as in the HCAL TDR. The hadron energy used for the isolation and had/em cuts was in the outer layer, effectively throwing away the inner layer and using it as an absorber. From the plots in Figure 4.17, we can see the effect of depth segmentation on the isolation and electromagnetic energy fraction had/em efficiencies for this background rejection, and this strongly suggests that this technique will be even more important at luminosities of 1 or 2×10^{34} cm^{-2}s^{-1} or higher where the in-time pileup is large.

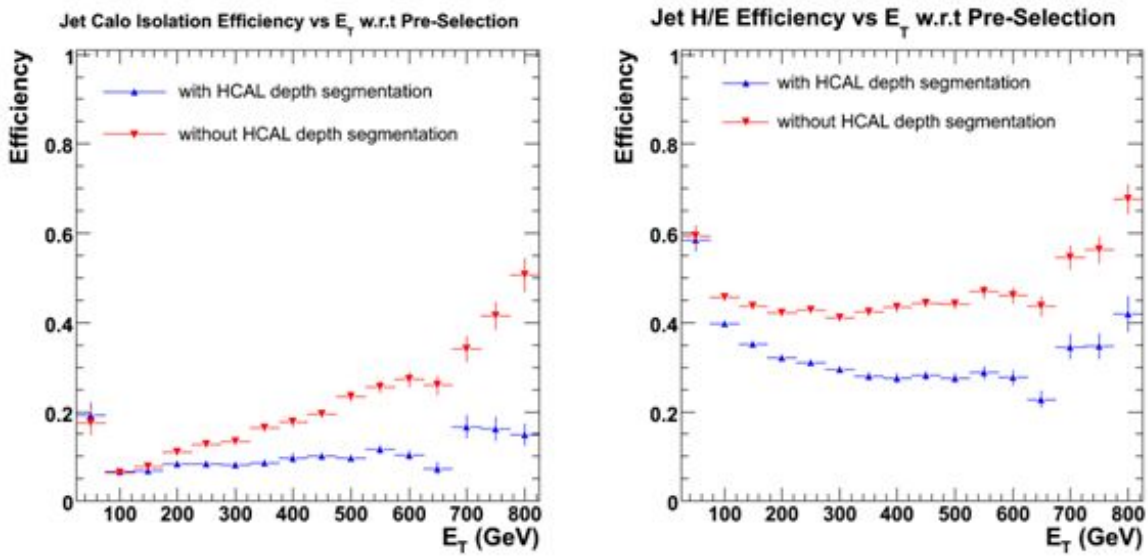

Figure 4.17: Effects from nominal depth segmentation in HCAL on backgrounds to isolated electrons

All of these issues (pileup, degradation of timing capability, sensitivity to smaller cross- sections, radiation damage, etc) can be mitigated by an upgrade that focuses on changes to the

front-end (FE) electronics by adding longitudinal segmentation and front-end electronics timing capability. This is detailed below.

4.2.3 Simulation Studies

Studies of physics processes are fundamental to optimize the design of the HCAL upgrade in the context of the combined measurement capabilities of the calorimeters, ECAL and HCAL, and tracking systems for doing physics at high luminosity. We are performing detailed studies to understand the expected improvements in triggering, isolation, energy resolution, and background rejection due to the increased longitudinal segmentation and TDC timing. These studies will provide input as to how to reestablish the current low-luminosity physics capabilities in the high luminosity era, and allow us to have a more powerful detector for triggering and offline analysis as the luminosity approaches several times 10^{34}, expected at the SLHC in Phase 2. Some of the analyses will need to be re-evaluated after CMS completes extensive data analysis from low-luminosity runnning. The upgrade path is designed with this flexibility in mind. For instance, the choice of longitudinal segmentation is not a constraint that impacts the fabrication of the front-end electronics and can be configured at a late stage in the upgrade timeline. The goals of the front-end simulation studies are to define the physics benchmarks to be used to form a straw-man definition of the required SiPM specifications, the front-end signal optimization, response time, digitization dynamic range and coding granularity, the choice of longitudinal segmentation and the performance optimization of front-end TDC measurements.

An initial setup for the simulation studies has been implemented in CMS software environment (CMSSW_2_2_13) and will be ported to a more recent version once the upgrade framework is supported in the standard software release. The HCAL upgrade software consists of layer-by-layer hit information to provide maximum flexibility in the study of possible configurations of the longitudinal segmentation and digitization parameters. The hit information is used to generate a calorimeter hit (PCaloHit) collection and is capable of feeding a new expanded set of channels (CaloDataFrames) incorporating multiple depths, improved signal-to-noise, SiPM pulse shapes, SiPM response time and TDC information. These CaloDataFrames are used to compute an expanded set of trigger primitives that will be able to feed the existing L1 trigger emulation software. Incremental improvements to the trigger primitives from replacing peak finding methods with TDC-based bunch-crossing identification can be studied directly. New quantities, such as lepton isolation cones, will be formed as part of SLHC L1 trigger primitive object and used to supplement the information of the existing L1 decision tree.

There are several possible schemes for longitudinal segmentation; Figure 4.18 illustrates two. The scheme on the left has finer segmentation where the energy density is greatest, and therefore optimizes the resolution, shown here for four depths of readout with the first depth consisting of layer-0, the second of layers 1-4, the third of layers 5-8 and the fourth of layers 9-16. This multi-depth configuration is referred to the 1-4-4-8 configuration. The scheme on right side of figure 4.18 optimizes redundancy and robustness by interleaving the rear two depths. The standard CMS simulation package does not record the energies deposited in the copper absorber plates and therefore the energy weighting studies have been performed with a separate standalone version of GEANT looking at different configurations for the purpose of improving jet resolution.

Simulation studies will focus on the SiPM device parameter requirements, the increased longitudinal segmentation and the ability to time the pulse to 1-2 ns within the 25ns window. This latter requirement stems from the fact that at high luminosity, out-of-time pileup (with average number of interactions per crossing increasing into the 100s) will preclude any pulse timing

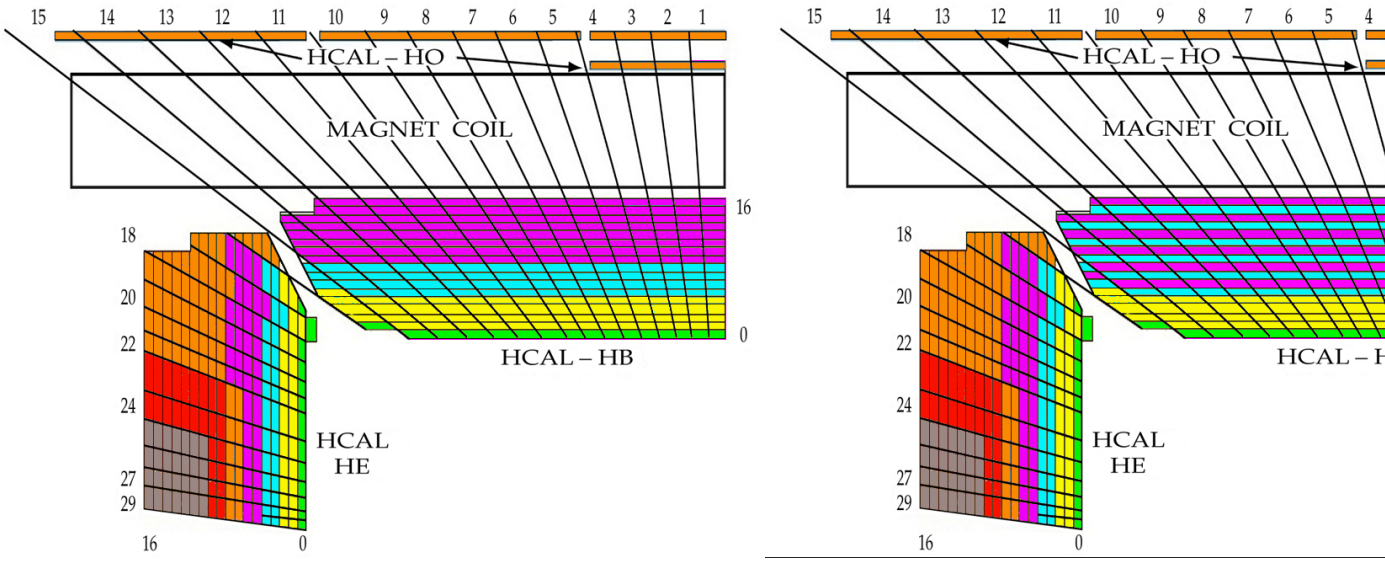

Figure 4.18: Two differing longitudinal segmentation schemes with each color code representing the layers that are grouped into separate readout channels. The one on the left maximizes resolution by concentrating separate readout channels to groups of layers where the energy density is highest. The one on the right maximizes redundancy and robustness of the calorimeter by providing two rear readout channels with interleaving sampling of the hadronic showers.

measurement with any accuracy below 10 GeV using the energy detected in 25ns buckets.

The largest performance improvement comes from the intrinsic signal-to-noise improvements from an SiPM photodetector and optimized readout electronics. Table 4.4 shows a preliminary comparison of the pedestal widths in GeV for the existing HPD and readout electronics for array of towers used for different purposes physics analysis and triggering: 1×1 for muon energies, 3×3 through 5×5 for isolation variables for electrons, muons and τs, and 12×12 and larger for jets, transverse missing energy and global energy sums. The reduction in noise levels shown in Table 4.4 corresponds to improvements of signal-to-noise from a factor of 3 summed over all longitudinal depths to a factor of 14 for the signal in Depth-1, consisting of layer-0 of scintillator. In the upgrades, the layer-0 neutral density filter would be removed in the upgrade yielding a factor of 2.4 more light for a given reference energy deposition in the scintillators. The purpose of the filter in the original design of the calorimeter was to reduce the signal in layer-0 at the hardware level to allow the signal to be added to subsequent layers optically without degrading the linearity of the energy response. With a separate readout, the full signal of layer-0 can provide a powerful tagging mechanism for non-interacting pions entering the HCAL barrel and for the detection of shower leakage from the ECAL for a more sensitive H/E discriminating variable. All layers will see a photoelectron light yield improvement currently approximated to be twice that of the current HPDs. In addition, the photoelectron equivalent of the pedestal noise will reduce from the current level of 3 photoelectrons to something closer to 1/3 of a photoelectron. For Depth-4, the 10% larger thickness of the rear absorbers can be separately applied and yields a corresponding 10% shift in energy scale to further improve response linearity of the calorimeter.

One of the most critical uses of the HCAL energy in the trigger is for the longitudinal isolation of electron and photon showers. This cut is traditionally placed between 2% and 5% of

Table 4.4: Pedestal widths (GeV) for HPD readout and SiPM readout with 4 depth segmentations in the 1-4-4-8 configuration.

	1×1	3×3	5×5	12×12
HPD	0.260	0.780	1.300	3.12
SiPM Depth 1	0.018	0.038	0.092	0.15
SiPM Depth 2	0.044	0.131	0.220	0.53
SiPM Depth 3	0.044	0.131	0.220	0.53
SiPM Depth 4	0.048	0.144	0.240	0.58
SiPM All Depths Summed	0.081	0.242	0.403	0.967

the total ECAL+HCAL energy. Some preliminary simulation studies on how to make use of longitudinal segmentation look promising. For instance, Figure 4.19 shows the effect of pileup on the ability to trigger on isolated leptons. At 2×10^{34}, with 40 multiple interactions per crossing on average, the pileup is large enough that there is a high probability for a particle to get through the ECAL into the first layer of the HCAL, compromising the EM fraction for an isolated electron. By eliminating the first HCAL layer from the trigger, we can recover an effective isolated electron capability. This is made possible by introducing longitudinal segmentation in the readout. This will become important towards the end of Phase 1 and even more so in Phase 2 where the number of multiple interactions is 5x that in Fig. 4.19.

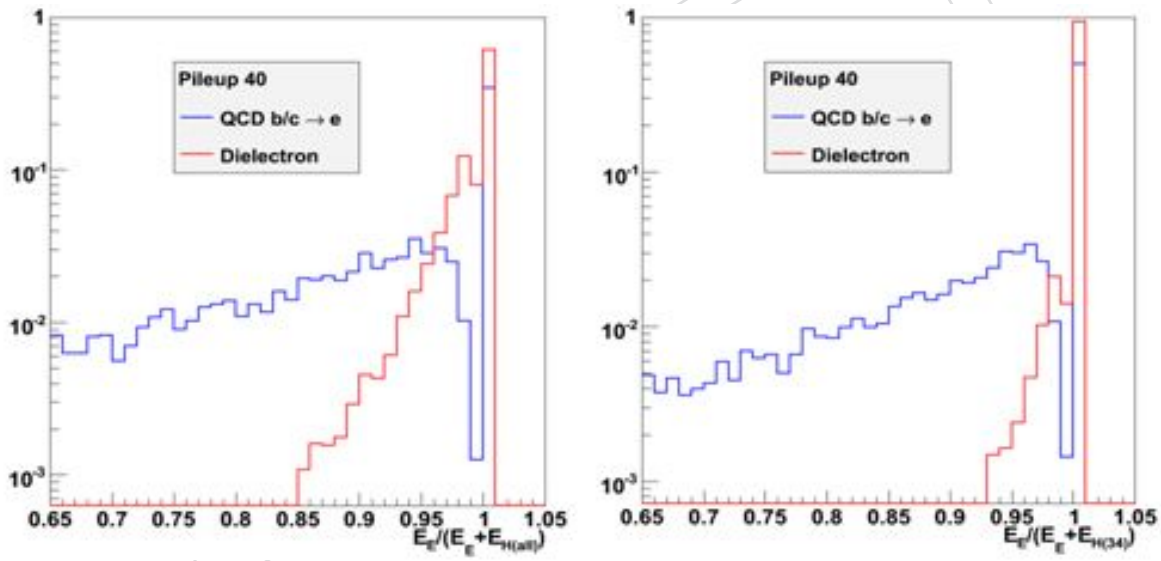

Figure 4.19: Pileup at 2×10^{34} can reduce the capability to trigger on isolated leptons. The left side of the figure shows the impact of using all HCAL layers in the determination of isolation; the right hand side shows how this improves when the first layer of the HCAL is not used.

Another way of seeing this effect is by looking at the shape of the single tower distribution for HCAL towers as a function of pileup. The results in Figure 4.20 clearly indicate that the electron/photon trigger path will suffer from luminosity-dependent inefficiency if it uses the full HCAL energy for isolation. It is better to exclude the first few layers. However, the jet and MET paths will likely be more stable with the inclusion of this energy. This motivates separate hadronic energy measurements for the jet and electron paths of the calorimeter trigger.

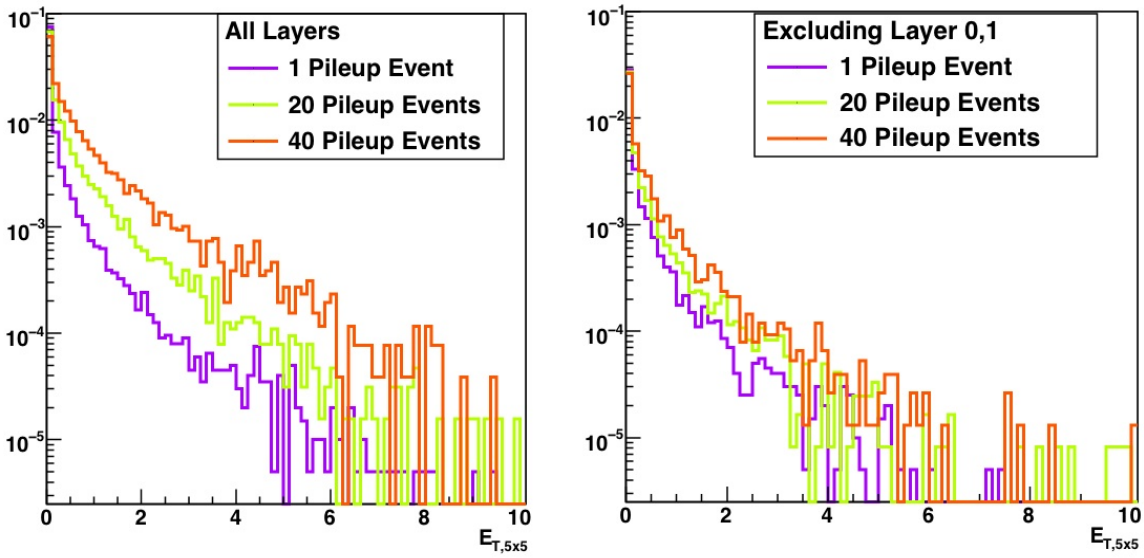

Figure 4.20: Energy distribution in the HB as a function of pileup when considering all layers (left) and when excluding the first two layers (right). The distributions are normalized to match the integral of the two leftmost bins, allowing a shape comparison.

4.2.4 Proposed Improvements and Upgrade Plan

4.2.4.1 Photodetector and front end electronics

The key element of the upgrade of the HB/HE is the replacement of the HPDs by SiPMs. A picture of a SiPM is shown in Figure 4.21. The devices have a high gain (up to 10^6 compared to 1500 for the HPD), a high QE (∼x2 over the HPD), and operate at much lower voltages (∼50V) compared to the HPD (∼7kV). The higher gain of the SiPM will reduce the electronic noise levels in the calorimeter, improving the sensitivity for low energy showers. The lower operating voltage should largely eliminate breakdowns, there is no vacuum hence no ion feedback, and the device is insensitive to magnetic fields, in contrast to the HPDs. SiPMs are linear up to the point where the probability for more than one photon per pixel gets large; however, this effect is mitigated by increasing the number of pixels (see Figure 4.22).

Our R&D plan is designed to identify candidate SiPMs that meet our requirements and that will be available commercially on the timescale needed at an affordable cost.

In setting the characteristics and performance requirements for the SiPMs to be used in CMS, some of the more important factors we identified are: 1) active area; 2) signal-to-noise; 3) photon detection efficiency; 4) insensitivity to magnetic field; 5) radiation tolerance; 6) linearity of response for single pulse; 7) rate capability; 8) lifetime; 9) temperature sensitivity; and 10) variation in operating voltage at constant gain for an ensemble of parts. We are currently formalizing the requirements document to present to the CMS electronics steering committee.

A very important part of the R&D will be to procure SiPM samples from various vendors for evaluation. Known vendors include Hamamatsu (Japan), FBK (Italy), CPTA (Russia), and Zecotek (Singapore). We plan to purchase sufficiently large samples of existing SiPMs and evaluate their performance. We will purchase larger quantities of promising devices and are prepared to work with the vendors to tailor them to our needs. In total, approximately 800 cm^2 of SiPM photodetection area is required for the barrel and endcap upgrade. Uniformity of the SiPM devices will be important for calibration and would therefore point to having at most

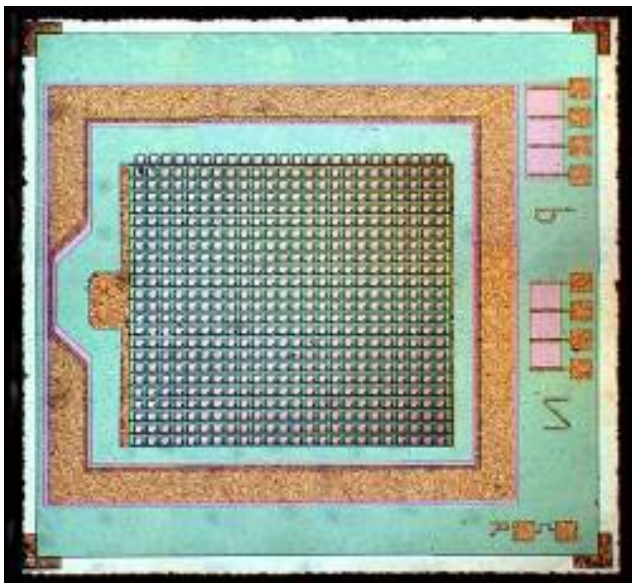

Figure 4.21: SiPM candidate chip from Hamamatsu

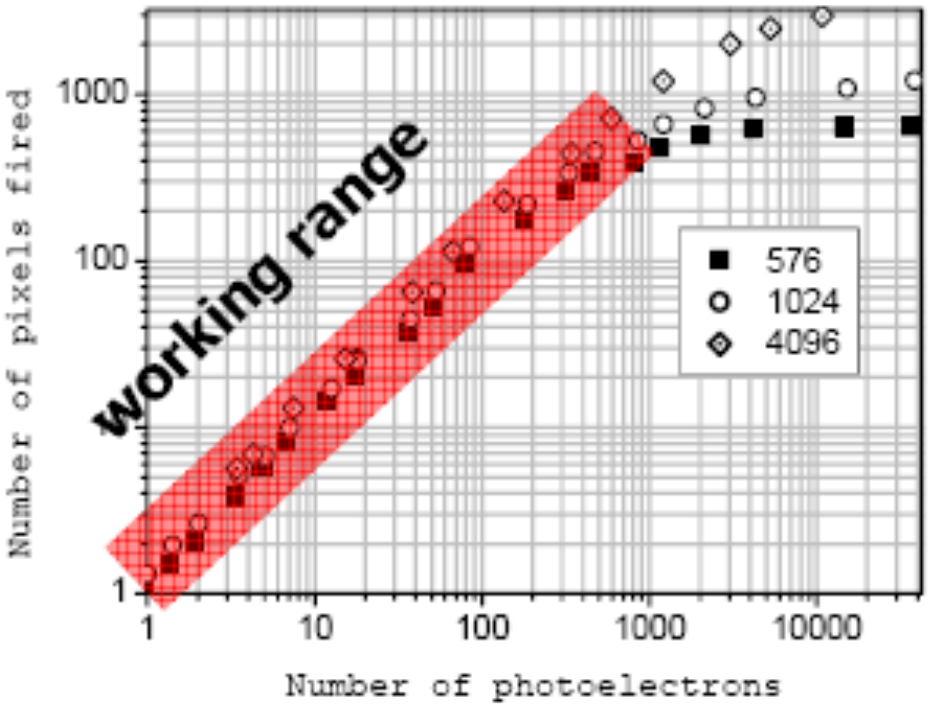

Figure 4.22: SiPM linear range as a function of the number of pixels per square mm.

one vendor for the entire barrel but with the possibility of potentially a separate vendor for the endcaps.

The integrated dose of neutrons with $E > 100$ keV during the lifetime of the SLHC is expected to be in the range $1 - 3 \times 10^{12}$ for HB/HE readout box regions. Neutrons in this energy range are particularly important as they have been shown to induce leakage current in silicon

devices. The SiPM and ADC must survive these doses with limited degradation. We have started exploring radiation damage to various SiPMs. Figure 4.23 shows relative loss in apparent QE/gain (ratio of peak of LED response) as a function of the dose, using protons with $E = 212$ MeV. We see that the candidate Zecotek devices (MAPD) look very promising.

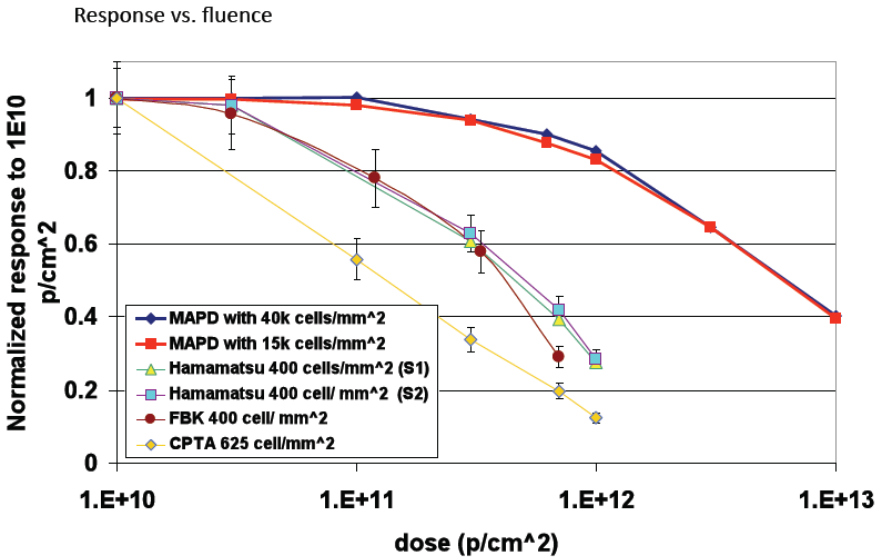

Figure 4.23: Change in LED peak value as a function of proton dose.

4.2.4.1.1 Longitudinal Depth Segmentation, Options for Optical and Electrical Decoder Units

To incorporate multiple depth segmentation in the calorimeter we will replace the ODU (Optical Decoder Unit) that receives the calorimeter analog optical signals from the scintillators and optically sums it into towers. We are investigating a new approach that allows us to read out each fiber with a SiPM and then make an analog sum of the output signals of the set of SiPMs (tiles) that would comprise the depth segment of the calorimeter. We believe that this will be both easy to build into the existing system, and would give us maximum flexibility in how we combine longitudinally. We call this new development the Electrical Decoder Unit (EDU). To build the EDU we need to create a design for the packaging that will allow the optical signals from the calorimeter to reach the SiPM and be formed into a readout segment. We will design the EDU to mate to the existing CMS HCAL fiber connectors, which consist of 18 individual 0.9 mm fibers.

Figure 4.24 shows the general concept of the EDU. Optical cables from the calorimeter are plugged into a mating array of SiPMs (linear array). These arrays are mounted on a PC board. Connectors couple the electrical signals from the SiPMs to electronics cards located below the readout electronics. The perpendicular arrangement of the readout card relative to the linear array allows for easy summation of fibers (tiles) into tower segments.

Figure 4.25 shows a detail of one of the SiPM linear arrays. In this implementation we would construct the linear array from individual packaged SiPMs bonded to a substrate. We plan on working with vendors to develop monolithic arrays of SiPMs. The first version would be 18 1mm diameter SiPMs in a linear array on a single piece of silicon. Having the integrated linear array rather than single parts will make handling easier, guarantee alignment, and reduce

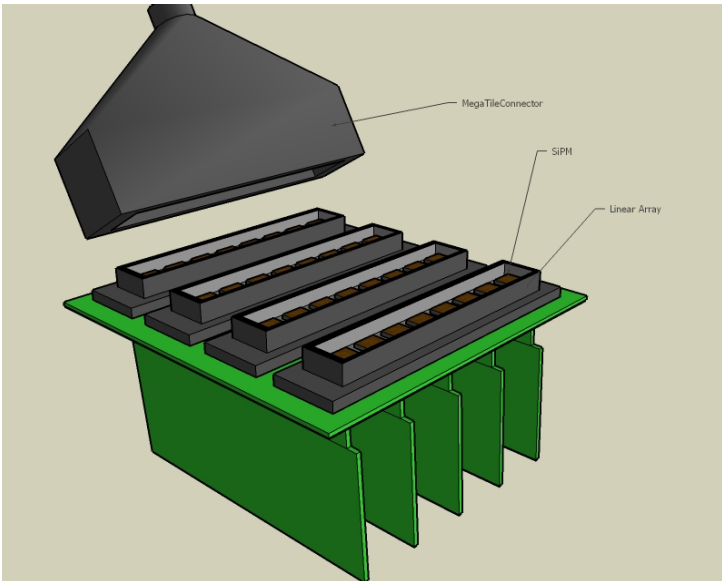

Figure 4.24: Electrical Decoding Unit (EDU)

3259 packaging costs. Figure 4.26 shows the details of the SiPM strip array packaging.

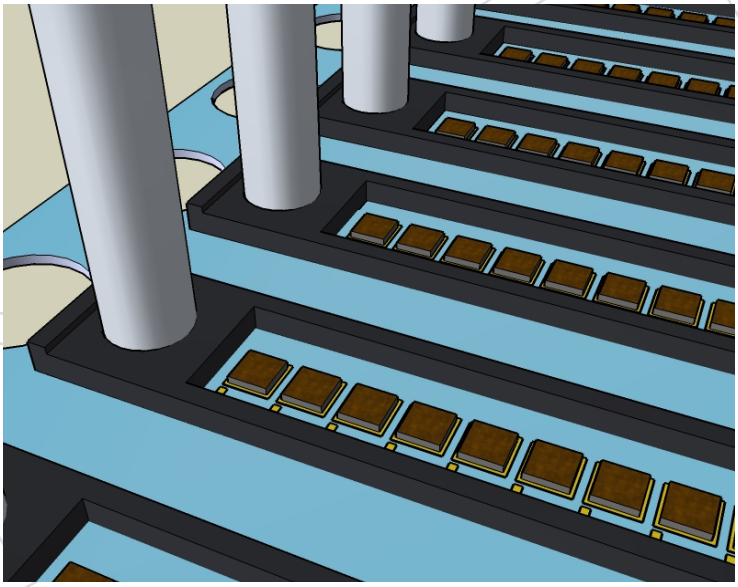

Figure 4.25: EDU detail showing linear arrays of SiPMs

3260 An important part of our R&D is to work with vendors to develop strip array SiPMs that would
3261 suitably mate to the analog optical cables from the calorimeter.

3262 Options for optical addition are also being explored. The advantage of optical addition is that
3263 any given fiber can be used to illuminate an incrementally larger photodetection surface with
3264 a correspondingly larger number of SiPM pixels. The total number of SiPM pixels sets the
3265 available dynamic range of the SiPM photodetector. This option is particularly important for
3266 devices where the feature size limits the pixel density to $\sim$5000 pixels/mm^2.

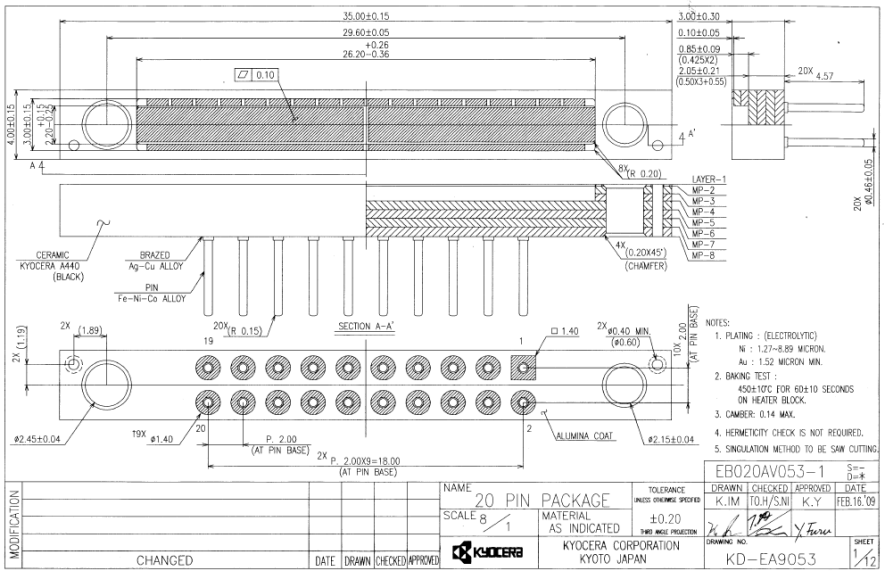

Figure 4.26: Kyocera strip SiPM package

4.2.4.1.2 Timing

We foresee the new front-end readout will incorporate TDCs on at least some of the channels. As stated above, we can learn from the experience of experiments at the Tevatron, where CDF has found that TDCs on the calorimeter readout are very useful in various background rejections. Additionally they open the door to new physics, for instance slow heavy stable particle detection. The TDC information has the potential to improve the bunch crossing identification accuracy over the current peak detection methods used for trigger primitive generation, especially for low energy quantities such as lepton isolation energies. We envision implementing a timing measurement in the FE electronics by first producing a fast discriminated pulse out of the QIE (see below), and then timing that pulse with a fast clock relative to the bunch crossing (BX) time, perhaps inside a radiation hard programmable logic chip. If the clock were to run at 320 MHz, or 8$\times$ faster than the BX clock, and use the leading and rising edge of the discriminator pulse, we could get a timing measurement to around 1-2 ns. We will be focusing part of our R&D effort in this area.

4.2.4.1.3 Readout

The current HCAL readout is via a charge integrating and encoding chip, called the QIE, developed at Fermilab. It has a large dynamic range, approximately 10^4:1, accomplished via input current splitting and comparison on 4 ranges, and digitizing the selected voltage representing the integrated charge with an FADC, and compressing by eliminating needless codes. Since the HCAL towers are large, the shaping is necessarily limited to short times to minimize out-of-time pileup. The sample-and-hold capacitors are necessarily very small in order to have a gain of approximately 1 fC/bin on the most precise scale. In order to make as linear a device as possible, a BiCMOS process was used for the current HCAL QIE (version 8, or QIE8), and at the time the QIE8 was developed the best process had a 0.8μ feature size.

For the upgrade we are exploring two possible ADC schemes for the readout: (a) an enhanced (and radiation hardened) QIE charge integration directly from the SiPM, and (b) a voltage following integrator similar to the ECAL scheme (called the MGPA/ADC). For the QIE, we will

propose an upgrade that will use a finer feature size (0.35μ), slightly greater functionality (e.g. some phase adjustments and fast discriminated pulse built-in), greater dynamic range ($\times 10$) and greater precision (6 instead of 5 bits on the FADC mantissa of the encoded output). For the MGPA/ADC option we will explore both the ECAL solution and commercial solutions. We note however that the ECAL solution was built for a detector that had 25x smaller tower sizes, and thus much less occupancy, which allowed stretching out the pulse to over 10 bunch crossings in order to make a precision measurement. Extending the length of the front-end pulse is not optimal for the HCAL; however, we want to consider all possible solutions that minimize the risk and cost. For either solution we will continue to compress the ADC output to save data bandwidth out of the calorimeter.

Both readout schemes are multi-range systems, but the dynamic range of the SiPM and its non-linear behavior at the high-end need dedicated studies to determine how best to match the SiPM with these different ADC systems. The channel density is also a major concern as the power and cooling of the existing services (the Readout Box, or RBX) are significant constraints. Our initial evaluation is that the QIE is most suitable for the SiPM HCAL upgrade. The QIE will therefore be our major focus for development in the short term. We will continue to study the MGPA as a possible solution. A test stand using ECAL VFE cards has been set up.

The performance of the SiPM system is closely tied to the ADC digitization for reasons of dynamic range and sensitivity. A new generation of the QIE is needed to match the SiPM gain ($\sim 5 \times 10^4 \rightarrow 10^6$ compared with $1 \rightarrow 2 \times 10^3$ for the HPD). As stated above, we plan on having the new QIE create a discriminated output pulse for use in an external TDC circuit.

The current HCAL QIE has an associated control chip, the CCA (Clocking Control ASIC). In the current implementation this is an ASIC. We plan to replace the CCA functionality with an FPGA that will implement some of the QIE control functions. It will also provide a digitized output for the TDC signal sent from the QIE. Additionally it will do error checking on the QIE. The FPGA will handle all QIEs in the readout module (18*4 = 72 channels) and format the data for the digital link. The options for the digital link are being explored in the context of the Cern Gigabit Transceiver (GBT) development group. For testing purposes, we are operating commercial off-the-shelf high-speed data links using FPGAs to serialize. We note that the exact format of the data stream feeding the front-end optical drivers can be defined relatively late in the upgrade plan in response to the needs and experiences with the first LHC collision data. In order to keep the high power electrical components in better contact with the readout box (RBX) cooling, we will build a separate board for the FPGA and optical drivers. Figure 4.27 shows a drawing of the layout of the new electronics cards in the Readout Module, showing 4 QIE cards plugged into a single FPGA card.

The SiPM needs stable bias voltage and temperature for optimal performance. We are developing a Cockroft-Walton circuit to generate the bias voltages. The circuit will also provide leakage current readback. The SiPMs in the EDU will be thermally isolated and solid-state (Peltier) coolers will lower and stabilize the temperature.

4.2.4.1.4 Front-end crate mechanics and cooling

The mechanical design of the FE package has several components. The optical decoding units must be redesigned to handle up to 4 readout depths that map to individual SiPM devices. The cooling pack for the ADC/TDC electronics needs to be expanded to handle the front-end channel increase. The outer mechanical case of the RM must accommodate the SiPM support and Peltier cooling and meet the outer dimensional requirements of the existing RBXs.

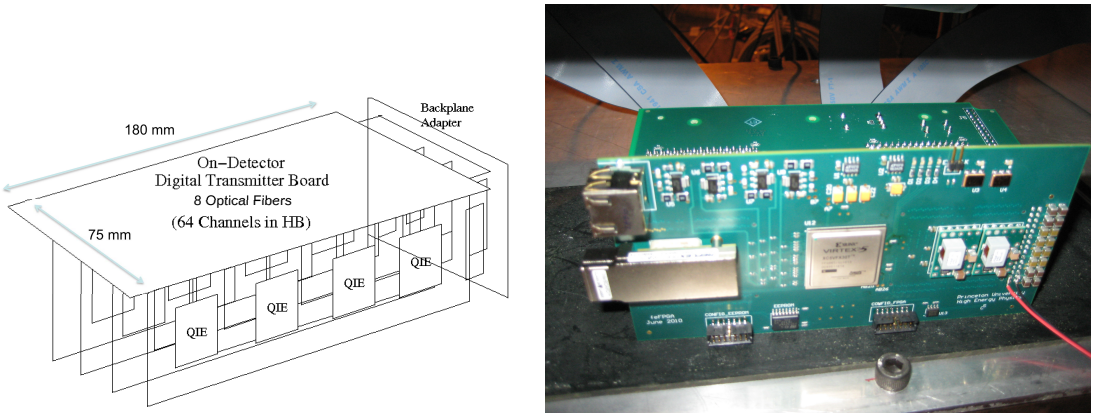

Figure 4.27: Layout of Readout Module boards, where the placement of the optical links and FPGA are optimal for the existing RBX cooling circuits. A functional schematic is on the left and a photograph of a prototype from the 2010 test beam is on the right.

The cooling capacity in the RBX is limited by the cooling plant and existing pipework. The layout of the readout cards should be optimized to ensure that additional heat load in the new front-end does not cause an increase in the chip temperatures, currently at about 25–30^{o}C.

We are studying a design modification to allow the highest power parts (GOLs/GBTs, FPGA, voltage regulators) to be very close to the heat exchange. Figure 4.27 above shows the proposed new layout. The heat exchange plates of the RBX are on top and bottom. Note the placement of the GOLs and FPGA close to this plate.

4.2.4.1.5 Front-end controls

The current front-end controls cannot accommodate an upgraded project using SiPMs, and it is envisioned that the TTC (Trigger Timing and Control) will evolve to something more powerful using the Cern Gigabit Transceiver (GBT) chips. Extensive R&D will be needed to design the controls upgrade. This includes accommodating the GBT on the front-end cards, interfacing the GBT controls signal to the rest of the front-end electronics in the RBX crate, and integrating the slow controls with the CMS runtime system.

4.2.4.2 HCAL Back-End (BE) Trigger/Receiver Upgrade

The calorimeter backend electronics are built to receive the data from the front-ends, ensure time alignment across the links, pass the necessary information to the trigger path, and collect the data in response to Level 1 Accepts. As outlined above, the HCAL Phase 1 upgrade makes major revisions to the front-end electronics that will result in more data (longitudinal segmentation and timing) transmitted to the back-end (BE). As the current HCAL Trigger Receiver boards (HTRs) cannot be modified to receive data at a higher rate, and as the upgrade to the front-end (FE) electronics will require transmitting more data on the same number of fibers, a new backend is required.

The BE upgrade will take advantage of progress in commercial technology since the HTRs were designed in 2002, specifically in programmable logic (FPGAs), increased integration (e.g. deserializers built into the FPGAs decrease the IO burden), and newer and more powerful infrastructure for crate data sharing and handling. At the same time this will allow a more powerful physics trigger. The system we envision should be optimal for HCAL, and scalable in ways that the current system is not. We will keep in close touch with the evolution of ECAL

and the CMS Level 1 trigger so as to be in a position to share technology and take advantage of economies of scale.

Given the higher luminosity and multiple interaction rate, we want to allow for increases in the BE capabilities that will allow CMS to do a better job of identifying jets. For instance, in the barrel and endcap region, the trigger primitives with a transverse granulaty of 0.087×0.087 in $d\eta \times d\phi$ are sent to the Regional Calorimeter Trigger (RCT) which subsequently reduces the granularity into larger 4×4 $\eta - \phi$ regions for physics considerations in the trigger. However, for the HF, the regions are constructed inside the HCAL HTR boards for historical reasons. Implementing a jet-finding trigger that will use a finer granularity than our current trigger will require hardware changes to both the HCAL BE and the RCT, both envisioned as part of Phase 1. We point out that by increasing the granularity in this region, we will be increasing the capability to trigger on jets right in the region where the jet cross-section from W-boson-fusion Higgs production diagrams is largest (see Figure 5.1): at the HE/HF boundary ($|\eta| \sim 3$). This particular production channel constitutes the highest cross-section for associated Higgs production,.

As a result of an increase in the number of multiple interactions, in-time and out-of-time pileup, and the effect on the trigger, the proposed structure of an upgraded HCAL backend must support an increased bandwidth between the HCAL front-end data and the electromagnetic and Jet/MET portions of the calorimeter trigger. Such an upgrade could be achieved in two ways. The straightforward option is an increase in the data volume from HCAL to the trigger system by 160% to accommodate electromagnetic object isolation variables. The second option is to combine HCAL data with ECAL trigger primitive data at an earlier stage, allowing the definition of electromagnetic energy and isolation bits to be made separately from the jet/MET energy definition. For the existing ECAL front-ends, this integration could be made relatively cheaply as the slow data links from the ECAL trigger front-ends can be received with conventional FPGA inputs, leaving optical receivers as the only hardware cost. If the ECAL front-ends are upgraded, a different design may be more reasonable. These issues are under investigation. Note that the baseline HCAL upgrade is to move forward with a new back-end that will accommodate a higher input bandwidth and a higher trigger (and DAQ) bandwidth as required, working in conjunction with the evolution of the calorimeter trigger and potential changes and upgrades to the ECAL back-end readout.

4.2.4.2.1 Electronics System Structure

To receive the data from the front-ends, the back-end electronics must accept the signals from the high-speed optical links. For the HCAL, these links will run over the current 850 nm multi-mode fibers, currently running at a speed of 1.6 Gbps (1.28 Gbps data rate). Since we will be increasing segmentation and sending more data, we will need to increase the data transmission rate, and we calculated that we will need a speed of 3.25 Gbps or higher. We will also utilize unused fibers in the existing fiber ribbons to increase the data throughput. The baseline proposal for the front-end upgrade includes the usage of the products of the GBT project at CERN. These components transfer data at a raw rate of 4.8 Gbps with a user data payload (after error correction and scrambling) of 3.28 Gbps. There is a possibility to increase the user data payload beyond 3.28 Gbps by using the 8B/10B transfer protocol. These products are expected to be radiation tolerant and to have adequate latency performance. The data link of the GBT will be received directly into a field programmable gate array (FPGA) using the high-speed deserializers built into these chips.

Time alignment, connection to the trigger, and the data acquisition system all require that the

back-end hardware be integrated into an architecture that allows for clock and fast control distribution as well as the local concentration of data before transmission to the DAQ system. In the original CMS electronics, the most common infrastructure solution was VME64, particularly the 9U-400 mm card format. VME is a parallel bus standard that has been used for years in high energy physics, but which is a poor match with the recent trends towards high speed serial data transmission for most interconnects. A commercial standard, the Micro Telecommunications Architecture (μTCA) is being considered, and this standard appears to match the requirements more closely. The μTCA standard specifies moderate-size cards (similar in size to 3U or 6U VME cards) that can communicate at high rates using up to twenty-one bidirectional high speed serial ports on each card. The interconnection of these ports is specified by the backplane, either by the construction of the backplane or by an active device such as a crosspoint switch. The active element is generally housed in a special hub slot of the backplane (called an MCH), but it can be integrated directly into the backplane as well.

The μTCA standard provides for the necessary high-bandwidth communication required for global data acquisition as well as a powerful local control and data acquisition path through gigabit Ethernet connections to each card. The standard is generic in many ways, however, and significant engineering effort is needed to resolve key issues such as the distribution and management of clocks (including the LHC clock) and the handling of fast controls. In particular, the HCAL backend electronics will likely be deployed before any upgrade of the TTC system is complete. Thus, the system architecture must be designed to allow for operation with the legacy TTC system until a new TTC system is available, then allow an upgrade if needed. This may be particularly relevant for next-generation DAQ designs.

The installation of upgrades in the running CMS detector will demand a serious attention to the physics risks of any change to the detector. At the point when the SLHC-related upgrades would begin, the detector would be acquiring high quality and high value physics data. One strength of the CMS HCAL design is the ability to access and upgrade it in a short shutdown. However, it would be very risky to replace the full front-end, back-end, and trigger electronics in a single short shutdown. Instead, the electronics must be capable of interfacing with older trigger electronics and the legacy front-ends, which allows flexible upgrade scenarios. In particular, the readout portion of the new system should be capable of running parasitically (using optical splitters to obtain a copy of the data sent to the existing electronics) to gain operational experience. These considerations add significant pressure to the back-end schedule. Rather than being a task to be attacked after the front-end is completely settled, as was basically the case for the original CMS electronics, the back-end production must be completed earlier than the front-ends.

The proposed structure for the upgraded HCAL backend electronics requires two separate classes of functionality, hosted on separate cards. These two cards may be physically identical depending on the requirements imposed by the backplane and external portions of the data acquisition and trigger system. One card has the role of receiving the front-end data, constructing and transmitting trigger primitives to the Level 1 calorimeter trigger system, and holding the pipeline of front-end data for data subpacket creation in the case of a Level 1 Accept. In analogy with the existing HCAL Trigger/Readout card (HTR), which has a similar function, the card will be called the UberHTR (uHTR) in this document. The second card has a dual role of collecting the subfragments from the UberHTR cards and building event fragments that are distributed to the DAQ and also of receiving the fast control and clock signals and distributing them to all the cards in the crate. This dual role is expressed in the term used for this card in this document: the DAQ and Timing Card (DTC).

As shown in Figure 4.28, each crate of the upgraded system would consist of twelve UberHTRs and a single DTC card. As a baseline, we consider the use of commercial crates that provide inter-slot connectivity through the backplane and through special "hub slots" that have enhanced connectivity to all slots. In particular, the baseline proposal specifies a crate with two MCH slots and twelve standard μTCA card slots. One MCH slot would be used for a commercial card providing the standard μTCA shelf management functionality, and a gigabit Ethernet connection to each site for use in configuration and control. The second site would be used by the DTC and would necessarily have three high-speed ports distributed to all μTCA cards (one for DAQ data, one for the legacy TTC, and the third for future fast controls). Additionally, the DTC will distribute a copy of the LHC clock to all cards over the backplane.

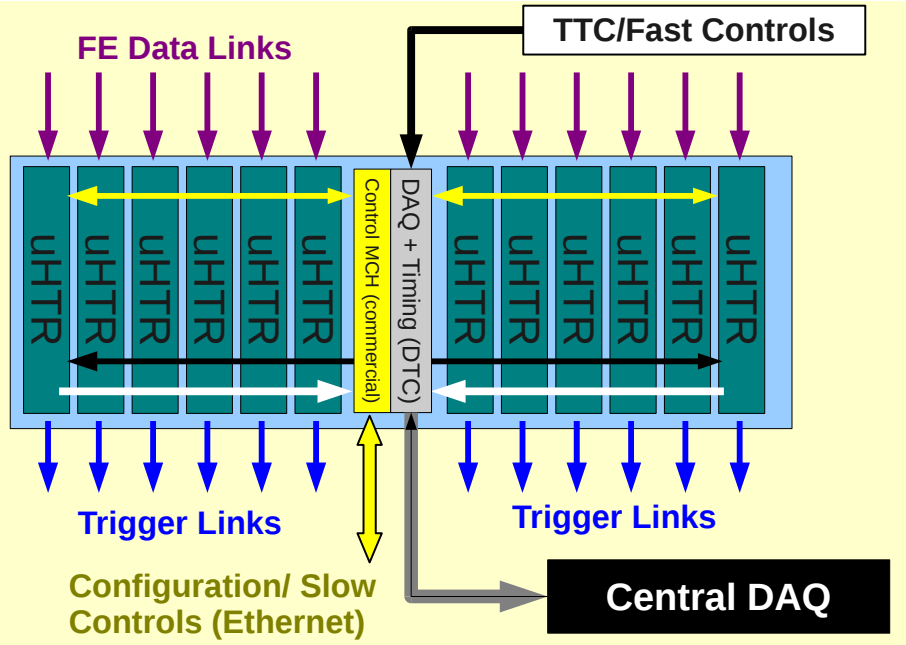

Figure 4.28: Conceptual design of μTCA crate with "UberHTRs" (receiver, trigger, pipeline buffer) boards combined with a DCC and trigger/timing card (DTC).

4.2.4.2.2 UberHTR Design Considerations

Much of the functionality of the UberHTR is set by the technological requirements of its inputs and outputs. The GBT links will be received using the high-speed built-in FPGA deserializers and decoded using firmware provided by the CERN microelectronics group. Sufficient memory will be available on the board to hold the data for the entire Level 1 decision time (which is expected to increase by a factor of 2 in Phase 2). The data must be formatted and transmitted to the DTC for inclusion in the full event fragment. There are two significant issues to be considered which require careful design work and new implementation effort. The first is the construction and distribution of the trigger primitives to the Level 1 calorimeter system. The second is the inclusion of regional zero suppression (sometimes called selective readout), which could have significant requirements for additional buffering and computation and is discussed later. The most challenging requirement for the HCAL backend electronics is the production of the trigger primitive information to be used in both electron/photon and jet/MET paths of the Level 1 trigger. These are custom-hardware systems operating under a strict latency budget. In particular, the Phase 1 upgrades do not envision replacement of the

Tracker pipelines, so the present Level 1 latency must be maintained even when the luminosity is increased.

UberHTR Detailed Prototype Design

While the final design for the UberHTR will depend on the results of ongoing research and development, a baseline proposal, shown in Figure 4.29, is useful to demonstrate the feasibility of the design and the applicability of the proposed technologies.

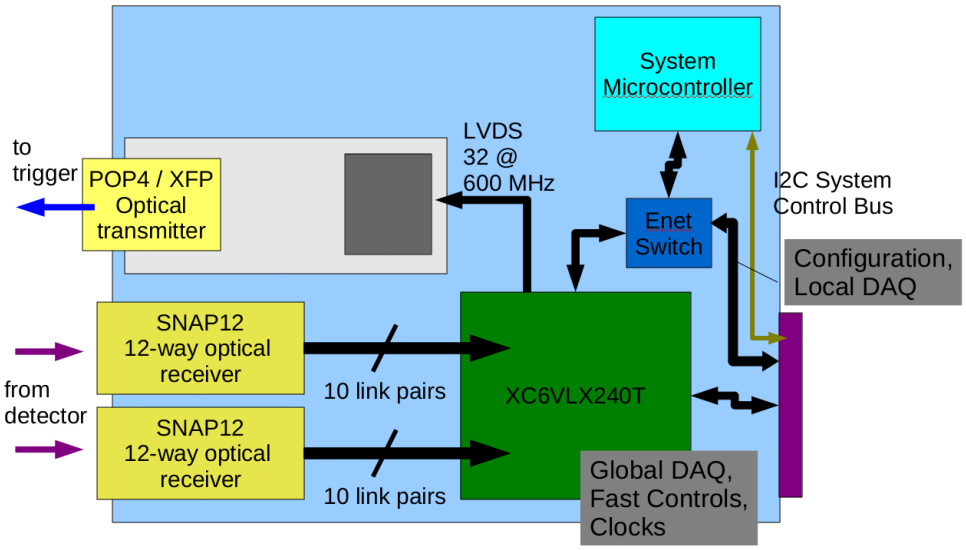

Figure 4.29: UberHTR conceptual design.

The UberHTR will receive eighteen front-end links using two SNAP-12 format parallel optical receivers. Nine links are necessary for a single HCAL wedge (18 towers in pseudo-rapidity), including the overlapping region between the barrel and endcap hadron calorimeters. This coverage also maps directly to the ECAL barrel coverage. The hadronic endcap will require fewer links as the number of towers is smaller, due to the change in ϕ-granularity from 5° to 10° which occurs at $|\eta| = 1.83$. If the UberHTR is to be built as a general-purpose card (appropriate for several uses within CMS), it would be appropriate to connect all 24 optical receivers to high-speed transceivers on an FPGA. However, there are a limited number of FPGAs that have sufficient resources to accommodate this number of links as well as the three additional links required by the system (Gigabit Ethernet control, data acquisition, and future fast controls). The baseline proposal, therefore, is the use of a 24 transceiver FPGA to receive up to 20 front-end links with four links for fast controls and data acquisition.

The link between the UberHTR and the trigger will be housed on a mezzanine card. This structure will allow the trigger link to be upgraded/adjusted as necessary as there are changes in the CMS trigger system. In particular, direct transmission at 10 Gbps is not supported by current FPGAs, but future trigger upgrades may take advantage of newer technology and require faster data links from the detectors. As a baseline proposal, the necessary trigger bandwidth could be provided by four fibers per mezzanine (e.g. POP4 connector). The mezzanine is proposed to use the same connector technology as the SNAP12 transceiver, which is robust and capable of very high data rates. The communication between the UberHTR main FPGA and the mezzanine would occur over a DDR LVDS bus, a solution that should be reliable and very low-latency.

The integration of the UberHTR into the μTCA crate will be supported by a microcontroller that will serve as the slow-control interface point for the system-management I2C bus. The microcontroller will be responsible for implementing the relatively complex "enumeration" process of the μTCA bus and for providing an emergency path for reprogramming the FPGA's flash memory chip. An I2C connection is necessarily only an emergency path given its low speed. Ideally, the microcontroller could use the Ethernet bus to provide faster programming (and become the primary solution), but most currently available microcontrollers do not support gigabit Ethernet or the μTCA standard. However, if a microcontroller with reasonable cost and complexity can be identified which supports gigabit ethernet, it might be most effective to pass the gigabit fast control stream through the microcontroller, which could save a high-speed transceiver on the FPGA.

4.2.4.2.3 DAQ and Timing Card (DTC) Design Considerations

As stated above, there will be a single DTC per crate to handle all DAQ and timing and clock signals, described below. At this time, an upgraded DAQ hardware interface has not yet been specified, therefore for prototyping we will provide 10 gigabit/sec class optical outputs with bandwidth 8-10 times the current FRL bandwidth. The existing S- LINK hardware is not readily compatible mechanically with μTCA, so we propose to develop a separate interface module for legacy DAQ operation. An S-LINK converter module would then be designed so that it could be housed in a separate chassis (perhaps surplus 9U VME crates). The DAQ output link would require a modest-bandwidth return path for backpressure. The legacy TTS outputs would also be mounted on the external modules that house the S-LINK source cards.

4.2.4.2.4 Selective Readout

The combination of the SLHC luminosity and the HCAL upgrade will significantly increase the HCAL data size. Considering simply the data volume, we expect to increase the data by a factor of more than four. This factor arises from the increase in channel count along with the additional TDC information that will be provided as well. On the other hand, the increase in luminosity at SLHC will significantly increase the average occupancy. The net result of these effects will be a requirement to significantly increase the amount of data sent from HCAL to the central DAQ (either more FEDs or faster SLINKs) and/or perhaps very stringent zero suppression requirements.

The ECAL experience has indicated that a balance between data volume and physics object quality can be achieved by a seeded readout scheme. Large energy deposits cause the cells around them to be read with reduced zero-suppression thresholds, a technique called "Selective Readout". Such a scheme would be ideal for SLHC, particularly if ECAL and HCAL were capable of cross-seeding. It is important to read out the HCAL energy directly behind electromagnetic candidates and it is also important to read out the ECAL with high precision in τ-lepton and some other classes of jet events.

The upgraded HCAL electronics should allow the DTC to participate in the selective readout process, at least to the level of accepting the selective readout bits from the ECAL selective readout processor (SRP). Depending on the behavior of the ECAL SRP at high pileup for taus and similar events of high interest, a bidirectional flow of selection information may be necessary. The integration of SRP will necessarily add latency to the DAQ-side of the processing (which is not considered a significant issue) and will increase the requirement for event data storage while the selective readout calculations are proceeding. This storage may be either on the UberHTRs or the DTC.

The UberHTR is proposed to maintain the same modularity as the current HTR (48 front-end channels), or possibly double the modularity (96 front-end channels). The front-end data volume is assumed to increase by about 4X as discussed above. For purposes of this document we assume that the double-density UberHTR option is taken, so the data volume increases by 8X.

It is realistic to send all non-zero-suppressed data from the UberHTR to the DTC. The current data volume from HTR to DCC is about 50 MByte/sec per HTR. Applying our 8X factor from above gives 400 MByte/sec, which is reasonable for a single μTCA fast backplane port.

4.2.4.2.5 Trigger, Timing and Fast Controls

The other major function of the DTC is to distribute triggers (L1A) and other time-critical control signals to the UberHTRs. Like the DAQ path, a well-defined legacy system (TTC) and the new (as yet to be finalized) replacement system (GBT timing features) must be supported. The most conservative approach is to distribute the encoded TTC stream on a dedicated backplane pair for legacy operation, and use a separate port to support a future fast controls path. The GBT provides a control path between the UberHTR and the front-ends, but the details of the fast control path are not well defined at this time.

In addition, one or more low-jitter clocks will be distributed by the DTC on the dedicated clock pairs allocated on the μTCA backplane.

4.2.4.2.6 Management Interfaces

The DTC will support both the I2C management interface and gigabit Ethernet. The details are similar to those discussed above for the UberHTR. Some additional work is needed in order to specify the details of Ethernet communication, high speed data input (e.g. configuration, look-up-tables, etc) and output (local data acquisition and monitoring) on the typical commercial backplanes. This R&D is underway.

4.2.4.2.7 Packaging

It is assumed that the DTC will be a double-width, full-height MCH-type μTCA module. There are two variations possible, depending on the type of backplane which can be obtained:

- DTC in MCH slot 1; commercial MCH in slot 2
- DTC in MCH slot 1 (performs essential MCH functions)

It is difficult to combine a commercial MCH and a custom DTC in the same MCH site, since no power supply connections are available on MCH connectors 2-4.

4.2.5 R&D for Phase 1

The following list summarizes the R&D needed for Phase 1:

1. Electrical and/or optical decoding unit (prototyping, production, assembly)
2. SiPM characterization and vendor determination
3. RBX mechanics (cooling, prototyping, production, assembly)
4. GBT validation and FPGA simulation

5. μTCA prototyping and production
6. QIE radiation characterization, redesign, prototyping and production
7. Front-end controls (CCM, slow controls, and TTC evolution)

4.2.6 Implementation and Infrastructure Issues

As discussed above, it is important that the back-end plan be staged in such a way that prototypes can be commissioned quasi-statically and run parasitically during the first phase of CMS running at the LHC. The key component in such a requirement will be the digital data on the current fibers, and the data rate that HCAL currently uses (1.6 Gbps 8B/10B encoding). To make the UberHTRs backwards compatible means that the prototype boards must be able to receive data at the current 1.6 Gbps rate and encoding scheme, and also at the higher rate using the CERN GBT rate of approximately 4 Gbps with an as yet unfinalized protocol (unfinalized but not expected to be the usual and current gigabit Ethernet physical protocol "8B/10B"). This requirement can, however, be implemented in one of the more current Xilinx or Altera FPGAs, which support differential high speed signals to be decoded by a built-in deserializer. The as-yet-to-be-finalized protocol for the GBT project will be handled with a logic core that will be supplied by the CERN GBT group, as is their commitment to CMS and HCAL. The new back-end will be designed so that it is capable of running with an existing HCAL front-end for a year to gain full confidence in the system.

The current electronics testing and commissioning facility in Building 904 will play an important role for the HCAL upgrade. Running prototype back-end systems will be brought up in 904 before moving to Point 5, and prototype front-end systems can be integrated and tested with the new back-end electronics. HCAL will therefore need a presence in 904 for the foreseeable future.

4.2.7 Alignment with possible Phase 2

The electronics upgrade for Phase 1, both front-end and back-end, will be constructed such that it will be able to be used for any possible Phase 2 upgrade. This requirement is fairly straightforward with respect to the electronics capability (bandwidth, etc), however it places a greater specification for radiation tolerance. HCAL will necessarily require that all front-end electronics meet with the radiation specification for 10 years of operation at 5×10^{34} cm^{-2}s^{-1} luminosity. We will update the projected radiation contour maps for this condition, and test all electronics to the appropriate levels for both total dose and instantaneous rate single-event effects.

4.2.8 Schedule

The Phase 1 HCAL upgrade is focused on producing new electronics on both the front-end and back-end. The front-end electronics will have new analog-to-digital conversion, new requirements for services in the existing front-end readout boxes, and new transmitters using the current fibers. R&D towards production will necessarily require extensive testing in test beams. The test beam schedule at CERN, typically with a run each summer, constrains some of the important milestone dates in the HCAL upgrade schedule. The following are plans for the next 3 slice tests that will result in a project that can be commissioned in 2015:

1. Summer 2009. Validate half density EDU with SiPM devices.

3648 2. Summer 2010. Test TDC circuits, prototype FPGA card and front-end to back-end high
3649 bandwidth communication with prototype μTCA readout.

3650 3. Summer 2011. Extensive comparisons between possible SiPM devices and possible ODU/EDU
3651 readout configurations. Test prototype cooling system for ADC and FPGA cards. Take
3652 data with first μTCA preproduction prototype crate and cards.

3653 4. Summer 2012. Test new QIE cards with pre-production front-end electronics cards, using
3654 μTCA prototypes. Test final candidates for SiPMs and ODU/EDU and finalize the analog
3655 section of the FE electronics. Evaluate GBT performance.

3656 5. Summer 2013. Pre-production prototype with final SiPM and final FE analog and digital
3657 electronics. Validate pre-production FE/BE electronics including all needed RBX services
3658 and integration issues.

3659 We indicate below those aspects most critical to the upgrade timeline.

3660 • RM assembly. Assembly of all boards into the RMs must begin by 2015 to be ready
3661 for extensive burn-in at the building 904 electronics integration center and the sub-
3662 sequent Phase 1 shutdown, when installation and commissioning begins.
3663 • Front-end boards. FE boards (FPGA + GBT + laser) must be ready for production by
3664 the end of 2013 so that RM assembly can begin in 2015.
3665 • GBT and front-end boards. The GBT project calls for production to begin in 2012,
3666 which means that the HCAL front-end boards have to be designed and ready for
3667 GBT inclusion in 2013.
3668 • Front-end controls. All FE control R&D must be completed by 2013 in time for inte-
3669 gration tests in the 2013 testbeam.
3670 • QIE. New QIE chips (QIE10) development began in 2009 and will finish in 2012
3671 for the analog section and in 2013 for the digital section, followed by 6 months of
3672 production, ending in early 2014.
3673 • QIE card. QIE card production, QC, and calibration begins in 2014, completing by
3674 late 2014 in time to meet the RM assembly, with contingency.
3675 • EDU/ODU. R&D, preproduction, and prototyping began in 2009, takes several test-
3676 beams to go through the development cycle, finishing in the summer of 2012, fol-
3677 lowed by 1.5 years of production and assembly and QC, finishing at the beginning
3678 of 2014 in time for RM integration.
3679 • SiPM. General R&D began in 2008. Vendor selection, procurement and delivery will
3680 begin in 2011 and last until January 2012. QC and assembly will being in mid 2012
3681 and last until the beginning of 2014, in time for RM integration.
3682 • μTCA. R&D and preproduction is already in progress, with increasing complexity
3683 tested during the 2009, 2010, and 2011 testbeams. Production and QC will begin in
3684 the fall of 2011, lasting until mid 2012 and take at least 1 year but will be in time
3685 for final installation and commissioning in advance of the 904 burn-in and Phase 1
3686 shutdown. Note that pre-production crates and electronics will be installed at Point
3687 5 to be used parasitically with real HCAL data following the 2012 shutdown.
3688 • Fiber optics. HCAL plans to keep the current fiber optics infrastructure, but we
3689 envision that a patch panel will be needed for the redistribution of the fibers. Plans
3690 call for the fiber patch panel R&D to begin in mid 2011 and take 1 year, to be ready
3691 for installation at point 5.

4.2.9 Conclusion

Recently CERN has defined the schedule for operations and shutdowns over the next two decades and has stated the goals for delivering luminosity during this period. The first phase of this plan will already require upgrades to the hadron calorimeters to deal with radiation damage and increased occupancy that would otherwise degrade the performance of these detectors, which play a key role in many CMS physics investigations. The key element in the upgrade is the replacement of HPDs with SiPMs, a new photodetector technology that has recently become available. The low cost, high gain, and compactness of the SiPMs permit the introduction of more longitudinal segmentation and the provision of detailed timing information. The SiPMs that are required for the HO are currently available. More R&D is required to obtain SiPMs that will satisfy the more demanding requirements for the upgrade of the HB and HE. The use of SiPMs to improve the CMS calorimeters result in more data to be read out and provides better information to the trigger. This in turn requires changes to all the front end and back end electronics. CMS has developed a strong plan to make these changes over the next 5 years. This plan will guarantee good performance from the hadron calorimeters through the Phase 1 period and will provide a solid foundation for an upgrade to handle the even higher luminosity of Phase 2.

Chapter 5

Forward Rapidity Calorimeter Systems

Introduction

The forward rapidity calorimeters make use of quartz radiators to produce Cherenkov light. The choice of quartz is driven by radiation hardness requirements. The rapid time response of Cherenkov radiation is also a benefit in the high occupancy environments of the forward calorimeters. As the Cherenkov process produces less light, the number of photoelectrons per GeV of energy deposited in the calorimeter is two orders of magnitude smaller than the plastic scintillating tile with WLS readout of the HB, HE, and HO calorimeters.

The forward calorimeter readout uses high gain photomultiplier tubes (PMT) and must contend with fringe fields from the CMS solenoid. The PMT window material and UV transmission sensitivity of the fibers and light guides are also affected by the high radiation environment of the forward rapidity regions. Due to the low yield of photoelectrons (due to the low number of photons) per deposited energy, currently 0.25 photoelectron per GeV in the HF, any interactions with the fibers outside of the calorimeter or with the photodetector window material can generate signals that are as large as those made by 1 TeV of energy deposited in the calorimeter. In fact, the 11m long decay path between the collision point and the HF detectors, allows in-flight decay from hadrons from minimum bias events to produce muons that pass directly through the photodetector window material with similar (though not identical) timing and signal-correlated properties as normal events. Other sources of anomalous signals in the forward calorimeters are also present. These non-calorimeteric sources of Cherenkov light in the readout system place additional constraints on the forward calorimeters that are further complicated by high instantaneous luminosity operation.

The following sections describe the current problems seen in the forward calorimeter systems and the plans for repairs, improvements, and upgrades to these systems through 2016. There are separate sections describing the forward hadron calorimeter (HF) and CASTOR. The 2012 shutdown work for the zero-degree calorimeter (ZDC) involves the installation of lifting equipment already foreseen in early running.

5.1 Forward Hadron Calorimeter (HF)

The Hadron Forward (HF) Calorimeters consist of two modules, located symmetrically at about 11 m from either side of the interaction point (IP), covering a pseudorapidity range of $3 \leq |\eta| \leq 5$. By extending the reach of the central calorimetry, the HF plays an important role in identifying tagging jets, determining missing E_{T}, and measuring the luminosity.

By providing forward jet tagging capability, the HF calorimeters enhance the CMS physics program. Of the major modes of Higgs production at the LHC, Vector Boson Fusion (VBF) is

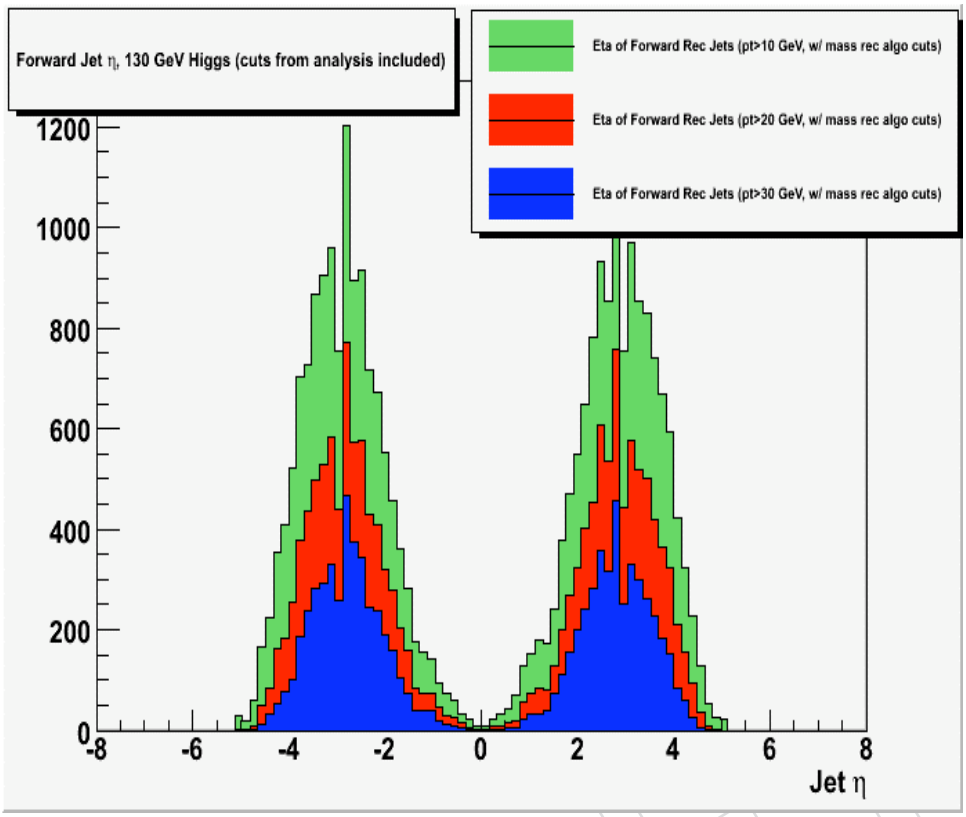

Figure 5.1: Forward jet η distribution for 130 GeV Higgs mass in the qqH channel. The analysis selection is applied, and the three different histograms indicate levels of the p_{T} threshold on the forward jets: $p_{\mathrm{T}} > 10$, $p_{\mathrm{T}} > 20$, and $p_{\mathrm{T}} > 30$ GeV/c.

the second most dominant mechanism for Higgs production. Forward jets (especially in VBF) extend Higgs boson coupling measurements and complement the measurement of the light Higgs boson width. Also, HF extends the $|\eta|$ coverage to 5 and thus provides better coverage for missing E_{T} measurements (important for many BSM searches). Figure 5.1 shows the η distribution of the forward jets after appropriate analysis cuts are applied to select the qqH final state. With a 10 GeV/c transverse momentum requirement on the jets, about 77% of the total events have at least one jet in the HF region. If the forward jet p_{T} cut is tightened to 30 GeV/cm, the fraction remains above 70%. This suggests that a precise forward jet measurement with HF is necessary e.g. for this particular Higgs discovery channel.

Each HF calorimeter consists of 36 steel wedges forming an approximately annular ring of absorber, extending from a radius of 12.5 to 120 cm, from the beam line in the forward direction, 11m from the interaction point. The length along the beam is 1.65 m or $10\lambda_{abs}$. Quartz fibers (QF), the active component of the calorimeter, are embedded throughout the steel absorber in evenly spaced grooves that run parallel to the beam axis. Half of the fibers in alternating grooves run the full length of the absorber; the other half, read out separately, start 22 cm back from the absorber front face. The fibers are bundled to divide the calorimeter into 13 segments in rapidity, and 72 segments in φ for a granularity of $d\eta \times d\varphi = 0.175 \times 0.175$, with the exception of the two innermost rings, which have half the φ segmentation. The fibers are read out with photomultiplier tubes. The segmentation of the HF gives a total of 864 readout channels per module for a total of 1728 channels.

The QF in HF are plastic-clad fibers (QPF), and the high $|\eta|$ ring (ring 10-13, η = 4.5-5.0) may

have 50% losses after 10 years at $\mathcal{L} = 10^{34}\,\mathrm{cm}^{-2}\,\mathrm{s}^{-1}$ which is about 1 Grad. These predictions do not take into account recovery of the fibers between exposures. We expect the fibers to recover at least 20% at each shutdown. There are fluorine-doped silica cladding fibers (QQF), which can stand ∼20 Grads, with ≤ 10% light loss, but the choice of QPF was driven by the cost (QQF fibers cost ∼5 times more than QPF fibers).

The photo-detectors in HF are PMTs manufactured by Hamamatsu (R7525HA), and they are well shielded. They have 8 stages of dynodes, a 25 mm diameter bialkali photocathode, a borosilicate glass window of average thickness 0.6 cm, and a maximum quantum efficiency (QE) at 450 nm of 22%. The PMTs would receive a radiation dose of about 8-10 krad/ 10 years at $\mathcal{L} = 10^{34}\,\mathrm{cm}^{-2}\,\mathrm{s}^{-1}$ ($\sim 10^{12} n/cm^2$/10 years at 10^{34}). The PMT windows (borosilicate glass) have significant damage (induced absorption with more than 20-30% loss of transmission at 420 nm) after ∼120 krad (gamma-irradiation); for neutrons, the effects are smaller except for fluences above $2.5 \times 10^{14} n/cm^2$.

5.1.1 Large Energy Events in HF PMTs

Although the HF detectors are hermetically shielded (by ∼40 cm of concrete, and 5 cm of polyethylene) from stray particles, a small fraction of the muons produced by the proton-proton collisions or by the cosmic rays are likely to reach the readout region and register signals that mimic very high energy events (referred to as PMT events). The PMT events occur when a muon or other energetic charged particle traverses the PMT window glass, producing a large number of Cherenkov photons. The PMT events can also be produced by charged particles from late showering hadrons in HF. These events can be tagged and rejected in off-line analysis with, on average, ∼80% efficiency (which is too low for sensitive searches for new particles). The PMT events can cause problems in trigger rates by producing fake missing transverse energy. Also, luminosity monitoring and minimum bias event triggering can be affected by PMT events. The real impact on physics is being investigated using detailed Monte Carlo simulations.

The HF PMT events were observed in the 2004 HF test beam data. The average signal recorded by a single calorimeter readout channel from an x–y position scan of muons passing through the entire system of iron absorbers, quartz fiber bundles, and the PMT window is shown in Figure 5.2. The figure clearly shows signal enhancement regions corresponding to interactions in the fiber bundle and a hot region corresponding to the PMT window. For 150 GeV muons traversing the PMT glass, the generated signals are equivalent to 120 GeV (Figure 5.3) pions impacting the HF absorber. This is equivalent to ∼30 photoelectrons. There is a long tail associated with these events that extends out to nearly a TeV. Such events have already been observed in the early running at the LHC.

HF is a stand-alone device. There is no tracker or electromagnetic calorimeter in front, no muon system behind, and only two quite non-independent segmentations. Furthermore, the DAQ system does not even remotely make use of most of the raw performance characteristics or most of the information produced by the PMT - fake events are easily identified using an oscilloscope. Reducing the fake events is therefore both crucial and possible.

5.1.2 HF PMT System Upgrade

We propose as an upgrade replacing the present R7525 with a new PMT having the following properties:

- a thin (< 1 mm) front window that reduces the amount of Cherenkov light;

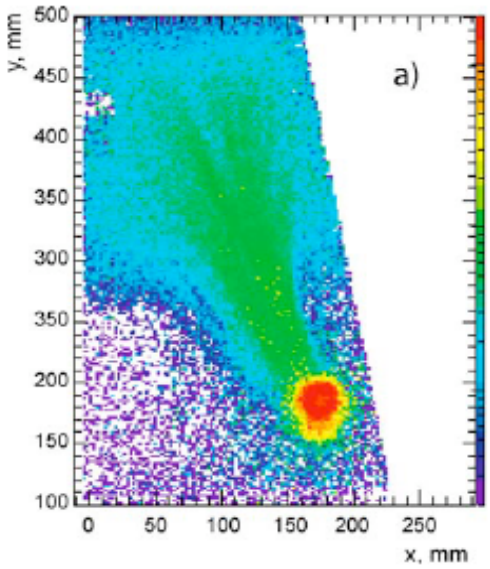

Figure 5.2: The average signal from muons passing through the entire system of HF iron absorbers, quartz fiber bundles and the PMT window, recorded as an x–y position scan with $2 \times 2\ mm^2$ resolution and using a single calorimeter readout channel. Signal enhancement regions from particles passing through the PMT window (red circle) and the quartz-fiber light guide bundle (green fan-shaped wedge extending from the PMT window upward and to the left) are clearly visible.

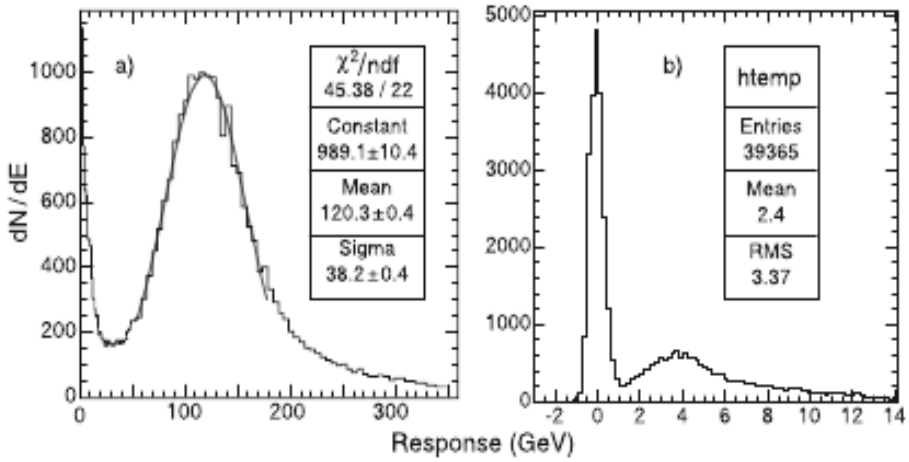

Figure 5.3: High energy muons impacting the PMT glass generate spuriously large energies (a). The response distribution clearly shows the single photoelectron peak at 4 GeV, as expected (b).

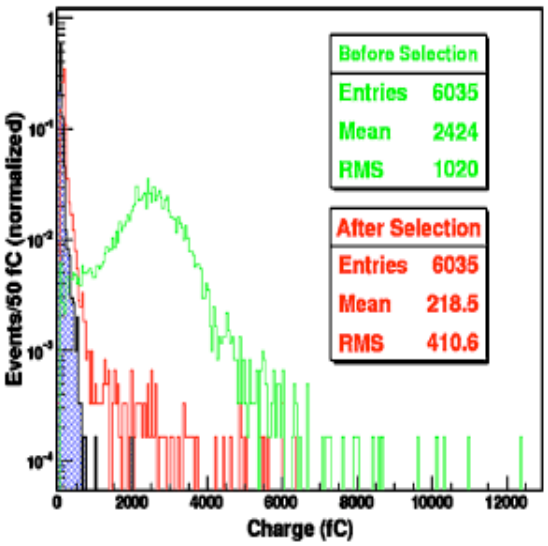

Figure 5.4: PMT window event selection and signal recovery for the four anode PMT with front incidence of muons. No pedestal subtraction was applied to the data. The blue, crossed area is the pedestal.

- a metal envelope that further eliminates Cherenkov light made by particles traversing the side of the PMT;
- 45% peak QE; and
- four-way segmented anodes that allow further rejection of PMT events by using the pattern of light distribution among the anodes, which is different than signals coming from energy deposited in the HF absorber.

We developed and tested a simple tagging and signal recovery algorithm for the four anode PMT. Figure 5.4 demonstrates the application of this algorithm to the front incidence data with a 150 GeV/c muon beam in the CERN H2 beamline. The algorithm proves to be more than 96% efficient. The initial proposal is to use the planned HCAL electronics upgrade to provide two readout channels per PMT, each channel being the sum of two anodes. A future upgrade allowing all four channels to be read out separately is not precluded.

5.1.3 Other Sources of Anomalous Signals in HF

While Cherenkov light from the PMT windows is the dominant source of anomalous signals in HF, there is a secondary contribution from broad scintillation signals tens of nanoseconds after the pp interaction due to albedo background at P5. The primary source of this scintillation is a short section of mirror material used in the connection between the light-guides and the PMTs. Possible other scintillation sources, such as the epoxy used in the fiber bundles, are believed to contribute much less to high energy anomalous signals.

The connection between the light guides and the PMTs will be replaced along with the PMTs. The new design will match the cross-section of the original light-guides to the new PMTs, and will utilize non-scintillating material.

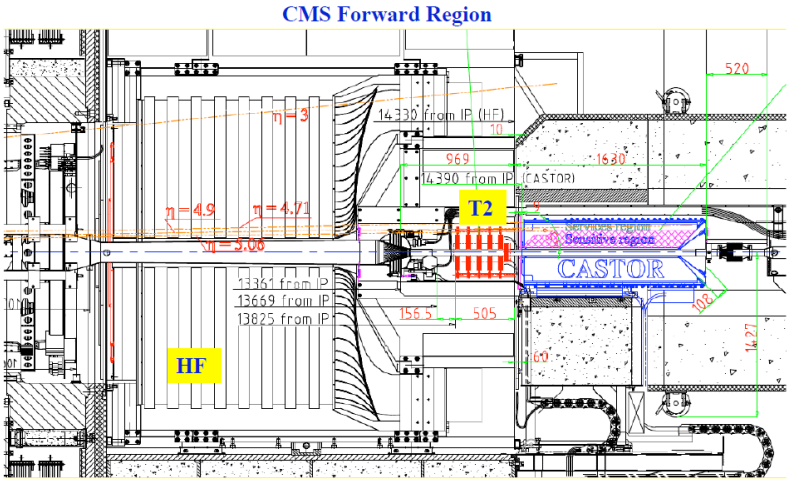

Figure 5.5: Location of CASTOR in the CMS forward region.

Figure 5.6: CASTOR calorimeter and support.

5.2 CASTOR

The CASTOR detector is a quartz-tungsten sampling calorimeter, installed at 14.38 m from the interaction point, covering the pseudorapidity range $-6.6 < \eta < -5.2$. The detector is designed for the very forward rapidity region in heavy ion and proton-proton collisions in CMS. The detector is built in two halves that surround the beam pipe when closed. The clam shell design allows the detector to be removed without disturbing the beam pipe or breaking the vacuum. It was proposed originally to have a CASTOR module on each side of the interaction region. For financial reasons, only one module has been built, and is installed on the negative rapidity side of CMS.

Figure 5.5 shows the location of CASTOR relative to other components of the CMS detector. The support system with CASTOR in the closed and open position is shown in Figure 5.6.

CASTOR is a Cherenkov-based calorimeter constructed from layers of tungsten plates as absorber interleaved with quartz plates as the active medium. It has two sections: an electromagnetic section (EM) with ten sets of 5.0 mm tungsten plates and 2.0 mm quartz plates; and a hadronic section (HD) with sixty 10.0 mm W plates and 4.0 mm quartz plates. The plates are inclined at 45° to maximize the collection of the Cherenkov light. The Cherenkov light from the

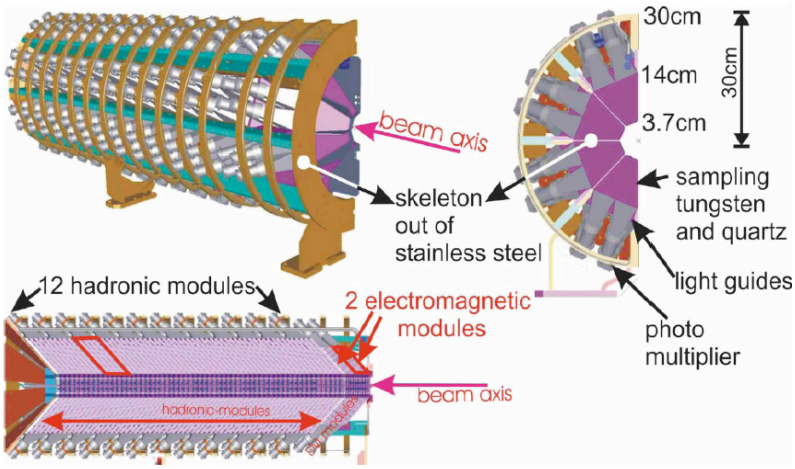

Figure 5.7: Details of the components and geometry of the CASTOR calorimeter

quartz is collected and focused by air light guides onto Hamamatsu R5505 phototubes. Each light guide collects the light from 5 quartz plates. Figure 5.7 shows the detailed layout of the detector.

CASTOR is installed in CMS and is operating for the 2010-2011 run. However, the fringe field in this region was found to be significantly higher than expected (see the discussion below). As a result, a different phototube model had to be chosen than the one originally planned, and the phototubes must be operated with high voltage settings and gains which are non-uniform.

The present phototubes must be replaced with more radiation hard phototubes for long term operation, and modifications to the magnetic shielding are highly desirable to achieve a more uniform detector response. Additionally, improvements are needed to establish good calibration and monitoring. The planned improvements are described below.

In order to carry out these improvements, CASTOR must be removed from the CMS collision hall and brought to the surface. Some of the work involves improving the mechanical stability of various support structures, improving the shielding from the fringe field of the CMS solenoid, and monitoring the position of the beam pipe, which is very close to CASTOR. These tasks are undertaken by CMS Technical Coordination in consultation with the CASTOR team.

5.2.1 Detailed description of tasks

5.2.1.1 Consolidation work on CASTOR

CASTOR was constructed and instrumented during the first 6 months of 2009. Under time pressure to complete the installation ahead of the final CMS closing and LHC startup, some of the work was not done at the design level. Although the calorimeter worked well during the 2009 and 2010 LHC run, some improvements are still pending. This work is enumerated below:

1. Exchange some of the EM and HAD light guides, which were slightly damaged during installation.

2. Exchange the damaged fibers and increase the number of the LED fibers that go to the light guides, as well as the fibers connecting the LED source to the patch panel.

3. Construct a new LED pulser with more outputs and independent firing, for a more efficient operation.

4. Construct a new patch panel using a PCB, for easier connection, possibility of changes and maintenance in situ.

5. Develop and execute procedures for gain/signal equalization of the new PMTs (see below), using the new LED system.

6. Repair the far side of the outer circuit of the cooling system, which developed a small leak after an accidental hit during the closing of the collar shielding.

5.2.1.2 Exchange R5505 PMTs with the equivalent radiation hard model R7494

The original information on the strength of the stray magnetic field in the CASTOR region predicted a field of the order of 10 Gauss. Based on this, the CASTOR team purchased the R7378A standard dynode, radiation hard PMT from Hamamatsu. However, it was discovered in 2008 that the B-field in the forward region was higher by a factor of more that 20. This necessitated the use of fine-mesh PMTs, capable of running in a high field environment. Due to the very short time and lack of money, DESY donated 250 units of the R5505 fine-mesh PMTs from the H1 SPACAL calorimeter. These PMTs have a borosilicate window and are not radiation hard. They are being used in the 2010-2011 LHC run, when the integrated luminosity is expected to be 1 fb^{-1} and the received dose within tolerable levels. The radiation environment near CASTOR and its PMTs is shown in Fig. 5.8. Irradiation results for the R5505 PMTs are shown in Fig. 5.9.

For the high luminosity pp and the subsequent heavy ion running beyond 2012, a radiation hard version, R7494, of the fine mesh R5505 is required. These PMTs, with synthetic silica window, will withstand the dose collected for more than 20 fb^{-1} of integrated luminosity. Irradiation tests on the similar window R7378A PMTs gave excellent performance up to 20 Mrad tested, as shown in Fig. 5.10.

The installation of the new PMTs will be followed by gain studies with LEDs and possibly with a radioactive sourcing system.

The funds for the purchase of these PMTs (cost $\sim$550 kCHF) are being collected. At present the amount of 310 kCHF has been secured from Brazil (210 kCHF) and Adana (100 kCHF). The remainder is expected to be pledged soon. The purchase order should be placed by the end of 2010 for full delivery and testing (at Adana) by end of 2011.

5.2.1.3 CASTOR Gain/Signal Equalization Issues

The adverse effects of the strong magnetic field still remain for $\sim$2-3 sections at the center of CASTOR (in the gap between the Collar and Rotating shielding), where the direction of the field is almost perpendicular to the axis of the PMT. To partially compensate for this, the HV to these PMTs was increased to close to the limit and the HV values of other PMTs were changed for signal equalization. These changes of the HV settings negate any gain/signal equalization, obtained in the absence of magnetic field (beam test, calibration with sources).

CASTOR faces a very difficult gain/signal equalization task, due to the strong variation of the response along the length of the calorimeter due to the fringe field of the CMS solenoid magnet. Therefore, any calibration should take place in situ with the solenoid magnet at 3.8T. The possible use of halo muons, with a specific muon trigger, is being investigated for such a study. The

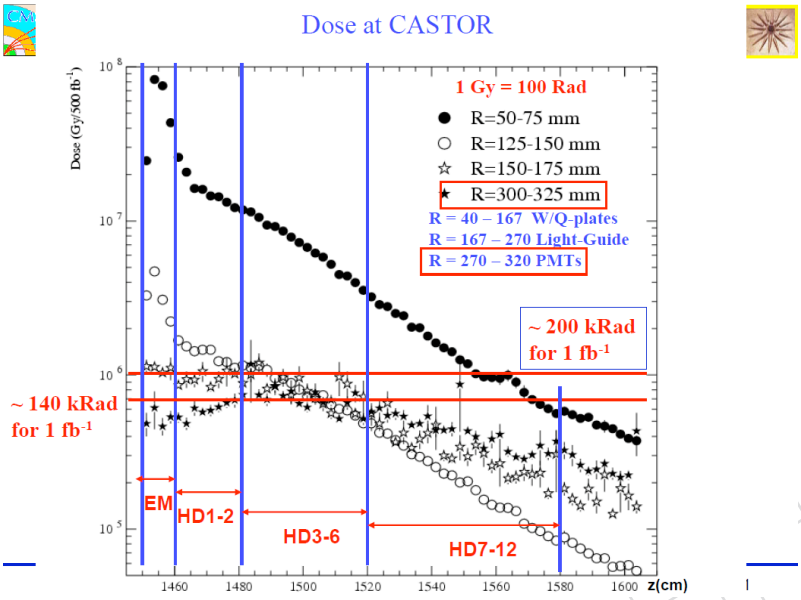

Figure 5.8: Radiation environment of CASTOR and its PMTs.

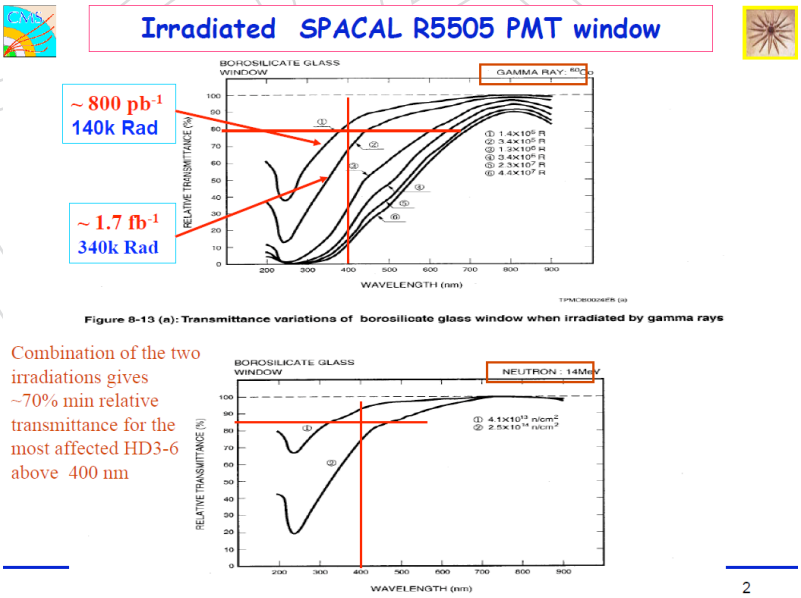

Figure 5.9: Irradiation results for R5505 PMTs.

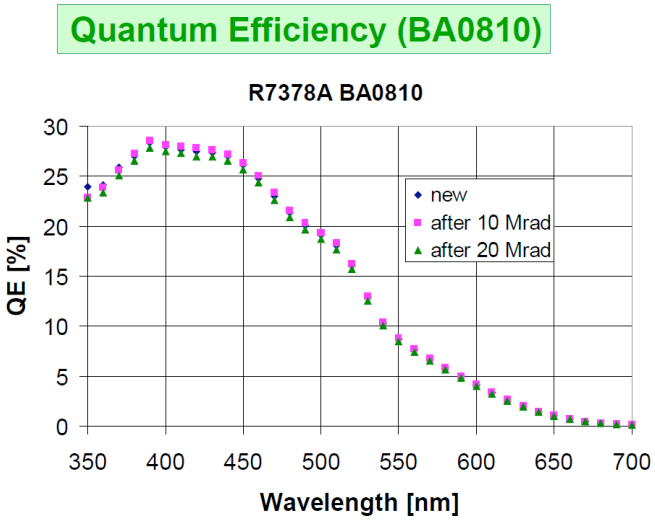

Figure 5.10: Gamma irradiation results for a R7378A PMT with synthetic silica window (same as in a R7494 PMT).

feasibility of a radioactive source system similar to the system used for HF is also being discussed. This source calibration would be accomplished during the 2012 shutdown. The most efficient solution, however, will be to minimize the stray field and this is being investigated. The idea is to fill this gap with thin iron sheets, a task that will be done during the 2012 winter shut down.

5.2.2 Work details and schedule

5.2.2.1 Work in 2012 with Castor moved to the surface lab

The various tasks and the institutional responsibility for them is listed:

1. Exchange light guides (DESY, Athens, Adana)
2. Exchange R5505 PMTs with the radiation hard version R7494 (Antwerp, DESY, Brazil)
3. Exchange LED fibers (Athens, Adana, Brazil)
4. New LED pulser (Antwerp, ITEP)
5. Exchange Patch Panels and check mappings (Antwerp, DESY, Brazil)
6. Signal/gain equalization with LED (DESY, Antwerp, Adana)
7. Repair water leak in half cooling system (CMS Technical Coordination)
8. Sourcing of full calorimeter (DUBNA, Athens, Adana)

Estimated time for this work is 5-6 months from the time when CASTOR arrives in the above-ground workspace.

5.2.2.2 Work coordinated with CMS Technical Coordination

In addition to the work described above, CMS Technical Coordination will make various improvements in the infrastructure supporting CASTOR. Some key elements of this work are:

1. Radiation-shielding box for calorimeter - This shielding box is not needed for the initial removal of CASTOR in 2012, but will be part of the installation and removal procedure thereafter. It must be ready before CMS closes again in 2012.

2. Improvement of the magnetic field situation in the CASTOR region. This will require new magnetic shield pieces to be installed in 2012.

3. Installation of monitoring for the beampipe temperature, local deformations, humidity, and possibly magnetic field.

Additional details may be found in chapter 10.

Chapter 6

Pixel Detector Improvements and Upgrades

At the heart of CMS is the silicon pixel detector [7]. It aims to provide three high-precision space point measurements to reconstruct charged particle trajectories. These three points are sufficient to produce good track information for the High Level Trigger (HLT) and for the efficient seeding of the reconstruction of longer tracks in the full tracker volume. The close proximity of the first detector layer to the interaction point (4.4 cm) minimizes multiple scattering effects and extrapolation uncertainties making the pixel information crucial for the reconstruction of the initial position and direction of the charged tracks. The pixel detector therefore plays a key role in the identification of primary vertices, secondary vertices, and secondary tracks. These elements are essential for the efficient identification of long lived particles, such as b quarks, and for the search for new physics at the LHC.

The present CMS pixel detector was conceived over 10 years ago and designed for a maximum luminosity of $1 \times 10^{34}\,\mathrm{cm}^{-2}\mathrm{s}^{-1}$. Following the Phase 1 upgrade of the LHC, the peak luminosity is foreseen to reach $2 \times 10^{34}\,\mathrm{cm}^{-2}\mathrm{s}^{-1}$ before the next long shutdown. The present pixel system will not be able to sustain such extreme operating conditions due to large data losses in the read out chip (ROC) and must be replaced in the long shutdown of 2016. This is the best, and perhaps only, opportunity to install and commission a new system before the luminosity will exceed $1 \times 10^{34}\,\mathrm{cm}^{-2}\mathrm{s}^{-1}$. The modular design of CMS allows good access to the pixel system, which can be extracted relatively easily, independently of the beam pipe or the strip tracker.

The baseline plan presented here is to replace the current system with an ultra-light pixel detector, with improved ROCs, having four barrel layers and three end-cap disks. The conceptual layout for the Phase 1 pixel detector is shown in Figure 6.1. The addition of the fourth barrel layer at a radius of 16 cm and the third forward disks will maintain the present level of tracking performance even in the high occupancy environment of the upgraded LHC. In addition, it provides a safety margin in case the first silicon strip layer of the Tracker Inner Barrel (TIB) degrades more rapidly than expected.

This upgrade of the pixel system will address all of the following shortcomings of the current detector:

- The most severe limitation is the ROC, which is just adequate at the LHC design luminosity of $1 \times 10^{34}\,\mathrm{cm}^{-2}\mathrm{s}^{-1}$. At this luminosity, buffer size and readout speed limitations are estimated to produce a dynamic inefficiency of 4% ($> 16\%$) if the bunch spacing time is 25 ns (50 ns). The dynamic inefficiency increases exponentially with increasing luminosity. At $2 \times 10^{34}\,\mathrm{cm}^{-2}\mathrm{s}^{-1}$ and 25 ns bunch spacing the ROCs in the inner region will suffer an inefficiency of 15%, leading to a major degradation of the overall level of tracking performance.
- The three-hit coverage of the detector is not completely hermetic, leading to 10-

15% inefficiencies at $|\eta| < 1.5$ and larger track seeding inefficiencies in the region $1.5 < |\eta| < 2.5$. This limits the efficiency of HLT tracking triggers and slows the full tracking algorithm. The situation will degrade even further at higher luminosities.

- The radiation hardness of the detector is not sufficient for operation up to the end of Phase 1, when the integrated luminosity will be around 350 fb^{-1}. Although the detector was constructed using the most radiation resistant technology known at the time of its fabrication, radiation damage will degrade its performance and necessitate replacement of the inner regions.
- The detector contains significant passive material that degrades tracking and calorimetric measurements due to multiple scattering, photon conversions and nuclear interactions.

The goal of the Phase 1 upgrade is to provide a pixel detector that can maintain a high efficiency at a luminosity of $2 \times 10^{34}\,\mathrm{cm}^{-2}\mathrm{s}^{-1}$, with less material, and will provide 4 hits over pseudorapidities up to 2.5. In the years since the design of the current detector, innovations in cooling, power distribution, mechanical support, CMOS electronics, and sensor materials enable the construction of a significantly more performant detector.

Radiation damage is still expected to significantly degrade the performance of the innermost regions during the three year Phase-1 run beginning in 2017. The position resolution of the detector will worsen by roughly a factor two after a fluence of $10^{15}\mathrm{n_{eq}cm}^{-2}$. The dynamic inefficiency is expected to be greater during the second half of this run as the luminosity increases. We are therefore considering the development of replacement parts based on smaller pixels, a more radiation-resistant sensor technology, and an improved readout chip based on a denser CMOS technology. The replacement would occur near the middle of the run and would ensure that detector performance increases rather than decreases during the period when the largest data samples are being acquired.

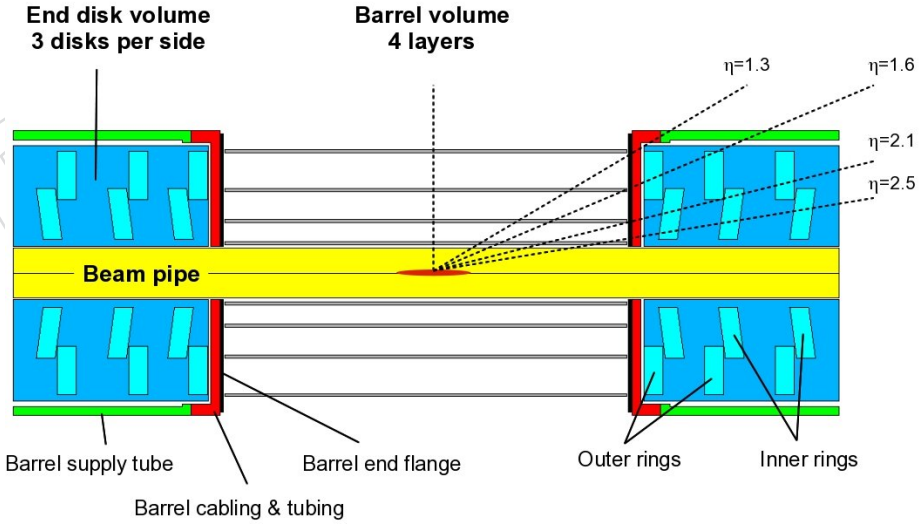

Figure 6.1: Schematic view of the Upgrade Layout. It consists of four barrel layers and three endcap disks on each side, with each disk separated into an inner and outer ring. The disks are placed in locations so as to maximize the 4-hit η coverage.

The implementation of the Phase 1 pixel detector would largely improve all aspects of CMS tracking:

- The addition of the extra layers will dramatically improve the efficiency and resolu-

tion of pixel-only tracks. Pixel tracks are a crucial part of the HLT and they are also used to seed the full tracking, leading to an increase of the efficiency and a decrease of the fake rate for full tracks.

- The decrease in the amount of material and the increase in the number of measurement points improve the resolution of all track parameters. In particular, the resolution of longitudinal and transverse impact parameters are significantly improved.
- The efficiency and resolution enhancements lead to much improved primary and secondary vertexing. Vertexing is essential to associate the final state particles with the correct primary vertex in the high pile-up LHC environment. Secondary vertexing plays a key role in b-tagging and the search for various long-lived exotic states.
- The improvements in tracking efficiency, fake rate, parameter resolution, and vertexing all contribute to significant improvements in the b-tagging performance of the tracker. The b-tagging performance for the present and upgraded detectors is shown in Fig. 6.2 for operation at an instantaneous luminosity of $2\times10^{34}\text{cm}^{-2}\text{s}^{-1}$ with 25 ns bunch spacing, or equivalently, $1\times10^{34}\text{cm}^{-2}\text{s}^{-1}$ with 50 ns bunch spacing. The upgraded detector would reduce the light quark background of the Combined Secondary Vertex Tag by about a factor of 6 for a b-efficiency of 60%, or conversely, it would increase the b-quark efficiency by approximately 30% at the fixed light-quark efficiency of 1×10^{-2}.

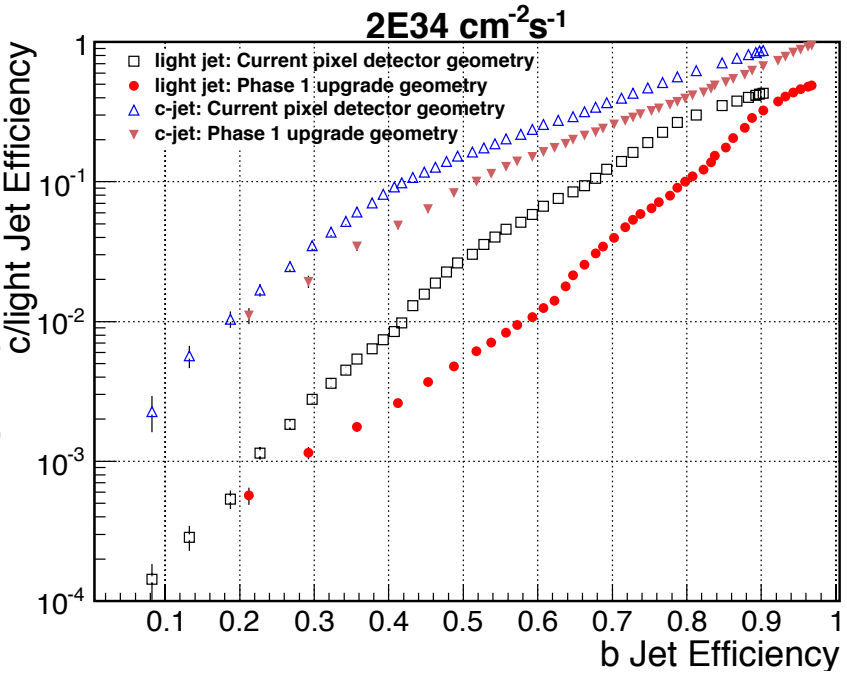

Figure 6.2: The light quark and b quark efficiencies of the Combined Secondary Vertex b-tagging algorithm are shown for the present and upgraded detector (with inner radius of 3.9 cm, 285 μm thick sensors and $100 \times 150\,\mu\text{m}^2$ pixels) at an instantaneous luminosity of $2\times10^{34}\text{cm}^{-2}\text{s}^{-1}$ with 25 ns bunch spacing.

In this chapter we outline the basic performance characteristics of the current pixel detector. We also point out some of the factors that limit its performance, and describe the proposed improvements to the mechanics, layout and electronics which would significantly enhance our physics capabilities during the first stages of the major upgrades to the LHC. This upgrade to the pixel detector significantly improves charged particle tracking for CMS and greatly en-

hances the experiment's physics reach during the crucial Phase 1 upgrade to the LHC when a large fraction of the luminosity will be delivered.

6.1 Performance of Current Detector

In this section, we discuss in more detail the performance of the current pixel detector and enhancements that the proposed detector upgrade will provide.

6.1.1 Electronics and Readout

The current pixel readout electronics were designed and optimized for the data rates and pixel occupancies expected up to the LHC design luminosity of $1 \times 10^{34}\,\mathrm{cm}^{-2}\mathrm{s}^{-1}$. There will be a dynamic inefficiency of about 4% from the current readout chip, PSI46v2, at this luminosity in the innermost layer. These losses are shown in Figure 6.3 as a function of the level-1 trigger accept (L1A) rate as measured in test beam runs with particle fluxes as expected for LHC design luminosity [8]. At the nominal L1A accept rate of 100 kHz, the data loss will increase to 16% in the innermost layer as the luminosity goes up by a factor of two (for 25 ns bunch crossing) to $1 \times 10^{34}\,\mathrm{cm}^{-2}\mathrm{s}^{-1}$. These losses are understood by simulations and characterizations of the PSI46v2 readout chip to be coming from two sources: the column drain dead time (0.8%) and readout-related losses (3.0%). Hit pixels are transferred using column drain readout to the chip periphery where the hits are stored in buffers during the L1 trigger latency (3.2 μs). If instead the LHC runs with 50 ns bunch spacing at $2 \times 10^{34}\,\mathrm{cm}^{-2}\mathrm{s}^{-1}$, then the data losses continue to increase almost exponentially, with losses on the order of 50% for the innermost layer for example.

Figure 6.4 illustrates the impact on performance of charged particle tracking from these data losses. In these simulated $t\bar{t}$ events at instantaneous luminosities of $2 \times 10^{34}\,\mathrm{cm}^{-2}\mathrm{s}^{-1}$ with 25 ns bunch spacing, we see substantial decreases in the tracking efficiency. These high luminosities also lead to a large fake rate even without the previously mentioned data losses. The degradation with 50 ns bunch spacing would be substantially worse. The conclusion is that the current readout chip is not able to cope with these rates in the innermost layers of the pixel detector.

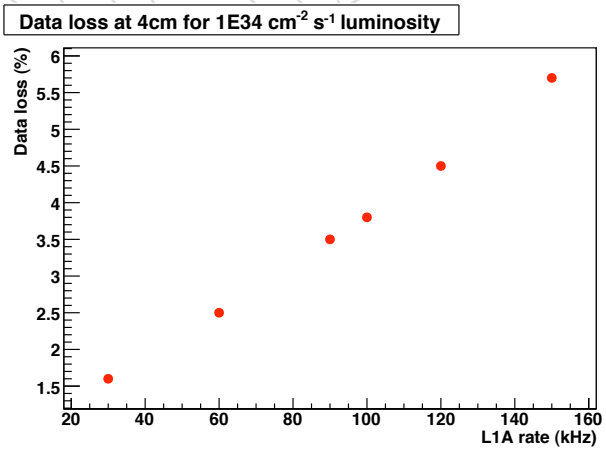

Figure 6.3: Left: Data losses as a function of the L1 accept rate of the innermost layer of the current pixel detector [8]. The instantaneous luminosity is $10^{34}\,\mathrm{cm}^{-2}\mathrm{s}^{-1}$ and the bunch spacing is 25 ns. CMS has been designed for maximum average L1 trigger rates of 100 kHz. The data points beyond this rate in the plot simply illustrate the linear nature of this data loss at this particular instantaneous luminosity with the PSI46v2 readout chip.

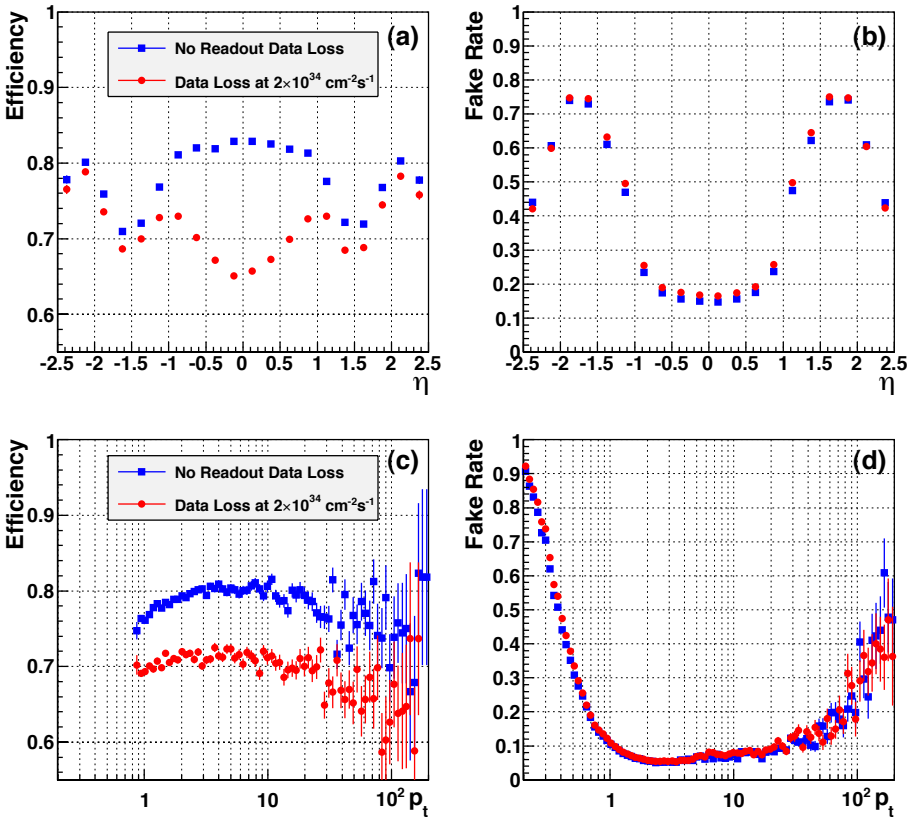

Figure 6.4: Performance of the current pixel detector in $t\bar{t}$ events at $2 \times 10^{34}\,\mathrm{cm}^{-2}\mathrm{s}^{-1}$ with no data loss (blue) and with the estimated data loss from buffer overflows mentioned in the text (red): (a) tracking efficiency vs pseudorapidity; (b) fake rate vs pseudorapidity; (c) efficiency vs p_{T}; (d) fake rate vs p_{T}.

In the present operation of the pixel detector events are observed with much higher pixel hit counts than expected from minimum bias event simulations. They are attributed to beam-gas collisions with charged tracks going almost horizontally through the barrel layers. These events can cause problems at the system level including the loss of event synchronization. By now, beam-gas events can largely be suppressed in the readout by excluding certain background triggers. However, the rate of these events scales with beam intensity and hence it could become more problematic in the future when we have to deal with high numbers of multiple collisions. Changes to the readout chip and downstream electronics would be one course of action to alleviate these problems.

6.1.2 Sensor Radiation Hardness

At the design luminosity of $\mathcal{L} = 10^{34}\,\mathrm{cm}^{-2}\,\mathrm{s}^{-1}$ the pixel system will be exposed to particle fluences of 3×10^{14}, 1.2×10^{14}, and 0.6×10^{14} $\mathrm{n}_{eq}/\mathrm{cm}^2/\mathrm{yr}$, at the first, second, and third layer, respectively. Fluences for the endcaps are comparable at the same radii. All components of the current system are specified to operate up to a total particle fluence of at least 6×10^{14} $\mathrm{n}_{eq}/\mathrm{cm}^2$. The sensors for BPIX and FPIX have been developed to operate efficiently up to this dose. They are n^+-on-n (n^+ implants on n bulk silicon) devices [9]. Electron collection has the advantage that after radiation-induced space charge sign inversion, the highest electric field is located close to the collecting electrodes, so even when the detector is not fully depleted after radiation

damage, the depletion zone is near the side that is read out. Moreover, since electrons have larger mobility and consequently a lower trapping probability than holes, electron collection leads to a higher charge collection efficiency (CCE) after irradiation.

Studies of the radiation damage effects on the performance of both the BPIX and the FPIX sensors have been performed. The barrel-type pixel sensors with their readout chips have been exposed to radiation fluences up to 5×10^{15} n_{eq}/cm^2 [10, 11, 12]. Charge collection of signals have been measured as shown in Figure 6.5. After a fluence of 1.1×10^{15} n_{eq}/cm^2 only about 50% of the charge is collected for $V_{bias} > 400$ V.

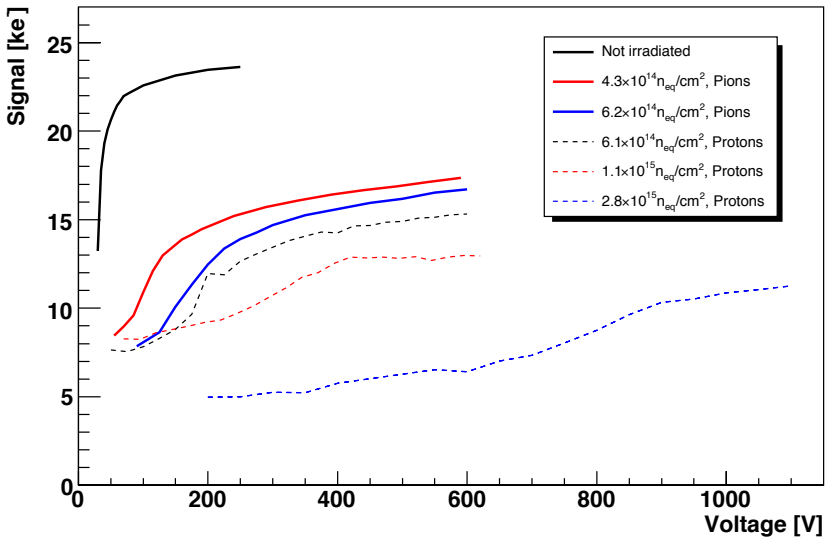

Figure 6.5: Most probable value of signal charge collected from single clusters as a function of the sensor bias for various irradiation fluences of barrel pixel sensors [10]. (It should be noted that biasing the sensor to 1000 V is not considered feasible with the actual detector and power supplies.)

Hit detection efficiency and resolution is expected to deteriorate with irradiation. For a radiation fluence above 10^{15} n_{eq}/cm^2 the hit efficiency measured in beam tests is below 97%. Figure 6.6 shows the simulated hit resolution as function of the track pseudorapidity before and after irradiation. The fluence 1.2×10^{15} n_{eq}/cm^2 is expected to be exceeded during Phase 1. After this exposure, the detector's hit resolution deteriorates by roughly a factor of two in the transverse plane and would require a replacement of the innermost layer. The Phase 1 upgrade pixel detectors must be designed to facilitate this partial replacement. This presents an opportunity to adopt more radiation hard sensors, if they can be developed in time.

6.1.3 Material In the Tracking Region

The services (including cables, cooling lines, printed circuit boards) and mechanical support structure (e.g. end flanges) for the current pixel detector introduce a non-negligible amount of material in the tracking volume. This reduces the track reconstruction efficiency and degrades the impact parameter resolution. The material distribution of the current pixel detector is shown in Figure 6.7 in terms of radiation lengths and nuclear interaction lengths as function of η.

Figure 6.8 shows the location of various parts and components for the current pixel detector along the z-direction. For BPIX, all the power and signal cables are routed to two end-flanges,

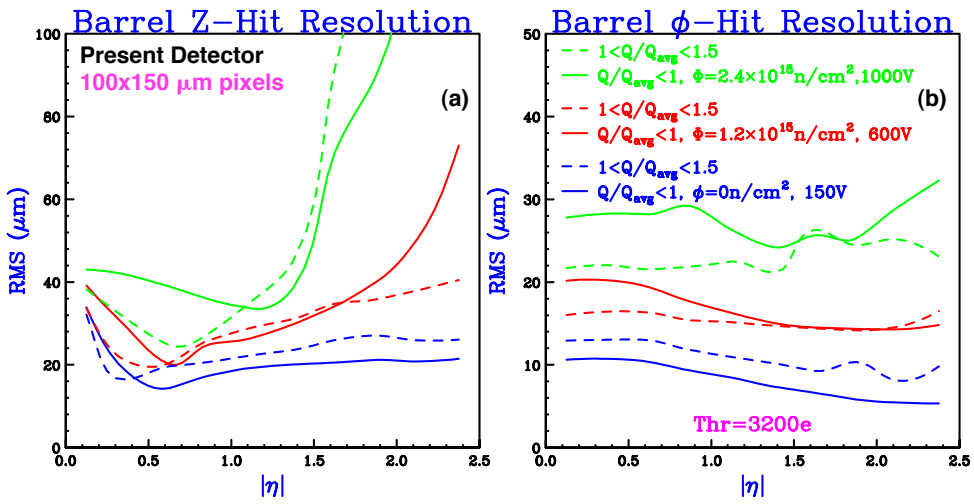

Figure 6.6: Hit position resolution (RMS) as function of the track pseudorapidity for an unirradiated (blue lines) and irradiated detectors (red and green lines). Longitudinal (a) and transverse hit resolution (b) are shown separately. The solid lines correspond to hits with total charge Q below the average charge. Dashed lines correspond to hits with total charge $1 < Q/Q_{avg} < 1.5$.

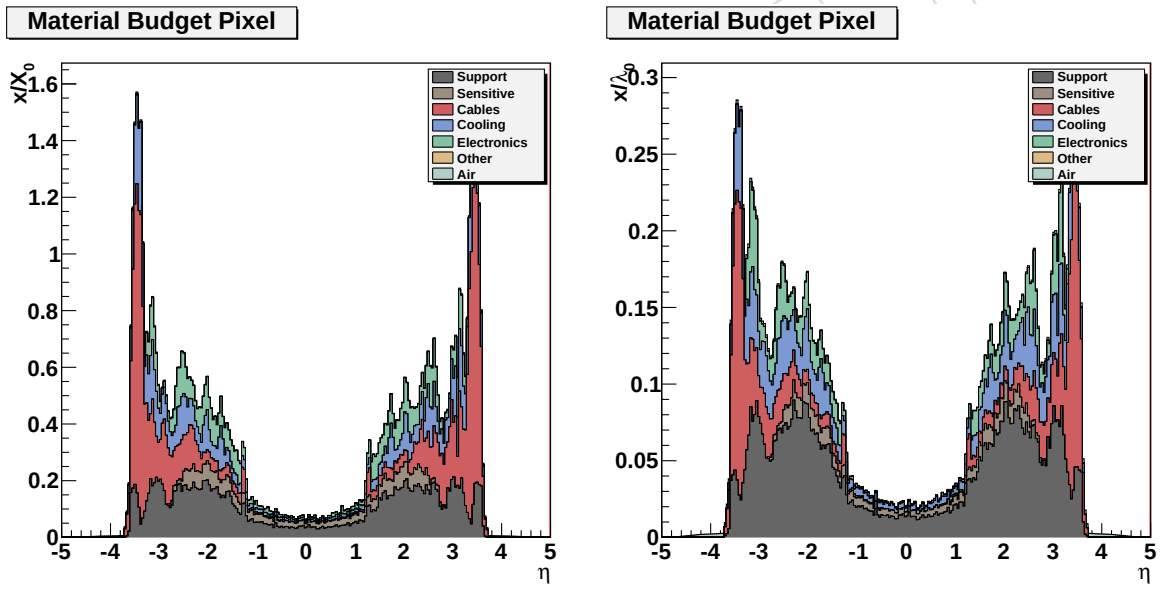

Figure 6.7: Radiation length (left) and nuclear interaction length (right) of current pixel detector.

behind both ends of the barrel region, and then directed to an optical link system that converts the electrical signals into optical. The signal is then sent over a 2 m long optical fiber to the patch panel on the tracker bulkhead. In the central region ($|\eta| < 1.2$), the main contribution to the total amount of material comes from the silicon sensors, the chips, the mechanical structure, cooling pipes, and Kapton flex cables. For $|\eta| > 1.2$, before getting to the FPIX, the main contributions are due to the cooling manifolds, the PCB end-flange print with more than 800 plugs and the Kapton cables. In addition, the cooling manifolds and the PCB end-flange are directly in front of the first forward disk of the FPIX system. Most of the material between $1.2 < |\eta| < 2.4$ is in the FPIX disks (brazed aluminum cooling loops) and electronics (ZIF connectors and adapter boards), and between $2.4 < |\eta| < 3.6$ in cables and cooling.

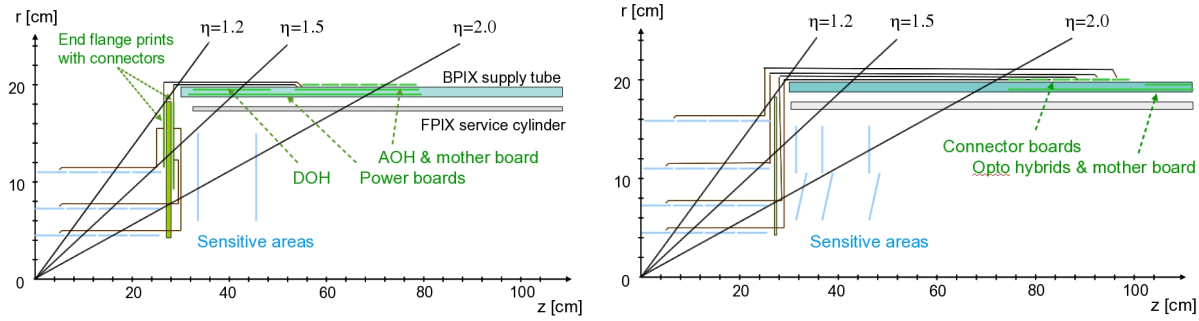

Figure 6.8: Location of components as a function of z and η for the current pixel detector (left), and for the proposed upgraded detector (right). In the current detector, there are a substantial number of connectors and electronics boards in the tracking volume, in particular at the end flange between the BPIX and FPIX. These have all been moved further downstream in z in the new design.

The passive material plays a visible role for tracks with low and intermediate momenta, as illustrated in Figures 6.9 and 6.10, which show the impact parameter resolutions as measured in recent collision data, compared to simulation, versus track η and ϕ [13]. At low momenta the transverse impact parameter resolution worsens at higher η due to the material traversed by the track. The impact of the 18 cooling pipes is clearly visible for lower momentum tracks versus ϕ.

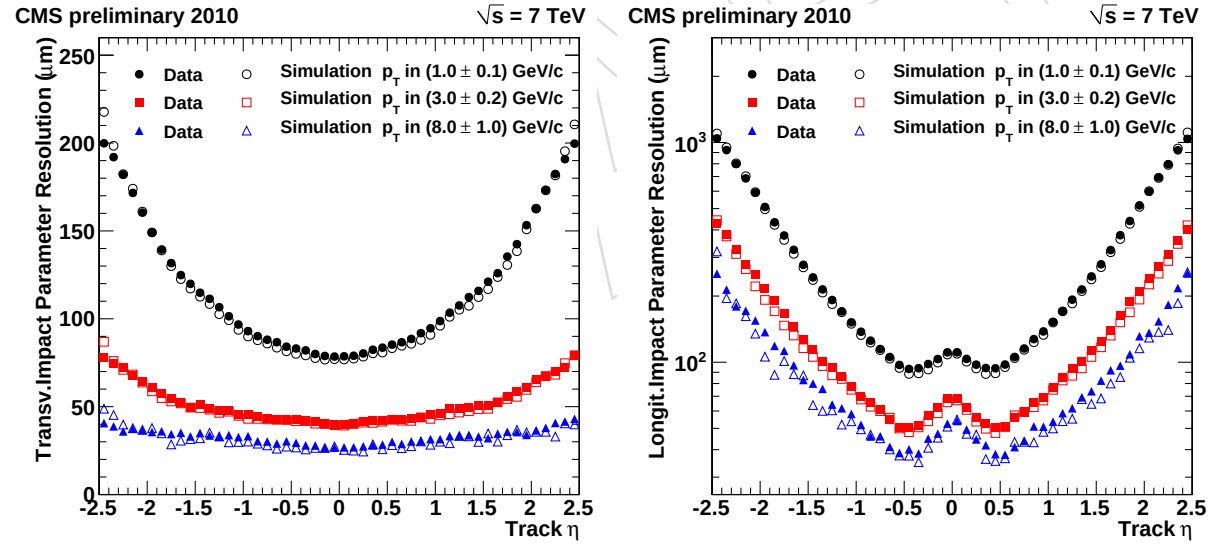

(a) (b)

Figure 6.9: Measured resolution of the track transverse (a) and longitudinal (b) impact parameter as a function of the track η for transverse momenta in $1.0 \pm 0.1\,\text{GeV}/c$ (circles), in $3.0 \pm 0.2\,\text{GeV}/c$ (squares) and in $8.0 \pm 1.0\,\text{GeV}/c$ (triangles). Filled and open symbols correspond to results from data and simulation, respectively [13].

6.2 Description of the Pixel Detector Upgrade

The design of the pixel detector must satisfy the following requirements and constraints:

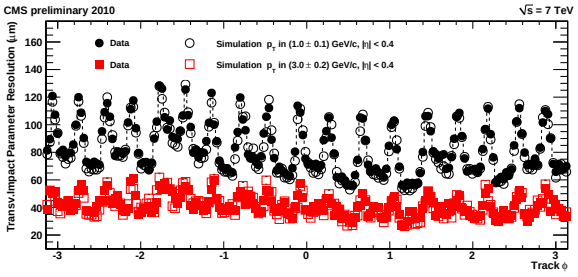

(a)

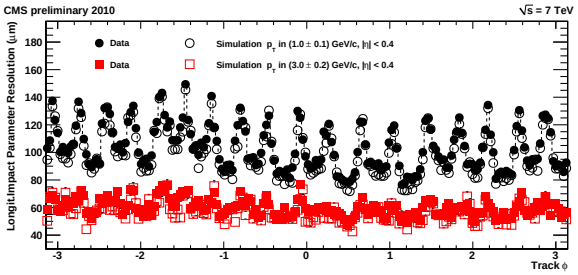

(b)

Figure 6.10: Measured resolution of the track transverse (a) and longitudinal (b) impact parameter as a function of the track ϕ for transverse momenta in $1.0 \pm 0.1\,\mathrm{GeV}/c$ (circles) and in $3.0 \pm 0.2\,\mathrm{GeV}/c$ (squares). Filled and open symbols correspond to results from data and simulation, respectively [13]. The 18 peaks correspond to the 18 cooling structures in the BPIX as described in the text.

- Minimize data loss due to latencies and limited buffering in high luminosity running;
- Minimize degradation due to radiation damage;
- Optimize detector layout for 4-pixel-hit coverage over the η range with minimal innermost layer radius;
- To reduce material, adopt two-phase CO_2 cooling and light-weight mechanical support, moving the electronic boards and connections out of the tracking volume;
- To reuse the current patch panel and off-detector services (cooling pipes, cables and fibers), adopt DC-DC power converters and higher bandwidth electronics;
- Reduce number of module types and interfaces;

The objective is to have the system installed and commissioned during the 2016 shutdown. In this section we describe our progress, as well as some of the R&D needed for the Phase 1 upgrade and how it relates to future upgrades.

6.2.1 Geometrical Layout

For the Phase 1 upgrade of the CMS detector, we propose a pixel detector with 4 barrel layers and 3 disks in each endcap. The 4 barrel layers are of equal length and are placed at radii of 3.9, 6.8, 10.9, and 16.0 cm. The three end-cap disks are placed on each side of the central barrel detector, with a radial coverage ranging from 4.5 to 16.1 cm. The location of the first disk along the beam line is at 29.1 cm from the interaction point, the second and third disks are located at 39.6 cm and 51.6 cm from the interaction point.

In the new design, there will be only one type of module with 16 readout chips in a 2×8 arrangement. They will be mounted on ultra-lightweight support structures integrated with the cooling distribution system. Two-phase CO_2 cooling will replace the current single phase C_6F_{14} resulting in significant material reduction. We plan to use thin-walled stainless steel pipes with a diameter of about 1.6 mm and wall thickness of 0.1 mm which will provide enough cooling power for each pixel sub-assembly based on a continuous loop. Further material reduction will be achieved by using longer twisted pair or light-weight flex-cables to carry the signals to the optical hybrid boards; these boards, as well as the port cards and cooling manifolds, will be moved out of tracking region.

The outer and inner parts of the detector will be designed such that they would allow the inner layers and rings to be easily replaced after radiation damage. For FPIX, this requires each half-disk be divided into an inner and outer ring. Figure 6.1 shows a cross-sectional view of the new pixel system and its sections. Similar to the current detector, the blades in the forward disks are rotated by 20° in a turbine like geometry to induce charge sharing. The separation of each half disk into an inner and outer assembly allows us to optimize the orientation and tilting to obtain the best position resolution in both radial and ϕ directions. Our baseline is to tilt the inner assemblies into an inverted cone at 12° towards the interaction point.

The upgraded pixel detector is constrained by the existing insertion volume and services. The cabling of the current CMS tracker detector, which includes the 200 m^2 silicon strip detector, was facilitated by the installation of two patch panels, denoted as PP1 and PP0, outside the tracker volume. This infrastructure will not be changed during the Phase 1 upgrade except for the cooling pipes between PP0 and PP1. Therefore, the upgraded pixel detector must use the existing power cables, fibers, and cooling lines from the cooling plant to PP1. Cables, fibers, and other required utilities are already installed up to PP0 for 3 forward disks; however, space for making changes to utilities between PP1 and PP0 is severely limited. The existing rail system for insertion and extraction will be used.

6.2.2 New Beam Pipe

To improve the physics performance of a pixel detector in terms of impact parameter resolution and vertex resolution the first active layer should be as close as possible to the beam, requiring a beam pipe of minimum possible radius. This requirement has to be balanced against the safe and efficient operation of the accelerator with minimum background in the experiment. For the safety of the detector, the last machine element in the interaction region should always be the point of smallest aperture. In addition, the minimum diameter is constrained by mechanical stability under vacuum. The CMS beam pipe spans over ±18 m from the interaction point to both ends of the experimental cavern. It is segmented into a central section and 4 sections on each end. The central section is 6.2 m long and consists of a cylindrical part of 1.8 m length and conical ends. The cylindrical piece is made out of 0.8 mm thick beryllium; the conical parts are of 0.8-1.2 mm thick stainless steel. The inner diameter at the interaction point is 58 mm.

The LHC machine group has studied the beam aperture for the LHC upgrade scenario. It was concluded that changing the minimum diameter of the central part of the CMS beam pipe from 58 mm to 50 mm will not cause any aperture problems in the CMS interaction region, provided all tolerances can be controlled to 11 mm. Therefore, it is proposed to install a new central beam pipe with an inner diameter of 50 mm together with the new pixel detector. The smaller beam pipe diameter allows the reduction of the first barrel layer radius from 4.4 cm to about 3.9 cm. A further reduction to 3.4 cm is under study. The opening angle of the conical part of the beam pipe will be preserved. The cylindrical part will be shorter by about 28 cm on each end. There

are two options for building the pipe. Either the conical part is again made out of stainless steel, leading to a shorter beryllium section, or we maintain the length of the cylindrical part of the beryllium section and connect the stainless steel section onto the conical beryllium ends. Detailed background studies have to be performed to judge the possible effect of a shorter beryllium section. The other solution, though in principle possible, is much more complicated from the production point of view. For both solutions detailed calculations using FEM have to be done to estimate the mechanical strength and the deflection. Also, the vacuum performance and the beam impedance have to be re-evaluated for the smaller radius.

6.2.3 Mechanical Support for BPIX

A comparison of the current 3-layer barrel and the new 4-layer system is shown in Figure 6.11. The addition of the fourth layer reduces significantly the gap between the pixel detector and the TIB. The BPIX mechanical support structure consists of 200 μm thick carbon fiber ladders, with cut-outs to reduce mass, glued onto the stainless steel cooling tubes. Each ladder is glued to two tubes. The end flange is made also of carbon fiber glued onto 4 mm thick Airex foam profiles. The bends of the tubes are made from 1.8 mm diameter 100 μm thick stainless steel soldered to the straight section. Figure 6.12 shows the prototype of the layer 1 mechanical structure.

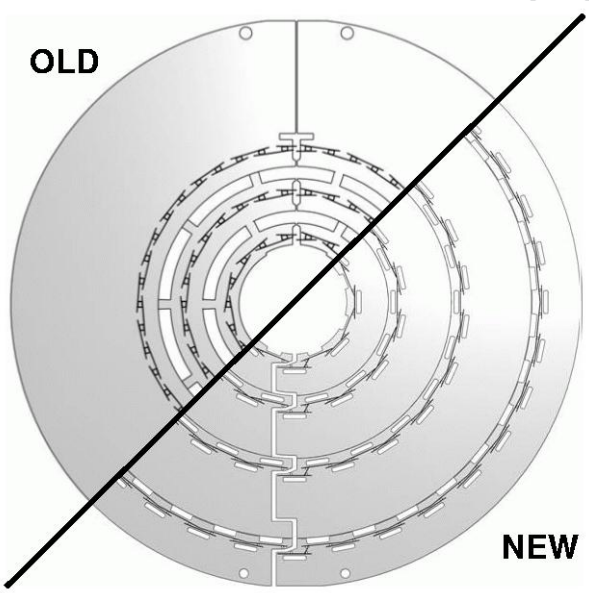

Figure 6.11: Cross sectional view of the old 3 layer barrel (top) and the new 4 layer system (bottom).

The electronic components of the services are moved to the forward direction, away from the active tracking region. The PCBs on the supply tubes are moved to $|\eta| > 2$ and those on the end flange have been removed entirely (see Figure 6.8). This has been made possible by the development of the low mass micro-twisted pair cables described later. Modules are now connected directly to the readout optical hybrids (ROH) which are about 1 m away. A new supply tube has been designed (see Fig. 6.13) to provide optimal η coverage between BPIX and FPIX. A prototype has been built, made out of carbon fiber ribs, panels, and tubes as well as Airex foam. The total weight of the supply tube is 2900 g.

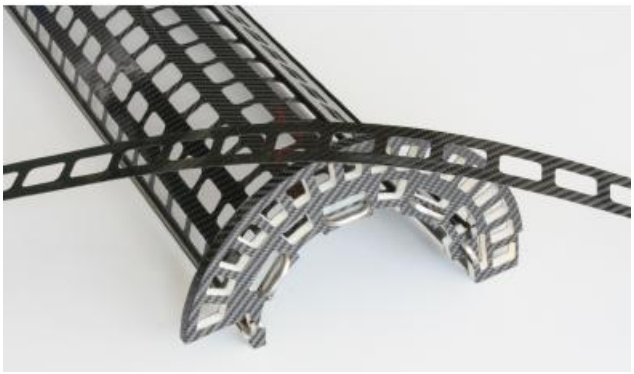

Figure 6.12: Prototype of the mechanical structure for the innermost layer. To illustrate its lightweight, a carbon fiber ladder is laid upon the half-barrel. The mechanical stability of the ladder is given by the cooling tubes.

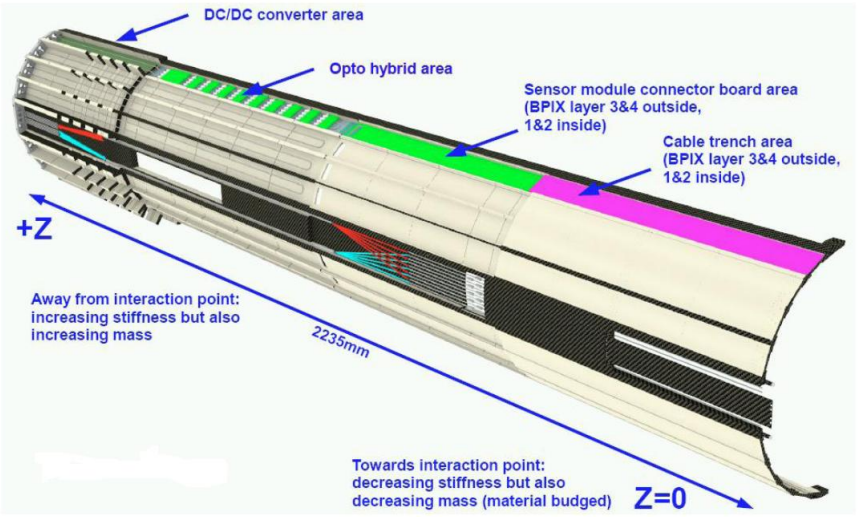

Figure 6.13: Schematic drawing of the new BPIX supply tube.

6.2.4 Mechanical Support for FPIX

The current FPIX detector has 7 module types on beryllium panels placed between $r = 59.7$ mm to 144.6 mm (there are a total 84 modules per half disk, or 540 ROCs per half disk). The upgrade layout uses only one module type (2x8 ROCs) arranged radially on panels placed between $r = 45$ mm to 161 mm (there are a total 56 modules per half disk, or 896 ROCs per half disk). Half-disks are divided into an outer ring with 34 modules and inner ring with 22 modules. The inner assembly is supported off the outer assembly by some rods and the two assemblies can be easily separated. The pixel modules are attached by a module holder to the substrate and are removable and replaceable without disassembling half-disks.

All the outer radius sensors are located to minimize the gap in 4-hit coverage between the end of the 4th-barrel layer and the innermost disk. The design maximizes the 4-hit coverage between the end of 4th barrel layer up to $|\eta| = 2.5$, for particles originating at the IP ± 5 cm, using a minimum number of modules.

Each blade will have one module placed on opposite sides of the same substrate (see Fig. 6.14). The radial orientation of the rotated turbine aligns the 150 μm dimension of each pixel in the radial direction and the 100 μm dimension in the ϕ direction, with more overlap between neigh-

boring sensors than in the current design. This will ease the spatial alignment for track reconstruction. We plan to use thermal pyrolytic graphite (TPG) for the substrates. TPG is a material with excellent in-plane thermal conductivity. The stainless steel cooling tubes for CO_2 cooling are embedded in the outer and inner assembly rings made out of light-weight carbon-carbon (C-C) material as shown in Figure 6.15.

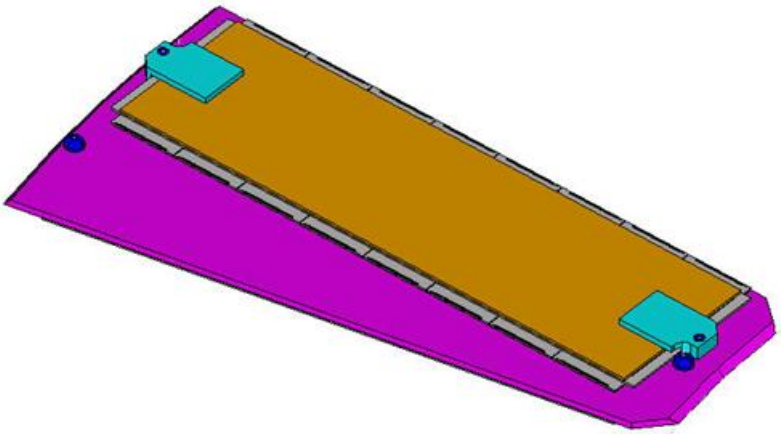

Figure 6.14: FPIX Upgrade Blade - identical blades are used in the inner and outer assemblies of all half disks.

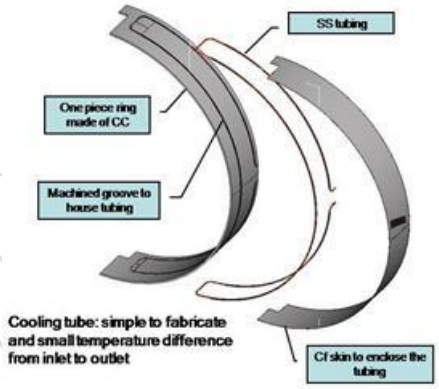

Figure 6.15: Edge Cooling Concept: cooling tube captured inside carbon-carbon ring with carbon fiber skins.

The design of the FPIX Upgrade blade is shown in Figure 6.14. It features:

- Solid TPG (0.68 mm thick) encapsulated with carbon-fiber facings (0.06 mm thick).
- All blades are identical with one 2×8 ROCs module mounted on each side.
- Each module has a pair of module holders made out of G9 glued at each end for attachment to the precision holes on the substrate.
- Cooling is provided at the end(s) of the blade by contact with the actively CO_2 - cooled ring(s).
- Each substrate is glued permanently to the rings so that the whole ring and substrate assembly with embedded cooling tubes could be constructed as a complete structure.

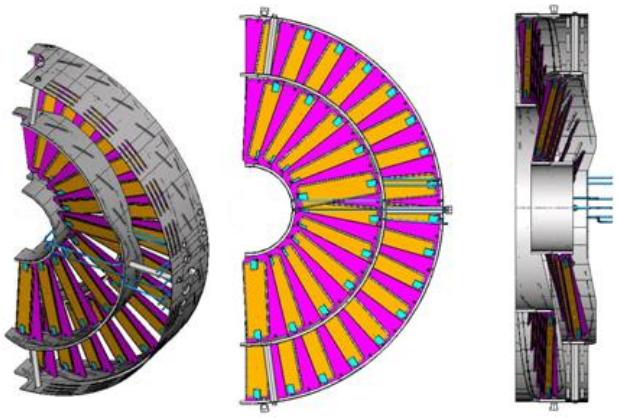

Figure 6.16: FPIX Upgrade half-disk design: Inner Blade assembly supported by Outer Blade assembly, with all blades attached permanently to the C-C assembly rings.

Figure 6.16 shows the complete half disk, with the inner assembly ring supported by the outer assembly ring.

6.2.5 CO_2 Cooling

In the present pixel detector, cooling pipes, manifolds, heat exchanger contacts and the C_6F_{14} coolant itself represent a major contribution to the overall detector material in the Tracker acceptance. CO_2 two-phase cooling has been identified as the most promising option to improve upon the present mono-phase fluorocarbon system, in order to achieve enhanced cooling performance with a lightweight system. CO_2-based cooling has been successfully adopted in other detectors, notably the LHCb VELO.

In general, CO_2 offers significant advantages compared to mono-phase fluorocarbon:

- Excellent thermodynamic properties for small channels: low mass, less viscosity, low liquid/vapor density ratio, low dT/dP, high heat transfer coefficient, and high latent heat;
- A factor of ~ 2 lower density, in liquid phase;
- At ~ 1 CHF/kg, it is substantially cheaper than C_6F_{14} (~ 100 CHF/kg).

The high heat transfer coefficient allows smaller heat-exchanger contacts. The high latent heat allows more heat load per channel, possibly reducing needs for manifolding and the size of the manifolds, as well as the size of the individual pipes. CO_2 also offers the required radiation hardness.

The development of the CO_2 cooling system for the pixel detector requires a substantial R&D program, covering the three main areas discussed below.

1. **Characterization of heat transfer.** The pixel detector cooling uses miniature pipes involving a domain of CO_2 heat transfer and two-phase flow for which very few experimental measurements exist, and available theoretical models do not give reliable predictions. A fundamental research line consists in performing laboratory measurements to characterize the process in the relevant domain, and improve the existing theoretical models accordingly.

2. **Optimization of the on-detector cooling.** The optimization of the on-detector part of the

cooling system is the key to reduce the detector material, and hence achieve the required improvement on its performance. The heat transfer from the silicon sensors to the structure, through the pipe walls into the coolant has to be maximized, while minimizing the amount of material and at the same time ensure reliable thermal joints with reproducible performance. The crucial aspects are the choice of the pipe material and size, pipe fittings and connection techniques, design of thermal joints and choice of thermally conductive materials.

3. **System design and integration in CMS.** Many aspects have to be addressed, including: (i) design of the cooling station, choice of the active components and of the accumulator; (ii) design of the control and monitoring system, choice of the instrumentation (especially of the active parts that will have to be installed in the experimental cavern), interface to the detector monitoring system; (iii) design of the cooling channels between PP0 and PP1 and choice of dielectric fittings in PP1; (iv) connection to existing cooling pipes from PP1 to the cooling station, and re-qualification of the pipes; (v) interface with surroundings in the UX cavern and with the main chiller in the US cavern; (vi) optimization and validation of system operation, including startup at warm temperature, study of safety issues and failure modes.

The first area of research is already well advanced, with several labs performing measurements in parallel on different setups. A large amount of data have been collected, analyzed and carefully compared, providing evidence that a suitable phase-space of working parameters is available, compatible with performance requirements and system constraints.

The optimization of the on-detector cooling is also advancing well; prototypes of mechanical structures of both BPIX and FPIX have already been tested with CO_2 cooling in realistic conditions, and extensive thermal modelling studies are underway. Although substantial optimization work is still to be done, the results collected so far indicate that suitable performance can be achieved with miniature pipes and lightweight contacts.

System design and integration studies will be a main focus for the coming 1-2 years. A full-scale system has been built in the CERN CryoLab, and will be used as test setup to qualify components for the cooling plant as well as the control and monitoring system; it will be also used to study system aspects with long pipe runs mimicking the geometry of the CMS service channels. Preliminary safety studies indicate that the installed pipes are compatible with the required operating pressure. Excellent progress has been made in updating as-built models of the existing cooling system and of the cavern infrastructure, which are the basis of the studies for the integration of the system in CMS.

6.2.6 DC-DC Conversion

The routing and installation of the current pixel detector's services (power cables, fibers, cooling lines) was a major technical challenge. Due to the space constraints of the conduits and other sub-detectors, it would be quite difficult to route additional power cables. The pixel upgrade will increase by about a factor of two the number of ROCs. Therefore, more power will be needed than in the current detector, supplied at a higher current. To limit resistive losses in the $\sim$ 50 m long power cables, a novel powering scheme based on the DC-DC conversion technique is proposed. The idea is to bring the power into the detector at a higher voltage but at a lower current (thereby significantly reducing the power losses in the cable) and to use a DC-DC buck converter close to the detector to convert the input voltages to the operation voltages needed by the pixel modules with high efficiency ($\sim$ 80%). A separate converter is used

for the digital and analog voltages. These converters need to be tolerant of both the radiation and magnetic field inside the tracker volume. Since commercial converters could not satisfy these requirements, a dedicated ASIC development is needed. A prototype is currently being developed. The DC-DC conversion chip and other components will be assembled on a small printed circuit board which will be placed on the support half cylinder, close to the pixel modules. Prototypes of these converter PCBs have been fabricated and tested for electromagnetic noise emissions in a set-up with silicon strip modules. The results of these tests are promising and indicate that the application of DC-DC converters in the pixel system should be feasible.

Tests are ongoing to study the performance of pixel modules powered by the same CAEN power supply modules currently in use and with the long power cables needed by the experiment with and without DC-DC conversion. As space is rather tight, it is also important to minimize the dimensions of the converters. Furthermore, since all the power to the detector will go through these converters which are closely packed, we have to understand the effect of temperature and provide a means of cooling to these devices.

Even with DC-DC conversion, there is concern that the current needed will exceed the ratings of the current power supply modules made by CAEN S.A (Italy). We have contacted the manufacturer to look into ways of modifying the low voltage supply power modules to have a higher rating that can meet our needs. An alternative that we are investigating is to use a two step conversion process. This involves a step-up conversion using commercial parts close to the power supply modules and then a step-down conversion close to the detector.

6.2.7 Front End Electronics

The pixel readout chip used in the current detector (PSI46v2) is well understood and tested. It is also sufficiently radiation hard to survive the Phase 1 integrated luminosity. However, as noted earlier, it will incur rate dependent inefficiencies in the inner regions when the peak instantaneous luminosity exceeds 10^{34} cm^{-2}s^{-1}. Although modifications are needed to allow for the luminosity that we will have for Phase 1 and possible operation with a 50 ns bunch spacing, we would like to keep its core unchanged as much as possible. Changes to the ROC are needed for two reasons:

- **Single hit efficiency:** To cope with the increased luminosity for Phase 1, the size of the internal data buffers must be increased. An additional internal buffer stage on the ROC will be needed which holds the Level-1 trigger verified hits until a readout token arrives. Doubling the buffers in the 0.25 μm process will increase the size of the chip periphery by 0.6 mm which can be accommodated in the module design. There is also good progress on designing an improved chip architecture with an additional buffering stage in the column periphery to reduce or eliminate the readout-induced dead time, which limits the efficiency of the innermost layer. This reduces dead time related to readout latency and allows for a more efficient use of the output bandwidth. Simulation shows that for the innermost layer at 3.9 cm, the peak inefficiency of this upgraded ROC at a luminosity of 2×10^{34} cm $^{-2}$s^{-1} is about 4.7% with an average over the whole LHC fill of 2.1%, assuming a fill lifetime of 10 hours, and a collision rate of 40 MHz (25 ns bunch crossing).
- **Fast readout:** Since we will have more modules than the current detector and the number of optical fibers is limited, we need to have a faster readout. The present readout uses 40 MHz analog links, with the pixel addresses encoded using six analog levels (2.5 bits), for an effective bandwidth of 100 Mbps. Increasing the clock rate on the analog links to 80 MHz presents a significant risk due to the limited rise time

of the ROC and Token Bit Manager (TBM) signals. Instead, we are developing a digital readout (with an on-chip ADC) from ROC to TBM at 160 MHz (160 Mbps). In addition, a multiplexing TBM combines two token rings into a 320 Mbps digital link, giving three times the throughput of the existing analog links on the same fiber plant. Besides increased bandwidth, advantages of the digital output from the ROC and TBM are lower power and less material in the cables.

The core of the ROC, including the pixel front end amplifier, threshold comparator with trimming and the column drain architecture remain unchanged. A phase-lock circuit (PLL) capable of up-converting the 40 MHz LHC clock to 80/160/320 MHz has been successfully tested. A successive approximation 8-bit ADC has also been tested; revised designs for both PLL and ADC have already been submitted and tested in 2009; further improvements to the ADC for higher clock rates are underway. With these functional blocks designed, laid out and tested, the redesign of the 0.25 μm ROC is on sound footing. The full layout for the upgrade ROC is expected to be ready in Summer 2011, with first test submission following shortly.

In case of a 50 ns bunch crossing scenario of the LHC, the data losses described above would increase by roughly a factor of two. A further reduction of these losses would require modifications to the complex circuit block in the ROC that manages the double column data buffers. Indeed, we intend to pursue such improvements to address readout-related data losses in a follow up submission of the ROC.

Changes are also required to the TBM to accept and produce digital signals. The TBM chip is needed to control a module. The core of this chip will remain largely unchanged. However, modifications will be needed to deal with the new fast up-link protocol. Only modest changes to the input and output stages are required, again using functional blocks already developed for new low-power electrical micro-twisted pair links between the module and downstream electronics. The TBM must also multiplex signals from two token rings run at 160 MHz into a single 320 MHz output to an optical link. The modifications that will be needed include replacing the analog switch drivers by digital multiplexers, a PLL for clock generation, and digital receivers and line drivers.

Digital signals would travel from the TBM on a new set of extremely low mass, flexible cables to an optical hybrid board, and then along optical fibers to the off-detector data acquisition electronics. Micro-twisted pair cable of copper-clad aluminum wires with 125 μm diameter have been developed. On these cables, signals are sufficiently robust over 1 m lengths, to allow the electrical to optical link boards for the barrel to be placed outside the fiducial volume. For FPIX, we are currently evaluating the use of a flat flex-cable made out of Al. Simulation shows good performance when operated digitally at 320 MHz. Prototypes of this cable will be available sometime in early Fall 2010. We are also investigating robust connectors for the both the Al cable and the micro-twisted pair cable.

The current Analog opto-hybrid (AOH) will be replaced with a new readout optical hybrid (ROH) to transmit the data through long fibers to the Front End Driver (FED). The current baseline is to build link boards similar to the existing analog optical hybrids, using 1310 nm lasers qualified for radiation hardness by the CERN Versatile Link project, intended for raw data rates of 5 Gbps, which is well beyond the required 320 Mbps for Phase 1. Several lasers in commercial TOSA packaging and attached fiber pigtails will be mounted on a common readout link PCB designed to fit in the service cylinders. Prototype lasers and link boards are expected to be available for testing in late 2010. Linear Laser Driver (LLD) chips from the CERN opto-electronics group were used in the original analog links and have been radiation qualified and tested at 320 Mbps. The baseline option is to use the LLD to operate these links at 320 Mbps over

approximately 100 m to the FEDs in the Underground Service Cavern, USC55, at CMS where most of the back end electronics is located. A suitable optical receiver has been identified and tested at 320 Mbps.

At the FED, the flash ADC and analog data packet decoder will be replaced by a deserializer, since the incoming signals will be fully digital. The existing FED design has a 9U VME motherboard with daughter cards hosting ADCs or FPGAs for data decoding and event building. One option is to replace the ADC daughter cards with a deserializer FPGA, leaving the architecture of the motherboard intact, where in fact changes are not likely to be necessary. If required, FPGA daughter cards can be replaced with faster FPGAs from the current generation of devices from Altera. A preliminary design for the replacement cards includes an extension for mounting the new optical receivers, leaving the old analog receivers intact. This may prove useful for prototyping and conversion of existing FEDs for digital readout. To accommodate the increased data rates at the FED output, the existing S-Link64 interface cards on the VME mezzanine boards would be replaced with new daughter boards implementing a new interface to the CMS DAQ system.

The downlink protocol for control and configuration of the detector is unchanged, both electrically and logically. New parts have to be procured for the digital control links and Front End Controller (FEC).

6.2.8 Sensor Module

A 4-layer barrel detector would comprise about 1200 full modules compared to the presently installed 770 full and half-modules. The number of pixels grows by a factor 1.7 from 48M to 80M. There are 672 modules in the upgraded 2×3-disk forward pixel detector, the same number as the current FPIX detector. However, since the size of each module will be larger, the number of pixels will grow from 18M to just under 45M.

The proposed upgraded pixel detector has only one type of sensor module with two rows of 8 ROCs each. This will simplify considerably the sensor production, module assembly, and testing. The active area of the module is 16.2 x 64.8 mm^2. The pixel size will remain the same as before, 100 x 150 μm^2. For the sensors our baseline is to use the same n$^+$-on-n technology as for the current detector. Nevertheless, there is some ongoing R&D activity to evaluate other radiation tolerant sensor technology. The sensor is bump-bonded to 16 ROCs which for Layers 1 and 2 for BPIX, will be thinned down to 75 μm. For the rest of the layers and the end-cap disks, the ROCs will be thinned down to about 200 μm. A high density interconnect (HDI) is glued on top of the sensor with wire bond pads to connect to the corresponding pads on the ROCs. Electrical signals will be sent from/to the ROCs through the HDI and then to the downstream electronics. The TBM chip will be mounted on the HDI as well. A small clip is glued to the ends of the module to allow the assembly of the module to its support structure.

For future replacements of the the detector innermost layers and rings we are considering other possibilities as outlined in Section 6.4.

6.2.9 Bump bonding

Bump bonding was a cost and schedule driver for the current pixel detector [14]. Since the number of pixels of the upgraded pixel system will increase by about 90%, some development work will be needed to increase the throughput as well as reduce the cost. For the current BPIX detector, bump bonding was done by PSI whereas for FPIX by two industrial companies. Industry is progressing steadily on bump bonding and lower cost processes for micro-bumps at 30 μm diameter and 100 μm pitch are becoming available. For example, at PacTech [15], pre-

fabricated solder balls are individually placed through a capillary and fused by laser-melting at a speed of 5–10 per second on a step-motor controlled machine. A special under-bump metal is still required, but the processing steps for the deposition and forming of Indium balls can be omitted. Any new vendor and process will have to be qualified to make sure that they meet our needs. In addition, the production yield and throughtput must be evaluated in a sequence of prototype runs.

6.2.10 Pixel Module Assembly and Testing

Starting from the bump-bonded pixel module, a high density interconnect will be glued onto the back of the sensor and wire bonded to the readout chips (about 700 bonds per module). Production of the necessary gluing and placement tools, based on assemblies used to build the current detector, has started. These assembly stations will include both manual and automatic procedures. The design and testing of fixtures, adhesive dispensing machines, and the necessary software are being commissioned.

Once assembled, the full modules then have to be fully tested and characterized at room temperature and at the foreseen operation temperature around -20°C. The tests include trimming the analog thresholds of all of the pixels to achieve uniform efficiency. The pixel detector achieves a point resolution of about 10 μm with 100 μm pitch by using the charge sharing induced by the Lorentz effect. The amplification is non-linear for small pulses and needs to be calibrated for each pixel using X-ray sources between 10 and 30 keV to reach the design resolution. The modules should also be tested at high rate, which can be done using an X-ray test stand.

In BPIX the final modules of one layer have to be mounted on a carbon-fiber frame which also includes the cooling pipes. A rotating fixture is needed, as adjacent ladders are mounted alternating from the inside and outside.

A system test of the fully assembled layer would require a CO_2 cooling plant of about 1kW, HV and LV supplies, optical links, control and readout boards, and a cosmics trigger.

6.2.11 Final integration and commissioning

Our plan is to do the final integration followed by system commissioning in the Tracker Integration Facility (TIF) at CERN. For BPIX, fully assembled layers will be transported from the various assembly sites to CERN. For FPIX, completed half disks and half cylinders will be shipped separately to CERN. At TIF, we will re-mount the half-disks to the half cylinders and carry out a commissioning of each half cylinder. Finally, extensive system tests of both BPIX and FPIX together will be performed at TIF prior to installation in CMS. Nine months are scheduled for this phase to minimize further commissioning in CMS for physics operations.

A program of high rate tests will be performed to uncover issues with the interoperability of the readout chain. This system test will allow us to exercise all firmware and software in the system. Cooling system tests will be performed to assure smooth, leak-free operation. In preparation for these tests, we will equip TIF with all the necessary electronics, power supply modules, as well as a CO_2 cooling system. The full readout and data acquisition chain will be present. We will also have a full control and safety system (DCS/DSS) installed and tested.

6.3 Performance Studies

The Phase I pixel detector has significantly reduced mass and significantly increased three-hit coverage. The net effect of these improvements on the amount of material, pattern recognition, track parameter resolution, vertexing, and b-tagging performance of the Tracker is summarized in the following sections.

6.3.1 Studies of the Effects of Material in the Tracking Volume

The upgraded detector will roughly double the number of pixels in the system. Despite this, we aim to reduce the amount of material in the tracking region by at least a factor 2 with respect to the current system.

The amount of material from the barrel pixel detector can be significantly reduced both in the active regions and even more in the service regions located in front of the pixel disks and the silicon strip tracker [16]. The use of serial CO_2 cooling with reduced density and pipe wall thickness is one important ingredient. This will reduce multiple scattering, photon conversions, and nuclear interactions. Within the region $|\eta| < 2.1$, the weight of the supply tube is 408 g and the total weight of the 4 barrel layers plus supply tube within this η region is estimated to be 7 kg, about a factor 2.4 less than the current BPIX detector with only 3 layers.

We estimate the overall mass of the FPIX detector can be reduced by $\sim$ 40%. The half disks contribute most to the FPIX material in the region $1.5 < |\eta| < 2.5$. It is feasible to remove 50% of the mass in the half disk by removing the very high density interconnect circuit (VHDI) and by using CO_2 cooling. The weight of the new half-disk is estimated to be 420 g, to be compared with the present 607 g. Within $|\eta| < 2.5$, the total weight of each half cylinder, including the three half-disks, cables, and cooling lines, is estimated to be 1.82 kg.

These reductions in material inside the pixel tracking volume are shown in Figure 6.17 and Figure 6.18 for BPIX and FPIX, respectively.

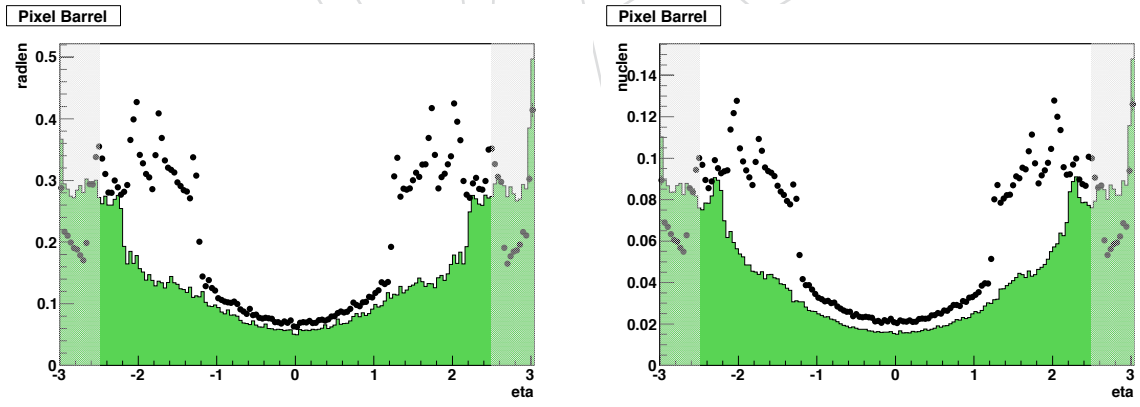

Figure 6.17: Radiation length (left) and nuclear interaction length (right) of current barrel pixel detector (dots) and proposed upgrade (histogram). The shaded region shows the material distribution outside the fiducial tracking volume.

Such reductions in the amount of passive material will have a large impact on charged particle tracking efficiency as well as electron and photon identification and resolution. For example, for a photon at $|\eta| = 1.5$, the probability that it would convert into an electron-positron pair inside the pixel volume (where the presence of pixel hits is crucial for distinguishing photons from electrons) is 22% with the current detector, but would be 11% with the proposed upgraded

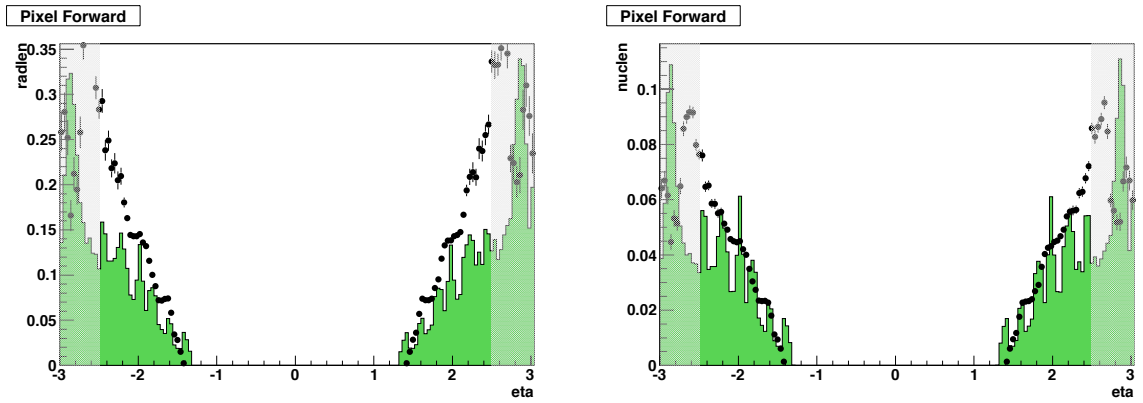

Figure 6.18: Radiation length (left) and nuclear interaction length (right) of current forward pixel detector (dots) and proposed upgrade (histogram). The shaded region shows the material distribution outside the fiducial tracking volume.

detector. Such improvements would have a positive impact on final state signatures involving photons, such as $H \rightarrow \gamma\gamma$.

6.3.2 Pattern Recognition and Efficiency Studies

The number of overlapping events during Phase 1 operation will be two to four times larger than during previous LHC operation. The interesting physics to be pursued during Phase 1 is likely to involve the reconstruction of tracks in high-p_T jets. These realities will emphasize the importance of reliable tracking in environments with high local hit densities. The challenge of maintaining high tracking efficiency and low track fake rate in dense hit environments has been studied as part of the CMS heavy ion program. It was found that seeding with three-hit combinations in the pixel detectors results in more precise initial estimates of the track parameters, which produces more reliable identification of the associated silicon strip hits and lower fake rates. Unfortunately, due to module boundary gaps in the current pixel detector with three barrel layers and two disks, this requirement leads to losses in efficiency. The new design with four barrel layers and three disks alleviates this problem by providing substantial redundancy for three hit seeds. The fourth layer also guarantees at least reasonable track seeding after high integrated luminosity. With four layers, even if the inner layer performance starts to degrade, the fourth layer will still provide three layer seeds.

In order to quantify the physics benefit that can be expected from the upgraded pixel detector, samples of jet events and $t\bar{t}$ events were generated for both geometries using the standard CMS simulation software and assuming an instantaneous luminosity of 2×10^{34} cm^{-2}s^{-1}. CMS has adopted an iterative tracking algorithm consisting of multiple steps. In the first step, hit triplets from the pixel detector or the innermost strip layer are used as seeds for the subsequent track finding and fitting. With the upgraded detector, in addition to triplets, quadruplets of pixel hits can also be used which cleans up the subsequent pattern recognition and reduces the fake rate. The left-hand plots of Fig. 6.19 show the track finding efficiency for the two geometries as a function of pseudorapidity and p_T. The track selection criteria are the same ones used in the recently released tracking performance studies [13] and represent the typical requirements used in recent physics analyses. The redundancy provided by the additional pixel layer in the Phase 1 geometry results in an increase of track seeding efficiency and a much lower fake rate. Losses due to nuclear interactions in the tracker material, which presently increases from about 0.4 X_0 in the central region to 1.8 X_0 at $|\eta| = 1.5$ (see Figure 6.7), and which is dominated by dead material of the strip detector, lead to a significant drop of efficiency towards

the acceptance limits of the barrel pixel detector. The comparison of the tracking efficiency in the two configurations demonstrates however that the gain in track seeding efficiency can be retained also for physics analyses.

The plots on the right-hand side of Fig. 6.19 show the corresponding fake track rate as a function of pseudorapidity for the current and Phase 1 detectors. Fake tracks are caused by the incorrect association of hits and are much more likely in regions with more passive material. They cause significant problems for b-tagging and are much reduced in the upgraded detector. The fake rate is also much reduced for lower momentum tracks.

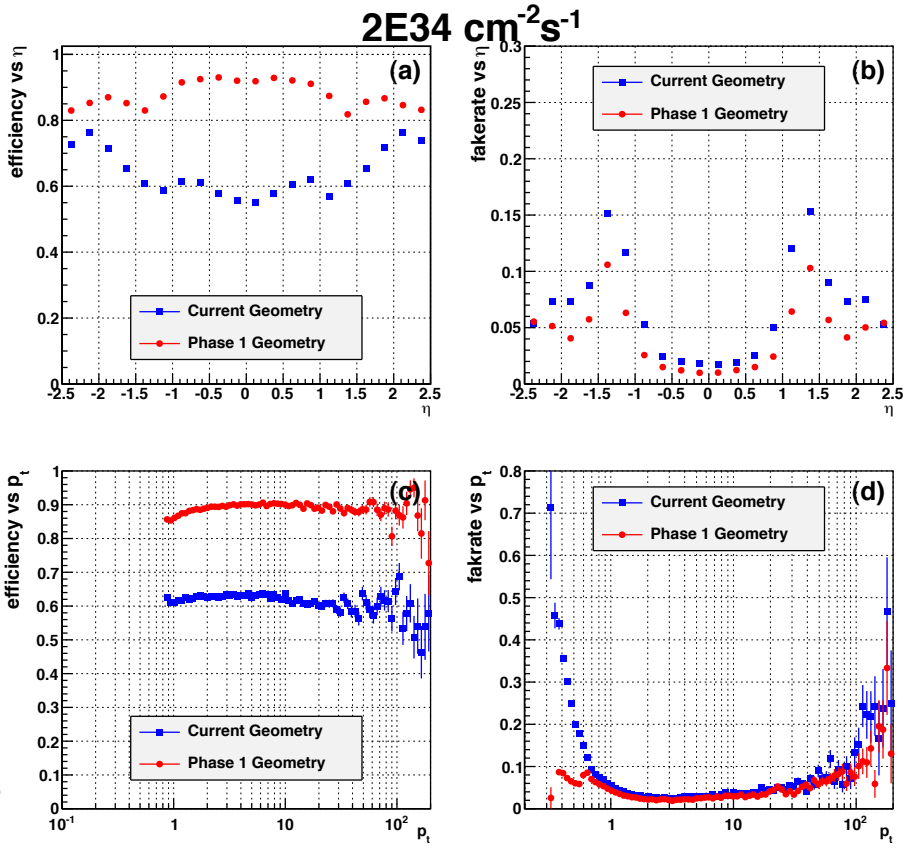

Figure 6.19: Comparison of tracking efficiency and fake rate for the current (blue) and upgraded (red) detectors in $t\bar{t}$ events at $2 \times 10^{34}\,\mathrm{cm}^{-2}\mathrm{s}^{-1}$ with 25 ns bunch spacing. The tracking algorithm with the current detector uses pixel triplets to seed pattern recognition, and pixel quadruplets and triplets with the upgraded detector. A "high purity" track selection is used which is similar to cuts used by analyses such as secondary vertex tagging [13]. Shown are: (a) tracking efficiency vs pseudorapidity; (b) fake rate vs pseudorapidity; (c) efficiency vs p_{T}; (d) fake rate vs p_{T}.

6.3.2.1 Recovery of TIB Inefficiencies

The inner layers of the barrel of the silicon strip tracker (TIB) are also important for pattern recognition and track reconstruction. There are a small number of cooling lines in this part of the tracker which cannot currently be operated as designed. So far, this has not resulted in any significant reduction in efficiency of the detector. However, if there were in fact some unforeseen premature degradation in the performance of the TIB, it would negatively impact the performance of track pattern recognition and reconstruction. The new four-layer pixel detector, with the fourth layer quite close to the first layer of the TIB, could significantly ameliorate such

degradations. To estimate the potential impacts of such degradations and a possible recovery by the new pixel detector, we simulated $t\bar{t}$ events similar to the studies in the previous section, but with a 20% random reduction in efficiency of the first two inner layers of the TIB. This was done for both the current pixel detector and the proposed upgrade. The results of this study are shown in Figure 6.20, which illustrates the impact such a degradation would have with the current detector and how the new pixel detector would recover most of the lost performance.

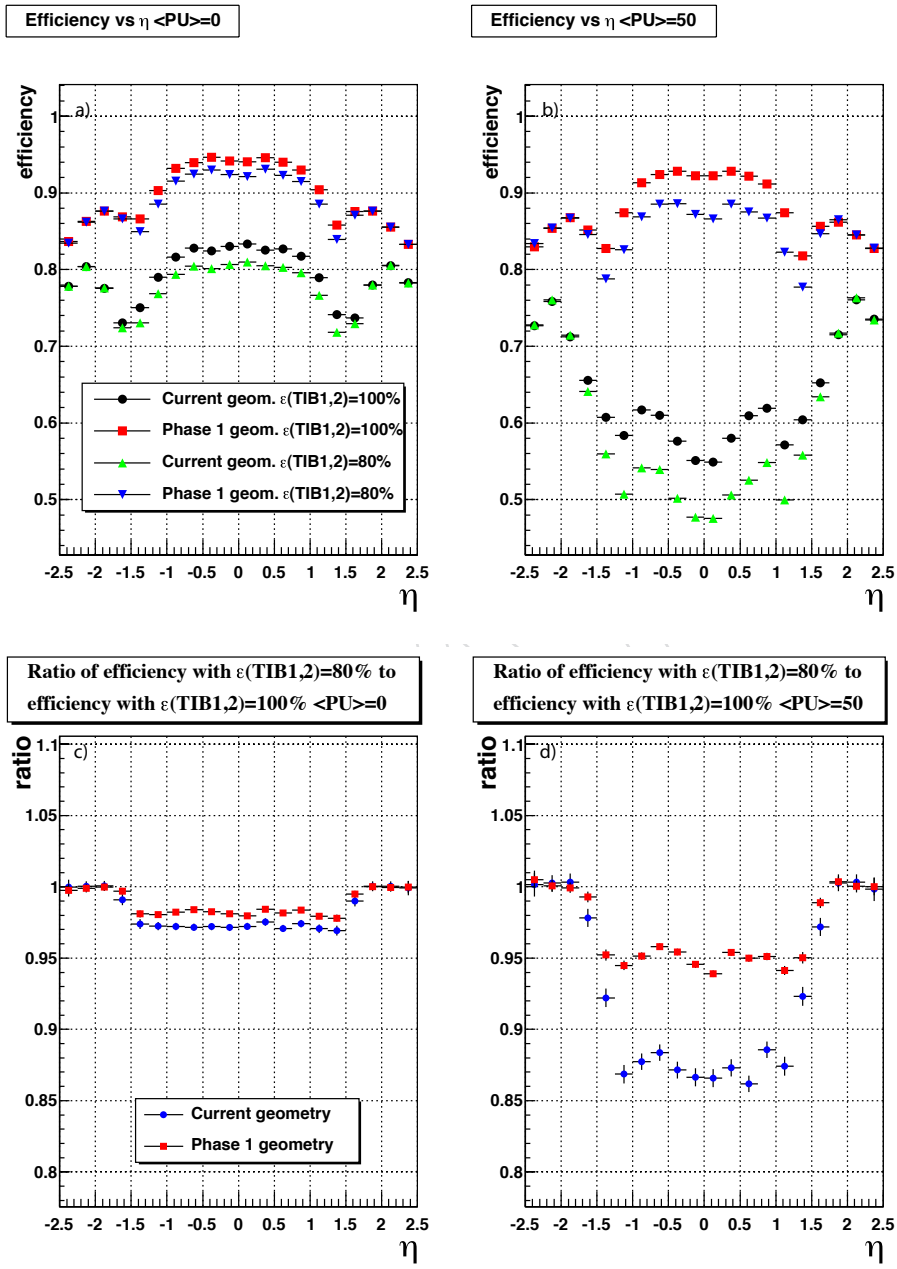

Figure 6.20: Effect of a 20% loss in efficiency of the TIB. The efficiency loss in track reconstruction is shown in (a) and (b) for low luminosities and 1E34 $cm^{-2}s^{-1}$. In (c) and (d), the ratios of efficiencies are shown. For the higher luminosities, this 20% loss in TIB efficiency would result in an overall relative reduction of 5% in the barrel region of the upgraded detector, but a 13% reduction in the current detector.

6.3.2.2 Muon Reconstruction with Tracker

Many analyses rely specifically on muon identification and reconstruction. In an effort to estimate the impact of the new pixel detector upon muon reconstruction in the tracker, single muons were embedded in pile-up events and the efficiency and fake rate to find such a muon as a function of transverse momentum and pseudorapidity were measured for the current pixel detector and proposed upgrade. The improvement in efficiency for the new detector is roughly 15% for muons across the momentum spectrum. Analyses which rely on two well identified muons would suffer an efficiency loss of $(0.85)^2$. This is shown in Figure 6.21.

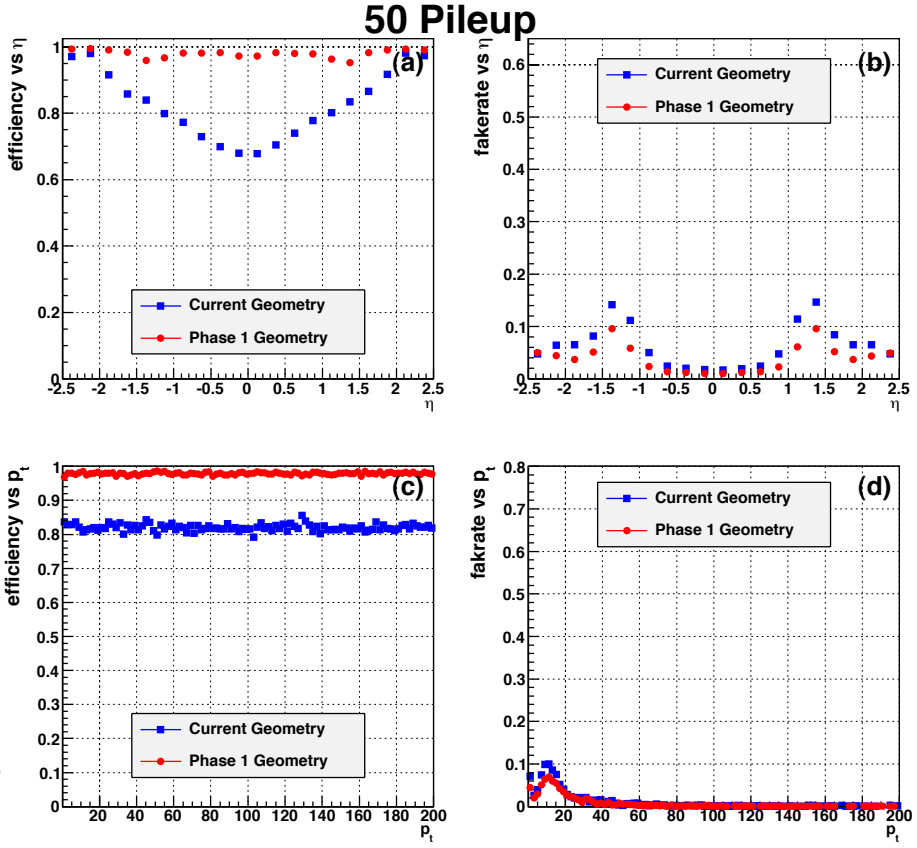

Figure 6.21: Single muon reconstruction in 2E34 $cm^{-2}s^{-1}$ events for the high purity selection.

6.3.3 Track Parameter Studies

The primary purpose of the pixel detector is to make precise measurements of the track direction and position before that information is degraded by multiple scattering. The increased sampling and reduced mass of the Phase 1 pixel detector also improve the track parameter resolution. The full-track impact parameter resolutions for the current detector and for the Phase 1 upgrade are shown as functions of pseudorapidity and momentum in Figures 6.22-6.23. Substantial improvement to the impact parameter resolution is a result of four main factors:

1. Reduced material in the tracking volume which reduces multiple scattering;
2. Moving the innermost layer closer to the interaction region;
3. Adding a fourth layer to the BPIX and a third disk to the FPIX which improves the track "lever arm" in the pixel region;

4. Improving the transverse impact parameter resolution in the forward regions by orienting the pixel sensors so that the 100 μm pitch (as opposed to the 150 μm pitch) contributes to the FPIX cluster resolution in the transverse plane.

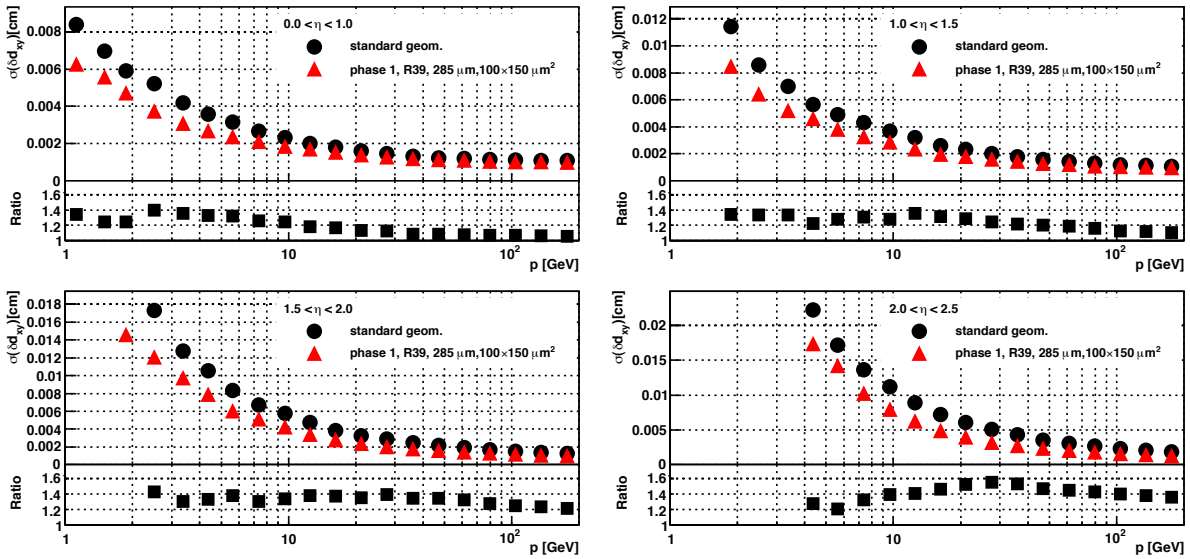

Figure 6.22: The transverse impact parameter resolution for the present and upgraded versions of the pixel detector as functions of track momentum in different pseudorapidity regions. The ratio plots at the bottoms of the subfigures show standard geometry resolutions divided by the upgrade resolutions, illustrating the relative improvement.

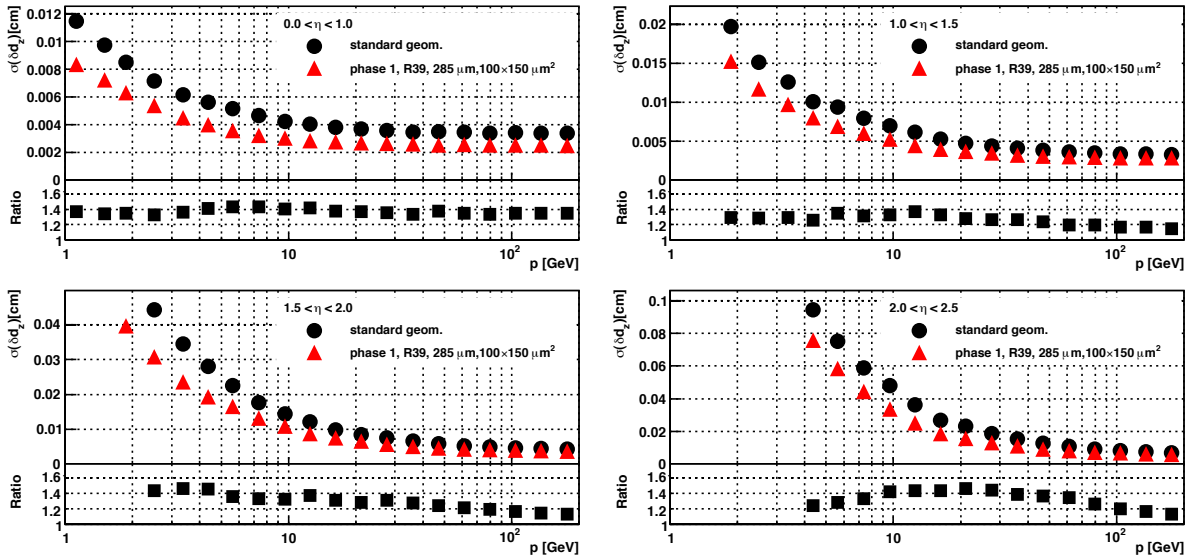

Figure 6.23: The longitudinal impact parameter resolution for the present and upgraded versions of the pixel detector as functions of track momentum in different pseudorapidity regions.The ratio plots at the bottoms of the sub-figures show standard geometry resolutions divided by the upgrade resolutions, illustrating the relative improvement.

As a consequence, vertex resolution and b-tagging performance also improve, as described in the following sections.

The addition of a fourth barrel pixel layer increases the measured radial track length by a factor two, thus improving the momentum resolution for stand-alone pixel tracks by a factor four.

This improves both the seeding and the extrapolation into the first layer of the strip tracker, and provides more powerful information to the HLT.

6.3.4 Vertex Resolution Studies

One of the primary functions of the CMS Tracker is to reconstruct primary and secondary vertices. It is expected that the Phase 1 detector will operate in an environment with a mean of 20-40 pp interactions per bunch crossing. Efficient and precise vertexing and the efficient association of individual tracks to vertices are essential to untangle the accidental coincidences of less interesting event topologies that could otherwise appear to signal important discoveries. The efficient and precise reconstruction of secondary vertices is a crucial element in b-tagging and in the search for possible long-lived exotic states. The longitudinal and transverse resolutions of simulated primary vertices are shown in Fig. 6.24 as functions of the number of tracks for the present detector and for the upgraded detector. Overall, the upgrade gives an improvement in the resolution of about 20%.

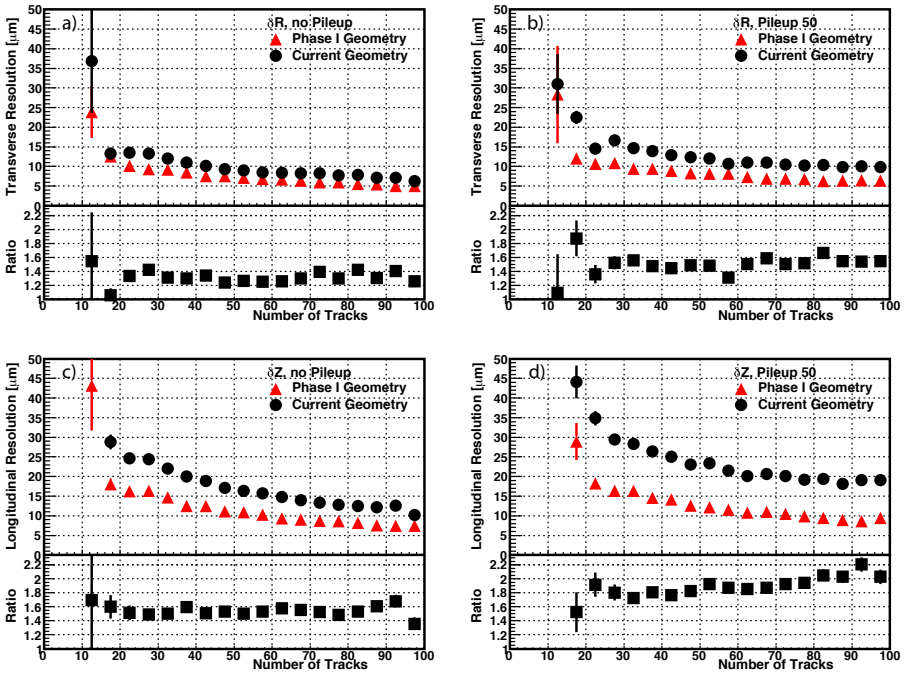

Figure 6.24: The transverse and longitudinal primary vertex resolutions for the present and upgraded versions of the CMS pixel detector as functions of number of tracks in simulated $t\bar{t}$ events. In (a) and (b), the longitudinal resolution is shown for no pile-up and $2 \times 10^{34}\text{cm}^{-2}\text{s}^{-1}$ at 25 ns bunch spacing respectively. Similarly, the same information is shown in (c) and (d) for the longitudinal primary vertex resolution.

6.3.5 b-tagging Studies

A number of interesting physics channels such as top quarks, Higgs bosons, and supersymmetric particles produce b jets in the final state. For example, a low mass Standard Model Higgs boson dominantly decays into a pair of b quarks, while the top quark decays almost exclusively into a W boson and a b quark. Various supersymmetric scenarios can produce final states with four or more b quarks. The efficient and pure identification of b jets is therefore a major element in the CMS physics program. The identification of b jets relies upon the relatively distinct properties of b hadrons such as large proper lifetime ($\tau \approx 1.5$ ps, $c\tau \approx 450$ μm), large mass, decays

to final states with high charged track multiplicities, relatively large semileptonic branching ratios, and a hard fragmentation function. Efficient track reconstruction, and in particular precise spatial reconstruction close to the interaction point, are thus key ingredients for almost all b-tagging algorithms. The performance improvements provided by the Phase 1 upgrade also enhance the b-tagging performance as shown in Fig. 6.25 for a sample of simulated $t\bar{t}$ events. Fig. 6.25a shows the detector performance for low instantaneous luminosity and Fig. 6.25b shows the performance for operation at an instantaneous luminosity of 2×10^{34} cm^{-2}s^{-1} with 25 ns bunch spacing. The b-tagging performance of the present detector is seriously degraded by the large number (~ 50) of overlapping interactions in each bunch crossing. The upgraded detector would reduce the light quark background of the Combined Secondary Vertex Tag by more than a factor of 6 for a b-efficiency of 60%, or conversely it would mean a relative 40% improvement in b-tagging efficiency for a fixed fake rate of 1%. The search for new physics frequently involves the identification of multi-b-quark final states. These searches would benefit by a factor of $(1.5)^n$ where n is the number of final state b quarks.

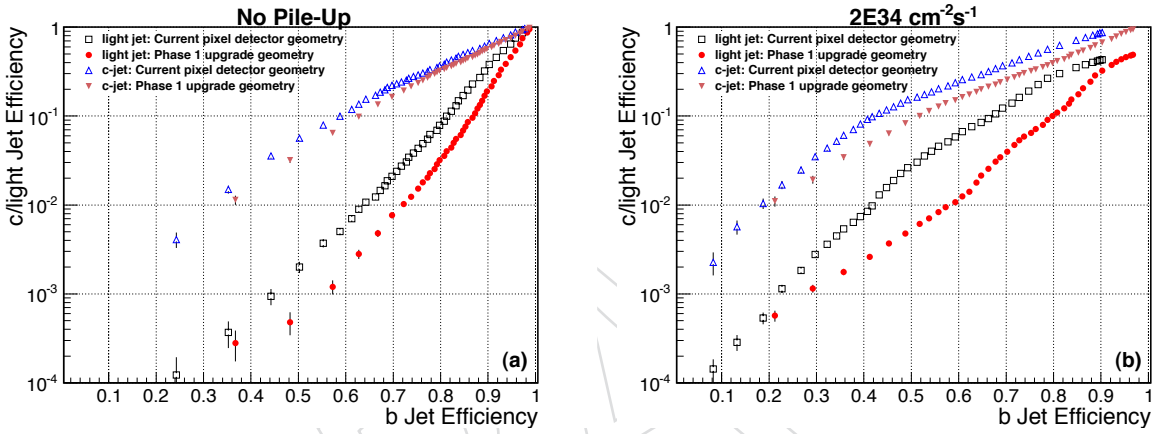

(a) (b)

Figure 6.25: The b quark efficiency of the Combined Secondary Vertex Tag is plotted versus the light quark (and gluon) efficiency for a sample of $t\bar{t}$ events in two different luminosity scenarios. The black points represent the performance of the current tracker and the red points represent the performance of the Phase 1 upgrade. (a) The instantaneous luminosity is assumed to be low enough that there are no multiple collisions. (b) The instantaneous luminosity is assumed to be 2×10^{34} cm^{-2}s^{-1} with 25 ns bunch spacing.

6.4 Further development for the innermost region

The innermost region of the pixel detector is expected to suffer degradation when the LHC reaches its high luminosity running in the later stages of Phase 1. The inner layers and rings have been designed, as described above, to be independently replaceable. An R&D line should continue for new detector modules with smaller pixel size and other enhanced features. The most important improvements target the module efficiency, radiation-hardness, and spatial resolution, aiming not only at better performance, but also more headroom relative to LHC conditions, or radiation backgrounds, which could exceed our expectations. The new modules must remain fully compatible with the rest of the Phase 1 mechanics, cooling and electrical systems.

6.4.1 Frontend electronics and sensors

Development of a new ROC is under consideration using CMOS technology of 130 nm or smaller. This will enable the engineering of a module with a smaller pixel size and lower readout thresholds. This will result in better spatial resolution and better ability to resolve tracks inside high momentum jets, where the present pixel size leads to overlapping hits in jets of energy above 100 GeV. The new ROC should also be able to operate with high efficiency with LHC operating conditions up to $2 \times 10^{34}\,\mathrm{cm}^{-2}\mathrm{s}^{-1}$ and 50 ns bunch separation.

The replacement of the innermost layers and rings also constitutes an opportunity to adopt sensors with greater radiation hardness. Recent measurements shown in Figure 6.26 show that sensors processed on mCz silicon collect the same signal at a lower bias voltage than those processed on FZ material. We are currently evaluating n-on-n and n-on-p single-chip pixel

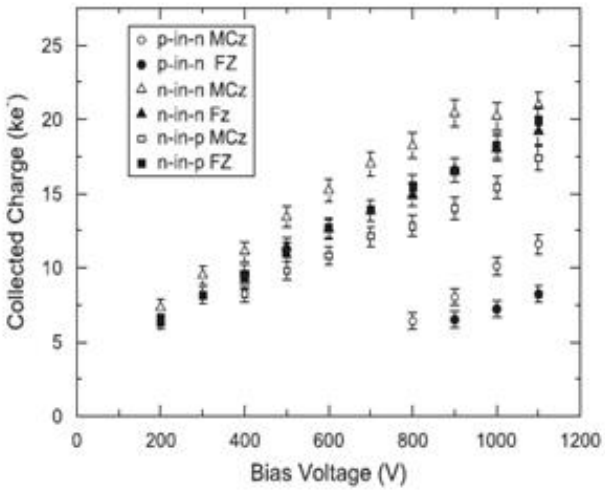

Figure 6.26: Collected charge as a function of bias voltage for six types of sensors irradiated with neutrons to $10^{15}\mathrm{n_{eq}}/\mathrm{cm}^2$ [17]

detectors processed on FZ, DOFZ and mCz material from different producers. A small number of n-on-p samples of FZ and mCz are available from Micron, IRST and CiS. A larger quantity of samples produced on different wafer types (FZ, mCz, epi) of different thickness and technology (n-in-n and n-in-p with p-stop and p-spray isolation) has been delivered recently by HPK and Sintef. Other options under consideration include the development of non-planar (so called 3-D) and diamond sensors.

6.4.2 Performance studies

The development of a readout chip with higher granularity and lower readout thresholds would offer the opportunity for further improving the detector later in Phase 1 in several key aspects:

- Enhanced hit resolution and detection efficiency after irradiation;
- Improved track parameter resolution;
- Improved jet reconstruction and b jet identification.

The pixel hit resolution is determined by the cell size, the charge sharing due to the combined effect of electric and magnetic fields, and by the readout threshold. The resolution can be improved by adopting pixel cells with smaller dimensions and front end electronics with lower

readout thresholds. Figure 6.27 shows the hit resolution after irradiation for a hypothetical scenario with a smaller pixel cell size, thinner sensors (220 μm) and lower readout thresholds (2000 electrons). We are considering further R&D on CMOS frontend electronics and sensors

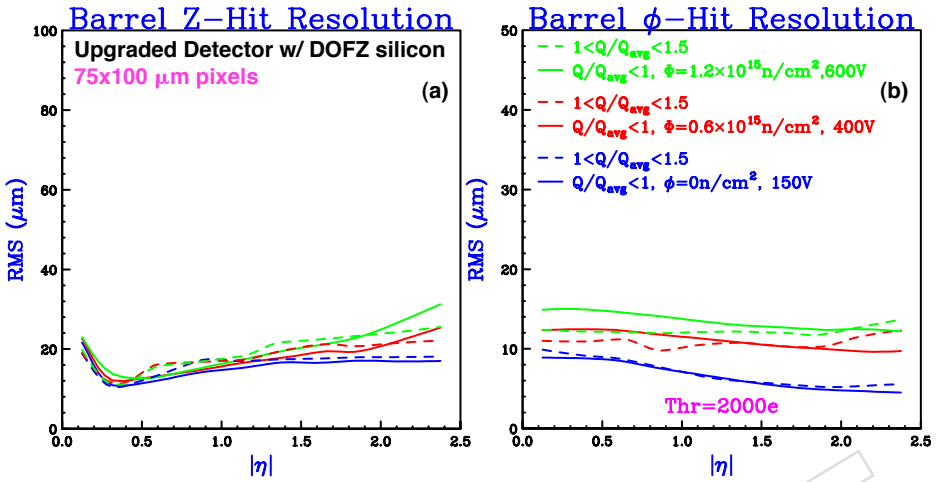

Figure 6.27: Hit position resolution (RMS) as function of the track pseudorapidity for an unirradiated (blue lines) and irradiated detectors (red and green lines). The pixel cell size is set to 75 $\times$ 100 μm^2 and the sensor thickness to 220 μm. (a) Longitudinal and (b) transverse hit resolution are shown separately. The solid lines correspond to hits with total charge Q below the average charge. Dashed lines correspond to hits with total charge $1 < Q/Q_{avg} < 1.5$.

in these directions.

At large momenta, the resolution on the track impact parameters and angles are largely determined by the hit resolution and radius of the innermost layer, and precision of the spatial alignment. For instance, with a hypothetical pixel cell of 75$\times$100 μm^2 in the 39 mm radius innermost layer, the longitudinal impact parameter resolution could be improved by 25%, as shown in Figure 6.28. Additional small improvements can be expected by further reducing the radius of the innermost layer. However, any reduction with respect to the baseline radius would require a careful assessment of the risks associated to the clearances during installation.

Primary and secondary vertex resolution is largely determined by the number of tracks associated to the vertex and resolution of track parameters. However, the hadronization of b quarks with large transverse momentum produces collimated jets which result in overlapping hits in the innermost pixel layer. In the current detector, for a 200 GeV b jet about 20% of the tracks have merged hits in the first layer. The effect produces a sizable deterioration of the b jet identification for jets with transverse momenta above 200 GeV. Future replacements of the innermost layer with sensors featuring smaller cell sizes, therefore, represent an opportunity to improve b jet identification in this upper kinematic range.

6.5 Schedule

Figure 6.29 shows a tentative schedule for the Phase 1 pixel upgrade.

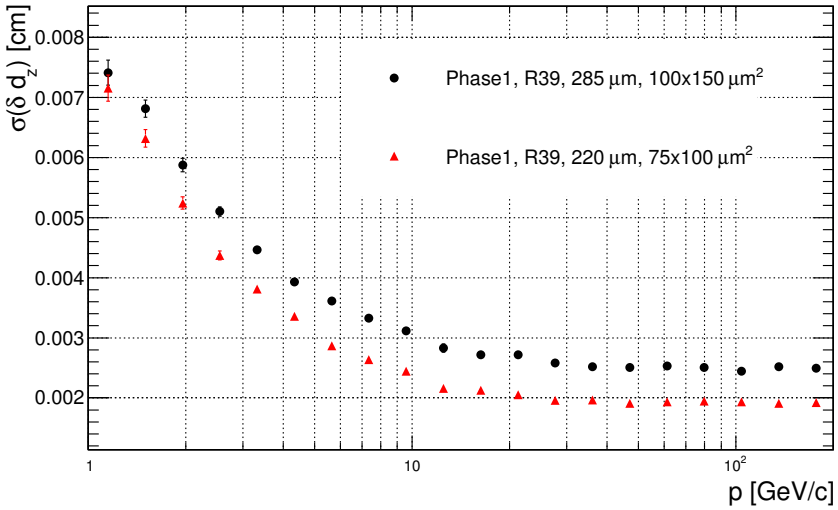

Figure 6.28: Longitudinal impact parameter resolution for the baseline upgrade scenario (black dots) and with a hypothetical replacement of the innermost layer adopting a reduced pixel cell size (red triangles).

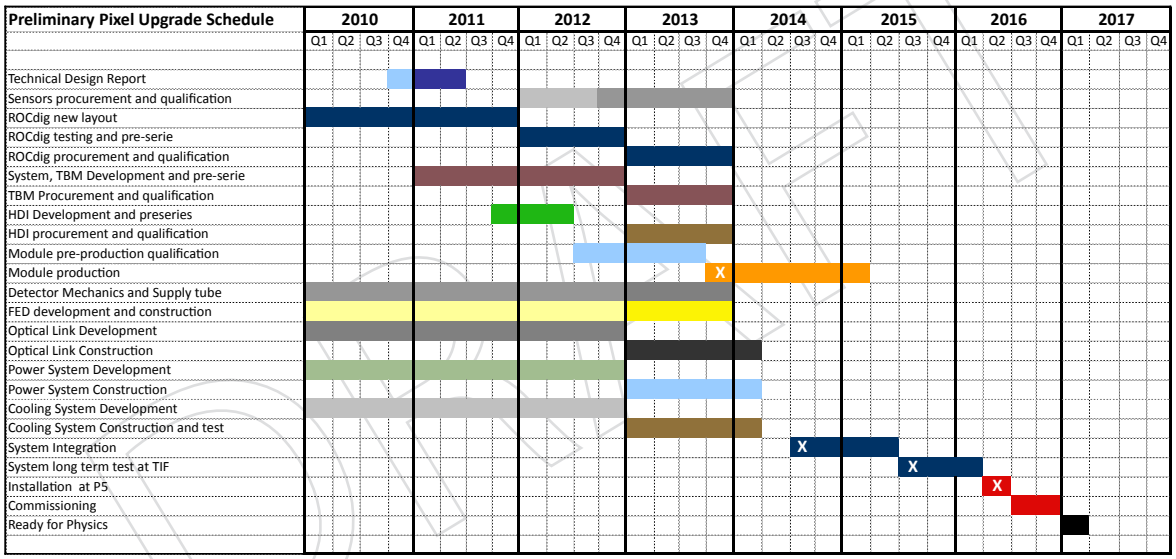

Figure 6.29: Tentative schedule for the Phase 1 upgrade pixel detector.

6.6 Conclusions

The Phase 1 upgrade of the LHC, starting with the long shutdown in 2016, presents CMS with both the requirement and the opportunity to upgrade the present pixel detector. The peak LHC luminosity after the Phase 1 upgrade is expected to reach up to 2×10^{34} cm^{-2}s^{-1} with a possibility of 25 ns or 50 ns bunch spacing. Such conditions are a factor two to four more intense than the nominal LHC conditions for which the present pixel detector was designed. The present system with its three-hit layout would suffer greatly in terms of performance in these conditions, severely compromising the ability of CMS to fully exploit the delivered luminosity from the upgraded LHC.

A thorough revision of the design of the ROC has been made, aiming to reduce the dynamic inefficiency to an acceptable level, while leaving the underlying architecture unchanged. So far,

a large reduction of inefficiency has been achieved with the new design, and effort will continue towards further reducing the data loss. The bandwidth of the readout has been doubled in the new design allowing the much larger system to be read out with the same number of fibers.

The addition of extra barrel and endcap layers will preserve our present excellent level of tracking performance even at the higher luminosity expected in Phase 1. Recent advances in CO_2 cooling, DC-DC powering, and readout links enable this ambitious proposal for the complete replacement of the present three-hit pixel system with a much larger ultra-lightweight system of four barrel layers and three endcap disks. The upgraded pixel system will have a reduced mass, a reduced innermost radius and increased lever arm, altogether resulting in a significant improvement over the present system in terms of tracking, vertexing and b jet identification.

Radiation effects will be of growing importance as the luminosity increases. The innermost detectors are expected to require replacement before the end of Phase 1 LHC operations. Such an intervention can be done during an LHC winter maintenance period. This replacement of the innermost layers presents a further opportunity to improve the detector performance at a later stage. Long term R&D is being done with the objective of having available sensors with greater radiation resistance. We are also considering designing a new readout chip in a more advanced CMOS technology, aiming to enhance the performance in terms of hit-efficiency and threshold, while also profiting from the potential to employ a smaller pixel size. There is a clear synergy here with R&D required for Phase 2 upgrade of the full Tracker system, which is also the case for the R&D on CO_2 cooling, power and readout systems.

The new system has to be commissioned and ready to take good physics data very soon after installation. The proposed schedule is compatible with having the detector integrated well in advance of the installation date, allowing time for extensive system tests at CERN and commissioning of large parts, if not the entire detector, prior to installation.

Chapter 7

Trigger System Improvements and Upgrades

7.1 Introduction

The present CMS trigger will work well up to the LHC design luminosity of $\mathcal{L} = 10^{34}\text{cm}^{-2}\text{s}^{-1}$ with the design bunch spacing of 25 ns, but will need significant modifications to operate above the LHC design luminosity. Due to the increased occupancy of at each crossing toward the end of Phase 1 of the LHC, when the luminosity will reach $2 \times 10^{34}\text{cm}^{-2}\text{s}^{-1}$, the Level-1 trigger systems will experience degraded performance of the algorithms presently planned to select 100 kHz of crossings from the input rate of 40 MHz (25 ns bunch spacing). For example, this increase in occupancy would cause electron and τ isolation algorithms to have reduced rejection at fixed efficiency and the muon trigger to have increased background rates from random coincidences. The same degradation would also occur if the LHC operates at design luminosity with a 50 ns bunch spacing due to the factor of two increase in occupancy.

While the modifications to the trigger systems described below will provide good trigger performance during the LHC Phase 1 operations or the LHC operating at design luminosity with a 50 ns bunch spacing, they also provide enhanced capabilities and improved performance at luminosities below the LHC design luminosity. Thus the modifications proposed provide the opportunity to increase the physics yield of the CMS detector by installing them before the LHC luminosity exceeds $\mathcal{L} = 10^{34}\text{cm}^{-2}\text{s}^{-1}$.

The modifications proposed for the Level-1 Trigger systems for Phase 1 must deliver the Level-1 trigger accept signal within the same time period as the present Level-1 Trigger systems since there is no possibility to increase this time until the present CMS tracker is replaced as part of Phase 2. This overall processing time constraint is independent of whether the LHC runs with 25 or 50 ns bunch spacing.

In order to meet the challenges for the DAQ of the higher LHC luminosity our approach is to hold the overall Level-1 trigger rate at the LHC design value of 100 kHz while increasing the DAQ readout bandwidth. This approach avoids rebuilding front-end and readout electronics as much as possible. However, maintaining a 100 kHz L1 rate during Phase 1 operations will increase the burden on the DAQ, which will need to transport more than the LHC design luminosity data size of about 1 MB per event.

The existing CMS Level-1 Trigger System shown in Figure 7.1 is organized into three major subsystems: the Level-1 calorimeter trigger, the Level-1 muon trigger, and the Level-1 global trigger. The calorimeter trigger combines information from the ECAL and HCAL, including the HF. The muon trigger is organized into subsystems that process the three different muon detector systems: the Drift Tube (DT) Trigger in the barrel, the Cathode Strip Chamber (CSC) trigger in the endcap and the Resistive Plate Chamber (RPC) trigger covering both barrel and endcap. The Level-1 muon trigger also has a global muon trigger that combines the trigger

information from the DT, CSC and RPC trigger systems and sends this to the Level-1 Global Trigger (GT).

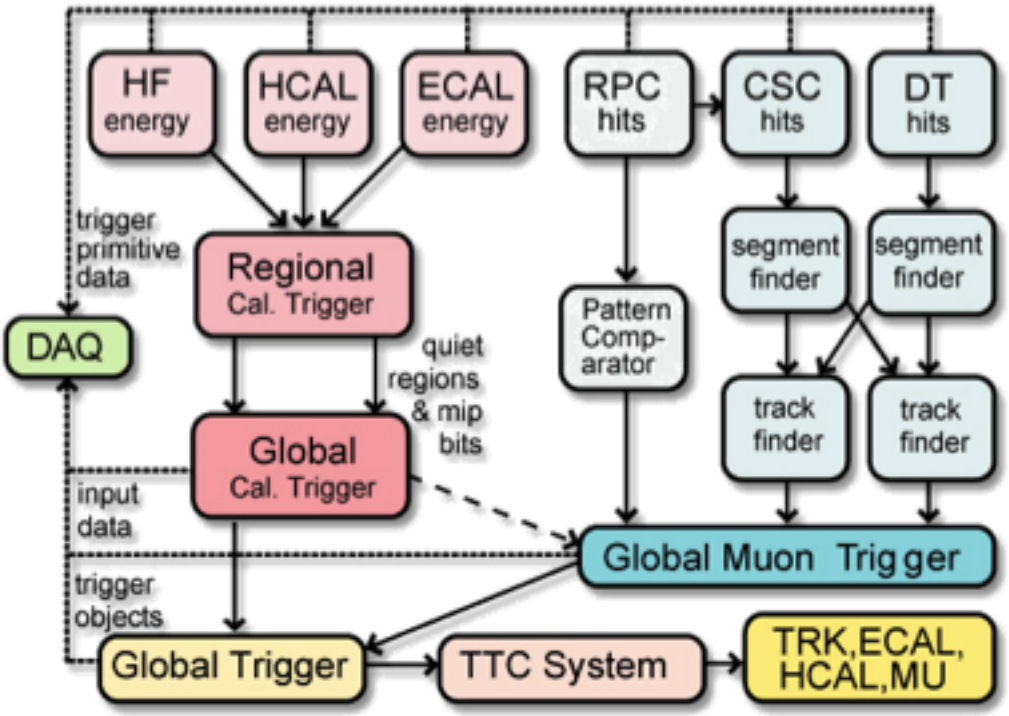

Figure 7.1: Overview of the present Level-1 Trigger System

In the following, we present the plans for upgrading each major trigger subsystem to improve the ability to maintain the system, to operate it reliably, and to handle the highest luminosities that will be experienced through 2020 with high efficiency and adequate rejection.

7.2 Calorimeter Trigger

7.2.1 Introduction

Increased luminosity results in several issues for the Calorimeter Trigger. First, the rate at which triggers fire goes up at least proportionately to the increase in luminosity. Second, the increased occupancy in the calorimeter renders some of the isolation cuts used in the calorimeter trigger less effective. This results in a decrease in the trigger efficiency, which can only be compensated by weakening the isolation requirement, which in turn results in a higher trigger rate. Third, multi-object triggers can also be affected by spurious coincidences of trigger objects in different interactions within the large number of pileup events. The net effect is that the trigger thresholds need to be increased, which may result in an inability to capture physics of interest for electro-weak symmetry breaking studies, even though the very highest p_{T} new physics is not affected.

To compensate for problems caused by high event occupancy the new calorimeter trigger upgrade design must significantly improve the efficiency and rejection ability of the Level-1 trigger algorithms. This is done by:

- Increasing the granularity of the calorimeter trigger *internal* processing. Due to limitations in the bandwidth and processing technologies available at the time of its

construction, the calculations of the present calorimeter trigger do not completely exploit the full (0.087×0.087 in $\eta \times \phi$) granularity of the ECAL and HCAL trigger towers transmitted to its inputs. The design of the upgrade calorimeter trigger completely exploits the full granularity of the ECAL and HCAL trigger towers in its calculations which enables improved algorithms that assure good performance up to twice the design luminosity or occupancy.

- Using the greatly increased flexible processing power in the new generation of FPGAs to implement sophisticated cluster algorithms that exploit the full trigger tower granularity. The raw trigger data can then be pre-clustered and the clusters then form the input to all calorimeter trigger algorithms. This improves dramatically the transverse energy resolution of the trigger output objects (Electrons, Jets, Transverse Energy Sums) and therefore makes the trigger thresholds sharper. Furthermore it allows for improvements in the isolation calculations, which (as shown below) exploit the full tower granularity to produce about a factor of two reduction in the trigger rate for the same efficiency.
- Using state-of-the-art Telecom technology to support the increased bandwidth requirements imposed by the higher granularity of the trigger input data.
- Providing the option to further exploit the higher granularity for eventual matching with a Level-1 Tracking trigger in Phase 2. Since the found calorimeter objects are located with significantly higher spatial granularity (half-a-trigger-tower resolution), there is the opportunity to enable matching with the tracking system at the highest granularity possible to better control the rates.

7.2.2 Present Calorimeter Trigger System Overview

The upgrade Calorimeter Trigger will replace the existing Regional Calorimeter Trigger (RCT) and Global Calorimeter Trigger (GCT). As shown in Figure 7.2 the existing RCT receives Trigger Primitives (TPs) consisting of eight-bit energies and a data quality bit for each calorimeter tower ($0.087\eta \times 0.087\phi$) from the HCAL and ECAL Trigger Primitive Generators (TPGs). The TPGs of both ECAL and HCAL use the Synchronization and Link Board (SLB). The RCT uses the TPs to find e/γ candidates and calculate four-by-four tower regional calorimeter sums that are sent to the GCT for sorting, jet finding, and calculating global quantities such as missing E_{T}. The RCT hardware consists of one clock distribution crate and 18 double-sided crates containing custom boards, ASICs, and backplanes. The Global Calorimeter Trigger (GCT) consists of 6 Source Card crates which convert the data to optical and a main crate which performs the jet finding and sorting, e/γ candidate sorting and calculation of all transverse energy quantities.

7.2.3 Calorimeter Trigger Upgrade Algorithms

The Phase 1 upgrade Calorimeter Trigger algorithms are based on the existing input trigger-tower granularity of $0.087\eta \times 0.087\phi$. The upgrade calorimeter trigger algorithms start with a particle-level cluster finder that makes 2×2 tower cluster sums along with setting of $e\gamma$-like or τ-like flags. The upgrade calorimeter trigger reduces the jet and missing energy trigger rates by clustering jets in multiples of 2×2 trigger towers: $6 \times 6, 8 \times 8, 10 \times 10$, with a sliding window that sums clusters of towers in one or two tower steps, and by the use of higher resolution scales with more precise geometry for missing energy.

The input information per tower consists of 8 bits of non-linear E_T information accompanied by a single feature bit determined from a fine grain analysis of the energy profile within the tower. For the ECAL, HCAL and HF, the feature bits indicate isolated electromagnetic energy,

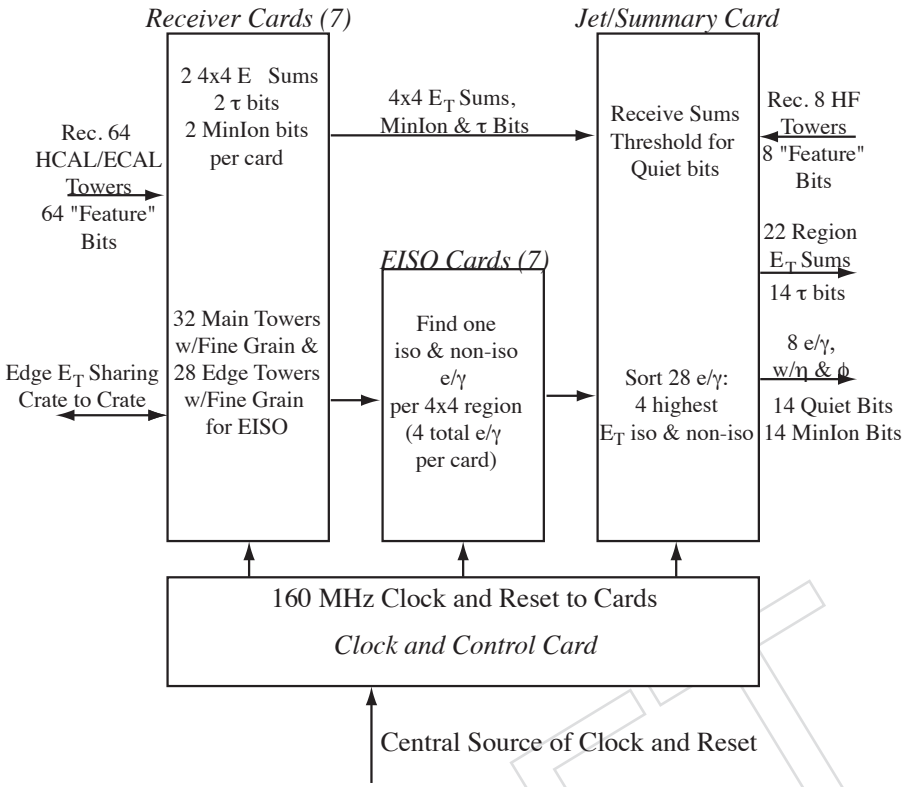

Figure 7.2: Schematic diagram of the present Regional Calorimeter Trigger data flow showing the trigger primitives entering from the calorimeters, the sharing of tower data between crates, processing for energy sums, jets, electrons and muons, followed by data transmission to the Global Calorimeter Trigger. MinIon refers to bits indicating the presence of a minimum ionizing particle; EISO refers to electron signals that are isolated from other nearby energy deposits; quiet means no energy present up to the threshold for minimum ionizing; Fine Grain refers to the bit set by the ECAL front end when the energy deposit in a 5×5 trigger tower of crystals is concentrated in one or two strips of 5 crystals; "Feature" refers to a single bit set in the HF indicating the energy in the trigger tower was concentrated in one or two HF cells.

minimum ionizing energy, and energy concentrated in a single tower, respectively. The output consists of the highest E_T objects in three categories: 4 electromagnetic objects, 4 τ objects and 12 jet objects, ranked by E_T, plus a set of global event characteristics: missing transverse energy (MET), total transverse energy (SumET), total jet transverse energy (HT) and missing jet transverse energy (MHT).

The algorithms create collections of isolated and non-isolated electromagnetic objects, isolated and non-isolated τ objects and jet objects. The algorithms are organized in several steps with progressive data reduction. These include a particle cluster finder that reconstructs overlapping clusters of 2×2 calorimeter towers and applies electron identification, a cluster overlap filter that removes overlaps between the clusters, locates local maxima and determines the cluster position; a particle isolation determination, jet reconstruction, particle separation and sorting that creates object collections sorted in E_T and passes on the highest E_T object in each collection to next step in Level-1 trigger processing; and finally the calculation of MET, MHT, and SumET from the cluster E_T values.

An initial series of studies of the algorithm performance used fast simulation with pileup of

4854 25 inelastic interactions per crossing. We defined two configurations of software, the existing
4855 CMS calorimeter trigger system and the upgraded calorimeter trigger. The initial simulation
4856 results indicate a factor of four reduction in rate for improved efficiency, as shown in Figure
4857 7.3. The output object location precision showing better than half-tower resolution is shown
4858 in Figure 7.4. The improved performance of the calorimeter trigger stand-alone algorithms is
4859 sufficient for Phase 1. This improved location precision will also be important for matching
4860 with tracker trigger information in Phase 2.

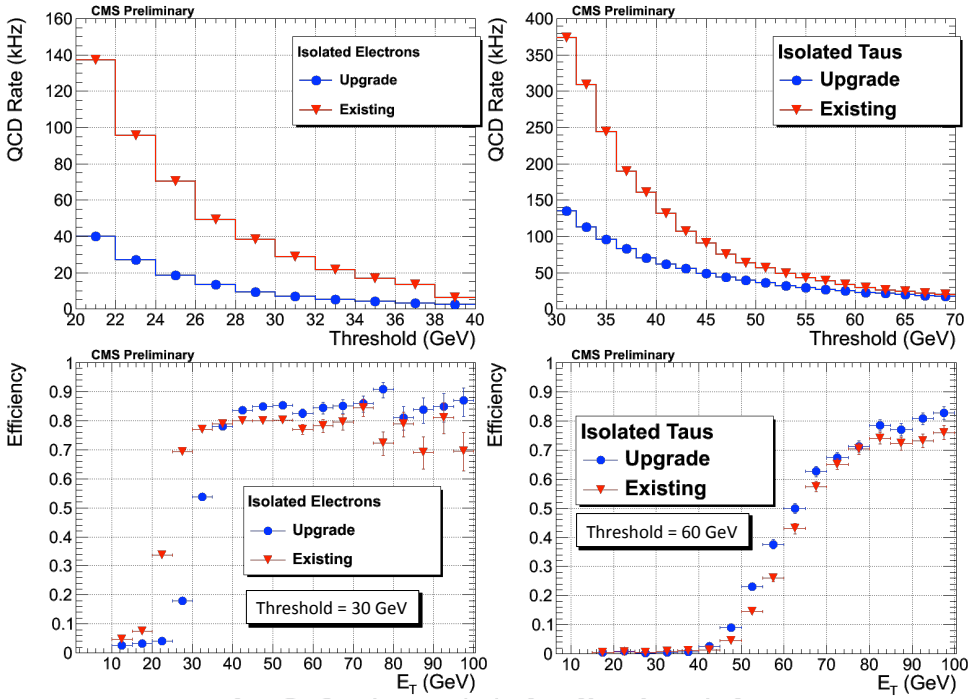

Figure 7.3: Integrated QCD trigger rate (kHz) for electron (top-left) and tau (top-right) triggers is plotted versus trigger E_T cut for the existing LHC and LHC Phase 1 Upgrade algorithms with improved clustering. Corresponding efficiencies for isolated electrons (bottom-left) and hadronically decaying taus (bottom-right) are also plotted for E_T thresholds of 30 and 60 GeV respectively.

4861 A sample Level-1 trigger table with thresholds and rates corresponding to 100 kHz total rate
4862 dominated by QCD (EWK) are shown in Table 7.1 for the case of instantaneous luminosity of
4863 10^{34} cm^{-2} s^{-1} where an average of 25 pileup events are seen. The thresholds values represent
4864 energies where there is 80% (75%) efficiency for the electron/photon (tau) object. The rates
4865 corresponding to these thresholds for the existing and upgraded calorimeter trigger system are
4866 shown. The total rate reduction is better than a factor of four. Note that the upgraded trigger
4867 system has more parameters that can be tuned to keep the rate at an acceptable level.

4868 7.2.4 Calorimeter Trigger Upgrade Hardware Strategy

4869 The LHC Phase 1 Upgrade trigger hardware will be based on modern FPGAs instrumented
4870 with fast Multi Gigabit Transceivers (MGTs) connected to optical links. The combination of
4871 large and fast FPGAs with Multi-GB/s optical links represents a revolution in online comput-
4872 ing and the signal processing industry. These state of the art devices combine very powerful
4873 computing capabilities with a large number of fast links which concentrate and process data
4874 very efficiently.

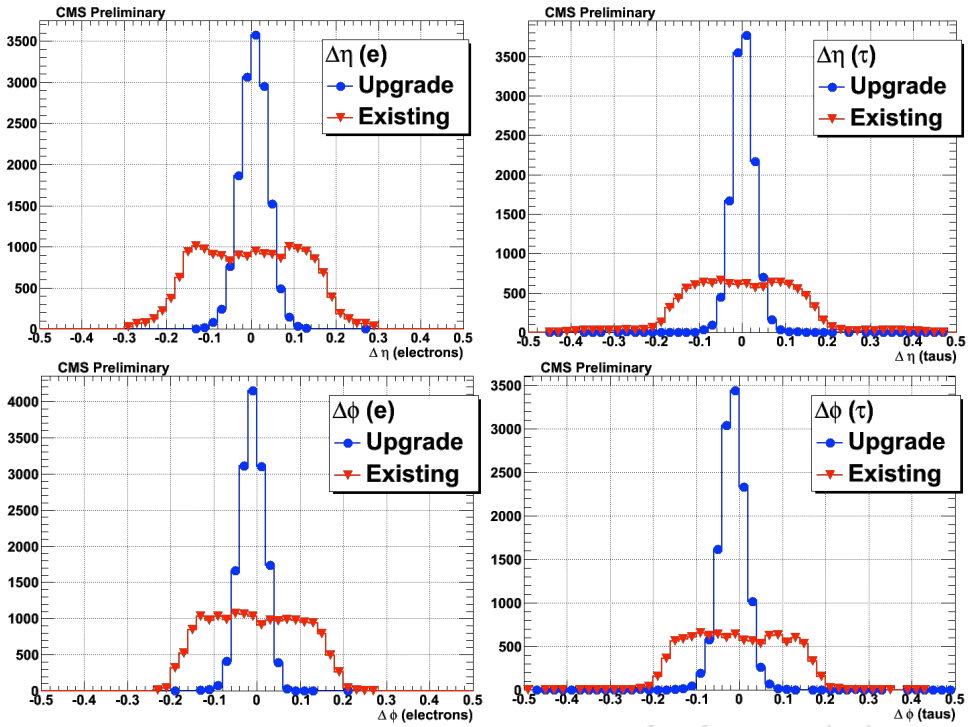

Figure 7.4: Position resolution of isolated electron, $\Delta\eta$, (top-left), $\Delta\phi$ (bottom-left) and hadronically decaying tau, $\Delta\eta$, (top-right), $\Delta\phi$ (bottom-right), for the existing LHC and LHC Phase 1 Upgrade algorithms with improved clustering, indicating better than half-tower resolution for the latter.

Trigger Object	Threshold (GeV)	Rate (kHz)	
		Existing CMS	Upgraded CMS
Single Photon	37	28	8
Double Photon	20	12	2
Single Electron	37	28	8
Double Electron	20	12	2
Single Tau	85	29	23
Double Tau	45	29	5

Table 7.1: A sample trigger table showing 80% (75% for τ) thresholds and rates which add up to 100 kHz at Level-1 for existing and upgraded CMS trigger systems.

FPGA capabilities in speed and capacity almost double with each generation. The most powerful devices on the market at present are Virtex-5 devices which are instrumented with 32 x 6 GB/s MGTs. Devices operating at 10-12 GB/s should be available in the next two years. These devices are ideal for all trigger algorithms and making the Level-1 Trigger (L1T) decision. Apart from technological advantage, they address a chronic problem in trigger systems, namely lack of standardisation. Speed requirements demand that L1T systems utilise custom electronics. For this reason L1T systems have limited capabilities but focus on fast execution of specific algorithms. They are adapted to the detector whose data they use and they are tuned for absolute minimum requirements sufficient for the physics selection. Thus hardware developed for muon triggers is not applicable for calorimeter triggers. The effect is that a trigger system consists of many different designs and technologies, which makes development, maintenance and

operation very slow and expensive. Many different pieces of hardware, software and firmware must be maintained by experts for the duration of the experimental programme, typically over ten years. The current CMS trigger system consists of at least one hundred different electronic cards, each requiring different maintenance, software and expertise.

Due to technology advances this trend of specific hardware for specific tasks is no longer necessary. Large FPGA parts with vast computing resources are readily available at reasonable prices. Modern FPGAs can cater to very different detector and physics needs. The physics applications are evident in the present CMS GCT where a complex system was designed quickly using essentially one processing board. This is capable, using suitable firmware, to execute all calorimeter trigger related algorithms, which range from electron sorting and missing transverse energy calculations to tau-jet finding. Thus, the use of different firmware on a single board type to service the various algorithm processing needs has already been demonstrated. While the opportunity to follow this strategy for the upgrade trigger does not justify the upgrade itself, its application to the upgrade will yield a more cost-efficient and easier to maintain system.

7.2.5 Calorimeter Trigger Upgrade Hardware Design

We propose to design the upgraded calorimeter trigger system based on FPGAs and Multi-GBit/sec links that adheres to the micro-TCA (μTCA) crate Telecom standard. Details about this industry-standard platform can be found in [18]. It is compact, hot swappable, and has a high-speed serial backplane. The capability will be built in for an eventual Phase 2 combination of the calorimeter trigger with tracker trigger information to enable both track matching for electron and tau objects, and provide tracker based isolation for photons, electrons and τs. The plan involves building the complete calorimeter trigger system based on high-speed optical interconnects and large FPGAs for data reception and processing.

We envision the new calorimeter trigger system to comprise up to 10 crates with up to 12 cards each. The goal is that the trigger processing cards will be uploaded with different versions of firmware each performing different processing tasks in the system. We will develop a new optical transmission system, which will connect the present calorimeter to either a new optical link or the present copper cable connections to the ECAL and HCAL Trigger Primitive Generation electronics and provide an additional output to connect to the upgrade calorimeter trigger so that both systems may be operated in parallel with physics data during a transition period. This can be done in a number of ways. As an example, a new optical Serial Link Board (oSLB) can replace the current SLBs on the HCAL and ECAL TPG electronics, and the current Receiver Mezzanine Card on the RCT Receiver Card.

The proposed platform for the upgraded Calorimeter Trigger processing is an Advanced Mezzanine Card (AMC)-style (μTCA) module (148.8mm high by 181.5mm deep). We are evaluating two possible architectures. One design uses three card types. The Input Cards will receive the TPGs and perform inter-region data sharing as needed. The Processing Cards will receive partial products from the Input Cards, perform second level sharing, complete the regional processing and deliver the output to the Summary Processing Cards that transmit their results to the Global Trigger. The TTC/DAQ card interfaces the crate to the Trigger Timing and Control (TTC) and DAQ systems, including the Trigger Throttling System (TTS) that provides back-pressure from the DAQ.

A block diagram of the above example of a new calorimeter trigger crate is shown in Figure 7.5. A single crate encompasses the full η-width from -5 to +5, including the full Forward Calorimeter (HF) granularity. A custom backplane would contain a combination of passive

and switched interconnections. The passive portion would be a good choice for the inter-crate sharing in η and the switches allow for some routing between the Input and Processing Cards.

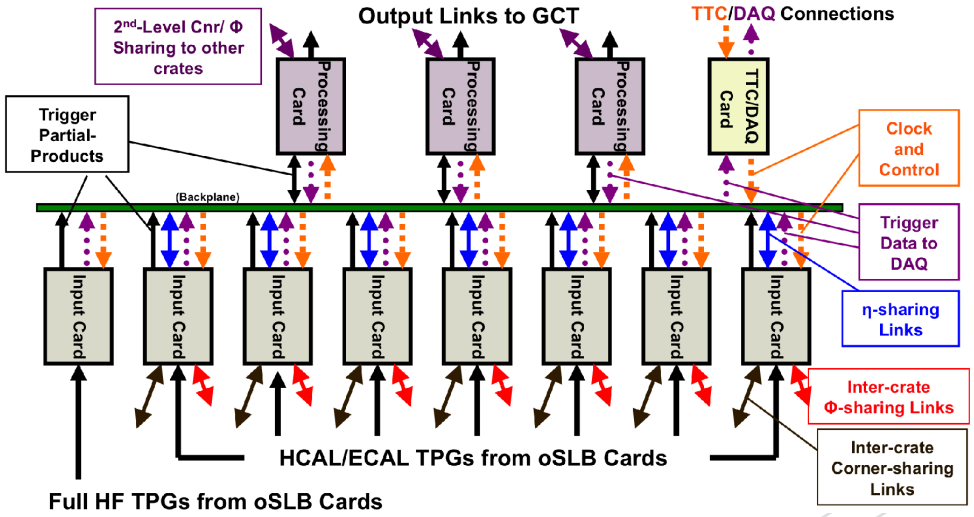

Figure 7.5: Block Diagram of an example of an upgrade RCT crate, showing cards and internal/external data flow. Eight Input cards will allow coverage in η from -5 to +5 and 30° in ϕ. Three Processing Cards would forward regional information to the GCT. A TTC/DAQ card would enable readout and handle Trigger Throttling System (TTS) interaction, receive the clock and control signals from the TTC system, and distribute these signals.

In order to verify that the upgrade calorimeter algorithms are implementable, firmware is being developed in Xilinx tools for these improved clustering and filtering algorithms with increased position resolution. The initial indications are that about 8×16 trigger towers worth of information can be processed in a single Virtex 5 FPGA using a good fraction of its 6.5 Gbps GTX multi-gigabit transceivers and 50% of the available logic. The processing can be done at or above 200 MHz with a latency of 185 ns, which would keep this processing well within the latency envelope of the present RCT calculations.

An alternative architecture, the Time Multiplexed Trigger (TMT), is also under evaluation. In a TMT data from a single bunch crossing (bx) are concatenated and delivered to a processing system over several bx. This approach requires several processing systems operating in a round-robin scheduling manner (i.e. processing system 1, takes bx = n, processing system 2, takes bx = n+1). The alternative architecture currently includes 10 of these processing systems.

An example of the TMT architecture is shown in Figure 7.6. Main Processor (MP) nodes are split across two cards (MP+ and MP- for $\pm\eta$). There are 10 of these MP nodes operating in a round robin scheduling manner, each only receiving data for every tenth bunch crossing. The two cards receive a single 9.6Gb/s link from each Pre Processor card in their respective η half. They also receive 4 links from the 4 adjacent towers in the opposite η half so that they have sufficient boundary information to build physics objects at the boundary between the two processing nodes.

The TMT Pre-Processor (PP) cards, that span the barrel and endcap, each receive ECAL and HCAL data in a ring that is 1 tower wide in η and spans the full ϕ circumference. The lack of ECAL data in the HF region enables these rings to be 2 towers wide in η. This requires 2×28 cards for the barrel and endcap and a further 2×28 for the HF and thus 72 PP cards and 92 cards in total. The total number of cards can be reduced to 56 if the calorimeter link speeds are

increased from 2.4 Gb/s to 4.8 Gb/s.

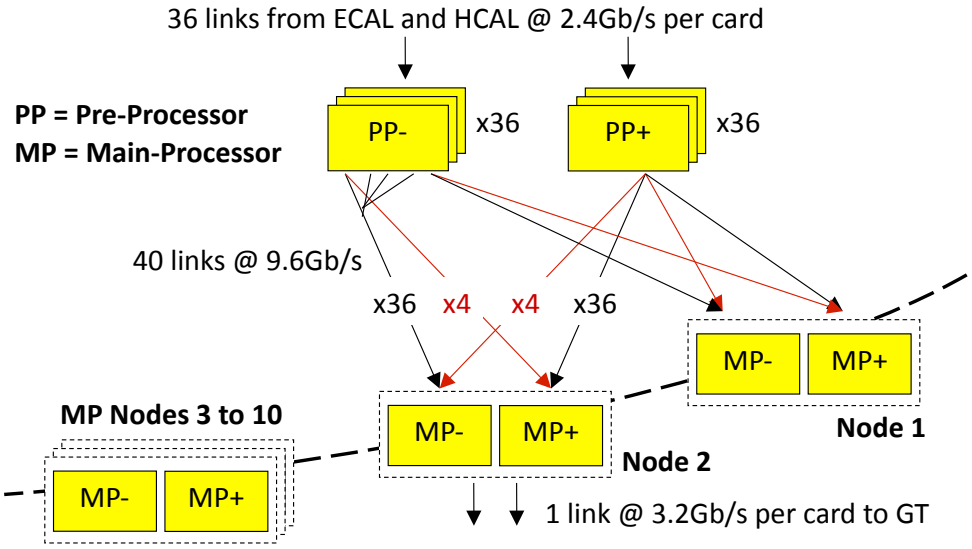

Figure 7.6: Time Mulitplexed Trigger Architecture.

The construction of the upgrade calorimeter also offers the opportunity, so far realized for only the ECAL, to apply a global calorimeter selective readout of both ECAL and HCAL using information from both ECAL and HCAL. This feature would enable the full-granularity readout of regions of the calorimeter with significant energy deposits and a more sparse readout of regions with minimal activity. This can be incorporated into the calorimeter trigger logic where energies from the ECAL and HCAL are summed and then processed by dedicated logic for transmission to the readout logic of the HCAL and ECAL.

7.2.6 Calorimeter Trigger Upgrade Hardware Demonstrators

The first step towards building the upgrade calorimeter trigger is to connect a number of μTCA prototype boards utilizing their configurable links according to a given architecture and build demonstrators for the Level-1 Triggers. The upgrade calorimeter trigger hardware technology has been validated through a successful program of hardware demonstrators based on μTCA modules and Xilinx Virtex FPGAs. Researchers at Imperial College London have built and tested a series of calorimeter trigger processing cards in order to evaluate the feasibility of the TMT architecture, gain experience in the latest technologies (e.g. MicroTCA) and develop the core firmware and software blocks that are common to both a TMT and conventional design. A double width, full height AMC card, MINI-T5, was designed, manufactured, tested and a TMT electron algorithm was implemented. The results show that the TMT design is consistent with the latency budget and the logic resources of a pipelined algorithm are, as expected, small. Researchers at University of Wisconsin Madison have built four trigger prototype cards integrated in a backplane fabric to demonstrate the running and data exchange of calorimeter trigger algorithms. Figure 7.7 shows photographs of these demonstrators.

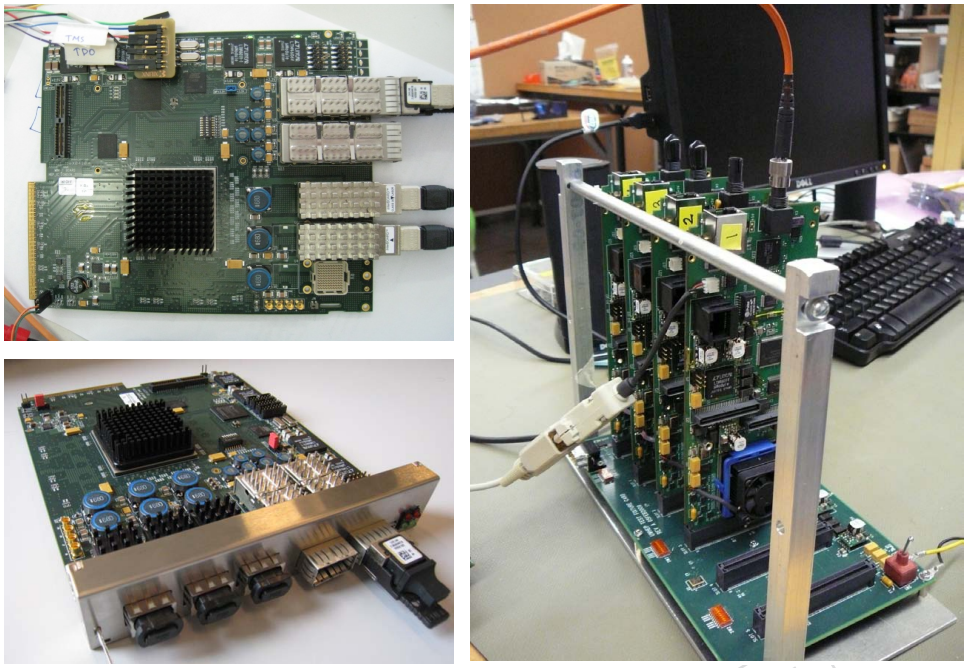

Figure 7.7: Photographs of modules built for the upgrade calorimeter trigger demonstrator program. Left: two of the Imperial College calorimeter trigger processing cards; Right: four of the University of Wisconsin calorimeter trigger algorithm test cards mounted on a test backplane fabric.

7.3 Muon Trigger

7.3.1 Introduction

Increased luminosity also results in several issues for the Muon Trigger. The single muon trigger rates as a function of the p_T threshold are shown in Figure 7.8 for LHC design luminosity (10^{34}cm^{-2}s^{-1}). The rates are shown separately for Level-1 (L1 Trigger information only), Level-2 (HLT reconstruction using full-resolution muon system data only, with isolation calculated from full-resolution calorimeter data), and Level-3 (HLT track momentum and isolation calculated from silicon strip and pixel tracking data), with and without isolation applied at Levels 2 and 3. Also shown is the single muon rate predicted by the event generator. A threshold of 31 GeV/c reduces the single-muon Level-3 rate to 50 Hz with isolation (100 Hz without isolation).

In Figure 7.8 the Level-2 rates have a reasonable reduction with increasing muon p_T cut up to 20 GeV/c, where the rate is 200 Hz. Above a p_T of 20 GeV/c, the reduction of rate with increasing muon p_T cut is very slow, dropping only a factor of 2 with an increase in p_T cut up to 60 GeV/c. Therefore if we bring the full power of the Level-2 algorithm performance (without tracking) to bear in Level-1, above a p_T threshold of 20 GeV/c the only effective method to reduce the rate with increasing threshold is to use Level-3 algorithms, which involve tracking. This motivates examining the eventual use of tracking information in the LHC Phase 2 Upgrade L1 trigger.

7.3.2 Present Muon Trigger System Overview

7.3.2.1 DT Track Finder

The Drift Tube Track Finder (DTTF) identifies muon candidates in the barrel muon detector and determines their transverse momenta, position and quality. The candidates are then sorted

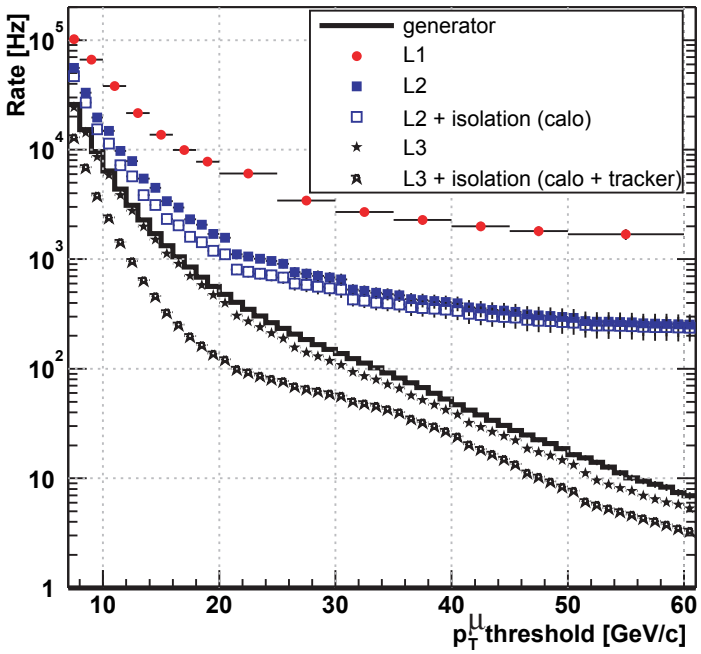

Figure 7.8: The HLT single-muon trigger rates as a function of the p_T threshold for a luminosity of $10^{34}\text{cm}^{-2}\text{s}^{-1}$. The rates are shown separately for Level-1, Level-2, and Level-3, with and without isolation applied at Levels 2 and 3. The rate generated in the simulation is also shown[19].

by rank (based on p_T and number of hits) by dedicated cards and the highest four are sent to the Global Muon Trigger. The track finding principle relies on extrapolation from a source track segment in one muon station to a possible target segment in another station according to a pre-calculated trajectory originating at the vertex. Target segments compatible with the expected extrapolation position and bending are linked to the source segment. Compatible segments form a track, to which a transverse momentum is assigned.

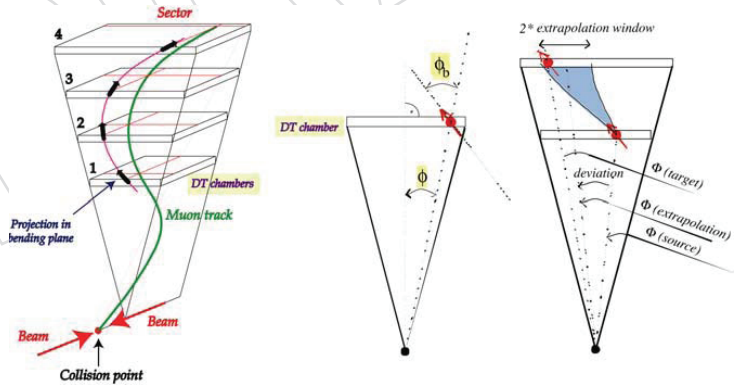

Figure 7.9: DTTF extrapolation scheme

The extrapolation principle is shown in Figure 7.9. The DTTF operates in the $r-\varphi$-projection. A coarse assignment of η is nevertheless possible by determining which chambers were crossed by the track. The DTTF works on sectors and wedges. The DT system is divided into twelve 30° wedges in φ. Each wedge is divided into six sectors in z. The central wheel is split into 2×12 half-width sectors, while the four outer wheels are each subdivided into 12 full-width

sectors. Every sector contains four DT chambers. The track finding is performed by 72 sector processors. Each sector processor receives at most two track segments per chamber from the DT local trigger (the Sector Collector card) through optical links. Each segment is described by its position in the sector local frame (12 bits), bending angle (9 bits), quality code (3 bits) and θ information (16 bits). The sector processors attempt to join track segments to form complete tracks. The parameters of all compatible segments are pre-calculated. Extrapolation windows, which are adjustable, are stored in look-up tables. Muon tracks can cross sector boundaries, so data are exchanged between sector processors. A cancellation scheme is incorporated to avoid duplicated tracks.

7.3.2.2 RPC Trigger System

An overview of the present RPC trigger system is shown in Figure 7.10. The analog strip signals are discriminated and formed into 100 ns binary pulses at the 7200 Front End Boards (FEBs) placed on the chambers (Figure 7.10). The signals are sent from FEBs in the LVDS standard through copper cables to Link Boards (LB). The LBs (1232 boards) are located around the detector (in the CMS cavern). The LB electronics synchronizes the signals with the clock provided by the TTC and compresses the data (zero suppression). The data from two Slave LBs are transmitted to the Master LB. The Master LB multiplexes the data from Slave LBs and from itself and converts them into optical signals (1.6 GHz) transmitted through a fiber to the Trigger Boards (TB) located in the Counting Room. In total there are 444 fibers varying in length from 20 to 80m. Since the data from every optical link has to be delivered to two or four TBs, the links are split by Splitter Boards (SpB, 60 pieces).

Each of 84 Trigger Boards receives signals from up to 18 links. On the TB the data are distributed through the OPTO Receiver FPGAs (6 chips on each TB) to the PAC FPGAs (3 or 4 chips on each TB, placed on the mezzanines; each PAC receives data from all links). The PACs execute the trigger algorithm based on the Pattern Comparator (PAC) strategy: the chamber hits are compared with predefined patterns of muon tracks obtained from simulations, the coincidence of hits in the same BX in at least 3 layers of chambers is required. In total about 110K RPC strip signals are compared with more than 2 million patterns in every BX across the entire system.

The muon candidates found by PACs are transmitted to the GBSORT chip. Since the PAC algorithm is performed for segments of the detector that overlap, the same muon can be found by several segments. Therefore, in the GBSORT, the muon candidates from neighbouring segments are suppressed (ghost-buster algorithm). Then remaining candidates are sorted according to their quality. Since the amount of data that has to be transmitted on the TB is large (432 bits per BX from six OPTOs to every PAC, then 432 bits from four PACs to the GBSORT), to reduce number of paths on the board the data are transmitted with fast LVDS lines with frequency of 320 MHz (i.e. one line transmits 8 bits during one BX).

The muon candidates returned by the GBSORT are further processed at the next levels of the ghost-busters and sorters tree: on the custom backplane of the Trigger Crate (TC GBSORT) containing the TBs, and then on the Half Sorter Boards (HSB) and Final Sorter Board (FSB) located in the Sorter Crate (SC). From FSB, up to 8 highest momentum muon candidates are sent to the Global Muon Trigger (GMT) every BX.

7.3.2.3 CSC Track Finder

The task of the CSC Track-Finder (CSCTF) is to reconstruct muon tracks in the CSC endcap muon system and to measure the transverse momentum (p_T), the azimuthal angle (φ), and

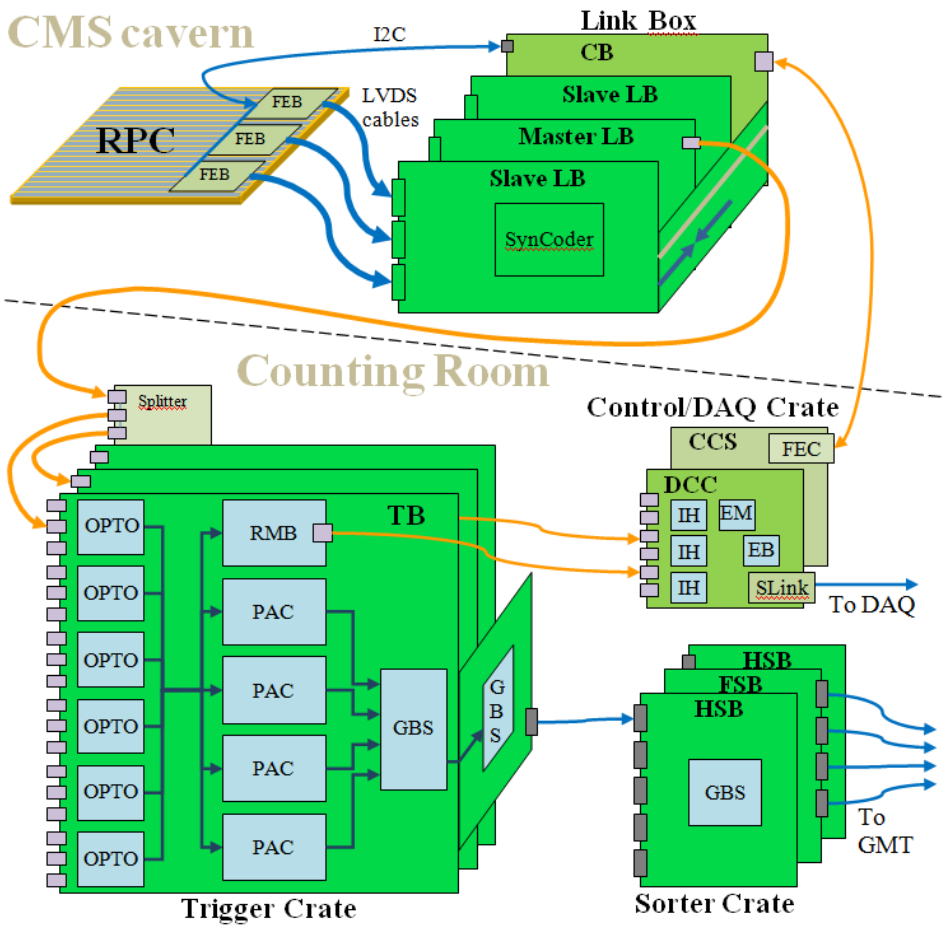

Figure 7.10: Overview of RPC Trigger System on the detector (upper) and in the underground counting room (lower).

the pseudo-rapidity (η) for each muon track. This objective is complicated by the non-axial magnetic field in the CMS endcap and by the expected high background rates already at LHC luminosities. Consequently, the design incorporates full three-dimensional (3-D) spatial information into the track finding and measurement procedures.

A block diagram of the CSC Track-Finder architecture is shown in Figure 7.11. The system is composed of the custom backplane and CCB (not shown), the Muon Port Card (labeled MPC), Sector Processor (SP) and Muon Sorter (MS) circuit boards. Front-end electronics boards (either mounted directly on the CSC chambers or in nearby crates) use pattern recognition firmware based on pattern templates to reconstruct track segments spanning the six layers within each CSC chamber. These segments, called Local Charged Tracks (LCT), are found independently in both the anode (ALCT) and cathode (CLCT) views, and are combined in the Trigger Mother Board (TMB). Up to two combined anode/cathode LCTs are sent from 9 TMBs to Muon Port Cards which reduce the number of LCTs delivered from each CSC sector to a maximum of three. The CSCTF receives data from several MPCs, reformats the data into tracking variables, applies alignment corrections, reconstructs tracks across the four endcap disks, and computes the p_T, η and φ. The processing in two of the boards (the MPC and the SP) includes sorting on quality indicators and elimination of low-quality track segments or tracks if necessary. The CSC trigger system is logically partitioned into 12 azimuthal sectors (6 per endcap) for the

purpose of regional track finding. Thus, 12 SP identify the three best muons (if present) in each 60° azimuthal sector. Each processor is a 9U VME card housed in a crate in the underground counting room of CMS. Each SP receives its data from MPCs resident in separate crates of the periphery of the CMS endcaps. The MPCs collect track segments from up to nine CSCs.

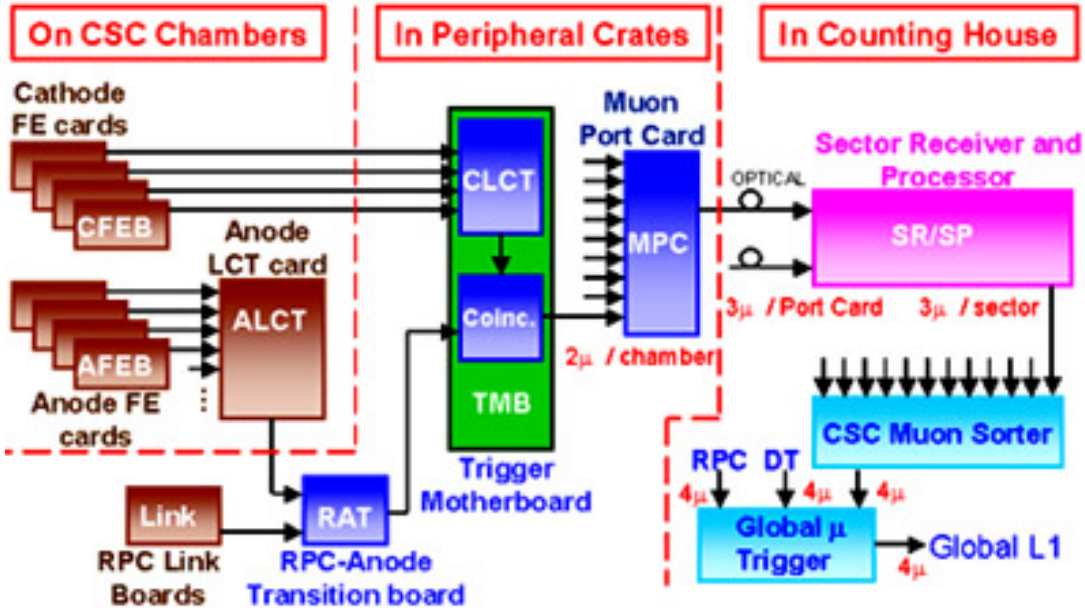

Figure 7.11: Schematic diagram of the CSCTF data flow.

A maximum of six track segments are delivered to an SP from the first muon station (ME1) of a sector. These track segments arrive from three MPCs, each delivering up to two track segments in a 20° subsector. For the other muon stations (ME2-ME4), one MPC per station delivers three track segments. In addition, up to four track segments from the barrel DT muon system are propagated to a transition board in the back of the crate and delivered to each SP as well. The output of the Track-Finder consists of the four best-identified muons together with their kinematic and quality descriptions. These are sorted by the Muon Sorter and then transmitted to the Global Muon Trigger (GMT). In the region near $\eta \sim 1$, the CSC and DT systems overlap and their respective Track-Finders exchange information to make composite tracks.

7.3.2.4 Global Muon Trigger System

The Global Muon Trigger sorts the RPC, DT and CSC muon tracks, converts these tracks into the same η, ϕ and p_T scale, and validates the muon sign. It then attempts to correlate the CSC and DT tracks with the RPC tracks. The final ensemble of muons is sorted based on initial quality (e.g. number of stations included in the track), correlation and p_T and then the 4 top muons are sent to the Global Trigger.

7.3.3 DT Trigger Issues and Upgrade

The highest priority in the design of the current DT Track Finder system was miminizing trigger latency. This required adopting specialized fast data transmission and processing techniques in the design. The adopted techniques have been found disadvantageous for production and maintenance, as experienced during trigger operation.

One of the critical issues for maintenance and operations is the data exchange between sec-

tors. A DTTF basic unit processes data from one of the 72 available sectors of the CMS barrel muon detector. The DTTF input data are transmitted serially through optical links from Sector Collector cards to the DTTF system, where they are decoded and processed. The Sector Collector cards are located on the CMS detector, and the DTTF crate is located in the Underground Counting Room (USC). To minimize latency, once received, the input data are always treated as a bit-parallel data stream forwarded on wide data paths. In order to reconstruct muons crossing sector boundaries, connections need to be made not only to the neighboring units in φ, but also the neighboring unit in z. The z connections between DTTF units are done through the backplane, but the φ connections are implemented with high density flat cables due to mechanical constraints on the backplane. This resulted in highly complex and error prone cabling. The complexity of the connections makes error detection and maintenance work very difficult.

Data transfer requirements put further constraints on the flat cable. On one hand, the transmission has to be completed in 25 ns, which sets the upper limit on its length. On the other hand, the mechanical arrangement inside the DTTF crate dictates its minimum length. The cable length has been designed to fulfill these constraints, but detector operations show serious problems with this design. Tests demonstrated that the present data transmission timing works at the physical limits. In addition, the noisy environment makes it difficult to establish an optimal data transmission.

7.3.3.1 Considerations for DTTF Redesign

The biggest motivation for a DTTF Upgrade is to eliminate drawbacks of the present design. Staying within trigger latency requirements with the available technology turned out to be more limiting than originally estimated. Faster FPGAs developed in the recent years allow more flexibility in distributing tasks. The possibility to re-prioritize permits the development of a new DTTF design that addresses most present problems.

Several DTTF upgrade approaches are considered. Each approach results in different system structures and requires different levels of changes. For all possible solutions, their technical feasibility and their impact on system performance will be investigated. The standard VME bus is subject to early obsolescence and there are CMS-wide efforts to find new standards. The μTCA system is considered the standard for most future developments. This standard offers high speed interconnects between boards and a fast, centralized control scheme. These qualities coincide very well with the needs of the DTTF system. Furthermore, we plan to investigate if fast interconnects or an extended JTAG structure for internal control and monitoring can be implemented more efficiently. The different upgrade schemes are depicted in Figure 7.12.

On the Trigger Primitive side, the Sector Collector (SC) electronics will be moved off the detector and into the underground counting room. This increases the flexibility of the new system. Moving the SC into the counting room provides more headroom in the latency budget, allowing a more generous design of the system-wide data flow. If the SC and the optical receiver are integrated, the double optical $\rightarrow$ copper, copper $\rightarrow$ optical transformation is omitted.

The biggest problem in the present design is the complexity of the Trigger Object distribution among the Track Finder boards. There are several possible solutions available to achieve a more "streamlined" system. All these solutions have a common point: the connections must use fast serial data transfer instead of the wide parallel data connections. This will help increase the signal quality and reliability, while simplifying data verification, monitoring and maintenance. There is no feasible solution to change or extend the present DTTF hardware design towards fast serial links because the entire electronics construction was designed around the required parallel connections.

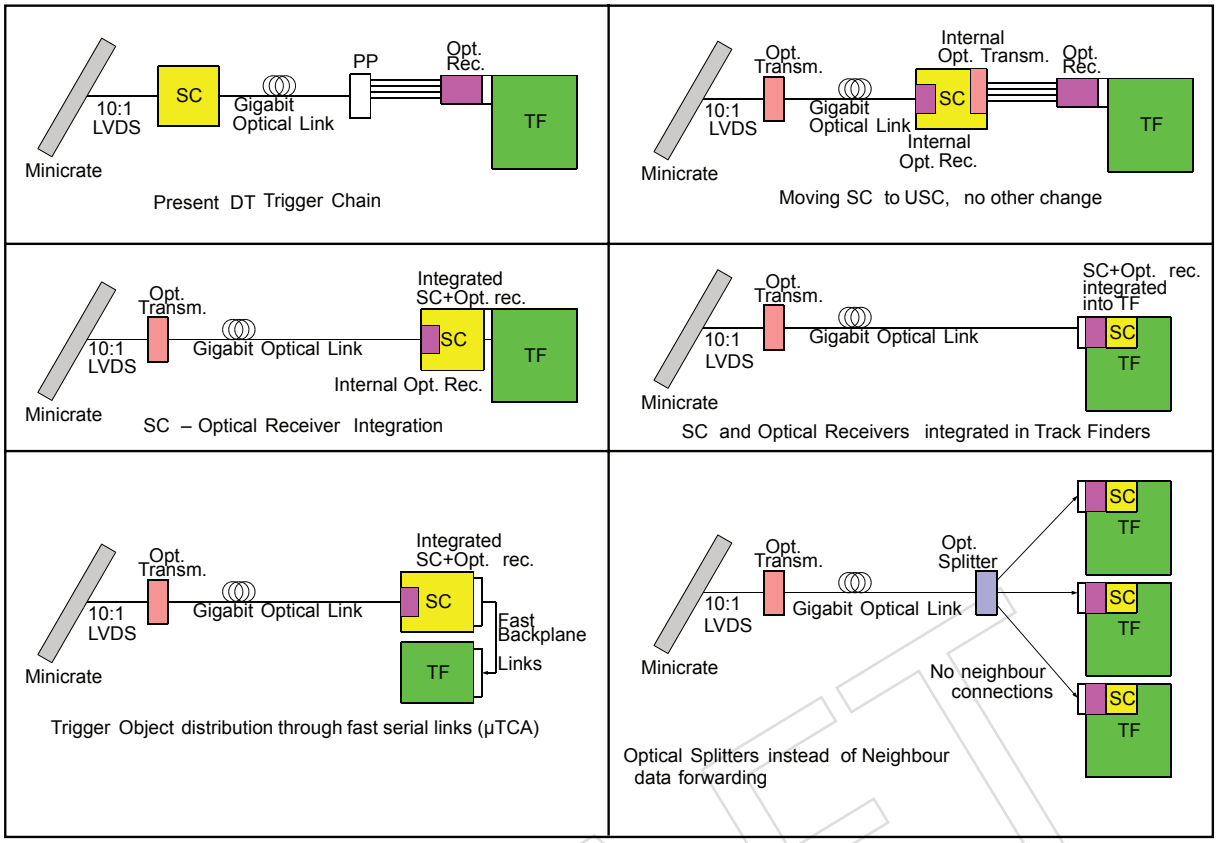

Figure 7.12: Possible layouts for the upgraded DT trigger scheme.

Conceptually, the simplest upgrade strategy is to keep the same data flow design of the DTTF system, but replace neighbour connections by fast optical links. This would require redesigning and rebuilding the TF boards; the number of boards would not change. The resulting system would have the same complexity and roughly the same cost as the present system. It would also not address the problems of the obsolete VME standard.

Another option being considered is an integration of DTTF and TSC functions. The upgraded DTTF could include the Optical Receivers and the SC functions. This solution would allow integration of TF processors for several sectors on a single board, decreasing the system size (number of boards, number of crates). The neighbour data exchange can be achieved using high speed optical links. This solution can not be implemented with the present backplane and crate structure. The possible integration of the Track Finding functions of several sectors into one board decreases the number of boards and thus crates.

A third option is to eliminate neighbour connections, but distribute the input data using optical splitters. In this design, all TF parts receive all information they use directly from the DT minicrate format. This also means the TSC functions would be multiplied for all inputs receiving optical links. The benefits and drawbacks of this solution must be clarified in a feasibility study.

7.3.3.2 System Layout

The most straightforward upgrade solutions foresee merging the TF functions of several sectors on one single electronics board. This merging task can be performed in several ways. Detailed

studies of different options will be performed in the context of a Feasibility Report that can be part of the future Upgrade TDR.

7.3.3.3 Demonstrators

In order to develop firmware for the upgrade, a demonstrator system must be built. Depending on the choice of system layout, this can be constructed on the present DTTF Prototypes or rather using a μTCA system. Demonstrator tests will determine the capacity of the fast serial connections, speed and bandwidth margins within a real hardware environment. Parallel developments should be avoided. Developments for the CMS Global Trigger and Calorimeter Trigger Upgrades should be taken into account; only hardware whose functionality cannot be achieved with the existing boards will be developed.

7.3.4 RPC Trigger Issues and Upgrade

The CMS RPC system is designed for highly efficient detection of muons with precise timing over the entire active area of the CMS detector. In order to save costs for the low luminosity detector, the CMS collaboration reduced the number of layers in the forward RPC system from 4 to 3 and the coverage in η from 2.1 to 1.6. The restoration of this original scope forms the two upgrades of the RPC trigger system. The first upgrade is adding station 4 for $|\eta| < 1.6$. This upgrade is trivial from the trigger point of view. The system is ready to include station 4, as soon as chambers and missing parts of the link system are available. The second upgrade extends the RPC coverage to $|\eta| < 2.1$. This requires that additional chambers be added to the detector. For the trigger, the upgrade requires building additional copies of the existing trigger boards. Roughly 20% additional boards need to be added. The fourth endcap plane upgrade is proposed for 2012-2013, and the expansion to $|\eta| < 2.1$ for 2016.

As the LHC approaches its design luminosity, the restoration to 4 layers of RPC in the forward direction will provide a substantial improvement in efficiency since CMS can require 3 planes out of 4 in coincidence instead of requiring 3 out of 3. The exact amount of rate improvement depends on the details of noise, neutron flux and charge particle flux. The increase in η coverage from 1.6 to 2.1 increases the discovery reach for new physics by increasing the available geometrical acceptance for muons by 31%. This η region also has the maximum muon bending power in the CMS endcaps, providing additional measurement power beyond the gain in acceptance. The present RPC system is built so that the additional RPCs are able to be installed in a straightforward manner. There are well-understood plans to incorporate additional planes into the trigger logic. There are additional on-detector Link Boxes that would be placed in reserved locations which would then connect to additional boards in provided locations in the trigger logic crates. Two additional trigger boards would be required for each of the 12 RPC trigger crates for a total of 24 plus spares. One additional Data Concentrator Card (DCC) would be needed to complement the present three. Since the RPC system uses the ECAL DCC, this is straightforward.

One possibility is the option of populating the forward region of η from 2.1 to 1.6 with more advanced gaseous detectors, which could be able to cope with high particle rates and hence provide CMS with enhanced physics performance at the highest luminosities. Micro-Pattern Gas Detectors (MPGDs) are being explored for the upgrade of the forward part of the muon system, as they can provide precision tracking and fast trigger information simultaneously, and they can be designed with sufficiently fine segmentation to cope with the high particle rates expected at LHC and its upgrades. If these detectors are used in place of the RPCs in this region, there would be further changes required in the RPC trigger system. In order to minimize these changes, the data produced by the MPGDs would be transmitted in a format

identical to that of the RPC data. Nevertheless, due to the higher granularity and therefore greater volume of the MPGD data, two additional TBs would be required for each of the 12 crates for a total of 48 instead of 24. In addition, the existing 12 TB crate backplanes would need to be extended to connect to the additional TBs. These 12 new backplanes plus spares would need to be manufactured and tested for the upgraded system if MicroPattern Gas Detectors (MPGDs) were selected. The Trigger Boards themselves as they presently exist should be able to handle the extra patterns since for the upgrade the focus is on high p_T muons whose straight tracks do not create as many additional patterns as low-p_T tracks.

7.3.5 CSC Trigger Issues and Upgrade

Detailed studies of the performance of the muon detector system upgrade are documented in Chapter 3. One of the key findings, shown again in Figure 7.13 is the importance of completing the coverage of the CSC detector to control trigger rates. The projected rate for a trigger threshold of 20 GeV/c drops from 60 to 20 kHz. From the CSCTF point of view, the improvement is due to the better resolution of the muon momentum measurement. Due to excellent shielding, the CSC system seldom reconstructs fake muons. The rate is driven by resolution effects, namely promotion of soft muons to high momenta by mis-reconstruction. Since the magnetic field is weak between stations 3 and 4, the reasoning for adding station ME4/2 to improve resolution is not completely intuitive.

Lacking ME4/2 coverage in the muon system, we cannot require LCTs in three muon stations without compromising efficiency. A two-LCT muon trajectory (CSC 2/3) uses three spatial measurements to fit the trajectory: the beam spot and the two LCT positions. This is not an over-constrained fit. Mis-matching a real muon LCT with a punchthrough LCT will cause the muon momentum to be randomly mis-measured. The trigger system, by construction, always keeps the highest momentum muon candidate. The highest momentum muon can be a mis-reconstructed combination of real muon and punch-through, thus promoting the event above trigger threshold. A three-LCT trajectory (CSC 3/4) is an over-constrained fit; wrong LCT combinations are rejected and therefore do not enter into the momentum fitting logic. So while the weaker field between stations 2,3 and 4 does not dramatically extend the fit lever arm, the third LCT "tags" the correct trajectory through the muon system. The significant rate increase from 20 to 60 kHz in Figure 7.13, shows that the loss of ME4/2 information cannot be compensated by the RPC trigger system.

In the following, we discuss the expected impact of both the high luminosity environment and the CSC detector upgrades on the design of the upgraded CSC trigger.

The occupancies of the Cathode Strip Chamber (CSC) system will increase with increasing luminosity. Detailed simulations of the occupancy of Local Charged Tracks (LCTs), which are the trigger primitives from the CSCs, indicate that due to prompt pile-up per Muon Port Card (MPC), approximately 0.05 LCTs per bunch crossing (BX) are expected for $2 \times 10^{34}\text{cm}^{-2}\text{s}^{-1}$, with large fluctuations at the level of 0.25. Therefore at 2σ, about 0.5 LCTs/BX must be accommodated in bursts. Simulation results on the number of LCTs/BX from 400 prompt pile-up events ($10^{35}\text{cm}^{-2}\text{s}^{-1}$ with 50 ns bunch crossing) are shown in Figure 7.14.

Additional LCT occupancy occurs from the neutron background, which is expected to grow faster than linearly with luminosity because of the limited penetration of the converted gamma rays (so that multiple random hits are needed to fire an LCT pattern). While highly uncertain until measured at the LHC, this background potentially can exceed the prompt pile-up background at the LHC Phase 1 Upgrade luminosities. Therefore, the MPC must be able to accommodate more than one background LCT per BX per sector, which exceeds the current

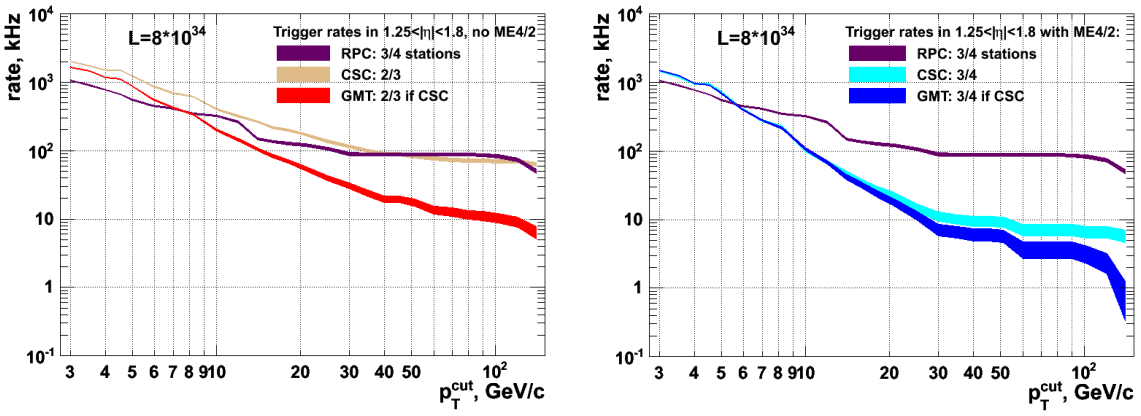

Figure 7.13: Simulated global muon trigger rates for $\mathcal{L} = 8 \times 10^{34}\text{cm}^{-2}\text{s}^{-1}$. The plot on the left (right) shows the trigger rates without (with) ME4/2 with the Global Muon Trigger requiring 2 out of 3 (3 out of 4) CSC planes on the track. The RPC curve shown corresponds to a configuration optimized for high efficiency and not for rate rejection.In this configuration, the CSC system with completed coverage drives the triggering rate. The muon trigger rates without full CSC coverage are significantly higher.

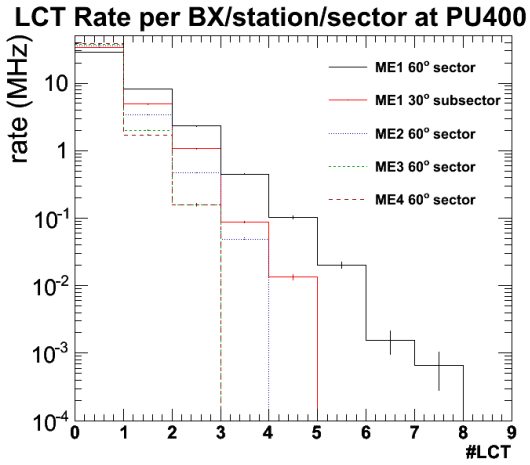

Figure 7.14: Number of LCTs per sector or relevant subsector expected for 400 prompt pile-up events, by station.

CSC trigger design assuming that a dimuon signal must be captured at high efficiency in the sector covered by the MPC. Since we target a single upgrade capable also for handling Phase 2 occupancies, the MPC should be capable of delivering the full 18 LCTs/BX for each trigger sector.

Additionally, the CSC Trigger Motherboards connected to the ME1/1 chambers need to be replaced in order to expand triggering to include the region $\eta > 2.1$. This also will increase the average number of LCTs sent to the MPC and transmitted to the Sector Processors. Therefore, additional bandwidth is needed to transmit LCTs to the Track-Finder crate, and additional processing logic will be required to identify and measure tracks in this higher occupancy environment.

The Muon Port Card (MPC) is a choke point in the CSC trigger path (designed that way to

reduce optical link costs for LHC). It sorts and filters up to 18 LCTs from 9 chambers in one 60 degree sector for one station to a maximum of only 3 LCTs. Assuming 2 LCTs are from a dimuon signal, allowing 1 additional LCT for background is not enough for Phase 1 occupancies beyond $\mathcal{L} = 10^{34}\text{cm}^{-2}\text{s}^{-1}$. Moreover, triggering on ME1/1a (high η region) will add still additional LCTs for the MPCs residing in ME1 peripheral crates. Therefore, the MPC needs to be redesigned to allow more throughput with additional sorting logic in a larger FPGA to transmit more than three LCTs, and using upgraded optical links to minimize cabling and inputs to the Sector Processors (already at a front-panel limit of 15 optical links). However, we must keep 3 optical links of the original type in addition to new links to maintain the existing CSCTF crate in parallel while commissioning the new one. This allows the new MPCs to act as an active splitter for the old and new Track-Finder crates. In total 60 Muon Port Cards must be replaced on the peripheral crates.

The 12 Sector Processors in the CSC Track-Finder crate in the underground service cavern also must be upgraded to accept the higher number of LCTs per BX from each MPC for robustness against Phase 1 occupancy. The optical receivers must be upgraded to match the higher bandwidth MPC transmitters, and the logic space must be increased to handle the additional combinatorics in the track-finding algorithm. Moreover, a new scheme for applying the geometry conversion in the FPGA logic rather than in numerous external LUTs as presently must be developed given the higher occupancy (otherwise there are problems with board space occupied by the memory chips).

The momentum resolution of the current CSCTF system is limited by the available onboard memory (2 Mb $\times$ 16 bits). The purity of the CSC track finder muons is very high; rate control is mostly driven by the track finder resolution. In the last five years, faster, smaller and cheaper memory chips have become available, and it makes sense to revisit the momentum assignment algorithm. We plan to investigate what highest p_T resolution we can ultimately reach at Level 1 by studying outputs of the offline standalone muon fit when using LCT coordinates as input. Should a significant improvement seem feasible, the next step is to understand what additional information or algorithm induces the strongest improvement to the momentum resolution.

The upgrade to the CSC Track Finder crate ideally should only be done once, so it should meet the design requirements of Phase 2 even though it is deployed with Phase 1. In Phase 2, the key new component in the trigger chain is the matching of pixel and silicon strip tracking information to CSC tracks, allowing track confirmation, isolation, vertex-finding and improvement on momentum resolution. To accommodate this, refined position information from the CSC Track-Finder ($\eta \times \phi$) is needed to match to the pixel and/or strip hits. In the current LHC CSC trigger design, this information is only reported on a ($0.05 \times 2.5^\circ$) granularity to the Global Muon Trigger for matching to calorimeter towers, although intrinsically the information is available on a much finer scale ($0.0125 \times 0.015^\circ$). In order to use this fine scale resolution more bits will be needed to be transmitted from the Sector Processors to a new Muon Sorter for eventual combination with the silicon tracker $\eta \times \phi$ information.

With finer information transmitted by the Sector Processors, the backplane and the Muon Sorter in the Track-Finder crate must be redesigned to accommodate the additional data transmission. Serialization of the data at frequencies higher than the current 80 MHz is necessary because the current Track Finder crate backplane design has utilized essentially already all available space for copper transmission lines. Therefore the Muon Sorter must be upgraded to handle the higher frequency transmission from the Sector Processors. It also needs the provision to send more than the current 4 CSC muons per BX to the Global Muon Trigger because of the higher occupancies which requires additional data lines in the output path.

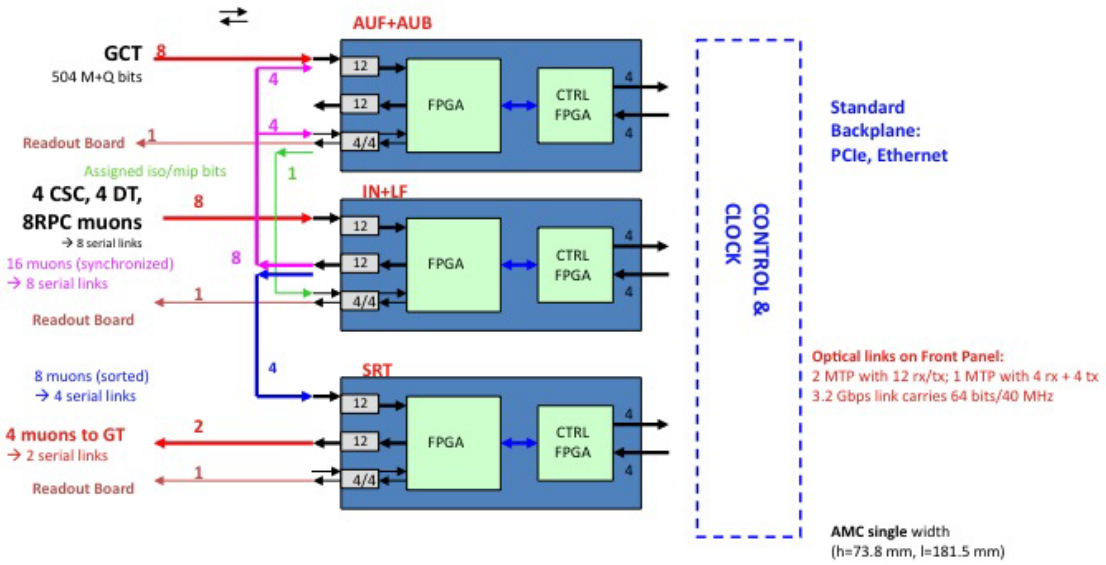

Figure 7.15: Global Muon Trigger.

7.3.6 Global Muon Trigger

As for the present GMT, the best muon candidates across the experiment must be determined. For this purpose information from the three muon subsystems and the Global Calorimeter Trigger is combined and analysed. The GMT combines the results of the muon subsystems making use of the quality information associated with the tracks from the regional triggers. The GMT generally forwards a candidate if it was seen by both RPC and DT/CSC system regardless of quality. If the candidate was seen by only one system quality criteria are applied to decide whether to forward it. Specific quality criteria can be applied depending on detector types, detector regions and transverse momenta.The best candidates are sent to the Global Trigger. The logic board will consist of a single width AMC module with a standard μTCA backplane (Figure 7.15).

7.4 Global Trigger and Central Trigger Control

7.4.1 Global Trigger

The upgraded Global Trigger will be designed to have the same basic categories of functions as the present GT, but will have more algorithms and more possibilities for combining trigger objects and technical triggers (e.g. independent trigger signals from detectors that are not combinable with other triggers):

- Synchronizing all trigger objects to arrive at the same time at the logic chip;
- Sending all trigger objects into one chip to make any correlation between them;
- Using an FPGA to change trigger conditions as required by physics;
- Calculating physics trigger algorithms in parallel (FPGA branch);
- Performing a final OR mask for all algorithm bits;
- Prescaler and Counter for each algorithm.

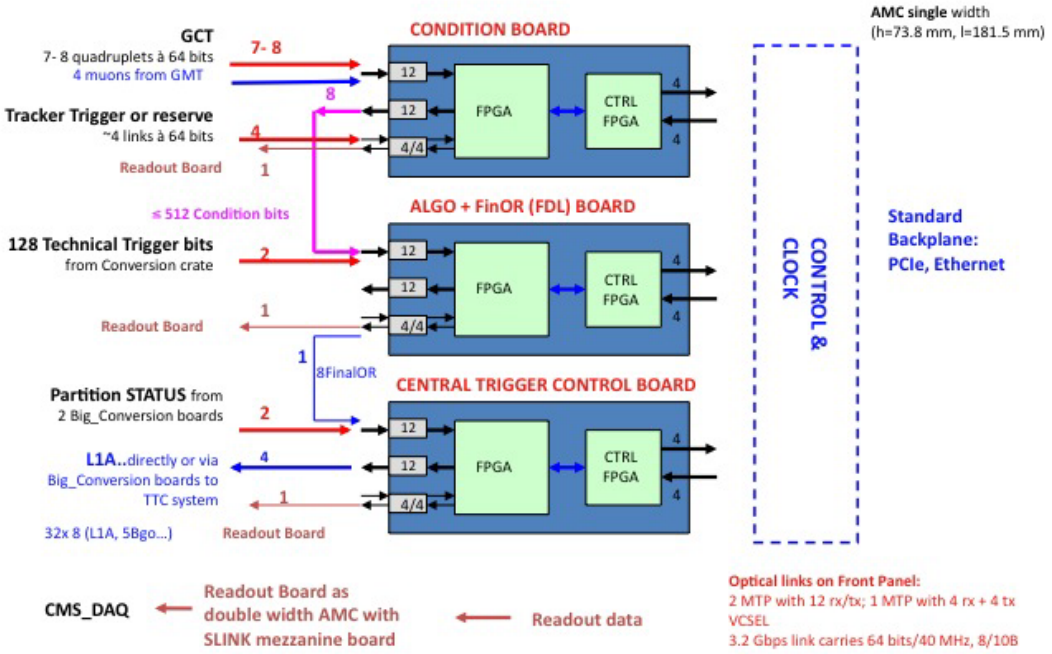

Figure 7.16: Upgrade Global Trigger Crate showing the inputs from the Global Calorimeter Trigger, provision for an eventual tracking trigger for Phase 2, and technical trigger bits from dedicated logic. Also shown are interfaces to the DAQ and TTC systems.

The upgraded GT will be able to process at least double the present 128 algorithms and 64 technical triggers. It may use the DSP cores now available on the newer FPGAs for complex triggers. These DSPs would enable firmware compilation of C++ code to produce triggers with constant latency. Each trigger object of 64 bits at 40 MHz will be assigned one optical link. The hardware will be realized in a single μTCA crate with a standard backplane.

The GT boards shown in Figure 7.16 will be single-width AMC modules. Apart from the condition board and the combined algorithm/final OR board the central trigger control board (section 7.4.2) is also housed in the GT crate. A second μTCA crate contains all required conversion boards connecting the Global Trigger and Central Trigger Control to the other trigger boards and later to the final trigger electronics which sends or receives 40 MHz differential data.

7.4.2 Central Trigger Control

The Central Trigger Control system, as at present, will receive status information from the Global Trigger processor, the detector partitions and the buffer emulators. It will transmit the L1 accept signal to the partitions and provide other control signals. It will be housed in two crates, the GT crate and a second crate called the Conversion Crate. The CTC module is located in the GT crate. The Conversion Crate will contain six double width interface boards with the functionality of the current GT Conversion Boards and L1AOUT modules that process the GT signals. There will also be two boards receiving the technical triggers from other subdetectors. It will have a standard backplane and carrier hub. Optical links provide the data transfer between the two crates. Figure 7.17 shows the setup.

For a gradual transition from the present VME-based trigger system we plan to mount a simple 9U interface board in the slot of the TCS board of the actual GT crate, which sends the current eight final ORs, four GT status bits and the reset signal to the conversion crate. In the final

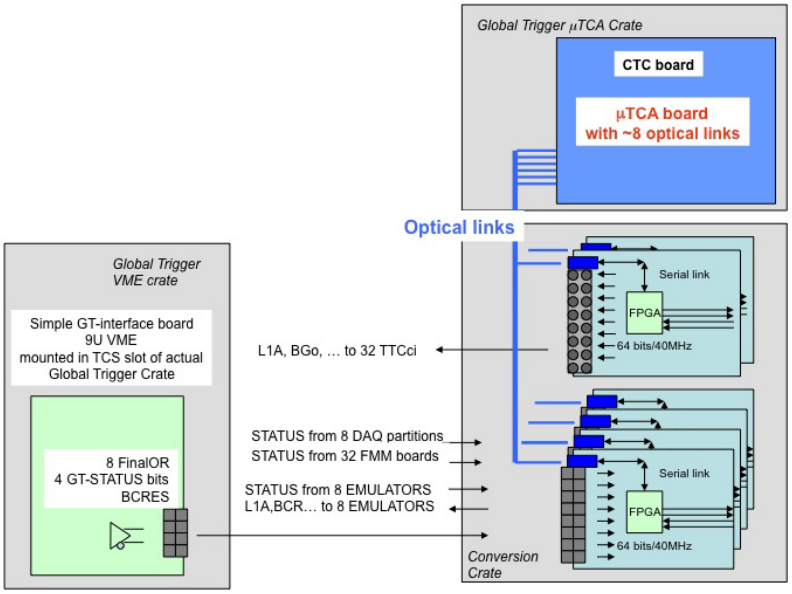

Figure 7.17: Central Trigger Control system with the interface to the current system.

version an optical link will transfer them directly to the CTC board.

7.5 Trigger Software

The current L1T system is supported by a large variety of software packages and components. These include online software and drivers for the setup and monitoring of the trigger components; diagnostic and monitoring packages for trigger tests; and offline software for trigger hardware emulation and performance estimation. The overall software system is large and complex, reflecting the nature of the hardware. Substantial effort is spent in maintaining and adapting the trigger software. This effort is needed well beyond the end of hardware commissioning, as it is essential for the maintenance and monitoring of trigger performance during LHC running.

As the trigger hardware moves towards the use of more similar hardware modules specialised for different purposes, an upgraded software system is required to support this. An analogous approach will be used, making use of a set of common software components specialised for different functions. The key design goals for the new system are: maximum commonality between the software supporting different hardware subsystems; maintainability through use of common components and good software engineering practices; reduction of effort through use of off-the-shelf libraries and drivers; and scalability, such that the same software approach may be used for Phase 1 and subsequent upgrades.

One key driver for the software upgrade is the adoption of ethernet-based control mechanisms in the μTCA hardware. This allows proprietary and/or custom hardware drivers to be replaced with standard network protocols using commodity hardware and standard OS drivers. Examples of candidate network technologies for this control and/or local DAQ applications are TCP/IP and Fibre Channel over Ethernet (FCoE).

A candidate upgrade software architecture is under development. Central components of this

new architecture include:

- Use of commodity GB/10GB ethernet switches and High Bandwidth Architectures (HBA) for high speed control and local DAQ.
- Firmware and embedded CPU software for direct ethernet communication with FPGAs, implementing a simple common protocol for memory-mapped access to hardware.
- A control hub component that arbitrates access to hardware, provides a common software interface for both ethernet-based protocols and legacy hardware (e.g. VME bus adaptors) and performs simple hardware monitoring functions.
- A higher-level C++ object model that allows trigger control / local DAQ applications to be written without detailed knowledge of the communications protocol or medium, and provides library functions for control of common firmware components.

Each of these layers will make maximum use of off-the-shelf components, e.g. software communications libraries and firmware cores for protocol decoding. In the critical areas (e.g. the control hub) proven components and software techniques from the telecommunications industry will be used in order to guarantee robustness and scalability. The new software must interface seamlessly with the CMS run control system, and provide a clear upgrade path for future redevelopment of existing trigger software as hardware is replaced or extended.

7.6 Schedule

7.6.1 Calorimeter Trigger

The Calorimeter Trigger schedule is based on installation of a prototype system that can run in parallel with the existing Calorimeter Trigger system during the 2012 shutdown and installation and testing of the final systems during the 2016 shutdown. The development and production of this system, including the selective readout capability, requires 4 FTE engineers, 4 FTE physicists, and 3 FTE technicians.

The development, design, production, test, integration and commissioning schedule is planned as follows:

- Technology demonstrator: July 2011;
- Prototype cards: July 2012;
- Preproduction and testing: Dec. 2013;
- Construction and testing: Dec. 2015;
- Installation and testing: Dec. 2016.

7.6.2 Global Trigger

The Global Trigger schedule presented below includes also the Global Muon Trigger and the Central Trigger Control. The development and production of this system requires 1 FTE engineer, 1 FTE physicist, and 2 FTE technicians.

The development, design, production, test, integration and commissioning schedule is planned as follows:

- Technology demonstrator: Dec. 2011;

- Design, firmware, software, test environment Prototype: Dec. 2012;
- Design, production, test environment, verification Production System: Dec. 2014;
- Full system test: Dec. 2015;
- Integration: July 2015;
- Commissioning: 2016.

7.6.3 Muon Trigger

7.6.3.1 DT Trigger

Taking in account the known LHC and CMS operation schedule the DTTF upgrade can only be planned for the 2016 shutdown. The development and production of this system requires 1 FTE engineer, 1 FTE physicist, and 1 FTE technician.

The development, design, production, commissioning and test schedule is planned as follows:

- Feasibility Report: Dec. 2010;
- Technology demonstrator: Dec. 2011;
- Design, firmware, software, test environment Prototype: Dec. 2012;
- Design, production, test environment, verification Production System: Dec. 2013;
- Full system test: Dec. 2014;
- Commissioning: 2016.

7.6.3.2 CSC Trigger

The CSC Trigger schedule is based on installation of a prototype system that can run in parallel with the existing CSC Trigger system during the 2012 shutdown and installation and testing of the final systems during the 2016 shutdown. The development and production of this system requires 1 FTE engineer, 1 FTE physicist, and 1 FTE technician.

The development, design, production, test, integration and commissioning schedule is planned as follows:

- Technology demonstrator: July 2011;
- Prototype cards: July 2012;
- Preproduction and testing: Dec. 2013;
- Construction and testing: Dec. 2015;
- Installation and testing: Dec. 2016.

7.6.3.3 RPC Trigger

The development, design, production, test, integration and commissioning schedule is planned as follows:

- Construction and testing: Dec. 2011;
- Installation and testing: Dec. 2012.

7.6.3.4 Overall Trigger Schedule

The schedule is designed for installation during the 2016 shutdown and commissioning and operation with first beam after that.

Trigger Component	Engineers	Physicists	Technicians
Calorimeter Trigger	4	4	3
Muon Trigger	3	3	3
Global Trigger	1	1	2
Total	7	7	8

Table 7.2: Estimate of FTE support required for upgrade of the CMS trigger systems.

Country	Calorimeter	Muon	Global
Austria			X
France	X		
Greece	X		
Italy		X	
Poland		X	
Portugal	X		
UK	X		
USA	X	X	

Table 7.3: Country interest in trigger upgrades.

- R&D and Prototype Phase: 2011-12;
- Pre-production and testing: 2013;
- Construction and testing: 2014-15;
- Installation and testing (incl. full system tests): 2016;
- Commissioning and Operation: 2017.

Table 7.2 shows the average estimated FTE support for the development, production and installation of the calorimeter, muon and global trigger systems. Table 7.3 presents the informal interest of the countries involved in the trigger upgrade. Personnel in these countries have experience with the present CMS trigger system and these countries were responsible for building most of it.

Chapter 8

Data Acquisition System Improvements and Upgrades

8.1 Introduction

The existing CMS DAQ system reads out data fragments from approximately 700 sub-detector specific Front End Drivers (FEDs), builds events from these data fragments using commercial network switch technologies, and provides these to the High Level Trigger computing farm where they are analyzed to generate a final trigger decision. Triggered events are temporarily stored before they are transferred to the Tier-0 Computing Center at CERN.

The system has been designed to work at a maximal first level trigger rate of 100kHz for an LHC accelerator operating at a peak luminosity of $10^{34}\,\mathrm{cm}^{-2}\mathrm{s}^{-1}$ with 25 ns bunch spacing. In this configuration the average event size was expected to be around 1MB.

The DAQ system can be divided into five major components:

- The Readout system built from custom electronics components. It comprises the SLINK64, the Front-end Readout Link (FRL) cards and the synchronous trigger throttling system (sTTS) implemented by the Fast Merging Modules (FMMs).
- The first stage of the CMS Event-Builder called the Fed-Builder. It is implemented by a commercial Myrinet network. Together with the Readout system this system is also called "Data to Surface" (D2S) system.
- The second stage of the CMS Event-Builder called the RU-Builder. It is implemented by a commercial Gigabit Ethernet switching network.
- The High Level Trigger (HLT) farm which is implemented by a computer cluster.
- The Storage-Manager (SM) which is implemented by two PC racks attached to a Fiber Channel SAN.

Figure 8.1 shows a vertical section through the DAQ system, called the DAQ column, which contains all DAQ components and its logical interfaces to the trigger system. Also shown are the logical networks used to implement the various functionality. Details can be found in[19][20].

Figure 8.2 shows a more detailed diagram of the Event-Builder. On a Level-1 trigger, every Front End Driver (FED) is sending data fragments via the SLINK to the FRL. In the Fed-Builder these fragments are collected and grouped together to form larger superfragments which are then distributed to eight Readout-Builders according to a simple round-robin algorithm. Superfragments on average contain eight FRL data fragments. The resulting 72 superfragments are then concatenated in the second stage (the RU-Builder) to form entire event data structures

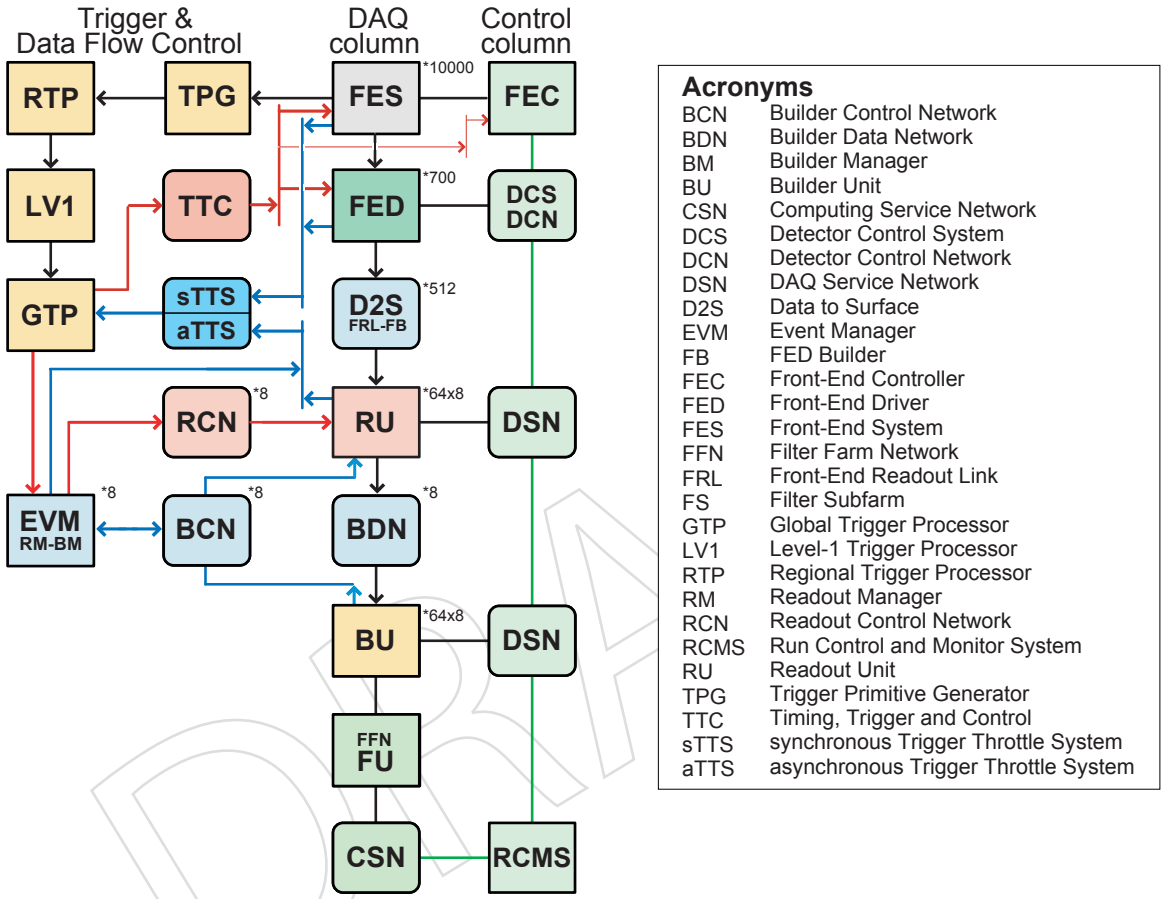

Figure 8.1: The Readout Column of the existing CMS DAQ system. A vertical slice of the DAQ system shows all logical components of the DAQ system and its interfaces to the trigger system. The small numbers next to the units indicate their multiplicity in the complete system. The event data flows vertically through the DAQ column. The data flow is shown up to the Filter Units.

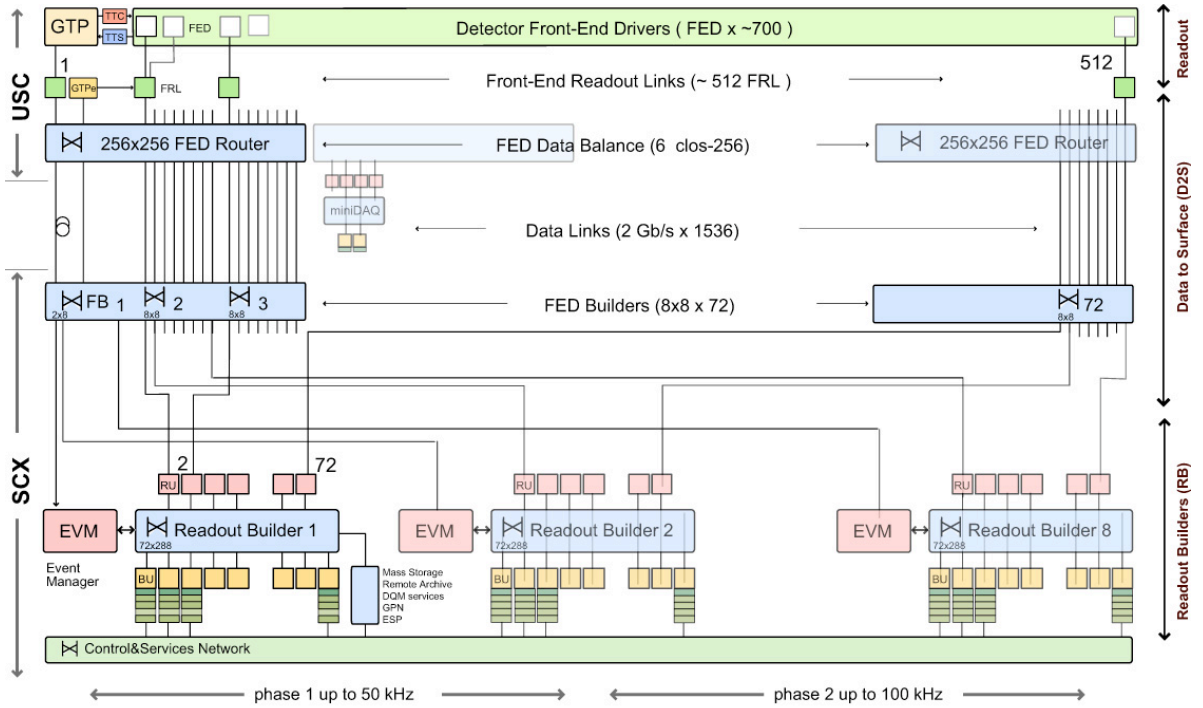

Figure 8.2: The two stages of the CMS Event-Builder.

in the Builder Units (BUs). There the events are analyzed by Filter Unit (FU) processes in order to find the High Level Trigger (HLT) trigger decision. Triggered events are then transferred to the Storage Manager where they are temporarily stored until they are transferred to the Tier-0 center.

8.1.1 Performance and limitations of the current system

The design of DAQ system was driven by the requirements of the CMS experiment operating at the design luminosity $10^{34}\,\mathrm{cm}^{-2}\mathrm{s}^{-1}$. The maximal first level trigger rate is 100 kHz. Table 8.1 summarizes the performance and the limitations of the various components of the current system. The network of the Fed-Builder is implemented by a Myrinet network. It consists of two switch fabrics operating in parallel. Every input port effectively runs at 240 MB/s. However due to the particular pattern of the network traffic in the Event-Builder where many sources transfer data to the same destination, in the worst case only half of this performance is available for event building[19]. Therefore in the table a performance of 120 MB/s per port is given.

8.1.2 Purchase and installation of the current system

The components of the central DAQ system have been installed and commissioned successively since 2005. Table 8.2 summarizes the purchase and installation of the various components which implement the current system.

The HLT farm currently contains processing power to handle 50% of the maximal data volume expected at $10^{34}\,\mathrm{cm}^{-2}\mathrm{s}^{-1}$.

Component	Quantity	Description	Performance
SLINK	≈ 700	Custom hardware readout	400 MB/s.
FRL	≈ 500	Data formatting and interface to commercial hardware. Input stage of the Fed-Builder.	400 MB/s.
Fed-Builder Network	Two 774×774 switch fabrics operating in parallel. ($\approx$ 500 of the 756 inputs currently used).	Data transfer from the underground area to the surface area. Data routing for the first stage of the Event-Builder.	120 MB/s for each input port. Every FRL is connected to 2 input ports (see text).
RU-Builder Network	8 slices with 72 RUs and 80 BUs and a multiple Gigabit network.	2nd stage event building.	360 MB/s via 3 Gigabit rails.
HLT farm	900 PCs with Intel Xeon-5430 Quad Cores CPUs (2.66 GHz) and 16 GB RAM	High Level Trigger algorithms.	See text.
Storage Manager	16 PCs and 2 hot spares with SAN	Temporary data storage.	220 TB storage. Performance Test: 2 GB/s writing and 1 GB/s reading concurrently.

Table 8.1: The performance of the various DAQ components currently installed in CMS.

Component	Purchase / Production	Installation	Remark
SLINK	2005	2006	custom hardware
FRL	2005	2006	custom hardware
FMM	2005	2006	custom hardware
Control PCs	2005	2006	Used to control custom electronics. No maintenance contract anymore.
RU PCs (PE2950)	2007	2007	Maintenance contract until 2012.
BUFU PCs (PE1950)	2008	2008	Maintenance contract until 2012. 50% of nominal Performance.
Myrinet Network equipment	2006	2007	
Gigabit Data-Network equipment	2006	2007	
Storage Manager hardware	rack1: 2007 rack2: 2008	rack1: 2007 rack2: 2008	Storage hardware on maintenance contract.

Table 8.2: Purchase and installation of the various components of the current CMS DAQ system.

8.2 Upgrade of the DAQ system

The upgrade of the DAQ system is different from the upgrade of other detector components for the following reasons:

1. The DAQ system is not involved in the process of generating data used for physics analysis but merely transports data produced by the sub-components of the experiment and provides the necessary CPU power in order to run the HLT algorithms. Therefore its upgrade is driven by the requirements in terms of data transportation and CPU power on one side, and the availability of affordable network and computing technology on the commercial market on the other side. The details of these requirements are unknown today. Neither do we have detailed designs for the sub-system upgrades, nor can we reliably estimate the expected data volumes produced by the subsystems. On the other hand data acquisition systems use commercial technologies which every year experience large performance improvements, since their development is driven by the requirements of growing markets like telecommunication. The upgrade of the DAQ system will profit from these improvements and once the requirements are well defined a suitable technology will be chosen to satisfy the needs at reasonable cost.

2. The DAQ system interfaces to all sub-detector systems and therefore needs to stay compatible with all of them i.e. with those being upgraded as well as with those not being upgraded. This excludes radical changes of its architecture.

3. To a large extent the DAQ system is built from commercial components. A large fraction of these are under maintenance contracts. The hardware needs to be replaced when it becomes obsolete in order to keep the reliability of the system high. Depending on the component being replaced this implies no or little work to be done on the system (e.g. when computers are being replaced by similar types) or major development work (e.g. when networking technologies have to be replaced).

4. The DAQ system continuously has to adapt to new running conditions. In particular throughout Phase 1 the luminosity is expected to gradually increase. This implies continuously changing operating conditions. In order to keep reliability of the system high, the DAQ software will undergo a smooth continuous upgrade which gradually improves the reliability of the system and deals with newly arising problems by improving fault tolerance and diagnostics.

8.3 Implications of LHC running scenarios and subsystem upgrades on the requirements for the DAQ system

The amount of data the DAQ system has to handle depends on the following factors:

- The rate of Level-1 triggers.This will stay 100 kHz in all upgrade scenarios.
- The data volume the DAQ system has to transfer for each event triggered by Level-1.
- The average processing power needed by the HLT to process an event.

The data volume of a single event has two contributions: A fixed term and a term proportional to the occupancy of the detector. The fixed term contribution can be determined by measuring the size of an empty event. These events contain contributions due to noise and a fixed overhead of the event structure.

In CMS the detector with the largest contribution to the event size is the tracker system (strips and Pixel). The occupancy of these detectors is proportional to the number of underlying minimum bias events. This in turn depends on the luminosity per bunch crossing. At 14 TeV and nominal luminosity of $10^{34}\,\mathrm{cm}^{-2}\mathrm{s}^{-1}$ and a bunch spacing of 25 ns approximately 19 underlying minimum bias events are expected for each bunch crossing. The DAQ system had been designed under the assumption that under these conditions the event size would be $\approx 1\ MB$. It follows that the system is capable of building events at 100 GB/s ($1\ MB \times 100\ kHz$).

8.3.1 Possible running scenarios of LHC for Phase 1

Up to the first shutdown in the years 2012/2013 the center of mass energy of LHC will stay at 7 TeV and the luminosity per bunch crossing will stay an order of magnitude below the nominal one. No significant pileup of minimum bias events is expected and therefore the DAQ system will be able to easily handle the data volume, even if triggering at 100 kHz.

After the first shutdown, the energy of the beam will be increased from 7 to 14 TeV and the luminosity is expected to first increase to $5 \times 10^{33}\mathrm{cm}^{-2}\mathrm{s}^{-1}$ with a bunch spacing of 50 ns and later to the nominal $10^{34}\,\mathrm{cm}^{-2}\mathrm{s}^{-1}$ but with 25 ns bunch spacing. Both scenarios have the same luminosity per bunch crossing and therefore in both cases 19 underlying minimum bias events are expected in each triggered event. The DAQ will operate at its originally foreseen performance.

After the second shutdown foreseen around the years 2015/2016, LHC might be able to deliver up to $2 \times 10^{34}\,\mathrm{cm}^{-2}\mathrm{s}^{-1}$ with 25 ns bunch spacing. In this case around 40 pile up events are expected and the occupancy of the detector will be proportionally higher. Moreover, additional readout channels will further increase the expected data volume to be handled. For example the data volume of the Pixel detector will increase by more than 50% due to the introduction of the fourth barrel layer and the third set of endcap disks. Similarly the data volume of the HCAL detector is expected to increase significantly from the introduction of longitudinally segmented readout. To continue to be able to trigger at 100 kHz the readout system, the Event-Builder and the HLT farm must be upgraded.

The design choices for the DAQ upgrade foreseen in the year 2015/2106 will have to be made around the years 2012/2013, i.e. leaving 3 years for prototyping, production, installation-testing and commissioning. At that time it will be impossible to design a system that would also fulfill the requirements of the Phase 2 upgrade at a reasonable cost. In addition, many components chosen for the 2015/16 upgrade will be obsolete by 2020.

8.4 Discussion of the DAQ components

The CMS DAQ system is implemented to a large extent with commercial computing hardware (e.g. PCs and network equipment). These components are purchased with maintenance contracts which provide efficient repair in case of failures. Once a product is declared obsolete, it is no longer possible to renew its maintenance contracts. The operation of obsolete equipment becomes a risk for the experiment, since a sufficient number of spares cannot be guaranteed anymore. The time before a given model of server PC becomes obsolete is typically 3 years. For network switching equipment this time is slightly longer (6-7 years). This defines a natural cycle when all the commercial DAQ equipment from the Fed-Builder to the Storage Manager is to be replaced.

A similar problem exists for custom hardware modules. After a given time components used in the modules cannot be purchased anymore. As soon as the number of functioning spare modules falls below a minimum, the operation of that hardware becomes a risk factor.

Modifications in all components of the DAQ system will be necessary in order to cope with the expected data volume after the second shutdown.

8.4.1 Hardware Control

The PCs currently used to control the custom hardware were purchased in 2005 (approximately 200 PCs). Their performance is sufficiently high but their maintenance contract terminates in 2011. These computers are essential to configure the readout electronics at the beginning of each run. It is foreseen to replace them in the shutdown 2012/2013.

The custom hardware in CMS is currently implemented in VME modules for the sub-detector specific electronics and in compact PCI modules for the FRL modules of the DAQ. The relevant crates are interfaced to the control PCs via commercial bridges (PCI to VME or PCI to PCI resp.). It is foreseen to replace these bridges together with the control PCs in the shutdown 2012/2013 with bridges connecting to a PCIe bus on the side of the host computer.

8.4.2 Readout links

For the 2016 shutdown a new custom readout link will be designed employing state of the art electronics components. It is expected that this link will be able to transfer data at a rate of about 10 Gbit/sec. The link will replace the old obsolete hardware of the current SLINK and will meet the requirements of the new readout link for higher data throughput. The link must be designed in a way that it can be interfaced to legacy FEDs of sub-detectors which do not need to be upgraded, and to newly designed FEDs which will be able to transfer substantially higher data volumes to the DAQ. Currently it is clear that the HCAL system will replace their FEDs with μTCA based FEDs in the second shutdown period. They are capable of delivering up to eight times more data than the current FEDs. In the trigger system, μTCA FEDs will also be added. The new Pixel detector will deliver substantially more data. However, it has not been decided yet if the FEDs will be rebuilt.

8.4.3 Fed-Builder

The Fed-Builder will be replaced in the second shutdown with modern network technology which can be interfaced reasonably easily to the custom hardware of the readout link. Similarly, the RU-Builder will be replaced by a state of the art network switch, based on multi-gigabit links, in order to be able to cope with the higher data throughput.

8.4.4 RU-Builder and HLT farm

The present filter farm that runs the Higher Level Triggers contains 720 Dual Quad Core Intel Xeon 5430 PCs running at 2.66 GHz and with 16 GB of memory. This provides about 5,000 instances of HLT processes running simultaneously. This is sufficient to process an input of 50 (100) kHz of Level-1 triggered beam crossings with each crossing taking 100 (50) ms on average to process. Figure 8.3 shows the Monte Carlo distributions of the average processing times, including both unpacking and algorithmic portions, for the nominal trigger menu for a center of mass energy of 14 TeV and a luminosity of $10^{32}\text{cm}^{-2}\text{s}^{-1}$ (where the pileup is negligible) for minimum bias events[21]. The mean value is 42.7 ms. Figure 8.4 shows a timing study taken with 30K minimum bias data events at an center of mass energy of 7 TeV and a luminosity of $5 \times 10^{29}\text{cm}^{-2}\text{s}^{-1}$ where the pileup averages about 1.2 events due to the small number of colliding bunches. The full HLT menu contains commissioning triggers that are being temporarily used to look at pixel tracks at the full Level-1 accept rate and has a mean time of 59 ms. When the commissioning triggers are removed, the mean time is 32 ms. Therefore we conclude that the

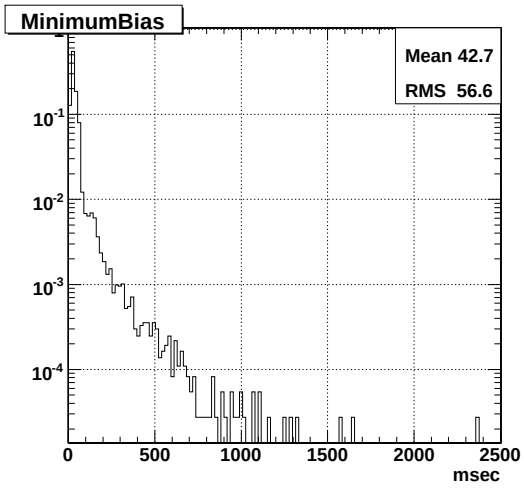

Figure 8.3: MC study of average processing-times (Core 2 5160 Xeon 3.0 GHz) for running the full HLT Menu including the data unpacking time. Measurements taken with L1-accepted un-binned minimum bias MC sample at a luminosity of $10^{32}\text{cm}^{-2}\text{s}^{-1}$[21].

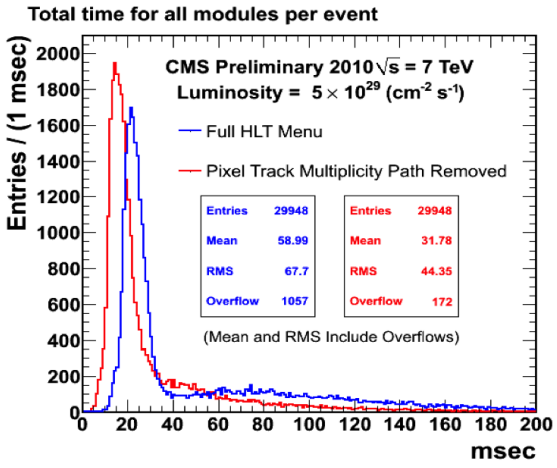

Figure 8.4: Average data processing-times (Core 2 5430 Xeon 2.66 GHz) for running the full HLT Menu including the data unpacking time. Measurements taken with 30K minima's data events from data at a luminosity of $5 \times 10^{29}\text{cm}^{-2}\text{s}^{-1}$.

present HLT CPU time is reasonably well understood with data and MC for events with small or negligible pileup and that the figure of 50 ms per event is a reasonable figure on which to base extrapolations to higher luminosities.

In order to do so, we use the present data with between 1 and 7 reconstructed vertices per event and interpreting each reconstructed vertex as a separate interaction as shown in Figures 8.5 and 8.6. The event size on average starts at 0.5 MB and increases by 20 KB per additional interaction. For the running period after the 2013 shutdown we expect a maximal luminosity of $10^{34}\,\text{cm}^{-2}\text{s}^{-1}$. With a bunch crossing interval of 25 ns one would expect 19 minimum bias events per bunch crossing resulting in an event size of $\approx$ 900 KB. From 2013 onwards LHC is expected to operate at the nominal energy, i.e. 14 TeV. Since the particle multiplicity scales approximately with the square root of the center of mass energy it is expected to increase by 41%. Assuming that a large fraction of the event size with only one interaction (0.5 MB) is constant, and only scaling the contribution due to the minimum bias events, we obtain a final event size of 1.1 MB.

Assuming that the required HLT processing power is proportional to the event size, the investigations above show that an enhancement in processing power of a factor 2 is needed in order to cope with the expected data volume at 100 kHz. This estimation neglects that the processing time of many HLT algorithms might have a stronger dependence on the event size. Experience in other experiments indicates that this effect might be more or less important (D0 and CDF). Therefore we add some margin and intend to increase the processing power of the HLT farm in the shutdown period 2012/2013 by a factor of 3.

The present computer rack infrastructure is only half populated with PCs since the PC's purchased had twice the CPU power used to specify the original infrastructure. Since the present PC's will be 5 years old at the 2012/13 shutdown, we will replace the existing PC's with new ones, rather than enlarging the existing farm. This will still leave still half of the infrastructure

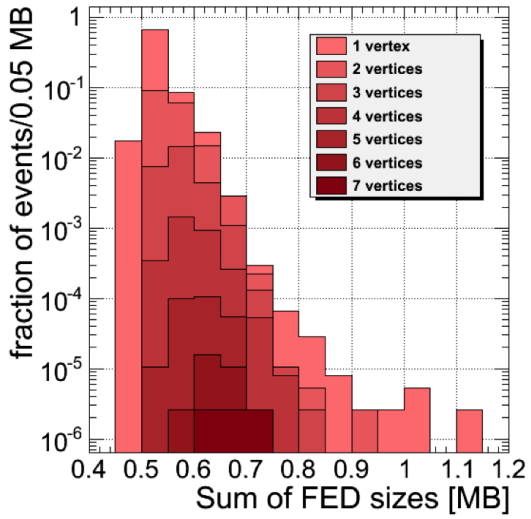

Figure 8.5: Event sizes for different numbers of reconstructed vertices from data at a luminosity of $5 \times 10^{29}\text{cm}^{-2}\text{s}^{-1}$.

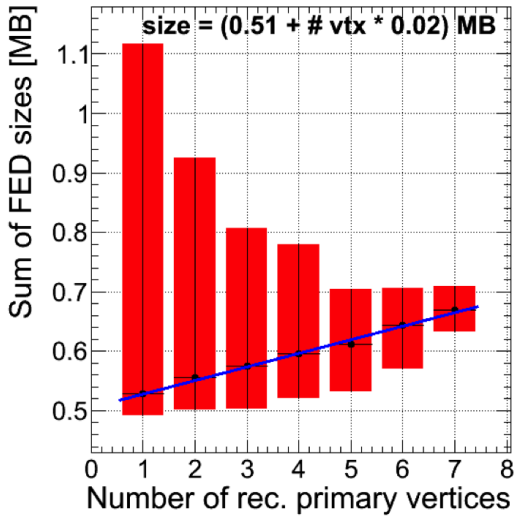

Figure 8.6: Event size dependence on number of reconstructed vertices from data at a luminosity of $5 \times 10^{29}\text{cm}^{-2}\text{s}^{-1}$.

unpopulated providing contingency in case of an unexpected increase in HLT CPU needs. In 2013 the cooling power of the SCX computer room will be increased to 1 MW as originally foreseen.

The next increment in HLT farm CPU power will be required during the 2016 shutdown, in order to provide the capability to operate at luminosities up to twice design luminosity ($2 \times 10^{34}\text{cm}^{-2}\text{s}^{-1}$). Forty minimum bias events per crossing are expected in this scenario. We estimate that this will require approximately 3 times the CPU power of the filter farm installed in 2012. Therefore, the plan is to replace all existing filter farm CPUs and to fill all of the rack infrastructure with PCs that are significantly more performing than those installed in 2012. In addition, the increased data will require an upgrade to the network switch infrastructure.

8.4.5 Storage Manager

The Storage Manager stores selected events temporarily on a local disk array and concurrently transfers the data to Tier-0. Once data has been verified at Tier-0 it is deleted from the Storage Manager disks. The transfer to Tier-0 is implemented with two 10 Gbit/s links. In normal operation only one link is used the other serving as a spare in case of failure of the first link. The two links can also be trunked together and operated simultaneously in order to increase the performance of the transfer system.

Currently the limitation of the CMS recording performance is given by the Tier-0 processing power that is limited to about 300 Hz event rate. Depending on the configuration of the tracker readout, the event size varies from 350 kB to 500 kB in the ongoing 2010 run. The total data volume written to disk depends on the configuration of the data output streams of the HLT.

In preparation of the Heavy Ion run during 2010 a series of performance tests have been carried out. During these the Storage Manager wrote 2 GB/s to disk and concurrently transferred 1 GB/s to Tier-0. This performance is estimated to be sufficient for the proton physics program and also for the initial Heavy Ion program of Phase 1 up to 2015.

It is necessary, however, to regularly replace the hardware of the Storage Manager to keep its

reliability high.

8.4.6 Online Database

The online database of CMS is implemented by an Oracle database. The hardware components (PCs and storage) will be regularly replaced to keep the reliability of the system high. In particular during the shutdown 2012/2013 it is foreseen to replace the hardware of the database. The required storage space will grow during the lifetime of the experiment. It is also expected that the total data rate written into, and read from the database will increase, since during the upgrade of the experiment the number of channels for various sub-detectors will increase. Therefore more parameters and conditions will be written to the database. During the lifetime of the experiment the performance of the database will need to increase in order to satisfy these requirements.

Chapter 9

Beam Instrumentation and Luminosity Monitoring Improvements and Upgrades

Comprehensive and flexible beam instrumentation was invaluable during the LHC startup in understanding beam conditions with a view to reducing beam losses and optimising LHC efficiency and luminosity. Moreover, the provision of beam instrumentation which protects the CMS detector against catastrophic beam losses which could damage the detector is absolutely essential. This is done by initiating a "beam abort" in the event of such dangerous losses.

The beam instrumentation installed for the startup proved flexible enough to fulfill all these roles as well as providing a stable and well-understood trigger to allow efficient data taking and resultant physics publications even during the initial period where all triggers were undergoing a thorough commissioning period. The CMS protection system similarly has worked seamlessly and invisibly, having been active and commissioned since the first LHC beams.

In the coming years, the expected intensities and beam conditions will develop rapidly. Additionally, there will be significant changes to the CMS detector configuration. To be able to continue to successfully protect and optimise conditions for CMS, it is necessary to consolidate the currently installed array of beam instrumentation to adapt to the changing machine conditions and detector configuration. Building upon the experience with the system so far, the changes necessary to do this are presented in this chapter.

In this chapter, first an overview of the present beam and radiation monitoring instrumentation is presented, followed by the motivation for improving the present system and a summary timeline for these improvements. Then each improvement is presented in some detail, starting with those which are most central to the primary aims of the beam instrumentation project. Finally, details are given as to the resources needed to undertake these upgrades in terms of manpower requirements, material costs and schedule.

9.1 Present Beam and Radiation Monitoring Instrumentation

The Beam and Radiation Monitoring systems (BRM) [20, 22, 23] perform both a monitoring and a protection function for CMS. To this end, multiple and redundant systems have been installed some of which can be used to initiate LHC beam aborts and/or CMS equipment control, others of which can be used for fast beam/detector optimisations. All systems will provide long term monitoring of the received radiation dose in various regions of the CMS detector.

The CMS experiment sits in an unprecedentedly high radiation field for a HEP experiment and much effort has gone into the design and construction of systems with very high radiation tolerance. Nevertheless the LHC is designed to run with 362 MJ of stored energy in each beam and with proton intensities in excess of 10^{14} per beam. Even very small fractional losses of this

beam risk causing serious damage to detector elements. Whilst the LHC itself has extensive instrumentation designed for machine protection, CMS requirements dictate that CMS must be able to detect beam-related problems as they develop and to assert beam aborts if required. In addition, CMS must be able to log data and perform post-mortem analyses in the case of accidents and understand the accumulated dosage and potential longer term damage to the detector elements. To this end CMS has implemented the BRM systems.

While radiation damage can lead to long term effects, the most likely damage scenarios involve very fast bursts of radiation/energy-dissipation in detector elements. Thus the protection systems must be sensitive to very fast changes in beam conditions; the BRM systems can detect changes at the 25 ns level, though the initially deployed protection systems will react in times of order 3-40 μs. Additionally the BRM systems provide monitoring and tuning data to permit operator intervention to diagnose and improve beam conditions. In addition, all BRM systems can be used to monitor integrated dose and detector component aging over the years of LHC operation.

CMS imposed several requirements on the design of the system:

- the systems have to be live at any time when beam is in the LHC independent of the state of CMS operations;
- systems must have readout and post-mortem capabilities very similar to those of the LHC machine protection systems; and
- they must possess a high degree of redundancy and a wide dynamic range for protection and monitoring scenarios.

Given these constraints, the system, which is summarised in Table 9.1, was implemented. The nomenclature and locations of the BRM subsystems in CMS are represented in Figure 9.1.

Subsystem (Sensor type)	Location Distance to IP (m)	Sampling Time	Function	Interface LHC/CMS type	# Sensors
Passives (TLD+Alanine)	CMS and UXC	$\sim$ months	Monitoring	N/A	>200
Medipix (Silicon pixel detector)	UXC and USC z=15 m, x=12 m	1 minute	Monitoring	CMS Standalone	3
RADMON (RadFets, PIN Diodes, SRAM)	CMS and UXC	1 s	Monitoring	Standard LHC	20
BCM2 (Polycrystalline Diamond)	TOTEM T2 z=$\pm$14.4 m	40 μs	Protection	Standard LHC	24
BCM1L (Polycrystalline Diamond)	Pixel Volume z=$\pm$1.8 m	5 μs	Protection	Standard LHC	8
BSC1 (Scintillator Tiles)	Front of HF z=$\pm$10.9 m	$\sim$ns	Monitoring	CMS Standalone	32
BSC2 (Scintillator Tiles)	TOTEM T2 z=$\pm$14.4 m	$\sim$ns	Monitoring	CMS Standalone	4
BCM1F (Single Crystal Diamond)	Pixel Volume z=$\pm$1.8 m	$\sim$ns	Monitoring	CMS Standalone	8
BPTX (Button Beam Pickup)	Upstream of IP5 z=$\pm$175 m	200 ps	Monitoring	CMS Standalone	2

Table 9.1: The subsystems deployed as part of the initial BRM. The table is ordered from top to bottom in increasing time resolution.

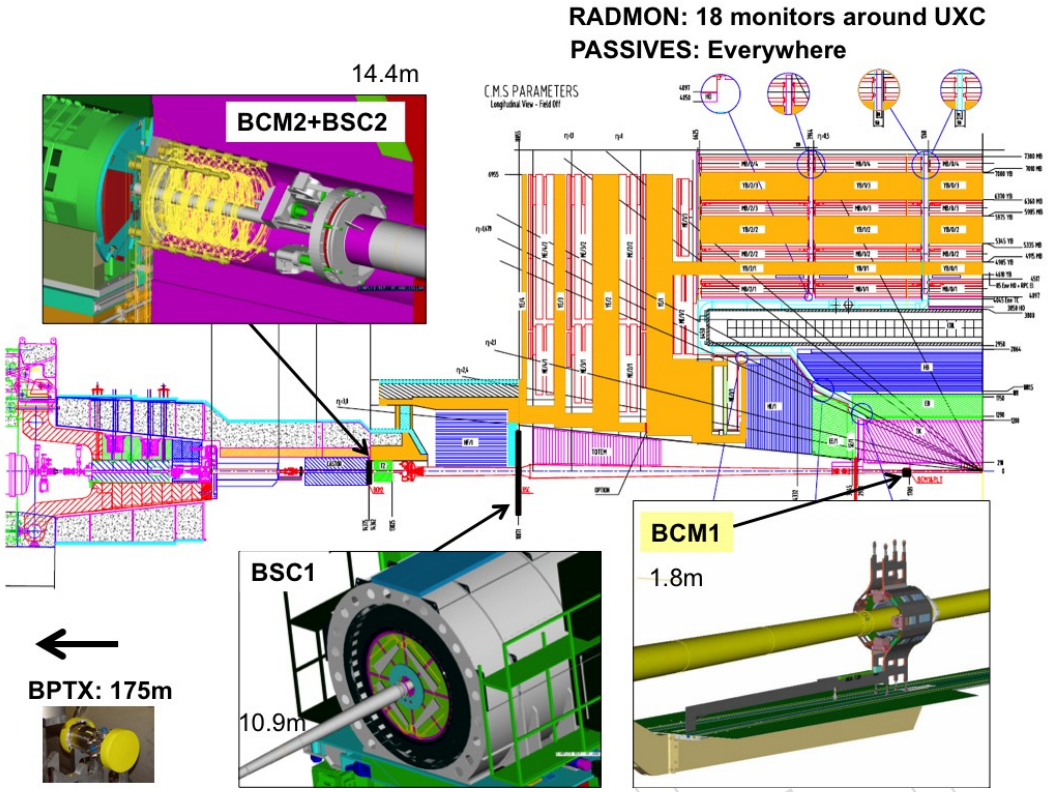

Figure 9.1: The layout of CMS BRM systems.

9.1.1 Protection Systems

The Protection systems are based on chemical vapour deposition diamond detectors [24, 25] similar to those that have been widely used in recent collider experiments [26, 27] where they have proven to be radiation hard [28], fast enough to match beam abort scenarios, and small enough to be inserted into areas close to key detector components without adding substantial material or services.

In CMS there are two protection systems foreseen for initial LHC operation [29**?**]. The first is the BCM1L which is four polycrystalline diamonds, each 10x10x0.4 mm, positioned on either side of the IP at Z values of $\pm$ 1.8 m close to the beam pipe and the pixel detectors at a radius of 4.5 cm. The second protection system is the BCM2. This is a set of twelve polycrystalline diamonds, each 10x10x0.4 mm, on either side of the IP behind the TOTEM T2 detector at a z position of $\pm$ 14.4 m. On each side of the IP, a set of eight sensors are deployed at an outer radius of 29 cm and an additional four at an inner radius of 5 cm. Here BCM refers to Beam Conditions Monitor, the index 1 or 2 refers to the two locations in z and the final character L indicates that these detectors are used in a leakage current measurement mode as relative flux monitors, typically integrating the leakage current over micro-second time scales. The BCM1L diamonds are arranged on the x and y axes. The BCM2 comprise eight diamonds at 45 deg intervals at large radius and four on the x,y axes at small radius.

The diamonds used for BCM1L and BCM2 are essentially identical, but the two systems differ in the readout methods adopted. The BCM2 uses a completely standard LHC Beam Loss Monitor (BLM) electronics and data processing [30, 31] that is read out asynchronously with the LHC orbit clock with a 40 μs sampling period. The BCM1L readout uses the same LHC BLM

backend electronics, but uses an alternative mezzanine card to provide sub-orbit sampling. The readout is synchronised with the LHC orbit clock, allowing user-configurable sampling over the 89 μs orbit so that the sampling can be matched to the bunch trains within the LHC orbit.

Using a set of thresholds in the readout systems and a combinatorial logic to reduce sensitivity to individual noise events, a hardware beam abort signal can be generated and transmitted to the LHC machine via the beam interlock system [32, 33], leading to the controlled extraction of the beams within 3-5 turns. A lower threshold value can be used to send hardware signals to CMS sub-detector clients to initiate high and/or low voltage ramp-downs.

In the event of a beam abort initiated by CMS, or any of the other LHC- or experiment- protection systems, a full history of the BCM1L and BCM2 signals is produced and transmitted to the LHC control room.

9.1.2 Monitoring Systems

Several monitoring systems are listed in Table 9.1. The BCM1F is also based upon diamond sensors, but with readouts able to resolve the sub-bunch structure; the Beam Scintillator Counters (BSC) are a series of scintillator tiles designed to provide hit and coincidence rates; the BPTX is designed to provide precise information on the bunch structure and timing of the beam; and the RADMON, MEDIPIX and Passives systems give calibrated information on the radiation field within the CMS cavern.

The BCM1F, BSC and BPTX are sensitive to time structure below the 25 ns level; as such they also provide several dedicated trigger inputs into the global Level-1 CMS trigger. In particular, the inputs from the BPTX and BSC will provide zero- and minimum- bias triggers respectively. Additionally, all three of these systems are sensitive to all machine intensities including the LHC pilot beam, where a single low intensity bunch is injected for studies or to confirm parameter settings prior to full intensity injection.

The BCM1F consists of eight single crystal diamonds, each 5x5x0.5 mm, four positioned on either side of the IP at z values of $\pm$ 1.8m at a radius of 4.5 cm, in close proximity to the BCM1L detectors. The purpose of the BCM1F is as a diagnostic tool to be able to flag problematic beam conditions resulting in "bursts" of beam loss over very short periods of time. Such beam losses are expected to be one of the principle damage scenarios for the CMS detector systems. The location for the BCM1F is close to the optimal position in terms of timing separation between ingoing and outgoing particles from the IP (i.e. 6.25ns from the IP). The gated rate information from the BCM1F therefore give a very good handle on the comparative rate of background from beam halo to that from lumonisity products. The sensor is connected to the JK16 radiation hard amplifier [34], after which the signal is transmitted to the counting room over an analog optical link built from the tracker optical components [35].

The detector and sensor is sensitive to one MIP and has a timing resolution for single hits of a few ns. The performance of the front end electronics is shown. Good separation can be seen between the signal and the noise. The pulse height was found to saturate at 100 V bias voltage across the sensor. The back end readout produces rate, multiplicity, timing and coincidence information independently of the CMS DAQ. However there is the possibility to feed information into the event stream via a standard CMS SLINK.

Beam Scintillator Counters are a series of scintillator tiles designed to provide hit and coincidence rates, with a design similar to those used at previous experiments [36]. The scintillators and PMTs used for the BSC are recycled from OPAL [37]. The BSC1 is located on the front of the HF, at $\pm$10.9 m from the IP, and consists of two types of tiles. Next to the beampipe are

the disks, segmented into 8 independent slices in ϕ with an inner radius of 22 cm and an outer radius of 45 cm. The primary function of the disks is to provide the rate information corresponding to the beam conditions. In addition, there are four larger area tiles further out, at a radial distance of between ca. 55 cm and ca. 80 cm, which in addition to providing rate information, will also provide coincidence information which can be used to tag halo muons passing through the detector for calibration purposes. The area covered by the BSC perpendicular to the beamline is about 25% that of the tracker; therefore these tiles can be indicative of activity within a bunch crossing, and is used to provide a minimum-bias trigger for commissioning and systematic studies as required. The BSC2 is located behind TOTEM T2 at $\pm$14.4 m from the IP. It consists of two tiles on each side of the IP, with an inner radius of between 5 cm and an outer radius of 29 cm. The primary function of the BSC2 is to distinguish between ingoing- and outgoing- particles along the beamline, as there is a 4 ns timing difference between them. The rates at this location can therefore be gated as to whether they are incoming (beam halo only) or outgoing (collision products and beam halo).

The Beam-Pickup Timing for the eXperiments (BPTX) [**?**] is a beam pickup device specifically installed to provide the experiments with the timing structure of the LHC beam. This beam pickup is a standard button monitor used everywhere around the LHC ring for the beam position monitors. Two are installed for CMS; 175 m left and right upstream of the IP. At this location, there are two beampipes, and so therefore the timing measurement is only of the incoming beam. To optimise the timing measurement, the four buttons (left, right, up, down) of the pickup have been electrically connected together, so there is no position information but the signal strength is maximised and hence the resolution on the timing.

An oscilloscope-based read out was chosen for the BPTX and developed in common with ATLAS [38]. The BPTX provides accurate information on the timing and phase of each bunch and its intensity. The phases of all the experimental clocks can be compared to the measured phase of each bunch at a precision better than 200 ps - presently variations at the level of 60 ps can be understood. This will also allow a z position for the interaction point to be calculated from the relative phases of the BPTX measurements on opposite sides of the IP. The BPTX also detects problems with the bunch structure, as well as measurements on the proportion of beam which has drifted into the neighbouring RF buckets.

In parallel to the oscilloscope based readout, the signals from the BPTX are discriminated, simple logical combinations are derived from this and sent as inputs to the CMS global Level-1 trigger. This will provide flags on each bunch crossing as to whether a bunch is present in each beam, either beam or both beams. The flag where bunches are present in both beams is indicative of whether collisions can occur in this bunch crossing, and therefore provides a zero-bias trigger for commissioning of the trigger system. This input is also essential to determine the relative timing between the LHC bunch clock and CMS experimental clock.

At 20 locations around the CMS cavern, RADMON [39, 40] detectors are installed. The RADMON detectors each provide calibrated measurements at these locations of the dose and dose rate using RadFETs; the hadron flux with energies above 20 MeV and the single event upset rate using SRAM; and the 1 MeV equivalent neutron fluence using PIN diodes. RADMON detectors are also installed all around the LHC ring, and in the experimental insertions. The RADMON detectors at CMS will be integrated into, and read-out via, the accelerator-wide LHC RADMON system.

The integrated radiation dose throughout the CMS cavern will be measured during each run period with passive dosimetry. This will provide a map of the radiation field throughout the cavern and will be used to validate the simulations of the anticipated doses. This gives an

absolute scale to the other measurements. The dosimeters chosen are TLDs and Alanine.

9.2 Motivation for Beam Instrumentation Improvements

The motivation for the improvements to the beam instrumentation proposed here is essentially to be able to provide a detailed monitoring capability as the expected beam intensities, luminosities and conditions evolve. In addition, there will be significant changes to the CMS detector configuration. As such, it is essential that the beam instrumentation adapts to the changing machine conditions and detector configuration.

The two CMS beam conditions monitors are the primary devices for protection of the CMS detector against adverse beam conditions. Within the CMS cavern, a span of ± 20 m they are only devices connected to the LHC ABORT system. Since there are therefore various categories of losses where the LHC protection system does not offer effective protection for the CMS detector, it is vital to ensure that the CMS protection system is maintained and active at all times. A detailed understanding of the detectors and their response is required to do this.

To ensure that the protection devices are always in optimal condition, during the LHC shutdowns, a preventative maintainance campaign is foreseen for both of the beam conditions monitors. Continued compatibility with the LHC Beam Loss Monitors is part of this strategy to ensure a system that is well understood. Additionally, it will be necessary to have a rebuild of the Beam Conditions Monitor 2 system during the 2016 shutdown, due to the changed geometry of the CASTOR region, with a larger beampipe being installed. Minor consolidation changes are also foreseen for the interlocks provided from the beam monitoring systems.

The beam monitoring system, scattered at various location in CMS, is invaluable in understanding beam conditions, to be able to understand sub-optimal conditions. The present system (consisting of the BCM1F, BSC and BPTX) is independent of the CMS DAQ, and always active, providing data for immediate online use, and also for later detailed offline understanding of beam conditions. Excellent timing resolution is a key aspect of the present system, as this is unavailable elsewhere within the CMS detector. The ability to feed into the L1 trigger has proved to be a strength during the initial run periods, and will be similarly useful in the future.

The improvements proposed here afford an improved monitoring capability throughout the LHC Phase 1 detector operations, based upon the strengths of the present system, and adapted for the increasing levels of luminosity, beam intensity and corresponding beam background. One notable improvement is through the provision of a trigger signal, which is designed to tag incoming beam background with a high purity and efficiency. Improvements in the instrumentation are proposed for the BPTX, BCM1F and BSC. Additionally, as an additional option to the core improvements proposed, a set of forward scintillators is proposed, which would extend the beam monitoring capabilities into the LHC tunnel, close to IP5. This is potentially interesting as it would allow the possibility of locating the origin of beam-gas interactions close to IP5.

The radiation environment in the CMS cavern is of particular concern for two reasons: first because high levels of radiation can damage sensitive electronics and second because the radiation will cause activation, particularly of materials close to the beam-pipe.

Every effort was made during the design and construction of the CMS detector to ensure that all sub-detectors are sufficiently radiation-hard for the anticipated levels of irradiation. The anticipated radiation fluences and doses were simulated using the design geometry. As an ongoing

effort it is necessary to validate these simulations against real data measured in the cavern, to ensure accuracy for the simulation results. Additionally, the simulations should be updated with the various upgrades and changes in configuration in the CMS detector. To be able to provide confidence in the simulation results, and ensure that they can always be validated against measured doses and fluences a suite of detectors, based upon those already available, is proposed to ensure that this is possible. Lastly, the levels of activation are a matter of concern, in particular for planning shutdown work based upon the ALARA principles. As such, it should be foreseen that each extended technical stop and shutdown give an opportunity to determine that the levels of activation are as expected, and that suitable detectors are available to measure this activation map with great accuracy.

The luminosity measurement is a key aspect of beam instrumentation that is used to monitor the LHCs performance in real time and to provide an overall normalization for physics analyses. The design goal for the real time measurement is to determine the average luminosity with a 1% statistical accuracy in 0.1 s. For offline analyses, the design goal is a systematic accuracy of 5%, although every reasonable effort will be made to produce a more accurate result. Both of these requirements must be met over a very large range of luminosities, extending from roughly 10^{28} cm^{-2} s^{-1} to 10^{34} cm^{-2} s^{-1} and possibly beyond. In addition to providing average luminosity measurements in real time and integrated luminosity values for offline analyses, the luminosity system will produce bunch-by-bunch luminosities useful for accelerator diagnostics and potentially also for accurate modeling of underlying event backgrounds. Other important and desirable features of the luminosity system include a capability for Always ON, operation and a bookkeeping system that is robust and easy to use. Always-ON operation means that luminosity information should be available for real-time monitoring of the LHC, whether or not the main CMS DAQ is operational.

The pixel luminosity telescope is designed to address all of these design goals, in particular it excels as an online luminosity monitor as it is independent of the CMS DAQ. The Pixel Luminosity Telescope(PLT) detector will be a dedicated luminosity monitor based on arrays of small angle tracking telescopes each consisting of three planes of diamond pixel sensors on each side of the IP. By providing a count of the number of three-fold coincidences seen in each bunch crossing, the pixel luminosity telescope will determine the relative luminosity of each of the 2835 bunch-on-bunch interactions occurring within the LHC to a statistical precision of 1% in a time period of $\tau = (0.55s)(L/L_0)$ where L is the luminosity and $L_0 = 10^{34} cm^{-2} s^{-1}$.

Additionally, the pixel luminosity telescope has considerable potential to vastly enhance the understanding of the beam dynamics, by being able to provide real-time online measurements of the luminous region, and of the relative rates and distribution of background within the pixel region. Having these parameters available online means that the LHC operators can potentially tune the parameters with feedback from data provided by the pixel luminosity telescope.

The pixel luminosity telescope is complementary to the HF luminosity measurement, in the sense that the method is a track-based rather than a calorimeter-based method. At the Tevatron, both CDF and D0 found advantages in measuring relative luminosity using tracks rather than calorimetric quantities.

Some of the upgrades proposed in this chapter also have a subsidiary role which improves the CMS physics reach for certain analyses. To a large extent, this is by improving the systematic understanding of the detector as a whole, in particular enabling absolute trigger efficiencies to be continiously measured with data, using the zero- and minimum- bias triggers provided by the BPTX and BSC respectively. Systematics can be further reduced by understanding the background conditions, as already motivated earlier in this section, with the beam background

triggers provided by the BSC and Forward Scintillator Counters (FSC) and diagnostics provided by the BCM1F. A small bandwidth dedicated to these triggers will allow high cross section analyses to be performed in the future. It is therefore vital to make sure that the BSC is upgraded to continue in its role as a well-understood minimum-bias trigger. In particular at every restart of the LHC after a shutdown, simple well-understood minimum-bias triggers are invlauable for an efficient recommissioning of CMS during the short low-luminosity phase that will occur during each LHC restart period.

The BSC also has an important role to play in the triggering for the heavy ion running. As the aim during the heavy ion running is to trigger on every event, it will be one of the key triggers for the run providing one of the two core minimum bias triggers. Additionally, more exotic triggers will be incorporated to select on certain event topologies (high multiplicity, forward-backward asymetries).

The forward scintillator counters option will add to the CMS physics reach in the forward region during both pp and heavy ion running. The counters will cover $7 \lesssim |\eta| \lesssim 11$, where $\eta = -\ln \tan\frac{\theta}{2}$ is the pseudorapidity, depending on the particle type and p_T. They extend the total rapidity coverage of the CMS detector to nearly $\Delta\Omega = 4\pi$. They will help increase our understanding of all high cross section processes, which is important for understanding the "underlying event" backgrounds to most physics searches. Full details of the proposed physics programme from the forward scintillator counters is given in [**?**].

9.3 Scheduled Plan 2012 and 2016 Shutdowns

The improvements are listed here, divided into the improvements which will be done prior to the 2012 shutdown, and those forseen for the 2012 and 2016 shutdown. The list prior to the 2012 shutdown will be done either during the 2011 extended technical stop, or parasitically during luminosity running in 2011.

Here is the list of improvements planned prior to the 2012 shutdown:

- Interlocks
- BPTX Trigger System
- Forward Scintillator Counters

Here is the list of improvements planned for the 2012 shutdown:

- Beam Conditions Monitors: Preventative Maintainance
- Beam Scintillator Counters Upgrade (Baseline)
- Pixel Luminosity Telescope
- Improvements to the instrumentation for validating the simulations (Passives, Medipix and Neutron Monitoring)

Here is the list of improvements proposed for the 2016 shutdown:

- Beam Conditions Monitor 2: Rebuild due to larger CT2 beampipe
- Fast Beam Conditions Monitor: Replacement
- Beam Scintillator Counters Upgrade (Possible Extensions)

It should also be bourne in mind that some R&D work will be needed for upgrades beyond the scope of this present proposal.

9.4 Beam Conditions Monitors

Studies of the radiation hardness of the diamonds and associated equipment in the LHC cavern show that they should all be sufficiently radiation hard to survive to the end of Phase 1. This is demonstrated in Table 9.2, where the expected lifetime of the equipment is shown in nominal LHC years. At all diamond detector locations, the expected lifetime exceeds that of the nominal LHC machine.

	BCM2I	BCM2O	BCM1F	BCM1L
DPA per pp	1.46×10^{-23}	5.92×10^{-23}	2.31×10^{-24}	4.95×10^{-24}
Error	1.14×10^{-24}	2.32×10^{-24}	5.22×10^{-25}	7.5×10^{-25}
Error %	7.82	3.92	22.62	15.16
Hardness factor	0.00835	0.03384	0.00132	0.00283
Seconds at nominal luminosity to reach 50% efficiency	1.06×10^{9}	2.61×10^{8}	6.68×10^{9}	3.12×10^{9}
In CMS years ($1 \times 10^{7} s/a$)	105.7	26.1	668.5	312.2

Table 9.2: Expected radiation damage for all beam condition monitor diamonds installed in CMS. Shown are displacements per atom (DPA), the hardness factor normalised to 24 GeV protons and the expected time in NOMINAL LHC Years to reduce the diamond detector efficiency to 50%.

9.4.1 2012: Preventative Maintainance

In 2012, while there will be access to both the BCM1L and BCM2 systems, it is not foreseen that any major work will be required. However, given the critical nature of the systems to the protection of CMS, it would be wise to foresee a campaign of work on a sub-selection of the diamonds to qualify that they are still in good working order. It is also necessary to anticipate problems that may occur between the present time and the 2012 shutdown. This work would entail, on a couple of diamonds from each system, checking wirebonds, the metallisation of the diamonds, the electrical connections, and the grounding of the system, as well as the state of cables and connectorisation and finally recalibrating the system in-situ. Assuming that nothing out of the ordinary was found, no further work would be done.

Similarly, given the critical nature of the Beam Conditions Monitors, and in particular the growing importance of the BCM inside the tracker region, it should be expected that both the Patch Panel boards in the service cavern and the BCM1L Readout boards should be replaced and upgraded based upon what is learnt in the first 2 years of running. The patch panel boards, as well as mapping the cables to the power suppy, provide filtering and correct treatment of the grounding. The BCM1L Readout boards are mezzanine cards with a sensitivity of $\sim$nA, despite being 100m away from the sensor. While already highly optimised, these cards have already been patched, and there is a great deal of recent understanding gained from analysis of the data. As such, further improvements in sensitivity and immunity to exterior noise sources can be expected if a new set of cards is produced.

A contingency item is the option to install a local UPS in the BCM racks with the aim of isolating the power supply from fluctuations on the mains grid. Experience over the first two years of running will show whether this is necessary.

9.4.2 2016: Preventative Maintainance and BCM2 Rebuild

Similarly in 2016, preventative maintainance should be carried out on the Beam Conditions Monitor systems, in a similar fashion to that done in 2012. However, in addition to this, three

major items should be foreseen:

1. Rebuild of the mechanics of BCM2
2. Possible replacement of the BCM2 "Tunnel card" Front End electronics.
3. Replacement of the VME crate interface board PCs.

The first of these items is required only if the CT2 beampipe diameter is increased subsequent to the removal of the CASTOR and TOTEM T2 sub-detectors at the end of the low luminosity phase of the experiment. This is likely to occur during the 2016 shutdown, but could take place as early as the 2012 shutdown. This would require a complete mechanical rebuild of the BCM2, as well as a replacement of the front end cabling for the BCM2, which would not survive such a rebuild intact. This was quite a delicate aspect of the original BCM2, requiring several attempts to produce a mechanically robust and radiation hard solution. Part of this work may be mitigated by the fact that it will be needed in some form for the work on replacing the BSC2 detectors. The rest of the cabling between the CASTOR table and the T2 rack on the HF platform is also likely to need some work due to the general overhaul of the HF platform. A simple replacement of this cabling should probably be foreseen.

The second item depends upon the LHC BLM group. At present, they plan to develop a new version of the tunnel card electronics in the next year or so. It is a possibility that they may install these in the LHC in the 2016 shutdown, and therefore a complete replacement of the tunnel cards should be reserved as a possibility for this shutdown, to remain compatable with the LHC Beam Loss Monitors. The change foreseen for the tunnel cards is from using a radiation-hard FPGA to an even more radiation-hard ASIC, based upon the present design of the tunnel card. This change will also remove the distinction between the dual ADC and CFC acquisition electronics, mis-matches of which cause minor degradation of the monitoring data from the BCM2 detector. Additionally, the upper-end of the dynamic range of the detector will be increased. The overall result will be a card with a single DAQ system with greater reliability for monitoring and simplicity in interpreting the data. Quite aside from the fact that this card should be changed for compatibility with the Beam Loss Monitor system, these simplifications will pay a dividend in understanding the beam from the monitoring. As the luminosity increases towards the nominal LHC luminosity, detailed understanding of beam background will be vital, as any deviations above the nominal expected background could decrease directly the luminosity reach.

The third item depends upon the LHC BLM and Controls groups. At present they are testing new board computers with Intel chips running LINUX as a replacement for the present RIO-3 Power PC boards installed all around the LHC. If, as is presently planned, these are replaced all around the LHC ring in front-end crates, it would be unwise not to follow these changes. In addition, it will be imperative to test extensively these devices prior to installation in the BCM2 system.

9.5 Interlocks

In addition to the beam permit (i.e. beam abort) functionality provided from the Beam Conditions Monitors, several other interlocks are provided to add to detector safety as well as an adaptable set of logic, to respond to developing needs in improving detector safety and smooth running. These tasks belong to the core responsibility of the Beam Instrumentation, and as such should be optimised for simple operation and maintainance as well as reliability.

Presently this adaptable logic is performed in a combination of two crates:

- A dedicated PLC crate to handle the Emergency Crash Buttons located in the CMS SX5 Surface Control Room at Point 5. The crash buttons are for the Beam Permit (i.e. Beam ABort) and for the Injection Inhibit.
- A dedicated VME crate, with standard CAEN logic cards to handle coincidence logic, and registering of safe hardware states sent by the machine, "Safe Beam Flags", as well as input into the Injection Inhibit based upon these states and a disable signal to the Pixel and Tracker CAEN Voltage crates, in case of bad beam conditions.

It is presently under review as to whether, during the 2010-11 extended technical stop, these crates should be combined into an expanded PLC crate, for the sake of simiplicity and ease of maintainance. A PLC crate is expected to also give a higher level of reliability.

9.6 Fast Beam Condition Monitors Replacement

9.6.1 Improvements to the BCM1F in the technical stop 2011/12

The DAQ and publishing software will be maintained and possibly upgraded, based on the experience acquired during running at higher luminosities. Also, the ring-buffer and post-mortem analysis tools will be implemented and further improved.

Hardware supplements foreseen are coincidences gated with the BPTX signal to separate collision products from beam halo and signals delayed with respect to the bunch-crossing time.

9.6.2 The 2011/12 Shutdown

Some limited damage is expected in the front-end readout of BCM1F. The form this will take is radiation damage of the FE ASIC and particularly of the laser diode for the analog signal transmission. Spare components, still available at CERN, should be prepared for this action.

The installation of a single GaAs sector, as described below, will be considered.

9.6.3 The 2016 Shutdown

The BCM1F system very likely will need a replacement after 2016 because of damage and current rate capability limits. A possible new system should be able to handle higher rates. The optical transmission of signals should have a wider dynamic range. Digital transmission will be the preferred option. The new system should explore existing or standard components because it is unreasonable to develop specific components for such a low number of detector modules. Standardization within CERN or CMS/ATLAS should be considered.

The baseline design should be for a replacement of the BCM1F system with a very similar detector design. There is an upgrade option under investigation, described below, for a significant enhancement of its capabilities.

9.6.4 Pad Detectors using GaAs Sensors

The possibility of the replacement or supplement of the inner BSC rings using GaAs sensors will be investigated. These GaAs sensors will be subdivided in pads of 5x6 mm^2, as shown in Figure 9.2, allowing particle flux measurements with finer granularity.

GaAs sensors are investigated within the BCM-DESY group. The signal to noise ratio is excellent and the leakage current per pad is at room temperature below 500 nA at an appropriate

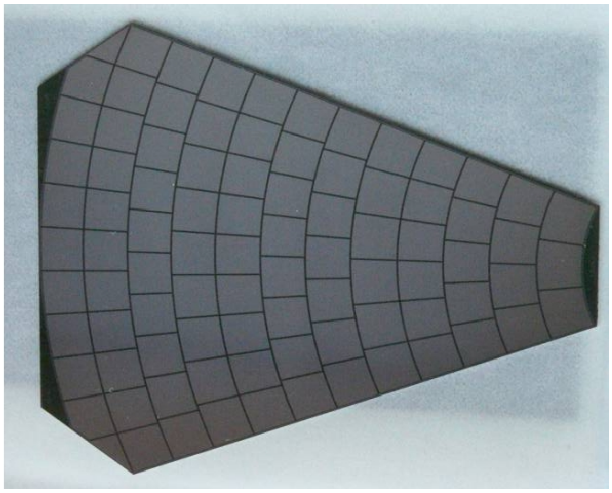

Figure 9.2: A prototype of a GaAs sensor sector with pads of about 30 mm^2 area.

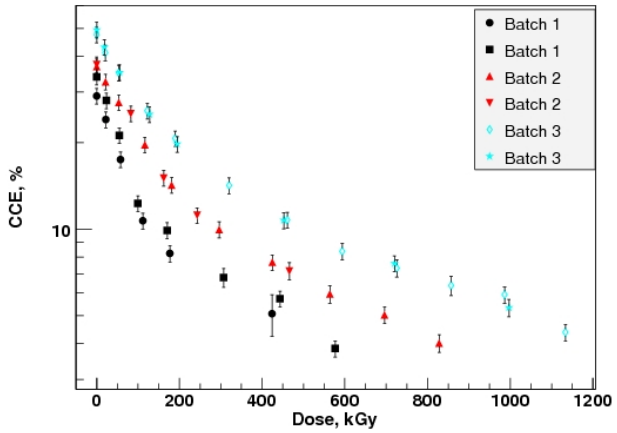

Figure 9.3: The CCE as a function of the absorbed dose for the GaAs sensors with different donor concentrations. The donor is Te for the batches 1 and 2 and Sn for batch 3.

operating voltage.

The radiation tolerance has been tested so far only in an high intensity electron beam up to depositions of 1 MGy. The result is shown in Figure 9.3. The signal amplitude dropped to 15% of the original one, but is still sufficient to count Mips. The leakage current at room temperature is only slightly increasing up to this dose, and still non-critical for operation of the sensor.

The R&D will be focused first on irradiation tests. Since radiation hard FE ASICS will be needed a close collaboration with other groups in or outside BCM will be necessary

9.7 Beam Scintillator Counters Replacement

It is foreseen to replace the beam scintillator counters in the 2012 shutdown, with an option to delay this replacement until 2016 depending upon their performance at the end of 2010 with a decision being taken during the 2010-2011 extended technical stop. If the replacement is done during the 2012 shutdown, there may be further optimisation during the 2016 shutdown to ensure that they function for the remainder of nominal LHC running.

For the replacement of the beam scintillator counters a number of proposals have been put forward; what is presented below is one example of how to construct such a replacement system. However there is an array of opinion as to what the functionality and scope of such an upgrade should be. A timeline of milestones in the foreseen decision process is outlined to achieve an engineering design review early in 2011.

9.7.1 Functionality of the Current BSC System

The Beam Scintillation Counter (BSC) is a simple, stand-alone CMS beam monitoring device. It uses polyvinyl-toluene (PVT) plastic scintillator tiles mounted on the Hadronic Forward Calorimeters (HF) facing the IP. The layout and photos of the installed tiles of the the 2 BSC stations are shown in figure 9.4.

The primary purpose for the installation of the BSC system is to monitor various aspects of the beam background during the early commissioning and low luminosity phases of the LHC in the region of the CMS experiment. However, the BSC became the most important minimum bias and beam halo triggering detector in CMS during the commissioning phases and remains an integral part of CMS data triggering. The BSC has provided the primary trigger for data analysis for some of the early CMS papers.

The BRM group have several subsystems installed, each focusing on a particular task while providing some redundancy between two or more sub-detectors[20, 22]. The BCM2 system at $\pm$ z = 14.36m is a safety system capable of monitoring relative halo and IP product rates by integrating the leakage current of the diamond sensors. The BCM1F provides beam monitoring on a bunch by bunch scale but with its position at $\pm$ z = 1.8m and 5×5mm diamond area, gives a relatively small field of view of the overall beam dynamics. The purpose of the current BSC falls somewhere between these two subdetectors with the aim of bunch-by-bunch beam monitoring in a position where beam background and collision product yields can be distinguished and compared. Measurements of beam halo timing and rate can be made from single bunches up to $\mathcal{L} = 10^{32}$ until radiation damage to the scintillator tiles becomes excessive or saturation of the channels due to large particle flux occurs.

The BSC can effectively be split in to three detector areas: the inner BSC1 tiles, designated D1-D8 in Fig. 9.4(a), which cover the η range of $3.9 < \eta < 4.4$; the outer BSC1 tiles, designated P1-P8 also in Fig. 9.4(a), which partially cover the η range of $3.2 < \eta <$3.4; and the BSC2 tiles, shown in Fig. 9.4(c) and (d), which cover the η range $4.5 < \eta < 5.7$ with a 30% coverage in ϕ.

9.7.1.1 Present Limitations

The BSC uses large area scintillator tiles which give it a high sensitivity required for the early phases of the LHC running when luminosity and bunch occupancy are low. When the luminosity increases, the signals will pile-up and result in a loss of some information of the beam halo and minimum bias events. A system with a dynamic range capable of coping with luminosities ranging from $10^{27} - 10^{35}$ will produce reliable data beyond the expected luminosities without losses due to saturation and be operational for the lifetime of CMS. The outer tiles of the BSC1 (see 9.4) are not complete in ϕ and have two different channel areas and radii making individual channel rates more difficult to equalize and complicating the geometrical acceptance. The timing of beam halo and collision products provides a method of differentiating particles arising from collisions at the I.P from those of beam halo and beam gas interactions. At the time of designing the BSC, the only possible position available for installation was on the HF front faces at a distance of $\pm 10.86m$. This is within 2.6ns of a point in Z where the incoming beam background passes through the outgoing collision products plus the beam background from

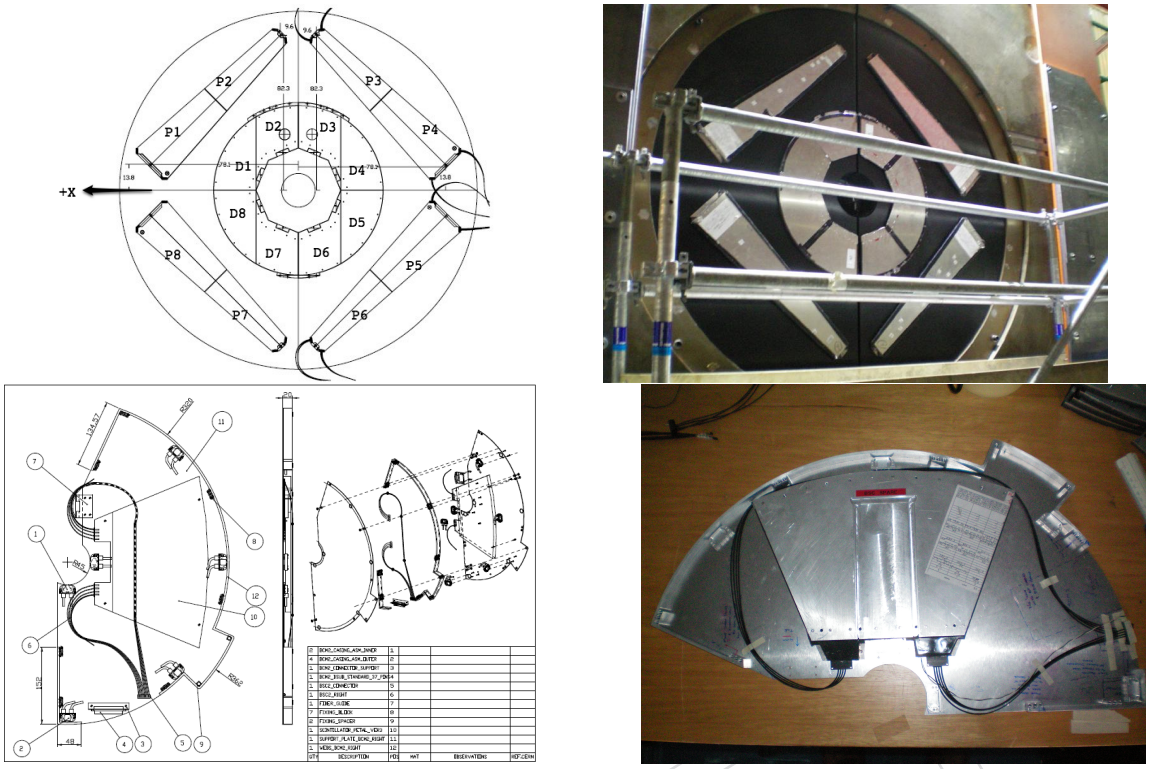

Figure 9.4: The BSC1 tile layout on HF. a) CAD Drawing of BSC geometry and channel names. b) Photo of installed scintillator tiles. c) BSC2 engineering drawing. d) BSC2 tile inside the BCM2 housing before installation.

the opposite direction (see section 9.7.2.3). With a time resolution of 3ns, it is difficult to differentiate between the two bunch categories and so the BSC2 tiles were installed in an attempt to reduce the ambiguity of identifying background from collision products. The scintillator tiles, fibers and PMTs will gradually become damaged by radiation. Indeed, after their use in the OPAL endcaps the condition of the hardware is not fully understood. There is no way of testing the front end system and calibrating for any loss of light output.

In summary, the present limitations of the BSC are:

- Failure of front end components due to radiation damage.
- Condition and Radiation hardness of PVT scintillators not fully understood.
- Lack of continuous symmetry in ϕ (outer tiles).
- Limited time discrimination due to proximity of bunch/beam background crossing region.
- Timing resolution is only just adequate for the current location (3ns).
- Will saturate at luminosities above $\mathcal{L} \approx 10^{32}$ and possibly for Heavy Ion runs.
- No *in-situ* calibration method available.

9.7.1.2 Future Functionality

No system yet exists for monitoring and triggering on beam background and minimum-bias products in the η = 3 - 5 region at nominal LHC luminosities. LHC operation during the past few months has shown that understanding beam dynamics is vital, as seen from the studies

on expected beam halo and beam gas [41**? ?**]. A detector that can trigger and veto on such events, as well as monitor them will be a very useful addition to the CMS triggering system as a whole. As minimum-bias events scale with luminosity, the upgrade system could be able to indirectly measure the luminosity in CMS. Many improvements can be made to the existing BSC design which are outlined in Table 9.3 along with the implications of these requirements. A more detailed note on possible future functionality is in preparation and will be released soon.

The BSC min-bias triggers have been extensively used in event trigging and offline anaylsis but, due to the incomplete coverage of the BSC (total $1.2m^2$ per end, not fully symmetric in ϕ), it is not a long-term solution when high-luminosities and Heavy Ion runs require that min-bias triggers and beam halo vetoing must be highly reliable and have a large acceptance. Therefore an upgrade with a larger, symmetrical coverage in ϕ and greater rapidity range will be beneficial.

Desired Features	Requirement	Details
Symmetrical coverage in ϕ	To increase the acceptance for monitoring and triggering	A complete 360° detector area encircling the beam pipe
Increased dynamic range	To provide proper operation up to maximum luminosity	More channels with smaller area and/or tunable sensitivity
Improved time resolution	To discriminate between collision products/halo with greater certainty	$\leq$ 2 ns front-end signals
Beam background/Collision product discrimination	Use time-of-flight information to monitor relative quantities of background and collision fragments	Determined primarily by installation location and hardware time resolution
Cost effectiveness	Must be financially viable for the lifetime of CMS	Radiation hard detector medium or replaceable cheaper options
Radiation Hardness	Front end materials must be able to survive more than 5 years of continuous running	Quartz or Radiation Hard plastic scintillators as a detector medium. Radiation hard PMTs or other readout devices
Maintanence	Minimal access requirements for repairs and replacements	Any exchangable parts must be easy to extract and replace for reasons of radiation safety
In-Situ Calibration	Ability to check and set up individual channel response	The channel occupancy for each event needs to be determined. A method of calibrating individual channels remotely is desirable

Table 9.3: Desired functionality of the BSC upgrade. These characteristics will help in deciding the correct channel geometry, material and method of readout. Additional to these aims, mechanical and environmental factors such as radiation hardness and required services must be considered.

In summary, the upgrade of the BSC detector should provide efficient, robust minimum bias and beam background triggering improving the readout of CMS and importantly, vetoing on beam gas events. It will also provide an online relative luminosity measurement by monitoring of the minimum bias rates. To provide this functionality up to the LHC design luminosity, an upgrade of the BSC system needs to be designed, built and installed during the 2012 shutdown. This should be done during the 2012 shutdown due to the age of the currently installed hardware.

9.7.2 Environmental Conditions

A major factor of the upgrade design is the environmental conditions that the BSC upgrade must operate in. The design limits are defined by the radiation flux, magnetic field strength, available space and the amount of extra infrastructure allowed.

9.7.2.1 Radiation Fluence & Dose

Probably the most important consideration in the design of the BSC upgrade is the radiation environment that the front end detector must be capable of operating in. Simulations of radiation fluence, calculated for 10 years of LHC operation have been made [**?** **?**] for various areas in CMS. The summary of these results that pertain to the BSC region are given in Table 9.4 and Table **??**. These numbers will govern the types of materials used and the geometry of the upgrade as detailed in section 9.7.6. Another important consideration is the likelihood of HF neutron induced activation of the polyethylene which will cause random events in the detector tiles if mounted directly on the front face. These *activation events* must be filtered out in some way without introducing a bias in the triggering. One method would be to use two detector layers separated by several radiation lengths of absorber and increasing the distance from the polyethylene face. Coincidences between the layers would allow for discrimination between real events and activation events while increasing the distance will reduce the amount of neutrons incident on the BSC detector elements.

η region	Average Energy	Avg Multiplicity per p-p collision
$0-3$	50 GeV	28
$3-5.3$	380 GeV	20
$5.3-7.8$	2110 GeV	13

Table 9.4: Multiplicity and energy of all particles in various pseudorapidity ranges[**?**]

The majority of the particle flux stems from collision products rather than beam background. Information of beam background and p-p collision products has been taken primarily from [**?**] and [**?**].

During LHC operation, the instantaneous luminosity varies by a factor of 10^7, from 10^{27} cm^{-2}s^{-1} for collisions between two nominal pilot bunches to the nominal LHC luminosity 10^{34} cm^{-2}s^{-1}. These instantaneous luminosities correspond to a rate of primary events of between 10 and 10^8 Hz. The corresponding expected particle flux at the HF front face varies from 1 cm^{-2}s^{-1} for luminosities of 10^{27} cm^{-2}s^{-1} to 10^7 cm^{-2}s^{-1} for nominal luminosity. Nearly 50% of the particles are charged pions. 25% is neutral pions. The rest is made of approximately equal quantities of neutrons, electrons, kaons etc [**?**]. The flux dictates the details in the design of the BSC upgrade in terms of channel size and materials. Channels which are too large could saturate and would not give useful information on channel occupancy. Choosing channels sizes that are too small would result in an expensive, complicated detector which gives no gains over one with the optimum channel size. The expected number of photoelectrons reaching the PMT is calculated using a 25cm^2 quartz tile ($\approx$100 photons per 1cm traversed material) with a 5% light collection efficiency and a 20% quantum efficiency of the PMT). Proposals of potential detector materials, sizes and front-end readout electronics are given in section 9.7.6.

9.7.2.2 Albedo Events

A phenomenon known as Albedo or "after-glow" has been noted in the BSC Minimum Bias triggers. These triggers are important for selecting minimum bias events and accidental trig-

gering could reduce the data taking efficiency of CMS[1]. These albedo effects cause the BSC Minimum Bias trigger to continue to fire with a low probability long after the instance of the bunch crossing. Figure 9.5 shows the number of triggers fired per bunch number (BX) summed over run number 123596 (Before) and 123818 (After). Figure 9.6 shows MC simulation results for 450GeV and 7TeV. It should be noted from the simulation that the effects are expected to be essentially independent of $\sqrt{s}$ and to first order only dependent upon the collision rate. However, the total sum of these late hits is expected to be 10 - 20% of the total and therefore a coincidence is not required for all tiles, as it is not expected to degrade the trigger performance of the BSC substantially.

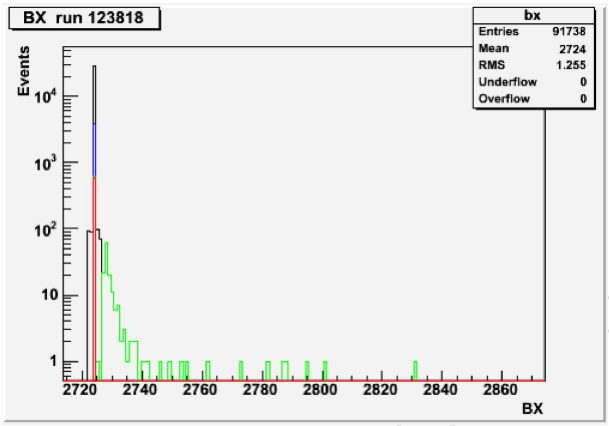

Figure 9.5: Histograms of the BSC Minimum Bias Triggers per bunch crossing (BX) where black is the distribution for all the Express Stream Events, blue for any BSC trigger, green for 40&41 and red for 40&41& (No BeamHalo BSC trigger)& (technical bit 0 (BPTX AND)) [**?**].

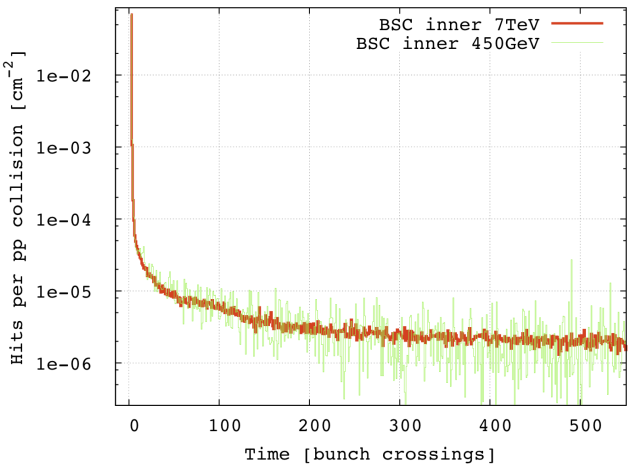

Figure 9.6: Results from MC simulations showing the long tails in arrival time for scattered particles. This may explain the higher incidence of late triggers seen in figure 9.5. [41]

It is suspected that the albedo effects are due to particle scattering and activation from the HF polyethylene face. Moving the BSC detector away from the HF face is therefore a worthwhile

[1]The L1 trigger rule prevents any subsequent triggering for 2BX (50ns) after the first trigger. A false trigger would lose data for up to 3 bunch crossings.

consideration. (See section 9.7.4).

9.7.2.3 Bunch Crossings in Z

With the two LHC beams traveling in opposite directions, there are several points along the beam-pipe axis where they overlap, crossing these points at precisely the same instance. By measuring the arrival time of a bunches (or more precisely, the beam halo[2] and collision products that travel with the bunches) with respect to the CMS bunch clock, it is possible to determine if the signals originate from outgoing halo and collision products, or incoming beam halo only. Therefore, in order to allow discrimination between the incoming and outgoing particle bunches, it is vitally important to avoid installing the upgrade detector on or close to any of these crossing locations. Figure 9.7 shows the locations of these nodes for 25ns bunch spacing. Optimal locations fall halfway between these locations and are given in Table 9.5 and Fig. 9.7.

Z location	Location in CMS
$\pm$ 1.875m	BCM1F locations
$\pm$ 5.625m	Inner barrel
$\pm$ 9.375m	Endcaps. T1 region
$\pm$ 13.12m	Middle of HF
$\pm$ 16.875m	Inside rotating shields
$\pm$ 20.625m	Inside TAS volume

Table 9.5: Optimum positions for the upgrade installation with regard to timing and then Beam1 and Beam 2 crossing locations.

The values in Table 9.5 were calculated by:

$$\Delta t = Min \left| \tfrac{2z}{c} - n(Bx) \right|$$

where z is the distance from the I.P, n = 1,2,3... and Bx = 25ns.

Some of these locations are unavailable or simply not practical. However, the current BSC2 location on the Castor table (Z = $\pm$ 14.36m) will be available as is the current BSC1 location on the HF front faces (Z = $\pm$ 10.86m). More details are given in section 9.7.4.

9.7.3 Performance of the BSC Minimum Bias Triggers

Using the openHLT ntuple data, an approximate calculation of the BSC minimum bias trigger performance can be made by looking at how they reacted in the presence or absence of true minimum bias events. The offline HLT software is capable of performing quick primary vertex reconstruction from the tracker and pixel data and stored the results in branches of a ROOT tree in terms of positions in x,y and z and also the number of primary vertices counted per event.

Figure 9.8 compares the *L1TechBSC_minBias_ threshold1*, *L1Tech_BSC_minBias_ threshold2* and *L1Tech_BPTX_plus_AND_minus* technical trigger bits with the existence or absence of one or more primary vertices, taken from the *recoVrtNtrk* branch. The zero bias trigger was the BPTX therefore the BSC numbers are unbiased.

[2] "Halo" here is used generally to refer to all beam losses which occur before the beam enters the CMS cavern. This is normally broken down in to 2 components; Inelastic beam gas events in the region 20m $<$ Z $<$500m; Elastic beam gas events and true beam halo which interact at the tertiary collimators (TCTs) 150m upstream of CMS.

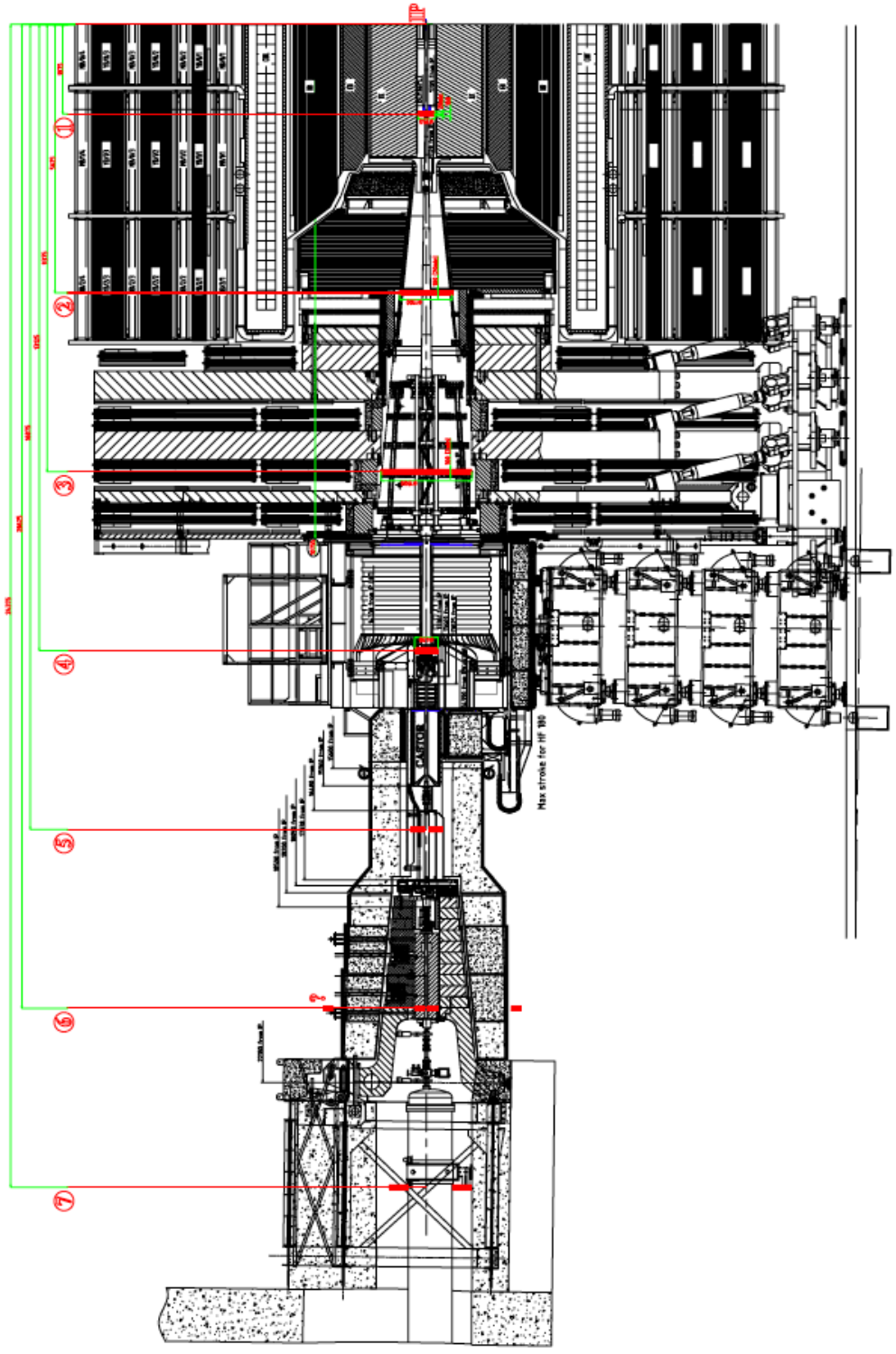

Figure 9.7: Sagittal view of one side of the CMS detector. The red lines indicate the locations where incoming background bunches have the greatest time separation from the outgoing collision products and background from the opposite direction. These locations are optimal to distinguish between the beam background and collision product yield using time-of-flight methods.

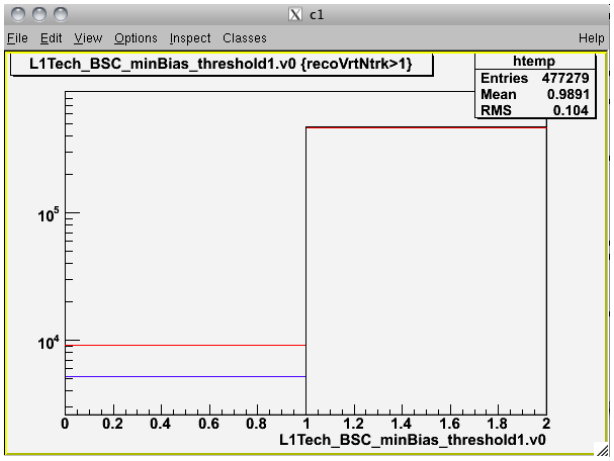

Figure 9.8: Performance of the BSC minimum bias triggers with the BPTX zero bias trigger. Events with one or more vertex are considered to contain a minimum bias event. Blue line: BSC MinBias Threshold1. Red line: BSC MinBias Threshold2. Black line: BPTX Zero Bias.

Trigger	% True Positives	%False Negatives
BSC MinBias Threshold1	99%	1%
BSC MinBias Threshold2	98%	2%
BPTX Zero Bias	100%	0%

Table 9.6: Performance of the BSC minimum bias and BPTX zero bias triggers during 2010.

The BSC minimum bias triggers have so far performed well, triggering on 99% of minimum bias events, as shown in Table 9.6, strongly suggesting that an upgraded detector specifically aimed at minimum bias triggering will be important for CMS.

9.7.4 Available Locations

It was initially foreseen that the upgrade detector would fill the space previously reserved on the -Z end of CMS for the Totem T1 sub-detector at Z $\approx \pm$ 10.7m. However, T1 installation is now expected to go ahead in the winter shutdown of 2010-2011 so the BSC upgrade will remain in the HF region between Z $\approx \pm$ 10.6m - 15m. This will be beneficial in terms of accessibility for additional services, for example, new and existing high voltage cables, signal fibers etc. However, as with the current BSC system, the possible installation locations are close to a p-p crossing node (9.375m, ΔZ = 1.49m) where incoming and outgoing beam halo and collision products are indistinguishable in time. This will need to be taken in to consideration if certain functions are to be carried out by the upgrade detector.

There is a 10 cm deep volume reserved within the Totem T1 detector volume [3]. This could allow the upgrade detector to be moved towards the I.P and away from the HF polyethylene face. This has two major advantages. First, it moves to a position where the incoming/outgoing bunch crossing Δt is increased from 2.6ns to 3.9ns, making the distinction of the two beams easier to achieve. Secondly, it moves the detector elements away from the activated HF calorimeter, thus reducing the back-scatter effects that could propagate in to the L1 trigger. If the detector was to be installed here, consideration would have to be given to the extent of the effect of the additional BSC material on the performance of the surrounding detectors.

For the BSC2 upgrade, there is some limitation on the minus-side of the CMS detector due to

[3] To be installed in the 2010-2011 shutdown on the +Z side of CMS only

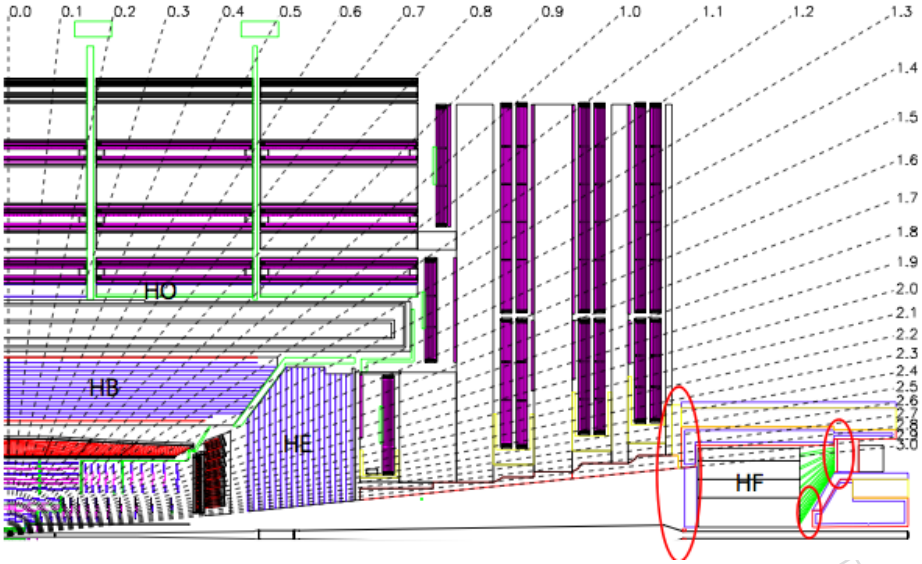

Figure 9.9: Longitudinal view of CMS showing the HF region and possible location(s) for the BSC upgrade.

the presence of Castor. Here, the upgrade detector must be located within the BCM2 volume, as it is now. On the plus-side, there is more available room and the upgrade detector could be located at various places along the Castor table, for example, a more ideal location near to Z = 16m. This also opens up the opportunity for a more elaborate double layered detector to reduce noise.

9.7.5 Read-Out System

For simplicity and reliability, the readout system will continue to use electrical signal cables as opposed to optical fiber. The front-end readout components must be able to withstand the harsh radiation and magnetic field environment in the CMS cavern. Silicon Photomultipliers (SiPM) are one possible choice provided they can be situated in a location where hadron fluxes are low. Radiation hard, multi-channel PMTs are another option. These could be situated in the PMT boxes of the current system where they would benefit from shielding due to the HF calorimeter.

The back-end readout of the upgrade requires that signals from individual channels are consolidated and their timing evaluated in logic to determine if they are minimum bias, Beam 1 background or Beam 2 background. The current trigger system uses cumbersome NIM logic to achieve this. For the upgrade, there are two possible modern solutions; a CAEN logic board or a generic trigger board. Either of these solutions would allow for more elaborate coincidence algorithms to be developed in software rather than in NIM hardware. The resulting outputs of the coincidence algorithms will then be sent to the Level 1 Global Trigger. For inserting monitoring and luminosity information in to the CMS event stream, there are a number of options to be investigated. These include the HCAL QIE, the PLT board and the SCal method which is under development. The current style of monitoring system, using VME based Analog-Digital Convertors (ADC), Time-Digital Convertor (TDC) and scalers could be built upon for the upgrade detector, keeping some compatability with the BCM1F detector.

9.7.5.1 Possible Detector Materials

The upgrade detector will be in one of the most extreme enviroments in CMS with regards to radiation flux and energy. For this reason, the choice of materials is vitally important and several are under inverigation at the present time. The present system uses PVT plastic scintillator tiles. These are relatively inexpensive and for the outer regions ($\eta \approx 3$) may be a sufficient material if changed every 5 years or so. Radiation hard plastic scintillators[4] also look like a promising option. Tests need to be carried out on some materials before they can be put in to CMS. Quartz with high OH content is known to be very radiation hard and is a perfect material to employ for the inner most channels, both in front and behind HF. The University of Iowa group is currently developing high-OH quartz plates with P-Terphenyl (PtP) coating to increase light yield.

9.7.6 Proposed Prototype System

The proposed system will fulfill the following:

- Provide absolute minimum bias rates and triggers from tiles located on HF at Z = $\pm$10.86m which are shielded from incoming background but almost in line-of-sight with the interaction region.
- Beam background monitoring and veto triggering from the tiles located on the Castor table at Z $\approx \pm$14m and inner ring of tiles on HF.
- Online relative luminosity monitoring from information of the minimum bias rates.
- 'Noise cancellation' from fake hits (activation events) by the use of two layers of detectors and coincidence detection.
- Feed data in to the CMS data stream via the CMS global trigger (L1-Level) and S-link, HCAL QIE or PLT readout board

Figures 9.10, 9.11 and 9.12 show the proposed Minimum-Bias/Beam Background detector with its geometry and channel layout. Table 9.7 lists the materials of interest to be used in the detector. The proposal is for 8 inner channels and 16 outer channels per end to replace the BSC1 system (HF front face) and a further 8 channels per end to replace the BSC2 tiles on the Castor tables. This gives a total of 64 channels.

Component	Options to be explore
Detector Material	High-OH quartz, PtP coated Quartz, Radiation Hard Plastic Scintillator(Outer Region), BC-408 plastic scintillator (Outer region)
Light guides	quartz core-quartz clad fibers, air-core fibers
Front End Readout	SiPM, Multichannel PMT
Back End Readout	VME modules, CAEN Logic board Generic Trigger Board (EUDET or Wiener)

Table 9.7: Materials under investigation for the upgrade front-end including detector materials and readout devices.

[4] Available from Amcrys' European distributors, Detec Europe. All documentation is currently only available in Russian.

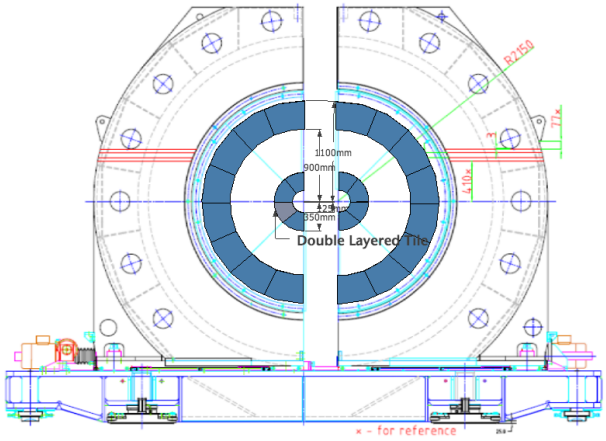

Figure 9.10: Simple concept drawing of the front-end upgrade for the BSC. Quartz or radiation hard plastic scintillator may form the inner annular ring while radiation hard scintillator or BC408 may form the outer annular ring. R & D will determine the number and size of segments as well as the boundary between the radiation hard detector material and scintillator.

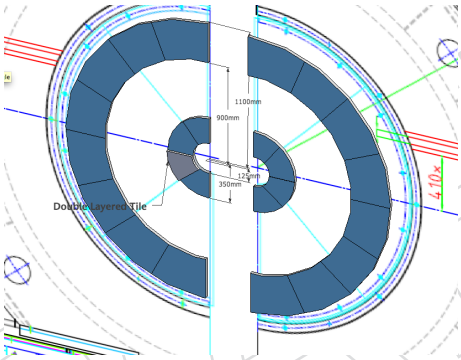

Figure 9.11: 3D view of the proposed upgrade geometry. One or more tiles can be fitted with an extra layer to enable discrimination (by coincidence detection) of true events and noise or activation events from neutrons emitted from the activated HF polyethylene material.

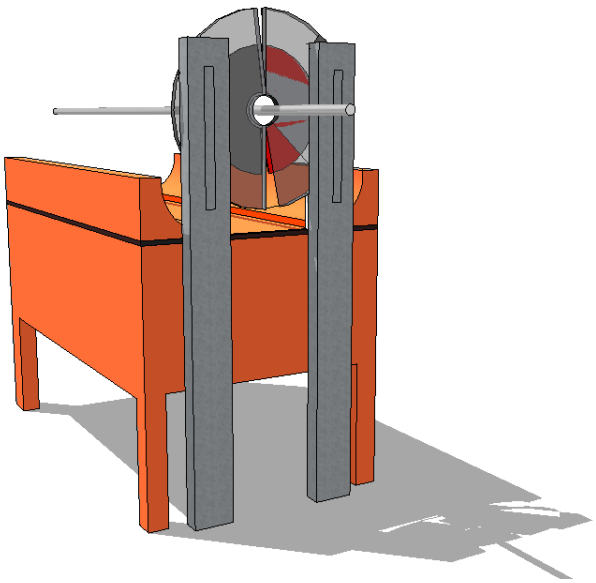

Figure 9.12: Inner BSC halo monitor situated on the Castor table (Z = $\pm$14.4m) with full ϕ coverage and appropriate tile segmentation. (concept drawing only; not final design.) As space is very limited on one of the Castor tables, the BSC2 upgrade should ideally fit within the BCM2 envelope. For the opposite Z end, a more elaborate detector could be installed in the available space in a more ideal location.

9.7.6.1 Triggering System

The proposed system has active detector elements (quartz plates, radiation hard scintillator) mounted on the I.P facing side of the HF calorimeters and on the Castor table, only a few centimeters from the beam pipe. The HF mounted elements will be in an ideal location to perform accurate minimum bias monitoring and triggering as they have an almost direct line-of-site to the I.P. The minimum bias trigger would be primarily achieved using these 48 channels and with the use of dedicated VME triggering boards which are configurable in software, a *majority over threshold* logic could be implemented that will make the minimum bias trigger highly tunable and accurate, even if several channels are not operating optimally.

The innermost of these elements will also be able to detect beam halo passing through the CMS detector. The elements situated on Castor will form the primary beam halo detector by using time-of-flight methods to determine the direction of halo. These channels, together with the inner channels on HF, will form a pair of two, three or four-fold coincidence beam halo triggers, resulting in a selection of veto triggers of variable sensitivity and accuracy.

9.7.7 Summary and Milestones for Beam Scintillator Counters Upgrade

It is clear that there will be an ongoing need from CMS for a BSC-type system for beam monitoring and triggering of minimum bias and beam background events, far beyond the lifetime of the currently installed system. The BSC has so far outperformed its expectations with a high triggering efficiency on minimum bias events. However, the detector was not designed to run beyond a few years or beyond $\mathcal{L} \approx 10^{32}\text{cm}^{-2}\text{s}^{-1}$. This document proposes a prototype design for the detector to replace the current system which will focus on the aim of triggering on minimum bias events and vetoing on beam halo with a high efficiency and purity. It should also be capable of providing an online relative luminosity measurement by monitoring the minimum bias rates and normalizing the data with the most recent Van-de-Meer luminosity scans.

A strong need for a replacement has already been indicated for the BSC system for a detector with powerful beam monitoring and triggering capability. It should be noted that the BSC has been the primary detector for monitoring beam conditions at CMS for the LHC and, as such, provides the 2 key figures of merit on background conditions at CMS for the CCC, which are subsequently reported on LHC page 1. This functionality will also be required from any upgrade. Informal discussions with members both inside and outside the present BRM project have indicated several groups who are potentially interested in collaboration on this upgrade. As the prototype develops, this collaborative effort should be encouraged and developed.

The expected list of milestones and decision points expected in the design and construction of the Beam Scintillator Counter Upgrade is given below:

- Sept 2010: CMS Note detailing functionality of the upgrade. The note will explain all detector components under consideration and the implications to be considered for each.
- Dec 2010: Report on the outcome of tests carried out of the various detector technologies for the upgrade. The note will give details regarding their performance, longevity, mechanical issues and designs of prototype channels.
- Feb 2011: Technical Design Report (TDR) for the BSC upgrade outlining the chosen design, its performance and construction which will lead to an Engineering Design Report (EDR).
- Jan 2012: HF Calorimeters will be in the garages allowing access to the current system and installation of the upgrade. Arrangements of work packages, manpower

and necessary special tooling will be made.

- August 2012: Installation of the completed Beam Scintillator Counters upgrade

9.8 Pixel Luminosity Telescope

The Pixel Luminosity Telescope (PLT) is a dedicated CMS luminosity monitor that is based on single-crystal, diamond, pixel sensors. It is designed to provide a high-precision measurement of the bunch-by-bunch relative luminosity on a time scale of a few seconds and a stable high-precision measurement of the integrated relative luminosity over the entire lifetime of the CMS experiment. The PLT is comprised of two arrays of eight small-angle telescopes situated one on each end of CMS. The telescopes are 7.5 cm long and consist of three equally-spaced planes of diamond pixel sensors. They are located 5 cm radially from the beam line at a distance of 1.8 m from the central collision point. Figure 9.13 shows a sketch of a PLT array and indicates its location within CMS. The telescope planes consist of single-crystal diamond sensors each with an active area of 3.6 mm $\times$ 3.8 mm that are bump bonded to the PSI46v2 CMS pixel readout chip.

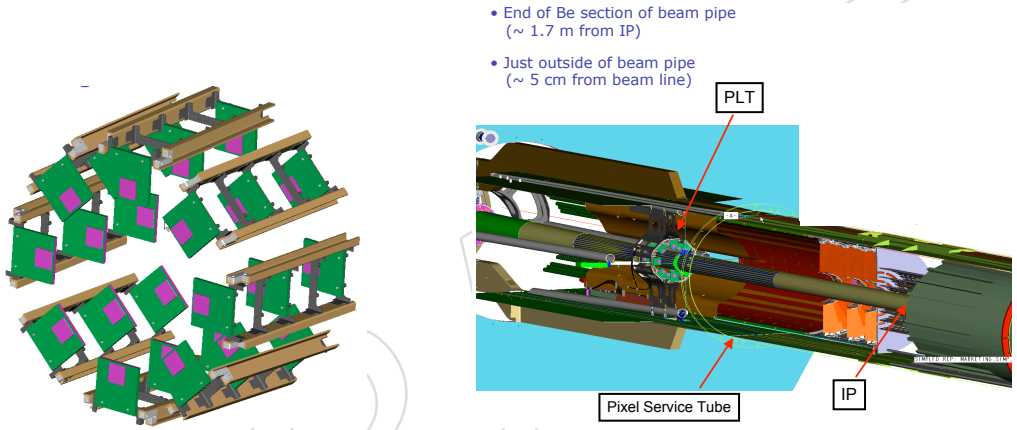

Figure 9.13: Sketch of one of the PLT telescope arrays and its location within CMS. The magenta squares on the telescope planes indicate the locations of the diamond sensors.

In addition to its primary luminosity function, the PLT will also provide important beam conditions monitoring. It will be sensitive to possible collisions occurring in the orbit gap. It will sample the beam halo just outside of the beam pipe and will locate the centroid of the beam collision point in real time in intervals of a few seconds.

9.8.1 Diamond Pixel Sensors

Diamond sensors are crucial for the PLT application since they will operate efficiently with only a moderate decrease in signal size over the entire lifetime of CMS. Studies have shown that the PSI46 pixel readout will also continue to function up to these exposures. Very importantly, unlike for silicon sensors, this radiation hardness does not require any cooling of the diamond sensors.

Single-crystal diamond is used for the sensor material rather than polycrystalline diamond since the distribution of pulse heights of single crystal diamond is large and well separated from zero, ensuring that any efficiency changes due to threshold drifts will be small. The single-crystal diamond sensors are Chemical Vapor Deposition (CVD) diamond with nominal thickness of 500 μm supplied by Diamond Detectors Ltd. Their physical area of 4.7 mm

$\times$ 4.7 mm is the largest size currently available for commercial, single-crystal, detector-grade diamond. Although a larger diamond size would be preferred for ease of handling during processing, the present area is more than sufficient for the solid angle coverage required for the PLT.

Before irradiation, a single crystal diamond yields full charge collection at an applied field of less than 0.4 V/μm with a leakage current less than 1 pA / cm^2. A minimum ionizing particle normally incident to the 500 μm diamond produces a mean signal of about 22,000 electrons well above the noise level in pixel electronics and well above the pixel threshold values of 2,000 to 3,000 electrons. At the location of the PLT just outside of the beam pipe, the particle fluence over the 500 fb^{-1} integrated luminosity expected during Phase 1 calculated by simulations is about 2×10^{15} particle / cm^2 / second. Although at this radiation dosage, single-crystal diamond show about a 40% loss in charge collection efficiency, the signal from a minimum ionizing particle is still well above the set threshold values. At this dosage, there is no increase in leakage current. Figure 9.14 shows the pulse height distribution from ^{90}Sr β particles incident on a 500 μm thick single-crystal diamond before irradiation and after an exposure of 1.5×10^{15} / cm^2 24 GeV protons.

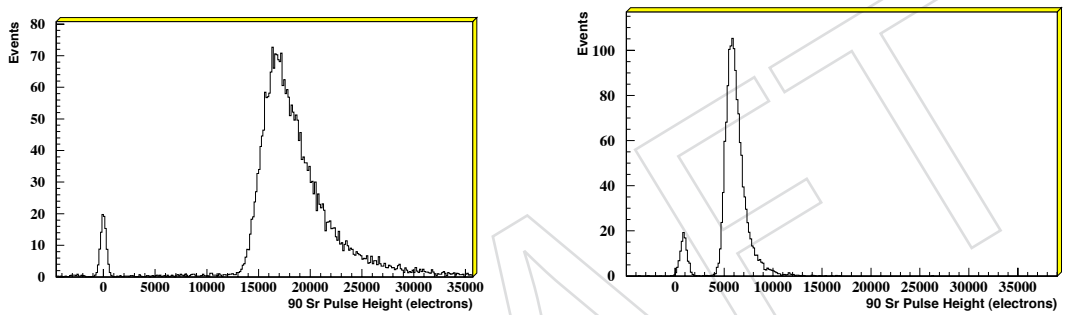

Figure 9.14: Pulse height of ^{90}Sr /*beta* particles in a 500 μm thick single crystal diamond. Before irradiation on the left and after exposure to 1.5×10^{15} / cm ^{2} 24-GeV protons on the right. Pedestal events are also shown to indicate signal separation form zero.

Deposition of the pixel electrode pattern on the diamonds and the bump-bonding of the diamond sensors to the pixel readout chips is carried out "in-house" at the Princeton Institute of Science and Technology Materials (PRISM) micro-fabrication laboratory. Following surface preparation, electrodes are sputtered onto the diamond surface using a Ti/W alloy target as an under bump metalizaztion (UBM). A 4 mm $\times$ 4 mm electrode is deposited on one side of the diamond using a shadow mask. On the other side, a pixel pattern is deposited using a standard lift-off photolithographic process. The pattern covers an area of 3.9 mm $\times$ 4.0 mm and consists of an array of 26 $\times$ 40 pixels with pitch of 150 μm $\times$ 100 μm matching that of the PSI46 chip. Each UBM pixel electrode is 125 μm $\times$ 75 μm with 25 μm gaps between electrodes. The pixelated diamond sensors are then bump-bonded to the readout chip using a flip-chip procedure. Approximately cylindrical indium bumps with diameters of 15 μm and heights of 7 μm to 8 μm are evaporated onto the pixel pads on both the readout chip and the diamond sensor. This step requires a thick layer of photoresist built up from two layers of intermediate thickness. Depositing the indium bumps on readout chip wafers using this thick photolithographic process is relatively straightforward since chips at the periphery of the wafer could be sacrificed. Depositing the indium bumps on the individual diamond pieces required considerably more development. It is necessary to remove a thick meniscus of photoresist that forms at the edge of the diamond during the photoresist spinning process without compromising the integrity of the pixel pattern close to the edge of the diamond. A procedure was developed for forming

a custom-fit frame around each diamond so that the photoresist would fully spin off the diamond onto the sacrificial frame leaving a uniform layer on the diamond. After indium bump deposition, the diamond sensors are then bump-bonded to the readout chip using a Research Devices MA-8 flip-chip bonder with an optically-controlled alignment precision of better than 2 μm. The electromechanical bond is then formed by applying pressure. The indium bumps are not reflowed. The readout chip has an array of 52 $\times$ 80 channels larger in area than the diamond sensors and the diamonds are bonded to columns 13 through 38 and rows 41 through 80 at the top edge readout chip. A completed detector mounted on a hybrid board is shown in Fig. 9.15.

+

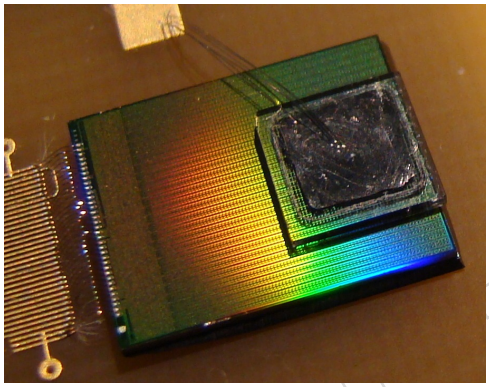

Figure 9.15: Bump bonded detector.

9.8.2 Readout

The readout of the PLT utillizes extensively the chips and VME electronic modules that have been developed for the CMS pixel detectors. The diamond sensors are bump-bonded to the PSI46v2 pixel readout chip that is used in CMS pixel detectors. This chip outputs a fast-or signal at each LHC bunch crossing (40 MHz rate) that indicates the number of double columns with pixels above threshold. This signal from each of the three planes in a telescope will be used to form a 3-fold coincidence indicating the number of particles traversing the telescope. The number of these 3-fold coincidences in the array of PLT telescopes provides the measure of the instantaneous luminosity. This luminosity will be recorded for each of the beam crossings in an LHC orbit.

In addition to the fast-coincidence information, the full pixel information will also be read out from the PSI46 chip at a triggered rate of about 10 KHz. This will provide information on the row and column address of the hit pixels and the hit pixel pulse height. This information will be very powerful in achieving low systematic errors on the luminosity. Two of the largest potential sources of systematics in the fast-coincidence luminosity measurement are coincidences caused by accidental hits leading to an over estimate of the luminosity and two-particle overlaps in a telescope leading to an under estimate. Both of these effects are proportional to the number of interactions per bunch crossing. Simulations have shown that each is a few percent at full LHC design luminosity. By using the pixel information, these effects can be measured and corrected to a few per cent of themselves. The full pixel information will also be used to diagnose the corresponding fast-or coincidence signals for those bunch crossing in which the full pixel readout is triggered.

Several custom circuits have been designed for the PLT. The hybrid board is a rigged-back flex circuit on which the telescope detector planes are mounted and wire-bonded. The hybrid boards have flexible pig tails that plug into the HDI circuit that forms the backbone of the telescopes. The HDI houses the CMS TBM chip that orchestrates the readout of each of the chips on the telescope planes and distributes control signals and bias voltage to the detectors on the hybrid boards. The HDI's from four telescopes, connect to a port card, a semicircular rigged-backed flex circuit, that is located on the PLT/BRM carriage at the rear of the telescopes. For each set of four telescopes there is also an optoboard located at the foot of the PLT/BRM carriage that houses the optical components, AOH's and DOH's, for the optical readout and control signals. The AOH and DOH optical hybrids are the same as those used in the CMS tracker.

The PLT will provide two types of data: full pixel readout at a few kHz, and fast-OR hit-counting information at the bunch crossing rate of 40 MHz. In the full readout mode, the data acquisition process will be identical to that of the CMS pixel detector. Data fragments consisting of addresses and pulse height information from each readout chip framed by header and trailer packets supplied by the TBM will be sent to the Front End Driver (FED), where the data will be digitized and merged into the CMS data stream. Both full pixel readout and fast readout will use the FED VME module developed by Vienna. The full readout chain will be the same as the existing CMS pixel system and therefore will not require any specialized development. The fast out used to extract luminosity information in realtime will require only modification of the firmware on the FED's FPGA. In particular, the system will need to fill a histogram having one bin for each of the 3564 bunch crossings. Data accumulated in this array will be shipped to a dedicated PC for further accumulation and distribution to the different luminosity consumers. See Fig. 9.16.

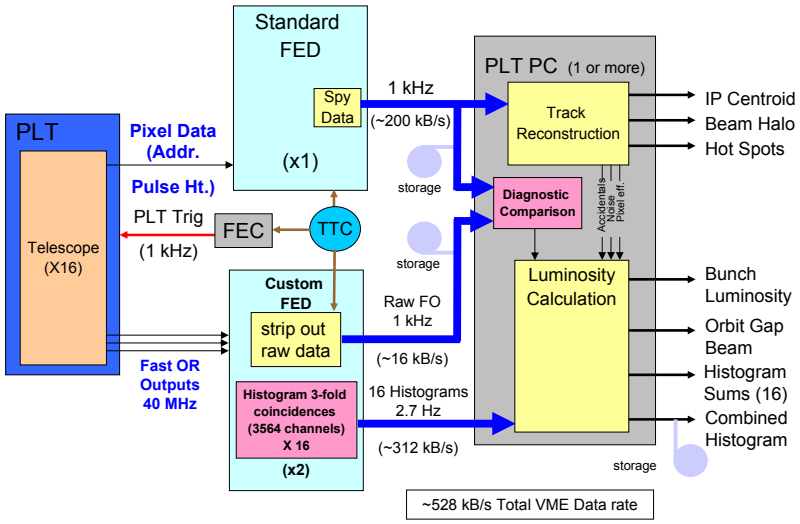

Figure 9.16: Schema diagram of the PLT readout.

The PLT data correspond to the number of telescopes that were hit during a bunch crossing. A similar logic design was completed for the HLX FPGA for the HF based luminosity. The firmware would take partially processed data from the ROCs and histogram it over a complete orbit, thereby providing a per-bunch representation of luminosity, including empty bunches. The occupancy histograms are transmitted to a PC via VME once roughly every 0.37 s, which is safely within the 5.8 s (worst case) histogram overflow time. The occupancy histograms comprise about 7 KB of data which is transmitted to the PC at a rate of approximately 0.16

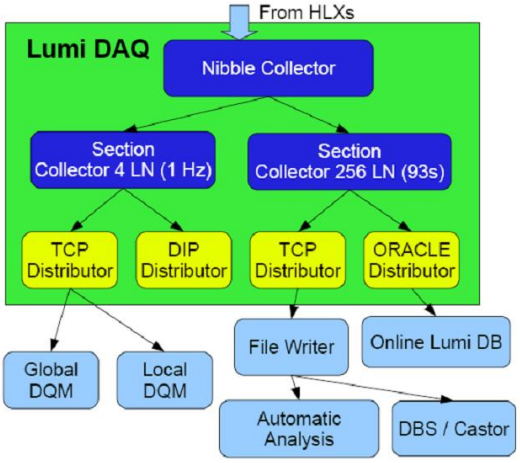

Figure 9.17: Software class hierarchy in HF based online readout framework.

Mbps. Many other design elements of the HLX firmware system, for example the handling of the LHC clock signals and the interaction with the CMS DAQ will be directly transferable to the PLT design.

The readout synchronization with the CMS DAQ system will also be similar to the HLX-based luminosity system. Luminosity histogramming begins on an OC0 command. Data is then accumulated for a programmable number of orbits (called a 'lumi nibble') and then shipped to the readout PC. Since this readout path is independent of the main DAQ system, the PLT will be able to provide realtime luminosity information even when the CMS DAQ is down—e.g., during the injection and ramping phases of LHC.

A large amount of online software for the handling of luminosity data has already been developed for the HF-based luminosity monitor. Most of this will be directly transferrable to the PLT. Dedicated online software was developed to process the raw data on a dedicated PC and to provide an interface with the CMS Database (DB), CMS and LHC. The class architecture of the online software can seen in Fig 9.17. Processing the histogram data is split into several classes. The NibbleCollector class is used for basic processing, such as the data integrity checks. Once this has been achieved, the data is forwarded to the SectionCollector class, where it is aggregated Once the desired number of nibbles has been collected, the data is forwarded to distributors, which output the data to various monitoring systems and in various formats, including CMSSW DQM, Oracle DB, ROOT, gif, and LHC DIP.

A effort has gone into developing software to log luminosity data and to make it available to users doing offline analysis. As is the case for the online software, the vast majority of this software will be directly applicable to the PLT data.

9.8.3 Performance

9.8.4 Status

The PLT project has undergone several CMS reviews and was approved for production at an Engineering Design Review held in November of 2009. The construction of the PLT is by now

well advanced and the project is on schedule for the PLT to be completed and ready for installation by the end of the year. Sixty diamond sensors have been ordered and delivered. Forty-seven of these have been characterized of which thirty-four have passed selection criteria. The ones that failed are being returned to the vendor for replacement. Twelve detector planes have been assembled with an additional eight planes ready in the first week of July. Twelve detector planes have been tested of which ten have passed the criteria for use in the PLT. The production rate has reached three planes per week and we expect the remaining planes to be completed and tested by the beginning of October. Prototype custom firmware for the fast-or FED has been developed by the Vienna HEPHY group and is currently under test. A full optical readout of a prototype telescope using prototype HDI's, port card and optoboard has been successfully completed and was used in a beam test at Fermilab in March. All of the final production hybrid boards have been delivered. All of the production HDIs have been delivered and will soon be under test. All of the production port cards type Version A have been delivered and have been successfully tested. Version B of the port card is currently under design. The optoboard has been designed and will be in production by the end of July. The design of the mechanical support cartridge for the PLT telescopes has been completed will be out for production by mid July. We expect a complete system with all of the final prouction components including firmware and DAQ software to be completed by the end of September.

9.9 Beam Position Timing for the Experiments

The Beam Position Timing for the Experiments (BPTX) are 2 LHC standard Beam Position monitors installed 175m upstream of the interaction points on the incoming beam pipes. These devices are absolutely essential for CMS, providing both the absolute reference timing of the beams, through a scope-based readout device, as well as jitter measurements of both the LHC beams and all LHC clocks with respect to each other. Additionally, they provide the zero-bias trigger to the L1 Global Trigger, and through this trigger determine the L1 trigger timing. This trigger is essential for understanding the absolute efficiency of all CMS triggers and will contribute to the studies determining and reducing systematic effects in the data. All of these triggers are presently tuned to have variations and jitters $<$500ps, insignificant given the phase measurements at the L1 trigger of 6.125 ns.

The present set of triggers was provided with a simple NIM logic, so that it was flexible to meet the highly variable needs in the first months of CMS running. This decision for flexibility was a considerable boon, which has resulted in 16 trigger inputs being provided from the BPTX device to the L1 trigger, indicating the success and reliability of the devices. These triggers, while still the main L1 trigger seed to the HLT at a luminosity of $10^{27} cm^{-2} s^{-1}$, will have an increased prescale at high luminosities. However, it is clear that for all periods of heavy ion running, and for all start-up periods following shutdowns, the zero-bias triggers will be essential for determining that CMS, in particular the trigger, is recommisioned efficiently, and to remeasure the absolute experimental timing.

To this end, it is foreseen, before the 2012 shutdown, to complement the NIM-based trigger system by a simple VME based trigger system. This will consist of VME-based discriminators, and a FPGA-based generic logic unit (CAEN V1495). This can be commissioned in parallel to the minimum system, so that no downtime is caused.

9.10 Validating and Updating the CMS Cavern Simulation: LHC RADMON, Medipix, Neutron Detectors, Passives and Activation Measurements

The impact of neutron radiation on the electronic equipment associated with the Large Hadron Collider, both for the experiments and the machine itself, is a worrying aspect of the accelerators operation. Damage caused by neutron radiation includes breaking inter atom bonds within materials and causing Single Event Upsets (SEUs), where the neutron causes a transistor to flip bits within a microprocessor or memory. SEUs are particularly worrying as they can cause data corruption and even destruction of devices. Measurements are currently made in the CMS cavern using LHC RADMON units, passive radiation monitors, the HF RADMON units and the experimental Medipix-based detectors using a USB readout system developed by the Czech Technical University. What is learned from these monitors in the 2010-11 running periods and beyond will be used to design the monitoring for the period beyond that.

9.10.1 Data from currently installed neutron monitors

The Medipix based detectors can give us the information absent from the RADMON system. Medipix chips were developed at CERN and evolved from the silicon pixel detectors used in many high energy physics experiments. The current version of the chip, Medipix2, features 65,536 pixels which each contain the necessary electronics for detecting the creation of a cloud of electron-hole pairs in the sensors semiconductor layer, which is bump bonded to the chip. The chip is able to determine the position of the incident particle as well as determine the particle's energy through the use of energy thresholds. Neutron radiation cannot be readily detected by the Medipix chip alone, so layers of neutron converter materials must be applied. For the ATLAS-MPX and CMS-MPX systems two types of neutron converters, Lithium Fluoride (LiF) and Polyethylene (PE), were applied over the chip by the Czech Technical University (CTU). Thermal neutrons impacting the LiF layers cause the emmission of -particles, while the PE layer will emit protons when hit by fast neutrons.

9.10.2 Proposed Improvements to Slow Monitoring

Given the danger of premature demise of equipment due to larger than expected fluxes of neutrons, it should be anticipated that an array of diagnostic tools might be needed to qualify simulated neutron flux maps of the cavern. As such it is currently foreseen, that looking to the upgrades in 2012 and 2016, the following devices will be made available:

- LHC RADMON units (or their successor)
- HF RADMON units.
- Medipix Gigabit-ethernet neutron cameras
- Passive neutron monitors (see section on passive monitoring).

The LHC RADMON units presently in use will continue to be so. The cabling and scope of these devices is such that they are already fairly flexible to be portable to any location in the cavern if a problematic region is suspected. If the LHC upgrades these devices, it is expected that the same will happen in the CMS cavern.

Also anticipated is the development of the Canterbury-CTU Neutron Camera, the next iteration of the Medipix based detection systems. It utilises the same Medipix chips as the current system but replaces the USB readout with the gigabit Ethernet-based MARS Readout board developed at Canterbury. The use of an Ethernet connection will allow for faster data transfer over greater

distances. It is foreseen that up to 10 of these devices will be installed in the CMS cavern during the 2012 shutdown. The Gigabit Ethernet connection and ability to read data at 100fps will allow for real- time radiation monitoring and particle identification. A prototype MARS readout has been operational for many months, with a production copy currently in the final stages of development.

9.10.3 Passives

The studies ongoing at the moment and also from reading the doses from the passives accessible during the 2010-2011 extended technical stop will highlight areas which are understood and those where there is less understanding or even disagreements, demonstrating gaps in the present shielding configuration. In particular, this will be used to qualify the simulations presently available for the radiation map in the CMS cavern. While the studies show so far that the level agreement between simulations and the measured radiation field in the cavern is good, there are several problematic areas. As such there will be a need to review for every long shutdown the positions chosen for the passive detcectors to get integrated fluxes. Similarly, there should be a flexible approach, to allow a quixk measurement of vulnerable electronics to determine the cause of operational problems. Additionally, as the integrated luminosity increases, and hence the integrated dose to electronics, vulnerabilities may be exposed. It should be possible to quickly rule in or out radiation as the cause of these problems. To enable a flexible approach to this problem, it should be foreseen to have a range of passives available for installation in case of need in both of these shutdowns.

9.11 Required Resources: Manpower Requirements, Schedule, and Expression of Interest By Institutes

9.11.1 Manpower requirements

Table 9.8 shows the required manpower for each of the proposed upgrades. These manpower estimates are given in Full Time Equivalent (FTE) Man-Years. They include only the required manpower to design, build, test and install the detectors. In all cases it is assumed that there is further manpower available to commission and utilise these detectors from the standard Maintainance and Operation.

Sub-detector	Manpower (FTE Man-Years)			
	Physicist	Engineer	Technician	Total
BCM	4	0.5	0.5	5
BCM1F	4	3	2	9
BSC	3-5	1	1.5	5.5-7
FSC	3	1	2	6
Medipix/Neutron	1.5	0	1	2.5
Passives	0.25	-	0.25	0.5
PLT	6	7	6	19
Total	21.75	12.5	13.25	47.75

Table 9.8: Manpower requirements for each of the proposed upgrades to the CMS beam instrumentation. This is broken down into three categories of manpower: physicist, engineer and technician. The allocation in the column is in terms of full-time-equivalent man-years(FTE MY).

9.11.2 Expression of Interest by institutes

Table 9.9 shows the matrix of the institutes (and a country-basis) against the proposed aspects of improvements on the beam instrumentation. All expressions of interest are at this stage provisional.

Country	Subdetector						
	BCM	BCM1F	BSC	FSC	Medipix/Neutron	Passives	PLT
AUSTRIA							X
BELGIUM				X			
CERN	X	X	X	X	X	X	X
GERMANY	X	X	X			X	
FINLAND							
ITALY				X			
NEW ZEALAND			X		X		X
RUSSIA				X			
USA	X		X	X			X

Table 9.9: Matrix of potential expressions in the proposals outlined in the text for the improvement of the beam instrumentation.

Chapter 10

CMS Common Systems, Infrastructure and Facilities

10.1 Introduction

This section describes the consolidation and upgrade programme for the common systems, infrastructure and facilities of the CMS experiment, which is planned between now and the end of the long LHC shutdown presently scheduled for 2016.

The individual particle and energy detection sub-systems deployed in the CMS experiment are the responsibility of sub-collaborations of institutes (in some cases including CERN), which take responsibility for their construction, maintenance and upgrade. Associated common systems, infrastructure, facilities and technical projects, which are needed to satisfactorily assemble and maintain the sub-detectors and to allow them to function together as a technically coherent scientific apparatus, are provided and maintained either by CERN as the host laboratory or using common CMS collaboration resources.

10.1.1 Overview of the CMS Common Systems

These systems, which form part of the responsibilities of the CMS central technical team, are listed below:

1. **Safety systems for the protection of personnel and equipment**
   - The Detector Safety System which protects the experimental apparatus.
   - Remote sensors including cameras, microphones systems and devices to measure position changes, mechanical strain, and environmental conditions.
   - The nitrogen, dry air and compressed air systems for inertion, environmental stabilization and pneumatic control.
   - Fire and smoke detection and fire extinguishing systems.
   - Radioprotection precautions, measuring devices and equipment tracability systems.
   - Access control.
   - Safety Training.
2. **Magnet** The 4T superconducting solenoid coil, including the power, cryogenic, monitoring, control and safety systems needed to operate it, along with field measuring devices and field simulations.
3. **Yoke, Shielding and Moving Systems** The segmented flux return yoke (which also forms the structural backbone of CMS), the radiation shielding system and the moving systems,

with the associated surveying or monitoring equipment needed to open and close these elements safely and efficiently for maintenance, repair, consolidation or upgrade.

4. **The Experimental Beampipe** This covers the beampipe in the range $\pm$ 18m either side of the interaction point; its support structures for operation, maintenance and bakeout; and the tooling necessary to install, remove and maintain it. Included in this category is also the set of removable radiation shielding necessary to protect maintenance personnel from regions of the beamipe and nearby detectors which will become progressively activated by collision products.

5. **The Beam Radiation Monitoring System** The beam radiation monitoring system consists of an array of active and passive devices, designed to monitor beam conditions and the radiation field at LHC Point 5. The purpose of the system is to protect the CMS detector from damage (via a beam abort and injection inhibit capability); to optimize collision conditions for data-taking; and to monitor the accumulated dose and induced activity throughout the detector.

6. **Logistics and Integration** This includes interfaces to subsystem tooling and the capability for controlling temperature and humidity in specific working areas.

7. **Experiment Service Infrastructure** This delivers power, IT network, cooling, operating gas, inertion gas, instrument air and dry air to the experimental cavern for the operation of the subsystems and the magnet. It includes the cooled rack systems in the experimental and service caverns and the piping and cabling network. It also includes the local counting and control rooms, including: the principal CMS control room in surface building SCX at LHC Point 5, the underground electronics cavern including the commissioning control room contained within it, and the surface DAQ barrack.

8. **Beam, Radiation, Cosmic Ray, or Environmental Test Facilities** These facilities are for investigating long-term performance or anomalous behaviour of installed detector systems and for testing detector systems proposed for consolidation or upgrade.

9. **Surface Assembly Buildings, Workshops, Laboratories, and Storage space** These are needed to sustain the construction, testing, maintenance, operation and upgrade of the subsystems. This includes areas capable of dealing with activated equipment.

10.1.2 Funding

Funding for CMS central systems, common projects and common facilities comes from several sources: the host laboratory provisions made by CERN; CMS Maintenance and Operation budgets; and, where applicable, CMS upgrade project budgets. Responsibility for coordinating such projects rests with Technical Coordination. The attribution of a given item to one or other of these funding sources is subject to interpretation. In this document, work is classified as a host laboratory expense if it is listed as such under the General Conditions for Experiments or, in the case of assembly buildings or experimental caverns, if it is independent of the specifications of the installed experiment. It should be noted that the provisions in the General Conditions are basic and restricted to providing an overall framework complying with basic personnel protection requirements and satisfying basic infrastructure and service needs. In particular, they do not cover equiping laboratory or experimental areas with infrastructure or services adapted to supplying detectors (specialised power, cooling, compressed air, network etc). Site-specific safety features, including those linked to the efficiency of operating or maintaining an experiment or assembly area, or protecting the experimental apparatus, are

also generally not included. Nevertheless, CERN departments generally make contributions beyond the basic minimum and reasonable precedents exist for all such attributions herein. Work can be charged to Maintenance and Operation budgets if they cover operation, repair or routine replacement of already installed equipment. This includes replacement of equipment which fails or becomes inoperable or un-maintainable before the end of its design lifetime. All other tasks, including consolidation, are attributed to the upgrade.

10.2 Safety Systems

Safety in the CMS surface halls and underground caverns at LHC Point 5 is considered the responsibility of the CMS Technical Coordinator with authority delegated to the GLIMOS, an Experiment Safety Officer appointed by the PH department head in consultation with CMS management and the Health, Safety, and Environment Unit.

10.2.1 General safety

Basic personnel protection is provided throughout CERN by the Level 3 alarm system, typically triggering evacuation and fire brigade intervention in response to smoke, flood, or oxygen deficiency sensors. Protection against beam-related hazards at CMS is provided by the LHC Access Safety System and the RAMSES radiation monitoring equipment. Additional protection systems, particularly against fire hazards, have been installed by CMS (and in several other experiments), many with the dual function of personnel and detector protection. Work is needed on further cavern-specific features including the safe areas and the evacuation route. Operational experience has shown that the installation of a magnetic-field tolerant public address system from surface control room to underground caverns is necessary at Point 5, because mobile phones are unreliable or inoperative in the fringe field of the CMS solenoid magnet.

10.2.2 Detector Safety System (DSS)

The Detector Safety System (DSS) is a hardware protection system, based on redundant PLCs and triggered by a relatively small number of sensors (smoke, temperature, pressure, humidity, current, etc). It applies a carefully reviewed and tested action matrix to initiate safety interlock actions when pathological conditions are detected. Its actions are generally applied at a coarse level (e.g. switching off racks, groups or racks, or even entire power systems) to protect the detector, an individual sub-component, or an ancillary system. These protective actions are not designed with rapid incident recovery in mind and expert intervention is generally required to release the applied interlocks. DSS is not a personnel safety system, although its actions may incidentally protect personnel as well as equipment. DSS and its sensor system are designed to be completely independent from the Detector Control System, which takes care of detailed monitoring and fine-tuning; the operational cycling between off, standby and on conditions; and should generally react to, or correct, abnormal conditions in sub-detectors well before DSS is triggered. The main improvement required is in the user interface, which, while suitable for specialists and adequate for commissioning, is unsuitable for use by trained, but non-expert, shift crew. Improvements are also desirable in the arrangement of the DSS system within racks at Point 5. Satellite systems should also be deployed to protect equipment at the electronics integration centre and at beam-test facilities.

10.2.3 Sensor systems

Although a certain number of magnetic field, position and environment condition sensors were incorporated in the original CMS design, the operational requirement for a sophisticated sen-

sor, camera and monitor network arose from unforeseen difficulties in CMS opening/closing; in magnetic field operation; in temperature pressure and humidity control; combined with various LHC and CMS technical incidents, notably the September 19 2008 LHC incident and the October 2009 CMS endcap cooling leak. Work is needed to consolidate and properly exploit the system and to extend it to give new diagnostic information in key areas within the detector and along the beampipe, using new developments in fibre-optic-based multi-parameter sensors.

10.2.4 Nitrogen, dry air and compressed air

A system of air compressors and liquid nitrogen dewars on the surface at Point 5 provides air and nitrogen for a variety of different purposes. Nitrogen or dry air are used by several subsystems to eliminate fire risk, maintain low humidity and exclude any possible helium contamination. In many cases this is, or will become, an essential year-round detector protection requirement. Since humidity is dangerous for Silicon sensors, operation of the Tracker at low temperatures from 2013 onwards will set much stricter requirements on dew point within the detector volume and in the volume within the solenoid vacuum tank between the endcap and barrel detectors. Nitrogen and dry air are also both used for instrument control in regions of high magnetic field, in particular for opening and closing valves in the subsystem gas and cooling distributions. This application is also clearly crucial for safe detector operation. Large amounts of liquid nitrogen are also needed to cool down the magnet cryogenic system from room temperature, but in future this activity will not factorize from subdetector commissioning and consequent high gaseous nitrogen demand. Lastly, a high flow gaseous nitrogen fire suppression system protects the detectors and cables in the inter-element spaces of the flux return yoke.

The proposed improvements consolidate the system, partially factorize the different functions and introduce spare capacity, increased reliability and redundancy. In particular it is proposed to purchase a nitrogen separation micro-plant (to reduce the cost/m^3 of nitrogen gas in view of the foreseeable increased demand) and to install higher capacity air compressors.

10.2.5 Fire prevention: detection, and extinguishing

Examples of CMS-specific systems installed in addition to the basic Level 3 requirements are non-magnetic fire extinguishers in high field regions; the sniffer system (aspiration and analysis of air from a network of tubes incorporated into the apparatus, recently re-designated by HSE as a Level 3 system); the water-mist local fire extinguishing system; the water-foam area fire extinguishing system; and the in-rack CO_2 fire extinguishers. Following a large investment during 2009, most of these systems meet the requirements of the initial CMS configuration and will be maintained and consolidated using M&O A budgets. However, as additions or expansions of existing CMS apparatus occur, corresponding expansions of these protection networks will be needed. The first and immediate case is the expansion of the rack fire detection and extinguishing system for the high level trigger processing farm, which needs expansion to cope with data rates expected from 2011 onwards.

10.2.6 Radioprotection precautions, measuring devices and equipment traceability

CERN as host laboratory takes responsibility for radioprotection, including the provision of procedures, qualified RP experts; measuring equipment; and the funding for local buffer zones and storage areas and central workshops, which can handle radioactive materials. These resources, while legally satisfactory, are not, however, sufficient to allow efficient maintenance

and operation of the experiments. Recognizing this problem, CERN has trained selected personnel (staff and users) from each LHC experiment as radio-protection experts and assistants (Swiss national qualification) which allows some RP screening procedures to be accelerated. In addition, CERN is supporting the creation of Class C radioactive workshop areas at Point 5, although the costs of tailoring this to CMS maintenance needs will have to be met from CMS M&O funds (see section on 10.9.2).

The logging, tracing, and RP screening of equipment moving in and out of the CMS experimental cavern is mandatory for radioprotection reasons. LHC experiments have developed equipment management databases with simple user interfaces, linked to required radioprotection procedures. Since these are generally applicable to equipment management, a fraction of the running and development costs (mostly in materials) is met by the experiment budgets. Similar arguments apply to the procedures and software developed to authorize and control interventions on the experimental apparatus.

Operational experience shows that much maintenance time is lost waiting for RP measurements from an overloaded central CERN RP service. In view of the expanding need for, and importance of, such measurements as activation levels increase, CMS intends to purchase RP screening equipment (such as a portable gamma spectroscope), which will allow these procedures to be streamlined or carried out locally.

10.2.7 Access control

Basic site and underground access control at Point 5, including the LHC access control system governing personnel and material access to the experimental cavern, is provided and maintained by CERN as host laboratory. Additional features necessary for the efficient maintenance, operation and protection of CMS equipment are the responsibility of the experiment. Examples are the expansion of the LHC access key delivery system capacity at Point 5 to allow more workers through each UXC access point and the addition of a modified anti-theft system to prevent workers accidentally leaving the site with access keys, which can bring re-start of the whole LHC complex to a halt. Assuring fast personnel access to the experiment service cavern (USC), adjoining the experimental cavern, during beam operation and shutdown is a fundamental CMS design assumption, although not an LHC-wide requirement, and some work remains to consolidate what will be a versatile and reliable system. Additionally, CMS will purchase an electronically operated key cabinet, linked to the personnel database, to give access to keys to sensitive areas or systems (e.g. RP veto) to authorized persons and will also wish, for security reasons, to implement access control on the projected new office building at Point 5 and the integration and production areas in Building 904.

10.2.8 Safety training

Training and refresher training of CERN personnel and users in specialized skills such as the construction of scaffolding or the use of harnesses, nacelles or lasers in the specific Point 5 environment is essential to completing complex, multi-activity maintenance or upgrade operations in the timescales available. Such training of additional personnel is the responsibility of the experiment. Similarly, specific training suggested by the CMS GLIMOS to reinforce the level of safety awareness and emergency reaction at Point 5 and in CMS surface assembly sites is also the responsibility of the experiment. Items include assistance in creation of the Point 5 specific L4C course and other documentation; safety signalisation (multi-lingual); experiment related safety equipment (harnesses, alarm panels, safety rails); safety-enhancing equipment (e.g. ladders with working platform), and training of CMS collaboration personnel to enhance

their own safety or that of the working team.

10.3 Magnet Consolidation and Upgrade

10.3.1 Introduction

The lifetime of the CMS solenoid will be limited by the number of cycles from zero to full field and back to zero, the cyclic strain from which will eventually lead to increased resistance of the pure aluminium stabilizer. In order to minimize unnecessary cycles, and in particular to further reduce the risk of fast discharges, modification to the cold box , the power breakers and the control system are envisaged.

10.3.2 Power systems

The key elements are:

1. The Power Converter (PC) which is made of 4 modules, with spare parts in hand to replace one module (thyristors bridge, transformer).
2. The Direct Current to Current Transformer (DCCT) arranged as a redundant pair and used for magnet current regulation. There is one spare.
3. The main transformer 18kV/400V (ERD1/55) for which there is no reserved spare. The reservation of a spare and the replacement time is being discussed with the EN-EL group.
4. The main 20kA DC switch breakers, and resistance contactors for which there are several sets of spare parts for the open/closed command circuit, plus spares to replace the electrical contacts.

10.3.3 Vacuum pumping systems

The key elements are:

1. The two primary pumping units, which are fully redundant and for which spare parts are available.
2. The two diffusion pumps, directly attached to the helium phase separator and to the magnet cryostat, located in the experimental cavern, which cannot be easily accessed. Replacement would require a warm up of the coil and thus an estimated 6 week period with no magnetic field availability. Spare components are available.
3. The Vacuum gauges for which spares are available.

10.3.4 Safety and control systems (MSS, MCS)

The system performs adequately, but two consolidations are considered necessary. A spare MSS chassis unit needs to be built with up-to-date electronics which can be more easily maintained and replaced. In addition, the 55V battery system needs to be modified by replacing the chargers and their supervision. This is the responsibility of PH-DT group and a cost estimate is pending. These upgrades/consolidations are in synergy with the needs for the M1 test facility (described in paragraph 10.8.3.1.5).

10.3.5 Cryogenic systems

Despite the solid performance of the system so far, three critical failures have been identified, any of which could cause the magnet to be unavailable for long periods (several months).

1. **Helium compressor units:** There are two compressors of different kinds, each working within a different pressure range and arranged in series, so that one cannot work without the other. Both compressors are designed for full maintenance every 40,000 hours. Taking an average run time per year of 8000 hours, the availability between major maintenance work is 5 years. At present, the first full maintenance is scheduled for 2012. Nevertheless, if one of the two compressors stopped and had to be repaired, the magnet would be stopped for the duration of the repair. Although, these compressors are still listed in the manufacturers catalogue, for construction to order, they are custom-built and not available off-the-shelf. In case a full replacement became necessary, the magnet would be unavailable for several months (procurement, manufacturing, installation, cool-down). If spare compressors were constructed and reserved for CMS, the magnet stop would be limited to the dismantling and replacement time. Installing these spares in SH5 would allow for compressor repair or revision without stopping the installation (and the magnet as a consequence) for any significant time. The available space in building SH5 and the layout of the compressor system were indeed designed to allow for two redundant compressors and full redundancy is the best solution to minimize the risk of extended magnet down-time. To take full advantage of this redundancy, a control process would be needed to allow the load to be transferred to the redundant compressors without stopping the cryoplant.

2. **Compressor lubricant separation unit** Periodic pollution problems have been observed in the whole installation, encountered with a frequency of one to 6 months, causing the magnet to be off, so far with no serious effects on data-taking. One possible explanation is that the helium compressor lubricant (BREOX) is found in the coalescers (4 stages) of the High Pressure unit, indicating that the separation is not efficient enough. This risk is likely to increase with time. Modification of the separation unit to cure the problem requires the installation to be stopped for a few months with magnet off. It has therefore to be implemented during the shutdown of 2012 or 2016. Clearly, the 2012 shutdown is more favorable, provided the decision is taken in due time and resources are made available. This is a problem common to the other LHC experiments and the machine. The study for the upgrade is being led by the CERN cryogenics group TE-CRG.

3. **Cold Box** The cold box contains 3 turbines. There is one spare unit covering turbine 1 and turbine 2, plus critical components to limit the time for major repairs (2 weeks instead of 6). There is no spare for turbine 3, as it is not considered as a critical element for the process. Nevertheless, when a regeneration of the turbine filter is necessary, turbine 3 is used to avoid a full stop of the cryogenics (which causes a magnet ramp down). This situation is considered adequate.

10.3.6 Miscellaneous

Spare parts are needed for small components and for the command and control systems (filters, seals, switches, transducers, etc.).

10.3.7 Field measurement and mapping

The magnet team is charged with developing and maintaining accurate maps of the magnetic field within the tracking volume, within the return yoke and in other regions where magnetic forces or field sensitivity might be significant. The mapping and simulation of the field within the tracking volume rapidly reached an accuracy of 1 part in 10^4. However, significantly more sophisticated simulations were needed to accurately reproduce the field in the return yoke. Unexpected field sensitivity of detector components led to the installation of a large additional network of Hall probes to provide additional detailed bench-marking data. Similarly, initial simulations underestimated the fields in some parts of the forward region by as much as a factor five, leading once again to unexpected field sensitivity. Although the current field models are extremely good, substantial work remains to fully implement the flux-loop measuring system in the return yoke and to both calculate and measure the substantial effect on the endcap field of introducing the extra shielding disk YE4 (part of the forward muon upgrade and described in section 10.4).

10.4 Yoke, Shielding, and Moving Systems

One of the unique features of the CMS design is the capability to quickly open and close the detector for repair and maintenance by separating the 13 major elements along the beam line, without removing the beampipe. Though proven to work, (for instance during the emergency cooling bushing repair of winter 2009-10), moving several thousand tons with clearances as small as 4 cm currently requires very many experts to be present and poses unnecessary risks to the beam pipe and detector components. In addition, several simple maintenance operations could be done dramatically faster if partial opening of the detector were possible with the beampipe still under vacuum.

Studies and tests are underway to make the movements safer and more reproducible, by improving the guiding, monitoring and hydraulic traction systems, concentrating on parts of the movements when elements are in close proximity. An example is the system proposed for making small relative movement between endcap disks, illustrated in Figure 10.1.

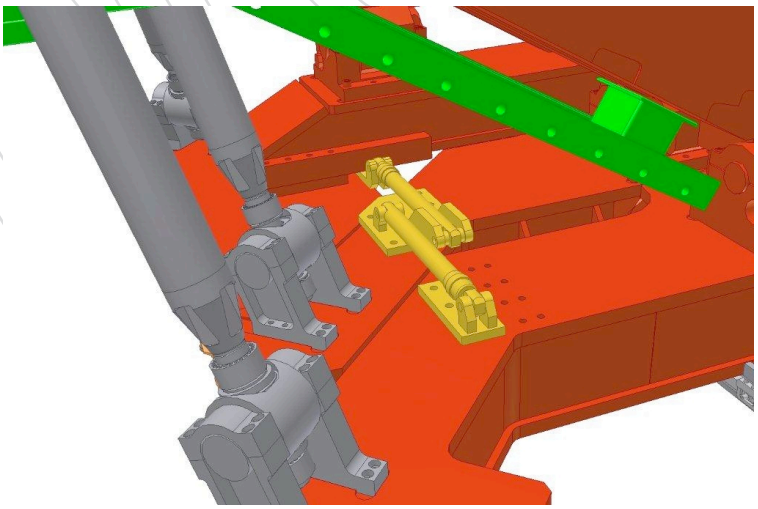

Figure 10.1: Inter-disk hydraulic jacks between YE1 and YE2 (act with symmetric pair on opposire side).

In the course of this upgrade the compressed air source should be changed for safety and economy reasons from bottles to a system of redundant compressors. The system must be redundant because a failure of pressurized air in the course of an opening or closing can result in uncontrollable movements of heavy detector elements.

10.4.1 YE4 Disks

At present, each endcap of the CMS magnet return yoke consists of three 12-sided, regular polygonal disks (YE1, YE2 and YE3), 14m in diameter with respective steel thicknesses of 600 mm, 600 mm and 235 mm, each supported on its own endcap cart and standing on either greasepads or, during opening and closing of the detector, on airpads. These disks also act as the support structure for the endcap detectors. The YE4 disks to be added at each end of the CMS yoke are supported from the YE3 cart as highlighted in Figure 10.2. They carry no detectors, but are part of the overall shielding design of the high luminosity CMS detector, described in the TDR and required for luminosities $> 2 \times 10^{33}$ cm^{-2}s^{-1} to reduce beam-related background in the forward muon system and, in particular, in the presently incomplete 4th stations of CSCs and RPCs, which are targeted for installation starting in 2012. The main backgrounds causing random hits in this station originate from leakage through gaps in the forward shielding structures (HF shielding, collar shielding and rotating shielding) needed to allow for closure tolerances. These leaking particles, which cannot hit the detector directly, cause background mainly due to albedo from the blockhouse shielding and the cavern endwalls. The thickness and composition of YE4 is optimized accordingly.

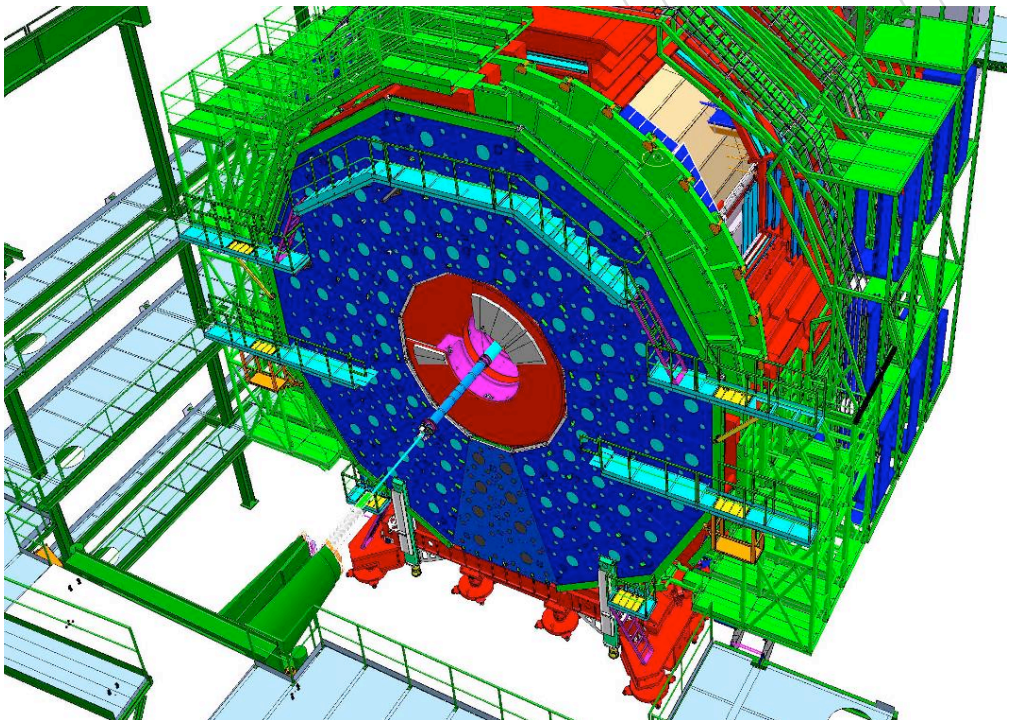

Figure 10.2: The YE4 disk.

To allow for assembly in the underground experimental cavern, where the crane capacity is limited to 20 tons, the 14m diameter, 125mm deep YE4 disks are each assembled underground from 12 hollow, trapezoidal, sector-casings with 25mm thick steel walls. Each casing will be filled with a specially adapted shielding concrete at CERN for a final weight of 6.8t. The Technical Specification for the YE4 disks in described in CERN EDMS Document CMS-SY-FS-0021.

Manufacturing drawings of the disks are complete and production has been launched in Pakistan. Assembly tooling drawings are nearing completion.

The assembly of the YE4 disks is one of the key activities determining the critical sequence in the 2012-13 shutdown. Assembly of a disk can only be achieved if the corresponding endcap is fully closed or with the disks fully together with YE1 in the 3.7m, partially-open position. This position is incompatible with most activities on the barrel or endcap detectors and completely at odds with the critical sequence planned for the 2016 shutdown (installation of new beampipe, pixel tracker, and HCAL front ends).

In the TDR concept, service work on the 4th endcap muon station is achieved by fully opening the corresponding endcap, to enable the YE4 disk support to be transferred from the YE3 cart to the blockhouse shielding of the cavern endwall. Partial re-closure of the endcap then opens the required working space. This procedure is cumbersome, particularly because it involves lengthy and delicate procedures such as opening and closing the corresponding YE1 disk (linked to YE2 and YE3 via cable chains). To improve flexibility for installation or maintenance of the 4^{th} muon station, a "YE4 push-back" jacking system is being designed. This will allow a YE4 disk to be pushed back from the corresponding YE3 by about 2.5m, without needing to open endcap disks 1 to 3. The concept is illustrated in Figure 10.3.

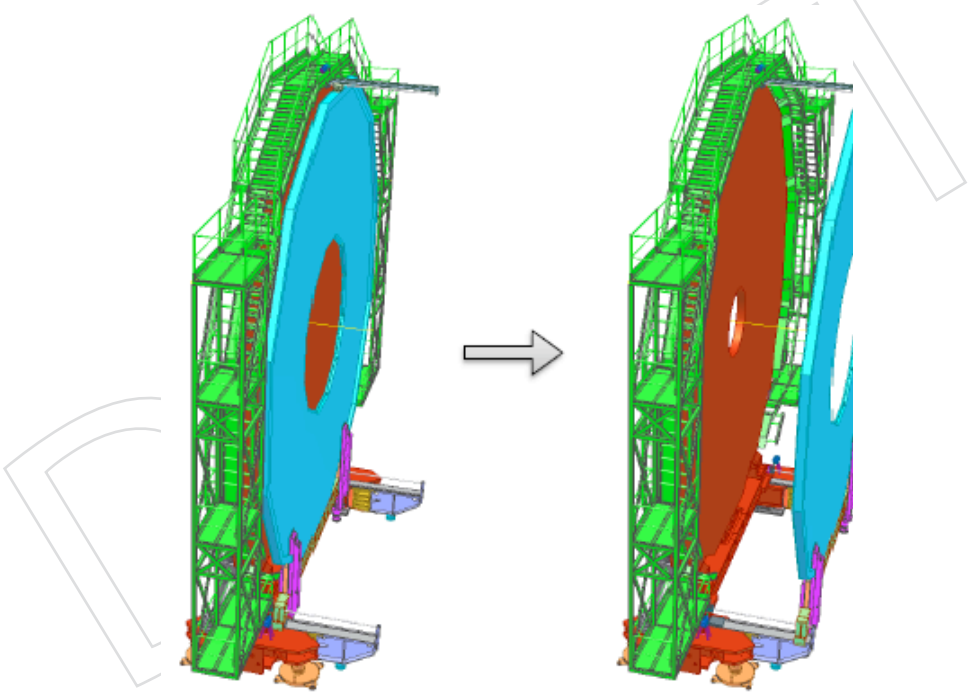

Figure 10.3: The YE4 push-back system.

10.4.2 Radiation shielding

When LHC is operating close to or at design luminosity, the severe radiation environment caused by collision products will cause substantial activation of the beampipe, the tracker bulkhead and the pre-shower disk. This means that appropriate shielding has to be available to protect personnel during maintenance and upgrade activities. Sophisticated shielding precautions already exist for the very forward ZDC detector, installed in the TAN at 150m from the interaction point, and for the HF, whose front face is equipped with lead shielding doors and is routinely stored in its shielded garage. After 2010, precautions will also be necessary inside the

main experimental cavern. The beam pipe, flanges and pumps and the CASTOR calorimeter will become particularly radioactive and will require shielding first.

An example of shielding for the HF beampipe and 13.5m flange is illustrated in Figure 10.4.

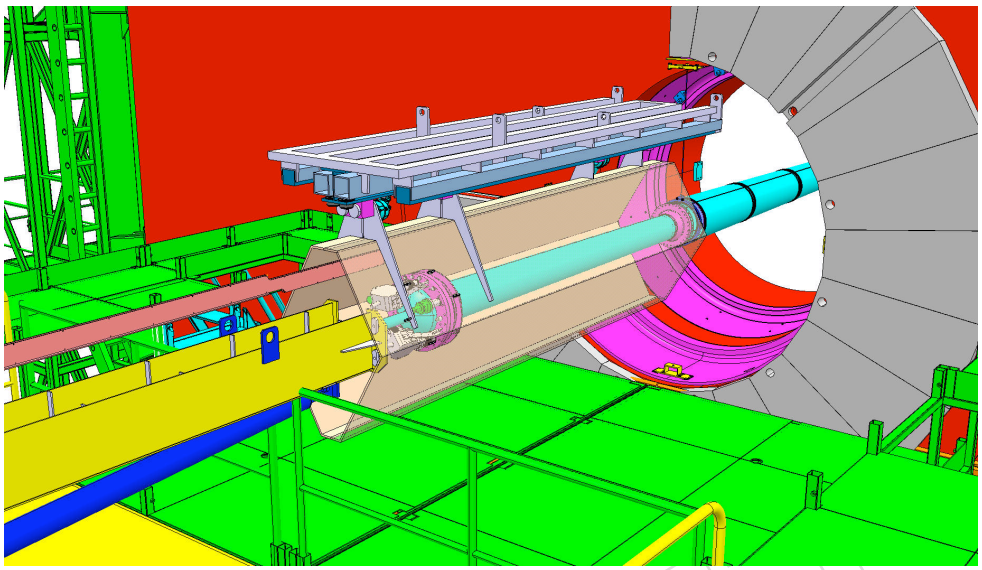

Figure 10.4: A possible design for shielding the beam pipe.

The endcap Electromagnetic Calorimeter crystals will also become activated and will have to be masked by shielding, especially during partially open maintenance configurations. The tracker bulkhead also contains easily activated materials and is expected to be accessed regularly during maintenance, thus a shielding disk has to be built that allows opening sectors for access. A modular shielding design is foreseen making it possible to add shielding plates as required. The support structures for these shielding elements and a first thin shielding layer must be ready for the 2012 shutdown. Design work is proceeding.

10.4.3 Forward Region

The Forward region containing the rotating shield and the HF tower, which supports the HF calorimeter, are far forward detectors and the collar shield requires a substantial revision. Operational experience revealed a variety of problems:

1. The first ramp up of the CMS solenoid after dismantling and rebuilding the HF tower leads to movements of the HF, its tower and the iron structures mounted on it, which are not fully predictable or reproducible. Since part of the beampipe support relies on stability of these structures, the risks are considerable. The mechanical tolerances in the set-up are large enough to cause the direction of forces between the HF and the iron yoke and those between the collar shield and the rotating shield to change several times during the field ramping. However, after the first ramp to operating field, the system settles and later ramps of the magnet do not cause problems. There is no easy mechanism in the current design to stabilize the tower sufficiently during the first ramp.

2. Before every opening of the yoke, a beam pipe support has to be mounted extending from 16.5m to 13.7m. The integrated installation time is 7.6 man hours of which the large majority has to be spent close to flanges or pumps. As soon as these are significantly activated this procedure can no longer be followed. Conceptual designs under study include

a permanent beam pipe support from the FIN, which will make any regular manipulation close to the flanges obsolete.

3. Maintenance or removal/re-installation of CASTOR, BCM2 or TOTEM T2 requires personnel to spend extended periods in very close proximity to the beampipe and to objects which will easily become activated. With the present radiation shielding structure (inner shell removed from the thin part of the rotating shielding to make way for CASTOR), CASTOR will have to be removed once the luminosity at Point 5 exceeds 2 x 10^{33} $cm^{-2}s^{-1}$ to maintain acceptable dose rates to systems in the experimental cavern.

4. The CASTOR detector cannot be adequately shielded from magnetic field due to the location of breaks between the different radiation shielding structures which also provide magnetic shielding.

An integrated solution is under study. It is already clear that any solution which could resolve all the issues listed above would require a radical re-design, with introduction of a second raiser structure (for whose jacks the provision was made in the initial CMS cavern design). The concept is illustrated in Figure 10.5.

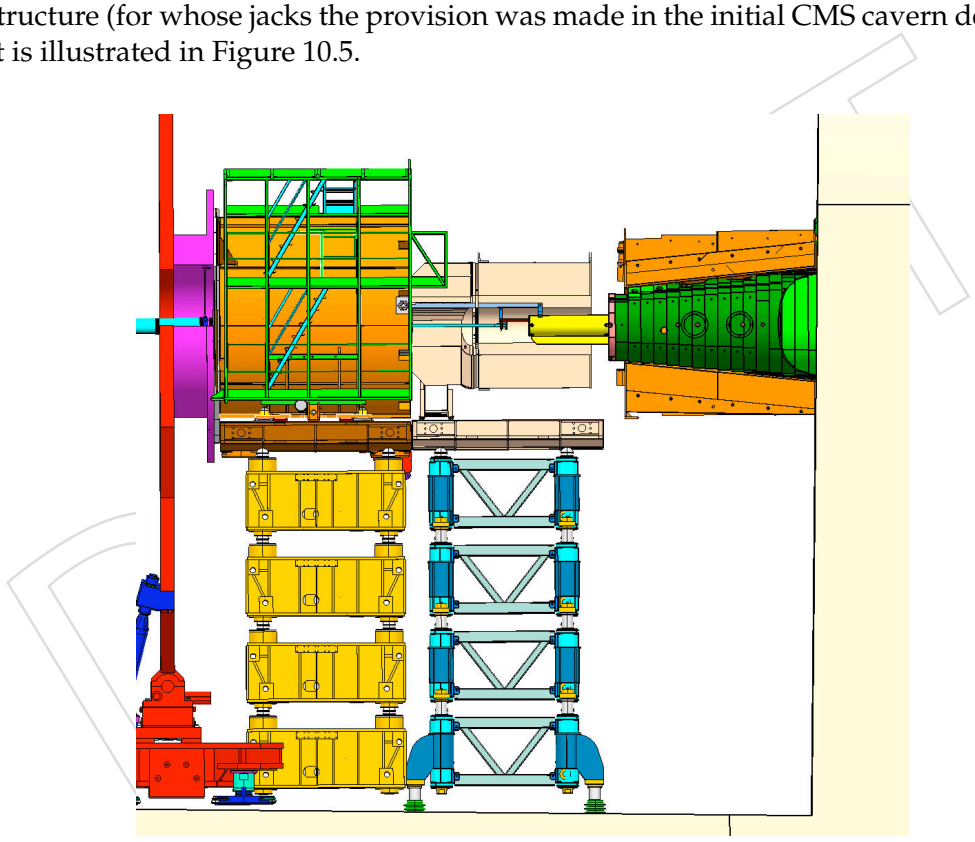

Figure 10.5: Concept for a revised forward region support and shielding structure.

10.5 Experimental Beampipe

The CMS beam pipe is a symmetrical structure extending 18m from the interaction point to either end of the experimental cavern as shown in Figure 10.6. It is constructed from a continuous central section and 4 additional sections at each end. The central pipe, spanning the interaction point, is 6.2m long and consists of an 0.8mm thick beryllium cylinder of 58mm bore, 3.8m in length and braised at each end to conical, end-pieces made of 0.8mm stainless steel. Each end

piece is attached, via a dual-bellow flange system, to a conical end-cap pipe, made of 0.8 to 1.2mm thick stainless steel, following the η = 4.9 cone and terminating in a thin window before a flange at 10.7 m which couples it to the HF pipe.

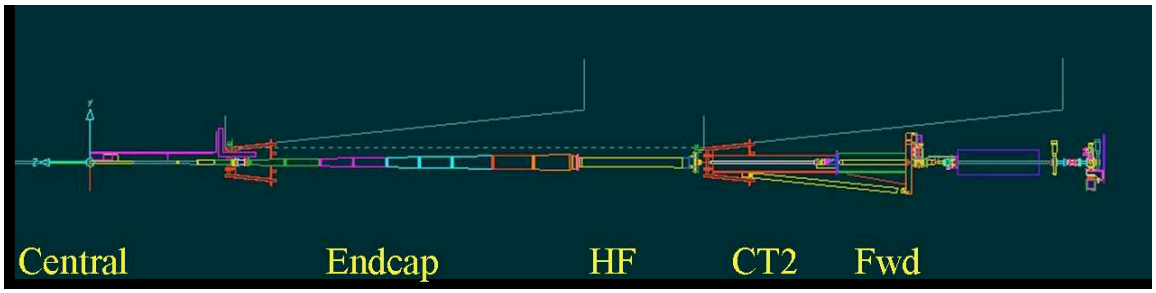

Figure 10.6: CMS beampipe from the interaction point to 18m.

The HF pipe is almost 3m long, also slightly conical, varying in diameter from 170mm to 208mm and is constructed from 1.2 mm thick stainless steel. It terminates in a thin window flange which carries 3 ion pumps and reduces the inner diameter to 58mm, for coupling to the CASTOR-T2 (CT2) pipe. This cylindrical pipe again terminates in a flange and bellow system, which couples it to the cylindrical, stainless steel forward pipe, 2.4 m long, which terminates at the junction to the TAS absorber at 18m.

The main features of the beampipe are:

- The Be central section which presents minimal material to particles emerging from the interaction point.
- The conical outer sections along lines of η (allowing the use of stainless steel while still minimising background in the muon system).
- The thin reducing window at the end of the endcap pipe.
- The HF and CT2 pipes which allow forward calorimetry up to η =7, external to the return yoke.
- The placement of pumps and flanges out of the detector acceptance.

The radius and thickness of the central beryllium section are important parameters affecting the physics performance of the CMS tracking system. The impact parameter resolution and vertex resolution could be substantially improved by fitting a re-designed pixel tracker, which has an additional fourth tracking layer within the limited space between the beampipe and the strip tracker, and thus ensuring the first measured point, given by the radius of the first layer, is as close to the beam line as possible. The support system proposed for the upgraded pixel tracker, which allows independent mechanical closure of the two half cylinders around the beam pipe, would already allow such a 4-layer system to be installed, but with installation tolerances so small as to pose a substantial risk. Reduced risk and better performance can be obtained if the beampipe radius can be reduced. This requirement has to be balanced against assuring a margin for safe and efficient operation of the accelerator and minimizing background in the experiment.

The required beam aperture determines the theoretically minimum inner diameter for any new beam pipe. During injection the beam occupies the largest aperture in the vertical plane and in case of an asynchronous beam dump the beam is largest in the horizontal plane. The dimension of the beam pipe must be chosen so that, taking into account all possible mechanical tolerances of the beam pipe, all installation tolerances and all possible movements of the pipe during operation, the wall of the pipe can never approach the beam closer than the limiting distance

required by the beam aperture. As a prudent precaution for the safety of the detector, no element of the beam-pipe within it should have a smaller aperture than the closest machine element to the interaction region, which in the CMS case is the TAS absorber, situated at 18m, which currently has an of inner radius of 18mm.

During the design of the currently installed LHC experiment beampipes, conservative aperture estimates lead to the request for a stay-clear cylinder of 14mm radius around the nominal beam line close to the interaction point. Operational experience with LHC shows that this estimate was indeed very conservative and investigations are ongoing to determine whether the diameter of the "stay-clear" zone can be reduced. The following mechanical factors have been considered to contribute to limiting the practicably achievable minimum inner pipe radius, such that the "stay-clear" cylinder is always contained within the physical pipe:

- Construction tolerances causing the pipe radius to be less than nominal.
- Mechanical sagging of the pipe between supports.
- The precision with which the pipe can be surveyed into place.
- Time-dependent movements of the beam pipe supports (attached through the Tracker, Tracker support and barrel Hadron Calorimeter to the central yoke wheel). These may be caused by displacements of the whole cavern with respect to the plane of the LHC machine, settling or flattening of the central yoke wheel, or distortions due to the magnetic field.

In Table 10.1 the original estimates of these mechanical contributions are compared with the values or upper limits inferred from measurements on the installed system.

Table 10.1: Mechanical contributions to displacements.

Quantity	**Original Estimate**	**Measurement**
Construction tolerance	2.6mm	$<$0.6mm
Installation tolerance	2.6mm	2.7mm
Sagging between supports	2.2mm	$<$3.0mm (r=25mm pipe)
YB0 yoke distortion	1.4mm	$<$0.5mm
Field-induced yoke distortion	1.2mm	$<$1.0mm
Cavern movements	5mm	$<$1.0mm
Linear sum	15mm	$<$8.8mm
Assumed "stay-clear" radius	14mm	14mm
Min Beampipe radius	29mm	$\sim$ 23mm

These figures indicate that a reduction in central beampipe inner radius by as much as 6mm may be achievable based on improvements in the knowledge and control of mechanical factors.

The LHC experimental beam pipes working group coordinates beam pipe aperture studies. The current target within this group is to demonstrate that a 50mm diameter central section inner diameter is possible for CMS and ATLAS in common. This allows for a comfortable safety margin. A preliminary review of aperture calculations has confirmed that the reduction from 29mm to 25mm inner radius at the CMS interaction region, is acceptable providing the sum of all uncertainties can be controlled to 11mm or better, still assuming a 14mm radius "stay-clear" cylinder.

The remaining factor limiting the minimum pipe radius is the vacuum impedance along the pipe and the consequent ability of the pumps at 13.5m and 18m to maintain a sufficiently low

residual pressure. Once again, preliminary calculations, combined with observations of the achieved pressure during 2009-2010, indicate that a 25mm radius would be acceptable.

Therefore the current baseline is to construct a new central beryllium beam pipe with an inner radius of 25mm, and to install it together with the new pixel detector in 2016. This will also require a revision of the support collars. For background minimization reasons, the η=4.9 opening angle of the conical part of the beam pipe will be preserved, leading to the cylindrical part being shorter by about 280mm at each end. Two options for this construction are being investigated. In the first case, the conical part would again be made out of stainless steel, leading to a shorter beryllium section. Detailed background studies have to be performed to judge the possible effects of this. Alternatively the length of the central Beryllium section would be maintained, and it would consist of a cylindrical part with conical ends connecting to the stainless steel conical sections at the same z as now. This is technically possible, but undoubtedly considerably more complex and expensive. For both solutions detailed calculations using finite element modeling have to be done to estimate the mechanical strength and the deflection.

Meanwhile, parallel calculations have been started to establish whether a 23mm inner radius would indeed be possible with acceptable safety margins. In this respect a review of the conservatively set 14mm radius "stay-clear" is eagerly awaited. Such a step would improve the pixel performance still further, as it is just sufficient to allow the close-fitting inner pixel layer to contract from a 16-sided polygon to a 12-sided polygon. A final decision on the pipe diameter is needed by CMS in late 2011, although if parity with ATLAS is considered an essential economy, the decision may have to be taken earlier.

10.6 Logistics and Integration

10.6.1 Cranes and rigging equipment

CERN provides and maintains the overhead beam cranes in the surface buildings such as 186 and 904. However, at the Point 5 site, the 2 x 80t surface cranes with 120m long cables and the single 20t underground crane are maintained by CERN at the expense of the CMS collaboration. Similarly, CERN provides a transport manager and a single crane driver, while all additional transport personnel (crane drivers, riggers, forklift operators) are charged to the collaboration. Typically one additional rigger is routinely needed to complete a minimum team and this rises to three during shutdown work, in order to have effective flow of material around the surface and underground areas. The specialized rigging equipment needed to lift, manoeuvre, install and remove detector and infrastructure elements has generally been designed by CMS engineers. The EN-HE group provides assistance in keeping track of equipment certification. Significant changes to the endcap muon tooling will be needed once the YE4 disks are installed.

10.6.2 Tooling and Working platforms

The modular design of CMS allows for access to many potential work areas simultaneously. However, the tooling to allow this is highly specialized. Heavy support structures, such as those needed for the very large platforms used for installation or maintenance of the beampipe, or major components within the solenoid vacuum tank, or on the endcaps, could reasonably be made using concrete blocks during assembly, but for future maintenance this is risky, time-consuming and incompatible with the low-dust environment needed once activation becomes a reality. Similarly, the intensive use of scaffolding during construction was cost- and risk-effective because of the long periods spent in static configurations, the need for access to entire surfaces simultaneously and the excellent relationship with a specialist scaffolding contractor

using a compression-clamp coupler system. The revised CERN frame contract for scaffolding provides exclusively for the rapid assembly, ring-lock type, secured by hammered wedges and unsuitable for use next to sensitive detector elements.

Various specialist maintenance structures, all designed to be installed and removed with the beampipe in place, were already constructed for use during the final stages of construction. These include a tubular structure for the support of the 20t installation platform, which gives a very stable work area at about 2m below the beamline between barrel and fully open endcaps, a set of telescopic towers which can be installed more rapidly to give access for lighter work at the same level and a multi-level cylindrical framework which fits inside the end of the solenoid vacuum tank. Maintenance on the mobile wheels and disks generally requires rapid access to very specific regions, and for this the ideal working platform for the barrel wheels is a specialized scissor-lift with a small footprint and 15m height range, while in the endcap varying designs of nacelle with 2-axis adjustable basket and a similar height reach are best suited. These scissor lifts and nacelles are, for the most part, unobtainable for rental locally, and have had to be purchased by CMS .

Purchase and maintenance costs are very high. Although invaluable, they do not cover all rapid maintenance scenarios. To provide additional access solutions, a range of custom-built, light weight platforms is being designed by the integration office to fulfill identified needs. These include light-weight platforms for use inside the solenoid vacuum tank and inside the endcap inner cones. In the medium term, it will become necessary to maintain the Tracker at low temperature even during maintenance periods (to arrest the effects of reverse annealing). This will necessitate the design and construction of an insulated, climate controlled enclosure incorporating the end of the solenoid vacuum tank, which should be easily mountable on heavy or light-weight platforms.

The currently available maintenance configurations of CMS are largely determined by the need to support the beampipe, which has support points at 3.7m, 6m, 10.7m and 13.2m. Maintenance structures for the endcap in a fully open position have to accommodate suitable support and many intermediate scenarios involve precise placements of the major elements so that they can form the basis of beamipe support. Engineering studies are underway for cantilevered support structures which may allow more freedom and increase the options for the 2016 shutdown in particular.

10.6.3 Logistics support teams

The estimated M&O A costs currently approved depend on an outdated LHC operating pattern in which an annual (approx 4 month) shutdown occurs from mid-November until mid-March. The estimates for mechanical support in particular were based on a model where, on average, one end of CMS was opened during each such shutdown and a single maintenance cycle is performed on moving equipment and access devices. It is estimated that extra logistic teams would be required from the Collaboration, from CERN contract Field Support Units (FSU), survey and beampipe support, and from other contractors during a 4 month period each year. In addition, the availability of 4-5 additional CERN staff technicians, who were involved in subsystem work until early 2010, to assist in heavy logistic activities has been taken for granted and halves the amount of spending needed on mechanical FSU.

In the current operating model, there is an estimated total of 34 months actual shutdown, (2+15+2+3+12) in the period 2010-2016. Experience shows that additional expenses actually start at least one month in advance of each winter stop or shutdown since manpower can typically be obtained for a minimum of 3 months. Thus there are 39 months of installation

and logistics activity. In a plan assuming no overtime and avoiding working at both ends of the detector simultaneously, then approximately 23 months follow the original model of M&O A financed shutdown and are roughly covered by the existing M&O A provision. This leaves a remaining 16 months of activity which is identifiably upgrade-related. For this period, workshop, survey and beampipe support requirements are assumed to be comparable to those needed during installation. Under these frugal assumptions, an additional 3M CHF would be needed to support the logistics of upgrade installation during the period 2010-1016. A more detailed breakdown of this estimate in given in Table 10.2.

Table 10.2: Logistic Support: 2010 - 2016.

Item	Upgrade	CERN/host	M&O A	M&O B	Totals
Crane drivers/riggers	184	351	266		801
Add. equipment/tooling maintenance	480		480		960
Collab. cabling/detector teams	800		900		1700
Contractors	200		180		380
Workshops	240	400	280		920
Survey & Beampipe	150		125		275
Field coordination	160		250		410
Technical staff/FSU	464	2925	565		3954
Stores & misc.	160		230		390
Totals .	2838	3676	3276	0	9790

10.6.4 Engineering Integration

10.6.4.1 Organisation

The Engineering Integration Centre (ENIC) in Building 904 is staffed by collaboration and CERN personnel and reports directly to Technical Coordination. It is organized as a joint project between the CERN electronics, engineering, infrastructure and experimental area management teams and has links to every detector subsystem through dedicated link persons. The centre is entrusted with defining and maintaining CMS standards of engineering coherence, quality, change control and documentation. It ensures that these standards are followed by all contributors, including CERN as host lab and CERN as institute and it supports all CMS systems in finding solutions to engineering problems. It also maintains the as-built model of the experiment, provides a CAD translation service and develops and maintains the Equipment Management Database.

10.6.4.2 Resources

The dedicated manpower, equipment and operating costs for the integration centre in the construction phase amounted to about 2M CHF/year and came from two main sponsor institutes (CERN and ETHZ), with the facilities dimensioned to allow project engineers, draughtsmen or subsystem link-persons from other institutes to integrate effectively for short or long periods. Entire integration responsibilities within particular geographical areas were delegated to partner institutes (e.g. Torino for the barrel wheels, Wisconsin-PSL for endcap disks) and several institutes provided engineering staff to the centre for considerable periods of time. The duties of the Integration Office are to optimise tooling and technical procedures, with an eye to schedule efficiency and ALARA constraints, as a component of the EAM and TC sequencing

and scheduling responsibilities. It must also maintain the as-built model drawings library, a CAD translation service and the Equipment Management Database essential for traceability. As far as upgrades are concerned, the ENIC will be responsible for ensuring the integration of infrastructure improvements and of new or modified subdetectors, considering them as black boxes with an envelope (possibly complex) and defined interfaces, including those with existing services. Much of the focus is likely to be on the integration of new and modified services, shielding and tooling, and on balancing subsystem physics optimisation with all the physical, electrical and thermal constraints imposed by the existing CMS detector. Of the current 1.2 MCHF foreseen budget for 2010-2016, (see Table 10.3), approximately 25% is funded by CERN to cover host lab responsibilities, 25% from M&O A to cover minimum collaboration requirements for consolidating, maintaining and operating the experiment, 25% from special institute contributions and the remaining 25% from existing upgrade projects. The equivalent resources for upgrade should be maintained at the current level of around 350-400 kCHF/year during 2011-12, allowing for the provision of the equivalent of two full-time engineers and one project associate (potentially through institute contributions). This level should be maintained until at least the end of 2016.

Table 10.3: Engineering Integration Center: Annual Operating Costs 2010-2016 (kCHF).

Person	**Category**	**FTE**	**Totals**	**CMS**	**CERN**	**M&O A**	**Upgrade**
EIC	Eng/App Phys.	100%	180	180	0	0	0
Librarian/sys support	CAD Draftsman	100%	96	0	0	96	0
Integration Eng. M&O	Eng./Draftsman	100%	120	60	0	60	0
Mu as-built consolid.	Engineer	20%	20	0	0	20	0
Upgrade Engineer	Engineer	50%	75	0	0	0	75
EMD manager	Developer/Eng	100%	150	0	150	0	0
EIC assistant	Sr. draftsman	100%	150	0	150	0	0
Beampipe supports	Engineer	50%	50	0	0	50	0
YE4 engineer	Engineer	100%	150	0	0	0	150
EMD assistant	Student Tech.	50%	40	0	20	20	0
CSC Upgrade Engineer	Engineer	75%	0	0	0		75
Short term visitors	Engs.& Assts.	50%	30	0	0	15	15
materials							
Computers/peripherals			35	0	10	15	10
Software licenses			15	0	0	15	0
Consumables			12	0	0	6	6
Physical Models			20	0	0	20	0
Totals .			**1218**	**240**	**330**	**317**	**331**

10.6.5 Electronic and Electrical Integration

The Electronic and Electrical systems Integration Centre (ELIC) in building 904 is described in Section 10.9.3.2. Consolidation and subsequent operation using M&O funds has been approved and is described in Section 9.

The Electronic and Electrical Systems Integration effort is combined with general electronics support and is led by an Electronic Systems Coordinator who reports to Technical Coordination. Additional host lab personnel consists of 0.5 FTE staff engineer (currently assigned mostly

to beam radiation monitoring), and two engineers supported by M&O A specialising in readout electronics and detector power systems respectively. Half of the costs of these last two should be transferred to upgrade from 2011,

10.7 Experiment Service Infrastructure

The infrastructure and common systems supporting operation of the CMS experiment at Point 5 were brought progressively into operation from 2006 onwards. Following partial commissioning in surface assembly building SX5, underground operation of detector elements began in late 2007, with progressively larger fractions of the detector and its associated systems becoming active. There were substantial periods with the full detector operational during 2008 and 2009, for both cosmic ray and beam tests. Since November 2009, the experiment has been in routine operation.

10.7.1 Responsibilities

Apart from primary power, raw cooling water, and the civil engineering structures (surface buildings, shafts and caverns), which are considered part of the infrastructure provided by CERN as host laboratory, the provision, maintenance and operation of the specific infrastructure and common systems needed for operation of the CMS detector and its surface facilities (which include control room, maintenance laboratories, etc.) is the responsibility of the CMS Collaboration. Contracts and service agreements with CERN departments cover key features of the industrial-scale infrastructure. The total CMS investment in the infrastructure and common installations needed for the low luminosity detector was about 40 MCHF, with an additional 6 MCHF spent on the power, cryogenic and control systems of the magnet.

10.7.2 Consolidation and Upgrade

The currently installed services infrastructure has proven to be adequate for operation of the current detector at reasonable efficiency at low luminosity. However, several systems have little or no margin and some weaknesses in design or implementation have become apparent with operational experience. Consolidation and upgrade will be needed to allow continued reliable operation and to cope with the significantly increased load expected from an upgraded detector, and from improving accelerator performance. Radiation damage and activation will make other changes necessary. Silicon-based detectors will require more power and additional cooling, including continued effective cooling during periods when the detector is being maintained. More processors will be needed to cope with increasing data-rates and this will require a substantial expansion in the number of cooled racks required to house them. By 2016, parts of the infrastructure will already have been operating for 10 years and obsolescence will become an increasing threat to reliability. As availability of spares and expertise (particularly for control systems) decreases and the MTBF becomes shorter, replacement of certain elements with up-to-date equivalents will become necessary to maintain reliable and cost-effective operation.

The following sections describe the actions currently being considered.

10.7.3 Cooling Systems

10.7.3.1 Chilled water for fluorocarbon plants

At higher radiation loads, silicon-based detectors are vulnerable to damage from reverse annealing, which can be halted by reducing the operating temperature and maintaining the detector cold even when not operational. For instance, it is believed that the Tracker will have to

be run with coolant temperature as low as -25°C to halt reverse annealing. Reliability of the cooling will become more critical to minimize radiation damage and ensure smooth operation. The fluorocarbon cooling systems of the silicon-based detectors (Pixel tracker, Strip Tracker and Preshower) are connected (for historical and budgetary reasons) to the same branch of the primary chilled water feed as the Heating, Ventilation and Cooling (HVAC) system serving the caverns and surface buildings. All other subsystems are fed by separate chilled water branches. This shared supply presents a reliability risk due to the radically different requirements and criticality of the Tracker and HVAC cooling functions. The detector circuit must be separated from HVAC, or alternatively a backup system must be provided, so that conditions in the Tracker are maintained even if the HVAC system is shut-down. This work should be done concurrently with revision of the primary coolant loop to allow operation at lower temperatures.

10.7.3.2 Computer farm

The cooling capacity for the event filter farm in the SCX building determines the maximum processing power available and hence the rate capability. The existing system, sized for a luminosity of a few x 10^{32}, was already observed to be vulnerable in high summer, since its maximum observed power consumption was 550kW, compared with the installed cooling capacity of 600kW. From 2011 onwards, with 50ns bunch-spacing and high bunch currents, pileup will already reach the design value. In order to maintain a steady build-up of processing capacity so that HLT performance can be maintained as luminosity increases, the cooling capacity must be increased to 1MW as soon as possible. This implies a complex intervention involving 3 CERN departments (GS,EN and PH). The concrete slab in the SUX building must be upgraded to house the bigger pumps (GS/SEM), which are sized to allow 150 m^3/h of water flow (EN/CV). The electrical distribution must be upgraded to power this new equipment (EN/CV) and it must be incorporated in the control system (EN/CV). Finally, monitoring instrumentation must be added (PH/CMX).

10.7.3.3 RPC Cooling

The operating temperature of the endcap RPC system, is observed to increase from layer to layer with distance from the barrel, reaching 22°C at the -z end, layer 3 and 21°C at the +z end layer 3. This is very close to the 24°C critical value at which the detectors are known to become unstable. The coupling of the endcap cooling circuit to the temperature sensitive areas of the RPC is quite poor. Attempts to improve the cooling system performance over the last year have typically gained only 3/4 degree and any further reduction of the cooling water input temperature from its current value of 16.5°C would entail insulation work on largely inaccessible pipework between USC and UXC, to prevent condensation. Several strategies are under investigation to improve this situation. Since the RPC temperature roughly tracks the cavern temperature, a reduction of the cavern temperature HVAC set-point to 19° or even 18°C should be attempted. (This corresponds to the original design value!). Forced circulation of cool, dry air between the second and third endcap disks is an interim measure for which a design study is ongoing, but the small, irregular gap will impede homogeneous cooling. The probable definitive solution is to re-design the RPC chamber cooling plate so that it couples to the whole outer surface of the RPC, not just to the electronics. Initial tests of this scheme have proven quite successful and it is likely to be implemented for the new layer 4 RPCs which are part of the forward muon upgrade (see Section 3.4)..

10.7.3.4 RE4 cooling

The common peripheral supply and return water cooling manifolds on YE3 are pre-equipped with connections for the CSC ME4 chambers, but not for the RPC RE4s. These manifolds will have to be either removed or modified in situ. The work involves drilling holes and welding half couplings to service the new distribution lines. A study of the temperature and pressure drops expected in the new circuits will determine whether an upgrade of the pump and heat exchanger is needed.

10.7.3.5 Leak tolerance/ detection/ suppression

The 9 October 2009 leak of a bushing in one distribution circuit fed from the YE1 peripheral cooling water manifold exposed the vulnerability of CMS to such leaks and emphasized the importance of detecting and shutting the leaking circuit rapidly to prevent serious damage to the detector as a whole. Since then, a very large investment has been made in replacing all the endcap bushings and installing leak detection cables and associated collector trays. 10 months of operation have since passed with no further leaks from the endcap disk manifolds.

However, a major vulnerability still remains. Of the 136 feed or return shutoff valves on YE1, 87 are inaccessible, meaning that a leak on one of these circuits would necessarily entail a shutdown of the whole YE1 manifold, which provides cooling for all CSCs and RPCs along with the cable trays of the endcap ECAL and the readout boxes of HCAL. Action to improve the disposition of isolating valves, at least on YE1, seems to be an essential mitigating action against this risk. This will involve an integration effort to find places for the new valves and careful planning of how to dismount the existing system and insert new components.

One further incident, a leak in the cooling of a peripheral rack mounted high on the outermost endcap disk on the z end, caused no damage, but highlighted the risk to the detector from leaks originating in any of the uppermost peripheral racks. A further extension of the leak detection system is needed to allow for early detection and prompt fixes.

10.7.3.6 USC rack system extension

Many subsystems and central systems plan major Trigger and DAQ upgrades in 2016. To allow for parallel commissioning of new systems alongside the old, and to accommodate expansion of the existing system, an extension of the rack service network (power/cooling/ control/fire detection) into the zone currently occupied by the commissioning control room will be needed. It is intended to install this infrastructure between 2012 and 2014.

10.7.3.7 SCX Control room

The cooling system of this Control room, the nerve centre of CMS, should be separated from that of the filter farm in the floor above.

10.7.4 Electrical Distribution

Power cuts and transients on the electrical network can damage power supplies, trigger and readout components and processors. The LHC power distribution system which feeds the underground areas is subject to both external and internal disturbances and transients. If such incidents are localized to the CMS experiment, or the experiment recovery time is longer than that of the LHC machine, then substantial amounts of collision data can be lost. In case of a loss of power, essential systems for the safety of the detector and personnel, as well as for shutdown

of the detector, are already backed up by UPS and a local diesel generator. However, operational experience has shown that maintaining full control of the detector is essential during any power incidents to allow a quick and safe recovery. As a consequence, it is proposed to extend UPS and diesel coverage to the entire surface control room in the SCX building.

Substantial work has also already been done to make the CMS system immune to common short-lived power transients, such as re-connection of the static var compensators (active filters) at LHC Point 6. Additional filters for rapid transients on the 400kV network are proposed to improve the immunity to very fast transients. To enable the detector system to ride through power glitches or very short outages safely, the on-board sub-detector low voltage systems are fed through a battery-stabilized UPS acting as a filter. Those systems not yet connected to this filter exhibit significantly higher down-time and damage rate. It is therefore proposed to extend the filter coverage to all low voltage, plus some high voltage, systems underground.

10.7.5 Heating, Ventilation and Air Conditioning (HVAC)

10.7.5.1 Ventilation

After the LHC incident on Sept 19 2008, authorisation for access to underground facilities at Point 5 was made contingent on achieving adequate shaft-USC, USC-UXC and UXC-LHC overpressures. The establishment and monitoring of these overpressures required sealing work and the installation of differential pressure sensors. Overpressure depends partly on optimising ventilation systems, but largely on making effective air-seals around cableways, doors and shielding. These seals must also be fire-proof. After consigning sealing work to a Swiss specialist company, CMS now has the best pressure differentials at LHC during beam operation. CMS is awaiting CERN-HSE advice about what pressure differentials need to be maintained during shutdowns for smoke protection. Depending on the result, substantial further work to revise the PM 54 and PM56 shafts and their safe areas may become compulsory, in which case these activities would be better classified under Safety and Safety Systems. CMS Technical Coordination already considers some modifications to be highly desirable, thus the main uncertainty is the budget to which this work can be attributed.

10.7.5.2 Cavern Humidity

In high summer, the underground cavern humidity has been observed to fall as low as 10%. This is not ideal for people, electronic systems and many adhesives. The HVAC system needs to be modified, if necessary using temporary portable humidifiers, so as to be capable of maintaining a minimum humidity of 30%.

10.8 Beam, radiation, cosmic ray or environmental test facilities

10.8.1 Introduction

Over the next decade, CMS will require the use of test beams and other test facilities for two main tasks. The first is to better understand the existing detector and may involve activities such as precise calibration, diagnosis of anomalous signals seen in the CMS detector, measurements of radiation damage, etc. The second is to research, develop and qualify replacement or upgraded detectors and to establish baseline calibration data. In the near future, these two activities will overlap, with the emphasis then gradually moving from understanding of the existing detector to preparations for the future.

10.8.2 Better understanding of the existing detector

The experience of previous collider experiments (e.g. ZEUS, CDF) has shown that once the initial debugging period is over, fine details start to emerge that require exercising realistic production elements of the installed system under controlled conditions. CMS has planned for this possibility and all CMS subsystems have either preproduction prototypes or spare modules that can be used, if and when a detailed study of a particular behaviour is needed.

Such studies typically take place in either cosmic ray or particle beam facilities, possibly combined with irradiation facilities to simulate background conditions or integrated radiation dose. As LHC approaches its design energy and luminosity, these measurements will be complemented and often surpassed in significance by real-life data coming from the experiment. By that time, R&D for new detectors will be approaching maturity and the irradiation and test facilities will continue to be used for the qualification and eventual calibration of the new devices.

10.8.3 R&D for Consolidation and Upgrade

Existing CMS subsystems have been designed and, as far as possible, qualified to operate for at least 10 years at LHC design luminosity of 10^{34} cm^{-2}s^{-1}. An exception is the forward muon system, where an additional station and a high η component were always foreseen for luminosities exceeding 2 x 10^{33} cm^{-2}s^{-1}. Parts of other subsystems may be replaced or revised because of poorer than expected performance, obsolescence, radiation damage or because technology and experience provide an opportunity to consolidate and improve the detector, so as to maximize the physics output from LHC Phase 1 (where luminosities $\sim$2 x 10^{34} cm^{-2}s^{-1} are eventually expected). For LHC Phase 2 (with target luminosities $\sim$5 x10^{34} cm^{-2}s^{-1} and 300fb^{-1} per year) CMS (notably the tracking systems) will have to be re-equipped with new detector technologies. Based upon experience from construction of the existing detector, the research, prototyping, development and production phases will likely require a full decade and thus must be started now.

The lively detector testing programmes of the last 2 years indicate that R&D for new detection techniques is already actively underway for the most vulnerable areas. CMS is currently studying silicon photomultipliers (SiPM), for HCAL readout,, forward RPCs constructed with different materials (due to an enforced supplier change), new silicon strip and pixel technologies, thick GEMs (Gas Electron Multiplier) for high η triggering and tracking, heavy fibers, new scintillating crystals, use of quartz plates in calorimetry and longitudinal segmentation of HCAL readout. Details are to be found in the chapters of this document concerned with individual subsystems. As in previous experiments, the important instrumentation used for beam monitoring and luminosity measurement (such as the recently tested diamond-tracking telescopes devices for luminosity monitoring) is likely to undergo R&D throughout the lifetime of CMS, in a continuous quest for better precision and robustness.

The facilities required for these test and calibration activities are summarized below.

10.8.3.1 Existing facilities, with examples of current use and investments proposed

10.8.3.1.1 SPS North area: H2 beamline: This is the location of a permanent combined calorimetry test apparatus consisting of a spare ECAL barrel supermodule, two HCAL barrel preproduction prototypes, sectors of HO, and a 20° sector of HE.

- **Description, status and recent applications** Following successful combined calorimetry tests which took place in 2006 for the barrel and in 2007 for the endcap, this

apparatus was used in 2010 with the explicit goal of finding and studying causes of single-crystal noise events in the ECAL barrel, which are observed in data from CMS. The installation uses an existing two-axis rotating platform that can precisely adjust the pion beam incidence on ∼100 t of equipment, allowing fine η-ϕ scans. A key feature of the H2 beam line is the available pion energy range from 2 to 300 GeV, achieved by using a very low energy tertiary beam that complements the secondary beam. Given the importance of a wide energy range for both energy resolution and detector linearity, CMS has equipped the H2 beam line with additional instrumentation (moving platforms, veto and TOF counters, and a Cerenkov counter for particle identification) which allows the available beam to be fully exploited. The calorimetry system is a likely candidate for further long-term study. The combination of a crystal ECAL and scintillator-brass sampling HCAL is highly non-compensating. In addition, ECAL readout electronics, cooling pipes and support rails appear as dead material between the two calorimeters, with a negative effect upon the precision of jet energy measurements.

- **Future requirements** In order to keep the setup fully operational, CMS will require preservation of this test area with a large energy spread of as many particle types as possible. This includes conservation of the very low energy tertiary beam line that is indispensable for good quality calorimetry measurements. Given the fragility of the optical fibres for readout and laser light injection, as well as the need to keep the same trigger and readout settings, CMS must retain exclusive use of control room HNA 370. In addition, an enclosure is needed to control the temperature of the ECAL detectors.

10.8.3.1.2 SPS North area H4 beamline: This area has an η-ϕ moving platform in an enclosure with controlled temperature and humidity, equipped with an interlocked hut housing a high power calibration laser, similar to that in use in the installed CMS experiment.

- **Description, status and recent applications** Studies of irradiated ECAL crystals are usually done in this facility. Environmental control is needed for high precision measurements because of the rather strong influence of environmental parameters on $PbWO_4$ crystal and avalanche photo-diode (APD) response, making such a controlled environment necessary for high precision measurements.
- **Future requirements** The major requirement in this area is continued maintenance of the already installed equipment: air-conditioning, moving platform, laser enclosure. CMS intends to continue using this facility at least for several weeks per year. At the moment the fixtures on the η-ϕ table in H2 allow data to be taken either with an ECAL barrel supermodule or an ECAL endcap setup of four supercrystals. A feasibility study is underway to see if modification of the existing structure could allow both modules to be mounted at the same time. The expected price for this custom modification is of the order of 100 kCHF.

10.8.3.1.3 Large area cosmic ray tracking telescope: This device is part of the RPC Muon effort and is located in an area at the ISR.

- **Description, status and recent applications** This telescope has been used predominantly for detailed performance optimization and production-testing of Resistive Plate Chambers (RPCs) and is currently been used to evaluate the efficiency of prototype RPCs with gaps made from bakelite panels sourced from a new manufacturer.

- **Future requirements** The existing hardware (scintillation counters and electronics) is over 30 years old and close to being unmaintainable. As CMS activities in the ISR have to be transferred to building 904 (Prevessin) to make way for a waste treatment facility, it is not cost-effective to move the existing telescope. A new large area telescope, with options for precision tracking, will be constructed in building 904, in time for production testing of RPCs assembled for the forward muon upgrade.

10.8.3.1.4 Irradiation Facilities

- **Description, status and recent applications** The CMS subsystems near the beamline close to the interaction point will be exposed to high levels of radiation from collision products. Similarly, the outer subsystems and all services in the underground cavern have to operate in a mixed radiation field of charged particles, photons and neutrons. During the R&D phase for the existing CMS detectors, they have all been qualified for long-term operation in such an environment by being exposed, in short periods at various irradiation facilities at CERN and elsewhere, to corresponding 10-year integrated doses of radiation. The key facilities presently available are:

  1. Gamma Irradiation Facility (GIF), presently standalone, but previously in a muon beam at the CERN SPS.
  2. IRRAD facility at the CERN PS.
  3. Intense low energy pion beams at PSI (Villingen, Switzerland).
  4. Low energy neutron irradiation facilities at various reactors worldwide.

  At least three ongoing projects are using these facilities: The first two are studying CMS subsystem behaviour in closer to realistic conditions, working with lower field intensities and mimicking the time between fills and during technical stops, when annealing processes can occur. One is performed with pixel detectors irradiated at PSI, the other with endcap ECAL crystals irradiated at the IRRAD facility. CMS is also participating in a common CERN-wide project to study filtering of any radiation-induced contaminants in RPC working gases. In view of the high cost of these gases, it is very important to recover as much as possible of the gas without compromising the detector performance. These tests are carried out in the GIF, which uses an intense Cesium source to simulate the background rate conditions under which muon detectors, in particular, are required to operate. It is to be expected that testing and qualification of any new gas-based detector, such as a micro-pattern gas detector (MPGD), will require the same facility.
- **Future requirements** Radiation dose rates and integrated doses for SLHC are going to be higher than for LHC, so all new detectors will have to be tested for radiation hardness. In addition to facilities outside CERN, the already existing CERN facilities such as GIF and the PS irradiation facility, for which various upgrades are planned, will continue to be needed. For continued usefulness, the GIF should be re-installed in an SPS extracted beam-line and the source should be replaced. In practice, the radiation shielding and shutter mechanism will also have to be replaced. A contribution from experiments is expected to be solicited. Data obtained during first few months of CMS running indicate that, as long suspected, the actual deterioration in detector performance may depend not only on the integrated dose, but also on the mixture of gamma, neutron and charged hadron fluences. From that aspect, a possibility to expose detectors and front end electronics to a realistic mixture of particles becomes very important. CMS thus expects more use for the mixed field

irradiation facility already existing at the PS and expects to be asked to contribute to construction of a more extensive facility.

10.8.3.1.5 High Magnetic Field Facility: M1 magnet This facility is in the SPS North Area beamline H2

- **Description, status and recent applications** The only test facility at CERN where a detector can be exposed to high energy particles in the presence of a strong magnetic field is in the H2 beam-line, where the M1 superconducting magnet recovered from NA22 experiment, which has a 1.40m bore, can reach fields of up to 3 T. This highly versatile facility was instrumental in confirming correct performance for numerous CMS components. Experience at CMS and elsewhere confirms that magnetic field tolerance should not be taken for granted, even when accounted for at the design stage. Recent tests at M1 investigated the behaviour of irradiated silicon pixel detectors, which are influenced by strong magnetic fields because of the effect on the drift paths of charge carriers in the silicon. Unfortunately, the last time the magnet was refurbished was in 1994 and the current state of both hardware and software is precarious. As the test programme of 2010 highlighted, almost the entire vacuum system and a large part of the control and monitoring system consists of equipment that is obsolete and is now becoming unreliable, risky to operate, very difficult to maintain and a drain on skilled personnel. Modern communication devices and analysis tools are strongly needed for safety and to limit the time spent by technicians for operation. The existing control software (written in Labview 2) should be replaced by the contemporary CERN standard-issue magnet control system built on top of a new hardware that will replace the existing CAMAC interfaces. Further operation is not possible until these revisions have been carried out.
- **Future requirements** Many new detectors and their front end electronics and power distributions will have to be tested in a strong magnetic field. The estimate for the hardware refurbishment of M1 is of the order of 400 kCHF, without taking into account manpower costs. As several non-CMS groups expressed an interest in using M1, a proposal is being made to CERN PH and TE departments and the EN-MEF group to share costs with CMS in order to create a general high-field test facility. Unfortunately, the magnet refurbishment is an extremely urgent matter for CMS, whereas an agreement on the modalities of cost sharing will probably take some time to arrange. For reasons of manpower availability, the ideal time to conduct such a refurbishment is during an extended period of LHC operation. In the near-term, this implies 2011 or the second half of 2013. In order to reduce the pressure on M1 refurbishment, with its consequent demands on skilled CMS manpower and to provide a simpler, cheaper solution to short term, high field validation tests of small objects such as pixel detector prototypes and electronic components, CMS proposes to purchase a small 4T magnet from a commercial vendor at an estimated cost of 70 kCHF (not including installation costs).

10.9 Surface assembly buildings, workshops, laboratories, and storage space

10.9.1 Introduction

The construction and assembly of new detector components and the maintenance and repair of existing ones requires substantial surface facilities at CERN. The large facilities at the ISR and

building 867 used for reception, assembly and testing of the muon detector and electromagnetic calorimeter of the low luminosity CMS have been re-assigned by CERN to other uses. The plan for future CMS surface facilities at CERN envisages a concentration of effort at a small number of sites in order to gain economies of scale in the provision of infrastructure, in communications, and in the use of host laboratory, or common CMS, facilities and personnel. For example, such concentration ensures that a CERN staff TSO and support technicians can be assigned to each of the sites, so that there is the best synergy with the priority activity of operating CMS efficiently and that the infrastructure of these few large sites can be accepted into the general site access control and monitoring. The provision of office and meeting space for CMS staff working permanently or intermittently at these sites is a key ingredient of the plan.

For maintenance of equipment exposed to beam in UXC (including activated material), activity will be concentrated at Point 5 (building SX5, 2000m^2, plus an external control barrack), which will be equipped with a Class C work area for lightly activated materials. Specialist electronic maintenance and mechanical work on activated objects, requiring workshop facilities rated better than Class C, will need access to the common specialist electronic and mechanical radioactive workshops being provided by CERN at Meyrin and Prevessin.

For upgrade activities (i.e. newly built equipment) and for maintenance and testing of non-activated equipment that do not originate from a defined zone around the beampipe, activity will be concentrated in buildings on the Meyrin and Prevessin sites (Meyrin building 186, 2000m^2, and Prevessin building 904, 2000 m^2). The Prevessin site offers transport access to SX5 without a border crossing and is therefore suitable for storing tooling, ready-use electronic spares, etc. It is also the site of the existing CMS centres for Electronics Integration and Engineering Integration.

10.9.2 Operation Support Centre (OSC) at Point 5

10.9.2.1 SX5 building

The SX5 hall is now being developed as the CMS Operation Support Centre. In the past this building was used for the surface assembly of CMS and, since the lowering of the CMS detector, has been used to store assembly tooling. The size of SX5 is 100 x 20 m^2 at 20m height. It contains 2 80-tonne cranes and a DAQ/control barrack. Work on the reconfiguration of SX5 was delayed by a protracted local planning process, which was needed because of previous environmental impact commitments. This centre is considered as an operational requirement for the existing detector, whether or not upgrades are carried out, and therefore it is funded by host laboratory and M&O A budgets only.

The proposed layout of the OSC is shown in Figure 10.7. The areas assigned to subsystems correspond to the minimum requirements requested by their field coordinators.

The SX5 hall will be divided longitudinally into sections. Starting from the left, the first is the PX56 shaft, normally closed by the 2m thick pit-head cover. Next to this, a section 20m x 10m with access doors on both sides, is devoted to logistics, transport arrivals and departures and staging, particularly of items to be raised and lowered from/to UXC. The next section, of area 65 x 18m, is access controlled and contains five subsidiary areas.

1. A logistics and infrastructure area.
2. A storage place for activated material, notably sections of the beampipe and shielding.

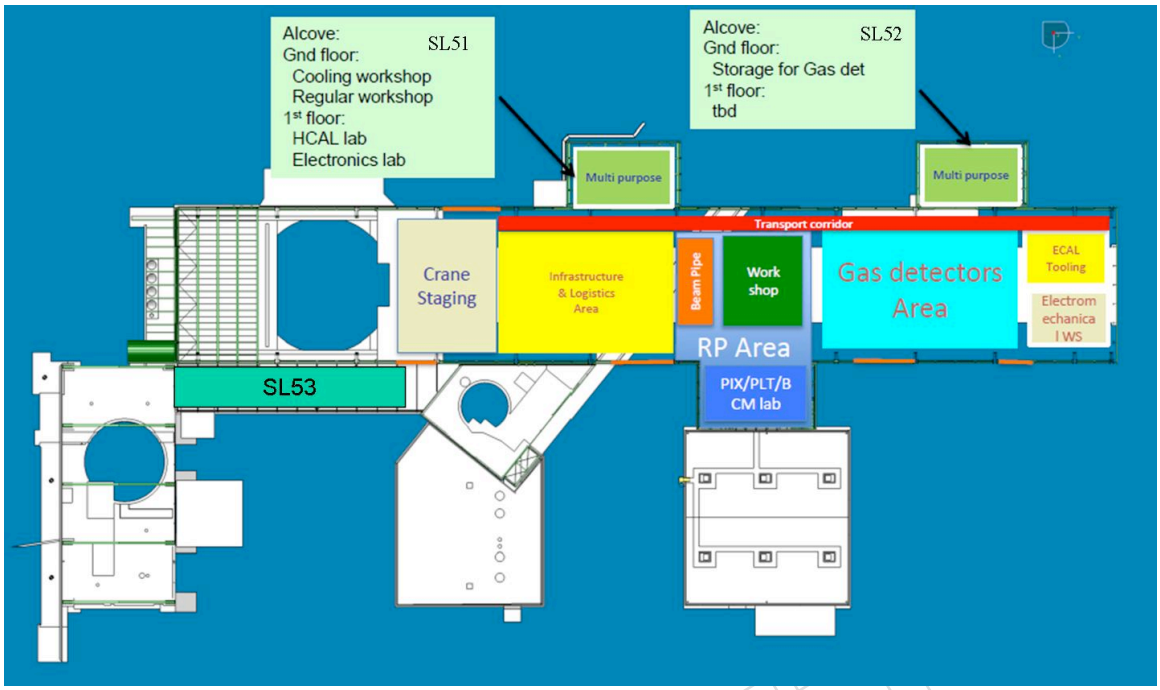

Figure 10.7: Proposed layout of the SX5 building showing the maintenance and operations areas.

3. A walled radiation laboratory (following broadly the Swiss Class C regulations: permitted total activity 1-100 x the limiting activity per isotope [LA] below which no special work area is required.). This work area covers the requirements of ECAL, HCAL and CASTOR calorimeters, TOTEM and the beampipe system. This area also acts as a buffer zone for the temporary storage and measurement of equipment removed from the UXC.

4. A area attached to the radiation laboratory in the SHL building consisting of a temperature-controlled semi-clean (∼class 100000), class C radioactive laboratory area (ground floor), with a room above for pixel trackers and beam monitors, equipped with a load platform to allow delivery and removal of objects by crane.

5. An area that accommodates 3 types of gas-ionization muon chambers (Drift tubes, Cathode Strip Chambers, Resistive Plate Chambers) and the alignment system. Facilities within this area will allow faulty units from the corresponding subsystems to be opened, diagnosed, repaired and re-qualified for installation. It is expected that spare drift tube chambers, spare cathode strip chambers and spare resistive plate chambers will also be kept under continuous active test in these areas.

The final 12m section is devoted to infrastructure support, especially electro-mechanics (e.g. rack system) and it concludes with a multi-level storage system, installed against the south end of the building. The alcoves on the north side, originally designed for Barrel HCAL assembly, will be modified. The upper floor of the SL51 (nearest PX 56) will be extended, equipped with a projecting loading platform and dedicated to electronics work; the lower floor will be a workshop (non-radioactive) for cooling and moving/hydraulic systems. The second alcove, SL52, is already occupied by the Point 5 general mechanical workshop and this will stay in place. A small, independently accessible user workshop will be added.

10.9.2.2 Green barrack

The "green barrack" (ex-OPAL experiment control barrack, recuperated as a control room for surface magnet tests) provides an on-site operation support room for the Tracker and Muon systems. It also features a rack room with sufficient racks to support the subsystem laboratories, which will be used to control data-taking in the test areas. An additional room has been loaned to the TOTEM experiment as a control room. The remaining room is used as a DAQ development facility and remains equipped as such, so that test data from the adjacent subsystem laboratories can be centrally recorded.

10.9.2.3 SL53 Offices

There is currently no permanent office space at Point 5. Two small laboratories and the small meeting room adjacent to the control room, along with the "green barrack" are used to support control room operations. The CMS collaboration obtained a surplus temporary barrack which has acted as the office quarters for the last 8 years, but which is now nearing the end of its useful life. During shutdowns, typically 50 technical team staff and collaborators are present daily at Point 5, along with several long-term contractor teams numbering up to 30 people. During operation, the technical team is reduced to a core of about 15-20, to which up to 20 support personnel from subsystems may be added, depending on the work programme. Office space is therefore needed for about 20 personnel plus a similar number of visitors. A conference room, with a capacity for about 60 people, is needed to allow the existing small conference room to be given over entirely to control room support/overflow.

CERN is committed to constructing a suitable office block on the existing foundation slab of the never-constructed SL53 building (see Figure 10.7), which was originally conceived for covered transfer of heavy material between SX5 and the PM54 shaft, a function now rendered superfluous by UPS installation blocking the pathway in SDX.

10.9.2.4 Visitor facilities

Outreach, in the form of welcoming VIP, funding agency, collaboration and public visitors to Point 5, is an additional consideration in designing the SX5 facility. The particular design features of CMS and the cavern system make underground visits feasible year round and visits to the experimental cavern frequently possible. Visitor facilities will be incorporated in the new office building SL53, which connects with a potential display area in the SDX building near the PM54 shaft and thence to the control room. Initiatives in partnership with the commune of Cessy, the Pays de Gex and the Department de l'Ain may result in a substantial science-tourism facility next to the Point 5 site, with the potential for shared facilities.

10.9.2.5 Funding for Point 5 reconfiguration

The OSC project is foreseen in four stages, which will maximum use of the availability of the resident technical staff, who will eventually run the facility.

- **Stage 1** This encompasses urgent items which could be needed as soon as the next extended technical stop or shutdown, plus preparation of the site for construction of the permanent office facilities. The total cost of this phase is estimated at 900 kCHF, approximately equally split between CERN host lab costs and CMS collaboration M&O A expenses.
- **Stage 2** This covers setting up the subsystem laboratories, for a cost of just over 500k CHF, approximately equally split between collaboration M&O A and M&O B.

- **Stage 3** This covers completion of the permanent offices and meetings rooms, plus basic visitor facilities, for a total estimated cost of 1.2 M CHF, of which the vast majority (1.0 MCHF) has been foreseen by CERN as host laboratory.
- **Stage 4** This is dedicated to providing handling facilities and working areas for subsystem materials which have been activated. The estimated cost of this final phase is 85 kCHF.

A breakdown of the estimated costs to complete the re-configuration in shown in Table 10.4. The host lab and M&O A contributions have been approved.

Table 10.4: Total Cost for the complete reconfiguraton (all numbers in kCHF).

	Total	**CERN**	**M&O A**	**M&O B**
Stage 1	974	425	499	50
Stage 2	530	0	270	260
Stage 3	1205	1000	205	0
Stage 4	85	0	85	0
Grand Total – all Stages	**2794**	**1425**	**1059**	**310**

10.9.3 Building 904, Prevessin

The principal laboratory area allocated by CERN to CMS in compensation for the loss of the laboratory areas centered on Building 184 (ISR) and in building 867, is Building 904 on the Prevessin site, which offers about 2000m^2 of contiguous laboratory space. Two large adjacent areas of about 1000m^2, each accessible with modern cranes of 12t and 20t lift capacity, are very well suited to house detector construction and assembly lines and diagnostic facilities for large detector components. An adjacent 800m^2 area is already in use as an Electrical systems, Electronics and Trigger test and integration centre. This is being upgraded using M&O A funds to provide a 5% DAQ slice, giving the opportunity to pre-test hardware or firmware modifications to Trigger and DAQ before deploying them in CMS at Point 5. A further, separated, 300m^2 laboratory with a light beam crane will become available in the medium term. The CMS Engineering Integration Centre has been established on the upper floor of 904 for almost 15 years and various offices and labs around it are scheduled to become available for CMS use.

10.9.3.1 Detector Assembly and Test Centre

Building 904 is foreseen to be the primary laboratory for all future calorimetry and muon upgrade projects requiring large amounts of space. The first production projects in this building will involve assembly and testing of Cathode strip Chambers (CSCs) and Resistive Plate Chambers (RPCs) for the CMS Forward Muon upgrade. All 72 CSCs of the ME4/2 layer will be assembled in building 904. Assembly of these trapezoidal chambers ($\sim$3.3m x 1.3m) requires large, precision machines which will be sent to CERN from a previous production site at Fermilab. A large fraction of the 200 RPC chambers planned for the CMS upgrade will also be produced in building 904. Acceptance tests, fault diagnostics and necessary repairs of RPCs built at other worldwide sites will also be done in 904. The projected layout during this phase is shown in Figure 10.8.

The basic building, as delivered, required substantial renovation and modification, which is being done by CERN (GS dept) as host laboratory overseen by the CMS Technical Coordination and Experimental Area Management teams.

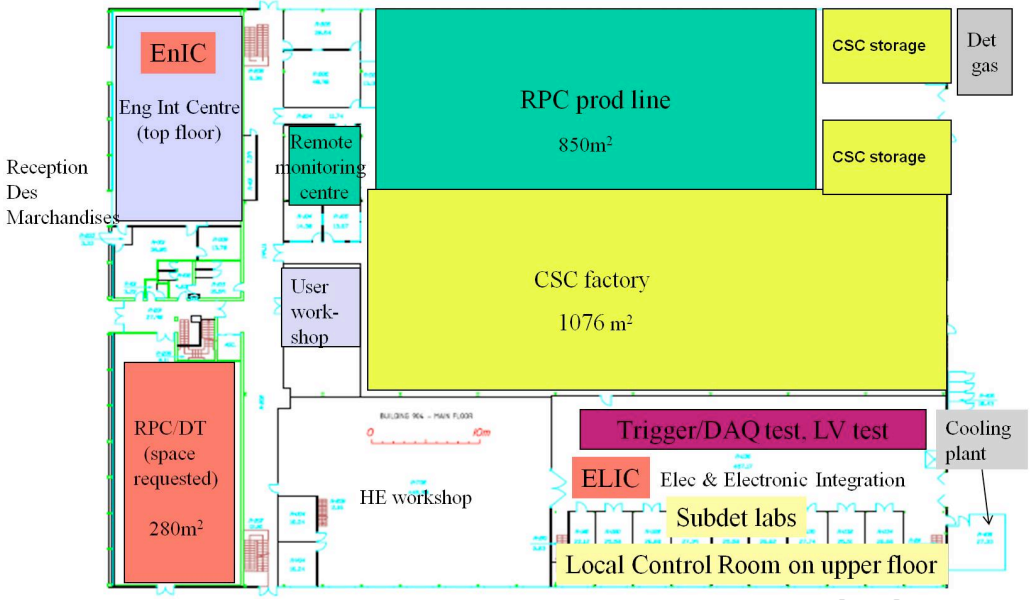

Figure 10.8: Proposed layout of Building 904 for the next 5 years showing the assembly areas for CSCs and RPCs, the CMS Integration Centre and the Trigger/DAQ test area.

This first stage of the 904 programme involves repairing the roof, filling-in inspection pits in the floor, installing fire protection systems, re-surfacing the floor, installing a storage platform and providing network hubs, This will be completed approximately on-time during Autumn 2010. Simultaneously a rigid storage tent will be installed an adjacent site to allow tooling and other installation equipment to be transferred from SX5 and building 904.

The assembly of Resistive Plate Chambers (RPCs), in particular, requires very strict environmental control. The required conditions, which are maintained naturally in the ISR, namely temperature of 21 ± 2 °C and relative humidity 40 ± 10 %, will be hard to reproduce in a building the size of 904 without a very large investment, which is probably not feasible on the timescale needed for the forward muon upgrade. CMS has made a proposal to CERN-GS department that would involve installing four laboratory rooms [∼10-15m x 6m x 3m] within Building 904 and controlling the temperature and humidity inside them using upgraded capacity from the existing cooling plant, which is already in use for the racks of the electronics, trigger and DAQ integration centre. The second stage of the Assembly and Test centre project will start with the installation of these huts and the construction of a framework for the specialized infrastructure for gas, detector-related cooling, detector electrical power and network connections for the assembly areas. These will be a shared responsibility of CERN (GS and PH departments). The next stage of moving facilities and equipment from ISR and SX5, installing the detector production lines and connecting the specialized services they require will get underway before the end of 2010. Any further insulation of the building shell (roof and walls) will continue as a fourth stage of the refurbishment, in parallel with, and factorized from, detector work inside the building.

10.9.3.2 Building 904 Electronics Integration Centre

The building 904 electronics integration centre consists of a central platform with installed electronics racks surrounded by a collection of several small laboratories equipped with the trigger and DAQ electronics for each of the main components of the CMS detector. The centre provides a unique environment for subdetector and trigger/DAQ experts to commission and integrate

new developments and upgrades into the central Trigger/DAQ system of CMS without affecting the operation of the experiment at SX5. With the upgrade of the building 904 services, as described above, corresponding improvements are needed in the electronics integration centre for central air, access control and other routine services.

Currently, a complete slice of the global calorimeter trigger (GCT) is permanently installed in building 904. This system receives input from the regional calorimeter trigger (RCT) and provides output to the global trigger (GT). The next components to be installed are a complete GT and the cabling up of the RCT. This work is foreseen to be completed well in advance of the 2012 shutdown. In particular, the building 904 setup will be used to pre-commission the Optical GT Interface (OGTI) from the GCT to the GT for 2011 operation. Similar developments on the central DAQ slice in building 904 will provide for a complete test bench for pre-commissioning of all hardware, firmware and critical software components before deployment in SX5.

For the Phase 1 upgrades, the common working area of the electronics integration centre will be extensively used to burn-in upgrade electronics. For the HCAL Phase 1 upgrades, approximately 1/3 of the entire front-end services and low-voltage power will be operated continuously to ensure data integrity and front-end stability. Known potential problems, such as slow control and monitoring induced noise sources, will be investigated and eliminated, if found, through the appropriate hardware, firmware and software modifications. The HCAL back-end readout based on the μTCA technology will begin its integration phase for the 2012 shutdown where optical splitters will allow the upgrade electronics to parasitically readout and generate trigger primitive information for data coming from the current front-end readout system. Effective integration and reliability of the HCAL upgrade depends on an extensive burn-in program for the front-end electronics based in 904 in advance of the 2016 Phase 1 upgrade and an upgraded back-end readout test slice for pre-commissioning in building 904 for subsequent parasitic operation in SX5 following the 2012 shutdown.

For the trigger Phase 1 upgrades, the integration of the serial link board (SLB) communication from the ECAL and HCAL back-ends to the RCT must be achieved in building 904 in advance of any modifications to the SX5 system. The hardware-level calorimeter trigger system is a critical online system whose data integrity must be maintained with high reliability. The DAQ integration for the trigger system also requires burn-in and testing in building 904 in advance of installing the system in SX5. The current 904 infrastructure has been extensively used for SLB testing between ECAL, HCAL and the RCT and a similar intense program of checks and burn-in is planned for the Phase 1 upgrades and 2012 shutdown maintenance and modifications.

10.9.3.3 Building 904: Offices and small laboratory/workshop areas

Some additional offices and labs are foreseen within or near building 904. Adjacent to the existing CMS mechanical integration centre, the current electrical workshop will be adapted as a pipework laboratory, and the electrical storage areas will be converted into storage for electronical components. The present "Kicker lab", 280 m^2, will be adapted as a detector development laboratory, which will contain activities such as the current prototyping test of Micro Pattern Gas Detectors.

Adjacent to building 904 and the tooling storage tent, barrack 933 will provide approximately 20 offices. Minor refurbishment costs (approx 10 kCHF) should be foreseen.

10.9.4 Other facilities

10.9.4.1 Building 892, Prevessin

The catacombs associated with ISR point 4 were converted into substantial locked storage enclosures for muon system spares. Material still required is destined to be transferred to the basement of building 892. Similarly one of the ECAL test benches currently in building 867, along with the mechanical workshop adjacent to it, will be transferred to the ground floor of building 892. Substantial refurbishment work to the shell of the building, a host lab responsibility, is estimated to cost 300k CHF and may be required during 2011. Detailed requirements are still to be negotiated.

10.9.4.2 Buildings 186 and 28, Meyrin

The size of building 186 is roughly 2000m^2 on 2 floors. This building contains the 600m^2 CMS-funded TIF clean facility used to commission the Tracker, preshower and beam monitors. It includes a scaled down readout system and infrastructure including rack water cooling and detector fluorocarbon cooling. It is adjacent to the PH department silicon facility. The upper floor contains smaller clean areas used for Tracker and Preshower component assembly and testing, pixel tracker final integration and testing, and beam scintillation counter and diamond beam monitor labs. All these facilities will be needed for upgrades. In extreme circumstances it is conceivable to transfer the Tracker back to the TIF if a major fault should occur before it is strongly activated.

However, as is the case for Building 904, the cooling plants are unreliable and the mini-DAQ now obsolete. The rough estimated cost of a basic refurbishment is 82 kCHF, whiich is to be split equally between CERN as host, CMS M&O A and CMS upgrade funds. Subsystems involved would take care of specific facilities from upgrade or M&O B funds as appropriate.

It is important to retain the use of offices, workshops and labs in the adjacent building 28.

10.9.4.3 Alignment test benches

The surveyed test benches used for calibration of alignment components on barrel muon drift chambers and of the MAB structures, which provide a link between barrel chamber layers, are needed during major shutdowns. They require an environment which is stable from the mechanical, temperature and humidity point of view. The environment should be lockable and relatively clean, with adequate lighting. The area adjacent to the ISR I4 collision hall met these criteria automatically. CMS is working with CERN departments to identify possible alternative areas. Costs of the transfer should be born by CERN as host lab.

10.10 Planning and Coordination

10.10.1 Organization

The coordination of technical operation and of maintenance, consolidation and upgrade activities during accesses, technical stops and shutdowns is the responsibility of the CMS central technical team. The present organization of this team is illustrated in Fig 10.9.

For those subsystems where major upgrade or revision work is anticipated, the currently dormant branch of subdetector coordination populated by the subdetector technical coordinators is expected to be restored. As in the construction phase, each will be responsible for planning and coordinating all technical aspects of the approved upgrade or revision project, according to

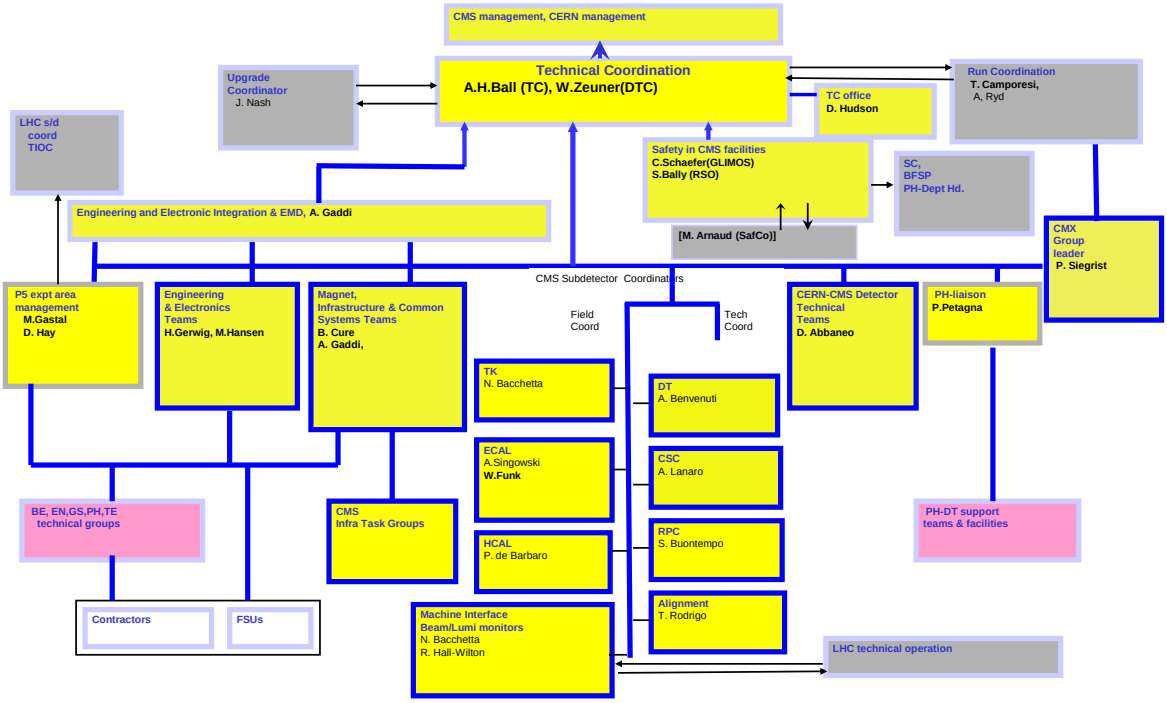

Figure 10.9: Organization of the CMS central technical team.

guidelines agreed with CMS technical coordination and scrutinized by the Engineering Design Review process. This responsibility includes QA/QC, delivery of finished items to point 5, pre-installation testing and any repairs or rework needed. The existing field coordination structure will deal with installation, post-installation testing, commissioning, integration into CMS, and subsequent maintenance and operation. Both arms of subdetector coordination, which depend on continuity of experienced personnel with project responsibility, were crucial to the success of the low luminosity CMS detector and must be maintained and supported. A small number (2-3) of additional central team task coordinators, drawn from the collaboration, will be put in place as soon as specific manpower plans for the central field teams are addressed.

10.10.2 LHC planning 2010-2016

The duration of the 2012 LHC shutdown is estimated at 15 months, a duration chiefly determined by the time required for splice consolidation to allow the LHC to operate at higher energy. The duration of the 2016 shutdown is currently considered to be around 1 year and determined by the needs of experiments, with the CMS request of 12 months currently the longest. Incorporation of LINAC4 into the injector chain, the main accelerator activity, is estimated to take only 6 months in 2016.

Extended technical stops are expected to occur at year-end 2013-14, with duration similar to the 9-11 weeks foreseen for 2010, and at year-end 2014-15, with duration estimated at 12 weeks. As has been demonstrated in 2009-10, rapid opening of CMS, giving a few days access for

light repair work in any location, followed by closing and a return to beam-ready condition, is possible in a 10-11 week shutdown. At least 3 weeks of this time is dedicated to the cycle of re-pressurizing the beampipe to 1 atmosphere with Neon and eventually restoring operating vacuum.

10.10.3 General constraints on planning

The possible timeframes for installation at Point 5 of the various consolidation and upgrade features is in most cases determined by their potential for readiness relative to the two major LHC shutdowns planned in 2012 and 2016. The pixel tracker and beampipe replacements are still being designed; clearly they will require a long shutdown and cannot be ready for 2012-13. In contrast, for many items in the forward muon upgrade, the design is mature, procurements are proceeding, assembly lines are being setup and construction is imminent. All modifications which involve significant individual or collective radiation dose to personnel must be completed as soon as possible (ALARA principle). The same argument applies to modifications or additions related to minimizing these doses. Where consolidation or upgrades are aimed at reducing or eliminating a large risk to the availability of the detector or the efficiency of data-taking, it is clearly prudent to execute them at the earliest opportunity after they are ready.

In order to repeat, in 2013 and 2017, the "unprecedented state of readiness" for first beam, achieved in 2009, the same integration of commissioning activities into the planning must be foreseen. The independently serviced wheels and disks of CMS allow for significant requalification tests and pre-commissioning work to be carried out concurrently with maintenance and installation activities, as was routinely the case from early 2006 onwards. In addition the detector must be closed, the magnet commissioned to full-field and extensive cosmic ray tests undertaken, early enough to leave sufficient margin before accessibility is lost to reopen and remedy any faults detected. The value of this was conclusively demonstrated by the MTCC in 2006 and the CRAFT exercises of 2008 and 2009. The planning being developed is therefore based on having partial or full infrastructure and services (HVAC, gas, cooling, electricity, DAQ) available continuously as soon as possible during each shutdown, so as to allow post-installation testing and commissioning of new detector parts to proceed smoothly and intensively. In addition, CMS will be closed and the magnetic field raised to 3.8T a minimum of 10 weeks before first beams are expected to circulate. It should be noted that this important safety margin may be hard to maintain in 2016, should all other shutdown activities indeed prove to require substantially less time than those at CMS.

The possible logistic configurations of opening CMS are severely limited by beampipe support requirements, the size of the experimental hall and the procedures for beampipe bake-out. The basic set of configurations available at either end of the detector are illustrated in Fig 10.10, Fig 10.11, and Fig 10.12. The possibilities for configuring the two ends differently vary from unrestricted to highly constrained, depending on what tasks are being done.

The attribution of activities to the two major shutdowns is determined by the constraints outlined above and particularly the logistic configurations needed for installation of the new beampipe and pixel tracker during the 2016 shutdown. Most of this shutdown must forcibly be spent with both endcaps fully open in configurations G through J. A further period is spent partially open (configuration E at both ends) for beampipe bake-out, during which, however, no other work on the detector is admissible due to safety constraints. Since installation of the forward muon upgrade requires very substantial periods of work in logistic positions C and E with closed, or partially closed, endcaps, this automatically leads to a requirement to complete

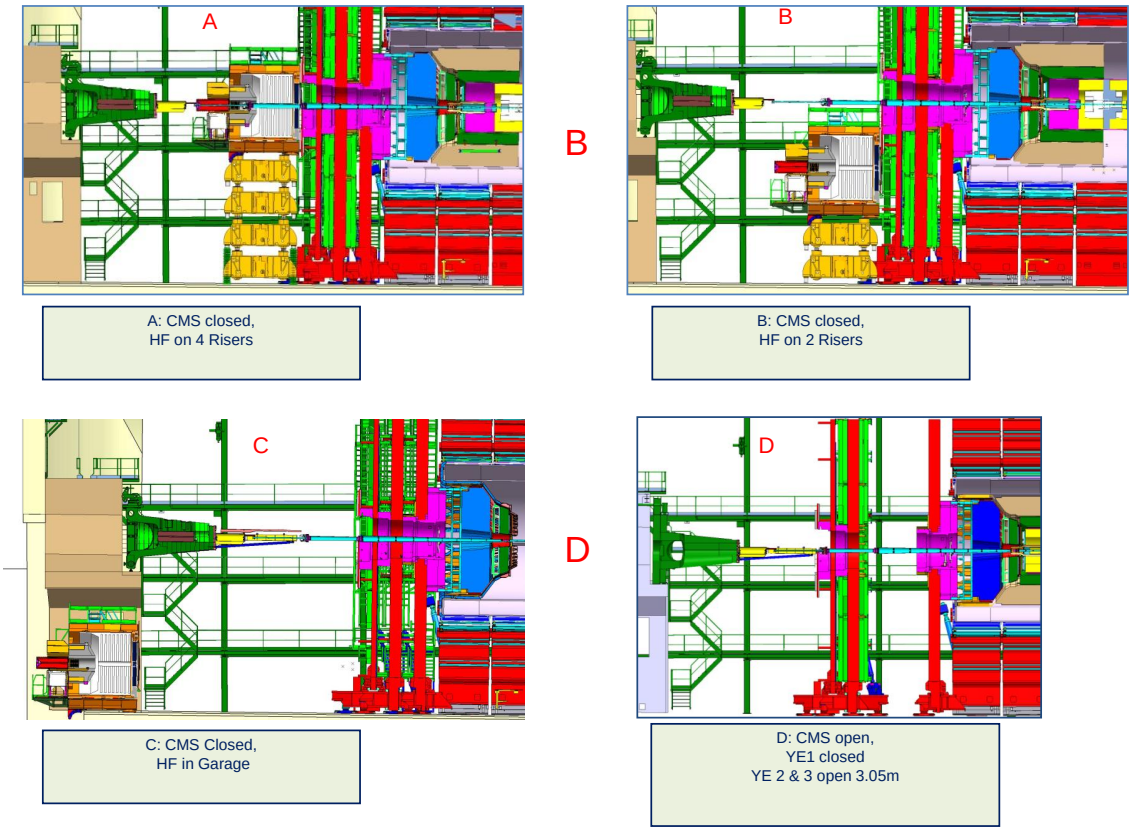

Figure 10.10: Possible opening configurations A - D of the CMS Detector.

this upgrade during the 2012-13 shutdown or in the technical stop(s) of 2013-14 and 2014-15. The work (particularly construction of the YE4 shielding walls) factorizes between the plus and minus z ends, so that the likely 2012-13 planning features sequential periods with the +z endcaps closed, then the -z endcaps closed.

It is essential to complete installation of the YE4 shielding disks at both ends before magnet re-commissioning starts in order to keep the magnetic field and forces symmetric. To accommodate the likely installation of these disks before the detector elements (CSC, RPC) of the forward muon upgrade are ready, the potential of the newly conceived YE4 pushback system (see Section 10.4.1) must be exploited to give rapid access for CSC and RPC installation without opening the yoke. Opportunities for completing the installation are envisaged in the 2013-14 or 2014-15 extended year-end technical stops,

Following the pattern established during construction, the detailed CMS planning being applied in the field must be flexible, ready to exploit opportunities presented by LHC schedule changes (even if not yet officially recognized) and factorized enough to be easily adapted to changed circumstances. Examples are the possible delayed start of the first long shutdown and the need to carry out currently unforeseeable maintenance work. Contingencies must also be kept in hand for effectively using any unforeseen machine repair stops of substantial duration, for reacting to late delivery of items to be installed and for accommodating maintenance work additional to what is now planned.

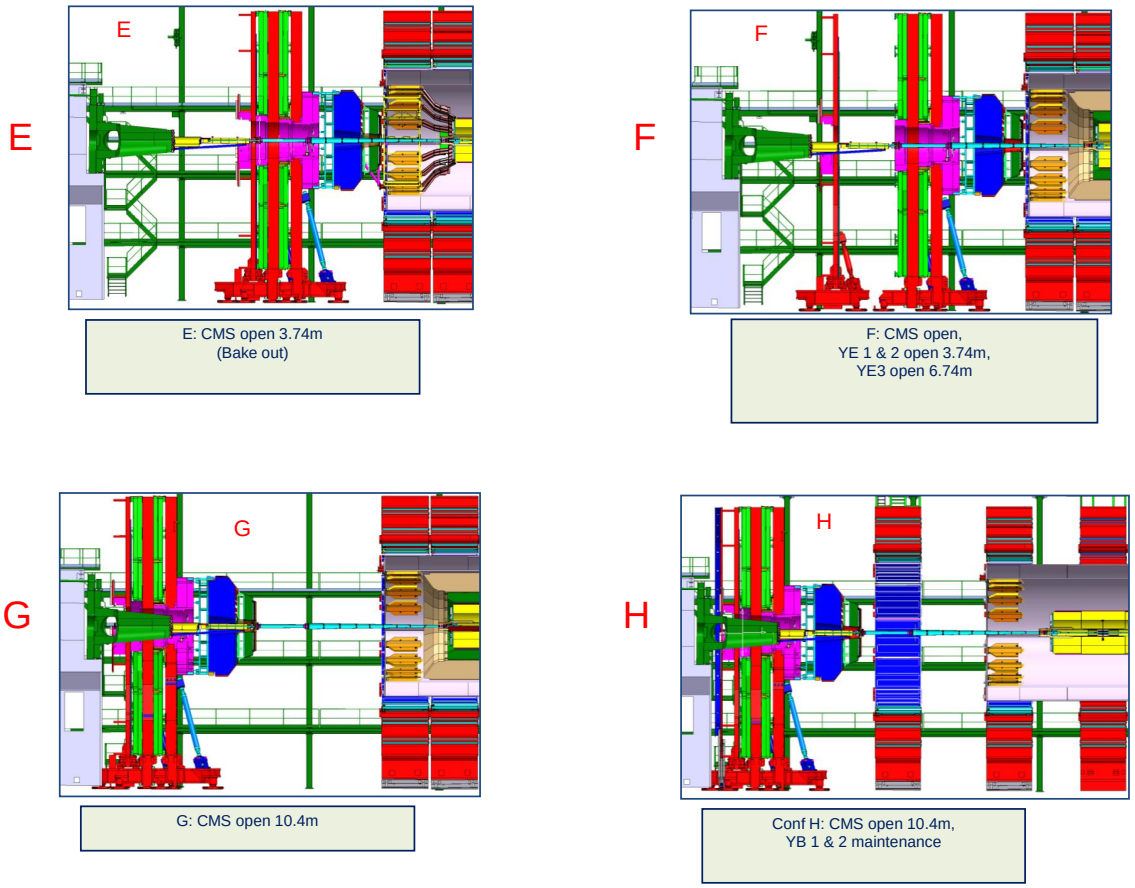

Figure 10.11: Possible opening configurations E - H of the CMS Detector.

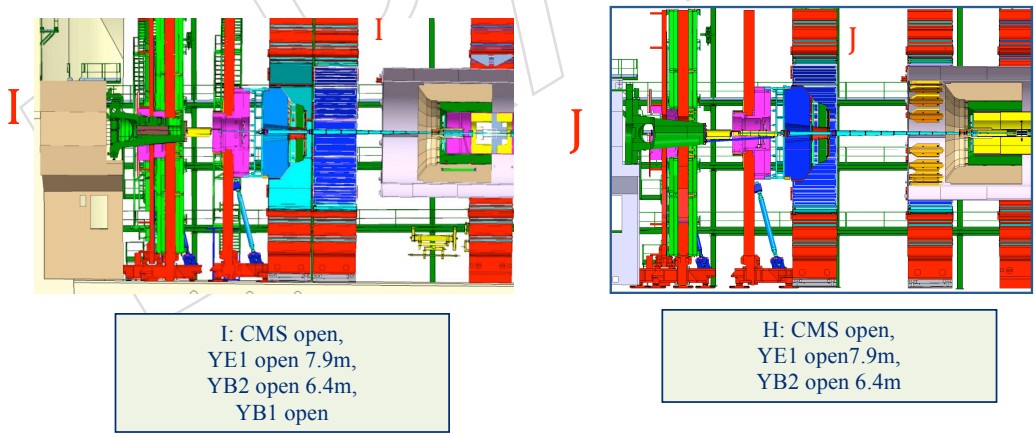

Figure 10.12: Possible opening configurations I - J of the CMS Detector.

10.10.4 Shutdown 2012-13

Assuming no force majeure constraints, such as an unexpected requirement for beam-pipe bake-out, the current list of detector activities in UXC during 2012-13 is:

- Improve barrel-endcap seal for cold Tracker.

- Test beampipe region RP shielding + opening under vacuum.
- Replace HO & CASTOR phototransducers.
- Build YE4+z shielding wall and install pushback system.
- Build YE4-z shielding wall and install pushback system.
- Install 4^{th} muon endcap station +z (ME+4/2, RE+4/2, RE+4/3) and possibly RE-4/2, RE-4/3 for -z)
- Replace HF phototubes +z and -z (while HF is in garage).
- Modify Forward Structures (for ALARA and so that CASTOR, TOTEM and ZDC are removable for pp running and re-installable for ion-ion or β^* = 1500m.). The most extensive modifications are needed at the -z end where CASTOR is installed.
- Remove and maintain one or both ends of the forward pixel system (with BCM removed).
- Install Pixel Luminosity Telescope (PLT).
- Install BSC extension, with possible installation of FSC stations.
- Install ZDC crane.

Very many infrastructure and common systems consolidations will be also be carried out. Perhaps the most critical are in the magnet cryogenic system where it is essential to reduce risks to the magnet availability and lifetime by improving contaminant filtering in the cold box and installing redundant compressors in the surface cryogenic plant.

After this shutdown CMS should be ready for beams at 6.5 TeV, instantaneous luminosity 2-5 x 10^{33} cm^{-2}s^{-1}, bunch-spacing of 25, 50 or 75 ns and integrated luminosity $\sim$ 50 fb^{-1}.

Fig 10.13 illustrates a likely critical sequence for activities on the +z end of the detector during the 2012-13 shutdown, assuming the shutdown starts on 5 Dec 2011. (note that the detailed planning developed from this summary already reaches 250 discrete tasks). The sequence shown is for the +z end. For the -z end, the periods in configurations E and H are interchanged and the period in configuration C is used in priority to install new forward support structures.

10.10.5 Technical stops 2013-14 (if applicable) and 2014-15

Exploiting the flexibility offered by the YE4 push-back system, and assuming no force majeure constraints forcing more extensive opening for maintenance, the current plan assumes the following critical detector activities during these technical stops.

- Install 4^{th} muon endcap station -z (ME4/2, RE4/2, RE4/3) (RE4 removal/re-installation if applicable).

10.10.6 Shutdown 2016

The current plan for detector activities in UXC during 2016 is:

- Remove pixel tracker, BCM and PLT.
- Remove part or all of the beampipe in the region (-18m $<$ z $<$ +18m).
- Re-install beampipe with new central Be section, radius 23-25mm (to be determined).
- Bakeout beampipe (-18m $<$ z $<$ +18m).
- Install 4 layer, low-mass pixel tracker, re-install BCM and PLT.
- Rebuild HB/HE front end +z and -z.

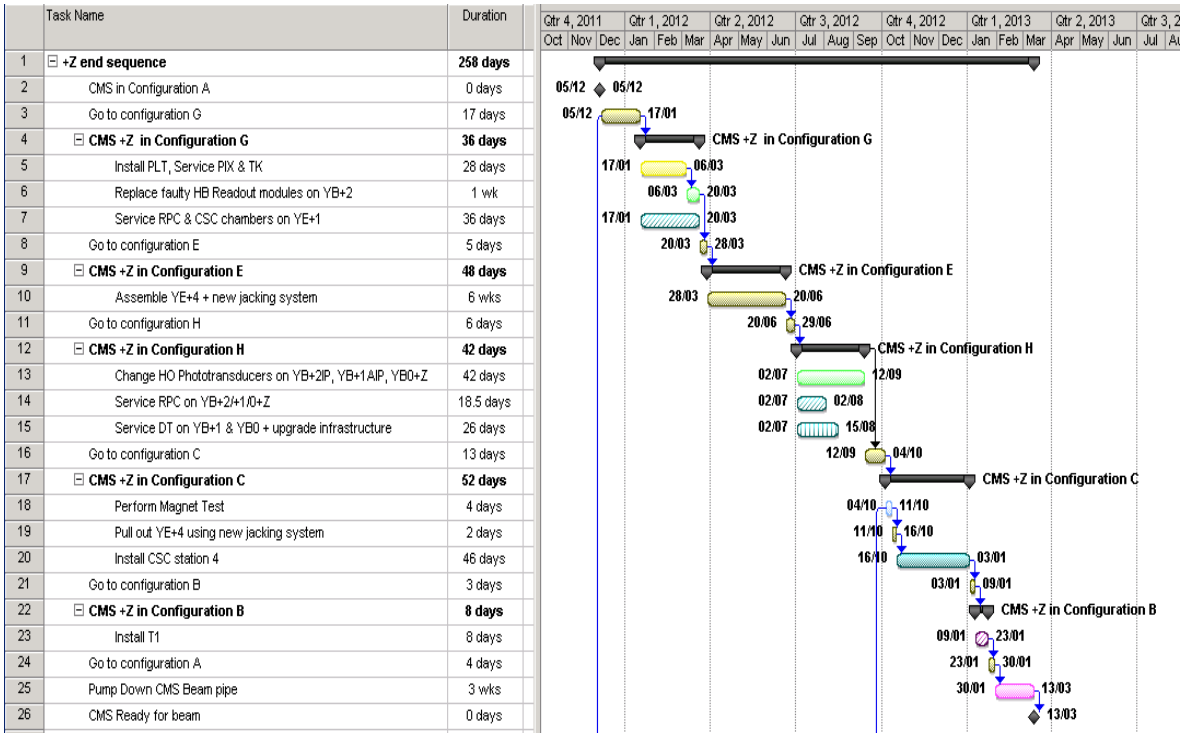

	Task Name	Duration
1	**+Z end sequence**	**258 days**
2	CMS in Configuration A	0 days
3	Go to configuration G	17 days
4	**CMS +Z in Configuration G**	**36 days**
5	Install PLT, Service PIX & TK	28 days
6	Replace faulty HB Readout modules on YB+2	1 wk
7	Service RPC & CSC chambers on YE+1	36 days
8	Go to configuration E	5 days
9	**CMS +Z in Configuration E**	**48 days**
10	Assemble YE+4 + new jacking system	6 wks
11	Go to configuration H	6 days
12	**CMS +Z in Configuration H**	**42 days**
13	Change HO Phototransducers on YB+2lP, YB+1AlP, YB0+Z	42 days
14	Service RPC on YB+2/+1/0+Z	18.5 days
15	Service DT on YB+1 & YB0 + upgrade infrastructure	26 days
16	Go to configuration C	13 days
17	**CMS +Z in Configuration C**	**52 days**
18	Perform Magnet Test	4 days
19	Pull out YE+4 using new jacking system	2 days
20	Install CSC station 4	46 days
21	Go to configuration B	3 days
22	**CMS +Z in Configuration B**	**8 days**
23	Install T1	8 days
24	Go to configuration A	4 days
25	Pump Down CMS Beam pipe	3 wks
26	CMS Ready for beam	0 days

Figure 10.13: Provisional planning for the sequence of major tasks on the +z end of the CMS Detector during the 2012-2013 shutdown.

- Replace ME1/1 endcap muon station readout electronics (both +z and -z) for improved granularity.
- Revise muon barrel front-end electronics.
- Replace BSC with rad hard solution in maintainable location.
- Replace BCM1 and BCM2.

In addition, very substantial modifications to the trigger and readout electronics in the USC are foreseen to prepare for higher luminosity and to address obsolescence issues.

After this shutdown, CMS should be ready for beam energies of 7 TeV, instantaneous luminosity 2 x 10^{34} and integrated luminosity 300 fb^{-1}.

References

[1] C. Collaboration, "The CMS experiment at the CERN LHC", *JINST* **3** (2008) 1–334, arXiv:hep-ph/XXXXXX. doi:10.1088/1748-0221/3/08/S08004.

[2] C. Collaboration, "Upgrade Projects under Development". https://cms-docdb.cern.ch/cgi-bin/DocDB/ShowDocument?docid=3096, November, 2010.

[3] M. Cacciari, G. Salam, and G. Soyez, "FastJet, A Code for fast k_t clustering, and more". hep-ph/0607071. http://www.lpthe.jussieu.fr/~salam/fastjet.

[4] Z. inc, "Web site". http://www.zecotek.com.

[5] H. inc, "Web site". http://www.hamamatsu.com.

[6] C. collaboration, "this is a place holder". http://www-cdf.fnal.gov.

[7] D. Kotlinksi, "Status of the CMS pixel detector", *JINST* **4** (2009) P03019.

[8] A. Dominguez, "The CMS pixel detector", *NIM* **A 581** (2007) 343.

[9] K. Arndt et al., "Silicon sensors development for the CMS pixel system", *NIM* **A 511** (2003) 106.

[10] T. Rohe et al., "Radiation hardness of CMS pixel barrel modules", *NIM* **A612** (2010) 493.

[11] G. Cerati et al., "Radiation tolerance of the CMS forward pixel detector", *NIM* **A 600** (2009) 408.

[12] Y. Allkofer et al., "Design and performance of the silicon sensors for the CMS barrel pixel detector", *Nucl. Instrum. Meth.* **A584** (2008) 25–41, arXiv:physics/0702092. doi:10.1016/j.nima.2007.08.151.

[13] CMS Collaboration , *CMS Physics Analysis Summary TRK-10-005* **TRK-10-005** (2010).

[14] P. Merkel, "Experience with mass production bump bonding with outside vendors in the CMS FPIX project", *NIM* **A 582** (2007) 771.

[15] "Pac Tech Packaging Technologies, Nauen, Germany". http://pactech.de.

[16] W. Erdmann, "Upgrade plans for the CMS pixel barrel detector", *to be published in NIM* **A** (2010).

[17] A. Affolder, P. Allport, and G. Casse, "Studies of charge collection efficiencies of planar silicon detectors after doses up to $10^{15} n_{eq} cm^{-2}$ and the effect of varying diode configurations and substrate types", *NIM* **A 604** (2009) 250–253. doi:10.1016/j.nima.2009.01.072.

[18] "PICMG μTCA website". http://www.picmg.org/v2internal/microTCA.htm.

[19] CMS Collaboration, "CMS: The TriDAS project. Technical design report, Vol. 2: Data acquisition and high-level trigger",. CERN-LHCC-2002-026.

[20] CMS Collaboration, "The CMS Experiment at the CERN LHC", *JINST* **3** (2008) S08004.

[21] CMS Collaboration, "Trigger Study Group: HLT performance",. CMS DP-2010/029.

[22] A. Bell, "Beam & Radiation Monitoring for CMS", in *IEEE Nucl. Sci. Symp. Conf. Rec.*, p. 2322. 2008.

[23] A. MacPherson, "Beam Condition Monitoring and radiation damage concerns of the experiment", in *Proceedings of the XV LHC Project Chamonix Workshop*, p. 198. 2006.

[24] R. Tapper, "Diamond Detectors", *Rep. on Prog. in Phys.* **63** (2000) 8.

[25] D. Chong et al., "Validation of synthetic diamond for a Beam Condition Monitor for the Compact Muon Solenoid Experiment", *IEEE Trans. Nucl. Sci* **54** (2007) 182.

[26] R. Eusebi et al., "A diamond-based Beam Condition Monitor for the CDF experiment", *IEEE TRans. Nucl. Sci* **2** (2006) 709.

[27] M. Brunisma and othes, "CVD diamonds in the BaBar radiation monitoring system", *Nucl. Phys. B* **150** (2006) 164.

[28] W. de Boer et al., "Radiation Hardness of Diamond and Silicon sensors compared.", *Phys. stat. Sol.* **204** (2007) 3004.

[29] L. Fernandez-Hernando et al., "Development of a CVD diamond Beam Condition Monitor for CMS at the Large Hadron Collider", *NIM A* **552** (2005) 183.

[30] B. Dehning et al., "The Beam Loss Monitor System", in *Proceedings of the XIII LHC Project Chamonix Workshop*. 2004.

[31] C. Zamantas, "The real-time data analysis and decision system for particle flux detection in the LHC accelerator at CERN". PhD thesis, Brunel University, 2006. CERN-THESIS-2006-037.

[32] R. Schmidt et al., "Beam interlocks for LHC and SPS", in *Proceedings of International Conference on Accelerator and Large Experimental Physics Control Systems, ICALEPCS, Gyeongju*. 2003.

[33] B. Todd, "A Beam Interlock System for CERN high energy accelerators". PhD thesis, Brunel University, 2007. CERN-THESIS-2007-019.

[34] J. Kaplon and W. Dabrowski, "Fast CMOS Binary Front End for Silicon Strip Detectors at LHC Experiments", *IEEE Trans. Nucl. Sci* **52** (2005) 2713.

[35] J. Troska et al., "Optical readout and control systems for the CMS Tracker", *IEEE Trans. Nucl. Sci* **50** (2003) 1067.

[36] J. Furletova, "Search for exotic processes in events with large missing transverse momentum in ZEUS at HERA". PhD thesis, Hamburg University, 2004. DESY-THESIS-2004-046.

[37] G. Aguillion et al., "Thin scintillating tiles with high light yield for the OPAL endcaps", *NIM A* **417** (1998) 266.

[38] C. Ohm, "Phase and intensity monitoring of the particle beams at the ATLAS experiment". PhD thesis, Linkoeping University, 2007. urn:nbn:se:liu:diva-9614.

[39] C. Pignard and T. Wijnands, "Radiation tolerant commercial of the shelf components for the remote readout of PIN diodes and Radfets", in *Proceedings of the RADECS Conference, Cap d'Agde*. 2005.

[40] T. Wijnands, "Radiation monitoring for equipment in the LHC tunnel", in *EDMS Document 565013*, `https://edms.cern.ch/`. 2005.

[41] S. Mueller, "Design, Commissioning and Performance of the CMS Beam Condition Monitor 2 and Simulation Studies of the Radiation Environment near CMS at LHC". PhD thesis, CERN/Karlsruhe University, 2010.

[42] V. A. Petrov, R. A. Ryutin, and A. E. Sobol, "LHC as πp and $\pi\pi$ Collider", *Eur. Phys. J.* **C65** (2010) 637–647, `arXiv:0906.5309`. `doi:10.1140/epjc/s10052-009-1202-0`.

[43] A. Szczurek, R. Maciula, and R. Pasechnik, "Diffractive exclusive production of heavy quark pairs at high energy proton-proton collisions", `arXiv:1007.1384`.

[44] A. E. Sobol, R. A. Ryutin, V. A. Petrov et al., "Elastic $\pi^+ p$ and $\pi^+\pi^+$ scattering at LHC", `arXiv:1005.2984`.

[45] V. A. Khoze, J. W. Lamsa, R. Orava et al., "Forward Physics at the LHC, Detecting Elastic pp Scattering by Radiative Photons", `arXiv:1007.3721`.

[46] CMS Collaboration, "Status of zero degree calorimeter for CMS experiment", *AIP Conf. Proc.* **867** (2006) 258–265, `arXiv:nucl-ex/0608052`. `doi:10.1063/1.2396962`.

[47] M. Raymond and G. Hall, "CMS microstrip tracker readout at the SLHC", in *Topical Workshop on Electronics for Particle Physicists*, p. 345. Naxos, 2008.

[48] P. Moreira et al., "The GBT, a proposed architecture for multi-Gbps data transmission in high energy physics", in *Topical Workshop on Electronics for Particle Physicists*, p. 71. Prague, 2007.

[49] L. Amaral et al., "The versatile link, a common project for super-LHC", *JINST* **4** (2009) P12003.

[50] B. Allongue et al., "Custom DC-DC converters for distributing power in SLHC trackers", in *Topical Workshop on Electronics for Particle Physicists*, p. 289. Naxos, 2008.

[51] CMS Tracker Collaboration, K. Klein et al., "System tests with DC-DC converters for the CMS silicon strip tracker at SLHC", in *Topical Workshop on Electronics for Particle Physicists*, p. 294. Naxos, 2008.

[52] M. Huhtinen, P. Lecomte, D. Luckey et al., "High-energy proton induced damage in $PbWO_4$ calorimeter crystals", *Nucl. Instr. and Meth.* **A 545** (2005) 63–87.

[53] P. Lecomte, D. Luckey, F. Nessi-Tedaldi et al., "High-energy proton damage study of scintillation light output from $PbWO_4$ calorimeter crystals", *Nucl. Instr. and Meth.* **A 564** (2006) 164 – 168.

[54] D. Renker, P. Lecomte, D. Luckey et al., "Comparison between high-energy proton and charged pion induced damage in $PbWO_4$ calorimeter crystals", *Nucl. Instr. and Meth.* **A 587** (2008) 266 – 271.

[55] CMS Collaboration, "The CMS Electromagnetic Calorimeter Project - Technical Design Report", *CMS TDR 4, CERN/LHCC* **97-33** (1997).

[56] F. Nessi-Tedaldi, "A parameterization of the anticipated evolution with delivered luminosity of the contribution to the CMS ECAL energy resolution from hadron damage to crystals", *ETHZ-IPP-2010-05* (2010).

[57] G. Dissertori, P. Lecomte, D. Luckey et al., "A study of high-energy proton induced damage in Cerium Fluoride in comparison with measurements in Lead Tungstate calorimeter crystals", *Nucl. Instr. and Meth.* **A 622** (2010) 41 – 48.

Appendix A

High Precision Spectrometer

A.1 Introduction

The goal of the High Precision Spectrometer (HPS) is to measure inelastic proton interactions at the LHC where one or both protons survive the collision. Such processes can take place when the interaction is mediated by the exchange of two colour-singlet objects such as "Pomerons" (two gluons in a colour-singlet state) and/or two photons. Although forward (anti)proton detectors have been used to study Standard Model (SM) physics in hadronic collisions for a couple of decades [**?**], the benefits of using proton detectors to search for New Physics at the LHC have only been fully appreciated within the last few years [**? ? ? ? ? ?**]. By detecting both outgoing protons that have lost a few per cent of their longitudinal momentum [**?**], in conjunction with a measurement of the associated centrally produced system using the current CMS detector, a rich programme of studies in QCD, electroweak, Higgs and Beyond the Standard Model physics becomes accessible, with the potential to make unique measurements at the LHC. A prime process of interest is Central Exclusive Production (CEP), $pp \rightarrow p + \phi + p$, in which the outgoing protons remain intact and the central system ϕ may be a single particle such as a Higgs boson. The measurement of the proton momenta can be used to determine the mass of the central system by means of the missing mass method.

The proposed High Precision Spectrometer (HPS) is a magnetic spectrometer which uses the LHC magnets between the interaction point and detector stations at $\pm$240 m and $\pm$420 m to bend protons that have lost a small fraction of their initial momentum out of the beam envelope. The detector stations consist of a silicon tracking system that can be moved transversely and measures the spatial position of these protons relative to the LHC beam line, as well as their arrival times. At 240 m the beampipes are in air and no modification of the beam-line is required, whereas at 420 m a new connection cryostat is required.

The HPS project started in 2005 within the joint ATLAS+CMS FP420 R&D project, which studied the feasibility of installing and operating spectrometers based on silicon trackers and fast-timing detectors in the LHC tunnel at about $\pm$420 m from the ATLAS and CMS interaction points. The joint FP420 R&D culminated with the publication of a report illustrating the feasibility of the project [**?**] and aiming at the independent installation of separate very-forward spectrometers at ATLAS and CMS. For the preparation of that report the support received from the accelerator (AB and AT) and technical (TS) departments of CERN was crucial. One of the key new aspects of the HPS proposal presented here with respect to [**?**] is that, in addition to stations at $\pm$420 m (HPS420), stations at $\pm$240 m (HPS240) are also proposed. Two major installation stages are thus foreseen:

1. "Stage One", with four prototype stations at $\pm$240 m, two on each side of IP5. Each station

would consist of a moving-pipe system equipped with a simple pixel tracker, and a fast timing detector (providing also the L1 trigger signal).

2. A second stage, referred to as "Stage Two", would consist of the installation of two detector stations at $\pm$420 m on each side of the CMS interaction point and of four stations at $\pm$240 m, two on each side.

Such a system has the following major technical aspects:

- Location: The areas at $\pm$240 m from the CMS interaction point are warm and empty LHC regions with just two bare LHC beam pipes over a distance of more than 12 m. Inspections as well as initial consultation with the LHC experts confirmed that nothing prevents installation of detectors there.

  In order to detect both outgoing protons at $\pm$420 m, detectors must be installed close to the outgoing beams in the high-dispersion region. The proposed instrumentation of the 420 m region entails the replacement of the existing 14 m long connection cryostat with a warm beam pipe section and a cryogenic bypass. To this purpose, a new connection cryostat (NCC) has been designed, based on a modified arc termination module, in order to minimize the impact on the machine.

- Tracking: The LHC magnets between the interaction points and the 240/420 m regions bend protons which have lost a small fraction of their initial momentum out of the beam envelope. The detector system is hence a magnetic spectrometer consisting of tracking devices, placed between the two LHC beam pipes. A measurement of the displacement and angle of the outgoing protons relative to the beam at several points in a $\sim$10 m region allows the momentum loss and transverse momentum of the scattered protons to be reconstructed. This in turn allows the mass of the centrally produced system to be reconstructed, irrespective of its decay modes.

  To obtain the desired resolution of around 2 GeV/c^2 on the mass of the centrally produced system, a spatial precision of $\sim$10 μm and an angular precision of 1 μrad are needed. To maximize acceptance for low momentum-loss protons, the detectors at 420 m must operate at distances between 4 mm and 7 mm from the beam centre over a region 20 mm wide, and be active as close to their physical edge as possible. This also poses a challenge in terms of radiation hardness. 3D silicon technology [**?**] has been chosen as the baseline detector technology best equipped to meet these requirements.

- Moving pipe: Because the detectors should be parked at a large distance from the beams during injection, acceleration and luminosity tuning, but must operate close to the beam centre during data taking, they must be moveable. Due to space constraints (the nominal distance between the pipes is 194 mm), the Roman pot technique cannot be used and an alternative solution for near-beam detectors, pioneered at DESY, has been chosen. The technique, referred to as "Hamburg pipe", consists of moving sections of beam pipe with integrated detectors. The motors and controls would be identical to those used for the LHC collimation system.

- Timing/Vertexing: The detector system must be able to operate up to the highest LHC instantaneous luminosities around 2×10^{34}cm^{-2}s^{-1} with about 20–40 inelastic interactions per bunch crossing. These overlap events can fake central exclusive production when a central event is combined with fast outgoing protons from other interactions in the same bunch crossing. There are various kinematic and topological constraints which can be used to suppress such a background offline. In addition, a measurement of the difference in the arrival times of the two protons at 420 m or

240 m with resolution in the 10 ps range allows for matching of the detected protons with a central vertex within 2 mm, which will enable the suppression of the residual overlap background, reducing it to a manageable level. In the case of 240 m, a trigger signal can be also included within the CMS L1 latency.

Two types of time of flight (ToF) counters are proposed, GASTOF (Gas Time Of Flight) and QUARTIC (QUARtz TIming Cherenkov). The former are gas Cherenkov detectors of about 15 cm length producing extremely fast light pulses, of a couple of picoseconds duration. These counters will be integrated in dedicated pockets along the Hamburg pipe. Both can be used as they have complementary features, and the combined measurement will be better than either; GASTOF is low-mass and can be in front of the final tracking station; QUARTIC has more mass and will be at the back. An essential component of the ToF system is a reference time signal without significant jitter and skew between the timing detectors located at the two different sides of the interaction point, separated by 240+240 m (420+420 m).

These technical issues are discussed in more detail in the sections to follow. We stress that for the Stage One HPS240 detectors already existing technologies will be used. The 240 m region is clearly less demanding from an engineering perspective than the 420 m one since a cryogenic bypass is not required and the moving pipes developed within the FP420 project can be integrated into the LHC collimator control system. The prototypes of fast timing detectors studied at various test beam in 2009 and 2010 could directly be modified for operation in Stage One. The timing readout electronics can be built using the CERN HPTDC chips of the muon system, or alternatively, using the commercially available PCI cards with picosecond resolution TDC channels. Finally, first simple tracking systems for Stage One could be built using the PSI-46 chips [**?**], about 300 m long optical links and pixels FEDs.

A.2 The physics case for forward proton tagging at the LHC

The HPS forward proton tagging capability can enhance the ability of the CMS detector to carry out the primary physics program of the LHC in various sectors and extensions of the Standard Model. In Stage One, this includes QCD in the diffractive, central-exclusive and photon-proton channels, as well as electroweak physics in two-photon interactions. In Stage Two, a prime motivation will be the measurement of the mass and quantum numbers of the Higgs boson, should it be discovered via traditional searches, and augmenting the discovery reach if nature favours certain plausible beyond SM scenarios, such as its minimal supersymmetric extension (MSSM).

By central exclusive production we refer to the process $pp \to p + \phi + p$, where the '+' signs denote the absence of hadronic activity (that is, the presence of a rapidity gap) between the outgoing protons and the decay products of the central system ϕ. The final state therefore consists *solely* of the two outgoing protons, which we intend to detect in the spectrometer, and the decay products of the central system which will be detected in the central CMS detectors. We note that gaps will not typically be part of the experimental signature due to the presence of minimum bias pile-up events, which fill in the gap but do not affect our ability to detect the outgoing protons. The main physics motivation is the production and study of Higgs bosons, but there is also a rich and more exotic physics menu that includes the production of many kinds of supersymmetric particles, other exotica, and indeed any new object which has 0^{++} (or 2^{++}) quantum numbers and couples strongly to gluons [**? ?**] or to photons [**?**]. The CEP process is illustrated for Higgs boson production in Fig. A.1 (left). The Higgs boson is produced as usual through gluon-gluon fusion, while another colour-cancelling gluon is exchanged, and

no other particles are produced.

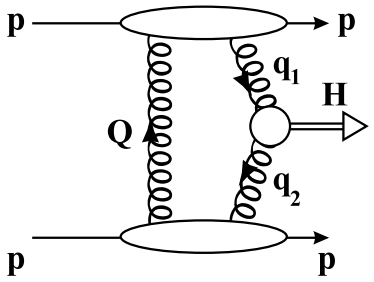

Figure A.1: Sketches of the relevant diagrams accessible to study with HPS: (a) Central Exclusive Production (CEP), $pp \to p + H + p$. (b) Exclusive photon-photon production, $pp \to \gamma\gamma \to p + X + p$. (c) Photon-proton production, $pp \to \gamma p \to p + X + Y$.

There are three important reasons why CEP is especially attractive for studies of new heavy objects. Firstly, if the outgoing protons remain intact and scatter through small angles then, to a very good approximation, the primary active di-gluon system obeys a $J_z = 0$, C-even, P-even, selection rule [**?**]. Here J_z is the projection of the total angular momentum along the proton beam axis. This selection rule readily permits a clean determination of the quantum numbers of any new resonance, which is predominantly 0^{++} in CEP. Secondly, because the process is exclusive, the energy loss of the outgoing protons is directly related to the invariant mass of the central system, allowing an excellent mass measurement irrespective of the decay mode of the central system. Even final states containing jets and/or one or more neutrinos can be measured with $\sigma_M \sim 2$ GeV/c^2. Thirdly, in many topical cases and in particular for Higgs boson production, a signal-to-background ratio of order 1 or better is achievable [**? ? ? ? ?**]. This ratio becomes significantly larger for Higgs bosons in certain regions of MSSM parameter space [**? ? ? ?**].

There is also a broad, high-rate QCD and electro-weak physics program; by tagging both of the outgoing protons, the LHC is effectively turned into a gluon-gluon, photon-proton and photon-photon collider [**? ?**]. Relevant diagrams can be seen in Fig. A.1. In the QCD sector, detailed studies of diffractive scattering, skewed, unintegrated gluon densities and the rapidity gap survival probability [**? ? ? ? ?**] can be carried out. In addition, CEP would provide a source of practically pure gluon jets, turning the LHC into a 'gluon factory' [**?**] and providing a unique laboratory in which to study the detailed properties of gluon jets, especially in comparison with quark jets. Forward proton tagging also provides, in particular, unique capabilities to study photon-photon and photon-proton interactions at centre-of-mass energies never reached before. Anomalous top production, anomalous gauge boson couplings, exclusive dilepton production, or quarkonia photoproduction, to name a few, can be studied in the clean environment of photon-induced collisions [**?**]. We discuss next succinctly the physics reach on these topics for each one of the two stages of operation of the HPS detector.

Physics for Stage One:

The full physics program outlined above will become accessible only with Stage Two but the initial Stage One will however allow one to start investigating central exclusive production in the high mass region above 200 GeV/c^2, as well as to learn about rates, backgrounds and operational aspects for the detectors. The mass ranges given are for 7 TeV beams, and scale with beam energy. Detectors at 240 m allow one to access various interesting and unique physics measurements:

- tagging, at low event pile-up, of single diffraction and high-mass photo-production;
- high energy two-photon exclusive production (the 240 m detectors accept about 50% of the events with invariant mass larger than 200 GeV/c^2, and more than 80% at around 400 GeV/c^2);
- the SM process $\gamma\gamma \to W^+W^-$, with the possibility to study quartic gauge-couplings as well as to study deviations from the expected $\gamma\gamma$ mass spectrum due to possible new BSM particles [**?**];
- the masses of the lightest-supersymmetric-partner (LSP) and light charged slepton pairs produced via exclusive photon-photon production [**?**];

In addition, the detectors at 240 m can be operated when ion beams are stored. This would allow some pioneering measurements of leading proton production in ion collisions [**?**] as well as interesting studies of ultra-peripheral ion collisions at the LHC [**?**]. Higgs production in two-photon processes has also been also proposed in proton-nucleus collisions [**?**]. The addition of HPS would allow one to measure the outgoing forward proton, improving the feasibility of the measurement.

Physics for Stage Two:

A major potential contribution of proton taggers to the CMS program is the possibility to exploit the $b\bar{b}$ decay channel of the Higgs particle, which is not available to standard Higgs searches due to overwhelming backgrounds. The combination of the suppression of the $b\bar{b}$ background, due to the $J_z = 0$ selection rule, and the superior mass resolution of the foreseen detectors opens up the possibility of exploiting this high branching ratio channel. Although the penalty for demanding two forward protons makes the discovery of a Standard Model Higgs boson in the $b\bar{b}$ channel unlikely despite a reasonable signal-to-background ratio, the cross section enhancements in other scenarios indicate that this could be a discovery channel. For example, it has recently been shown that the heavy CP-even MSSM Higgs boson, H, could be detected over a large region of the $M_A - \tan\beta$ plane; for $M_A \sim 140$ GeV/c^2, discovery of H should be possible for all values of $\tan\beta$. The 5σ discovery reach extends beyond $M_A = 200$ GeV/c^2 for $\tan\beta > 30$ [**? ? ?**].

In addition, for certain MSSM scenarios, proton taggers provides an opportunity for a detailed lineshape analysis [**? ?**]. In the NMSSM, the complex decay chain $h \to aa \to 4\tau$ becomes viable in CEP, and even offers the possibility to measure the mass of the pseudoscalar Higgs boson [**?**]. Another attractive feature of the proposed programme is the ability to probe the CP-structure of the Higgs sector either by measuring directly the azimuthal asymmetry of the outgoing tagged protons [**?**] or by studying the correlations between the decay products [**?**].

A.3 LHC Optics and detector acceptance

The configuration of the LHC beamline around the interaction points is shown schematically in Fig. A.2. The proposed forward detector stations are to be installed in the regions located at approximately 240 m and 420 m from the IP5 interaction point in both beamlines downstream of the central detector. Here protons that have lost energy in the primary interaction are able to emerge from the beamline. The acceptance and the ultimately achievable experimental resolution of the forward detectors depends on the LHC beam optics and on the position of the detectors relative to the beam.

The FP420 Collaboration has written two independent proton tracking programs, FPTrack [**?**]

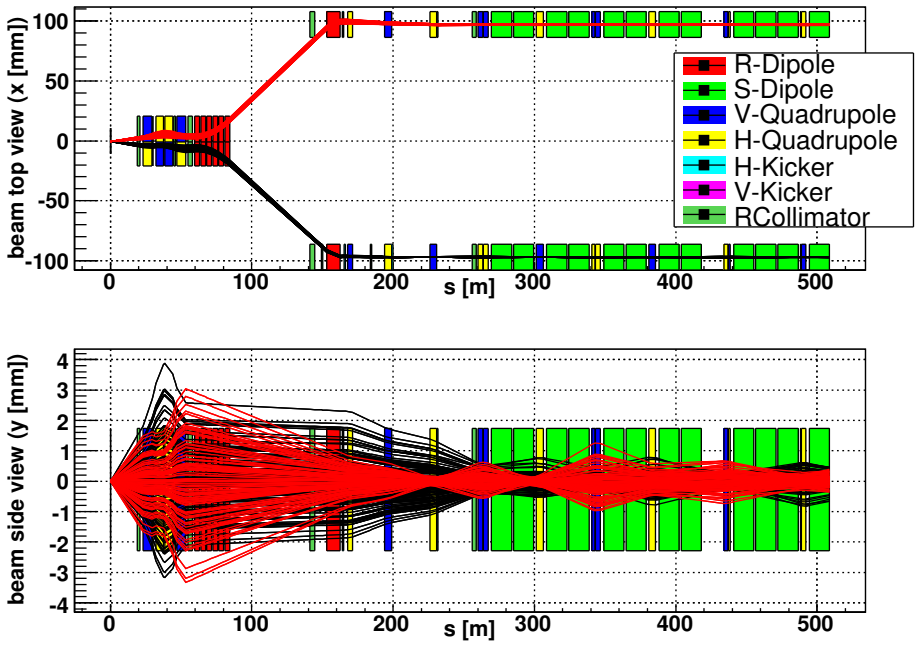

Figure A.2: Schematic plan view and side view of the beamline at IP5; the horizontal curvature of the beamline has been straighted out for purposes of simplification here.

and HECTOR [**?**], and implemented a model of the LHC beamline into the package BDSIM [**?**] in order to simulate machine-induced backgrounds (see Section A.4). The three simulations, FPTrack, HECTOR and BDSIM are in good agreement with each other and with MAD-X, the standard LHC beam transport program used at CERN. All the programs perform aperture checks through each of the LHC optical elements.

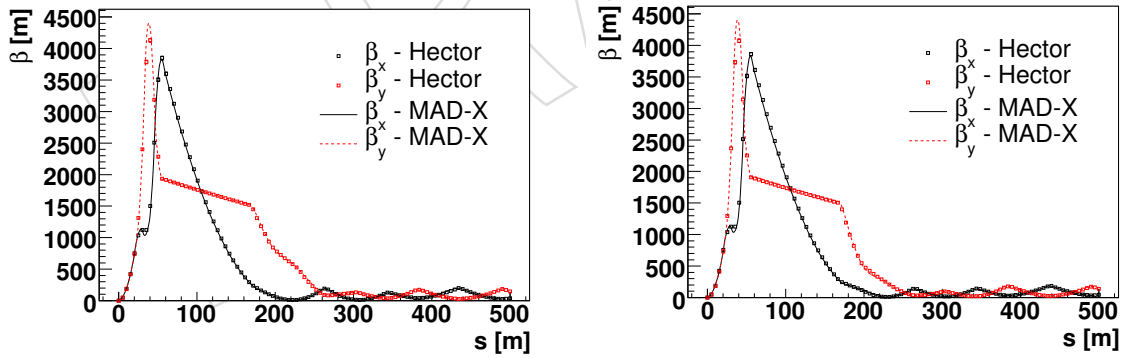

Figure A.3: Beta functions β_x (horizontal) and β_y (vertical) for LHC beam 1 (left) and beam 2 (right) calculated by MAD-X (lines) and HECTOR (squares).

The position and direction of a proton in the 240 m and 420 m detectors (for a given LHC optics) depend on the energy and scattering angle of the outgoing proton and the z-vertex position of the collision. The energy and scattering angle are directly related to the kinematic variables ξ, the fractional longitudinal momentum loss of the outgoing proton, and $-t$, the square of the four-momentum transfer.

The ExHuME Monte Carlo [**?**] was used to generate outgoing protons from the central exclusive production of a SM Higgs boson, although the results apply for any centrally-produced

system of the same mass. FPTrack follows the trajectory of the protons using version 6.500 of the LHC optics files with: $\beta^* = 0.55$ m; angular divergence $\sigma_\theta = 30.2$ μrad at the IP; crossing angle = 142.5 μrad in the horizontal plane; beam energy spread $\sigma_E = 0.77$ GeV. Full details can be found in [**?**]. The energy spread of the 7000 GeV beam is an irreducible limiting factor on the mass resolution that can be obtained by proton tagging detectors at the LHC. Figure A.4 shows the corresponding acceptance in the ξ-t plane for the 240 m and 420 m regions for beam 1 and beam 2 respectively, around IP5.

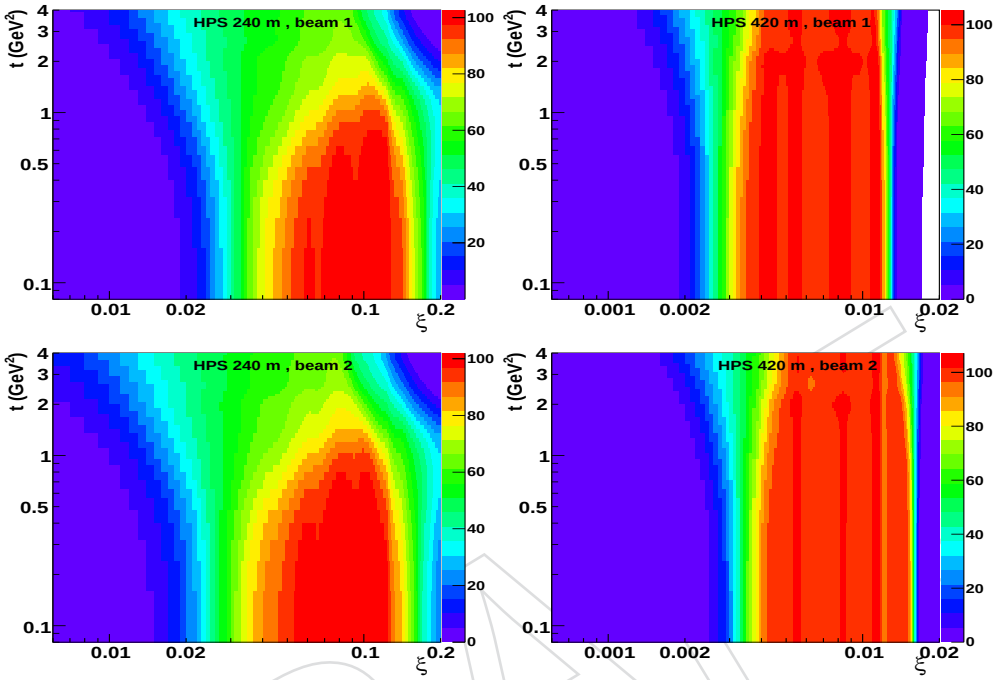

Figure A.4: Acceptances in ξ (fractional energy loss) versus t (squared-momentum transfer) for protons to reach planes at 240 m (left) and 420 m (right) for beam-1 (top) and beam-2 (bottom) around IP5, computed with FPtrack. No detector effects are included here.

In Figure A.5 we show the global features of the acceptance for central systems produced in CEP and photon-photon interactions, where the central system is required to be produced within rapidities $|y| < 2$. Roughly speaking, 420+420 accepts exclusive systems with masses in the 50–150 GeV/c^2 range, 420+240 in the 200–500 GeV/c^2 domain, and 240+240 above 400 GeV/c^2. For central masses above 150 GeV/c^2 or so, the combination of 240+420m detectors becomes necessary. Clearly, acceptance for new heavy particles requires 240-m stations. In general, both stations have larger acceptance for central systems in photon-photon than in CEP interactions. The CEP plot (left) has been obtained with Silicon distances at 5 mm for 420 m and 3 mm at 240 m (there is an extra "dead" interval of 0.8 mm inside these values to allow for some dead inner edge region). Operating at 2.5 mm (dashed lines in the plot) increases somewhat the acceptance for measurements involving the 240 m but not 420 m detectors. The photon-photon plot (right) corresponds to 420 m detectors operating at 5 mm and 240 m detectors at 2.5 mm from the nominal beam position.

A.4 Machine induced backgrounds

The machine-induced background contributions at 240 m are very similar to those measured by the TOTEM Roman Pots at 220 m, with real data during the 2010 proton-proton run. The LHC provides extremely clean beams at this position with very small single-station contributions

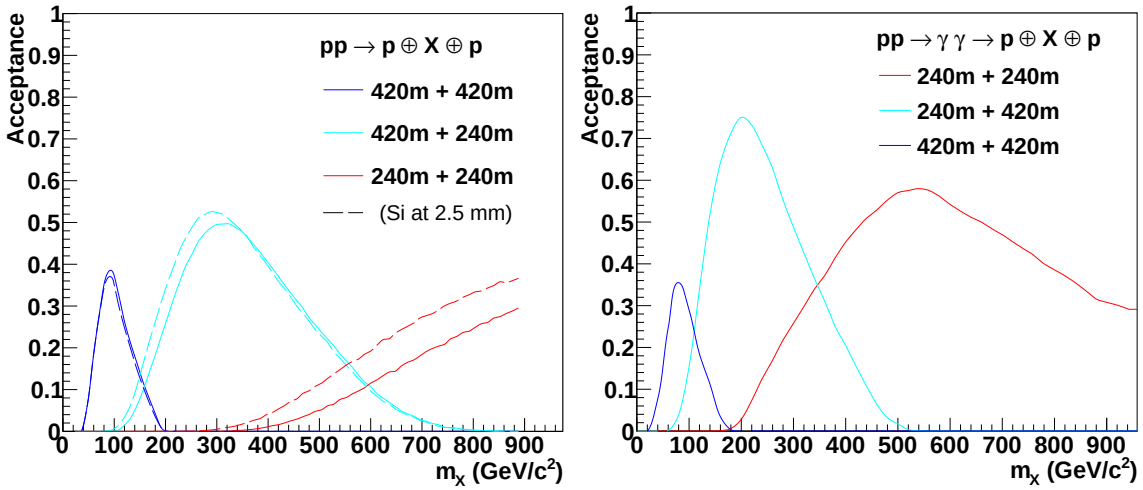

Figure A.5: Acceptances as a function of centrally produced mass for CEP (left, computed with the ExHume MC and the FPtrack beam transport code) and photon-photon (right, computed with MadGraph and the HECTOR proton transport program) processes, for HPS detectors at 240+240 m, 420+420 m, and combined 240+420 m. No detector effects are included here.

from beam halo and beam-gas collisions, as well as from interactions with the collimators and proton losses [**?**].

At 420 m, the background contributions from near beam-gas and the betatron cleaning collimation is expected to be small, due to the arguments given in [**?**]. However, there is a contribution to the background rate arising from far beam-gas, the momentum cleaning collimators and proton loss in the beamline. The first two of these contributions give a proton background which is described by a peak determined by the momentum cleaning collimator settings, and a tail dominated by far beam-gas halo protons. The combined distribution is shown in Fig. A.6. At detectors transverse distance of 5 mm or greater, the expected integrated number of protons from beam halo is expected to be less than 1 per bunch crossing. The proton loss background contribution is a mixture of charged and neutral particles produced immediately upstream of 420 m. The BDSIM estimate of the neutron rate is 0.11 neutrons per bunch crossing at 420 m.

A.5 Hamburg beam-pipe

The technique of moving sections of the beam-pipe with integrated detectors is known as "Hamburg pipes" and was developed within the ZEUS collaboration in 1994 to measure very forward-scattered electrons as a signature of photoproduction [**?**]. The concept was inspired by the moving pipes used in the PETRA wiggler line to allow for beam-line aperture changes. The ZEUS version involved small electromagnetic calorimeters attached to the moving pipe (44 m from the interaction point). The detectors were retracted during beam injection, but could be positioned close to the beam axis during stable beam conditions, and thus measure scattered electrons with reduced energy, which exited the pipe through special thin windows. Since the detectors were located outside of the machine vacuum, they could be easily maintained and were successfully and routinely used for six years, providing data essential for several publications [**? ? ?**]. The detectors were positioned remotely by the HERA shift crew, which inserted the detectors at the working position, typically about 15 mm from the coasting electron beam, using the HERA slow control system.

Prior to installation at HERA, the Hamburg pipe system was tested by making several thou-

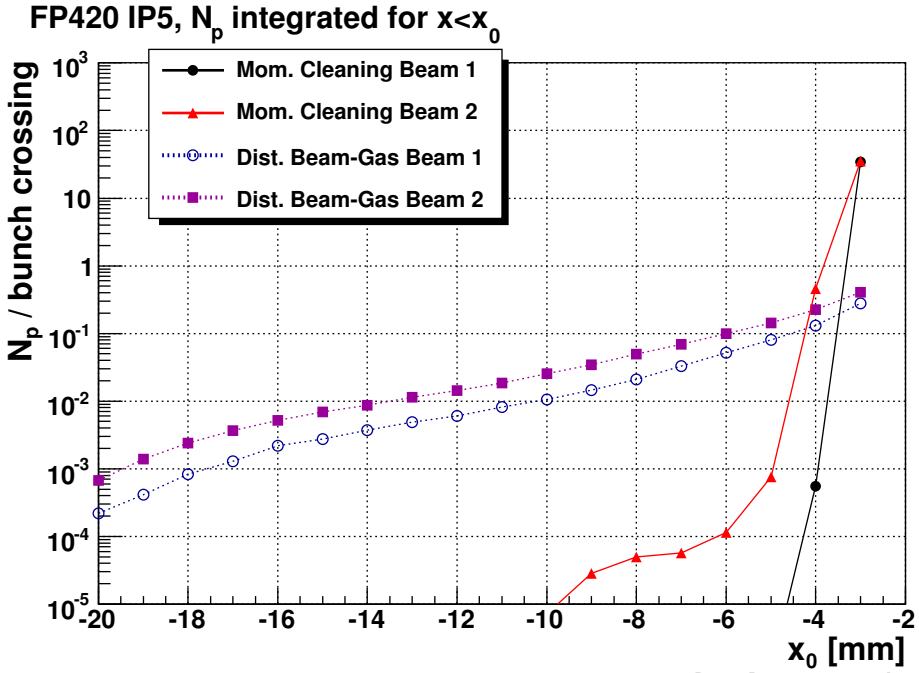

Figure A.6: Total amount of beam halo protons predicted at the 420 m regions for different detector horizontal positions.

sand displacement operations. No significant radio-frequency (RF) effects on the electron beam were observed due to the modified beam-pipe geometry. It should be noted that no special RF screening was used; it was sufficient to have the so-called RF fingers providing good electrical contact across the connecting bellows.

The moving pipe technique has many advantages with respect to the Roman Pot (RP) design. It allows much simpler access to detectors and provides direct mechanical and optical control of the actual detector positions. In addition, unlike the RP case which involves forces from pressure differences as the detectors are inserted into the vacuum, the Hamburg pipe maintains a fixed vacuum volume. This results in much less mechanical stress, consequently allowing a very simple and robust design.

A.5.0.1 Stage One moving pipe

The moving pipe design for Stage One is driven by the wish of maximal robustness, safety and simplicity. Each station will consist of one 30 cm long pocket, common for the tracking and timing detectors. There will be one detector box, providing secondary vacuum, with a lid giving access, and feed-throughs. The moving pipe support tables and interfaces to the LHC beam-lines will be designed in such a way as to allow for using bigger, more complex detectors in Stage Two. In particular, use of two pockets in one station, and installation of the moving BPMs will be possible.

A.5.0.2 Stage Two moving pipe

A modified connection cryostat (Section A.10) has been designed with approximately eight meter long warm beam-pipes, providing adequate lateral space to install the HPS detectors. Figure A.7 shows the layout of the connection cryostat including two detector stations and the support table. The entire detector arm is fixed on the support table, which is attached to the

tunnel floor, independent of the cryostat. Both ends of the detector arm are equipped with vacuum pumping and control stations and isolation valves. Figure A.8 shows one of the two detector stations equipped with timing and silicon detectors, a LVDT (Linear Variable Differential Transformer) for position measurement and one moving and one fixed beam position monitor (BPM). The support table and motion system are shown in Fig. A.9.

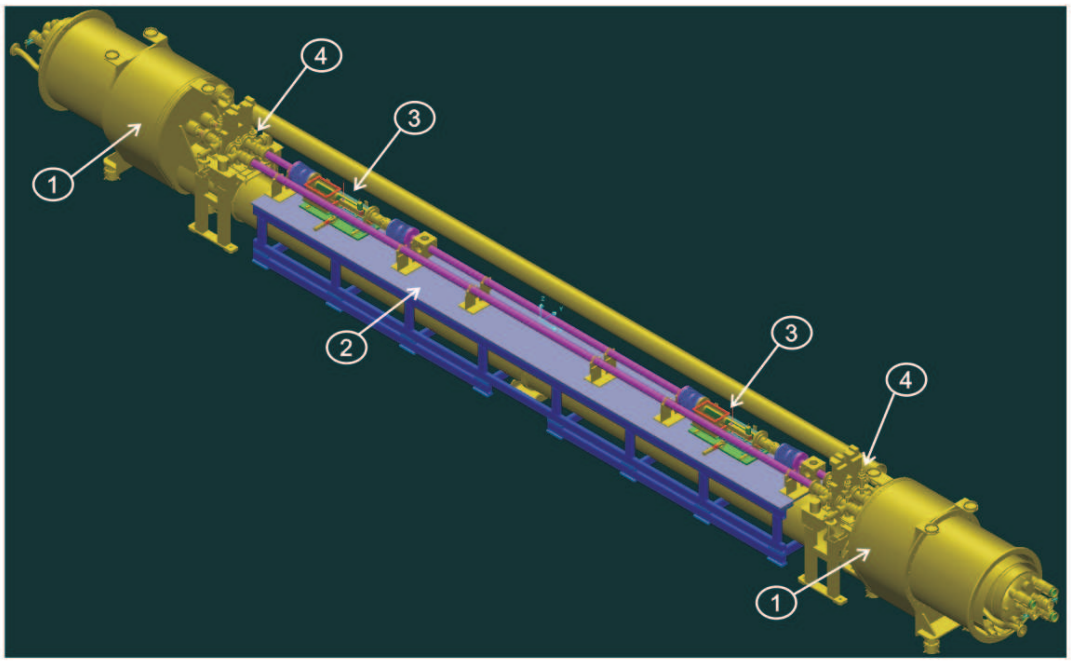

Figure A.7: Schematic view of the connection cryostat (1) and detector arm with support table (2), two detector sections (3) and vacuum pumping sections (4).

The basic dimensions of the stations are defined by the LHC standard beam-pipe diameter, the required lateral detector translation, and by the longitudinal dimensions of the detectors. Each station is composed of a beam-pipe with inner diameter of 68.9 mm, wall thickness of 3.6 mm and a length of about 1000 mm, fixed on a motorised drive. Rectangular thin-walled pockets are built into the pipe to house the different detectors that must be positioned close to the beam. The displacement between data taking position and the retracted or parked position is about 25 mm. The ends of the moving beam-pipes are connected to the fixed beam-pipes by a set of two bellows. Inside, these may be equipped with moving RF-contacts to assure electrical continuity. In general, this design allows significant flexibility in the configuration of the detectors stations, allowing optimization of the detector operation, scattered proton detection, kinematical reconstruction, and alignment.

A number of tests were performed on the detector pocket fabrication and welding techniques to a beam pipe. The best results were achieved for the pockets produced by electro-erosion and then laser welded. A high quality prototype was produced, ready for the next system and integration tests in laboratory and at test beams. Exploratory studies were carried out of production by electro-erosion of beam-pipes in one piece, without need of the pocket welding. This has been suggested as a next, very promising step in the development of the final HPS prototype.

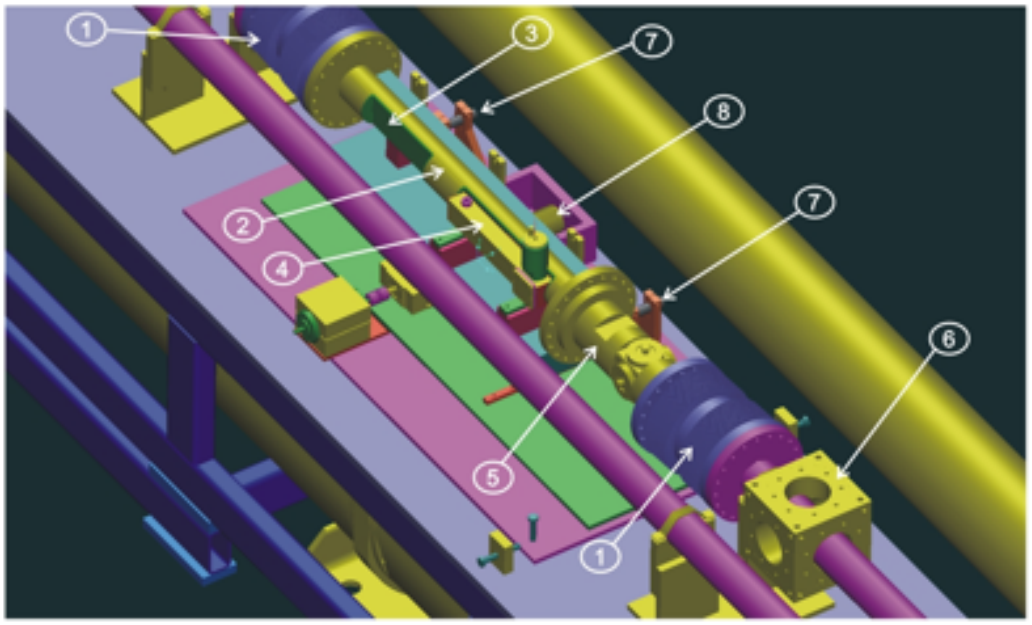

Figure A.8: Top view of one detector section: bellows (1), moving pipe (2), Si-detector pocket (3), timing detector (4), moving BPM (5), fixed BPM (6), LVDT position measurement system (7), emergency spring system (8).

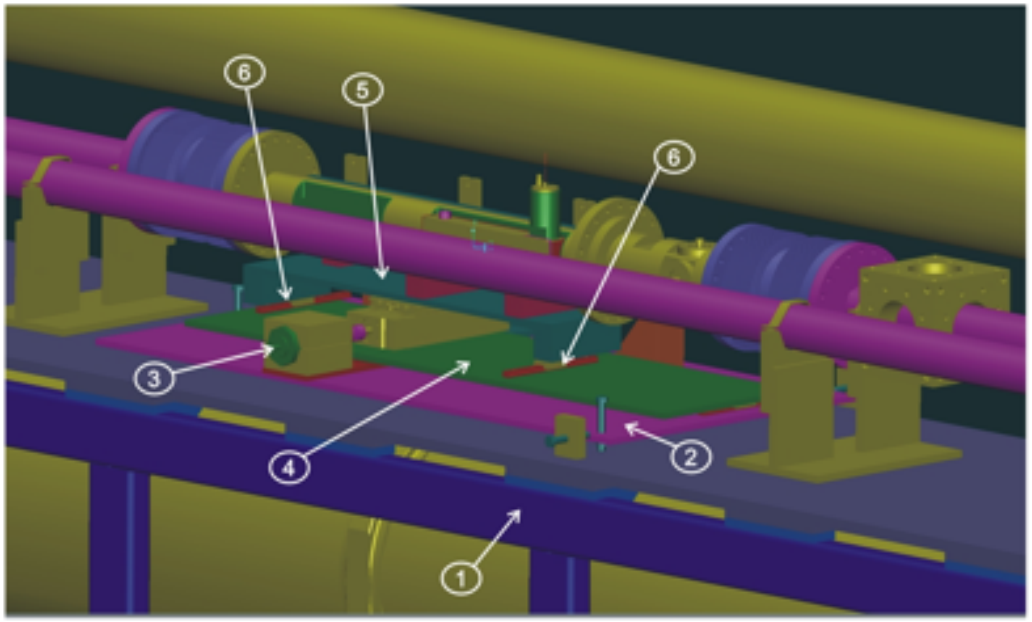

Figure A.9: Support table (1), drive support table with alignment system (2), drive motor (3), intermediate table for emergency withdrawal (4), moving support table (5), and linear guides (6).

A.6 RF impact

The single pocket geometry has been characterised in terms of coupling impedance. Numerical simulations, analytical calculations and laboratory measurements showed consistent results, all indicating that this design will have a small impact on the total LHC impedance budget.

Tapering of the beam pipe indentations is recommended because it does reduce the impedance significantly, as measured both with the single pocket and double pocket designs. Since an effective tapering can be done outside the beam orbit region (i.e. above and below the 500 μm thin window), this design modification can be implemented at no cost in terms of the forward proton signal to background ratio. With a double pocket station design, the beam pipe section between the two pockets can also be electrically connected outside the beam orbit region, in order to provide a good RF contact and minimise the effect of beam pipe cross section variation. This could not be tested in the laboratory, due to the difficulty of accessing the region after beam pipe fabrication. Simulations and laboratory measurements of a new prototype, modified according to the RF studies completed so far, will be continued.

The resulting effective longitudinal impedance follows from the convolution of the results presented here with the LHC beam spectrum. The beam harmonics at 2 GHz are expected to be below 10^{-2} of the main harmonic at 40 MHz and well below 10^{-3} at 2.5 GHz. This provides a further indication of the expected minimal impact of a HPS station on the LHC impedance. One of the consequences is that, according to the available analytical models, the horizontal tune shift induced by a station is expected to be almost imperceptible when compared to the tune stability region defined by the available LHC octupoles magnets.

In addition, the worst case considered in these studies refers to the positioning of a station at 3 mm from the circulating beam, whereas recent acceptance (Section A.3) and background (Section A.4) calculations indicate that 5 mm is a more likely distance of closest approach. This implies that the results are conservative in terms of disturbances to the beam. Further studies are ongoing in order to determine the characteristic loss factor, which will provide an estimate of the power dissipated due to electromagnetic coupling.

A.7 Silicon tracking detectors

A.7.1 Stage One detectors

The tracking detectors in Stage One will be based on the (barrel) pixel detectors. Each station will consist of four or five planes, where each 8 mm $\times$ 32 mm plane is readout by four PSI46 ROCs. Each tracker station will be enclosed in a box with secondary vacuum, and will be cooled by Peltier elements. The corresponding DAQ system will be just another branch of the present pixel DAQ system, with about 300 m optical links, in place of about 100 m long fibers in use now.

A.7.2 Stage Two detectors

In order to detect at 420 m from the IP protons from the production of central systems of masses $\sim$ 100 GeV/c^2, the detector edge has to approach the beam axis to a minimum distance of 5 mm. This represents a challenge for the radiation hardness and radio-frequency pick-up in the detector and the nearby front-end electronics, as described in Sections A.4 and A.6. The detector system has to be robust, and for satisfactory control of systematic uncertainties its position has to be aligned and maintained to a positional accuracy of 10 μm in order to achieve the required track angular precision of 1μrad.

With a typical LHC beam size at 420 m of $\sigma_{beam} \approx 300$ μm, the window surface of the Hamburg pipe can theoretically safely approach the beam to $15 \times \sigma_{beam} \approx 4.5$ mm. However, this distance will ultimately be determined by the LHC collimator settings, since for beam 2 in particular the halo can extend to $\sim$ 5 mm with the nominal collimator positions. The window itself adds another 0.2 mm to the minimum possible distance of the detectors from the beam. To maximise the acceptance for low momentum-loss protons, the detectors should therefore be active as close to their physical edge as possible. In general, planar silicon detectors have a wide (0.25 mm – 1 mm) insensitive border region around the sensitive area which is occupied by a sequence of guard rings. This ring structure controls the potential distribution between the detectors sensitive area and the cut edge to remove leakage current. Planar silicon detectors designed for a heavy radiation environment or generally for operation at high bias voltages, contain multi-ring structures with typically about $\sim$20 rings.

The key requirements for the HPS tracking system are

- To track efficiently as close as possible to the sensor's physical edge.
- To have extreme radiation hardness. A design figure equivalent to or better than the vertex systems used for ATLAS or CMS will be required, i.e. better than 10^{15} 1-MeV equivalent neutrons per cm^2.
- To operate at the highest LHC luminosity and be robust and reliable.
- Individual detectors should have a spatial precision of $\sim$10 microns. The tracking system angular precision should be 1 μrad.
- At 420 m the tracking detector needs to cover an area of 25 mm $\times$ 5 mm.

3D silicon technology has been chosen as the baseline detector technology best equipped to meet the above requirements. Until recently, 3D detectors have been operated only with ATLAS readout electronics [**?**]. A first production of 3D sensors compatible with the CMS pixel chip PSI46 [**?**] has been completed at SINTEF (Norway) as a joint effort amongst ATLAS, CMS, and Medipix [**?**]. More CMS-compatible sensors are being fabricated at IRST-FBK (Trento, Italy), SINTEF, and CMN (Barcelona, Spain) and will become available in the next months. Part of the planning and the testing is being (and will be) carried out together with the CMS pixel upgrade group, which is also exploring this novel technology.

In a test beam at Fermilab in March 2010, two 3D sensors from SINTEF were successfully tested. Since then, some more 3D sensors have been assembled and are being tested. One of them was tested in conjunction with the timing detectors. Since then, two more 3D sensors have been assembled and tested in the laboratory. A collected charge of about 24K electrons was measured, approximately what is expected for a 280 μm thick silicon detector. Full charge collection was obtained at 40V.

A.8 Fast Timing Detectors

A.8.1 Overlap background and kinematic constraints

The HPS detectors must be capable of operating at the LHC design luminosity of $\mathcal{L} \approx 10^{34}$ cm^{-2}s^{-1} in order to be sensitive to femtobarn-level cross sections in the central exclusive channel [pXp]. At these luminosities overlap background from two single diffractive events superimposed with a central hard scatter ([p][X][p]), as shown in Fig. A.10(a), becomes a significant concern, especially in dijet final states. The 2-fold overlap coincidence backgrounds, shown in Fig. A.10(b) and (c), also must be considered however; as they scale with $\mathcal{L}^2$ instead of $\mathcal{L}^3$ they

are less of a concern in the high luminosity limit. Fortunately, there are a number of techniques we can employ to reduce this overlap background. It can be substantially reduced at the high level trigger stage, or offline, by employing kinematic constraints. These factors include consistency between the central system and the protons in rapidity and mass, and also use the fact that the number of particle tracks associated with the event vertex is much smaller for exclusive than generic collisions. Even after the significant background rejection afforded by these constraints, overlap backgrounds are still expected to dominate the signals without the additional rejection provided by precision timing of the protons, as detailed below.

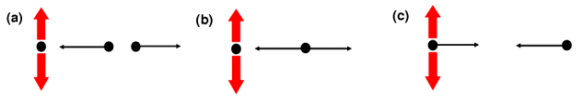

Figure A.10: A schematic diagram of overlap backgrounds to central exclusive production: (a) [p][X][p]: three interactions, one with a central system, and two with opposite direction single diffractive protons (b) [pp][X]: two interactions, one with a central system, and the second with two opposite direction protons (c) [p][pX]: two interactions, one with a central system and a proton, the second with a proton in the opposite direction.

A.8.2 Timing

High-precision time of flight (ToF) detectors at 420 m can be used to obtain a large reduction in overlap (or pile-up) backgrounds [**?**]. We need only measure the *relative* arrival time of the two protons, $\Delta t = t_L - t_R$. Under the assumption that they originate from the same event, the z-position of that event can be calculated as $z_{pp} = \frac{1}{2}\Delta t \times c$. The uncertainty on z_{pp} is $\delta z_{pp} = \frac{c}{\sqrt{2}}\delta t$, where δt is the (r.m.s.) time resolution of the proton measurement. For example, δt = 10 ps implies δz_{pp} = 2.1 mm. We then require a match between z_{pp} and the vertex position from the central detector, z_{vertex}, which is known with extremely good precision ($\approx 50\ \mu$m) [**?**].

In the case of the overlap backgrounds, the protons do not originate from the same event as the hard scatter and so the vertex reconstructed from time-of-flight information will, in general, not match the vertex observed in the central detector, which implies that a large rejection factor can be obtained. This rejection factor depends on four parameters; the timing resolution δt, the spread in interaction points σ_z, the vertex window size (i.e. the degree to which the vertices are required to match) and the luminosity. As the luminosity increases, the probability of there being more than one proton in an arm of HPS increases. If any of the subsequent timing measurements results in a vertex that coincides with the central vertex, then these protons would be chosen as the 'correct' protons. Hence the rejection factor degrades slightly with increasing luminosity. The vertex window size is a trade-off between high signal efficiency and high background rejection. Clearly a smaller vertex window results in a higher background rejection but will also lead to more signal events failing the vertex matching requirement. Common choices are that the vertices must coincide to within 1, 1.5 or $2\times\delta z_{pp}$, which corresponds to a signal efficiency of 68%, 87% and 95% respectively. Finally, the rejection factor increases if the spread in vertices increases and is also approximately linear with δt.

We have calculated the background rejection for the three overlap cases shown in Fig. A.10 (a) [p][p][X] (b) [pp][X] and (c) [pX][p]. For example, if δt = 20 ps (δz_{pp} = 4.2 mm) and the spread in interaction points is $\sigma_z \approx 50$ mm [**?**], we obtain a rejection factor of 21 for the first two cases and 15 for the third if the vertex measurement from proton time-of-flight is required to fall within $\pm$4.2 mm ($\pm 1 \times \delta z_{pp}$) of the vertex measured by the central detector. Case (a) dominates at high luminosity and consequently for δt = 10 ps, we would be able to obtain a rejection factor of greater than 40 (for a $\pm 1 \times \delta z_{pp}$ vertex window), enabling HPS to effectively

cope with the large overlap backgrounds at the design luminosity. For the nominal crossing angle of 250 μrad, the vertex spread exceeds 5 cm, and in addition, the expected growth in σ_z would result in an improved rejection. The final choice of vertex window will be optimised based on the analysis goals and instantaneous luminosity. For example, a discovery measurement would likely maximize signal to background, while a measurement of a state's properties, might demand very low background at the expense of signal efficiency.

In addition to detector performance, there are other factors that could impact the overall timing precision. If the path length of protons were to vary significantly, this could degrade the vertex measurement accuracy. We have determined that even for the largest energy loss for protons in our acceptance compared to the beam protons, the path difference amounts to less than 30 μm, corresponding to a 100 fs time difference (an even smaller effect is expected from proton velocity differences). A second concern is that a precise measurement of the arrival time difference between deflected protons in the ToF detectors requires a reference timing signal at each detector with a $t_L - t_R$ jitter that is small enough not to contribute significantly to the overall time resolution. Our reference timing system is described in Sec. A.8.4.

The absolute calibration of the ToF detectors z-coordinate measurement will be determined and monitored with double pomeron exchange (DPE) physics events to correlate the vertex position measured with the central trackers with the vertex measured by the HPS420 timing detectors. Since it is not possible to trigger on the protons at Level-1 (trigger signals from 420 m, transmitted with cables, reach the L1 boards slightly later than the 3.5 μs L1 latency), it will be necessary to add a double Pomeron filter at the High-Level-Trigger to the highest cross section candidate DPE processes that pass the Level-1 trigger, dijets and dileptons, for example, to select an adequate sample of events. Given the high cross section for DPE dijets, it will be possible to collect hundreds of such events per hour.

A.8.3 Timing detectors

We are developing two types of ToF counters for HPS, GASTOF (Gas Time Of Flight) and QUARTIC (QUARtz TIming Čerenkov). Prototypes of both types of detector have been built and tested.

A schematic diagram of the GASTOF detector developed at UC Louvain is shown in Fig. A.11. It has a gas radiator at 1.1 – 1.4 bar in a rectangular box of 20 – 30 cm length, with a very thin wall adjacent to a specially designed flat pocket in the Hamburg beam pipe (Section A.5). The protons are all essentially parallel to the axis. A thin 45° concave mirror at the back reflects the light to a MCP-PMT. The gas used in the tests, and which we propose to use in HPS420, is C_4F_{10}, which is non-toxic and non-flammable, and has a refractive index $n = 1.0014$ between 200 nm and 650 nm, giving a Čerenkov angle ($\beta = 1$) of about 3.0°. C_4F_{10} is used in the RICH1 detector of the LHCb experiment.

The in-line material in a GASTOF (thin windows, mirror and gas) is minimal and does not cause significant multiple scattering. It can therefore be placed before the final tracking detectors. GASTOF is intrinsically radiation hard, the only sensitive element being the MCP-PMT. Lifetime tests on gain, transit time spread, and quantum efficiency under laser light irradiation were carried out on Hamamatsu and Budker Institute tubes by the Nagoya group [**?**]. At 2.8×10^{14} photons/cm^2 some gain decrease occurred, recoverable by increasing the HV, but the transit time spread (TTS) was not affected. However, a significant deterioration of the photocathode quantum efficiency (QE) was observed. Such an effect could be remedied by increasing the gas pressure and thus the number of Čerenkov photons – for a 30 cm GASTOF and the nominal QE, the mean number of photoelectrons can exceed 10.

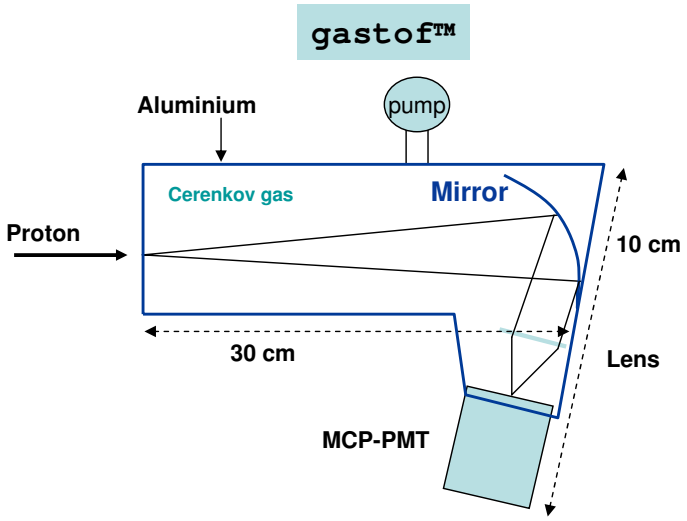

Figure A.11: Schematic of GASTOF, a gas-based Čerenkov counter proposed by Louvain-la-Neuve, as described in the text.

The QUARTIC detector, which utilises fused silica (artificial quartz) bars as radiators, is being developed by the University of Alberta, Fermilab, the University of Texas, Arlington and Louvain-la-Neuve groups. Figure A.12(a) shows the concept: a proton passing through the silica bars radiates photons which are measured by the MCP-PMT. Figure A.12(b) shows the 4 $\times$ 8 array of bars with a 6 mm $\times$ 6 mm cross section and length ranging from about 110 mm for the first bar hit by the proton to 70 mm for the last, and will be flush with the surface of the MCP-PMT. The bars are oriented at the average Čerenkov angle, $\theta_c \approx 48^\circ$, for isochronous (equal time) light on the QUARTIC detector. Figure A.12(c) shows a third generation single-row prototype used in the June 2008 CERN test beam. The final four-row version will have a very thin wall adjacent to the beam pipe, matching the dead area of the silicon detectors, to ensure full acceptance for all measured tracks.

Since the GASTOF and QUARTIC detectors have complementary features we are proposing to use both: one GASTOF detector will be located in its own beam pipe pocket after the first silicon detector pocket and two QUARTIC detectors will be located in their own pocket after the final silicon tracking detector, to mitigate the impact of multiple scattering.

Both the GASTOF and QUARTIC devices have developed considerably recently:

- In a test beam at Fermilab in June 2009 a time resolution of 18 ps was achieved with a QUARTIC detector consisting of two Photek PMT210s, each reading out one 6 mm $\times$ 6 mm bar.
- Beam tests at Fermilab in March 2010 were made of two QUARTIC detectors, each with three rows of five quartz bars in line inclined at the Cherenkov angle onto a Photek PMT240. Resolutions of 15.5 ps and 16.3 ps were measured for the two detectors, respectively, and of 11.2 ps for the combined detector. These prototypes are already suitable for use in HPS.
- As discussed in the previous section, in March 2010, data were taken for the first time with a QUARTIC prototype together with CMS pixel planes and one 3D-Si plane.
- The most recent GASTOF prototypes equipped with the Hamamatsu R3809 and Photek PMT210 tubes were tested in 2009 at the Louvain cosmic-ray stand. The

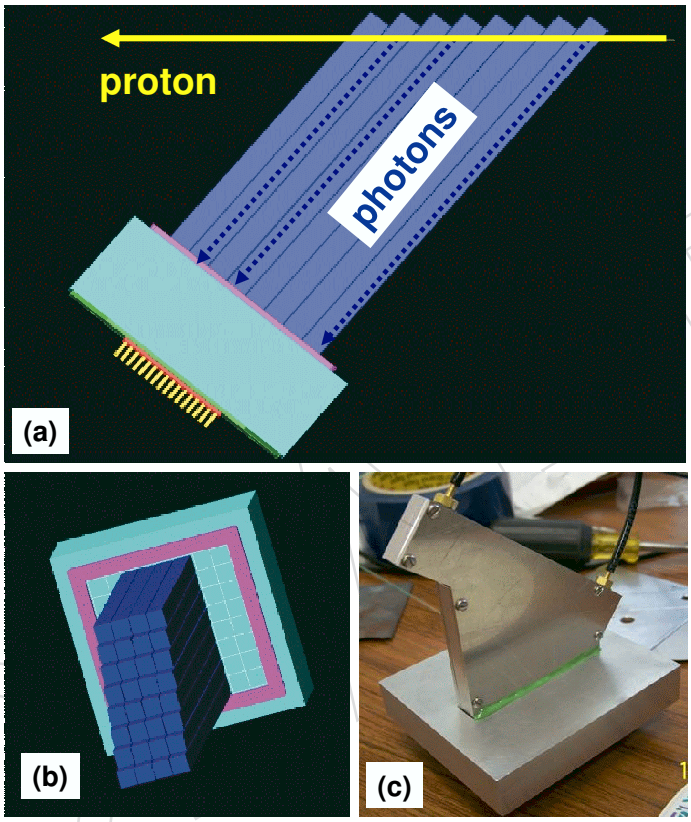

Figure A.12: Conceptual drawings of a QUARTIC detector, (a) showing the proton passing through eight bars of one row in x providing eight measurements of the proton time (b) showing the 4×8 layout of QUARTIC bars (c) A photograph of the prototype detector used in the June 2008 CERN test beam.

results obtained with the Hamamatsu 6 μm pore MCP-PMTs confirmed a 13 ps timing resolution determined from the 2008 CERN test beam data [**?**]. Moreover, the cosmic ray data obtained with the Photek 35 μm pore MCP-PMTs demonstrated the expected resolution below 10 ps [**?**]. Also these prototype detectors are already suitable for use in HPS.

- Four single-channel MCP-PMTs, two Photek PMT210 and two Hamamatsu R3809, are being now characterized at a dedicated picosecond laser stand. The first results allowed building an accurate and efficient model of the MCP-PMT response [**?**]. Dedicated constant fraction discriminators were developed for HPS which showed excellent performance, notably an intrinsic time jitter below 10ps.

A.8.3.1 Stage One Timing Detectors

The timing detectors for Stage One are being prototyped at the moment. The baseline configuration assumes in each arm two detectors, a GasToF in the front station and a Quartic in the back one. A quartic is a detector with one MCP-PMT as an independent unit. Each has 4 (rows) $\times$ 8 (bars), making 64 channels per arm. With the two quartics mounted in opposite directions ('up' and 'down') the time sum is independent of y-position which can be a useful check. Two types of DAQ systems for Stage One are being investigated. The first is based on commercially available PCI cards containing TDC boards with better than 4 ps resolution [**?**]. It would however require transmission of the signals produced by fast constant fraction discriminators over 300 m. Another solution relies on the HPTDC chips providing about 20 ps resolution – this assumes near-detector TDC boards and sending the digital data over 300 m long optical links.

The L1 HPS trigger signals will be produced by the timing detectors, and combined in such a way as to provide one bit input to the central trigger for each arm of HPS. Special, high-quality and fast cables will be installed to ensure arrival of the HPS trigger signals within the L1 latency limit.

A.8.4 Reference timing system

We have two solutions for the reference time signal propagation. One possibility is a monomode optical signal derived at IP5 from the LHC RF, and sent along optical fibers to the stations at positive and negative z values, where it is converted into pECL electrical pulses to use as START or STOP signals for the detector TDC. This is the scheme presently used by the LHC timing signal system. The only relevant parameter is the short term (pulse-pulse or minute-minute) jitter, which is not significantly present in the optical signal transmission, but only in the conversion from optical to pECL. If necessary, this can be reduced by splitting the optical signal more ways (one is returned to the source), without introducing any jitter, and thereby making several reference timing signals locally.

The second scheme takes the 400 MHz LHC RF signal itself, splits it at IP 5 and sends it along two 7/8" cell-flex RF cables to the detector stations. This scheme has been presented to us by Brian Chase (Fermilab Accelerator Division). The temperature coefficient at 20^oC is 1 ppm/^{o}C, and the loss over 400 m at 400 MHz is 12.7 dB. The phases can be fixed by a phase-locked loop, which is a standard procedure.

An actual demonstration of a resolution below 10 ps is still needed. However, much higher performance than we require has been demonstrated, for example in the RF phase and time distribution system for the NLC [**?**]. Another demonstration with much higher performance used mode-locked fiber lasers as master oscillators [**?**]. Tests in an accelerator environment over 500 m with length-stabilised fibers have demonstrated a residual timing jitter caused by

the fiber link to be 10 fs (sic) rms at frequencies from 1 kHz up to 20 MHz.

A.9 Trigger

This section summarises some of the trigger studies performed by CMS and TOTEM [**?**] relevant to FP420. More details can be found in Chapter 6 of [**?**]. Although these studies are based in proton detectors at 220 m, the trigger differences are minimal for our HPS Stage One detectors at 240 m from IP5.

Central exclusive production of a Higgs boson is used as an example, $pp \to pHp$, with Higgs mass close to the LEP direct current exclusion limit. The selection efficiencies for other diffractive processes are also presented.[1]

Events from $pp \to pHp$ and $H(120\,\mathrm{GeV/c^2}) \to b\bar{b}$ can be triggered on at L1 by exploiting their muon-rich final state by means of the existing CMS trigger slots, also at the highest instantaneous luminosities. An additional L1 trigger stream can be realised, based on the presence of two jets in the central apparatus and, if 220 m detectors are available, a proton in the 220 m detectors. This stream is discussed in detail in Sect. A.9.1. With the addition of this stream, the trigger efficiency more than doubles to 20-30%, as discussed in Sect. A.9.2.

Table A.1 shows the main features of such additional stream: the requirement that the E_T of the event be concentrated in the two jets gives a factor 2 suppression, independent of the instantaneous luminosity. With a L1 bandwidth [2] of 10 kHz, this is sufficient to reach instantaneous luminosities of $10^{33}\,\mathrm{cm^{-2}\,s^{-1}}$. An additional factor 10, at $2 \times 10^{33}\,\mathrm{cm^{-2}\,s^{-1}}$, is obtained by requiring the presence of a signal at 220 m with $\xi < 0.1$. If the leading proton spectrum normalisation is taken from [**?**] or [**?**], the reduction becomes larger by a factor 3 to 6. A further factor of 2, independent of luminosity, can be obtained with a simple topological condition discussed in Sect. A.9.1. In short, the requirement of jets along with a proton in the 220 m stations, assuming a L1 bandwidth of 10 kHz, could be used up to luminosities in excess of $10^{34}\,\mathrm{cm^{-2}\,s^{-1}}$.

The main reason for the trigger rate increase at high instantaneous luminosities is the pile-up. HPS420 is instrumental in keeping this under control at the HLT. Simply requiring the presence of a proton in both arms of the HPS420 spectrometer yields a reduction by a factor 150. Further, major suppression of the pile-up backgrounds can be obtained by applying offline-type conditions, similar to those discussed elsewhere in this document: the information from the protons and the central event can be required to match and the information from the timing detectors can be used. A simple implementation of the former, discussed in Chapter 7 of [**?**], brings a factor of order 10^3. Timing information brings another factor 40.

[1] The present studies assume that the near-beam detectors are 100% efficient in detecting all particles that emerge at a distance of at least $10\sigma_{beam} + 0.5$ mm from the beam axis (1.3 mm at 220 m and 4 mm at 420 m; the latter condition, as discussed elsewhere in this document, can be loosened without prejudice for the physics capability of FP420). The results were obtained with the full CMS detector and trigger simulation package. They do not depend on the specific hardware implementation of the TOTEM detectors. QCD background events were generated with PYTHIA, and so were the diffractive events contributing to the pile-up. For the latter, the correction to the PYTHIA leading proton spectrum described in [**?**] was used. This condition implies a leading proton rate a factor of about 3 higher than suggested in [**?**] and a factor ranging between approximately unity (in the ξ region covered by the HPS420 detectors) and 5-6 (in the region covered by the 220 detectors) higher than that of PHOJET [**?**], used for other studies in the present document. The rates given here can therefore be taken as an upper limit.

[2] Note that Table A.1 assumes a maximum L1 bandwidth of 1 kHz. By raising this to 10 kHz the reduction factors required at a given instantaneous luminosity are lowered by a factor 10 and the instantaneous luminosity reachable for a given set of conditions increases by a factor 10.

A.9.1 2-Jet and Forward Detector Conditions at L1

As seen in Table A.1, demanding that a proton be seen in the near-beam detectors at 220 m results in excellent background suppression in the absence of pile-up. The suppression reduces to a factor $\sim 4(2)$ at $2 \times 10^{33}\,\mathrm{cm^{-2}\,s^{-1}}$ ($10^{34}\,\mathrm{cm^{-2}\,s^{-1}}$), see Table A.1, where the effects of conditions based on the HPS420 detectors are also shown. They are of interest both in the L1 trigger for special, long-latency runs and, in normal running conditions, for the HLT. By applying a cut $\xi < 0.1$, the suppression becomes 10 (3) at $2 \times 10^{33}\,\mathrm{cm^{-2}\,s^{-1}}$ ($10^{34}\,\mathrm{cm^{-2}\,s^{-1}}$).

The following additional trigger conditions were studied:

- Condition based on central CMS detector quantities. Requiring that essentially all the E_T be concentrated in the two central L1 jets with highest E_T, i.e. $[E_T^1 + E_T^2]/H_\mathrm{T} > 0.9$ (H_T condition), corresponds to imposing a rapidity gap of at least 2.5 units; here H_T indicates the scalar sum of the E_T values of all jets. This condition reduces the rate of QCD events by approximately a factor 2, independent of pile-up and with only a small effect on the signal efficiency.
- Topological condition. The 2-jet system has to balance the total momentum component of the two protons along the beam axis. In signal events with asymmetric ξ values, the proton seen on one side in the 220 m detectors has the larger ξ and thus has lost more of its initial momentum component along the beam axis. Hence the jets tend to be located in the same η-hemisphere as the near-beam detectors that detect this proton. A trigger condition requiring that $[\eta^{jet1} + \eta^{jet2}] \times \mathrm{sign}(\eta^{220m\ det}) > 0$ reduces the QCD background by a factor 2, independent of pile-up, and with no loss in signal efficiency.

Luminosity $[\mathrm{cm^{-2}\,s^{-1}}]$	Pile-up events per BX	Level-1 2-jet rate [kHz] for $E_\mathrm{T} >$ 40 GeV	Total reduction needed	Reduction when requiring track in det at					
				220 m	220 m $\xi < 0.1$	420 m	220 & 420 m (asymmetric)	220 & 420 m (asymmetric) $\xi < 0.1$	420 & 420 m
1×10^{33}	3.5	26	20	7	15	27	160	380	500
2×10^{33}	7	52	40	4	10	14	80	190	150
5×10^{33}	17.5	130	100	3	5	6	32	75	30
1×10^{34}	35	260	200	2	3	4	17	39	10

Table A.1: Reduction of the rate from standard QCD processes for events with at least 2 central Level-1 jets with $E_T > 40$ GeV, achievable with requirements on the tracks seen in the near-beam detectors. Additional rate reductions can be achieved with the H_T condition and with a topological condition. Each of them yields, for all luminosities listed, an additional reduction by about a factor 2. A maximum L1 bandwidth of 1 kHz is assumed. By raising this to 10 kHz the reduction factors required at a given instantaneous luminosity are lowered by a factor 10. It should be noted that the reduction factors when using HPS420 can only be realised at the HLT because the signal from the detectors at 420 m do not arrive within the L1 trigger latency. Table from [**?**].

Table A.1 summarises the results; it shows that reduction of the QCD rate to levels compatible with a L1 output target rate of $\mathcal{O}(1)$ kHz appears feasible when introducing a single-sided 220 m condition for luminosities up to *at least* $2 \times 10^{33}\,\mathrm{cm^{-2}\,s^{-1}}$ assuming the conservative leading proton spectrum normalisation of [**?**]. Using the normalisation from [**?**] or [**?**], $5 \times 10^{33}\,\mathrm{cm^{-2}\,s^{-1}}$ becomes possible. For a 10 kHz bandwidth, $10^{34}\,\mathrm{cm^{-2}\,s^{-1}}$ is feasible.

A.9.2 Level-1 Signal Efficiencies

For this study, signal samples with central exclusive production of a Higgs boson were generated with the Monte Carlo programs EDDE [**?**] (version 1.1) and EXHUME [**?**] (version 1.0); consistent results were obtained.

A.9.2.1 Central Exclusive Higgs Production $H(120\ \mathrm{GeV/c^2}) \rightarrow b\bar{b}$

About 20% of the $H \rightarrow b\bar{b}$ events have a muon in the final state. Of these, about half can be triggered by implementing a 1 muon + 1 jet trigger with thresholds of 3 GeV/c on the muon p_T and 40 GeV on the jet E_T. The efficiency can be more than doubled to 30% (20%) if the 2-jet requirement (2-jet plus single-arm 220 m) is implemented with a 40 GeV E_T threshold. For 30 GeV threshold in the 2-jet plus single-arm 220 m condition, the total efficiency becomes more than 30%.

A.9.2.2 Central Exclusive Higgs Production $H(120\ \mathrm{GeV/c^2}) \rightarrow WW$

For SM Higgs masses above 120 GeV/c^2, the $H \rightarrow WW$ branching ratio becomes sizable; in this case the final state contains high-p_T leptons, and triggering is easier.

Efficiencies are in general high. About 23% of the events have at least one muon in the final state. Approximately 70% of these (i.e. 16%) are retained by requiring at least one muon with a p_T threshold of 14 GeV/c. An extra $\approx$ 10% (i.e. 2%) would be retained by implementing the muon/jet slot discussed above with thresholds of 3 GeV/c on the muon p_T and 40 GeV on the jet E_T.

A.9.2.3 Single diffractive hard processes

Double-Pomeron exchange processes constitute only a small part of the diffractive cross section. Hard single-diffraction, $pp \rightarrow pX$, where only one proton remains intact have much higher cross sections than hard double-Pomeron exchange events. Yet, hard SDE can only be measured with no PU, requiring low instantaneous luminosities. Efficiencies have been studied for $pp \rightarrow pX$, with X containing a W or a Z boson that decays to jets and to muons, as well as with X containing a dijet system. The POMWIG Monte Carlo generator [**?**] (version 1.3) was used.

For four example processes, Fig. A.13 shows the efficiency as a function of the L1 threshold value, normalised to the number of events (in the muon rate case to the number of events with a muon in the final state) and $0.001 < \xi < 0.2$. Three different trigger conditions are considered: trigger on central detector quantities alone (i), trigger on central detector quantities in conjunction (ii) with the single-arm 220 m condition, and (iii) with the single-arm 420 m condition. Also shown is the number of events expected to pass the L1 selection per pb^{-1} of LHC running. There, a gap survival probability of unity was assumed. However, at the LHC this factor is expected to be $\mathcal{O}(0.1)$.

A.10 The new connection cryostat at 420 m

The LHC beamline layout downstream of an interaction point consists of a triplet of low-beta quadrupole magnets, two beam separation dipoles and a matching section of quadrupoles up to quadrupole Q7. This is followed by a dispersion suppressor region of standard dipoles and quadrupoles and finally the periodic lattice of the arc. In the dispersion suppressors there is a 14 m drift space, sometimes called the "missing magnet" drift space, which is approximately

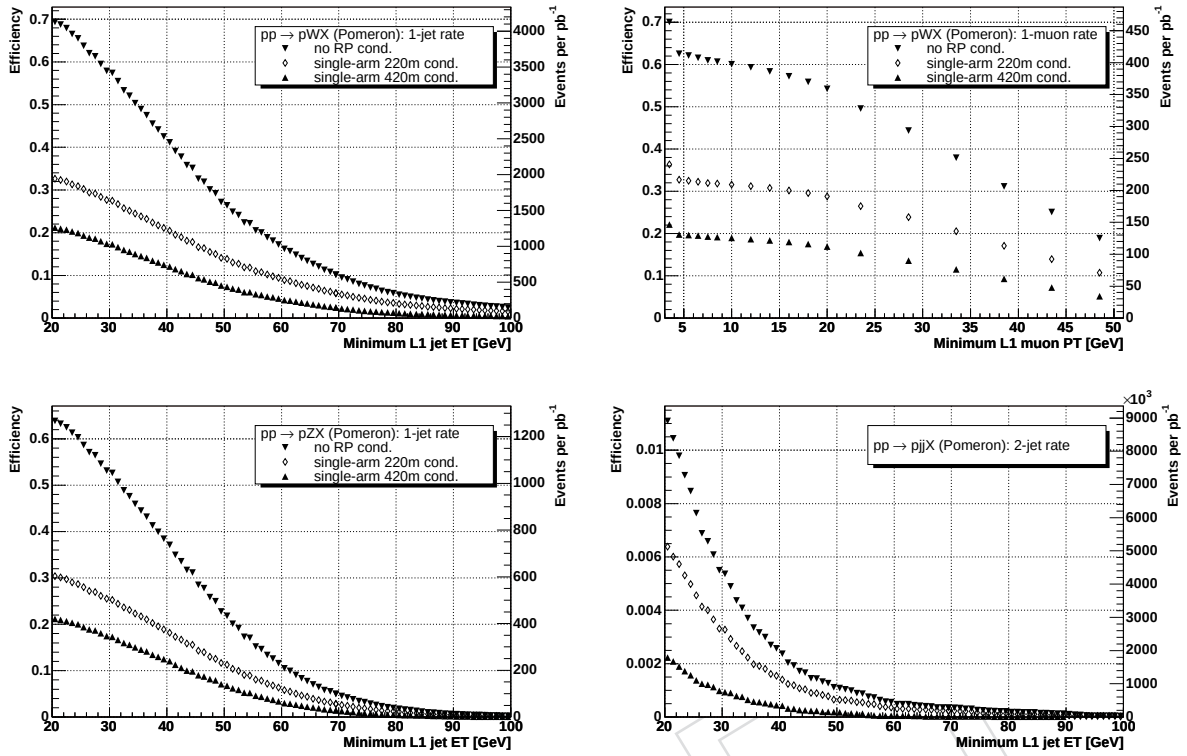

Figure A.13: Selection efficiency as function of the threshold value for $pp \to pWX$ (upper left and upper right), $pp \to pZX$ (lower left), $pp \to pjjX$ (lower right). At least one L1 jet with E_T above threshold is required (upper and lower left), at least two L1 jets with E_T above threshold are required (lower right), at least one L1 muon with p_T above threshold is required (upper right). The normalization of the efficiency curves (left y-axis) is explained in the text. The number of events expected to pass the L1 selection per pb^{-1} of LHC data (right y-axis) does not take into account the gap survival probability which at the LHC is expected to be $\mathcal{O}(0.1)$. All plots are for the non-pile-up case. Figure from [**?**].

420 m downstream of the IP. In the LHC it was decided, mainly for cost reasons, to place the dispersion suppressors and arc magnets in one continuous cryostat from Q7, all the way to the symmetric Q7 quadrupole upstream of the next IP [**?**]. At the position of the missing magnet, 420 m downstream of each IP, there is a 14 m long Connection Cryostat (CC) which contains cold beam-pipes, the 2K heat exchanger, or X-line, and various cryo-lines which run throughout the continuous cryostat, as well as the superconducting busbars and nearly 100 superconducting cables of the main bending magnets and corrector magnets. There are sixteen CCs in the LHC, each made to be as similar as possible to a standard arc cryostat, as far as interconnection and handling are concerned. At this 420 m point, the dispersion function D, with the standard high luminosity optics, is approximately 2 m and hence protons from the IP which have lost around 1% of their momentum are well separated from the circulating beam, as described in Sec. A.3. Placing detectors directly inside the 1 m diameter cryostat at a temperature of 2K was considered, but ultimately dismissed, primarily because of the inevitable very high local heat load on the LHC cryogenic system and accessibility problems. The alternative is to replace the existing connection cryostat with a warm beam-pipe section and a cryogenic bypass. As a matter of fact, a cryo bypass solution is already planned at IP3 for collimators at $\pm$420 m. At the end of each arc cryostat of the LHC there is a special short cryostat called

an Arc Termination Module (ATM) which includes cold to warm transitions for the beampipes and connects cryo-lines and superconducting busbars and cables to the electrical feed boxes. A New Connection Cryostat (NCC) with approximately 8 m of room temperature beam-pipes has been designed using a modified ATM at each end.

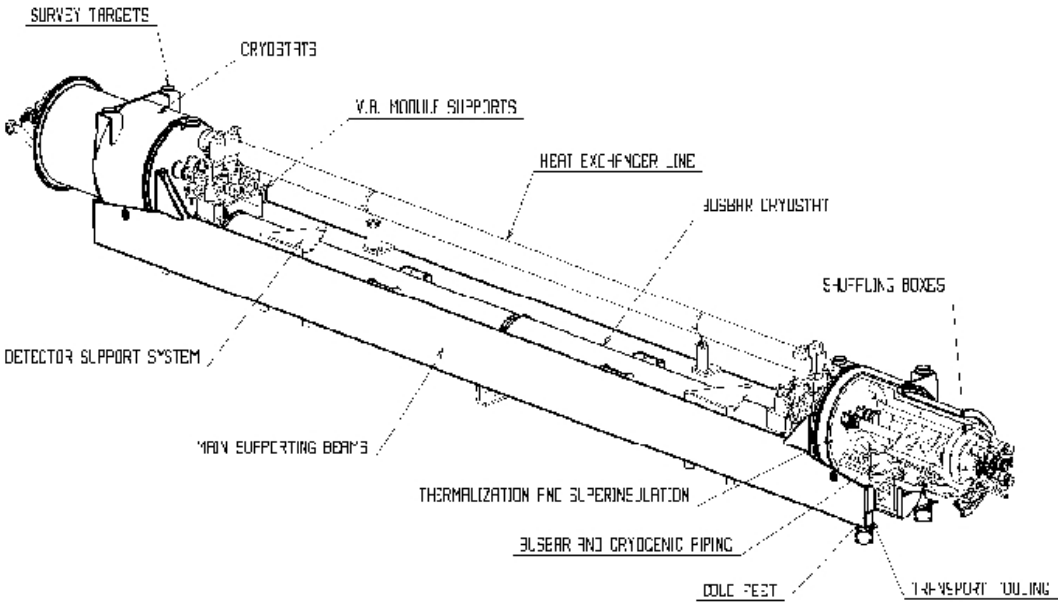

Figure A.14: The new connection cryostat.

In addition to the two modified ATMs and warm beam-pipes, the NCC shown in Fig. A.14 has a small cross section cryostat below the beam-pipes carrying all the cryo-lines and superconducting circuits and a new specially designed cryostat for the X-line. All this is supported by two longitudinal beams to make a single unit which can be directly exchanged for an existing connection cryostat. The passage of the X-line through the ATM modules is the main modification needed to the standard ATMs, but the geometrical layout of this passage has been arranged to be as far away as possible from the downstream beam-pipe and hence leave adequate space for near-beam detectors and their associated equipment.

The existing connection cryostat contains a box structure of lead plates of 15 mm thickness enclosing the two beam-pipes to reduce the radiation field in the tunnel, essentially replacing the shielding provided by the cold mass in a standard arc dipole cryostat. The same thickness of lead shielding will be provided around the warm beam-pipes and detector stations of the NCC.

There are also short lengths of cylindrical shielding in the form of collars around the beam-pipes at each end of the existing connection cryostat to limit the risk of quenching adjacent superconducting magnets. These same collars will be incorporated into the modified ATM's at each end of the NCC in order to ensure that the performance of the NCC is also equal to the existing cryostat in terms of influence on the local radiation fields.

The engineering design of the new connection cryostat was carried out by the EN/MME group and validated. The design aim was to meet or exceed the same specifications as the existing

	Normal Days
Warmup from 1.9K to 4.5 K	1
Warmup from 4.5K to 300 K	15
Venting	2
Dismantling interconnection	10
Removal of the connection cryostat	2
Installation of the cryostat	5
Realization of the interconnections	15
Leak test and electrical test	4
Closing of the vacuum vessel	1
Evacuation/repump	10
Leak test	2
Pressure test	4
Cool-down from 300 K to 4.5 K	15
Cool-down from 4.5K to 1.9 K	3
Total [days]	89

Table A.2: The estimated time in days required to install one NCC.

connection cryostat, whilst providing the maximum useable space for the detectors. Such design design offers acceptable solutions for all cryogenic and mechanical engineering aspects as well as integration into the LHC environment [**? ?**]. Simulations show that during LHC operation the NCC actually has a lower dynamic heat load than the existing connection cryostat, because in the 8 m long warm section synchrotron radiation will be absorbed at room temperature. Therefore the additional static heat load arising from the two additional cold to warm transitions will be tolerable for the LHC cryogenic system.

As regards construction of the NCC's, the sixteen ATM modules of the LHC were assembled at CERN in a dedicated workshop in Building 110, under the responsibility of Ramon Folch (TS/MME). His team has prepared a preliminary construction schedule and cost estimate for the new cryostats [**?**].

The cutting and removal of the existing connection cryostat and its replacement by an NCC is very similar to the replacement of a standard LHC dipole and has been evaluated by the group responsible for all the LHC interconnections. As mentioned above this is the same group that took responsibility for the design installation and performance of the existing connection cryostat.

Table A.2 shows the sequence of operations and the estimated time needed in normal working days to complete the exchange of a connection cryostat from start of warm-up to being ready for beam. It is thus conceivable that the installation of modules consisting of an NCC cryostat and associated detectors could be completed in an annual long shutdown. A preliminary study of the transport aspects has shown that adequate tooling exists and it can be expected that the time needed will be in the shadow of other operations shown in Table A.2. However, the number of connection cryostats that can be replaced in a standard annual shutdown will depend on the number of LHC magnets requiring replacement and the work load of the interconnection teams.

A.11 Cost estimate

A preliminary estimate of the costing of the major components of HPS 240 and 420 detectors is given here as an indication. A detailed costing evaluation is still being performed.

Stage One, two full HPS240 stations:

- Silicon tracker including the electronics and mechanical parts: 0.7??? MCHF
- Quartic timing detectors, including electronics, 100 kCHF for 4 detectors.
- GASTOF timing detectors, including electronics, DAQ, slow controls and cables: 150 kCHF.
- BPMs and beampipe mechanics: 380 kCHF.
- High voltage/Low Voltage: 160 kCHF.

This leads to a approximate grand total of 1.5 MCHF for equipping both sides with HPS240 detectors.

Stage Two, two full HPS420 stations:

- Two new connecting cryostats, amounting to a total of 1.5 MCHF.
- Silicon tracker including the electronics and mechanical parts: 0.7 to 1.0 MCHF.
- Quartic timing detectors, including electronics, 100 kCHF for 4 detectors.
- GASTOF timing detectors, including electronics, DAQ, slow controls and cables: 150 kCHF
- BPMs and beampipe mechanics: 380 kCHF
- High voltage/Low Voltage: 160 kCHF

This leads to a approximate grand total of 3.0 MCHF for equipping both sides with HPS420 detectors.

Appendix B

Forward Region: the MPGD (MPGD) Detector

B.1 Introduction

The CMS Forward Muon system comprises four stations located on the disks YE1 to YE3. The first three stations are instrumented with Resistive Plate Chambers, and the fourth station RE4, initially de-scoped, is being up-scoped with both CSC and RPCs detectors.

The Forward Muon RPC trigger system is equipped with detectors at $|\eta| < 1.6$. For this low η region, extensive tests were performed over several years in order to validate the RPC technology and the gas mixture for particle rates of $\sim$10 Hz/cm^2. A sophisticated gas system was commissioned in order to recuperate the expensive components of the gas and to filter the pollutants and contaminants produced during chamber operation. The tests carried out showed that the detectors are suitable for operation in the low η region, while concerns remained about the possibility of achieving stable operation with the radiation conditions expected at $|\eta| < 1.6$. Thus the high η region of CMS has no RPC chambers and presents an opportunity to instrument it with a detector technology that could sustain the environment and be suitable for operation at the LHC and its upgrades.

The high η region presents hostile conditions, with particle fluence of several 100 Hz/cm^2 for an LHC luminosity of 10^{34} cm^{-2}s^{-1}, which may go up to several kHz/cm^2 depending on the upgrade scenarios. In addition the rates of thermal neutrons, low energy protons and γs must be taken into consideration. Hence the most stringent requirements for a detector at high η which can sustain operation in the upgraded LHC, are given in table B.1.

Table B.1: Requirements for a detector at high η.

Rate capability for charged particle rates	10^4 Hz/cm^2
Aging dose at one year of continuous operation	$>$7 mC cm^{-2}
Discharge probability	10 discharges cm^{-2}year^1
Space resolution	250 μ - 500 μ
bx identification efficiency	95%

Over the past six months an effort has been focused on looking for options, and Micro-Pattern Gas Detectors (MPGDs) seem to be a valid choice for this region.

B.2 Present experience with MPGDs

An investigation of MPGDs as candidate technology to instrument the vacant zone in the forward part of the CMS detector, namely $1.6 < |\eta| < 2.4$ (see Figure B.1), is undertaken. The

objective is to develop a detector with enhanced and optimized readout granularity ($\eta - \phi$), and a rate capability improved by two orders of magnitude compared to RPCs, to improve the muon trigger efficiency and combine triggering and tracking functions.

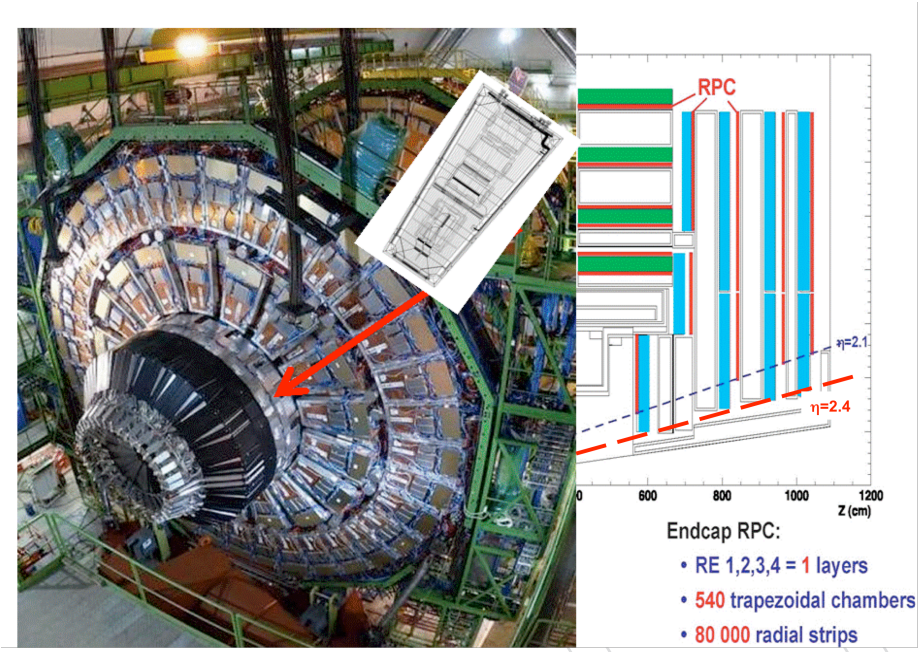

Figure B.1: The position of the high η chambers within the CMS Forward Muon system. The CSC chambers cover up to η = 2.4, as indicated by the large-dash red line. RPC chambers were originally expected to cover up to η = 2.1, as indicated by the small-dash blue line.

Two types of micropattern detectors have been considered: the micromegas and the gas electron multiplier (GEM). The micromegas is a gaseous detector made with a metallic mesh exploiting the exponentially increasing Townsend Coefficient at very high electric fields. The gas electron multiplier on the other hand is a thin metal-coated polymer foil perforated with a high density of holes (50-100/mm^2); each hole acting as the multiplication region. GEMs can be used in combinations thus making a double or triple GEM detector delimiting the gas volume with a drift cathode and customized readout anode. Both technologies have the potential for production of large area detectors (1m x 2m) with cost effective industrial processes.

Micromegas and triple GEMs have been installed at the COMPASS experiment in 2002 and were also operated for one week with a 25 ns LHC-like hadron beam with the intensity on the detector of 5 x 10^6 pions per spill of 5 s on a surface of approximately 1cm2, similar to the one expected in CMS for an LHC luminosity of 10^{33} cm^{-2}s^{-1}. The COMPASS collaboration reports good performance of the GEM detectors, with no evidence of deterioration. Triple GEMs have been installed in the first LHCb muon station, while ATLAS is considering the micromegas for its muon upgrade.

On a COMPASS triple GEM operated at the gain of 2 x 10^4,a charge of 20mC/mm^2 has been integrated on the readout board with no sign of aging. Operation at lower gain (for example 8000) can further enhance the robustness of the detector for high particle rates, in view of the high luminosities that may be achieved with the LHC upgrades. For Triple GEMs, with a gain of 2 x 10^4, very good gain stability was measured up to a photon flux of about 5 x 10^7 Hz/cm^2, and extensive aging measurements have been performed in the past.

As all gaseous detectors, GEMs have a finite probability of exhibiting a breakdown of the gas

rigidity or discharge. Systematic investigations have been carried out by LHCb; the most significant study is the measurement of the discharge probability of a triple GEM detector in a high intensity, low energy beam at PSI, the beam that best simulates the conditions expected at the LHC. It has been demonstrated that the detector does not deteriorate after multiple discharges with large repetition rates, provided that the amplifiers of the GEM electronics are properly protected.

B.3 Outline of the R & D Project

The R & D project is structured in the tasks listed below. To moderate workload and cost, tasks II-V are restricted to a single technology, taking as case study the RE1/1 station.

1. **Comparison of small-size prototypes in the two technologies** – Two small detectors of identical size and built with comparable quality, are compared for various aspects of performance and robustness.
2. **3D modeling of a full-scale detector and services integration** – Detailed Catia modeling of a full-scale detector, to support construction of mock-up (task III) and functional prototype (task IV). Analysis of the integration of power and readout, including routing of cables in CMS.
3. **Construction of full-scale mock-up** – Mechanical prototype to study handling and integration aspects.
4. **Construction and test of a full-scale functional prototype** – Demonstrate performance of a real-size detector with realistic readout electronics. Investigate in detail all construction aspects.
5. **Evaluation of a possible construction project for the whole high-η region** – Provide first estimates of the resources needed for a full construction project and its timescale. Collect expressions of interest from Institutes that may participate in the project, along with estimates of the resources they may contribute.

As the R & D project is underway, some of the tasks are already partially completed. Status and plans are given in the next section.

B.4 Present status, plans, and schedule

B.4.1 Study of small-size prototypes

One small (10 x10cm^2) prototype of each technology, namely one micromegas and one triple GEM, were constructed. The cost of work and material was shared between Ghent University and CMX-DS. Both prototypes were produced at the surface treatment workshop at CERN (EN-ICE) and they were subsequently tested in the DT RD51 Lab. The two detectors were characterized by measuring the gain and pulse height spectra with radioactive sources and Cu X-rays from a generator, using standard gas mixtures. Efficiency plateaus were measured and the operational voltages were determined (Fig. B.2). The two detectors were then exposed to a π/μ beam in October 2009. The triple GEM was equipped with VFAT electronics from INFN Siena-Pisa, while the micromegas with GASSIPLEX from RD51. These two detectors along with three other triple GEMs of similar size (from RD51) formed the beam telescope. The analysis is still ongoing; preliminary results show good efficiency, cluster size and space resolution (Fig B.3) for the triple GEM, while the micromegas showed a substantial discharge probability (as reported below), and hence the data quality is poor.

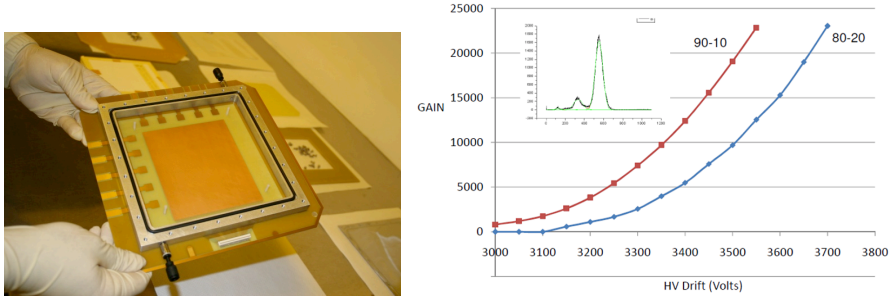

Figure B.2: (a) Triple GEM prototype, (b) gain measured with X-rays in two different gas mixtures: Ar-CO_2 90%-10% and Ar-CO_2 80%-20%.

Discharge probabilities of the two detectors were measured in the lab; for the triple GEM a probability of 10^{-6} was measured up to gains of 20 x 10^4, while the micromegas was discharging with a probability of 10^{-4} at a gain of less than 2000; such results are consistent with previous studies. It was decided to continue the R & D program with the triple GEM technology, on the basis of these results and previous knowledge (Section 2).

Further beam tests are planned in 2010 with the triple GEM small prototype. The main goals are to establish space and time resolution as function of incident angle and magnetic field, fine tuning the operational parameters. This is pertinent in view of the fact that the zone $1.6 < |\eta| < 2.1$ on the CMS endcaps has maximum bending power for muons and must be exploited.

A technique of using honeycomb spacers is being studied in another small 10 x 10 cm^2 prototype made by DT-RD51. The main purpose of this detector is to evaluate possible efficiency losses, first in the lab using cosmics, and later also on a beam.

The full understanding of the operation of GEM detectors in high neutron and gamma fluxes, as expected in the high η region, demands further studies which are not included in this R & D proposal, namely Monte Carlo simulations of neutron effects, complemented with tests of a triple GEM prototype in neutron and gamma beams.

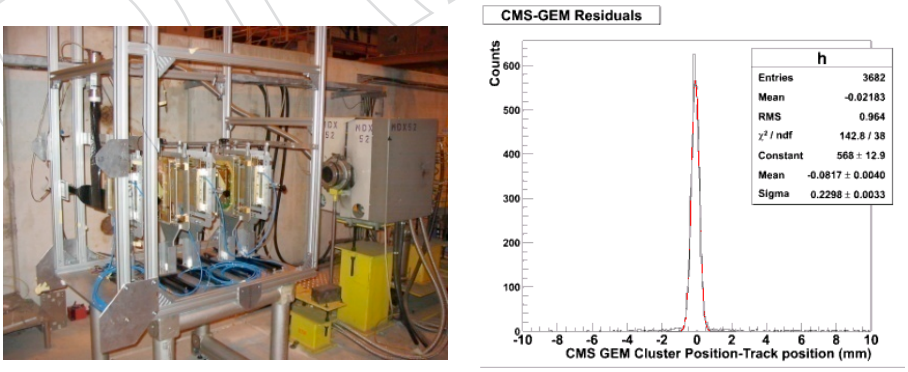

Figure B.3: (a) Beam tests of the Triple GEM and Micromegas prototypes shown mounted on a test bench; (b) preliminary space resolution of the GEM prototype.

B.4.2 Modeling of full-scale detector and services

A detailed design of a full scale detector is mandatory to investigate the impact of size on the detector properties and performance, as well as to address all the issues related to the powering

scheme, and the integration of gas, HV, LV and cooling supply services. The development of a complete 3D CATIA/Autocad model has been launched; as a starting point, the detector size has been matched to the nominal RE1/1 envelope ($|\eta| < 2.1$ (see Fig. B.4), the possibility to extend further the coverage to higher rapidity (ideally, up to $|\eta| < 2.4$, if possible) will be investigated later. A basic model of the detector using CATIA is already available and has been transferred to the surface treatment workshop; it will be completed within the next month, and will serve as basis for the construction of the full scale prototype. Then, in parallel with the construction of the detector, the model will be further evolved to study the integration services; this part of the work is expected to be completed by the end of the year.

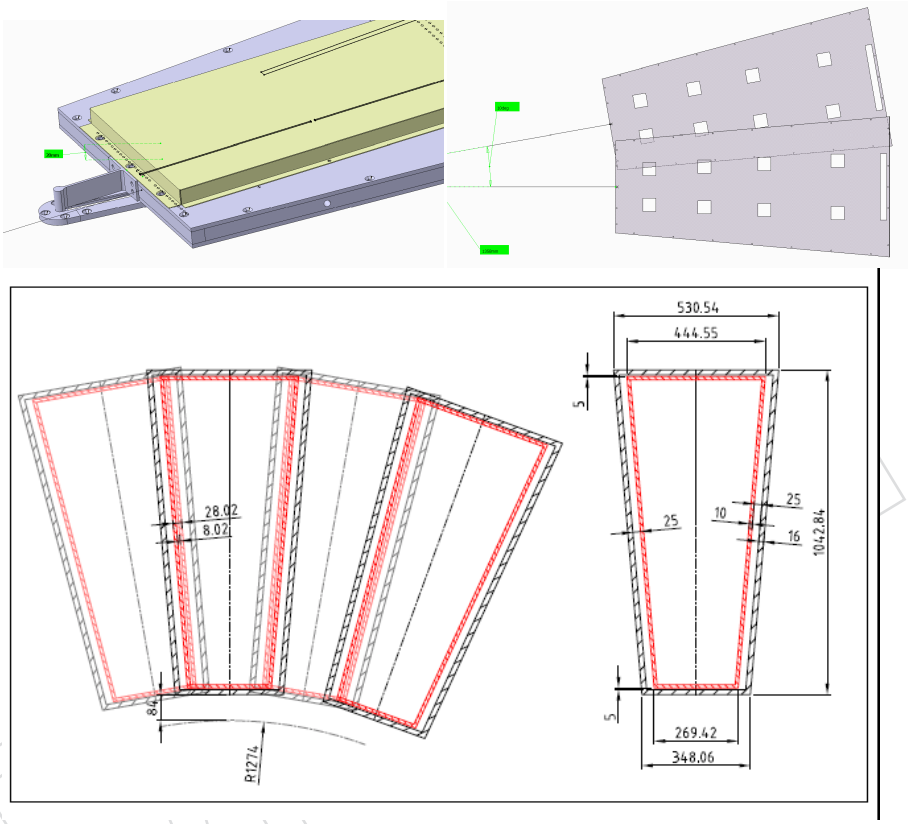

Figure B.4: Catia model of a Triple GEM detector for the YE1 disk. This design is for the nominal RE1/1 envelope.

A model of gas flow within the detector module has been initiated by importing the CATIA model into ANSYS, and optimization studies for inlet and outlet pipe diameters, volume exchange and gas flow rates have been launched.

B.4.3 Construction of a full-scale mock-up

The construction of a full-scale mock-up has been launched, based on the 3D model. Fine tuning of the distribution of HV on the GEMs and connection to the HV divider is being presently worked out. This mock-up has been prepared within the CMX-DS team and is providing vital information regarding services inside the detector module. Definition of readout strips and placement of connectors for readout electronics are important elements to be understood for the construction of an operational detector. The mock-up should be completed soon and the lessons learnt will be injected into the 3D model and used for the construction of the full-scale operational prototype.

B.4.4 Full-scale functional prototype

With the analysis of data from lab and beam tests on the small prototypes, and after the completion of the 3D model and the construction of the full scale mock-up, most of the technical specifications needed for the construction of a full-scale functional prototype will be available. These include placement of GEMs inside the supporting envelope, HV divider and distribution in respective sectors of the three GEMs, gas pipe layout, inlet and outlet diameters, support and connectors for HV, LV and front end electronics, cabling layout.

The surface treatment workshop (EN-ICE) has demonstrated fabrication of large size GEMs for the (LNF-RD51) KLOE-II experiment. The DT-RD51 group has validated a pioneering method of framing GEMs using a thermal technique, while the Frascati group has established the technique for stretching large GEMs over frames. After an evaluation study to choose the most suitable technique, we will customize it for the trapezoid shape required for this application. Additionally, if honeycomb spacers are proven to be a valid option, they could allow piling the triple GEM sandwich without the need for stretching the foils, which would be an important step for large-scale production.

The geometry of the readout strip plane can be optimized to maximize the trigger and tracking performance of CMS. For the purpose of the construction of the prototype, a pragmatic choice of strip widths will be made based on the number of electronic channels available in time for the tests. If time permits studies will be performed using the PSpice simulation software, in view of further optimization.

The electronics that we will use for the prototype is being developed by INFN (Siena and Pisa), based on the TOTEM VFAT chip. The VFAT is a digital on/off chip and has an adjustable threshold for each of the 128 channels; it uses 0.25 micron CMOS technology and its trigger function provides programmable fast OR information based on the region of the sensor hit. This can be used for the creation of a trigger while tracking function provides precise spatial hit information for a given triggered event. Some improvements are foreseen in the VFAT2 chip in preparation, but that does not impact this feasibility study.

Within one year we expect to have relevant results from tests with the full-scale prototype, and we plan to write a final report on the basis of those results (see below). Additional tests in magnetic field and long-term tests will be significant, but are not planned in this time frame.

B.4.5 Evaluation of the construction project

The main deliverable of this R & D project will be a report summarizing the work done, and providing a first evaluation of a possible construction project aiming at equipping the high η vacant zone of the CMS muon system with triple GEM detectors.

In addition to the tasks described above, a complementary engineering study will be performed to explore the possibility of extending further the η coverage towards $\eta = 2.4$, and to investigate the implications of the slightly different geometry of the disks YE2 to YE4 compared to YE1 (as mentioned above, the full-scale prototype will be built for the YE1 geometry, and for the nominal RE1/1 envelope covering up to $\eta = 2.1$).

The final report will address the following points:

- Design of detectors, including electronics and services, and their integration in CMS. Details of the full-scale prototype, modifications required to extend the rapidity coverage and to adapt to the YE2-YE4 stations.
- Data collected using small prototypes and full-scale prototype, providing evidence

for adequate performance and robustness. Additional tests required and possible remaining open issues. Additional studies required for optimizing the detector design (notably granularity).

- First estimates of resources needed for a full construction project (material cost, personnel, facilities); first assessment of a realistic construction schedule.
- List of Institutes interested in a possible construction project and resources that they could provide (financial contribution, personnel, facilities and infrastructure, specific competence).

Such report is intended to provide sufficient information to evaluate the feasibility of a possible construction project. Simulation studies to quantify the improvement in the muon tracking and trigger performance of CMS and evaluate the benefits for the reconstruction of specific physics channels are currently not part of this R & D project.

B.5 Participating institutions and available resources

The R & D project is presently supported by the following groups:

- CERN CMX-DS (CMS collaborators)
- CERN PH-DT, EN-ICE
- Laboratori Nazionali di Frascati dell'INFN (CMS)
- University of Ghent (CMS)
- Peking University (CMS)
- INFN Pisa/Siena

Other Institutes have expressed interest in contributing to the R & D, and to a possible future construction project:

- BHU India
- NISER India
- Delhi University India (CMS)

An overview of contributions to the different tasks is given in Table B.2. The R & D project, as structured today, appears to be reasonably well covered; however additional contributions could be integrated and would be highly beneficial as they would allow the performance of some of the additional studies previously mentioned which are not part of the current work plan. A tentative schedule showing the different tasks and main activities is presented in Fig. B.5.

B.6 Conclusions and outlook

We have presented an R & D project with a clear work plan and schedule; the purpose of the R & D is to establish the feasibility of a possible construction project to populate the high η part of the CMS RPC system, currently empty, with triple GEM detectors. The tasks currently included in the work plan are reasonably well covered by the resources contributed by the participating Institutes, and should provide sufficient information for a first evaluation of a possible construction project. Additional aspects might be studied in the time frame defined if other groups join the effort.

Table B.2: Participating institutes and resource sharing

Item	CMX	PH-DT	Fras	Siena	Gent	FT	Peking
small-size prototypes							
construction work		x					
material cost	50%				50%		
tests & data analysis	x				x	x	x
Modeling of full-scale detector							
dev. of 3D Catia model	x						
gas simulation studies	x	x	x				
integration of services	x	x					
Full-scale mock-up							
construction work	x	x					
material cost (1 kCHF)	100%						
full-scale functional prototype							
detector construction work	x	x					
detector material cost (30 KCHF)	50%				50%		
electronics components				x			
electronics assembly & testing				x			
electronics cost (10 KCHF)				x			
tests and data analysis	x	x	x		x	x	x
evaluation of construction project							
resources, cost, schedule	x	x					

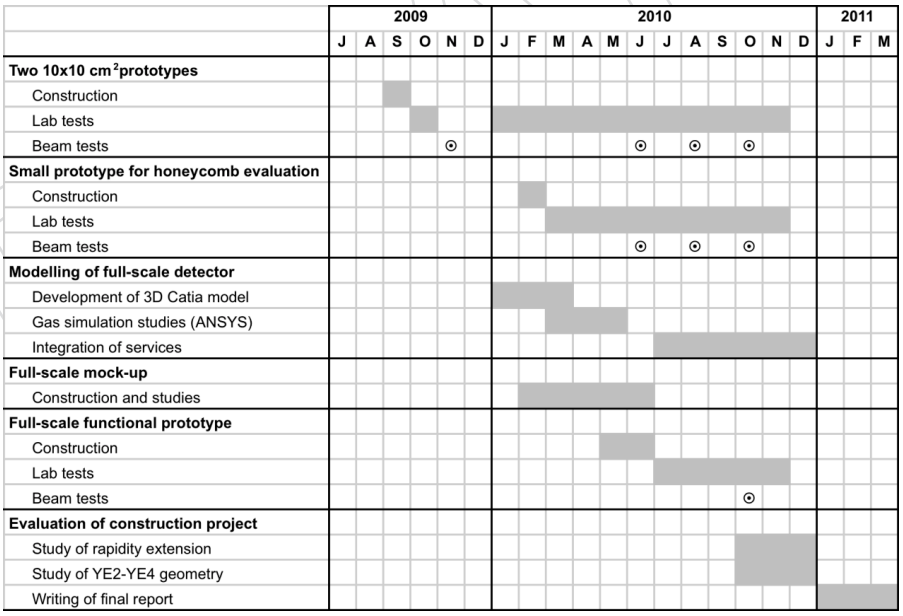

Figure B.5: Tentative schedule for the evaluation of the prototypes. The final report is expected to be submitted in Spring 2011.

We expect to present a final report in Spring 2011 summarizing the outcome of the work planned. A possible continuation of the activities will depend on the interest of the CMS community.

Based on current knowledge, we expect that production of mpgd detectors for the high-η region could be handled by two production centers working in parallel for two years. Hence a construction project aiming for installation during the long shutdown planned for the middle of the decade is possible. The expected cost scale is between 10 and 20 MCHF. More reliable estimates will be possible after the experience of building and operating the prototypes.

Appendix C

Phase 1 ECAL upgrade

C.1 Motivation

The effect of ionizing radiation on the electromagnetic calorimeter has been well documented in the ECAL TDR [**?**]. It was written in the early days of construction, but now with production complete much of our understanding at that stage remains the same. In summary the main points are:

- Radiation does not affect the scintillation mechanism
- Low energy neutrons do not give any visible damage effects
- Gamma radiation causes the creation of colour centres at sites where there are already existing crystal defects
- The colour centres recover at a rate that is temperature dependent, with higher temperatures giving shorter lifetimes for colour centres
- The loss of the optical transmission under gamma irradiation stabilizes at a level that is determined by the rate of color centre creation and their recovery

Since the time of the TDR there have been several further refinements to our understanding [**?**]. Firstly, it has been demonstrated [**?**] that large fluxes of high-energy hadrons damage the optical properties of the crystal by creating some quasi-permanent colour centres, with lifetimes of years rather than days. This effect is attributed to nuclear interactions and is distinct from the effects due to ionizing radiation. For brevity we will refer to it as 'nuclear damage.'

All damage effects, created by gamma irradiation or by charged particles, are fully mitigated by exposure of the crystals to high temperatures ($\approx 300^{o}$C) for several hours.

It has also been observed that the injection of light can reduce the number of colour centres. This process is known as "stimulated recovery" or "optical bleaching".

In this appendix we describe a potential upgrade to the endcap electromagnetic calorimeter (EE) that we are considering in the light of these recent observations. We describe the program of tests that ECAL is currently conducting to quantify the stimulated recovery process as applied to crystals in EE, the changes to EE that would be required to exploit it, and the decision process to determine whether or not to proceed with any changes.

C.2 Effects of Radiation Damage

The radiation-induced damage effects estimation, presented in the TDR, was made for the "nominal" LHC operation: 10 years at peak luminosity $10^{34}\text{cm}^{-2}\text{s}^{-1}$, for an integrated luminosity of 500fb^{-1}. The expected total doses and dose rates in ECAL are given in table C.1

	eta	Ionizing radiation dose rate, Gy/h	Integrated Ioniz. Rad. dose kGy.	Integrated neutron fluence, cm^{-2}	Integrated charged hadron fluence, cm^{-2}
EB	0	0.18	2.5	$1.2x10^{13}$	$2x10^{11}$
	1.48	0.28	4	$2x10^{13}$	$3x10^{11}$
EE	1.5	0.29	4	$5x10^{13}$	$3x10^{11}$
	2.6	6.5	90	$7x10^{14}$	$2x10^{13}$
	3	15	200	$1.8x10^{15}$	$4x10^{13}$

Figure C.1: Expected total doses and dose rates in the ECAL for nominal LHC operation

The new Phase 1 operation scenario divides LHC operation into three periods:

- Period 1 (2010-2011). Beam energy 3.5 TeV, peak luminosity $10^{32}cm^{-2}s^{-1}$, integrated luminosity of $1fb^{-1}$
- Period 2 (2013-2015). Beam energy 7 TeV, peak luminosity $10^{33}cm^{-2}s^{-1}$, integrated luminosity of $100fb^{-1}$
- Period 3 (2017-2019). Beam energy 7 TeV, peak luminosity $10^{34}cm^{-2}s^{-1}$, integrated luminosity of $700fb^{-1}$

The corresponding dose rates and total doses of hadrons, and the associated light losses induced are given in tables C.2, C.3 and C.4. In these tables the light yield loss induced by gammas is the steady state level that will be reached during running, estimated from the dose rate. The light yield loss induced by charged particles is the estimated value of the light yield at the end of the running period, with the value being determined by the integrated hadron flux.

	eta	Ionizing radiation dose rate, Gy/h	LY loss induced by Ioniz. Rad. %	Hadrons, integrated fluence, cm^{-2}	LY loss, induced by nuclear interactions, %
EB	0	0.000018	0	$4x10^{8}$	0
	1.48	0.000028	0	$6x10^{8}$	0
EE	1.5	0.000029	0	$6x10^{8}$	0
	2.6	0.00065	0	$4x10^{10}$	0
	3	0.0015	0	$8x10^{10}$	0

Figure C.2: Expected total doses and dose rates for "Period 1" of LHC operation

	eta	Ionizing radiation dose rate, Gy/h	LY loss induced by Ioniz. Rad. %	Hadrons, integrated fluence, cm^{-2}	LY loss, induced by nuclear interactions, %
EB	0	0.018	0	$2x10^{10}$	0
	1.48	0.028	0	$3x10^{10}$	0
EE	1.5	0.029	0	$3x10^{10}$	0
	2.6	0.65	3	$2x10^{12}$	25
	3	1.5	5	$4x10^{12}$	40

Figure C.3: Expected total doses and dose rates for "Period 2" of LHC operation

	eta	Ionizing radiation dose rate, Gy/h	LY loss induced by Ioniz. Rad. %	Hadrons, integrated fluence, cm^{-2}	LY loss, induced by nuclear interactions, %
EB	0	0.18	4	$3x10^{11}$	6
	1.48	0.28	5	$4x10^{11}$	10
EE	1.5	0.29	5	$4x10^{11}$	10
	2.6	6.5	10	$3x10^{13}$	80
	3	15	23	$5.8x10^{13}$	90

Figure C.4: Expected total doses and dose rates for "Period 3" of LHC operation

As can be seen in the tables we expect there to be no damage to either calorimeters during the first period; effects, especially in the high eta region, begin to appear in second, and some significant light losses in the third period in the endcap calorimeters will be seen in the last period.

While we characterize the damage in terms of light yield loss, there is an additional effect: the uniformity of light collection as a function of the longitudinal position of its emission is compromised. This adds to the constant term in the energy resolution. Since nuclear damage tends to be more uniformly distributed along the length of the crystal, the light collection will hence be non-uniform in crystals for which the optical absorption length is of the same order as the length of the crystal.

As discussed in the TDR, we have included in our design a laser monitoring system to track the short-term changes in the optical transmission in the crystals. The expected changes in EB are within the range, covered by the ECAL precise light monitoring system design, and we ought to be able to correct for these varaiations with the required precision of 0.3%. The situation is less clear as the changes in the optical transmission EE will be more severe than anticipated in the TDR, due to the addition of the hadron damage.

It is clear that at high eta, with the expected high levels of radiation fluence, the monitoring and correction of the changes in the crystal properties will pose a considerable challenge to the experiment.

C.3 Stimulated Recovery

The first reports of stimulated recovery application to $PbWO_4$ crystals were made by the CMS Caltech group [**?**], where it was observed that blue light improved the crystal's transmission and that UV light damaged them. More recently the GSI group, in the context of the Panda experiment [**?**], observed that crystals that had been exposed to ionizing radiation recovered faster when illuminated with near-infrared light than would be expected by thermal recovery alone. This result has been confirmed by further experiments performed by a GSI-INP (Minsk) collaboration with help from the ETH Zurich group. That collaboration observed indications of stimulated recovery in the range of wavelengths from 465 nm to 1550 nm. The rate of recovery for the same optical power is observed to be greater for shorter wavelengths [**?**]. At shorter wavelengths the light itself damages the crystals, as was observed by Caltech.

While it is clear that there is a direct benefit from the stimulated recovery of colour centres created with ionizing radiation, it is less clear that it can be used to aid in the annihilation of colour centres created by nuclear interactions. The GSI-ETH-INP groups have observed the partial op-

tical recovery of EE-type crystals, irradiated by hadrons to a fluence of 10^{13} protons/cm^2.

C.4 Current R&D results and plans

To address the question of the viability (and utility) of using stimulated recovery to stabilize the crystal performance there are three areas that will be investigated thoroughly:

- We need to quantify the effect of the stimulated recovery, addressing such questions as how much optical power is required to usefully reduce the radiation damage effects
- We need to understand the requirements for the installation and operation of the system, and estimate the time, cost and personnel resources required to execute it
- We need to establish that the injection of infrared light will not have any adverse effects on the existing system

The ECAL community has begun an extensive program to investigate this effect using a matrix of endcap crystals at the H4 test beam. The steps that we have so far completed are:

- Extensive measurements of the light output of crystals with varying levels of radiation damage by hadrons. [**?**]
- Measurement of the energy resolution observed in heavily damaged crystals at H4. (November 2009)
- Measurement of stimulated recovery with an 800 nm LED after irradiation with gammas and electrons. (July 2010)

In parallel we have irradiated at the CERN PS twelve endcap crystals with 10^{13} protons/cm^2. These will subsequently be incorporated into a crystal matrix for studies in the H4 beam of their performance and to investigate the effects of stimulated recovery on these hadron damaged crystals. In addition we will conduct bench tests to determine the optimum light injection parameters (wavelength, power and delivery mode).

For the design of a suitable light injection system it seems, based on bench tests and initial results from beam tests that the current light injection system, used to inject laser light into the crystals, will not be sufficient since the light injection system delivers only one ten thousandth of the laser light to the crystal. As initial estimates put the required delivered optical power at a level of $\sim$ 20 mW this reduction factor makes the use of the laser distribution fibers unfeasible. The next possible injection method is through a 5 mm diameter hole at the front face of each crystal, that was used during construction for single channel testing. This method would require the placement of fibres and routing to the outside of the endcap volume. It would also require the routing of the fibers to a point where a light injection system could be set up. The planning, design and cost estimate of this will begin once the optical power level required is better understood from the beam tests and bench test measurements.

Before we decide to proceed with this upgrade we will also conduct extensive bench and system tests to make sure that the injection of infrared light into the crystal does not have a deleterious effect on the crystal or the VPT. One possible effect, which will need to be thoroughly tested, is the slow degradation of the VPT. This could be caused by, for example, a slow evaporation of the photocathode.Only when these three parts of the program are complete will we be in a position to judge the benefits and the feasibility of doing it. We expect that this decision point will be reached by the end of 2011. While we recognize that any modification to the endcap calorimeter requires a considerable amount of work and resources to achieve, and will

be accompanied by associated risks, we consider that in the light of the possible severe degradation to the light output of the crystals that we can expect to occur, we need to investigate thoroughly this possibility to mitigate the effects.

Appendix D

ZDC Shower Maximum Detector

The transverse distribution of forward neutrons from pp collisions is sensitive to the gluon distribution within the proton. For proton - proton collisions forward neutron distributions probe the proton wave-function at low Feynman X [42, 43, 44] while the distribution of photons can be used to deduce the total pp cross section [45].

The ZDCs are two identical small, forward calorimeters located between the two LHC beam pipes at approximately $z = \pm$ 140 m, on each side of the CMS interaction region, [46]. They reside in special detector slots in the neutral particle absorber, the TAN, which is designed to protect the first superconducting quadrupole from synchrotron radiation. A photograph of one of the detectors is shown in Fig. D.1. The Flow Detector is a segmented layer of the ZDC near shower maximum that will allow CMS to increase its physics reach in the very forward region.

Figure D.1: A photograph of ZDC- in the the TAN absorber. The CMS interaction region is 140m to the left of the detector.

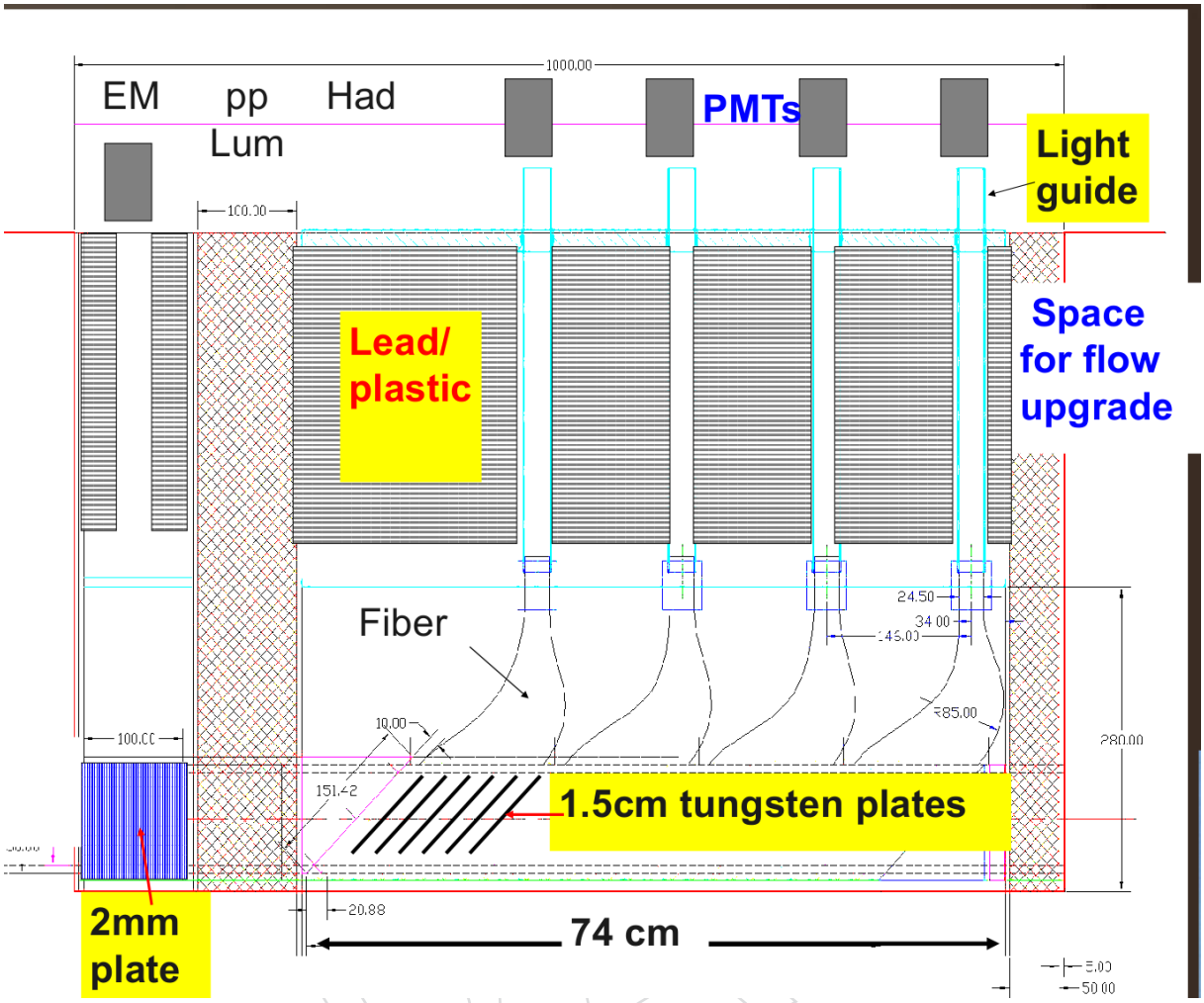

Figure D.2: A side view of the ZDC showing the EM and HAD sections.

As such it plays on a natural strength of CMS, its almost complete angular coverage.

The ZDCs are designed to detect neutral particles, mainly photons and neutrons, with pseudo-rapidity $|\eta| \geq 8.3$. Each ZDC is a sampling calorimeter with tungsten plates for the absorber and quartz fibers, organized into ribbons as the active medium. Each ZDC has two sections: an electromagnetic (EM) section optimized for photon detection and energy measurement; and an Hadronic (HD) section measure the energy of neutrons. The EM section is segmented into 5 vertical strips which can give a measure of the X position of incoming photons. The hadronic section is divided into 4 depth segments. The two sections are separated by the BRAN, a copper ionization chamber which serves as a luminosity monitor.

Figure D.2 shows the schematic layout of one ZDC while Fig. D.3 is a picture of the hadronic section. In the hadronic section the tungsten plates are tilted by 45^o in order to optimize collection of the Cherenkov light. There is no room for this in the EM section and so these tungsten plates and fibers run vertically. Individual fiber ribbons are grouped together to form a readout bundle which is compressed and glued into a circular shape. From there an air light guide carries the light through radiation shielding to a Hamamatsu R7525 phototube.

The slot in the TAN is 10cm wide and 100cm long. When the ZDC was designed 5 cm was reserved for the flow detector. We are now ready to use this space to measure the transverse

Figure D.3: Photograph of the ZDC HAD section during construction showing the gray tungsten plates, the sheets of quartz fibers and the light guides. The lead/boronated polyethyene shield that lies above the tungsten plates was not yet installed.

Table D.1: Main parameters of PMT.

Quantum Efficiency at 350 nm	43%
Gain	2000000
Dark Current, max (after 30 min)	2 nA/ch
Rise Time	0.6 ns
Transit Time	6.8 ns
Rate Capability	0.1 MHz
Pixel-to-pixel cross talk	<5%

position of incoming particles by instrumenting a plane near the maximum of the showers. The flow detector will have an active area of ∼79 mm in width and ∼90 mm in height. The granularity of the detector is matched to the Molare radius of tungsten. We are investigating whether to use strips or pads using a GEANT simulation. Initial results suggest that we can attain a position resolution less than 1cm. This will be sufficient to measure the transverse distribution of neutrons. We plan to use quartz fibers to carry the light to Hamamatsu multi-anode photomultipliers located on the top of the TAN.

Given the rising LHC luminosity the detector t must be radiation hard and so the active medium will be quartz or perhaps GSO. The shower maximum layer is not designed to measure energy but merely the transverse position of the showers. Since an unbiased ensemble of collisions is azimuthally symmetric the detector is essentially self calibrating.

D.1 Design Requirements

One possible configuration of the shower maximum plane is shown in Figure D.4. We plan to use 32 readout strips (10 strips in X and 22 Y strips in two layers, 11 Y strips for each layer) with width and thickness of 7.5 mm. Wavelength shifting fibers of diameter 0.83 mm will be embedded in each strip or pixel and will transport light to to the photodetector at the top of the detector. Each strip or pixel will be wrapped with reflective aluminized Mylar tape.

D.2 Photodetector

As a photodetector we are planning to use the 32-pixel HAMAMATSU H7260 - 200 photo-multiplier. We found that the performance in cross talk, timing, effective quantum efficiency and dynamic range to meet our needs. The performance of this phototube is summarized in Table D.1.

The PMTs will be delivered with a complete resistive base. For heavy ion running the current will be less than 6 μA but for pp running we expect the current to be significantly higher. It may therefore be necessary to install a voltage divider across the secondary cathodes of the photo-tube. During running, the gain will be monitored with a Laser system, which will distribute light pulses to each pixel. The PMTs with the HV base, high voltage and signal connectors and short high voltage and signal cables will be located on the upper level of the detector enclosure.

Our design requires 64 HCAL QIE channels. We believe that these can be spare HCAL modules. The high voltage can be generated at the tube by a special Hammatsu supply that only requires a 15V input. The ZDC already has a laser system which sends light from the HCAL laser room to a distribution near each ZDC. The input light is currently heavily attenuated and we have plenty of spare light which could be used to monitor the shower maximum detector. All that is

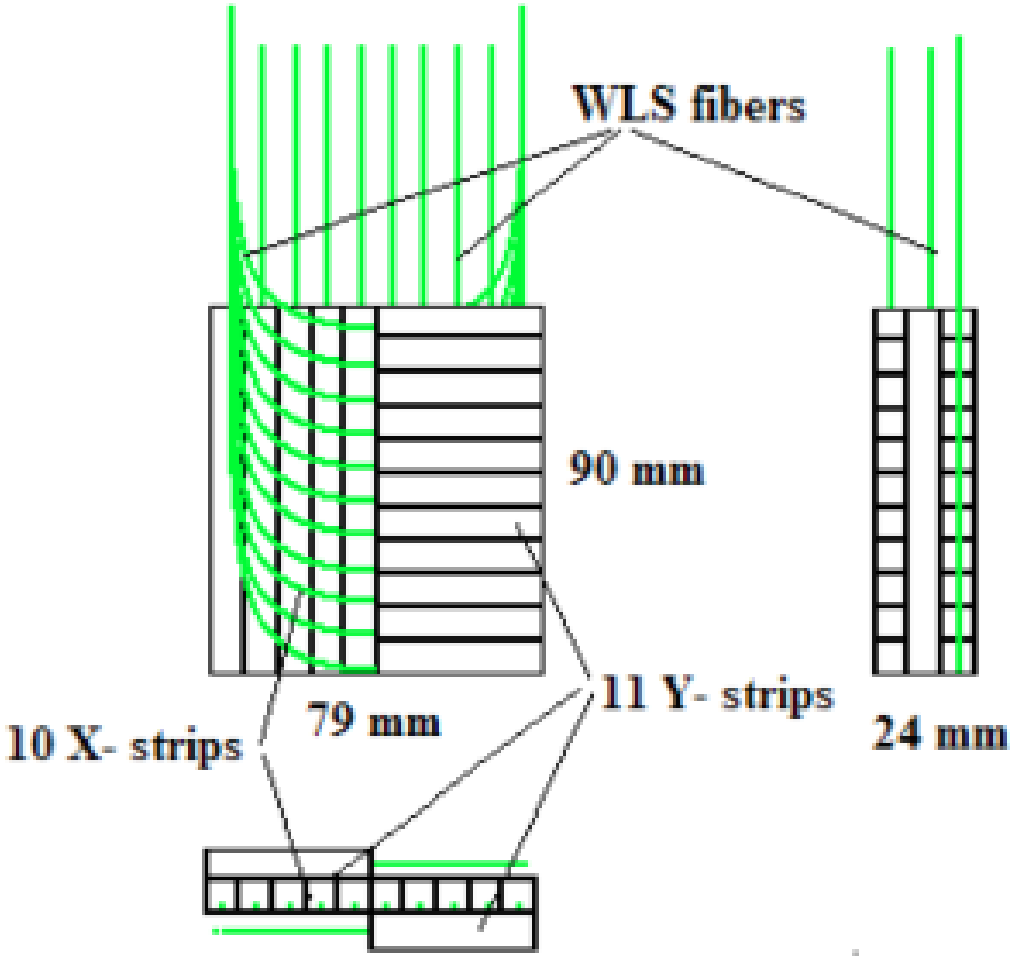

Figure D.4: The active area of the Flow Detector for the ZDC.

necessary is to build new light distribution boxes with more outputs.

If possible we will bring the signals out to the underground service cavern. This is very convenient in terms of setting up and maintaining but at Chf 5/cable/m laying 64 200m cables would cost Chf 64 K. We believe that we can transmit 8 signals per line on multicore cables. Alternatively we may install the QIEs in the ZDC bunkers. The are small rooms made from concrete blocks that will be used to store the ZDCs when they are not being used. They are situated at the junction between the main tunnel and the bypass tunnel, about 10m away from the ZDCs.

D.3 Detector Preparation

The first prototype will be built and tested in a dedicated beam line (FNAL, BNL or CERN) in 2011. Generally, a compromise among a few parameters is needed. These include signal-to-noise ratio, gain and rate performance. These issues will be addressed specifically during bench and the beam tests. The prototype will be checked for uniformity of gain response using radioactive sources in a test bench prior to beam test. Because the prototype will be the full-scale detector, it is extremely important to prove the overall mechanical integrity of the detector in such aspects as thickness, width, light leak-tightness, etc.

D.4 Project scope, cost, and schedule

The project comprises the following elements: the active detector itself with the optical read-out system, monitoring and high voltage system. In detail, the scope includes the following:

1. Detector, mechanical structure and installation: Active area and mechanical structure, Detector assembly
2. Photo detector readout system: Light tight enclosures and optical distribution system, Photo detectors, HV and control, calibration and monitoring system, system assembly, Signal and HV cables
3. Test beam: infrastructure, DAQ, data collection and analysis
4. Electronics: Crate, Digitizers, Controller, Interface card, Slow control interface card, HV power supply
5. Bench test: Radioactive sources, DAQ, HV Power supply and control

A cost estimate is shown in Table D.2 .

Table D.2: Rough cost estimate for the flow detector upgrade.

Item	Quantity	Unit Price	Total
QIE Channels	64	from HCAL	0
CCM Module	1	from HCal	0
HTR Module	2	from HCAL	0
Signal cables	10	$ 3/m * 200m * 10	$6 000
HV Cables	2	$1/m * 200m	$400
Laying Cables	12	$5/m * 200m	$12 000
32 Channel PMT	2	$6150	$12 300
Hamamatsu HV	2	$1000	$2 000
Laser splitter	2	$500	$1 000
Detector	2	$10 000	$20 000
Total			$53 700

Appendix E

Forward Shower Counters

This proposed upgrade is a scope extension to the core of the present beam instrumentation. However it adds a very powerful tool to the beam diagnostics available to CMS. To a certain extent, the forward shower counters can be seen as an extension of the beam scintillator counters along the beampipe outside the CMS cavern.

It is proposed to add very forward shower counters closely surrounding the beam pipes with 59 m $\lesssim |z| \lesssim$ 140 m from IP5 on both plus (+) and minus (-) sides. These locations are beyond the Tertaiary Absorber of Secondaries (TAS) which defines the extent of the CMS cavern and before the Tertiary Absorber of Neutrals (TAN) and the Zero-Degree Calorimeter (ZDC), and where both incoming and outgoing beams are in a common pipe. Over much of this length the beampipe is warm and accessible in some places. These counters are termed the Forward Shower Counters, FSC; they do not detect primary particles directly from the pp collisions, but showers produced by small angle and high energy ($\sim$ TeV) particles that hit the beam pipes and surrounding material.

Similar forward shower counters have been used in CDF, ZEUS [**?**] and elsewhere. The Collider Detector at Fermilab, CDF, included a similar set of counters (called Beam Shower Counters) used in veto at level 1 for some physics (central exclusive production). These detectors made several valuable contributions to the physics output.

The counters will cover $7 \lesssim |\eta| \lesssim 11$, where $\eta = -\ln \tan\frac{\theta}{2}$ is the pseudorapidity, depending on the particle type and p_T. By nearly completing the rapidity coverage of CMS, the total solid angle approaches $\Delta\Omega \sim 4\pi$, and almost all inelastic collisions will be detected. In the next section we discuss possible locations.

Primarily they will be important for understanding beam-related backgrounds (beam-gas, beam halo-pipe, etc.), complementing other monitors such as the BSC. In addition they give added value to the CMS physics programme. References [**? ? ?**] present the physics case for the counters.

E.1 Baseline Design

The baseline design for the counters is to have two at each of several z locations, one above and one below the beam pipe. The scintillator chosen is NE110 equivalent, and the proposed PMT is Electron Tubes XP2020 (Previously a Philips PMT). Four prototype stations are already available, with a active area of 20x10cm with 1cm thick scintillator material. Each station has a complete weight, including shielding of about 5kg.

It is also proposed to add a few (perhaps two on each side of CMS) directional Cherenkov counters (DCC) [**?**]. These are simply cylindrical rods of cast acrylic plastic, about 5 cm in

diameter and 12 cm long, closely adjacent and parallel to the beam pipe. With a PMT at each end, incoming and outgoing particles (or showers) can easily be distinguished by the pulse height asymmetry. Placed close to a scintillator that can distinguish incoming and outgoing showers by timing, each can monitor the performance of the other.

The counters should be mounted in the tunnel, using standard support stands already in use for beam instrumentation in the tunnel, such as the beam loss monitors or RADMON devices. No services will be required for the counters, except HV supply and signal cables, and possibly a fibre for calibration.

E.2 Locations in LHC tunnel

A discussion of the possible locations (in z) of FSC counters is presented in the accompanying note [**?**]. Here we briefly mention seven positions shown in Table 1 (in each of the + and - directions) in front of and behind the MBX magnets, where the warm elliptical beam pipe is accessible, see Fig **??**, and detectors can be placed. Beyond those locations there are further places out to 140 m where the vacuum pipe flares and the TAN is located, but the (circular) beam pipe there has larger diameter, 22.5 cm. There are 3 m concrete shielding blocks at z = 107.2, 118.2 and 131.2 m, and their front face, as well as the front face of the TAN, may be good locations, shielded from incoming particles. Some locations are best placed to distinguish incoming and outgoing beam halo using timing; with 50 ns between bunches the maximum time difference Δt is 25 ns, easily distinguishable. We will show some MARS simulations of coverage for counters in these MBX locations. Further simulations are now being done to choose z-locations that maximise the forward coverage (e.g. for the total inelastic cross section, and for low mass diffraction). Also, some z-positions may be more useful than others for beam background monitoring. A location closer to the interaction point, e.g. between the quadrupole triplet and the TAS, will also be considered, mainly for background tagging.

Location	z(mm)	Δt (ns)
1	59426	3.8
2	63751	0.0
3	68026	3.5
4	72301	7.0
5	76576	10.5
6	80851	11.0
7	85126	7.5

Table E.1: Possible locations of counters on each (+ and -) beam pipe around the MBX magnets, as used in the simulations, and the time difference Δt between incoming and outgoing bunch passes. Additional locations beyond the MBX magnets with 12.5 ns bunch separation are available.

The FSC counter locations are close enough (closer than the ZDC) for their signals to be included in level 1 triggers. The minimal (and probably sufficient) trigger signal is a logical-OR of all the FSC on each arm. These will be used both in a positive requirement and as a veto, together with a central signal Y, where Y = central $\sum E_T$, di-leptons, jets, etc., sometimes in combination with E_T or E sums from the HF (again, either positive or in veto). The possibility to use simple logical combinations of these counters is kept open at this time. It is also foreseen to provide a background tag for incoming background from the LHC tunnel to the CMS detector, using hit timing as a discriminant, to be used as a background veto should it be required. This

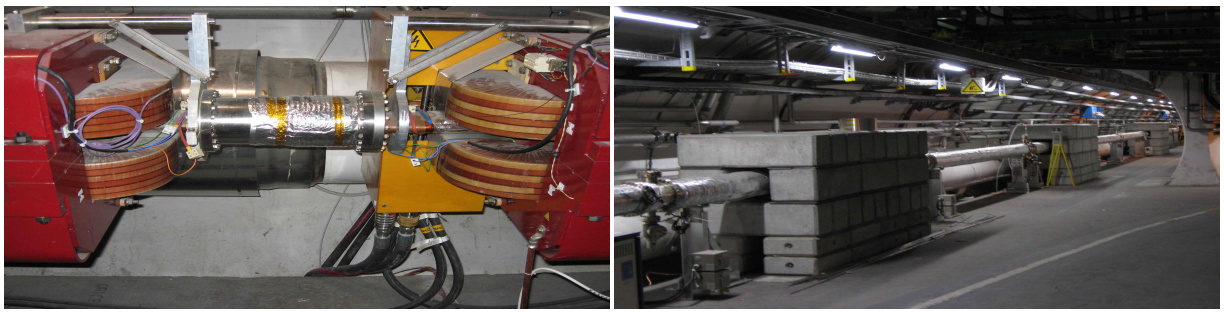

Figure E.1: A region between MBX magnets where FSC counters can be placed (left) Region in the LSS beyond the MBX magnets where FSC counters could be placed (right).

background tag should be particulary informative in terms of locating the origin of beamgas events.

E.3 Towards 4π coverage for CMS, and σ_{inel}

At present there is no detector at the LHC that has very close to complete coverage for inelastic collisions. Experiments cover a large fraction of the 4π solid angle but not the small polar angles, θ, where the particle density is high, as are their typical energies. At the highest energy at which these cross sections have been measured, the Tevatron with $\sqrt{s}$ = 1800 GeV, σ_{tot} = 72 − 80 mb, and $\sigma_{elastic}$ = 16-20 mb, implying (although it has not been directly measured) σ_{inel} = 52-64 mb.

The existing detectors of CMS from $\eta = 0$ to the forward edge of the HF calorimeter at $|\eta_{HF}(max)|$ = 5.2, are essentially free of cracks and have good efficiency for detecting all events that have particles in that region. Beyond that, CASTOR (on one side only) with $5.2 < \eta < 6.4$ is a deep electromagnetic and hadronic calorimeter. The beam (true) rapidity at $\sqrt{s}$ = 7 (10) (14) TeV is 8.9 (9.3) (9.6).

E.4 Simulations (MARS)

We have used the MARS simulation [**?**] for the generation of forward particles in pp collisions, as well as of beam halo and beam losses in the region, with a detailed simulation of particle showering in all materials (beam pipe, collimators, magnets etc.). This enables us to predict particle fluxes in the FSC detectors from both incoming and outgoing beam-generated showers, and to calculate the probability for collisions that non-diffractive and diffractive pp collisions have counts in this region, i.e. their efficiency at rejecting pile-up and their efficiency at detecting rapidity gaps. A similar exercise needs to be carried out to calculate the efficiency of tagging beam gas and beam halo backgrounds.

The dimensions of the counters used in the simulation were ±12.5 cm horizontally (x) and ± 25 cm vertically (y) centred on the beam pipe, and at the z locations given in Table 1, around the MBX magnets.

Figure E.2 shows (colour) a map of energy deposition in fluxes (cm^{-2}s^{-1}) for electrons (left) and hadrons (right) in showers. Figure E.3 shows the average deposited energy per pp-collision for the seven locations; it is higher above and below the beam because of the elliptical pipe together with a strong dependence on the distance from the beams. The spectra of different particle types in the showers is shown in Figure E.4 on the inside of the LHC ring (i.e. towards the LHC centre; up and down and outside are similar).

The radiation levels are calculated to be about 1750 Gy/fb^{-1} for the left and right detectors, and about 730 Gy/fb^{-1} for the up and down detectors. However the absorbed dose is a factor ≈ 25 higher close to the beam pipe than at the outer edges, as shown in Figure E.2. Radiation hard scintillators can survive up to about 10^4 Gy, so they may need replacing after a few fb^{-1}.

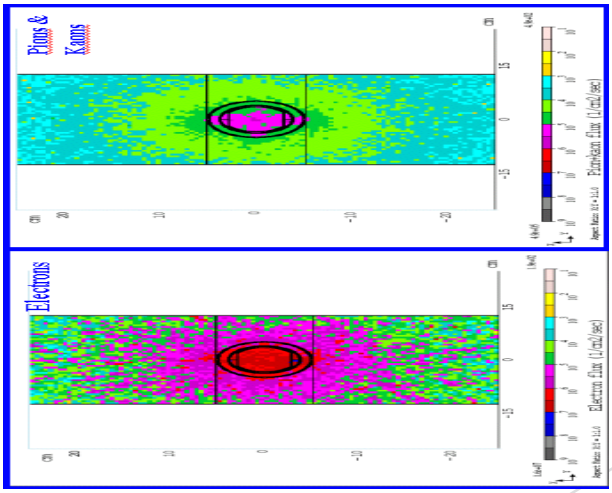

Figure E.2: Transverse (x, y) view of deposited energy at a luminosity of 10^{32}cm^{-2}s^{-1}. Electrons and photons (left) and pions and kaons (right).

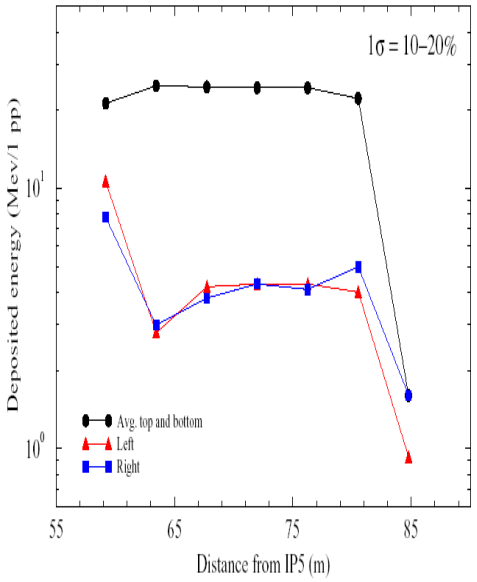

Figure E.3: Average deposited energy, in MeV per pp-collision, at the seven locations simulated and separately for the inside (L) and outside (R) of the ring, and up and down (averaged).

E.4.1 Single particle efficiency of FSCs

The FSC detection efficiency for incident particles ($\pi^{\pm}$, π^0) was calculated as a function of pseudorapidity η. The requirement was at least one hit (alternatively at least five hits) in any of the FSC counters. A transverse momentum (p_T) distribution of the form $e^{-6.7p_T^2}.dp_T^2$ was assumed for the incident primary particles, corresponding to that obtained from PYTHIA 6.2 [**?**]. The efficiency of the FSCs for detecting charged particles from showers induced by the primary $\pi^{\pm}$ and π^0 is shown in Figure E.5. For charged pions the efficiency is ~70% for $|\eta| > 9.5$, and it

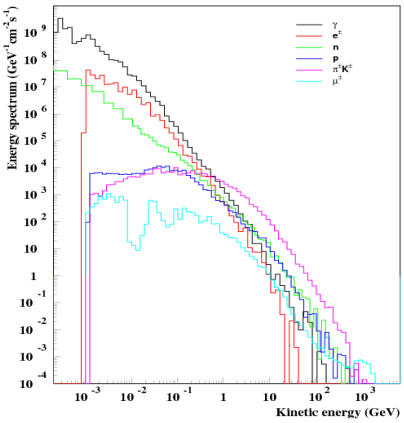

Figure E.4: Rate of different particles above 1 keV in showers generated by different particles at location 1, on the inside of the ring.

is nearly independent of the number of hits, for 1 - 5 hits per detector plane. For π^0 between $8 < |\eta| < 9.3$ the efficiency exceeds 65% (50%) when at least 1 (5) hits are required. From the results presented in the following sections, this is sufficient for most anticipated physics studies.

E.5 Installation issues and schedule

These counters are probably most useful for diffractive physics while single interactions are still frequent ($L \lesssim 10^{33}$ cm^{-2}s^{-1} for 25 ns between bunches), and most useful for understanding beam halo and conditions "immediately", i.e. as soon as they can be installed. Their background monitoring function is of course not dependent on no-pile-up conditions, and this is especially true of the directional Cherenkov counters. If approved quickly they could be ready for an installation in a short ($\sim$ 4-6 weeks) shutdown in early 2011. They offer the possibility of vetoing backgrounds already during 2011 running if required.

The counters are a low risk activity for installation. The only items required for installation in the tunnel are HV and signal cables, the scintillation counters and their supports. Neither gas nor cooling is required, and there should be no maintenance required on shorter than annual time scales. Once installed and checked out, such photomultiplier-based systems usually need no access. The supports will be simple and safe, requiring no special tooling, and will be designed for easy, fast access. It is foreseen that the supports will be based on structures already used by beam instrumentation in the LHC tunnel. The readout will be standard and identical to that used already by HF, ZDC and BRM, and the trigger logic is simple (based on YES/NO logic).

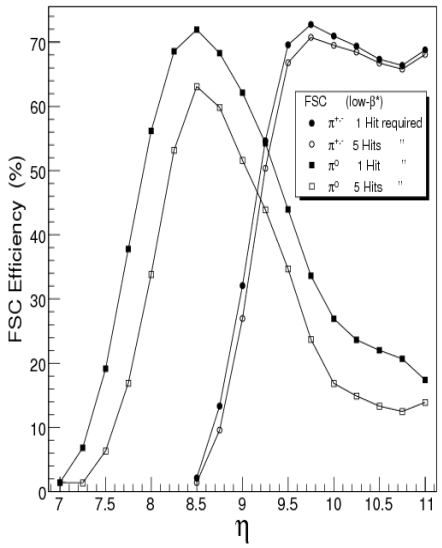

Figure E.5: The efficiency (%) of the forward shower counters (FSC) for registering particle showers induced by primary $\pi^{\pm}$ and π^0 as a function of their pseudorapidity η (low β^* conditions).

Appendix F

Phase 2 R&D

While this document concentrates on upgrades before the major shutdown in 2020, signficant R&D is required to handle the instantaneous and integrated luminosity that will follow. The Phase 2 R&D will build on the design of the Phase 1 upgrades. In some cases, the Phase 1 upgrades produce detectors that can operate successfully throughout Phase 2; in other cases, they provide an infrastructure that can facilitate the additional modifications necessary for Phase 2; and finally, the demands of Phase 2 may require the complete replacement of some detectors or electronic systems. Another coupling between the Phase 1 upgrade and the R&D for the Phase 2 upgrade is that they take place over the same 5 to 6 year period from 2011-2016. During this period, they will compete for human and financial resources. It will be a challenge for CMS to manage these two activities together so that CMS will retain the formidable physics capabiity that in possesses today not only throughout the next decade but for the one following it.

To provide a complete picture of the upgrade activities that CMS will be carrying out in the first half of this decade, we outline the requirements for Phase 2 R&D in this appendix.

F.1 The Phase 2 Tracker Upgrade

F.1.1 Introduction

An increase of the LHC luminosity well above its original design figure of 10^{34} cm^{-2}s^{-1} requires a substantial upgrade of the CMS Tracking system to cope with the much more demanding requirements and implement additional functionalities. A scenario with instantaneous luminosities of 5x10^{34} cm^{-2}s^{-1} at a rate of 40 MHz, corresponding to approximately 100 pileup events per bunch crossing, results in an integrated luminosity of up to 3000 fb^{-1} after several years of high-luminosity operation. The tracking system has to be enhanced in three main aspects: (i) higher radiation resistance, with respect to both instantaneous and integrated levels; (ii) higher readout granularity, to keep the channel occupancy at an adequate level; (iii) ability to contribute information for the Level 1 trigger. This will allow CMS to achieve the enhanced discrimination required by the increased pileup.

In addition, the new tracker concept has to comply with constraints coming from the existing CMS detector, services, infrastructures and available space in the underground caverns. It is currently foreseen to re-use the services (cables, fibers and pipes) running from the patch panel "PP1" to the back end. Since they are interleaved with those of other subdetectors, replacing them would add considerable complication and risks, and would substantially increase the length of the required shutdown. This constraint translates to a limit in the total available cross section of conductors, cooling pipes, and number of optical channels.

Such requirements and constraints drive a series of challenging developments:

- Silicon sensors have to maintain adequate performance after accumulated radiation levels $\sim$ 10 times higher than the requirements of the present Tracker. Thus higher granularity and thinner sensors are required everywhere, and radically different options may be useful for the innermost pixel layers.
- More advanced ASIC technologies have to be used. The main challenges are to cope with the high instantaneous rates in the inner pixel layers, to limit the power consumption with the higher granularity, and to implement the new trigger functionality.
- Novel powering schemes have to be employed to reduce the cross section of conductors inside the tracking volume and take full advantage of the lower operating voltage of the front-end ASICs, while remaining within the constraint of the existing supply cables.
- More efficient cooling methods have to be used to reduce the mass of cooling pipes and heat exchangers, as well as the mass flow of the coolant, and to cope with the constraints from the existing pipes.
- High-speed data links are required to handle the increased data volume generated by the increased granularity and by the trigger output, and still maintain compatibility with the installed optical fibers.
- Novel module concepts and electronics architectures need to be developed to implement on-detector data reduction, which allows the trigger functionality to be implemented while maintaining the bandwidth at an acceptable level.

Some details about these developments are given in the following sections, along with some preliminary ideas of possible detector concepts.

F.1.2 Sensor development

The sensor R&D for a SLHC Tracker Upgrade is obviously a key issue. Three main phases can be identified:

1. Evaluate different sensor technologies.
   (a) A large campaign to evaluate planar technology with different substrates has started and will go on for about 1.5 years.
   (b) Two submissions are ongoing to evaluate the 3D technology for the innermost pixels.
2. Wafer submission with all relevant geometries and connection schemes to evaluate close-to-final designs (planar and 3D if needed).
3. Pre-series of the final design.

The first phase concentrates mainly on the issue of radiation hardness, but addresses already several geometry, design, connectivity and final testing strategy issues. Fig. F.1 presents the wafer design used in the evaluation campaign on planar technology (item 1.a above), while the different types and thicknesses are shown in Table F.1.

All structures of the wafer will be subjected to neutron and proton irradiation to evaluate the materials with their final mixed fluences which mimic the conditions at different radii. This procedure emphasizes the real operational conditions of the chips and has been developed together with RD50 representatives. Basically, all structures will be evaluated for Signal/Noise after the different irradiation and annealing steps. This evaluation should be finished by the beginning of 2012. It is designed to be exhaustive, and the most relevant parts are briefly described below.

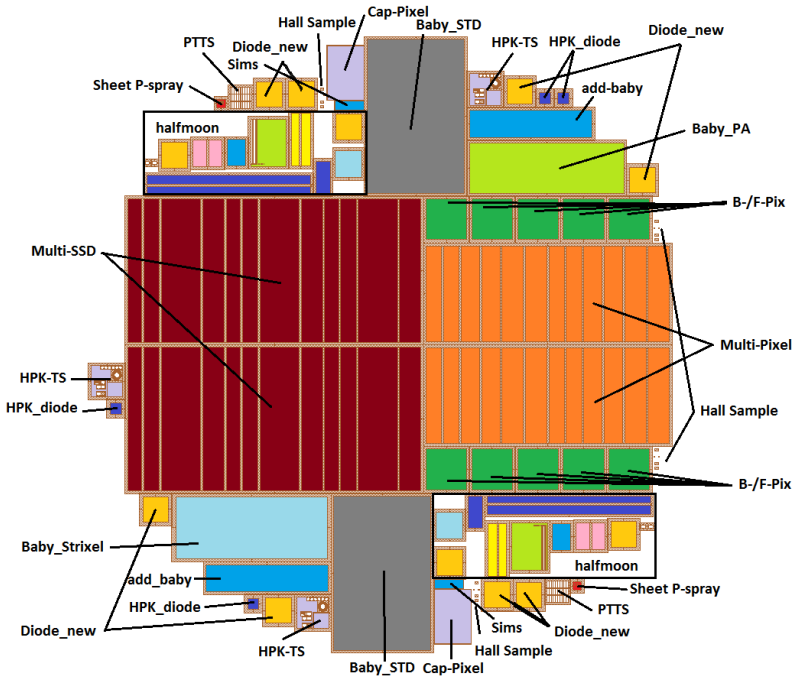

Figure F.1: HPK wafer design

Table F.1: Summary table showing the number of wafers ordered for the different combination of materials, thicknesses and production technologies. FZ stands for FloatZone, MCz for magnetic-Czochralski and EPI for epitaxial.

Substrate Type	FZ			MCz	EPI		
Active thickness (μm)	100	200	300	200	I50	100	Total
p-in-n	6	6	6	6	6	6	36
n-in-p (p-stop)	6	6	6	6	6	6	36
n-in-p (p-spray)	6	6	6	6	6	6	36
p-in-n (double metal)		6					6
n-in-p (p-stop; double metal)		6					6
n-in-p (p-spray; double metal)		6					6
Total	18	36	18	18	18	18	126

The multi-geometry strip structures represent the future outer strip detectors; they have different pitches and strip widths to evaluate and optimize inter-strip capacitances and inter-strip resistances as well as breakdown behavior. The multi-geometry long pixel structure has 1.25 and 2.5 mm long pixels to evaluate a possible use in the intermediate layers. We are testing different pitches, widths and different bias schemes. The halfmoon, also known as standard test structure, is an improved version of the former CMS one. It is designed to evaluate the process quality of the future vendor, and to investigate if it can also be used to evaluate the process parameters before and after irradiation. The minisensor has been introduced mainly to evaluate the radiation and annealing behavior. The Lorentz sensor is a standard sensor to evaluate the Lorentz angle with respect to different technologies, irradiation levels, temperature and voltages. The diodes will give us information about depletion voltage, trapping field configuration and Signal/Noise. The double metal pieces will allow us to evaluate different routing schemes, as well as the Baby_PA and Long Pixel structures, where we try to insert the PA into the sensor. Pixel detectors have been submitted to evaluate the n-in-p types. These

sensors are also valuable to test potential new bump bonding companies. At the end, one or two of these technologies will be chosen.

We are evaluating in a parallel workflow (item 1.b) the 3D technology, where we are working with two different producers. We are testing the double-sided double type column technique (DDTC). One submission has been received already and is partially bump bonded. The second submission is in the design stage, and larger sensors will be produced to enable full pixel module qualification.

In the second phase of the testing we will submit real size structures in the chosen technology (e.g. 2.5 cm and 5 cm long strips) as well as another larger field of long pixels, but with a geometry that should be similar to the final one where the pitches and widths will be defined. At that point we should have a conclusion on whether the planar technology (e.g. EPI) can give sufficient signal, or if trapping requires 3D sensors.

As a last phase we intend to order final design sensors in a pre-series to allow, if needed, a last opportunity for minor changes before we order the full series production. This scheme has proved to be very useful during the sensor production of the current CMS Tracker.

F.1.3 ASIC development

The ultra-high luminosity at the SLHC, with proportional increases in occupancy and radiation levels, presents severe challenges. For occupancy reasons the granularity will have to increase in all regions of the tracker. However, the present average trigger rate of 100 kHz must be maintained at SLHC to avoid major modifications to other sub-detectors and triggering systems, which implies that tracking information will have to be included in the L1 trigger decision.

F.1.3.1 SLHC FE chip-specific challenges

The biggest challenge for the on-detector readout is power, both consumption and provision. Advanced CMOS technologies will help, but power savings per chip will depend on functionality, which may increase. At present, it is assumed that 130 nm CMOS technology will be used for SLHC. MPW (multi-project wafer) access to the technology has recently been negotiated, and it has already been characterised for HEP applications. Mass production of readout chips has to start several years before installation, so the proposed development is timely, and the technology appears to be adequate and affordable, although more expensive than the present 0.25 μm CMOS.

Power provision is a major challenge. Since 130 nm chips operate at half the supply voltage of 0.25 μm, the supply current doubles even if the total SLHC tracker power remains the same as at the LHC. The result is increased power dissipation and voltage drops in cables. Hence the need for a more advanced power distribution, and the choice to develop on-detector DC-DC conversion, which has implications for FE chip design. Front end specifications have been developed. A number of relevant issues are still open and are the subject of wider tracker R&D. Some examples are:

- Sensor signal polarity (n-side readout of p-substrate or vice-versa).
- Solutions for each signal polarity seem essential to optimise power consumption and limited dynamic range available for the reduced supply voltages.
- Sensor-FE chip coupling: DC coupling simplifies sensor design and reduces cost, but requires the FE chip to sink or source leakage currents.

- Sensor strip lengths and pitches: capacitance and leakage current, hence noise, depend on length and pitch, requiring optimization of the amplifiers.
- Local DC-DC conversion implies stringent requirements on power supply rejection performance, which still need to be fully explored.
- Control and readout interfaces must be defined using standard electrical and signalling protocols.
- Module assembly and interconnect technology have to be optimized for large scale manufacture. Bump-bonding may be preferred, although it reduces flexibility during prototyping.
- The provision of suitable data for the L1 trigger logic, and the study of system issues permitting this to be achieved with adequately low power and impact on material.

The exact architecture of the final chips will depend on the studies of the performance of designs matched to different sensor choices, and also on system level constraints. The overall readout system must be well integrated, so the whole system must be considered early in its definition, specification and evaluation.

F.1.3.2 CMS Binary Chip (CBC) development

The current strip tracker readout system uses non-sparsified analog readout and analog data optical transmission, with digitization and zero-suppression performed off-detector. The non-sparsified approach allows a robust and simple synchronous system, where simple checks can be incorporated to identify front end chips which may go out of synchronisation. The biggest challenge for the SLHC on-detector readout is power consumption. Higher granularity means more front end chips. Un-sparsified binary readout has been taken as baseline readout architecture for the strip tracker at SLHC. Although this means giving up pulse height information, we can retain the simplicity and robustness of the present system with known, occupancy independent, data volumes. The relative simplicity of the front end chip should also lead to the lowest power solution. The CMS Binary Chip (CBC) prototype has recently been submitted for fabrication in 130 nm CMOS [47]. The CMS tracker has adopted on-detector DC-DC conversion as a baseline option, which has implications for the FE chip design. In particular, the front end amplifier can be sensitive to supply noise likely to be present in DC-DC power systems, and the CBC incorporates on-chip regulation to provide robustness against this.

The main CBC specifications are: (i) both signal polarities can be accommodated; (ii) sensor coupling can be DC or AC, tolerating up to 1 μA DC leakage; (iii) noise must be less than 1000 e^- for a sensor capacitance of 5 pF; (iv) power consumption must be less than 0.5 mW / channel for 5 pF sensor capacitance; (v) pipeline is 256 deep (latency up to 6.4 μsec), plus 32 deep buffer for triggered events.

The CBC prototype chip occupies an area of 7×4 mm^2 and has been designed for wire-bonding at 50μm input pad pitch. We expect to learn a lot from this prototype including functionality and performance issues such as noise, power, radiation hardness (ionizing and single-event effects). This will provide valuable input to further chip and system developments. These may include adapting the chip for different input pitch and/or bump-bonding to simplify module construction and remove the need for separate pitch adapters. System aspects have also been considered and while the first prototype will not contain all the features required for interfacing with the envisaged GBT-based off-detector link, a clear route is identified to future compatibility. Fig. F.2 shows a model of a module with two hybrids carrying CBC chips.

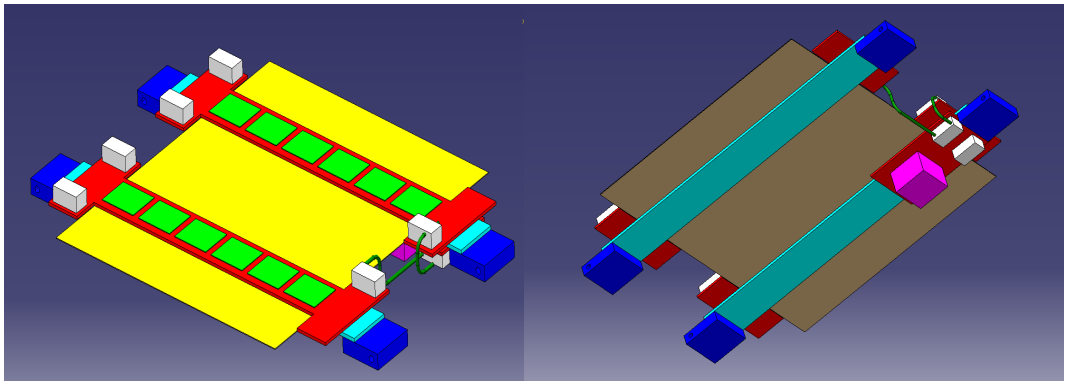

Figure F.2: Model of a possible readout module based on the CBC chips. Two readout hybrids are mounted on a sensor with $\sim$ 2.5 cm long strips. In this version the DC-DC power converter is integrated on the opposite side.

F.1.3.3 Summary and outlook for ASIC developments

The evaluation of the CBC prototypes will provide valuable input for further development of the chip, but also for issues of general interest like noise rejection and the integration of on-chip DC-DC conversion. In parallel with the CBC design, progress is being made to define the required functionalities for modules that should provide information for the L1 trigger, which will require the development of more complex ASICs.

For the innermost pixel detector, the most important requirement is to be able to cope with the high instantaneous rates without data losses. Benefits in the tracking performance could be obtained by utilizing smaller pixels, if the chip were able to operate with substantially lower thresholds. Such goals should be achievable using more advanced ASIC technologies. The final chip will have to be optimized depending on the sensor choice (i.e. planar vs 3D technology).

F.1.4 Data links

F.1.4.1 The GigaBit Transceiver

The need for increased bandwidth to transfer the data from the front-end chips to the back-end electronics is addressed by the development of the GBT chipset [48]. In addition to the larger data rates, the SLHC environment imposes more severe requirements in terms of radiation tolerance.

The operation of the Tracker requires the transmission of data from three systems: the Data Acquisition (DAQ), the Timing Trigger and Control (TTC), and the Slow Control (SC). The GigaBit Transceiver architecture allows us to transmit data simultaneously from the three systems in the same link, aiming at a total bandwidth of $\sim$ 5 Gb/s in the version currently under development. Such requirements can be met using deep submicron CMOS commercial technologies; the GBT chipset is being designed and fabricated in 130 nm.

The GBT architecture offers clear advantages in terms of development, production, installation and maintenance, since all functionalities are combined in a single system. It offers the possibility of a drastic reduction in the number of optical fibers, thanks to the large bandwidth. In addition, early modelling studies clearly show beneficial simplifications by using a single system, as compared to the current ring-architecture for the controls, which required a non-trivial matching of the granularity of control and readout as well as a rather complicated integration of the services.

The link consists of bidirectional point-to-point optical fiber links between the counting room and the detector electronics. In the counting room, which offers a radiation-free environment, transmitter and receiver are implemented in commercial off-the-shelf components and FPGAs. At the front-end, the GBT chipset is composed of the GigaBit Transceiver ASIC (GBT13), the GigaBit Laser Driver (GBLD) and the GigaBit TransImpedance Amplifier (GBTIA), which are all developed in 130 nm CMS technology.

The GBT frame is composed of 120 bits transmitted over a single bunch crossing interval (25 ns), resulting in a line data rate of 4.8 Gb/s. Of the 120 bits, 4 bits are used for the frame header, and 32 bits for the for the Forward Error Correction. This leaves 84 bits for data transmission, corresponding to a bandwidth of 3.36 Gb/s available for the user. Of the 84 bits, 4 are reserved for the Slow Control, 16 for the TTC and 64 for the DAQ, corresponding to bandwidths of 160 Mb/s, 640 Mb/s and 2.56 Gb/s, respectively.

The error correction capability is necessary for robust operation in the SLHC environment. The high radiation levels result in relatively high rates of Single Event Upsets (SEU). In addition to errors in the internal ASIC logic, particles can generate spurious events in the photodiodes, faking the arrival of a data bit. Errors tend to occur as bursts, rather than isolated events, which makes error correction more difficult. The option chosen in the GBT allows correction of up to 16 consecutive wrong bits, and the decoding of the error code is done well within one bunch crossing interval, hence with minimal impact on the latency.

It is conceived that communication between the GBT and the front-end ASICs may be implemented through serial bidirectional links, ("e-links"), allowing the GBT to serve several front-ends with bandwidths multiple of 80 MB/s. Such flexibility will allow the GBT to be used efficiently in different regions of the detector producing different data rates.

F.1.4.2 The Versatile Link

The GBT is complemented by the Versatile Optical Link, which allows developing and qualifying the optical part of the link [49]. The project is composed of a Versatile Transceiver (VTRx) in the front-end, plus back-end components and passive optical components (fibers and connectors). Some details about the Versatile Transceiver are given below.

The VTRx is the only component of the Versatile Link which requires custom development due to the stringent and exotic requirements deriving from operation inside the detector volume (minimal size and mass, high radiation environment, operation in strong magnetic field). It is developed starting from a commercially standard transceiver of the SFP+ family, which is well-suited for the required customization. The VTRx includes (i) a Transmitter Optical Sub-Assembly (TOSA), which features a laser diode qualified for use in the HEP environment and the laser driver developed in the context of the GBT project (GBLD); (ii) a Receiver Optical Sub-Assembly (ROSA), which contains a p-i-n photodiode qualified for use in the HEP environment, and (iii) the Trans-Impedance Amplifier developed in the context of the GBT project (GBTIA).

The design of a customized VTRx involves the following main aspects: (i) minimize mass and volume by avoiding metals wherever possible; (ii) avoid any magnetic material; (iii) qualify commercial photodiodes in terms of bit error rate from SEU; (iv) optimize choice of photodiode and design of GBTIA and ROSA; (v) derive requirements for the Forward Error Correction.

F.1.4.3 Outlook

The ongoing developments are expected to be concluded in 2012. The links will be used for the upgrade of other CMS subdetectors and will support the system developments for the upgraded Tracker. Given the timescale for the full Tracker upgrade, a further iteration in the link development is possible; the phase space for upgrades involves higher bandwidth and/or reduced power and mass. A possible target for bandwidth would be 10 Gb/s per link, which is the current performance limit of commercially available SFP+ Transceivers. This increase in bandwidth would require the design of a new chipset in a more advanced CMOS technology, as well as redesign of PCBs. Reduction of power can be pursued through careful revision of the chips design, as well as link components and architecture.

F.1.5 Power distribution

The 130 nm CMOS technology currently envisaged for the front-end electronics of the Upgraded Tracker requires 1.2 V for the analog circuitry, while the digital part can operate at significantly lower voltage (e.g. 0.9 V). The total load current is likely to be significantly higher than for the present system due to the higher granularity and increased functionality required, although the power requirements for the digital and the analog parts are expected to be of the same order. In addition, the optoelectronics components will require a voltage of 2.5 V at least, with substantially lower current. These basic facts, combined with the constraint from installed power cables and the need for minimizing the cross section of conductors inside the tracking volume define the basic requirement for the power distribution: (i) support the distribution of different voltage domains; (ii) decrease the current in the conductors from the power supplies to the load.

F.1.5.1 DC-DC converters

A power distribution based on DC-DC converters has been chosen as baseline for the Tracker Upgrade [50]. The main conversion stage is provided by a buck converter, bringing the voltage down from 10-12 V to the operating voltage, or else to an intermediate voltage (e.g. 2.5 V). Since ferromagnetic materials cannot be used in the magnetic field, the converter has to rely on air-core inductors. The chip implementing the power switches and the control circuitry must be developed in a technology capable of sustaining 12V with some safety headroom. Two technologies have been identified which provide the required high voltage transistors and are compatible with the radiation levels, and prototype ASICs have been fabricated in both technologies, thus demonstrating that the required conversion ratio and efficiency can be achieved. A close-to-final ASIC prototype with an efficiency target of $\sim$ 90% is expected during 2011.

In parallel, a switched capacitor converter has been designed in 130 nm technology, which could serve as an on-chip stage to further divide by two the voltage, in a scheme with two conversion steps.

F.1.5.2 System aspects

Besides the ASIC development, the implementation of a power distribution based on DC-DC converters requires the study of substantial system issues, as well as the optimization of the distribution scheme [51].

Both the buck converter and the switched capacitor converter have the potential of injecting significant noise into the system, thus compromising the functionality of the readout electronics. A lot of progress has been made in investigating system issues related to the integration

of a buck converter, as well as the optimization of the PCB design and the possible need of shielding. Studies have been made using spare sub-assemblies of the present tracker as a test case. For the on-chip switched capacitor, a significant series of tests are planned with the CBC prototypes.

The overall optimization of the conversion scheme is a very complex topic, involving several different aspects that can have substantial impact on the detector quality, such as overall complexity of the system, susceptibility to noise, robustness wrt to failure of individual components, power consumption, and mass of the conductors. Since we are close to a definitive proof of the feasibility of this option, the focus in the future will move from ASIC development to system design, which will have to be optimized for the chosen detector concept.

F.1.6 CO_2 cooling

The upgraded CMS Silicon Tracker will most likely dissipate at least as much power as the present one (if not more), while silicon sensor operation will require more stringent temperature control to limit the leakage current in the high radiation environment of the SLHC. CO_2 two-phase cooling appears to be a promising option to improve upon the present mono-phase fluorocarbon system, since it will achieve enhanced cooling performance with a lightweight system. Some of the main advantages of CO_2 cooling are: (i) the high latent heat allows the use of small pipes, as well as large heat load per single channel, possibly reducing needs for manifolding; (ii) the high heat transfer coefficient allows smaller heat-exchanger contacts; (iii) CO_2 is a natural substance, which is more environmentally friendly and less expensive than fluorocarbons. The use of CO_2 cooling will contribute to an improved detector quality, while automatically ensuring compliance with the constraint of the cross section of the installed pipes.

The R&D for the Tracker Upgrade will move from the design and construction of the cooling plant to the pixel "Phase I" upgrade.

The first phase of the R&D consists of (i) characterizing through laboratory measurements the heat transfer and mass flow of two-phase CO_2 in small channels using the parameter range relevant for operation in CMS, (ii) deriving guidelines for detector cooling optimization (dimensions of the pipes and heat exchangers, and operating pressure), (iii) developing numerical models that correctly describe the flows and heat transfers relevant for the CMS tracker. This part, which is now well underway, will provide all the information needed for the pixel and for the whole tracker cooling design.

Some aspects of the engineering design, such as compliance with the installed pipes and with safety aspects related to the installation in the CMS cavern, will also be studied and solved for the pixel plant, which will then be applicable in a straightforward way to the full tracker system. Most of the effort will go into the design and engineering of the system, and analysis of system aspects such as manifolding, which will pose novel challenges due to the much larger scale of the system.

F.1.7 Modules with trigger functionality

Besides maintaining the current tracking performance in the more congested SLHC environment, a novel and most challenging requirement has been identified for the Phase 2 Tracker upgrade, namely the contribution to the Level-1 trigger. The trigger system needs to maintain an output rate of 100 kHz despite the 10-fold increase in luminosity, and that appears to be impossible to achieve using only information from the calorimeters and muon detectors. At present, tracking information is used in the High Level Trigger where it achieves a rate reduction of a factor of $\sim$ 100 in the muon rate. Unfortunately, a flattening of the Level-1 rate as a

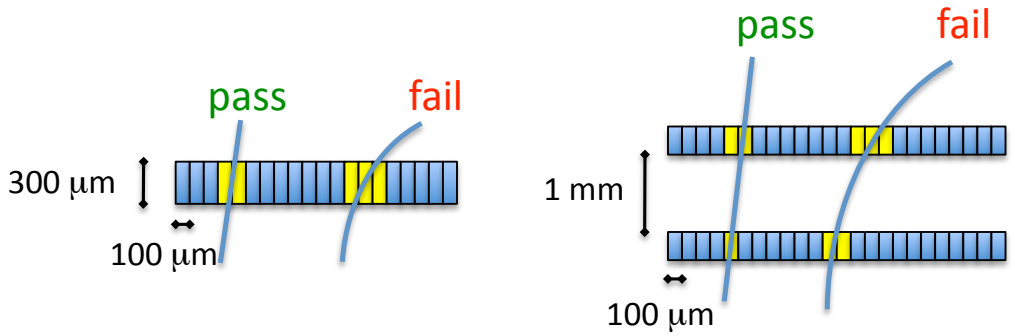

Figure F.3: Sketch showing the principle of p_T discrimination in a single sensor (left) and in stacked sensor pairs (right).

function of p_T is observed, which suggests that increasing the threshold will not help unless tracking information is included. Similar evidence is found for electron, tau, and jet triggers.

Delivering information for the Level-1 trigger involves sending out signals at 40 MHz, which requires data reduction to keep the overall bandwidth at an acceptable level. The strategy that is being pursued in CMS exploits the strong bending power of the 3.8 T magnetic field to design modules that are able to reject, in real time, signals from low-p_T particles. The discrimination can be done within a single sensor, based on cluster width, or by correlating signals from stacked sensor pairs, as shown in the sketches of Fig. F.3. A correlated pair of hits in a sensor stack is called a "stub". Rejecting hits from tracks below a p_T threshold of 1 GeV (or larger) yields a reduction of the data volume by one order of magnitude, and this makes data transmission at 40 MHz feasible.

Different implementations of p_T modules are under study, and briefly discussed below.

F.1.7.1 Strip p_T modules

Two variants of strip p_T modules based on stacked sensors have been studied. In both options, the two sensors are wire-bonded to a single hybrid. This implies that the segmentation along the strips cannot be more than two, since the hybrid needs to be placed at the edge of the module (and not on top of it), in order to access both sensors. A sketch of a possible module is shown in Fig. F.4. These types of sensors could be suitable for the outer part of the Tracker (e.g. $R > 40$ cm) due to the relatively long strips, which would cause too large an occupancy at the inner radius.

In the first variant, corresponding strips on the two sensors are bonded to neighboring channels on the readout ASIC. In the second variant, top and bottom strips are bonded to the same readout channels (see sketches in Fig. F.5). Both versions have been developed using spare sensors and hybrids from the current Tracker and tested in a cosmic telescope setup, where the discrimination logic has been implemented offline. The performance of the discrimination logic has also been measured on LHC data from Tracker Outer Barrel stereo modules by using the tracking information to account for the stereo angle of those those modules. All results indicate that the required data reduction can be achieved for both module variants. These studies represent the first validation of the p_T module concept on real data. The second variant has half of the readout channels, which is obviously an advantage. However, the first variant allows for more flexibility in the implementation of the discrimination logic, and it also allows reading out both sensors for tracking, hence providing more redundancy. Also, in the first variant, the readout pitch required is half of the sensor pitch, which leads to a straightforward

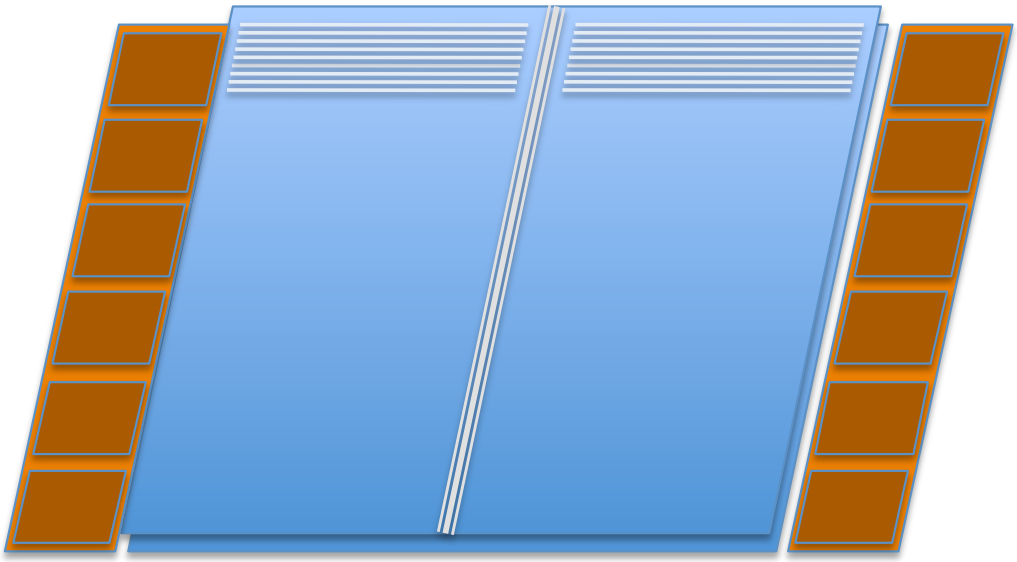

Figure F.4: Sketch of a possible strip p_T module based on two stacked sensors. The two sensors are read out at the edges by the same hybrid. Assuming that the sensor is made out of a 6″ wafer, the strip length is $\sim$ 5 cm.

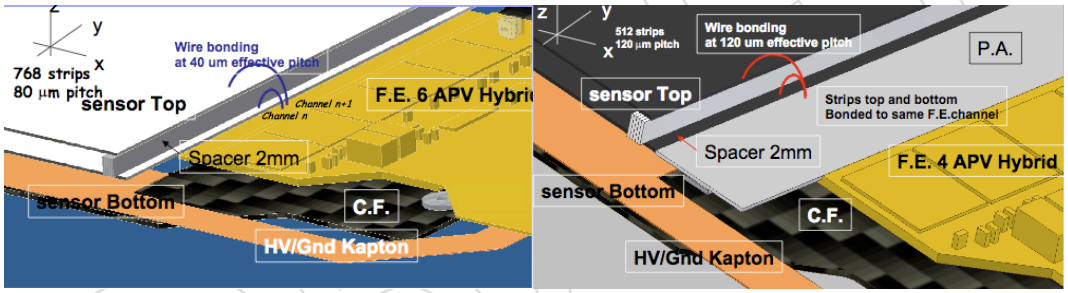

Figure F.5: Left: strip p_T module first variant; the two sensors are directly bonded onto a readout hybrid, top and bottom strips are bonded to neighboring readout channels. Right: strip p_T module second variant; the two sensors are bonded to a pitch adapter, top and bottom strips are bonded to the same readout channel.

module assembly without a pitch adapter (Fig. F.5).

An even simpler p_T module could be designed by selecting clusters on the basis of their width in a single sensor. In this case, the hybrid could be placed on top of the sensor and therefore the strip length could be shorter than 5 cm. This type of module would only be suitable for use at large radii, since the track curvature is measured only over the sensor thickness (Fig.F.3), and hence the achievable data reduction is lower, which is not suitable for the most congested regions. In addition, the p_T rejection efficiency in such an option is, in principle, affected by radiation damage, as it depends on the depletion depth and the Lorentz angle.

In conclusion, strip p_T modules based on stacked sensors appear to be a solid option to build modules with trigger capability, since basic technologies are in hand, and the interconnection between the two sensors uses wirebonds, the lightest and most power-economic way. The design of a front-end chip with the required functionalities and the development of an optimized

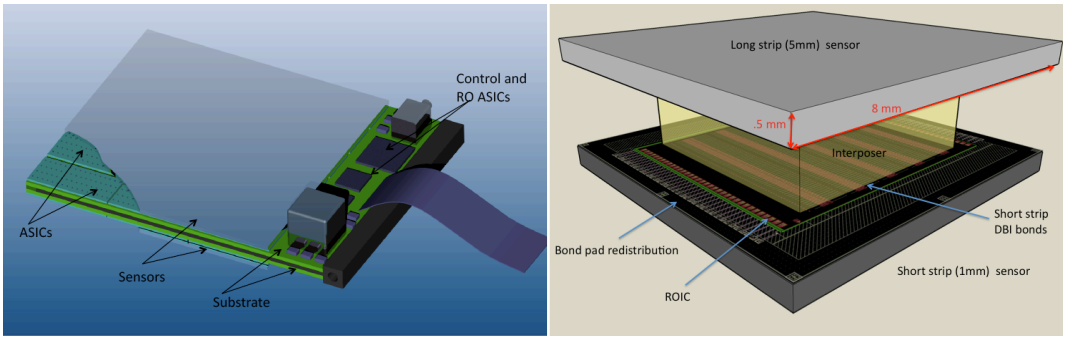

Figure F.6: Two possible implementations of pixellated p_T modules (see text).

electronics architecture is nevertheless a challenging project requiring substantial investments.

F.1.7.2 Pixellated p_T modules

The possibility of developing pixellated p_T modules is also being pursued with substantial efforts. Compared to strip p_T modules, pixellated modules would also be suitable for use in the intermediate radial region ($20 < R < 40$ cm) and would provide tracking information in the z view, possibly allowing for some primary vertex discrimination at Level-1. However, the development of pixellated p_T modules is substantially more difficult, and requires the use of more advanced technologies. The challenge is the connectivity between the two sensors of the stack, which needs to be implemented through an "interposer" or "substrate". The high granularity and the complex connectivity naturally lead to higher mass and power consumption.

Two possible implementations of pixellated p_T modules are shown in Fig. F.6. In the first version (left), each sensor is connected to the ASICs which are in turn connected to a substrate carrying power and signals. A foil of conductive material (e.g. TPG) in the center of the assembly removes the heat. The substrates are connected together at one edge, while at the other edge they extend out of the sensor surface, and carry the auxiliary electronics. ASICs in one layer are programmed as "transmitters", in the other layers they operate the correlation logic and send trigger data out. A pixel size of $\sim 0.1 \times 2$ mm^2 is envisaged, leading to an overall module size of $\sim 48 \times 48$ mm^2 (or larger, if the interconnection technology is proven to be reliable on large surfaces). The connections sensor-to-ASIC and ASIC-to-substrate could be done with direct oxide bonding and bump bonding, respectively; or both with bump bonding, with through silicon vias on the ASIC. Alternatively, low-height wirebonds could be used between ASIC and substrate, which would not require through silicon vias on the ASIC.

In the second version (Fig. F.6 right), there is only one layer of ASICs bonded onto a "master sensor" with finer granularity (e.g. $\sim 0.1 \times 1$ mm^2) with analog connections through an "interposer" to a "slave sensor" with longer channels (e.g. $\sim 0.1 \times 5$ mm^2). Since the electronics are only on one side, the module could be cooled from the side of the master sensor. Options and issues for the interconnection sensor to ASIC and ASIC to interposer are similar to the first version.

In addition to the design of an ASIC with a much higher level of complication, the development of these types of modules requires validating the chosen interconnection technologies on large surfaces, and addressing delicate system issues related to the high densities of interleaved analogue and digital lines. Such developments require both substantial efforts and financial resources.

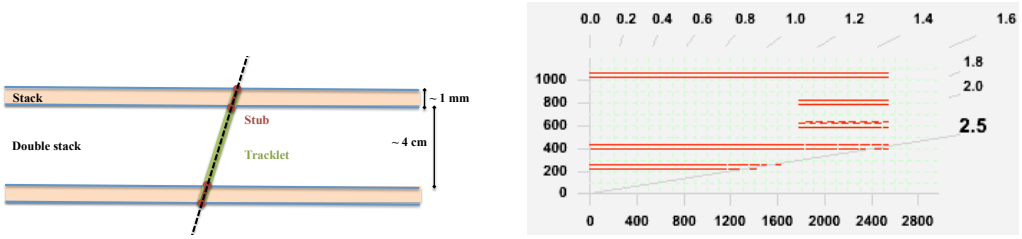

Figure F.7: Left: sketch showing the principle of the double-stack geometry; stubs are reconstructed from two hits in a stack; the two layers in the double-stack are sufficiently close in space that stubs can be correlated to form tracklets, which are then extrapolated out to the next double-stacks. Right: example of Tracker layout based on double-stack barrel-only geometry.

F.1.8 Detector concepts

The module designs presented in the previous section are suitable to send out for every bunch crossing the coordinates of "track stubs" generated by particles above a certain p_{T} threshold, where the thresholds can be typically between 1 to 2 GeV, or more. This is still an enormous amount of information to be processed at Level-1. Two main approaches can be envisaged:

1. Use the information of Tracker stubs to refine trigger primitives from calorimeters and muon system (improve the momentum estimate of muons and confirm electron candidates).
2. First combine Tracker stubs to form Level-1 tracks, and then combine the tracker primitives with information from calorimeters and muon detectors.

For the second approach (i.e. aiming at reconstructing all the tracks of the bunch crossing at Level-1) the combinatorics are likely to be too prohibitive to be solved in a few clock cycles, unless the detector geometry is optimized for the purpose. For this reason, the "double-stack geometry" has been proposed.

Double-stack geometry. A double stack consists of two layers of p_{T} modules (built out of stacked sensors), placed at a distance of few cm; the two layers of the stack have the same ϕ segmentation (i.e. the inner layer is a shrunken version of the outer one). With such geometry, it appears possible to correlate stubs reconstructed in the two stacks and to form "tracklets". A tracklet should have sufficient precision in the determination of the direction and the momentum (measured over a few cm distance) to extrapolate to a sufficiently small region onto the next double-stack, and correlate with tracklets reconstructed there (see Fig. F.7). The extrapolation is obviously affected by the multiple scattering in the detector material.

An example of a tracker layout entirely based on pixellated p_{T} modules with double-stack geometry is shown in the right sketch of Fig. F.7. Such a detector concept is optimized to reconstruct all tracks at Level-1. Its feasibility and performance as a tracking device critically depend on the possibility of building lightweight pixellated p_{T} modules in a reliable technology with moderate power consumption and an affordable price.

The left sketch of Fig. F.8 shows an option where pixellated p_{T} modules populate the inner part, in a single-stack barrel geometry, while the outer part is populated with "standard" readout modules. This option would aim at improving the Level-1 trigger with the "stubs" from the p_{T} modules, while limiting overall power consumption and cost, and possibly improving tracking performance with a lightweight region dedicated to tracking only.

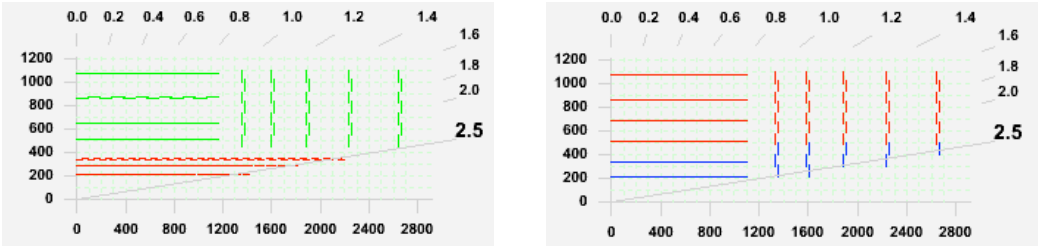

Figure F.8: Left: Tracker layout with single-stack pixellated p_T modules in the inner part (in barrel geometry), and "standard" readout modules in the outer part. Right: Information for the Level-1 trigger comes from strip p_T modules in the outer part (in barrel or endcap geometry), while the inner part is populated with stereo strip modules, or with long pixels, to provide some precise coordinates in the z view.

The right sketch of Fig. F.8 shows an option where the information for the Level-1 trigger comes from strip p_T modules in the outer part (in barrel or endcap geometry). The inner part could be populated with stereo strip modules, or with long pixels to provide some precise coordinates in the z view. This option should provide good tracking performance due to the use of the lightweight strip p_T modules, and offers substantial advantages in terms of feasibility and cost. Its viability as a solution for the Level-1 trigger has to be investigated. It should be noted that the double-stack geometry is not applicable exclusively to pixellated p_T modules since it could be employed also for strip p_T modules, if required.

All these sketches assume an inner pixel detector with approximately the same boundaries as the present one. Moving the boundaries to large radii and adding one more layer in the inner pixel detector may or may not be beneficial, depending on whether the first layers of the outer tracker will be pixellated or not. It has been recently proposed to investigate the possibility that the inner pixel detector contribute to the Level-1 trigger, reading out only "regions of interest" determined by the calorimeter triggers.

Dedicated software tools are being developed to facilitate the modelling of these detector concepts, and to characterize them in terms of basic properties (such as power consumption, material, expected occupancy and tracking performance) prior to the full detector simulation. Effort has started also to model the full chain of data processing for the Level-1 trigger, at least for some of the proposed options. Design, modelling and simulation studies are the key for choosing the optimal option for the CMS Tracker Upgrade, together with the R&D on the hardware components.

F.1.9 Outlook

The upgrade of the CMS Tracker for the high-luminosity operation of the LHC is a formidable challenge. A substantial amount of R&D is already ongoing, and all major aspects are receiving attention. Some of the developments, in particular those addressing the most advanced technologies, may soon be confronted with the lack of financial resources. Together with the R&D on the components, design, modelling and simulation studies (for tracking and trigger) are the key for an optimal choice of detector concept. The progress in the next two years will be crucial for the project, as it will lead to the choice of the detector concept to be designed and built.

F.2 Calorimetry in the High Luminosity LHC Era

F.2.1 Introduction

By the end of the current decade, the CMS calorimeters will have recorded an integrated luminosity of over 300 fb^{-1}, will have operated for more than ten years, and will be operating at an instantaneous luminosity of 2×10^{34} $\text{cm}^{-2}\,\text{s}^{-1}$ leading to pileup of $\sim$40 overlapping interactions per bunch crossing. Around the year 2020 a long shutdown will allow modifications to the LHC that will increase its instantaneous luminosity by around a factor of 5. This Phase 2 upgrade (also called HL-LHC), will provide an integrated luminosity, using luminosity leveling techniques, of around 300 fb^{-1} per year, leading to a total integrated luminosity of about 3000 fb^{-1} over the following decade. The radiation damage to the calorimeters during this era will be far beyond the initial design specifications. It is thus highly likely that significant changes to the calorimeters will have to be made.

The currently implemented CMS electromagnetic calorimeter (ECAL) consists of a barrel section covering $0.0 < |\eta| < 1.45$ and two endcaps covering the region $1.45 < |\eta| < 3.0$. Lead tungstate scintillating crystals are used in both regions, with silicon avalanche photodiode light detectors (APDs) glued to the barrel crystals and vacuum phototriodes (VPTs) glued to the endcap crystals. Each endcap also includes a $3X_0$ thick lead-silicon sampling preshower detector placed in front, covering a slightly smaller fiducial area of $1.653 < |\eta| < 2.6$. The total radiation expected after 3000 fb^{-1} in the barrel region is 5 MRad with a hadron fluence of 6×10^{13} cm^{-2} at $\eta \approx 0$ and 10 MRad with a hadron fluence of 1.2×10^{14} cm^{-2} at $|\eta| \approx 1.45$. In the endcap calorimeters the expected total doses and fluencies are considerably higher ranging from 10 MRad at the barrel-endcap interface to 30 MRad with a hadron fluence of 3×10^{15} cm^{-2} at $|\eta| = 3$. The hadron fluences are mainly low energy ($E > 100$ keV) neutrons.

The currently implemented CMS Hadronic calorimeter (HCAL) consists of barrel (HB) and outer barrel (HO) sections covering $0 < |\eta| < 1.3$, two end caps (HE) covering $1.3 < |\eta| < 3.0$ and two forward detectors (HF) covering $3 < |\eta| < 5$. These subsystems are described in Chapters 4 and 5 of this document. The HB and HE are sampling calorimeters with a layered structure of brass absorber plates interleaved with plastic scintillator megatiles. The photosensors, currently Hybrid Photodiodes (HPDs), are located within the CMS solenoidal magnet, but far from the interaction point and deep in the calorimeter in regions of low radiation dose. The HPDs are optically connected to the megatiles through wavelength shifting and optical waveguide fibers. The HO system samples hadronic showers that penetrate through the CMS magnet, and consists of one or two layers of scintillator read out by SiPMs and/or HPDs. In Phase 1, the HPDs used in these subsystems will be fully replaced with SiPMs. The HF resides in the area of greatest integrated radiation dose. To meet the demands of this environment, the HF detectors are composed of steel absorber instrumented with polymer-clad Quartz fibers and readout with photomultiplier tubes.

Our basic working assumption is that we will want to maintain robust calorimetry coverage to $|\eta| < 5$ during HL-LHC operation. Meeting this requirement poses challenges in the barrel region for electromagnetic calorimetry and in the forward region for electromagnetic and hadron calorimetry.

For calorimetry in the barrel and endcap regions, the anticipated operating conditions will have hardware consequences – due to radiation damage, material activation, detector lifetime and software consequences for the trigger and for event and pattern recognition in the face of very significant pileup. There may also be operational concerns, similar to the present observation of anomalous signals in the ECAL, that will manifest themselves over the next few years of

initial running as CMS reaches higher and higher levels of integrated and instantaneous luminosity. The Phase 1 upgrade will address the needs of Barrel Hadron Calorimetry (HB and HO subsystems) and allow these to operate effectively into the HL-LHC era. These upgrades are described in the main body of this Technical Proposal. The Phase 2 upgrade will address the needs of the Barrel Electromagnetic Calorimetry (EB) and Forward Calorimetry (EE, HE and HF subsystems) and these are described here.

This appendix is divided into two sections, the first describing the modifications that we are considering to the barrel ECAL, and the second describing changes to, or replacements of, the calorimeters in the forward region. These sections summarize some of the questions and concerns that need to be addressed and outline some of the R&D programs that CMS is (or is considering) following to ensure effective calorimetry for HL-LHC operations. This list is not exhaustive but rather is meant to give a flavor of what work lies ahead in the coming decade.

Based upon experience from our development and construction work and operations of the current CMS Detector, we anticipate 5 years of intensive preparation including all necessary R&D and decision-making about the configuration of the various ECAL and HCAL detector components. This will be followed by a construction project that will also last about 5 years, in order to have the full calorimetry upgrades ready for installation during the shutdown around 2020 and subsequent HL-LHC operations. The length of this shutdown is expected to be between 18 and 24 months, which is actually relatively short and could limit some potential upgrade options. The preparation phase includes identification of the physics drivers that are expected to be important in the HL-LHC era, and development and use of simulation tools to study radiation damage, pile-up effects, and material activation. This effort is already underway. Such activities will inform the development of one or a few select detector designs/modifications to meet the physics goals. In parallel with these efforts, extensive R&D on detector elements and systems must be performed, as well as the development of the engineering strategies for handling the removal and replacement of highly activated detector subsystems, particularly in EE and HF. These activities will result in a technical design report that will form the basis of a HL-LHC Calorimetry Construction Project, expected to start circa 2015.

F.2.2 Barrel Electromagnetic Calorimeter in the HL-LHC Era

Although the $PbWO_4$ crystals are relatively radiation tolerant, there are some effects that, over time, will reduce their performance. In addition, the APDs will suffer from radiation damage. The effects we anticipate include:

- Hadronic interactions in the crystals that will reduce the transparency of the crystals [52, 53, 54] affecting the ECAL performance in two ways:
  - through an overall increase in the stochastic term, due to the lower amount of light detected, and
  - through an increase in the constant term due to induced absorption in the crystal which modifies the light collection uniformity
- In the barrel, an increase in the noise term due to bulk damage in the silicon of the APDs increasing their dark current.
- An increase in the noise term due to a decrease of the signal-to-noise ratio.

Although the barrel performance will degrade over time we expect that its degradation will be insignificant when compared to other effects, such as the equivalent noise introduced into the energy measurements due to the pileup of a very large number of overlapping minimum bias

events per bunch crossing at HL-LHC.

F.2.2.1 Anomalous Calorimeter Signals

Since the beginning of LHC operation in late 2009, large energy deposits have been observed in isolated single crystals in the barrel ECAL. The most likely source of these "anomalous calorimeter signals" (ACSs or "spikes") is hadronic interactions in the APDs. For LHC operation during the coming years, the particular topology and timing of these events allows a majority to be removed at the trigger stage (at either Level-1 or in the HLT) without affecting the performance of the ECAL for real physics objects. It is currently unclear how these signals will evolve with increasing LHC intensity and energy, but it is highly likely that, unless certain physics triggers (e.g. single EM deposits above 40 GeV or higher) are removed from the Level-1, some hardware intervention on the barrel ECAL will be necessary.

As mentioned previously, the hardware changes possible are limited by the amount of time available. In addition, the time available to work on the detectors will be restricted by the very significant levels of activation of the ECAL. The dose rate expected for the endcap calorimeters will be around 500 mSv/hr at 30 cm from the detector, even after a cool down period of two months. This level of activity precludes any option to perform work on the calorimeter without a complex, and expensive, remote handling system.

In discussing any modifications to the barrel calorimeter it is important to understand that the detector is divided into two sections separated by an aluminum grid that acts as a thermal screen. On the inner side, or inner radius, of the grid are the crystals and the APDs. Polyimide cables connected to the APDs pass through the grid and connect to the front-end electronics. Accessing anything on the crystal side of the grid requires a complete dismantling of the detector, while reaching the electronics is comparatively easy. Current estimates are that once a supermodule (SM) is removed from the detector, any intervention on the APDs will require about 8-9 weeks for dismantling and re-assembly, while interventions on the electronics would take about 2 weeks. In both cases the time of the intervention itself is not included.

As discussed above, the main concern is to limit the effect of the Anomalous Calorimeter Signals. Various potential remedies requiring hardware interventions on the barrel ECAL are under consideration; in order of decreasing complexity they are:

1) To read out each APD separately. Although each crystal is equipped with two APDs, their signals are combined upstream of the front-end electronics making it impossible to distinguish signals in a single APD. By reading out each one individually we believe we could almost completely eliminate the ACS problem. However, to do this would require a complete dismantling and re-assembly of the whole calorimeter.
2) To modify the very-front-end analogue electronics to exploit the difference between the risetime of the signals from the ACS and from crystal scintillations. Because of their different origins, the ACSs have a faster rise-time than signals from energy depositions in the crystals. This difference could be used to identify the ACS at the individual crystal level. This would require a complete redesign of the electronics and most likely the off-detector electronics.
3) Leave the very-front-end electronics intact and change the Front-End boards. This board currently generates the trigger primitives and stores the data until a Level-1 Trigger Accept is received. It could be replaced with one that uses higher bandwidth data links (e.g. 10 Gbs) to send crystal-level information to the off-detector electronics with every bunch crossing. With this the Level-1 decision could include the

off-line ACS suppression techniques but will require a re-design of the off-detector electronics.

As a prelude to this work we will evaluate the activation level of the barrel at each stage of LHC operations and prepare plans for handling the supermodules. We will conduct an engineering study on how to extract supermodules from CMS in order to understand the different operational steps and to define the required tooling. We will also estimate the precise time required and the risks of each of the options listed above, as well as evaluating the possibilities of parallelism of the various tasks.

If and when we have decided which of the above options to pursue, we will begin the development program of the new version of the readout. This will entail design and prototyping steps, followed by testing and qualification with our spare supermodule in beam tests. We anticipate that this last phase will begin no earlier than 2015.

In addition there are other changes to the on-detector read-out electronics that might be necessary. One of these is to reduce the risk of failure of the control system. Currently, groups of up to 200 crystals are controlled by a single "ring" and, although there is some redundancy built-in, it is possible that they can fail. New chips are currently being designed at CERN (the GBT project), and ECAL will participate in the system design. The new architecture is point-to-point with redundancy, so the chance of losing large fractions of the detector due to failure of the control system is greatly reduced.

There are other possibilities that are being discussed, that would require modifications to other sub-detectors. For example, one or two fine-grained outer tracker layers equipped with lead absorbers – to act as a barrel Preshower – could possibly aid in distinguishing ACS from normal signals. This possibility, along with others, will be examined through simulation in the coming months.

In summary, an upgrade to the barrel detector is motivated by the presence of the Anomalous Calorimeter Signals and the danger that, at the highest luminosities, they will use up much of the available trigger bandwidth. Possible upgrades to the read-out electronics to improve redundancy and to introduce high speed data links need to be investigated. We will prepare plans for intervention on the supermodules for the different options. Substantial effort will needed to evaluate in detail the feasibility of carrying out any of these options.

F.2.2.2 Minimum R&D for the ECAL Barrel Upgrade

a. Detailed engineering studies of the mechanics of removing the supermodules and performing any intervention on them.
b. Electronics R&D to prepare possible changes to the readout to address the anomalous signals and improve redundancy, and to develop high speed links.
c. The development of radiation tolerant low voltage regulators for the endcap electronics and a more robust control system architecture.

F.2.3 Forward Calorimetry in the HL-LHC Era

The calorimetry elements, both ECAL and HCAL, forward of $|\eta|$ greater than 1.5 represents a very challenging situation in terms of radiation damage and pileup relative to the barrel regions of ECAL and HCAL. To identify and deal with the challenges to Forward Calorimetry in the HL-LHC era and to develop a common strategy for a new ECAL-HCAL endcap, a joint ECAL/HCAL taskforce has been established to address:

(1) the physics objectives that will be relevant for Phase 2 of LHC operatioons;

(2) the identification and execution of the relevant R&D for the new technologies required to properly inform credible subdetector designs; and

(3) the production of a technical design report in which designs for calorimetry in the endcap/forward region are presented that can meet the challenges of the physics objectives in the 2020 era;

The Taskforce activities have led to a consensus that most of the elements of forward calorimetry will require upgrade or replacement by 2020.

Figure F.9 shows the radiation map expected for the forward calorimetry. Shower maximum is located within the EE and hence the highest integrated doses for $|\eta| < 3.0$ are expected in the $PbWO_4$ crystals. The HE benefits from lying in the shadow of the EE so the region most affected by radiation exposure is the inner most layers at smallest (r, z)-values corresponding to $2.2 < |\eta| < 3.0$ as shown in Figure F.10. The proximity of HF to the beam and its forward location $3 < |\eta| < 5$, mean intense doses, shown in Figure F.11, are expected there.

As the integrated luminosity of the LHC increases and as the EE is increasingly exposed to radiation – from both electromagnetic and hadronic sources [55] – attendant reduction in subdetector performance is expected in the $PbWO_4$ crystals and VPT photosensors of the ECAL endcap and Preshower endcap detectors. As already mentioned in Section F.2.2 in the discussion of radiation damage of the $PbWO_4$ in the ECAL barrel, there will be loss of transmission of light in the crystals. The VPTs will suffer from a darkening of the front window and a reduction of the quantum efficiency of the photocathode and dynode surfaces. These effects are anticipated and are being quantified. The noise term in the resolution function σ/E dominates the resolution up to ~300 GeV for 500 fb^{-1} and still dominates above 1000 GeV for 3000 fb^{-1}. In the Preshower, bulk damage to the silicon will increase the leakage current and lower the charge collection efficiency, resulting in a decrease of the signal-to-noise ratio.

Moreover, the activation of the materials of the EE will make repairs very difficult. While CMS is investigating robotic repair possibilities should the crystal calorimetry configuration be maintained, it is likely that the present EE will need to be replaced with an appropriate calorimeter whose technology is to be decided by physics objectives.

The radiation effects to the HE and HF subdetectors were anticipated during the design and construction of CMS. We expect at minimum considerable repair and refurbishing of these devices beyond that accomplished in Phase 1 upgrades with radiation hard components and photodetectors able to withstand the instantaneous and integrated luminosity of the HL-LHC.

Tools using MARS and Fluka codes exist and are able to estimate the radiation load and activation of materials at any point in the calorimeters if the materials, location, and beam luminosity are provided. These tools are appropriate for the work of designing new EE, HE, and HF detectors and will be utilized by the Taskforce. This issue is particularly important for any replacement strategies for the EE. An example of the power of this tool is shown in Figure F.12 and demonstrated for $PbWO_4$ in [52].

F.2.3.1 Physics Simulations for the Forward Calorimetry

The simulation effort is directed toward deciding on the important physics objectives for which the forward calorimeter is needed and finding solutions for each of the many challenges that the forward calorimeters will face. The design possibilities that deal with the challenges listed above range from a forward calorimetry configuration that preserves the excellent EM resolu-

tion of the present $PbWO_4$ crystal calorimeter to a configuration that emphasizes jet or MET resolution by optimizing compensation in a combined ECAL-HCAL endcap. The choices are to be based on physics objectives.

To assess the effect of forward calorimetry on HL-LHC physics, several physics processes have been identified that are regarded as likely to be important for study in that era. These include

- Standard Model benchmarks
  - rare top decays,
  - triple gauge boson production,
  - triple differential cross section for jets, and
  - observation of Higgs boson decays to Z γ.
- new physics processes
  - SUSY b-jets or photons plus missing E_T,
  - compositeness and vector-vector scattering.

These event topologies must be simulated with both radiation damage effects and event pileup included. Toward the Higgs to Z γ final state, work is progressing on an initial study of $Z \rightarrow e^+e^-$ with event pileup, to assess where the performance of the current CMS detector begins to deteriorate – with and without radiation damage. Studies of the other processes will follow. The nature of the needed instrumentation to address the physics relies on the simulations to answer whether powerful EM calorimetry is required, whether high quality jet energy measurement (and missing energy measurement) are preferable, or both are needed. If either of the latter is essential, then it is likely that compensating calorimetry will be the concept of choice.

One complication, as mentioned earlier, in the study of the effect of radiation damage, is that during the accretion of radiation damage the detector performance will be degraded by increasing pileup. At an instantaneous luminosity of 5×10^{34} cm^{-2} s^{-1}, pileup of 100-200 interactions per bunch crossing is to be expected, a truly daunting challenge. Pileup and radiation damage studies will be done in concert to ascertain which is the dominant source of detector performance degradation at any point of operation at a given integrated and instantaneous luminosity.

Work is in progress on developing a version of the CMS fast simulation MC that has incorporated in it detailed radiation damage test beam results [56] as a function of fluences at different luminosities as a function of η. This version of fast simulation already is capable of any level of pileup that CMS will experience. This tool will be used to generate the effects of the radiation damage and pileup at different instantaneous and integrated luminosities on different critical aspects of CMS calorimetry function such as mass and energy resolution and missing transverse energy in different types of physics signals.

F.2.3.2 Strategies for Implementing the Forward Calorimetry

Very different strategies for implementing the forward calorimetry and a different detector R&D will be necessary depending on the physics objectives. These will be determined by a combination of Monte Carlo studies and analysis of the data that CMS is presently accumulating and will depend upon whether we want to achieve excellent EM resolution or emphasize jet or MET resolution by optimizing compensation in the combined ECAL-HCAL endcap. The correct configuration of the forward calorimetry is probably somewhere in between these two poles.

If the objective is to obtain the best EM resolution, one approach would be to rebuild the EE in more or less the same configuration as the present CMS endcap but with new radiation hard crystals and photodetectors. The HCAL detectors in the forward region would remain essentially the same with perhaps improvements based on radiation hardening in certain limited areas of the HE and HF.

Another strategy would be to enhance the particle-flow capabilities of the endcap region covered by the central tracking system ($1.3 < |\eta| < 2.4$). This could be done using a fine granularity EE, introducing an HE with finer transverse and longitudinal segmentation and reducing the dead material between the EE and HE components.

At the other pole of design options, solutions that produce an endcap compensating calorimeter would require development of techniques to equalize electron and hadronic response by using detectors combining scintillation light emission and detection and Cerenkov light and detection, such as could be achieved by addition of Cerenkov (EM) sensitive layers to the hadron calorimeters. A second approach would be to use wavelength filtered photosensors to read out crystals. GaAs and GaInP Geiger mode APDs are possible photosensors that can be used to image light of different wavelengths with good efficiency.

F.2.3.3 Forward Calorimetry Technology R&D

Development of appropriate technical designs for accomplishing the various configurations for forward calorimetry for HL-LHC operation will require significant R&D on new radiation hard detector technologies, radiation hard front end electronics, fast triggering and readout, This effort must start early in the current decade. In order to inform any decision on calorimetry for 2020, several areas of investigation are underway or planned. We divide the various initiatives into three categories: detector R&D specialized to the best possible electromagnetic resolution; R&D specialized to producing a compensating forward calorimeter; and R&D which would be required no matter which of these two directions the physics objectives indicate. As might be expected, since a major amount of R&D must go into developing radiation hard components, most of the R&D will fall into the third category. Some of the listed R&D are useful for the barrel ECAL also.

I. Detector R&D aimed at optimum electromagnetic resolution:
   a. R&D to select a replacement radiation hard crystal to replace the present $PbWO_4$ crystals. Two candidates are currently under investigation, LYSO(Ce) and PbWMO. While LYSO(Ce) is attractive because of its brightness, speed and radiation hardness, its relatively high cost would restrict its use to a limited volume of the EE. The less costly PbWMO option requires further study of its radiation hardness. A further crystal type, CeF_3, is under consideration. This material has been demonstrated to be extremely radiation hard, but no industrial production is currently available [57].

II. Detector R&D specialized to developing a compensating calorimeter:
   a. Techniques to equalize e/h by using detector layers combining scintillation light emission and detection and Cerenkov light and detection. Possible options for Cerenkov (EM) and scintillation sensitive layers include Quartz plates, crystal plates, crystal fibers, and liquid scintillator in Quartz tubes.
   b. Techniques to equalize e/h using wavelength filtered photosensors to read out crystals. GaAs and GaInP Geiger mode APDs are possible photosensors that can be used to image light of different wavelengths with

good efficiency.

III. Detector R&D to develop radiation hard components common to Approaches I and II:

a. Studies of use of SiPM and GaAs photodetectors in the existing HE and HF. With the use of more extensive longitudinal sampling, the radiation damage to the innermost layers of the HE – where waveshifted scintillation light levels would be reduced – could be reweighted appropriately. Photosensor noise issues can be improved by using smaller pixel sizes in the devices or through cooling.

b. R&D on new materials to replace the plastic scintillation tiles in regions where these are vulnerable. Options include LYSO(Ce) crystal plates, quartz tiles coated with waveshifter, aluminum or quartz cells containing liquid scintillator that can be filled and flushed, and quartz tubes containing liquid scintillator.

c. R&D on new readout fibers, necessary to transmit the light from tiles to the SiPMs. The current approach employs a photosensor readout that is located remotely and connected via waveshifting fiber. Existing waveshifting fibers are vulnerable to radiation damage and must be replaced with an alternative. Possibilities include use of liquid-in-capillaries, novel waveguide structures, and crystal fibers.

d. Development of gas calorimetry options. Several approaches might be used to replace existing vulnerable layers in the HE. These include GEM detectors or planar structures.

e. R&D on secondary emission ionization calorimetry for its speed and radiation hardness.

f. Use of quartz core-quartz clad (QQ) fiber to replace the existing quartz core-polymer clad (QP) fiber in HF.

g. The development of more robust light sources for calibration and tracking of the calorimetry gains.

h. The development of radiation tolerant low voltage regulators for the endcap electronics and a more robust control ring architecture.

F.3 Muon System Phase 2 Upgrades

F.3.1 R&D Issues for the Muon Drift Tubes in Phase 2

For the Phase 2, the DT detector itself should be able to cope with the higher luminosity, but the DT electronics will need to be revised. First, the luminosity increase will cause a worsening of the radiation environment. The radiation tests carried out on the current front end DT electronics indicate that some regions will experience an unacceptably high a rate of single event upsets and some regions eventually will not survive the total irradiation dose. Second, the Level-1 trigger system will have to cope with high rates. The only effective way to increase the trigger rejection power will be an improvement of its p_{T} resolution, in order to limit the feedthrough of mismeasured low momentum muons to high momentum, as is now done at normal LHC luminosities in the High Level Trigger. Since the p_{T} measurement is intrinsically limited by the multiple scattering in the material in front of the DT system, a big improvement in trigger rate control will come from the use of the Tracker data. Different possibilities to get Tracker hits and improve transverse muon momentum resolution by matching them to the DT

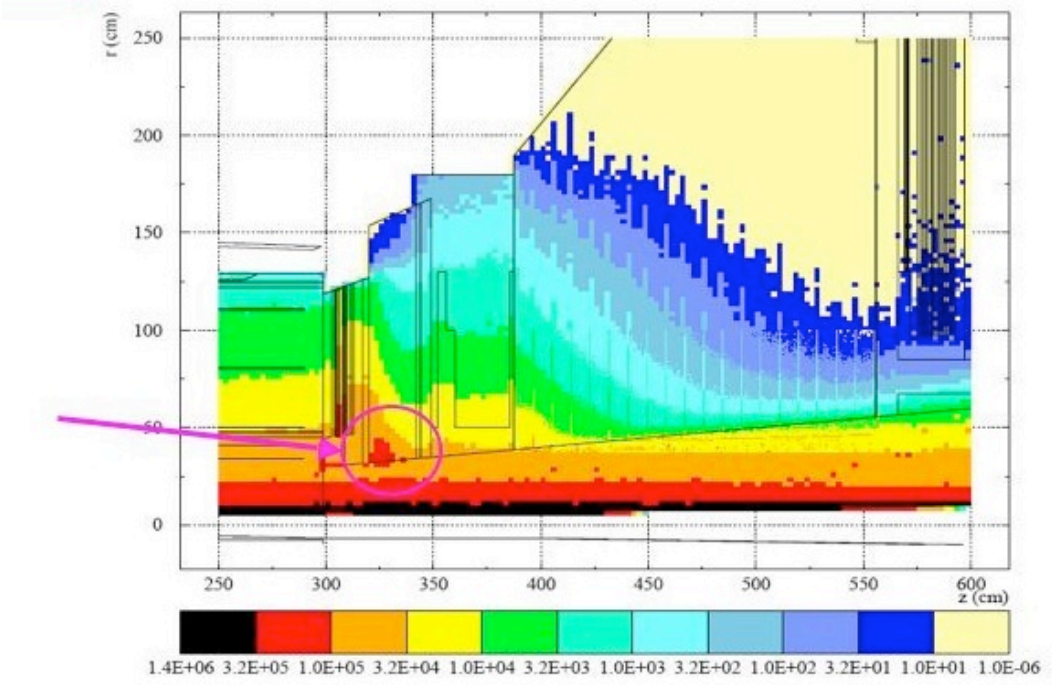

Figure F.9: A map from Fluka of the radiation field in the endcap region including EE and HE detectors. Dose units are Gy. The dose is clearly greatest at smallest values of (r, z)-coordinates.

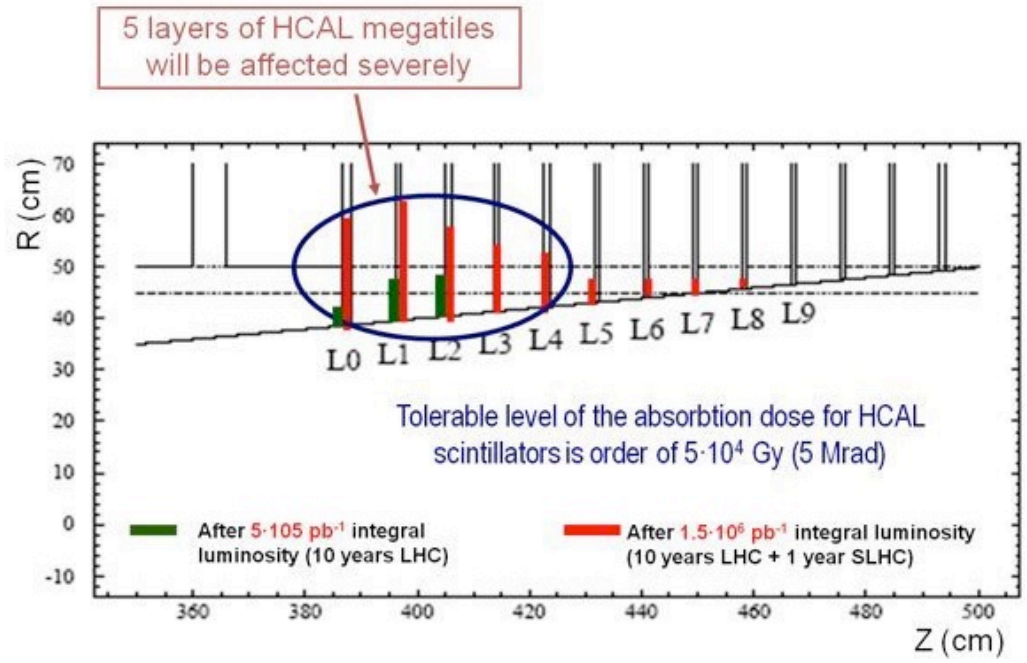

Figure F.10: A schematic of the HE detector showing layers suffering significant radiation damage. The regions of HE most vulnerable to damage are at the smallest (r, z)-values. The angled boundary corresponds to $\eta = 3$.

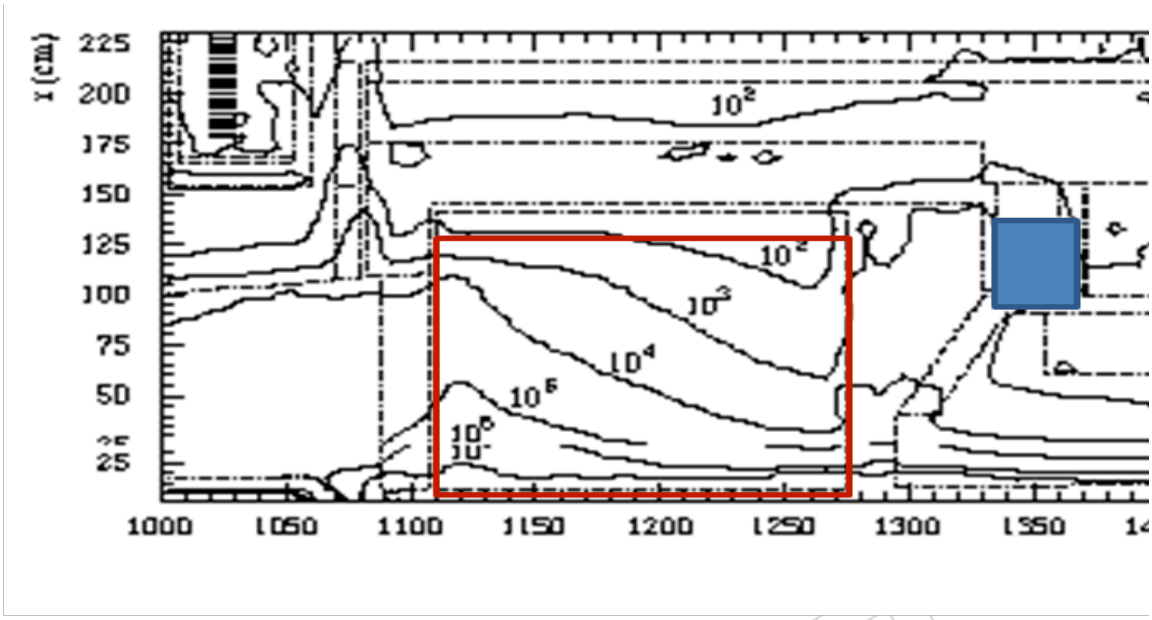

Figure F.11: Radiation fields in the HF detector. Doses are in Gy. The horizontal axis (z) is in centimeter units and the collision point is to the left. The blue highlighted region represents the location of the PMT readout.

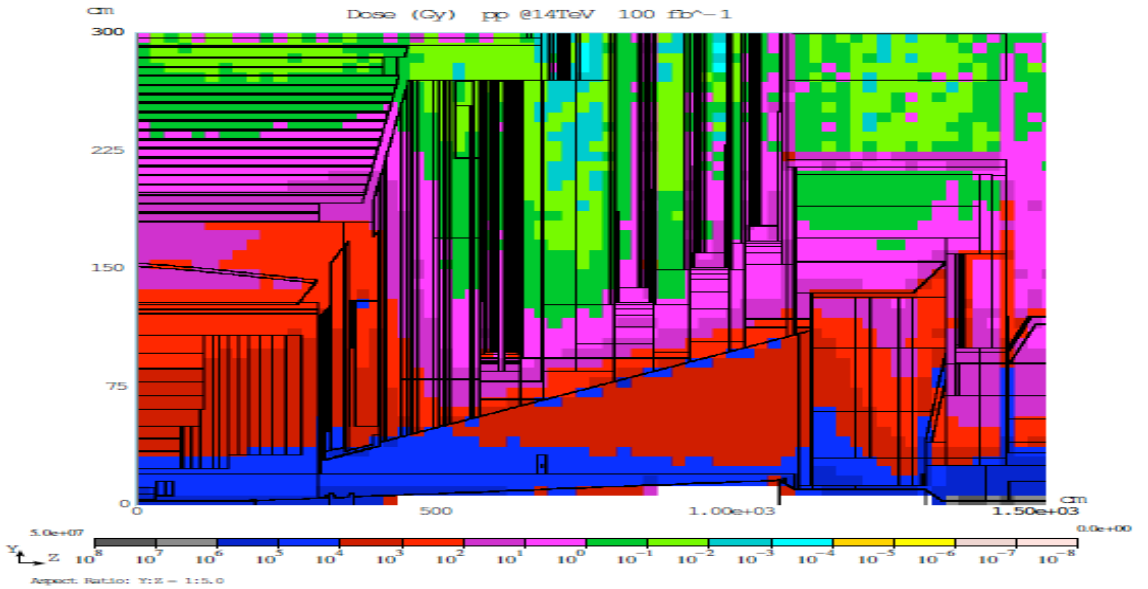

Figure F.12: A MARS code representation of the radiation field for the CMS endcap and forward regions. The calculation assumes pp collisions at 14 TeV with an integrated luminosity of 100 fb^{-1}.

trigger primitives are under study. Several technical solutions can be worked out, but these are strongly dependent on ultimate choices of the new Tracker design.

F.3.2 RPC Phase 2 Upgrades

The CMS Forward Muon system comprises four stations, namely RE1 to RE4. At this time only the first three are instrumented with Resistive Plate Chambers, since the fourth station RE4 was initially descoped. The phase 1 upgrade will add the RE4 station which provides coverage up to $|\eta| = 1.6$.

The RPC muon system provides both a level 1 high p_T trigger and an offline muon identification. The trigger consists of the coincidence of at least three RE stations which provides the bunch crossing identification. The RE system as presently configured covers the region $0.9 < |\eta| < 1.6$. For this η region extensive tests were performed over several years in order to validate the RPC technology, the gas mixture and operational characteristics, namely particle rates of the order of few 10 Hz/cm^2. These were successful in concluding that this η region could be successfully instrumented with the current design of RPC chambers. However, in the high particle rate environment and radiation conditions at a higher $|\eta| > 1.6$ region additional studies would be required. Thus the high η region of CMS is presently vacant and presents an opportunity to instrument it with a detector which would be suitable for operation at the Phase 2 luminosity of the LHC.

The high η environment of the phase 2 LHC presents hostile conditions of particle fluence rates of several 100 Hz/cm^2 up to several kHz/cm^2 at a luminosity of 10^{35}cm^{2}s^{-1}. In addition, the rates of thermal neutrons, low energy protons and γs must be taken into consideration.

Careful studies will be undertaken to simulate the expected background for $|\eta| > 1.6$. As part of this simulation, the increase of the CMS physics capability in this region must be quantified. This preliminary study must also clearly define the ideal detector requirements for safe operation.

At this time, Micropattern detectors (MPGDs) seem to be a promising candidate technology to instrument the currently vacant zone in the forward part of CMS ($1.6 > |\eta| > 2.1$), although other options could be possible in case the background would be consistently lower than foreseen now. Using MPGDs with enhanced readout granularity in $\eta - \phi$, and an improved rate capability by two orders of magnitude, one could complete the forward RPC system with good trigger and tracking efficiency. While there are several types of MPGDs, two types look promising for this application, namely the micromegas (MM) and the gas electron multiplier (GEM). Both these detectors have the potential for producing large area (1m x 2m) detectors with cost effective industrial processes. They have demonstrated stable, long term operation and have negligible discharge probability. Both types of MPGDs have already been installed successfully in other experiments. In the LHCb first muon station, where expected rates are $\sim$500 kHz/cm^2, triple GEMs have been installed, and ATLAS is considering the micromegas for its muon upgrade.

The full understanding of the operation of GEM detectors in high neutron and γ fluxes, as expected in the high η region, require additional studies in CMS. The main topics of investigation are:

- Large size detector prototyping and performance studies.
- Ageing studies.
- A detailed mechanical design.

- Integration studies for mechanical envelope services and routing in CMS.

F.3.3 CSC Phase 2 Upgrades

For LHC Phase 2, a new track trigger in conjunction with the existing CSC muon information should be sufficient to allow Level-1 muon triggering at an acceptable rate and momentum threshold. Therefore, the potential Phase 2 upgrades for the CSC system are more oriented towards handling high particle and background rates. Depending on experience with these rates at various luminosities, deployment of the upgraded cathode (DCFEB) boards could be expanded from the ME1/1 chambers to other types of chambers as well, in order to dramatically improve their high-rate capability. Likewise, expansion of the use of replacement TMB mezzanine cards to other types of chambers would result in better trigger-level spatial resolution in addition to higher rate capability. The anode (ALCT) on-chamber boards could have their mezzanine cards swapped with new ones containing high-performance logic (FPGAs). This could allow for dramatically better position resolution, as well as improved time resolution that could enable a slow-particle trigger if desired. The CCB boards would need replacement only in the case that the clocking of the experiments via the TTC system needs to be changed. Finally, the CSC system data flow is most concentrated in several crates of DDU and DCC readout modules, and replacement is only contemplated if there are surprises with background particle rates. The numbers of the boards mentioned are: 2268 DCFEB, 468 TMB mezzanine, 540 ALCT mezzanine, 60 CCB, 36 DDU, and 4 DCC.

F.4 Trigger R&D for Phase 2

F.4.1 Introduction

In order to meet the challenges of Upgrade Phase 2 operation the suggested approach is to hold the overall Level-1 trigger rate at the LHC value of 100 kHz by increasing the readout bandwidth. This approach avoids rebuilding front-end and readout electronics as much as possible since these were designed for an average readout time of less than 10 μs. It also permits use of front-end buffers for an extension of the Level-1 Accept (L1A) latency rather than for more post-L1A storage before readout.

Operating the LHC with 50 ns bunch crossing spacing at 5×10^{34} implies a pileup 200 min-bias events/crossing. This is a factor of more than 10 greater than the LHC design luminosity (10^{34}) figure of 20 min-bias events per 25 ns bunch crossing and will degrade all occupancy-dependent trigger algorithms that rely on forms of isolation to identify electrons, muons, taus and missing energy signals. Since running the SLHC at 40 MHz will be retained as an option to mitigate these difficulties, we require that all CMS detector and electronics designs for SLHC upgrades work with a 25 ns bunch spacing and handle an occupancy consistent with 5×10^{34} at 50 ns bunch spacing. This requires a more performant trigger with additional information, such as tracking data, used to reduce the trigger rates against the much higher backgrounds. The size of regions sampled for trigger decisions will need to shrink to handle the increased backgrounds.

F.4.2 Upgrade Phase 2 Trigger Strategy

The strategy for the upgrade follows the present strategy of TriDAS evolution during LHC running of first operating any hardware Level-1 (L1) trigger virtually in the Filter Farm Higher Level Trigger (HLT) code using emulation compared with the data read from the L1. During the first phase of CMS LHC operation, the L1 algorithms involve data from the calorimeter and

muon systems. Once the trigger rate reduction power of these subsystems is fully exploited, the next step is to use tracking information.

The CMS Upgrade Phase 2 Trigger R&D centers on integration with a L1 tracking trigger for identification of tracks associated with calorimeter and muon trigger objects. The track information provides a sharp momentum threshold and also is used for isolation. This information would be used to combine with the calorimeter at L1 to reject π°s and reject jets from pileup. The tracks would be used to sharpen p_{T} thresholds and reduce accidentals and wrong crossing determinations in the muon system. Implementation would not only require rebuilding the tracker, but also rebuilding the calorimeter and muon trigger systems in order to provide outputs with suitable granularity and other information to combine with the L1 tracking trigger.

For the Upgrade Phase 2 the L1 trigger data would need combination between tracking and calorimeter and muon triggers at a regional level with finer granularity than presently employed. After this regional correlation stage, the physics objects made from tracking, calorimeter and muon regional trigger data would be transmitted to the Global Trigger. The important new feature is that some of the tracking, isolation, and other regional trigger functions would be performed in combinations between regional triggers in a new hardware layer composed of regional cross-detector trigger crates.

The additional layer of processing for combination of tracking information, increased algorithm complexity and larger trigger data volume due to finer trigger granularity motivates an extension of the present CMS 3.2 μs L1 latency. A longer latency would also be needed for use of FPGA embedded serializers and deserializers, addition of more serialization and deserialization steps to use high speed serial links or use of buffers to incorporate commercial serial links running asynchronously with respect to the LHC clock. The CMS L1 latency is limited by the front-end analog storage capacity of the tracker and preshower electronics. Since it is expected that these detectors will be replaced for the SLHC, it is reasonable to assume that their electronics will be replaced also and that this limitation can be removed. The next limitation is the ECAL digital memory depth of 256 40 MHz samples corresponding to time of 6.4 μs. This is proposed as the CMS SLHC L1 latency baseline.

F.4.3 Upgrade Phase 2 Track Trigger R&D

A source of trigger primitives not used in the current CMS L1 trigger system is the strip and pixel tracker. Presently this information is added only in the HLT, where it effectively reduces rates and backgrounds. For the proposed Phase 2 upgrade the complete tracking systems will need to be replaced due both to radiation exposure and to be able to handle the higher occupancy in collisions with 200 to 400 interactions. This complete rework of the tracker opens up the possibility to read out trigger primitive information from the tracker for use in the L1 trigger.

The tracker can provide information of four types: (1) the simple presence of a track match validates a calorimeter or muon trigger object, e.g. discriminating electrons from hadronic (π°) backgrounds in jets; (2) adding precise track hits improves precision on the p_{T} measurement, sharpening thresholds in the muon trigger; (3) the degree of isolation of an e, μ or τ candidate; and (4) the primary z-vertex location within the 30 cm luminous region derived from projecting tracks found in trigger layers, providing discrimination against pileup events in multiple object triggers (e.g. in lepton plus jet triggers, jets inconsistent with the lepton z vertex could be rejected). In the HLT, track matching to electron L1 objects reduces the rate by a factor of 10. A similar rejection factor is achieved for muons by adding tracker measurements for isolation and p_T. We would like to retain the ability at SLHC luminosities of 10^{35} cm^{-2}s^{-1} to have an

open L1 trigger for single electron and muons with thresholds in the range from 20 to 30 GeV.

Different concepts for tracking trigger primitive generation are currently explored by the tracker community. Most effort is currently put into studying modules that will provide p_{T} discrimination in the front ends by correlating hits in two closely stacked sensors. Current indications are that two or more layers of these modules will be required in order to provide useful information to enhance the current L1 electron, μ, and τ triggers. To maintain the eta coverage of the current trigger and control the rate, the track trigger has to cover the full eta range -2.5 $< |\eta| <$ 2.5. The most straightforward way to accomplish this is to have long barrel modules at radii less than $\sim$50 cm. The trigger primitives considered are the stubs that are formed by pairs of hits in the closely stacked sensors, or tracklets that are obtained by linking up stubs. The stubs provide only minimal p_{T} information as the lever arm for two hits separated by 1 to 2 mm only allows the possibility to apply a threshold to remove hits from low momentum tracks. However, the tracklets that link up two stubs allow a much more precise momentum determination. At these small radii the sensors naturally have to be (long) pixels of no more than a few millimeters in z in order to keep the occupancies low. This fine segmentation in z allows determination of the track vertex along the z-axis with a precision of about 1 mm.

Another area of active research is development of algorithms to use of tracking trigger primitives to accomplish track matching, isolation, p_{T} measurement and z vertex determination. We are pursuing conceptual designs for the interfaces to the calorimeter and muon triggers that allow their Phase 1 upgrades to add tracking trigger primitives when they become available. The improvements in the calorimeter and muon trigger to report more precise $\eta - \phi$ coordinates are important for the performance of the track trigger in order to reduce road sizes and reduce the combinatorial problem when linking the coarse information from the outer detectors with the very precise information from the tracker.

F.4.3.1 Upgrade Phase 2 Calorimeter Trigger R&D

The primary idea to reduce the Phase 2 SLHC rate by an order of magnitude is to use tracking in the Level-1 trigger system to identify the lepton tracks, isolate them from other tracks in the event, and perhaps also to ascertain that all the lepton tracks and jets triggering the event originate from the same interesting primary vertex. To reduce the volume of data examined by the trigger system, the calorimeter trigger can provide seed information for the objects found by it. The better position resolution calorimeter trigger provides, the better it is for the tracker trigger processing.

We would like to design and implement the upgraded calorimeter trigger with the best possible position resolution already at Phase 1. The reason for such an early implementation of position resolution is primarily for Phase 2 matching with tracker. Our early studies indicate that we are able to specify the electron and τ object position to half-a-tower resolution (0.04 in $\eta - \phi$).

The Phase 2 SLHC related R&D that we propose to conduct is:

- Simulation studies to determine the best position resolutions for electron, τ, jet and MET objects that can be achieved.
- Identify data flow and bandwidth required to carry the position information for all objects between the various cards.
- Prototype cards with sufficient number of links with appropriate bandwidth between cards to carry the position information

F.4.3.2 Upgrade Phase 2 CSC Muon Trigger R&D

The high luminosity of Upgrade Phase 2 CSC Trigger will require a Level-1 muon trigger for the endcap that can handle increased occupancy by at least a factor 10 (for 50ns bunch spacing and L=5×10^{34}), and possibly higher due to larger than linear growth effects in the number of chamber-level trigger patterns fired due to neutron backgrounds. In addition, to take advantage of the increased luminosity for physics, generally one needs to maintain similar p_T thresholds as used for LHC running, and this will require improving the momentum resolution of the trigger because the rate predominantly comes from mis-measured real muons. Therefore, data points from an inner silicon tracking device are also required to be matched to Level-1 muon candidates, and a refit of the momentum to improve the momentum resolution. To seed the tracker regions to include into the trigger, refined η, ϕ, and p_T information is required from the CSC trigger.

The R&D required to prepare a Phase 2 Muon Trigger includes high bandwidth serial links (optical from the Muon Port Cards on the detector, and copper between the Sector Processor and Muon sorter track-finding cards in the underground counting room), and very large FPGAs to accommodate the increased functionality and much higher number of logic tests required in the track-finding (scales approximately as the square of the number of segments used). Naively scaling the existing track-finding algorithms to 20 times higher input occupancy does not seem feasible, thus accurate simulations and projections are required to ascertain the expected background levels, and new methods of track-finding should be investigated. Thus, a third R&D area on alternative CSC track-finding algorithms is proposed, such as using a pattern-based approach rather than a cut-based one. This could be implemented into high density FPGAs, or possible dedicated ASICs such as the AM++ associative memory design, into the Sector Processor design.

For the serial link technology, 10 Gbps would solve the need for the optical link connections from the detector. Thus investigation and prototyping of serializer-deserializer (serdes) chips (possibly using those embedded into FPGAs) and opto-transceivers approaching that bandwidth are planned. Additionally, R&D on backplane communication using serial links is foreseen. For implementation of logic into large state-of-the-art FPGAs, the Xilinx Virtex-5 and Virtex-6 chips will be taken as starting points for the research.

This hardware R&D will complement the simulation studies we are conducting to evaluate the performance of the upgraded CSC trigger with estimated Upgrade Phase 2 background levels. Moreover, the improved precision of the muon candidates will be used in studies with tracker stubs to contribute to the conceptual design for a second stage regional muon track-finder linking and fitting tracker stubs.